IAHR 2017

37th IAHR WORLD CONGRESS

13-18 August, 2017

Kuala Lumpur, Malaysia

Supported by Spain Water and IWHR, China

FLOOD MITIGATION AND CONTROL

GREEN WALL AS URBAN FLOOD MITIGATION

DARRIEN YAU SENG MAH[(1)], JING TECK LAU[(2)], HAFIZAH MARIAH MOHD ABUSEMAN[(3)] & FANG YENN TEO[(4)]

[(1,2,3)] Department of Civil Engineering, Faculty of Engineering, Universiti Malaysia Sarawak, 94300 Kota Samarahan, Sarawak, Malaysia
ysmah@unimas.my, dante.lau91@hotmail.com, 30292@siswa.unimas.my
[(4)] Department of Irrigation and Drainage Malaysia, Jalan Sultan Salahuddin, 50626 Kuala Lumpur, Malaysia
teofy@water.gov.my

ABSTRACT

This study intends to look into modular-typed green wall, specifically with coconut peat as the growing medium. Commonly, such design is attached to vertical outdoor wall. Therefore, it is suggested to direct roof runoff to the green wall as an urban flood mitigation strategy. Characteristics of coconut peat are investigated through experimental works. The application as urban runoff control is demonstrated through a modelling case study of a typical commercial lot. SWMM model is developed by taking the advantage of its low impact development interface to apply bio-retention system as a green wall. Scenarios of using dry and saturated coconut peats are subjected to intense 15-minute 10-year ARI storm event. Outputs of the model suggest that a straight column of green wall modules in 700 mm wide, 200 mm thick and 12000 mm high is capable to fully capture the 6.3 m^3 of total roof runoff generated by the design storm. Hence, the idea of adopting green wall for urban flood mitigation is encouraging.

Keywords: Bio-retention; growing medium; hydraulic conductivity; runoff; stormwater.

1 INTRODUCTION

Green wall is increasingly argued as a way to solve the issue of impervious area in cities. On top of the popularity of green wall solely for aesthetic value, it could have another added value as stormwater detention system. Roof runoff outlet on the roof may need minor modification to direct the rainwater to the green wall. Discharge outlet of the green wall is equipped to discharge excess water to nearby drain and it may need modification of its size to accommodate passing of rainwater. Loh (2008) stated that runoff could be reduced through percolation of rainfall within living walls, thus offering true benefits to urban stormwater management. Several preliminary studies suggested that these systems retain as much as 45 to 75% of rainfall (Webb, 2010). Besides, researchers like Kew et al. (2013) mentioned that, green walls might become one of the effective stormwater management via vertical planting systems as wall area far exceeds roof area especially in the urban developing areas.

There are many types of green wall. In this paper, the green wall is referring to modular cells of quadrilateral in shape (see Figure 1). Such module is assembled from durable lightweight interlocking panels. Each module has a large face with a grid of conveniently spaced openings to support vertical planting. The thickness of module varies to accommodate different media depths and volumes to cater for the needs of a wide variety of plants.

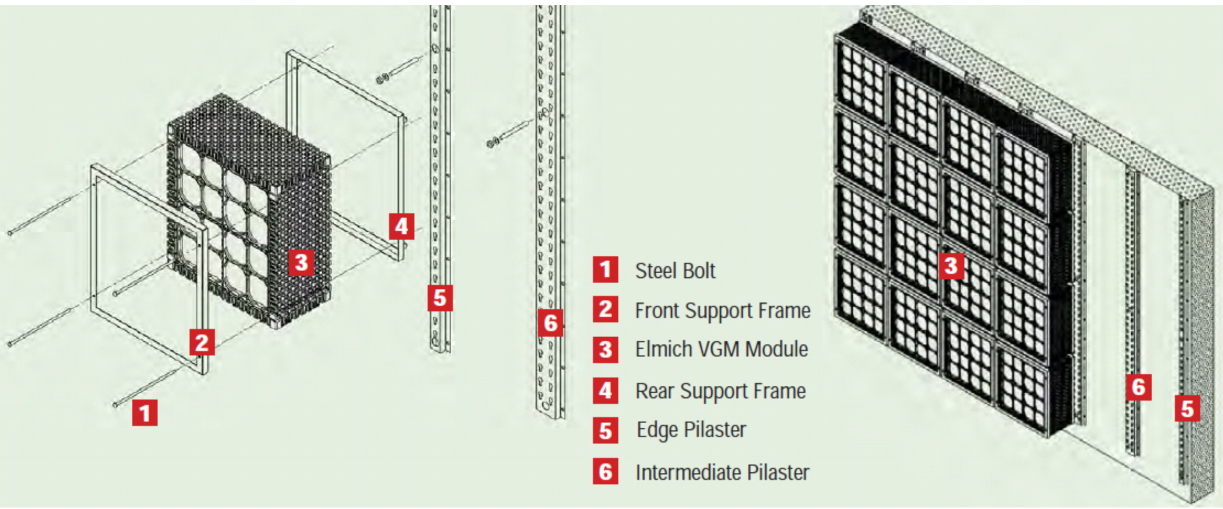

Figure 1. Green wall module (Elmich, 2008).

2 MOTIVATION

Green wall is similar to a bio-retention system, but structured in a vertical manner on a façade or wall, without the traditional requirements of space by sacrificing built-up area. If conventional bio-retention system is a component of urban runoff control, then theoretically green wall should be able to have the same function.

Bio-retention system is highly dependent on growing medium to support growth of plants as well as to capture runoff and to allow infiltration process to take place in the system. Therefore, this paper is looking at a particular type of fairly new growing medium available in the market – coconut peat. Its light and organic in nature have been proven good for gardening. However, its ability for runoff control is unknown at the moment. Laboratory investigations on coconut peat are carried out based on the principles of bio-retention system. Then, a case study of modelling a green wall based on the same principles is presented to better demonstrate the application of green wall as urban flood mitigation strategy.

3 GROWING MEDIUM

Artificial soils are often used as the growing medium for green wall. Coconut peat is chosen as it is one of the available artificial soils other than mineral or organic soils. It is made from coconut husks and primarily consists of coir fibre or coir dust. This can be obtained by processing coconut husk and removing the long fibres. Coconut peat is able to hold a large quantity of water similar to a sponge. It is best used as a replacement for traditional peat in soil mixtures and also used for plant cultivation as a soil-less substrate (Global Coirs, 2014; Mason, 2003).

4 EXPERIMENT

Five (5) parameters of the coconut peat were tested through laboratory works. Firstly, hydraulic conductivity indicates the speed of water infiltration through a soil layer (Arshad *et al*., 2013). Coconut peat is packed into porous bag that could be fitted to a single green wall module. Experiments were conducted on a hydraulic bench by passing water through different depths of coconut peat to determine the flow rate with and without the artificial soil. The values of hydraulic conductivity for dry and saturated coconut peats are tabulated in Table 1. Generally, dry coconut peat drains faster compared to saturated coconut peat. The saturated form is demonstrating the desired performance to be able to hold water longer and yet its hydraulic conductivity does not differ much compared to the dry form.

Table 1. Hydraulic conductivity for coconut peat.

Depth of Coconut Peat (mm)	Hydraulic Conductivity (mm/hr)		
	Dry	Saturated	Difference (%)
100	86.5	106.3	+ 22.9
200	191.3	187.6	- 2.0
300	283.4	249.1	- 13.8
400	333.4	372.0	+ 11.6

Other than hydraulic conductivity, the remaining characteristics of coconut peat are tabulated in Table 2. Suction head is to assess the quality of the soil, estimate in-situ effective stress and the realistic application of the unsaturated soil mechanics. It is measured by using mini disc infiltrometer (Decagon Devices, 2014). Porosity is the volume of soil voids that is able to be filled by water or air. Field capacity is the amount of water in the soil after being wet or free drainage has ceased in soil. Wilting point of the soil occurs when most plants unable to recover their turgor upon rewetting and when the volumetric water is too low for the plant to remove water from the soil (NCCRA, 2008).

Table 2. Other characteristics of coconut peat.

Parameter	Value
Suction Head (mm)	60
Porosity (fraction)	0.277
Field Capacity (fraction)	0.043
Wilting Point (fraction)	0.023

5 MODELLING CASE STUDY

The data collected above is required to simulate the movement of runoff down a bio-retention system as green wall (see Figure 2). Storm Water Management Model (SWMM) under the sponsorship of US Environmental Protection Agency (EPA) has its version 5.0 updated with functions of low impact development (LID) controls (Rossman, 2010). Storage and underdrain are not applicable in this case. However, the soil layer as the dominating component is increased many folds to resemble a green wall.

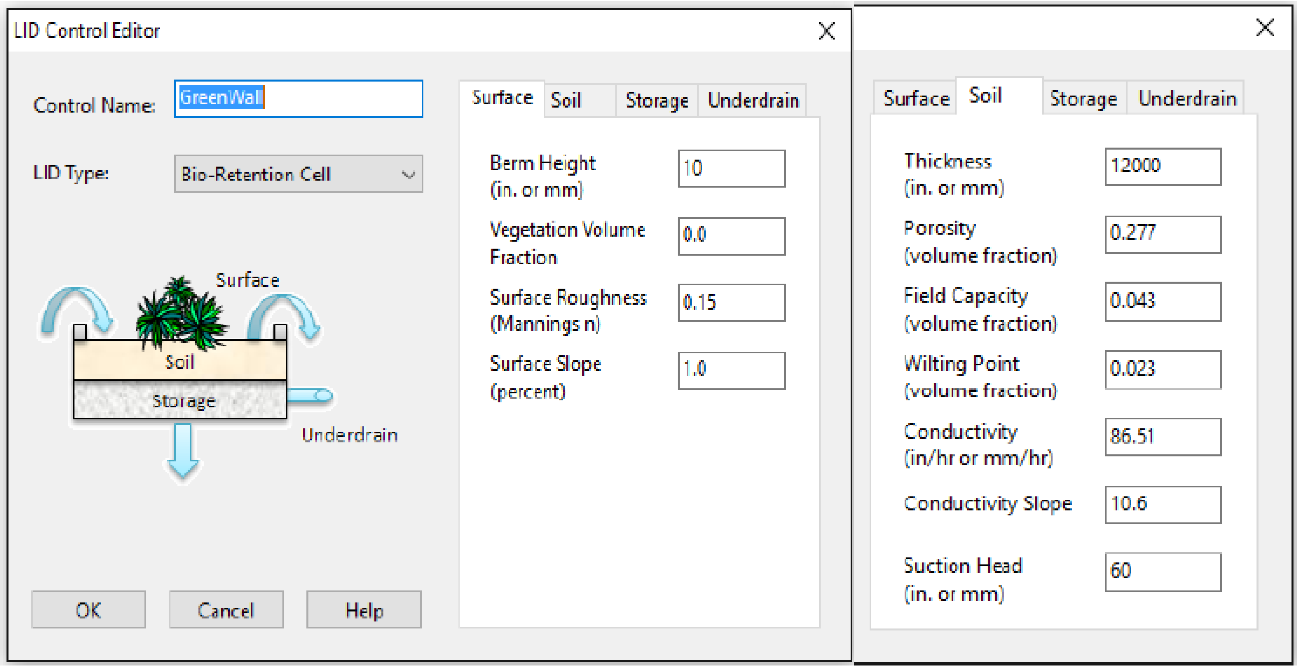

Figure 2. Bio-retention interface in SWMM version 5.0.

A green wall is proposed just in front of a column of a typical commercial lot as shown in Figure 3. The top would receive runoff from the roof, then the water is to slowly infiltrate by gravitational force to the ground level, lastly, flows into the culvert and road side drain. The width and height of building column is measured to be approximately 750 mm and 12000 mm respectively. The size for a single green wall module is 700 mm in height, 700 mm in width and 200 mm in thickness. Therefore, there are a total of 17 modules to be assembled as a straight column which is approximately the building height.

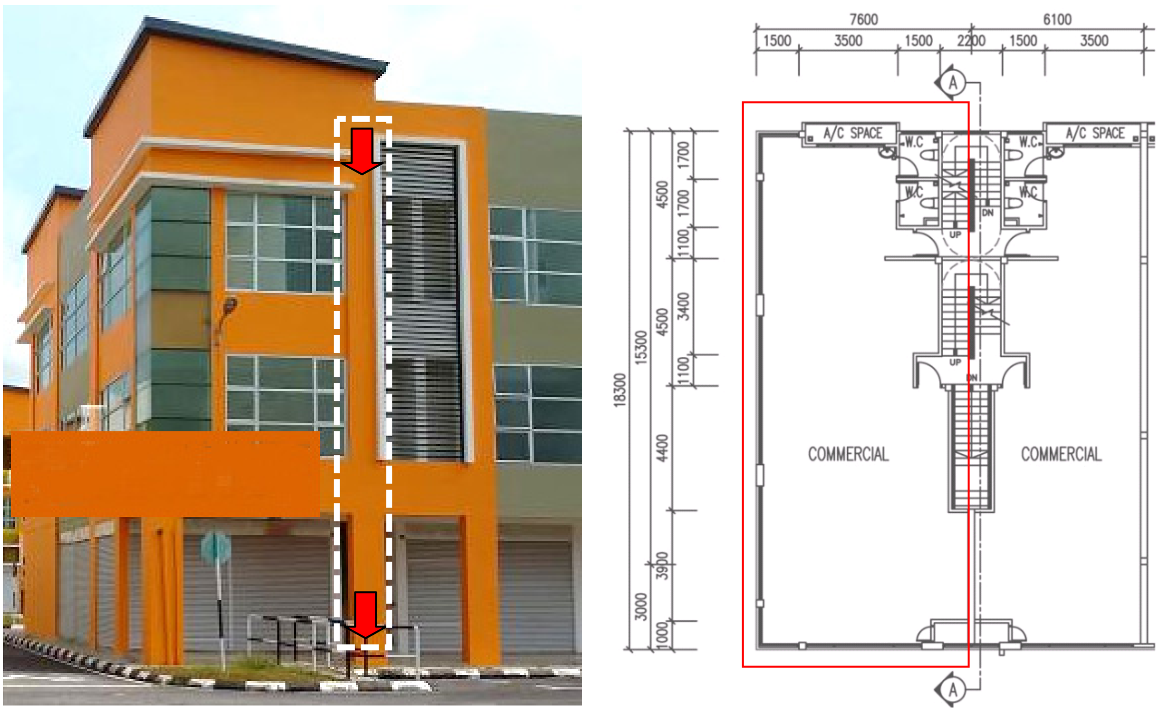

Figure 3. Proposed green wall for typical commercial lot.

A SWMM model is developed based on the case study above using the interface of bio-retention system as green wall. Two scenarios are developed, namely using dry and saturated coconut peats following the experimental works. Due to small catchment, the scenarios are subjected to 15-minute 10-year ARI storm based on local weather pattern in Kuching. Such storm event is very intense with 180 mm/hr of rainfall and 45 mm of rainfall depth over 15 minutes. The roof catchment would produce a peak runoff of 0.00702 m^3/s.

The outcomes are presented in Tables 3 and 4. It shows the assumptions used in the modelling of considering only 100, 200, 300 and 400 mm of coconut peats at the top of the green wall. Once the filling capacity of the artificial soil is met, the running water shall be directed to outlet. Each depth is using the hydraulic conductivity obtained from experimental works. The hydraulic conductivity increases with the depth of soils, and the model estimated the coconut peats are retaining water as its depth increases. Thus, it is suggesting that coconut peak could adsorb even more water if the depth was to further increase.

Based on the above-mentioned statements, the authors extrapolate the graphs in Figure 4 to reach 100% of runoff reduction by assuming status quo for the capability of coconut peat in draining water. It is estimated that it would requites about 1500 mm deep of dry coconut peat to hold 6.3 m^3 of total roof runoff, while about 3000 mm deep of saturated coconut peat to do the same.

Table 3. Modelled output for dry coconut peat.

Parameter	Depth of Coconut Peat (mm)			
	100	200	300	400
Roof Runoff (m^3/s)	0.007020	0.007020	0.007020	0.007020
Runoff from Green Wall at Outfall (m^3/s)	0.006196	0.005772	0.005334	0.004903
Runoff Detained (m^3/s)	0.000824	0.001248	0.001686	0.002117
Reduction (%)	11.73	17.78	24.02	30.16

Table 4. Modelled output for saturated coconut peat.

Parameter	Depth of Coconut Peat (mm)			
	100	200	300	400
Roof Runoff (m^3/s)	0.007020	0.007020	0.007020	0.007020
Runoff from Green Wall at Outfall (m^3/s)	0.006453	0.006331	0.006015	0.005800
Runoff Detained (m^3/s)	0.000567	0.000789	0.001005	0.001220
Reduction (%)	8.08	11.24	14.32	17.38

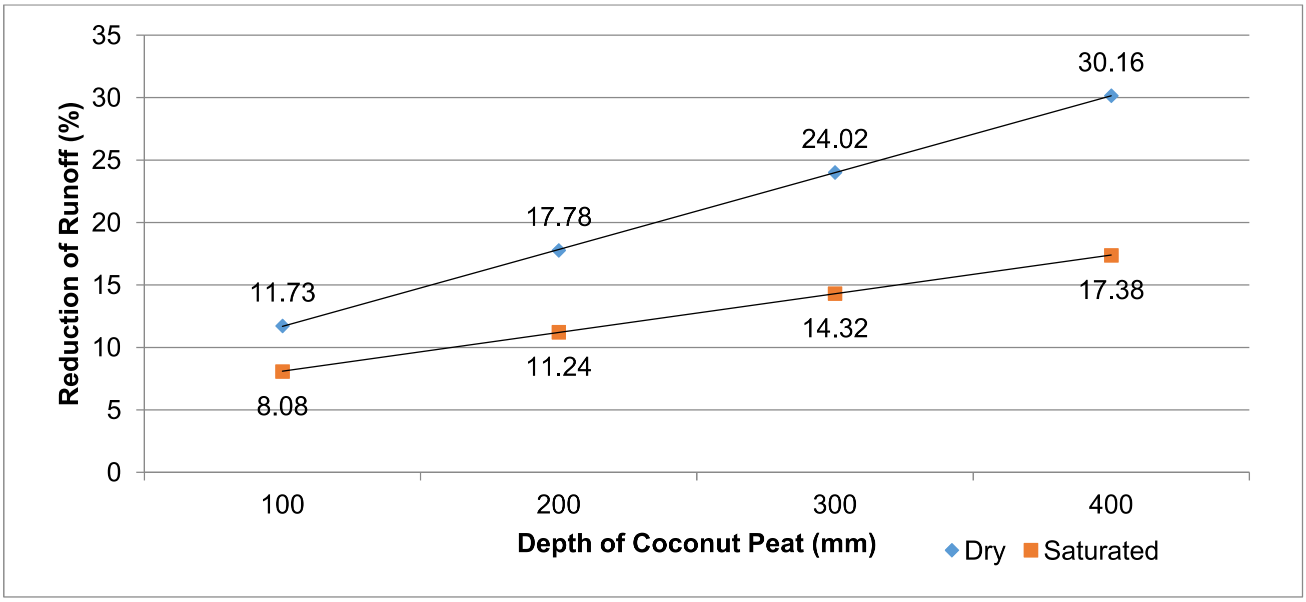

Figure 4. Peak runoff reduction for different depths of dry and saturated coconut peats.

6 CONCLUSIONS

Based on the results, the reduction of runoff is increasing as the soil depth increases. The height of the green wall of 12000 mm could hold the volume of water for 15-minute 10-year ARI storm event for both dry and saturated coconut peats. Both meet the objective of urban runoff control to slow down and detain temporarily the roof runoff. It shows that green wall is possible to be adopted as urban flood mitigation strategy. However, the factors of plant and its roots are not included in the analysis. Therefore, further testing with live plant is needed to reflect a more realistic representation of green wall.

ACKNOWLEDGEMENTS

This project was funded by SpGS Grant F02/SpGS/1405/16/6 rendered by the Universiti Malaysia Sarawak. The authors wish to thank the Department of Irrigation and Drainage for their continuous support.

REFERENCES

Arshad, R.R., Gharabaghi, B., Mosaddeghi, M. & Sayyad, G. (2013). Predicting Saturated Hydraulic Conductivity by Artificial Intelligence and Regression Models. *ISRN Soil Science*, 201, 1-8.

Devices, Decagon. (2014). Mini Disk Infiltrometer User's Manual. Available at http://www. decagon. com/products/hydrology/hydraulic-conductivity/mini-disk-portable-tension-infiltrometer/ [Accessed 12 May 2014].

Elmich (2008). *Elmich Green Wall*. Available from http://www.elmich.com [Accessed 2 February 2015].

Global Coirs (2014). Coco Peat. Retrieved from http://www.globalcoirs.com/coco-peat.html [Accessed 5 June 2017].

Kew, B., Echols, S. & Pennypacker, E. (2013). Green Walls as a LID Practice for Stormwater Mitigation: Can Green Walls Provide Similar Attributes as Green Roofs? *6th International Conference of Education, Research and Innovation*, Seville, 18 November, 2598-2607.

Loh, S. (2008). *Living Walls - A Way to Green the Built Environment*, BEDP Environment Design Guide, 1 (TEC 26), 1-7.

Mason, J. (2003). *Sustainable Agriculture*. BPA Print Group, Australia.

Northeast Region Certified Crop Adviser (NCCRA) (2008). *Competency Area 2: Soil Hydrology AEM*, Cornell University.

Rossman, L.A. (2010). *Storm Water Management Model User's Manual Version 5.0,* US Environmental Protection Agency.

Webb, V. (2010). Green Walls: Utilizing & Promoting Green Infrastructure to Control Stormwater in Mobile, Alabama. *Emerging Issues along Urban/Rural Interfaces III: Linking Science and Society*, 256,130-136.

Proceedings of the 37th IAHR World Congress
August 13 – 18, 2017, Kuala Lumpur, Malaysia

ROAD INTERSECTION AS STORMWATER DETENTION BASIN

DARRIEN YAU SENG MAH(1), SIEW LING LOH(2), GABRIELLA SABATINI ANAK POUL(3) & WAN HASHIM WAN IBRAHIM(4)

(1,2,3,4) Department of Civil Engineering, Faculty of Engineering, Universiti Malaysia Sarawak, Kota Samarahan, Sarawak, Malaysia

ABSTRACT

This study is exploring the potential of transforming road junction with dual functions in supporting traffic flow and accommodating stormwater detention. High loading capacity in specialist concrete could be used to construct precast concrete modular units, as it could be strong enough to allow passing of vehicles. It could also be molded to form hallow chambers that function as temporary stormwater storage. A modelling case study is presented to showcase the application of such stormwater on-site detention system. Initial modelling has indicated that the design could reduce the flow of urban runoff by 40-50% on road surface; and the running water could be fully captured within a height 0.4 m of underground storage.

Keywords: Flash flood; junction; road drainage; subsurface; pavement.

1 INTRODUCTION

Nowadays, cities are becoming busier with more and more vehicles each year. Hence, road drainage is one of the important necessities to have well-managed roadways. During the rainy season, rainwater can accumulate rapidly on the road surface and thus causing the occurrence of flash flood. The phenomenon that called “stripping”, well explains the problem of water damage to asphalt pavements (Kandhal et al,, 1989). This could cause the road to crack and forming potholes on the road. These situations should be avoided because it can be costly to observe maintenance on the roads. Besides, stormwater runoff forms a thin film of water and as it flows at the edge of the road pavement, its speed increases. It is also known as hydroplaning.

In the particular case in Figure 1, the road junction has a wide impervious surface area. This causes the time taken for the stormwater runoff to discharge out of the site to be longer. Therefore, ponding happens on the road junction for a certain period of time. The infiltration process is not possible on this particular land cover because road pavement is made of asphalt. The ponding on the road junction can be a disturbance because it can cause accidents, washouts, and delay to drivers and pedestrians. Besides that, it is known to cause deterioration to the road structures after repetitive flash flood events.

Figure 1. Surface runoff on the road (http://www.straitstimes.com, Published 10 Dec 2015).

2 MOTIVATION

In addition to poor road drainage, road junction, as according to JKR Sarawak, suffers damages quite often due to the traffic loads of reducing speed at traffic lights instantly and picking up speed when the traffic light changes the cycle to red or green. There is a request to improve the strength of the pavement materials for the road junction. Thus, this study is attempting to solve both problems simultaneously using precast concrete units under the road junction for pavement and urban runoff control.

3 STORMWATER ON-SITE DETENTION

On-Site Detention (OSD) is a structural component in the drainage system that controls the discharge of urban runoff using a temporary storage as an outlet restriction device near to the source. Mascararenhas et al. (2005) had reported underground reservoirs could be applied as alternative to urban runoff control. There are many forms of the so-called underground reservoirs. One of popular materials is the use of precast concrete as the road pavement and at the same time, providing the mentioned reservoir under the pavement.

Mah et al. (2014; 2016) had reported a possible case of merging urban road with stormwater detention. They suggested modular precast concrete units, in which the top cover could be functioning as road pavement, the middle section is cylinder with hallow chamber for stormwater detention and the bottom cover for monolithic footing (see Figures 2, 3 and 4). The concrete design includes a high load carrying capacity that could withstand crushing load up to 100 kN/unit. For the aspect of stormwater detention, it could fully capture 3-hour continuous 10-year ARI storm event.

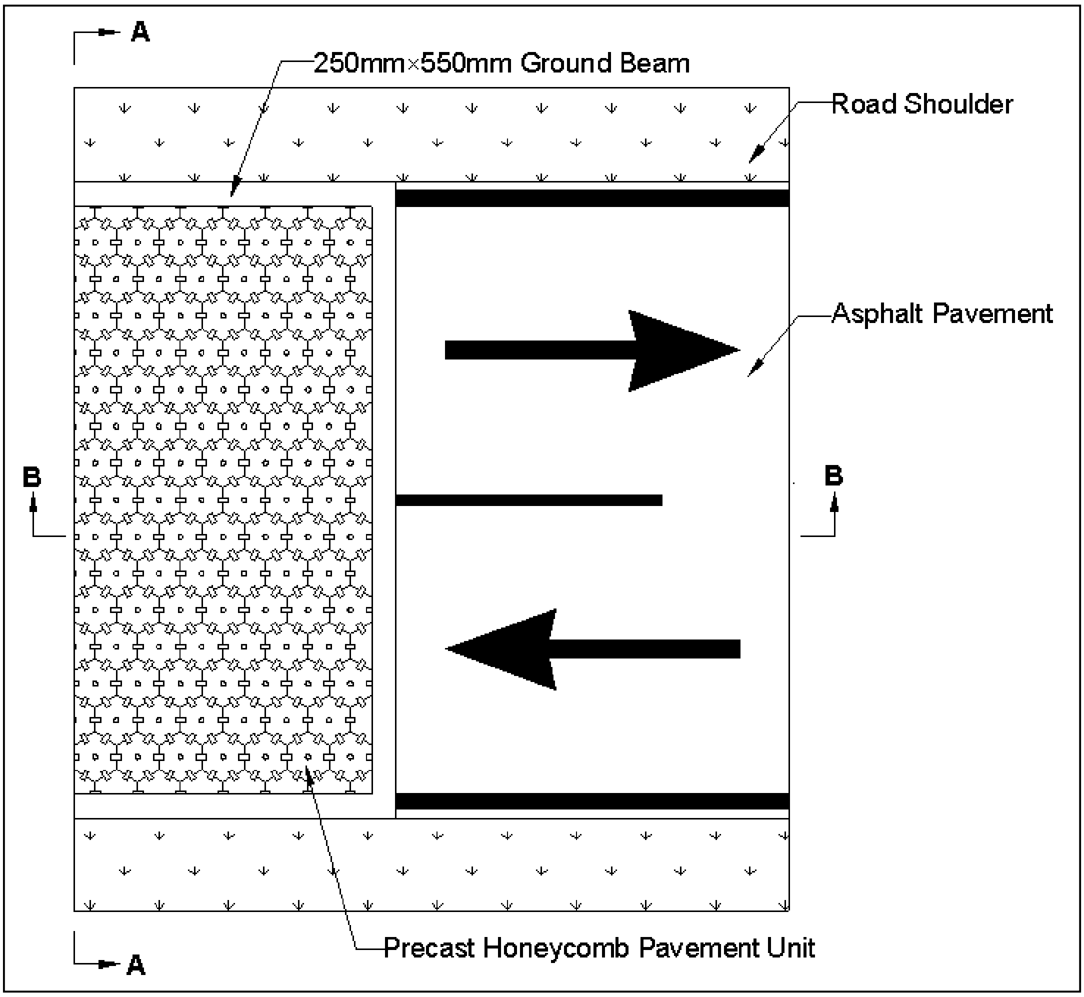

Figure 2. Precast concrete units as pavement (plan view).

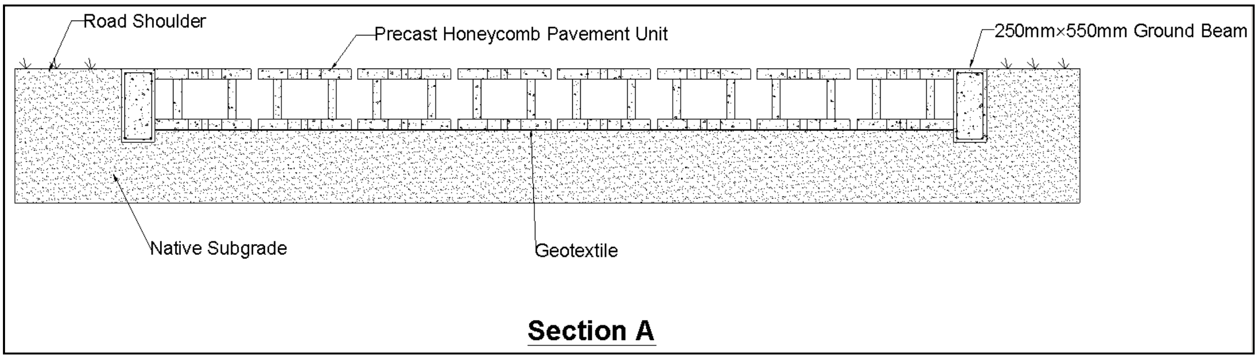

Figure 3. Precast concrete units as stormwater detention (sectional view).

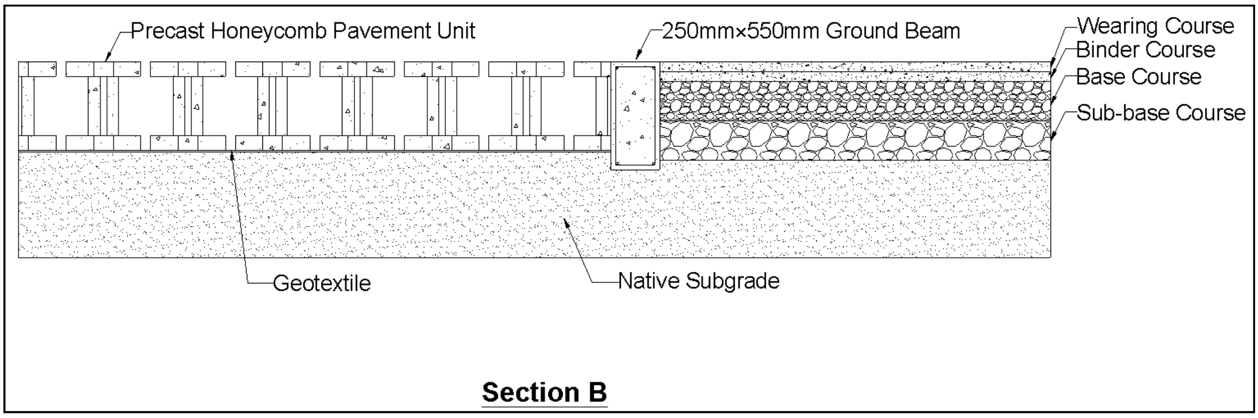

Figure 4. Precast concrete units compared to conventional road (sectional view).

4 MODELLING CASE STUDY

In this study, the road junction at the crosses of Jalan Tun Razak – Jalan Foochow 1 (Figure 5) is selected for case study. The sizing of the road junction is 31m in length and 25m in width and this sizing of road junction is a more typical design that can be found in Kuching city.

Figure 5. Satellite view of Jalan Tun Razak – Jalan Foochow 1, Kuching City (http://www.wikimapia.org).

By using the Storm Water Management Model (SWMM), there are a few inputs of parameters that should be considered in the modelling design and also to investigate the efficiency of the precast concrete modular units that can be constructed for road junctions. Stormwater that flows onto the road junction acts as the catchment area. The runoff shall be directed to hallow chambers and to the outlet. By using the diversity of ARIs, the design rainfall depths and intensities were determined to ensure the adequacy of the design. The storm duration for this particular case was taken at 15-minutes due to small catchment size of road junction. Rainfall intensities from 2-, 5-, 10-, 20- and 50-year ARI for Kuching City were considered.

Scenario 1 acts as an element which is used to compare with the next scenario on how much urban runoff that can be reduced with the OSD system. This could determine the sizing of the modular unit under the road junction. The results of the peak runoff from the existing condition are presented in Table 1. In this case study, it shows that the existing condition of the typical design of road junction has the highest peak runoff discharge of 0.0378 m3/s for 15 minutes of 50-year ARI storm. The urban runoff from road catchment is directly discharged into drainage system.

Table 1. Modelled peak runoff for Scenario 1.

ARI (year)	2	5	10	20	50
Peak runoff at outfall (m^3/s)	0.0276	0.0308	0.0330	0.0352	0.0378

In Scenario 2, the precast concrete modular units were constructed under the road junction in order to capture the urban runoff. The modular units would fill up within the dimension of 9.5m x 10m x 1m. The study area indicated here is small ($775m^2$/0.0775ha). The parameters of the storage unit such as the area, depth and the invert of the elevation were input based on the proposed OSD. Five simulations are developed by taking 15-minutes storm duration to run in SWMM simulation and to determine the depths to fully detain the stormwater in the storage. The results of the peak runoff after implementing the OSD tank under the road junction and depth of fully detained stormwater in the storage are tabulated in Table 2.

Table 2. Modelled runoff for Scenario 2.

ARI (year)	2	5	10	20	50
Peak Runoff at OSD (m^3/s)	0.0202	0.0222	0.0232	0.0242	0.0253
Reduction of Peak Values (%)	36.6	38.7	42.2	45.5	49.4
Depth of Fully Detained Stormwater (m)	0.24	0.27	0.29	0.31	0.33

By allowing infiltration to the underground hallow chambers during the course of storm event, the peak runoffs accumulated on the road surface were expected to decrease by 40-50%. The volumes of urban runoff are fully captured by the storage layer. The depth of storage was first set at 1 m in the model. Modelling outputs have demonstrated that it could be further reduced according to ARIs. To cater for weather variability, some 20-30% of extra height should be provided. Take the 50-year ARI, it could be provided at 0.4m. This depth is reasonable to be constructed, as conventional road laying required about the same thickness of aggregates. Therefore, the tank itself could be alternative to sourcing aggregate for road laying in the future.

5 CONCLUSIONS

In this research, by using SWMM model in virtually implementing an OSD system under the road junction at Kuching City has been carried out. The simulations of the study area are based on the existing condition of the study area; and with the inclusion of OSD system. Then, this study determines the effectiveness of the OSD system under road junction. Two scenarios have been used to compare the outcomes on implementing the OSD system. The results show that the peak runoff could be reduced close to 50% in 50-year ARI storm.

In conclusion, the OSD system is possible to be implemented in cities in the future as this could be a form of control so that urban runoff from the road could be detained to mitigate flash flood in the cities.

ACKNOWLEDGEMENTS

This project is funded by SpTD Grant F02/SpTDG/1440/16/3 rendered by the Universiti Malaysia Sarawak. The authors wish to thank the Department of Irrigation and Drainage for their continuous support.

REFERENCES

Kandhal, P.S., Lubold, C.W. & Roberts, F.L. (1989). *Water damage to asphalt overlays: case histories,* NCAT Report No. 89-1. Nashville, Tennessee: National Center for Asphalt Technology.

Mah, D.Y.S. (2016). SWMM Modelling of On-Site Stormwater Detention System underneath Urban Road. *International UNIMAS STEM Engineering Conference*.

Mah, D.Y.S., Putuhena, F.J. & Rosli, N.A. (2014). Environmental Technology: Potential of Merging Road Pavement with Stormwater Detention. *Journal of Applied Science & Process Engineering*, 1(1), 1-8.

Mascarenhas, F.C.B., Miguez, M.G., Magalhães, L.D. & Prodanoff, J.H.A. (2005). On-site stormwater detention as an alternative flood control measure in ultra-urban environments in developing countries. *IAHS-AISH Publication*, *293*, 196-202.

Proceedings of the 37th IAHR World Congress
August 13 – 18, 2017, Kuala Lumpur, Malaysia

A HYDROLOGY AND HYDRAULIC CASE STUDY ON JANUARY 2015 FLASH FLOOD IN UNIGARDEN, KOTA SAMARAHAN, SARAWAK

HAUZHI ER(1), LEONARD LIK PUEH LIM(2) & CHARLES HIN JOO BONG(3)

(1,2,3) Department of Civil Engineering, Faculty of Engineering, Universiti Malaysia Sarawak, Kota Samarahan, Sarawak, Malaysia
hauzhi@hotmail.com; llpleonard@unimas.my; bhjcharles@unimas.my

ABSTRACT

This study investigated the possible causes for occurrence of flash flood in UniGarden by looking into the hydrologic and hydraulic factors. This study consists of the assessment of water balance (precipitation, surface runoff, and infiltration) as well as the suitability of the hydraulic capacity of the existing earth drain based on MSMA guidelines. The site works involved analysis on precipitation, measurements of size of the earth drain and the corresponding flow velocity, and water quality testing. The consistency in annual rainfall and comparison between storm in year 2007 and 2015 indicated that precipitation was not the main cause of the flash flood. The infiltration of both storm events were limited due to precipitation few days prior to the extreme storm event that partially saturated the previous ground. There was a 45% increase in the average peak flow in 2015 than that in 2007. The TSS in both low flow and high flow were relatively low, providing estimated sediment loading up to 84.81 g d^{-1}, which is not likely to have a direct effect on reducing the earth drain size. Rapid vegetation growth slow down flow, reduced free flow area of the earth drain, thus decreased its hydraulic capacity. Lowest invert level point of the drain was found to be located some distance away from the outlet, indicating potential backflow of water. These findings suggests that the increase in runoff, decrease in hydraulic capacity, and the improper invert level of the earth drain contributed to the flash flood in UniGarden on 18 January 2015. This finding is essential in providing insight to the incident as well as call for consistency review of drainage network in land development policy and decision making.

Keywords: Drainage design; hydraulic capacity; vegetation; water balance.

1 INTRODUCTION

Flash flood affects the lives of people and environment by disrupting the mobility of residents, damaging infrastructures, and endanger public health and safety. Flash flood is also a strong indication for hydrological review of a catchment area, especially developed for area with proper drainage system. Therefore, this study was conducted to investigate the cause of flash flood in UniGarden on 18 January 2015. The accumulation of the surface water in the main earth drain preceded the flash flood. It was observed that the excess surface water overflow from the main earth drain towards the apartment and commercial areas (Figure 1a, b), give rise to submergence of the main access road (Figure 1b) and nearby compounds. The accumulation of surface water was observed during and after the storm (Figure 1c, d).

In this study, the flash flood is reviewed based on 5 areas of study, namely on precipitation, surface runoff, sedimentation, vegetation growth, and drainage design. It is anticipated that, should the intensity of precipitation increases, the runoff generated is more significant as the ground is fully saturated with water and all excessive precipitation is turned into runoff (Yuan et al., 2015) and hence precipitation should be studied. Ground cover and land use also directly influences the occurrence of flash flood. Rapid developments and removal of vegetation and protective layers from the earth result in generation of greater runoff volume as the impervious ground surface increases and the soil become more compact. The runoff also travel with higher velocity on bare surfaces such as bare earth and impervious surfaces. All these contributes to larger peak flow and result in a flash flood (University Corporation for Atmospheric Research, 2010) and hence should be studied. The main purpose of drainage system in a developed or urbanized area is to convey the excessive runoff from the area to the outlet in a timely and hygienic manner. It must be capable of either rapid removal of excess surface runoff, storage on site, or temporary detention and hence its design should be studied. Excessive sedimentation in the water body due to heightened sediment loading may threaten the water quality, disrupt aquatic biota and affects the hydraulic capacity of a conveyance system such as river (Bong et al., 2014; Douglas, 1995) and hence should be studied. Vegetation growth drastically influences water levels and flow patterns in lowland rivers (Doncker et al., 2009) and hence should be included in the study as well.

Figure 1. Photos of flash flood hitting UniGarden on 18 January 2015 (a) and (b) and accumulation of surface water during a storm event (c) and (d).

The project site comprises of 6% and 94% of commercial and residential area, respectively UniGarden residential area, Central View residential area (under construction), Uni Square commercial area and Uni Vista residential area. The project site has undergone rapid development for the past ten years. This development consequently increased the total impervious area in the catchment area, and consequently increased the total surface runoff into the main earth drain. Nevertheless, the main earth drain was not enlarged or revised to accommodate the increase in surface runoff until after the flash flood on 18 January 2015. The impervious area in the project site expanded significantly to 4.51 × 10 m^2 (71.6%) of the total catchment area at 2015, a 3 fold increase as compared to the development condition at 2005.

Table 1. Earth cover condition and discharge at year 2007 and year 2015.

Parameter	**Year 2007**			**Year 2015**		
	A[1]	**B[2]**	**C[3]**	**A[1]**	**B[2]**	**C[3]**
PE Units	1,390	421	400	6,515	1,104	400
Impervious Area (10^5 m^2)	1.31	0.14	0.05	4.09	0.37	0.05
Pervious Area (10^5 m^2)		4.80			1.79	
Total Area (m^2)	6.3 × 10^5					

[1]A = Residential Area (5 PE per house)
[2]B = Commercial Area (3 PE per 100m^2 area)
[3]C = 4-Storey Apartment (5 PE per unit, 4 units per floor)

2 METHODOLOGY

The study methodology revolves around the determination of hydrologic and hydraulic parameters, qualitatively or quantitatively. For hydrologic factors, the precipitation, infiltration, and surface runoff were determined quantitatively. For hydraulic factors, the discharge capacity of the drains and culverts were determined quantitatively.

2.1 Hydrologic

In hydrologic review, the main focus was on the analysis of precipitation pattern over the past 10 years to identify any possible trend, as well as on the change in water balance within the project site. The rainfall data over the past 10 years were obtained from Department of Irrigation and Drainage (DID Sarawak), which is a regulatory body involved in the field of hydrology and flood mitigation works including urban drainage works for urban development, and were analyzed to identify possible changes in precipitation pattern over the past 10 years. The water balance in the catchment was estimated based on Welty (2009) equation as shown in Eq. [1];

$$P=Q+ET+I+G \qquad [1]$$

where, P is the precipitation (m^3), Q is the surface runoff (m^3), ET is evapotranspiration (m^3), G is net groundwater outflow (m^3), and I is infiltration (m^3). The component of Evapotranspiration is often considered as negligible in areas which are highly developed due to the lack of vegetation (Welty, 2009). The precipitation data was obtained by analyzing the rainfall data obtained from DID Sarawak rainfall station. The surface runoff was computed using Eq. [2];

$$Q=\frac{CiA}{360} \qquad [2]$$

where i is the rainfall intensity (mm h^{-1}), A is the area of catchment (Ha), and C is the runoff coefficient of the surface (dimensionless). The C value for impervious surface is 1, and 0.35 for undeveloped, vegetated area with bush cover according to Table 2.5, Urban Stormwater Management Manual for Malaysia (MSMA) 2nd Edition (DID, 2012) which is a design guideline used in Malaysia for urban drainage system design. Effluent discharge is 225 L per capita per day according to Malaysia Standards (MS) with ratio of 1228:1991, which is a design standard for wastewater treatment design in Malaysia. A hydrograph for the previous storm event was plotted.

2.2 Hydraulic

In hydraulic review, the main focus was on the hydraulic capacity of the earth drain, which is controlled by its dimension, invert level, and gradient. Insufficient hydraulic capacity was one of the major factor causing buildup of surface water and flash flood during a storm event. The sizing, invert level, and the gradient of the earth drain was determined using a Total Station. The discharge capacity, Q_d of the earth drain was then determined using Manning's method as shown in Eq. [3];

$$Q_d = \frac{1}{n}AR^{\frac{2}{3}}S^{\frac{1}{2}} \qquad [3]$$

where A is the flow area (m^2), R is the hydraulic radius (m), s is the longitudinal slope of the drain (m m^{-1}), and n is the manning's roughness coefficient (dimensionless), which can be obtained from Table 2.3, MSMA 2nd Edition.

2.3 Water sampling

In this section, the main focus was on the concentration of Total Suspended Solids (TSS) present in the water. Higher TSS concentration indicates a higher sediment loading and higher sedimentation rate, which may then, decreases the hydraulic capacity of the drain through promoting vegetation growth and reducing its dimensions. Water samples were collected during low flow and after storm events and were tested in the laboratory to identify the concentration of TSS in the water. TSS sample was prepared by filtering 100 mL of water samples through an 11 µm filter paper, using Rocker 300 vacuum pump. The sample remaining on the filter paper was dried in a Medcenter Einrichtungen Incucell model oven at 105°C for 1 hour. The difference in the dried mass before and after filtration divided by the volume of water sample filtered will provide the TSS in mg L^{-1} (see Eq. [4]).

$$TSS = \frac{B-A}{V} \times 1000 \qquad [4]$$

where, A is the mass of dried filter before filtering (mg), B is mass of dried filter after filtering (mg), and V is the volume of sample used (mL).

3 RESULTS AND DISCUSSION

The outcome of this study focuses on the discussion of changing precipitation pattern, surface runoff, sedimentation, vegetation growth and adequacy of existing drain and their relationship with the January 2015 UniGarden flash flood.

3.1 Precipitation

The 10 years precipitation record from year 2005 to 2015 at the nearest station (8 km) showed neither increasing nor decreasing trend in term of annual precipitation, ranging between 3024.5 mm to 4587 mm; mean of 3778 mm and a standard deviation of 21.8% (Figure 2). Based on the analysis, there was not much variation in the amount of precipitation received by the catchment, and thus the existing earth drain should still be able to accommodate for the rainfall. There was greater variation in the daily rainfall with standard deviation of 57.9% (Figure 3), and this led to the study of extreme storm events over the 10 years duration.

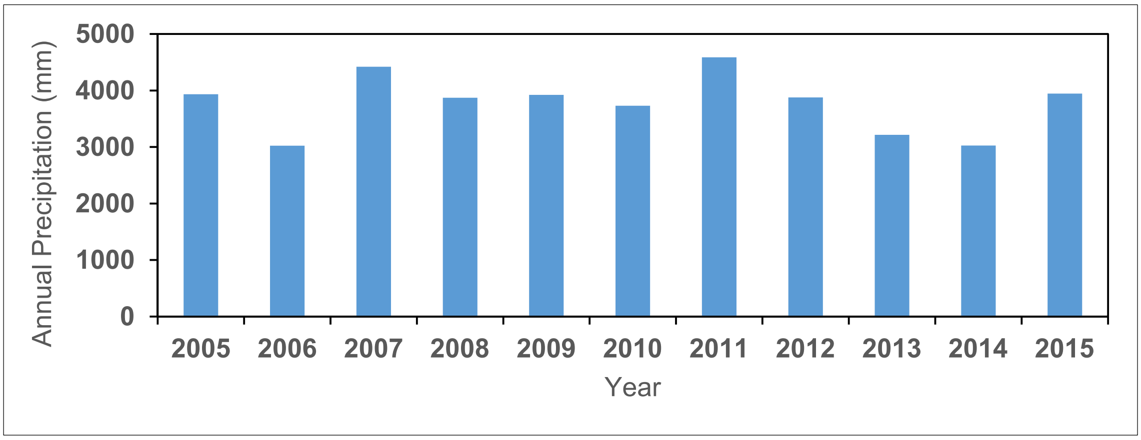

Figure 2. Annual precipitation from year 2005 to 2015 (Max: 4587.0 mm, Min: 3024.5 mm, Mean: 3778.0 mm).

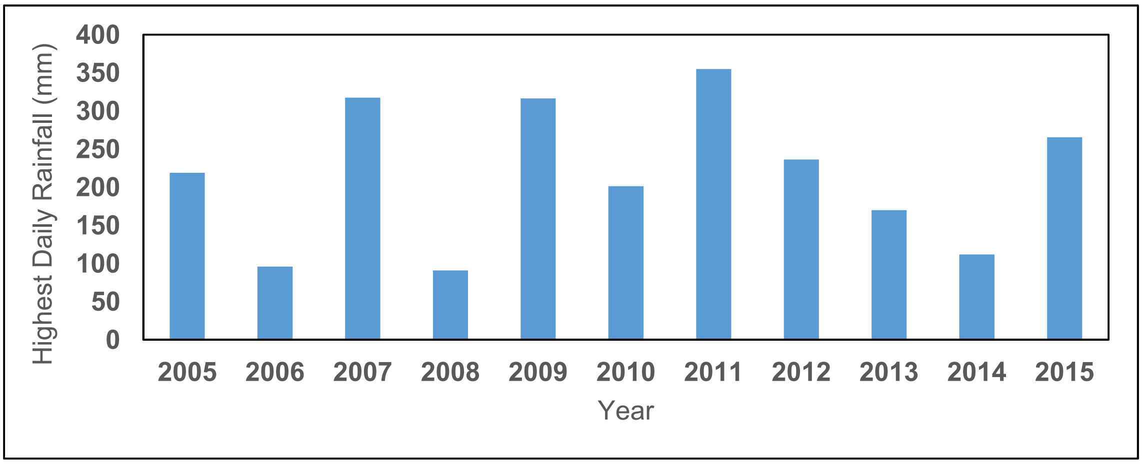

Figure 3. Highest daily rainfall from year 2005 to 2015 (Max: 355 mm, Min: 91 mm, Mean: 216.4 mm).

Table 2 shows the rainfall data record for selected extreme storm events. The 18 January 2015 storm lasted 52 hours, which is 85% from the total duration of the flood event. The flash flood occurred after 27 hours of rain, with a total of 237.5 mm, about 50% of the of the total precipitation, over the duration of 27 hours and with an average intensity of 8.80 mm h^{-1}. The total precipitation of this storm is 471.0 mm, with an average intensity of 9.06 mm h^{-1}. The investigation on the rainfall data were conducted by reviewing continuous heavy storms' rainfall intensity. It revealed that the duration of previous storm event ranged from 50 to 69 hours, with an average intensity ranging from 8.07 to 8.80 mm h^{-1}. The intensity and duration of the previous storm events are consistent with that of the 18 January 2015 storm. Therefore, the storm event on 18 January 2015 was compared with that of 30 November 2007, being the most extreme storm in the 10 years record, with a total rainfall of 607.0 mm over the duration of 69 hours (28.9% higher than 18 January 2015 storm), and had an average rainfall of 8.80 mm h^{-1} (2.9% lower than 18 January 2015 storm). Both storms had similar intensity, and the 30 November 2007 storm had greater total rainfall, but yet flash flood did not occur then.

Table 2. The record of rainfall data during selected extreme storm events.

Date	Duration	Total Rainfall (mm)	Average Rainfall (mm h^{-1})	Highest Hourly Rainfall (mm h^{-1})
17 Jan 2015 – 19 Jan 2015	52	471.0	9.06	43.0
30 Nov 2007 – 4 Dec 2007	69	607.0	8.80	71.5
27 Jan 2009 – 30 Jan 2009	50	403.5	8.07	48.0
25 Dec 2011 – 27 Dec 2011	53	446.5	8.42	67.0
4 Jan 2012 – 9 Jan 2012	68	578.5	8.51	56.0

The consistency in rainfall intensity and pattern shows that precipitation was not a factor contributing to the flash flood in UniGarden on 18 January 2015. This suggests that the flash flood could be due to other factors such as variation on surface runoff and this led to the investigation on the land development in the catchment area over the past 10 years which can vary the surface runoff.

3.2 Surface runoff

The equations for peak discharge for year 2007 (see Eq. [5]) and 2015 (see Eq. [6]) were derived from Eq. [2] by summing the surface runoff from both impervious and pervious surface, using the coefficient Table 2.5, MSMA 2nd Edition. The rate of effluent discharge for both equations was not included as it is insignificant (less than 1%) of the total discharge during a storm event.

$$Q_{2007} = 0.1014\, i \text{ m}^3 \text{ s}^{-1} \qquad [5]$$

$$Q_{2015} = 0.1474\, i \text{ m}^3 \text{ s}^{-1} \qquad [6]$$

For any given rainfall intensity i, the peak discharge in year 2015 Q_{2015} was about 45% greater than that in year 2007 Q_{2007}. Substituting i with the average daily rainfall of respective storm event, the discharge and infiltration for year 2007 and 2015 were determined (Table 3). The percentage of infiltration volume during a storm event was reduced by 61.9% from year 2007 to 2015, highlighting that the increasing impervious surface limited the infiltration process and converted more precipitation to surface runoff.

Table 3. Comparison of water balance in term of precipitation, surface runoff, and infiltration in the project site.

Year	P (10^5 M^3)	Q (10^5 M^3)	I (10^5 M^3)
2007	3.82	2.22 (58%)	1.60 (42%)
2015	2.97	2.50 (84%)	0.44 (16%)

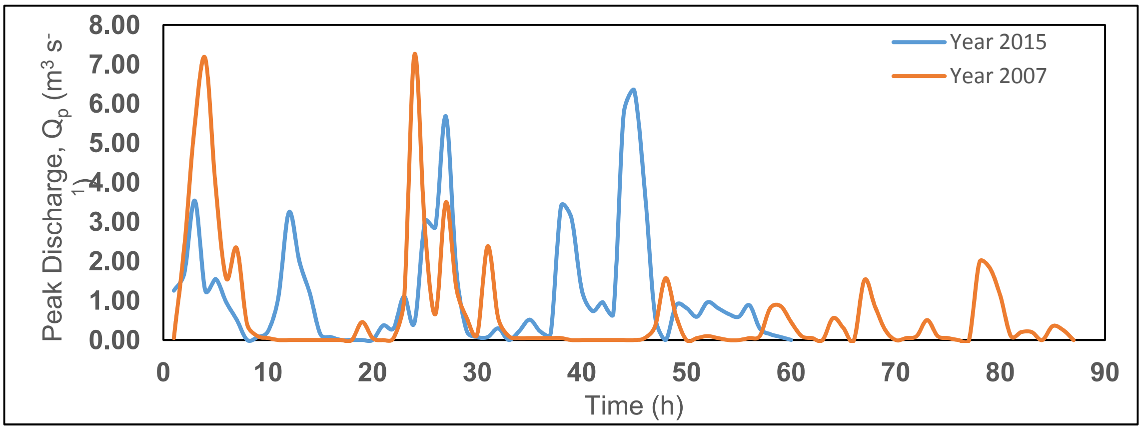

Figure 4. The hydrograph for year 2007 and 2015 storm event.

Figure 4 shows that the highest peak discharge during the 30 November 2007 storm event was at the 24th hour, with a precipitation value of 71.5 mm and a peak discharge of 7.25 m^3 s^{-1}, which is 14.4% higher than that happened at the 45th hour during 18 January 2015 storm, with a precipitation value of 43.0 mm and a peak discharge of 6.34 m^3 s^{-1}. Comparing in terms of the precipitation value and the generated peak discharge, the precipitation value in the year 2015 was lower by approximately 39.9 % as compared to the year 2007. Where else, the 2015 peak discharge is only lower by 12.6% when compared to year 2007. This suggests that the increase of impervious ground area (Table 1) contributed to the increase of the peak discharge. It is also worth noting that the peaks during 18 January 2015 storm had shorter intervals than that of the 30 November 2007, which also contribute to the rapid buildup of surface water.

3.3 Sedimentation

Laboratory testing showed an average TSS value of 33 mg L^{-1} during sunny day, and 73 mg L^{-1} after a storm event. When there is no rain, the average sediment loading along the earth drain is 0.26 g d^{-1}, and can reach up to an estimated 84.81 g d^{-1} during the January flash flood event. The deposition of sediment depends on settling velocity V_s of the suspended sediment particles, and the horizontal velocity V_h of the flowing water. If V_h is faster than V_s, sediments will not deposit, and vice versa. V_h can be reduced by bend and infrastructure interruption (Figure 4.6 a). The flow velocity was measured to be approximately 0.01 m s^{-1} during low flow and approximately 0.10 m s^{-1} during high flow. The fastest settling velocity of the largest particles, namely fine sand, is 0.03 m s^{-1}, this indicates that sedimentation were highly unlikely to occur during high flow where the flow velocity is greater than the settling velocity, and indicated that deposition occurred mainly during low flow period.

The Semenyih river, Selangor, which was used as drinking source for more than a million of population, recorded a TSS value of 11.7 mg L^{-1} to 58.1 mg L^{-1} (Al-Badaii et al., 2013), which is quite similar to that of the runoff in the earth drain. Also, according to the National Water Quality Standards (NWQS) for Malaysia, the TSS value during low flow is within the limit of Class IIA/IIB, and as Class III during high flow. Both indicating that the TSS value presents in the earth drain was of low level.

The low TSS values in both low and high flow, and slow deposition rate of sediment indicates that the reduction in drain dimension due to sedimentation was not significant and was ruled out as a factor contributing to flash flood.

3.4 Vegetation growth

The slow flow of the water, with an approximate flow velocity of 0.01 m s^{-1} during sunny day and 0.10 m s^{-1} after a storm event, allow rapid growth of vegetation. According to MSMA (Clause 14.2.4.3), the minimum flow velocity of 0.6 m s^{-1} is needed to prevent excessive sedimentation and vegetation growth. In this case, the flow velocity was not sufficient to limit the vegetation growth. It only takes 2 months for a cleared earth drain to be fully covered by vegetation again (Figure 5a, b). Excessive vegetation reduced the free flow area of the earth drain, thus slow down the flow velocity resulting in reduced size and hydraulic capacity of the drain.

(a) (b)

Figure 5. The condition of earth drain right after clearing (a) and 2 months after clearing process (b).

3.5 Adequacy of existing earth drain

For the purpose of this study, a survey work to determine the mean longitudinal invert level and cross section of the earth drain was done for a length of 800 m and divided into 5 sections according to the outlets from the catchment to the earth drain as shown in Figure 6. Figure 7 shows the mean longitudinal invert level for the earth drain as well as the flow direction. From Figure 7, the lowest invert level is section 3 where Uni Square (the commercial area) is located. Flows from the direction of Central View and Uni Vista is directed into section 3, causing flooding at the commercial area as well as surrounding areas. Comparison in terms of the discharge capacity of the earth drain with the generated peak discharge on 18 January 2015 has shown that most of the earth drain section could not cater for the peak discharge (see Table 4) and overflowed.

Figure 6. Catchment area of the study area, flow direction of main drains and earth drain.

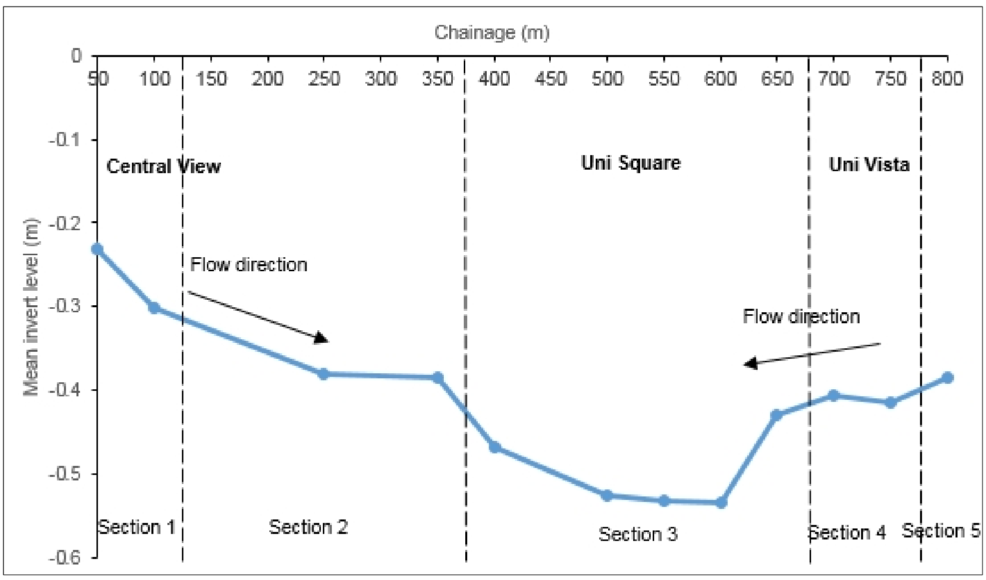

Figure 7. Mean longitudinal invert level for the earth drain.

Table 4. Comparison between the earth drain section with the peak discharge on 18 January 2015.

Section	Drain section	Q_{drain} ($m^3 s^{-1}$)	Q_{peak} ($m^3 s^{-1}$)	Remarks
1	1	4.39	6.34	Overflow
	2	2.01	6.34	Overflow
	3	2.45	6.34	Overflow
2	4	3.78	6.34	Overflow
	5	1.94	6.34	Overflow
	6	6.83	6.34	Ok
	7	2.96	6.34	Overflow
	8	2.13	6.34	Overflow
3	9	5.00	6.34	Overflow
	10	13.78	6.34	Ok
	11	13.246	6.34	Ok
	12	0.95	6.34	Overflow
	13	0.479	6.34	Overflow
	14	2.82	6.34	Overflow
4	15	2.23	6.34	Overflow
5	16	0.53	6.34	Overflow

4 CONCLUSIONS

From this study, it was observed that there are several factors that contributed to the flash flooding on 18 January 2015 at UniGarden. These factors are increased of impervious areas due to rapid development, improper invert level directed towards the Uni Square commercial area and inadequacy of existing earth drain cross section to carry the peak discharge. Excessive vegetation growth with no maintenance prior to the flooding may have also played some role in exacerbating the flash flood. Further study is needed to check on the existing culvert capacity and the outlet connections of the earth drain. Besides that, the probability of backflow in the earth drain as well as the flow direction in all the other connections towards and out of the earth drain when section 3 (the lowest point) overflowed also need to be studied.

ACKNOWLEDGEMENTS

The author would like to thank the Department of Civil Engineering, Universiti Malaysia Sarawak for the use of the survey equipment in this study.

REFERENCES

Al-Badaii, F., Suhaimi-Othman, M. & Gasim, M.B. (2013). Water Quality Assessment of the Semenyih River, Selangor, Malaysia. *Journal of Chemistry*, 2013, 10.

Bong, C.H.J., Lau, T.L. & Ab. Ghani, A. (2014). Sediment Size and Deposition Characteristics in Malaysian Urban Concrete Drains – A Case Study of Kuching City. *Urban Water Journal*, 11(1), 74-89.

De Doncker, L. Troch, P., Verhoeven, R., Bal, K. Desmet, N. & Meire, P. (2009). Relation between Resistance Characteristics Due to Aquatic Weed Growth and the Hydraulic Capacity of the River Aa. *River Research and Application*, 25(10), 1287-1303.

DID (2012). *Urban Stormwater Management Manual for Malaysia* – 2 Editions, Department of Drainage and Irrigation Malaysia, Kuala Lumpur.

Douglas, I. (1995). *Sediment Transfer and Siltation.* The Earth as Transformed by Human Action: Global and Regional Changes in The Biosphere over The Last 300 Years, Ed. Cambridge University Press, Cambridge, 215-234.

Malaysian Standard (1991). *MS 1228:1991 Code of Practice for Design and Installation of Sewerage Systems – Section 1: General*, Standard & Industrial Research Institute Malaysia, Kuala Lumpur.

University Corporation for Atmospheric Research (2010). *Flash Flood Early Warning System Reference Guide,* Washington DC, USA: National Oceanic and Atmospheric Administration, U.S. Department of Commerce.

Welty, C. (2009). *The Urban Water Budget. The Water Environment of Cities*, Ed. L.A. Baker, Springer, NY, 17-28.

Yuan, Z., Chu, Y. & Shen, Y. (2015). Simulation if Surface Runoff and Sediment Yield under Different Land-Use in Taihang Mountains watershed, North China. *Soil and Tillage Research,* 153(1), 7-9.

Proceedings of the 37th IAHR World Congress
August 13 – 18, 2017, Kuala Lumpur, Malaysia

USING A MIXED SIMULATION-OPTIMIZATION METHOD FOR MULTI-RESERVOIR FLOOD CONTROL OPERATION

XINYU WAN(1), YANGYANG ZHANG(2), YANDONG JING(3), MIAOYAN SUN(4) & PING'AN ZHONG(5)

(1,2,3,4,5) College of Hydrology and Water Resources, Hohai University, Nanjing, China,
wanxinyu@hhu.edu.cn; 2479006161@qq.com; jingyd@hhu.edu.cn; smy472835162@163.com; zhongpa@yahoo.cn

ABSTRACT

Multi-reservoir flood control operation is an important nonstructural measure for reducing flood damage. With the increase in the number of reservoirs in watersheds, multi-reservoir operation is becoming increasingly difficult. There are three commonly used approaches to build simulation, optimization, and mixed simulation-optimization models for multi-reservoir operation. However, an optimal solution cannot be obtained using simulation models, a complex system is often simplified to excess using optimization models, and the computation burden of optimization models with the same scale as simulation models is usually high. Hence, a new mixed simulation-optimization method for multi-reservoir flood control operation is presented. Firstly, an overall simulation model was constructed based on the reservoir routing method and the reach routing method. Secondly, the downstream flood control effectiveness of each reservoir was analyzed, and the main reservoirs with an obvious flood control function were identified. Thirdly, operation of each main reservoir was set to the optimal mode to minimize the water volume exceeding the downstream safety release. The reservoir iterative algorithm was used for solving the optimization model. Finally, the mixed simulation-optimization model was applied to multi-reservoir flood control operation of Huai River, China. This case study demonstrated that the method improved flood control effectiveness, and decreased the computation burden.

Keywords: Huai River; flood control; multi-reservoir; optimization; simulation.

1 INTRODUCTION

Flood events frequently occur under climate change conditions, and intensify loss of life, damage to land, properties, and infrastructure. Many structural measures are used to effectively reduce flood damage, such as levees, flood walls, flood diversion structures, flood control reservoirs, and detention basins (Graber 2009; Thampapillai and Musgrave 1985). In large-scale watersheds, these structures form a complex flood control system, which has dimensionality, stochasticity, and nonlinearity. This complexity often provides opportunities for an integrated flood control system. Hence, for maximizing the efficiency of complex flood control systems, it is necessary to optimize flood control operation. In general, there are three approaches to solve this issue: optimization techniques, simulation modeling, and mixed simulation-optimization.

During the last 50 years, optimization techniques have been widely adopted for planning, design, and managing complex flood control systems, including linear programming (LP), dynamics programming (DP), nonlinear programming (NLP), network flow programming, stochastic programming, genetic algorithms (GA), simulated annealing (SA), and ant colony optimization. There are several highly regarded reviews of the application of optimization techniques in flood control operation (Labadie 2004; Rani and Moreira 2010; Wurbs 1993, 2005; Yeh 1985). Although optimization models can automatically search for an "optimal" solution that meets all system constraints, they require mathematical expression of all aspects that can influence the decision-making process, and only define a simplified description of the real system (Sechi and Sulis 2009). This simplification can make optimization models mathematically tractable and computationally efficient; however, it amplifies the gap between theory and application, especially in large-scale complex flood control systems.

To overcome these limitations, many simulation models have been developed and applied in real cases, such as HEC-ResSim, Mike Flood, and CCHE2D. Simulation modeling is used to reproduce the behavior of a real system on a computer, and describes all features of the system, largely through mathematical or algebraic formulation. Given certain inputs, such as inflow data, reservoir parameters, and operating rules, a simulation model can provide information on the corresponding response of the system, which can help decision makers assess the consequences of various scenarios. Simulation models are different to the above-mentioned optimization models in that they are more flexible, interactive, and versatile; however, simulation modeling limits decision making to a finite number of options (Yeh, 1985).

Although optimization models and simulation models each have their own merits and limitations, they can also complement each other very well. Recently, the combination of optimization techniques and simulation models has been the mainstay of water resources studies, including flood control operation. For example, Yazdi and Neyshabouri, (2012) coupled the MIKE-11 simulation model with the NSGA-II multi-objective optimization model to determine the optimal design of structural and nonstructural flood mitigation measures. Bayat et al.(2011) combined particle swarm optimization (PSO) and a river flood routing model to optimize the operation of river-reservoir systems under flooding conditions. Most models contain elements of both approaches, and the distinction between them is somewhat obscured. Many complex, largely descriptive simulation models use optimization algorithms to perform key computations. Various strategies are employed for combining simulation and optimization models. Firstly, optimization algorithms are embedded within many major reservoir-system simulation models to perform certain computations. Secondly, an optimization procedure may involve iterative executions of a simulation model, with the iterations being automated to various degrees (Rani and Moreira 2010; Wurbs 1993; Yeh 1985). Usually, a simple model of the problem to be solved is built using an optimization model as a screening tool, and then further detailed analyses are undertaken via simulation (Mousavi et al., 2004; Wurbs 1993).

In the process of combining optimization and simulation modeling techniques, little attention has been given to the difference in model scales between optimization and simulation techniques. In many previous studies, both models had the same scale. However, in large-scale flood control systems involving many reservoirs, reaches, detention basins, and control points, it is unrealistic to build an optimization model at the same scale as a simulation model. The main reservoirs significantly impacting on the downstream control point must be selected to simplify the optimization model. This paper aims to present criteria for choosing the main reservoirs for the model, and to integrate the multi-reservoir flood control optimization model based on downstream flow rates with river-reservoir simulation models.

This paper describes a simulation-optimization model involving reservoir routing, reach routing, and development of a multi-reservoir flood control optimization model, and presents a computation algorithm for the optimization model. Next, a case study of the river-reservoir system operation in the upper basin of the Huai River, China, is used to demonstrate the model.

2 SIMULATION-OPTIMIZATION MODEL

2.1 Simulation model

Simulation models address flow routing in the river using either hydrologic or hydraulic routing models. In this paper, hydrological routing was adopted, which consists of computing the outflow hydrograph corresponding to a given inflow hydrograph. For a time interval, Δt, the continuity equation is written as

$$\frac{S_2 - S_1}{\Delta t} = \frac{I_1 + I_2}{2} - \frac{O_1 + O_2}{2} \qquad [1]$$

where I is the inflow from the routing model. O is outflow from the routing model. S is the storage volume in a reservoir, river reach, or other container. Subscripts 1 and 2 refer to the beginning and end of the computational time interval Δt.

Hydrologic routing is based on combining Eq. [1] with the relationship between storage and discharge. Alternative methods differ by the form of the storage-discharge relationship. Two alternative methods are often used: (1) storage outflow, and (2) Muskingum. The storage-outflow approach is usually applied to reservoirs, and is often called level-pool reservoir routing. Muskingum routing was developed specifically for streams and rivers.

The computational algorithms for level-pool reservoir routing are based on rearranging Eq. [1] with the unknowns, O_2 and S_2, grouped together as follows

$$\left[\frac{2S_2}{\Delta t} + O_2\right] = I_1 + I_2 + \left[\frac{2S_1}{\Delta t} - O_1\right] \qquad [2]$$

At each time step, the terms to the right of the equal sign are known, and the $(2S/\Delta t + O)$ term on the left is computed. The relationship between the term on the left of Eq. [2] and outflow O

$$\frac{2S}{\Delta t} + O \quad \text{versus} \quad O,$$

is required to determine O.

For a reservoir, the S versus elevation, and O versus elevation, can be combined to form a relationship between S and O. This relationship also allows simple computation of the relationship between O and $(2S/\Delta t + O)$.

Muskingum routing is based on the assumption that the storage volume in a stream reach at an instant in time is a linear function of the weighted inflow (I) and outflow (O). Eq. [1] is combined with the following relationship

$$S = K[xI + (1-x)O], \tag{3}$$

to obtain the Muskingum routing equation

$$O_2 = C_1 I_2 + C_2 I_1 + C_3 O_1 \tag{4}$$

$$\begin{cases} C_1 = \dfrac{0.5\Delta t - Kx}{K - Kx + 0.5\Delta t} \\ C_2 = \dfrac{0.5\Delta t + Kx}{K - Kx + 0.5\Delta t} \\ C_3 = \dfrac{K - Kx - 0.5\Delta t}{K - Kx + 0.5\Delta t} \end{cases} \tag{5}$$

where K and x are Muskingum model parameters. The parameter K has units of time, and Δt must have the same units as K (e.g., minutes, hours, or days). The weighting factor, x is a dimensionless number between 0.0 and 1.0 representing the relative influence of I versus O in determining S. For most natural channels, x is in the range of 0.1–0.3. Detailed information on hydrologic routing can be found in Wurbs and James (2001).

2.2 Optimization Model

An optimization model, based on the downstream flow rates, was developed with the aim of reducing flood damage in the watershed. The model minimizes the flow peak at the downstream control point. The objective function may be written as follows

$$\min \sum_{i=1}^{T} \left(\sum_{j=1}^{N} O'_{j,i} + Q_{l,i} - q_a \right)^2 \tag{6}$$

where $O'_{j,i}$ refers to the responding flow rate of the release from reservoir j at the downstream control point in time period, i, which can be evaluated using the Muskingum method; N is the number of reservoirs; $Q_{l,i}$ is the lateral inflow from uncontrolled watershed areas below the dams in time period, i; q_a is the maximum allowable flow rate at the downstream control point, which is a constant; and T is the operation horizon.

The model constraint set includes continuity constraints for each reservoir and control point, and reservoir release capacity, in each time period (Needham et al. 2000; Watkins et al. 1999), as well as the maximum stage of each reservoir. Among these constraints, the maximum stage constraint, $Z_{\max}$ can be determined through the allocation model of flood waters exceeding “bank-full” stream capacity. The model is described as follows.

As shown in Figure 1, at some time periods when the hydrograph flow is greater than the maximum allowable discharge at the downstream control point, the water volume exceeds the maximum allowable flow rate, and this can be expressed by Eq.[7].

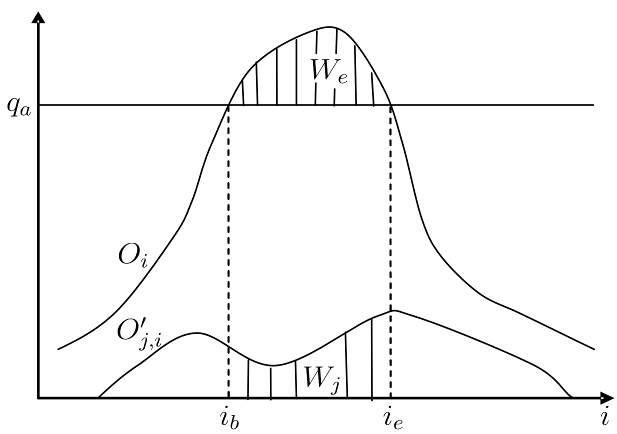

  / ISSN 1562-6865 (Online) - ISSN 1063-7710 (Print)

Figure 1. Sketch of flood waters exceeding bank-full stream capacity at control point.

$$W_e = \begin{cases} \sum\limits_{i=i_b}^{i_e} (O_i - q_a)\Delta t & \text{for } O_i \geqslant q_a \\ 0 & \text{for } O_i < q_a \end{cases} \quad [7]$$

where W_e denotes flood water exceeding the maximum allowable flow rate at control point; i_b and i_e are the beginning and end of time periods, respectively, in which the discharge is greater than the allowable flow rate; O_i refers to the natural hydrograph flow at the control point in time period, i without the influence of upstream reservoirs.

Hence, if $W_e > 0$, water must be held in upstream reservoirs as much as possible by effectively employing the flood control storage capacity of each reservoir for releasing downstream flood control stress.

In Figure 1, $O'_{j,i}$ is the responding flow of upstream reservoir j inflow at the control point in time period, i. W_j expresses the water volume of hydrograph flow from reservoir j in time interval $[i_b, i_e]$, that is

$$W_j = \sum_{i=i_b}^{i_e} O'_{j,i}\Delta t \quad [8]$$

If $\sum_{j=1}^{n} W_j \geqslant W_e$, then W_e can be completely held in upstream reservoirs; if $\sum_{j=1}^{n} W_j < W_e$, then W_e is only partly stored. The stored flood water volume in each reservoir not only relates to W_j, but is also limited by the reservoir real-time status. In reservoir j, under current stage conditions, the remaining flood control storage capacity is V_j, which can be used for subsequent operations. Then, for both natural and engineered conditions, the flood water volume, $W_{j,s}$ stored in the reservoir j should be:

$$W_{j,s} = \min\{V_j, W_j\} \quad [9]$$

Hence, the maximum water volume held in all reservoirs is

$$W_s = \min\left\{W_e, \sum_{j=1}^{N} W_{j,s}\right\} \quad [10]$$

According to the safety balance principle, the water volume stored in each reservoir can be determined by the allocation coefficient, λ_j

$$\lambda_j = \frac{W_{j,s}}{\sum\limits_{j=1}^{N} W_{j,s}} \quad [11]$$

For the real-time operation procedure, if the future precipitation can be forecasted, then it must be considered for allocating the flood water volume, W_s. Assuming the precipitation is p_j in the controlled watershed of reservoir j whose area is A_j, then the future precipitation is approximated by the net precipitation, the future reservoir inflow volume is $p_j A_j$, and the flood storage for future precipitation ΔV_j is

$$\Delta V_j = p_j A_j - \Delta W_j \quad [12]$$

where ΔW_j denotes the release volume from reservoir j in the computational time period.

Based on an overall analysis of nature, engineering, and future precipitation, the flood water volume, $W_{j,s}$ stored in reservoir j should be:

$$W'_{j,s} = \min\{V_j - \Delta V_j, W_j\} \quad [13]$$

Under these conditions, the maximum water volume held in all reservoirs is

$$W_s' = \min\left\{W_e, \sum_{j=1}^{N} W_{j,s}'\right\} \qquad [14]$$

and the flood water allocation coefficient for each reservoir is

$$\lambda_j' = \frac{W_{j,s}'}{\sum\limits_{j=1}^{N} W_{j,s}'} \qquad [15]$$

Then, by considering the location, free storage capacity, inflow hydrograph and future precipitation of each reservoir, the flood water volume stored by each reservoir is

$$\Delta W_j = \begin{cases} \lambda_j W_s & \text{if not considering future precipitation} \\ \lambda_j' W_s' & \text{if considering future precipiation} \end{cases} \qquad [16]$$

2.3 Selection of Reservoirs for Optimization Operation

In a large-scale watershed, there are usually many reservoirs. For example, 38 large reservoirs, and other smaller reservoirs, have been built in the watershed of Huai River, China. When the optimization model is constructed for multi-reservoir flood control, it will greatly increase the burden of model computation when all the reservoirs are included in the model. For a given downstream control point, each upstream reservoir does not have a significant flood-control effect. In general, if the reservoir is larger and closer to its downstream control point, then its flood control effect is more significant. On the contrary, if the reservoir is smaller and farther away from its control point, then it has a smaller effect. Hence, when building a multi-reservoir flood control optimization model, not all reservoirs need to be included in the model, because it is sufficient to include only those reservoirs with a significant effect.

A change in the reach peak stage can reflect the flood control effect of upstream reservoirs on downstream control points. Supposing the peak stage at the downstream control point is equal to Z_{um}, in conditions where all upstream reservoirs release their maximal flow, if one of them changes, and its operating rule and those of the other reservoirs do not change and the peak stage is Z_{cm}, then the flood control effect of the changed reservoir can be formulated as

$$\Delta Z = Z_{um} - Z_{cm} \qquad [17]$$

where ΔZ is the change value of the downstream peak stage after changing the operation rule. If ΔZ is greater than a threshold value ΔZ_{th}, then the reservoir has a significant flood control effect on the downstream control point. The value of ΔZ_{th} is affected by the real-time flood condition, river levee stress, and capability of decision makers.

2.4 Computation Algorithm

There is a number for multi-reservoir flood control optimization model computation methods, such as dynamic programming (DP), and linear programming (LP). However, if the number of reservoirs increases, then the model computation is extremely inefficient. For example, DP has the problem of dimensionality. In this paper, the reservoir iterative algorithm for each reservoir was employed according to the following steps:

i. For determining the reservoir iterative sequence, a concept, dynamic regulating performance, is presented. The dynamic regulating performance, α_j of reservoir j is determined by Eq.[18].

$$\alpha_j = \begin{cases} 1 - \dfrac{\min(W_j, V_j)}{V_j} & \text{if not considering future precipitation} \\ 1 - \dfrac{\min(W_j, V_j - \Delta V_j)}{V_j - \Delta V_j} & \text{if considering future precipiation} \end{cases} \qquad [18]$$

ii. When α_j is greater, the dynamic regulating performance of reservoir j is higher. Reservoirs were sequenced from poor to good in terms of their regulating performance (with priority given to the reservoir with shortest traveling time when the regulating performance is the same);

iii. Conduct compensation scheduling on reservoir 1 (which has the poorest regulating performance). By taking the minimum value of maximum water flow in the flood control cross-section as the target, the target function of compensation scheduling is

$$\min F_1 = \sum_{t=1}^{T} \left[O'_1(t) + Q_a(t) - Q_s\right]^2 \qquad [19]$$

where T is the number of intervals in the scheduling period; $O'_1(t)$ is the response discharge of release of reservoir 1 on the flood control cross-section; $Q_a(t)$ is the interval runoff process; and the other variables are defined as described above.
Constraint conditions such as water balance, release ability, and the highest water level of the reservoir in compensation scheduling should be taken into consideration.

iv. Conduct compensation scheduling on reservoir i. By taking the minimum value of maximum water flow in the flood control cross-section as the target, the target function of compensation scheduling is

$$\min F_i = \sum_{t=1}^{T} \left\{O'_i(t) + \left[Q_a(t) + \sum_{j=1}^{i-1} O'_j(t)\right] - Q_s\right\}^2 \qquad [20]$$

where $O'_i(t)$ is the response process of release of reservoir i on the flood control cross-section; $Q_a(t) + \sum_{j=1}^{i-1} O'_j(t)$ is the sum of interval discharges and the response discharge of aerial drainage of reservoir 1 to reservoir $i-1$ on the flood control cross-section; the other variables and constraint conditions are defined as described above.

v. Repeat the operation until the compensation scheduling of the last reservoir (i.e., the one with the greatest regulating performance) is completed.

3 CASE STUDY

The above simulation-optimization method is applied to optimize multi-reservoir flood control operation of Huai River basin, which is located in the east of China. This basin has an area of 27×10^5 km^2, and has complex and varied terrain and landforms. There are many tributaries to the river basin. Under the influence of tropical oceanic air masses and polar continental air masses, flood events frequently occur, which result in significant economic losses, especially in the midstream Lutaizi reach. On each tributary of the upstream basin of the Lutaizi control point, 20 large-scale reservoirs have been built with a total flood control area of 2.2×10^5 km^2 and a total storage capacity of 154.09×10^8 m^3. These reservoirs prevent the Wangjiaba, Runheji, and Lutaizi control points from flood damage. This study focused on the optimization of these 20 large-scale reservoirs for the flood control operation and safety of the Lutaizi control point. Figure 2 shows the 20 large-scale reservoirs on the Huai River, and Table 1 lists the main design parameters of each reservoir.

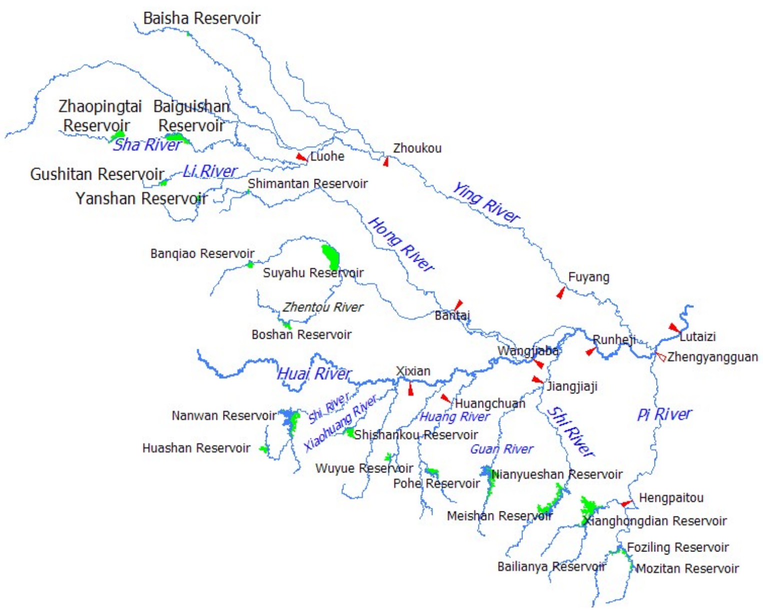

Figure 2. 20 large-scale reservoir locations upstream of Huai River, before the Lutaizi control point.

Table 1. Main parameters of 20 large-scale reservoirs on the Huai River.

Reservoir	Basin Area (km^2)	Safety Discharge of Downstream (m^3/s)	Compensation Elevation (m)	Conservation Pool Level (m)	Maximum Historical Level (m)	Design Level (m)
Huashan	129	200	/	237.00	236.77	240.50
Nanwan	1100	800	104.17	103.50	105.53	108.89
Shishankou	306	600	79.50	79.50	80.75	80.91
Wuyue	102	500	89.30	89.30	89.90	90.02
Pohe	222	1250	82.50	82.00	82.10	83.01
Nianyushan	942	2000	111.10	107.00	109.31	111.42
Boshan	580	2000	110.00	116.60	122.75	122.10
Banqiao	768	2800	112.50	111.50	117.94	117.50
Suyahu	4498	1800	54.00	53.00	57.66	57.39
Gushitan	285	1400	155.50	152.50	158.72	157.07
Zhaopingtai	1430	2500	174.81	174.00	177.30	177.89
Baiguishan	2740	3000	104.00	103.00	106.21	106.19
Baisha	985	500	226.00	225.00	230.91	231.85
Yanshan	1169	1900	107.00	106.00	/	114.60
Shimantan	230	350	108.53	107.00	110.11	110.65
Xianghongdian	1400	2500	129.00	128.00	134.17	139.10
Meishan	1970	1500	129.00	126.00	135.75	139.17
Foziling	1840	3750	128.26	124.00	130.64	125.65
Bailianya	745	/	/	208.00	/	209.24
Mozitan	570	4000	204.00	187.00	204.49	201.19

According to the hydraulic connections among the reservoirs, reaches, and control points, a multi-reservoir flood control operation simulation model for Huai River was built based on the reservoir routing model and the reach routing model. An appropriate operation mode can be selected for each reservoir, such as a traditional mode, maximum release mode, and optimal mode. The optimal operation mode minimizes the downstream flood peak by using multi-reservoir operation. As previously stated, if the optimal mode is selected for each of the 20 reservoirs, then the optimization computation burden would be very high. Hence, the reservoirs with significant flood control effectiveness were first selected.

Nine historical floods of Huai River were chosen to simulate the operation. The operation mode of each reservoir was changed sequentially, and the change in the flood peak at the Lutaizi control point between the maximum release mode and the optimal mode was analyzed. The reservoirs with significant downstream flood control effectiveness were identified, and their operation was set to the optimal mode. The computation results of the model were discharge hydrographs, which were transformed to water stage hydrographs according to the stage-discharge relationship of the downstream control point, before analyzing the stage change of the downstream flood peak. As discussed with the Huai River Water Resources Commission, a reservoir will have significant flood control effectiveness at the downstream control point if the stage change of the flood peak at that control point exceeds 10 cm. After analyzing and evaluating the results, we found that Suyahu, Nianyushan, Meishan, Xianghongdian, and Foziling reservoirs were significantly effective at controlling the flood peak at the Lutaizi control point.

In the flood control simulation-optimization model of Huai River, the above-mentioned five reservoirs used the optimal operation mode for dam safety, and the other reservoirs still used the traditional operation mode. In order to compare the model with the real operation procedures, the same beginning stage and the same maximum stage as historical floods were used as the control conditions for each reservoir in the model. The control conditions of the five reservoirs are shown in Table 2.

4 RESULTS AND DISCUSSION

Using the above simulation-optimization approach and model parameters, we optimized the flood control operation for nine historical floods of Huai River, and compared the optimization results with the real operation results. The results are shown in detail in Table 3, 4, and 5.

Table 3 shows the real flood control effectiveness for the nine floods. In the real flood control operations, the large-scale reservoirs had already implemented the flood-control function. The peak discharges of nine floods at the Wangjiaba, Runheji, and Lutaizi control points significantly decreased when deploying the joint flood control of upstream reservoirs. The average peaks in the reduced rates were 10.8%, 19.1%, and 22.2%, respectively.

As shown in Table 4 and Table 5, the flood control effectiveness was improved by using multi-reservoir flood control operation based on the mixed simulation-optimization model. This model minimized the flood peak of the downstream control points. Under optimal operation mode conditions, the reduced rates in the average peak of nine floods at the Wangjiaba, Runheji, and Lutaizi control points were 13.7%, 23.0%, and 25.5%, respectively, and were an improvement over real flood control operation by 2.92%, 3.84%, and 3.30%, respectively. These results demonstrate that the optimal operation mode presented in this paper was effective. Therefore, under the current operating conditions, the flood control effectiveness at downstream control points can be improved by optimizing the flood control operation mode of the main reservoirs.

Table 2. Control conditions of five important reservoirs.

Flood No.	Control Condition	Suyahu	Meishan	Nianyushan	Foziling	Xianghongdian
19680713	Beginning Stage (m)	51.38	/	/	109.06	101.55
	Maximum Stage (m)	53.69	/	/	114.28	107.97
19690708	Beginning Stage (m)	/	125.21	/	121.03	120.37
	Maximum Stage (m)	/	133.35	/	130.62	130.66
19830721	Beginning Stage (m)	51.47	125.62	103.70	/	125.02
	Maximum Stage (m)	52.77	130.43	105.82	/	126.46
19910611	Beginning Stage (m)	52.18	129.48	105.21	117.99	126.68
	Maximum Stage (m)	53.17	135.75	107.16	125.59	134.17
19960628	Beginning Stage (m)	53.34	122.41	104.77	113.51	117.27
	Maximum Stage (m)	53.81	126.99	107.75	118.03	121.35
20030627	Beginning Stage (m)	51.56	123.58	105.10	113.89	/
	Maximum Stage (m)	54.20	125.92	106.75	115.78	/
20050708	Beginning Stage (m)	52.57	/	/	110.34	120.28
	Maximum Stage (m)	53.94	/	/	114.97	122.45
20050821	Beginning Stage (m)	53.69	122.98	105.83	112.71	124.36
	Maximum Stage (m)	54.60	129.90	108.21	121.94	130.41
20070702	Beginning Stage (m)	52.13	113.80	97.96	/	118.78
	Maximum Stage (m)	54.76	123.93	104.90	/	119.98

Table 3. Real flood control effectiveness of large-scale reservoirs for downstream control points.

Flood No.	Wangjiaba			Runheji			Lutaizi		
	Nature Flood Peak (m^3/s)	Real Flood Peak (m^3/s)	Peak Reduced Rate (%)	Nature Flood Peak (m^3/s)	Real Flood Peak (m^3/s)	Peak Reduced Rate (%)	Nature Flood Peak (m^3/s)	Real Flood Peak (m^3/s)	Peak Reduced Rate (%)
19680713	19500	17600	9.74	21000	17500	16.70	18300	15300	16.40
19690708	5080	4660	8.27	7640	6720	12.00	8420	6940	17.60
19830721	9520	8670	8.93	10800	8220	23.90	9080	6960	23.30
19910611	6870	5900	14.10	9430	6350	32.70	12100	7480	38.20
19960628	5760	5370	6.77	7330	6590	10.10	7850	6710	14.50
20030627	8460	7400	12.50	8630	7160	17.00	10400	7890	24.10
20050708	8350	7170	14.10	6600	5560	15.80	6930	5980	13.70
20050821	6510	5620	13.70	6380	4990	21.80	9390	6680	28.90
20070702	8750	7950	9.14	9640	7520	22.00	10400	7970	23.40
Maximum	19500	17600	14.10	21000	17500	32.70	18300	15300	38.20
Minimum	5080	4660	6.77	6380	4990	10.10	6930	5980	13.70
Mean	8756	7816	10.80	9717	7846	19.10	10319	7990	22.20

Table 4. Optimal flood control effectiveness of the large-scale reservoirs for downstream control points.

Flood No.	Wangjiaba			Runheji			Lutaizi		
	Nature Flood Peak (m^3/s)	Optimal Flood Peak (m^3/s)	Peak Reduced Rate (%)	Nature Flood Peak (m^3/s)	Optimal Flood Peak (m^3/s)	Peak Reduced Rate (%)	Nature Flood Peak (m^3/s)	Optimal Flood Peak (m^3/s)	Peak Reduced Rate (%)
19680713	19500	17400	10.80	21000	17340	17.40	18300	15100	17.50
19690708	5080	4660	8.27	7640	5910	22.60	8420	5910	29.80
19830721	9520	8160	14.30	10800	7660	29.10	9080	6500	28.40
19910611	6870	5900	14.10	9430	6180	34.50	12100	7380	39.00
19960628	5760	5230	9.20	7330	6020	17.90	7850	6290	19.90
20030627	8460	7330	13.40	8630	7160	17.00	10400	7890	24.10
20050708	8350	7060	15.40	6600	5550	15.90	6930	5980	13.70
20050821	6510	5020	22.90	6380	4700	26.30	9390	6200	34.00
20070702	8750	7420	15.20	9640	7147	25.90	10400	7970	23.40
Maximum	19500	17400	22.90	21000	17340	34.50	18300	15100	39.00
Minimum	5080	4660	8.27	6380	4700	15.90	6930	5910	13.70
Mean	8756	7576	13.70	9717	7519	23.00	10319	7691	25.50

Table 5. Flood control potential of large-scale reservoirs for downstream control points.

Flood No.	Wangjiaba		Runheji		Lutaizi	
	Potential of flood peak reduction (m^3/s)	**Potential of peak reduced rate (%)**	**Potential of flood peak reduction (m^3/s)**	**Potential of peak reduced rate (%)**	**Potential of flood peak reduction (m^3/s)**	**Potential of peak reduced rate (%)**
19680713	200	1.06	160	0.70	200	1.10
19690708	0	0	810	10.60	1030	12.20
19830721	510	5.37	560	5.20	460	5.10
19910611	0	0	170	1.80	100	0.80
19960628	140	2.43	570	7.80	420	5.40
20030627	70	0.90	0	0	0	0
20050708	110	1.30	10	0.10	0	0
20050821	600	9.20	290	4.50	480	5.10
20070702	530	6.06	373	3.90	0	0
Maximum	600	9.20	810	10.60	1030	12.20
Minimum	0	0	0	0	0	0
Mean	240	2.92	327	3.84	299	3.30

5 CONCLUSIONS

In summary, we presented a mixed simulation-optimization model for multi-reservoir flood control operation. The simulation model included a reach routing model and a reservoir routing model; the objectives of the optimization model were to minimize the downstream flood peak, as well as to incorporate constraints such as water balance, release ability, and the maximum water level of the reservoir. An optimization algorithm by reservoir turns was used to build the optimization model. Using a demonstration case study, we found that:

i. For a large-scale basin with many reservoirs, it is effective to use a mixed simulation-optimization method to optimize multi-reservoir flood control operation.
ii. Reservoirs with significant flood control effectiveness can be identified by comparing changes in the downstream flood peak. Mixed simulation-optimization models that use only the main reservoirs can decrease the computation burden.
iii. By optimizing the operation mode of the main reservoirs, the flood control effectiveness at downstream control points can be improved.
iv. Under the current operating conditions, the large-scale reservoirs in the basin of Huai River are effective at flood control; however, there is considerable potential for improvement.

ACKNOWLEDGEMENTS

This research was supported by the National Natural Science Foundation of China (Grant No. 51379055), the National Key Research and Development Program of China (No. 2016YFC0400909).

REFERENCES

Bayat, B., Mousavi, S.J. & Namin, M.M. (2011). Optimization-Simulation for Short-Term Reservoir Operation under Flooding Conditions. *Journal of Water Supply Research and Technology-Aqua*, 60(7), 434–447.

Graber, S.D. (2009). Generalized Numerical Solution for Detention Basin Design. *Journal of Irrigation and Drainage Engineering-Asce*, 135(4), 487–492.

Labadie, J. (2004). Optimal Operation of Multireservoir Systems: State-of-the-Art Review. *Journal of Water Resources Planning and Management*, 130(2), 93–111.

Mousavi, S.J., Zanoosi, A.G. & Afshar, A. (2004). Optimization and Simulation of a Multiple Reservoir System Operation. *Journal of Water Supply Research and Technology-Aqua*, 53(6), 409–424.

Needham, J.T., Watkins, D.W., Lund, J.R. & Nanda, S.K. (2000). Linear Programming for Flood Control in the Iowa and Des Moines Rivers. *Journal of Water Resources Planning and Management-Asce*, 126(3), 118–127.

Rani, D. & Moreira, M.M. (2010). Simulation-Optimization Modeling: A Survey and Potential Application in Reservoir Systems Operation. *Water Resources Management*, 24(6), 1107–1138.

Sechi, G.M. & Sulis, A. (2009). Water System Management through a Mixed Optimization-Simulation Approach. *Journal of Water Resources Planning and Management-Asce*, 135(3), 160–170.

Thampapillai, D.J. & Musgrave, W.F. (1985). Flood Damage Mitigation: A Review of Structural and Nonstructural Measures and Alternative Decision Frameworks. *Water Resources Research*, 21(4), 411–424.

Watkins, D.W., Jones, D.J. & Ford, D.T. (1999). Flood Control Optimization using Mixed-Integer Programming. *WRPMD'99: Preparing for the 21st Century*, American Society of Civil Engineers, USA, 1–8.

Wurbs, R.A. (1993). Reservoir-System Simulation and Optimization Models. *Journal of Water Resources Planning and Management*, 119(4), 455–472.

Wurbs, R.A. (2005). *Comparative Evaluation of Generalized River/Reservoir System Models*. Texas Water Resources Institute, College Station, Texas, Technical Report No. 282.

Wurbs, R.A. & James, W.P. (2001). *Water Resources Engineering*. Prentice-Hall, USA.

Yazdi, J. & Neyshabouri, S.A.A.S. (2012). A Simulation-Based Optimization Model for Flood Management on a Watershed Scale. *Water Resources Management*, 26(15), 4569–4586.

Yeh, W.W.G. (1985). Reservoir Management and Operations Models: A State-of-the-Art Review. *Water Resources Research*, 21(12), 1797–1818.

Proceedings of the 37th IAHR World Congress
August 13 – 18, 2017, Kuala Lumpur, Malaysia

HYDRAULICS OF DENDATE FLIP BUCKET WITH AN AERATOR

FEI MA(1), CHAO LUO(2) & JIAN-HUA WU(3)

(1,2,3)College of Water Conservancy and Hydropower Engineering, Hohai University, Nanjing, China
mafei921@163.com

ABSTRACT

Flip buckets have been widely used in release works due to its simple structure and economics. For purpose of enhancing energy dissipation and avoiding flow choking, the dentate flip buckets with an offset are developed in this paper. The model tests results indicated that, the gap at the dentate flip bucket center separates the flow into two branches. Correspondingly, the flow regimes of the jets include overlapping jets, transition jets and separating jets. The aerator at the gap may protect the dentate buckets from cavitation damage due to air entrainment. Comparing with the traditional flip buckets, the energy dissipation is improved about 15% for the dentate flip buckets. Base on the analysis of the influencing factors on the energy dissipation rate, the expression of the energy dissipation for the dentate flip buckets is provided in this paper.

Keywords: Dentate flip bucket; aerator; flow regime; energy dissipation.

1 INTRODUCTION

Flip bucket is a usual element of release works of hydropower projects, which can jet the flow far away from the release works, and guarantee that the structure is safe. Most release works have adopted the flip buckets due to its simple structure and economics.

In past decades, a significant number of studies were published on the hydraulic futures of flip buckets (Juon et al., 2000; Schmocker et al., 2008; Steiner et al., 2008; Pfister et al., 2009, 2014; Ma et al., 2016). In addition, a variety of flip bucket kinds were proposed by previous researchers. In condition of low Froude number approach flow, the flow may choke at the flip bucket. In this case, the jets from the bucket immediately collapses once leaving the bucket, and this might lead to dam toe scour or submerging at the outlet of discharge tunnel. Currently, there are many works which paid attention to flow choking for the flip bucket (Heller et al., 2005; Wu et al. 2015; Ma et al., 2015). Meantime, many new type flip buckets were developed for solving different practical problems about energy dissipation (Khatsuria, 2005; Lucas et al., 2013; Wu et al., 2014).

The dentate flip buckets usually gain good effect of energy dissipation, and it may avoid flow choking due to the gap between buckets teeth. However, cavitation damage often occurs at the dentate flip buckets. The matter mentioned above limits the dentate flip buckets to be used more widely. In this paper, an aerator is designed at the gap of dentate flip bucket, which will entrain air into flow and thus protect the bucket from cavitation damage. In order to separate the jets from the dentate flip bucket, here, the gap floor is no longer arch, but is planar. When the flow passes the bucket, a part of discharge flow though the gap and another part flow on the two bucket teeth, and thus two separated jets will be generated. The present paper describes the flow regimes of the jets, and presented and discussed the experimental results related to onset of cavity filling below the aerator, energy dissipation rate and the dynamic pressure futures for the dentate flip buckets.

2 EXPERIMENTAL SET-UP AND INSTRUMENTATION

The experiments were conducted in the high-speed flow laboratory of Hohai University (HFL-HHU). The experimental setup consisted of a feed basin, a short chute, and a tailwater channel connected to an underground reservoir and a pump for providing water recirculation from the underground reservoir to the feed basin. At the end of the chute, a dentate flip bucket made of plexy glass is settled.

Figure 1 is the definition sketch of the dentate flip bucket used in the present work. It mainly includes two arch bucket teeth, a planer gap in the center of bucket, an offset and the ventilation holes. There are many geometry parameters of the dentate flip bucket as follows: R - the radius of bucket teeth 1 and 2; θ – the radius angle of the bucket teeth 1 and 2; b - the gap width; t - the height of offset; and α - the slope angle of the gap floor. Here, the width of chute is a constant 0.15m, and the radius bucket teeth 1 and 2 is fixed as 0.50m. The vertical difference between chute bottom and tailwater channel floor （s） is 1.05m. The width of the ventilation hole is 0.05m, and the height of the ventilation hole is same as the offset (see Figure 1).

Flows of variable approach (subscript 0) flow depths 0.030, 0.062 and 0.100m and Froude numbers $F_0 = V_0/(g \times h_0)^{0.5}$ within $2.33 \leqslant F_0 \leqslant 10.49$ were generated with a jet-box, where V_0 is the approach flow velocity and g is the acceleration of gravity, allowing for an independent variation of h_0 and F_0. Table 1 lists the model

  / ISSN 1562-6865 (Online) - ISSN 1063-7710 (Print)

parameters of the dentate flip buckets, cases M2, M3 and M4 are used to investigate the effect of the offset height *t*, whereas cases M4 and M5 are used to investigate the effect of the bottom angle α. M1 is traditional continues flip bucket, which is used to compare with the dentate flip bucket.

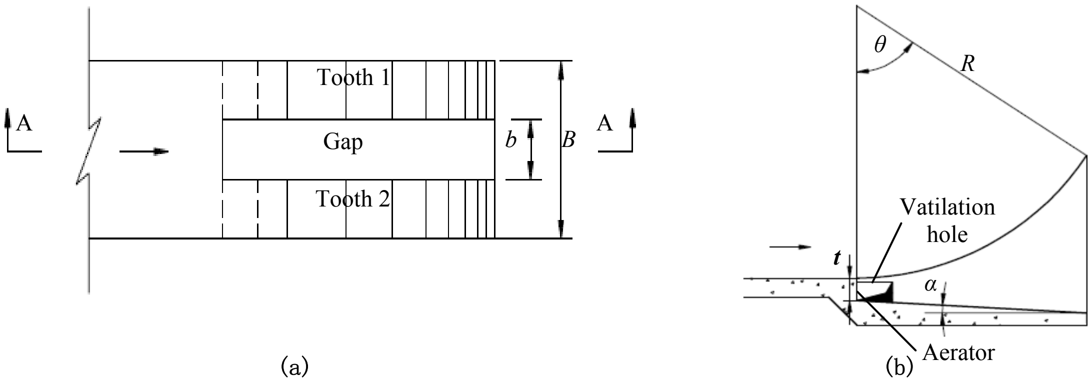

Figure 1. Definition sketch of dentate flip bucket (a. Plan of the flip bucket; b. A - A section).

Table 1. Model parameters of flip bucket.

CASE NUMBER	θ (°)	b (cm)	t (cm)	α (°)
M1	35	0	0	0
M2	35	7	0	0
M3	35	7	2	0
M4	35	7	4	0
M5	35	7	4	10

3 RESULTS AND DISCUSSIONS

3.1 Jet characteristics

Figure 2 is the jets pattern for M4 at the different approach flow Froude numbers and h_0 = 0.030m. When the flow passed the dentate flip bucket, it was separated into two jets. The upper jet flowed through the bucket teeth, and the lower passed through the gap. Between the upper and lower jets, a fin is formed due to shock wave. In the case of low Froude number approach flow, the flow velocity at the end of bucket teeth was remarkably smaller than that at the gap end due to the increase of potential energy. As a result, the upper jet collapsed and fell down on the lower jet, and two jets combined together (Figure 2(a)). Therefore, this flow situation is named overlapping jets. Whereas in condition of large Froude number approach flow, the take-off velocities of the upper and lower jets are similar but their take-off angles are significantly different, thus two jets individually dropped into downstream river (Figure 2(c) and (d)). Therefore, this jets pattern is called separating jets. Figure 2(b) shows the critical jets pattern between overlapping jets and separating jets when the footprints of upper and lower jets are adjacent. For these jets patterns of dentate flip bucket, separating jets is undoubtedly the better flow regime, because it was already proven that more scattering jets can gain more energy dissipation for ski jump.

In flow observation for the traditional continues flip bucket M1, flow choking occurred when h_0 = 0.030m and F_0 = 5.12 (Figure 3). Previous studies indicated that the flow passing the flip bucket may choke as the approach flow Froude number is lower than the critical Froude number value. However, flow choking did not occur all the while for dentate flip bucket. It is demonstrated that the dentate flip buckets have good performance of anti-flow-choking.

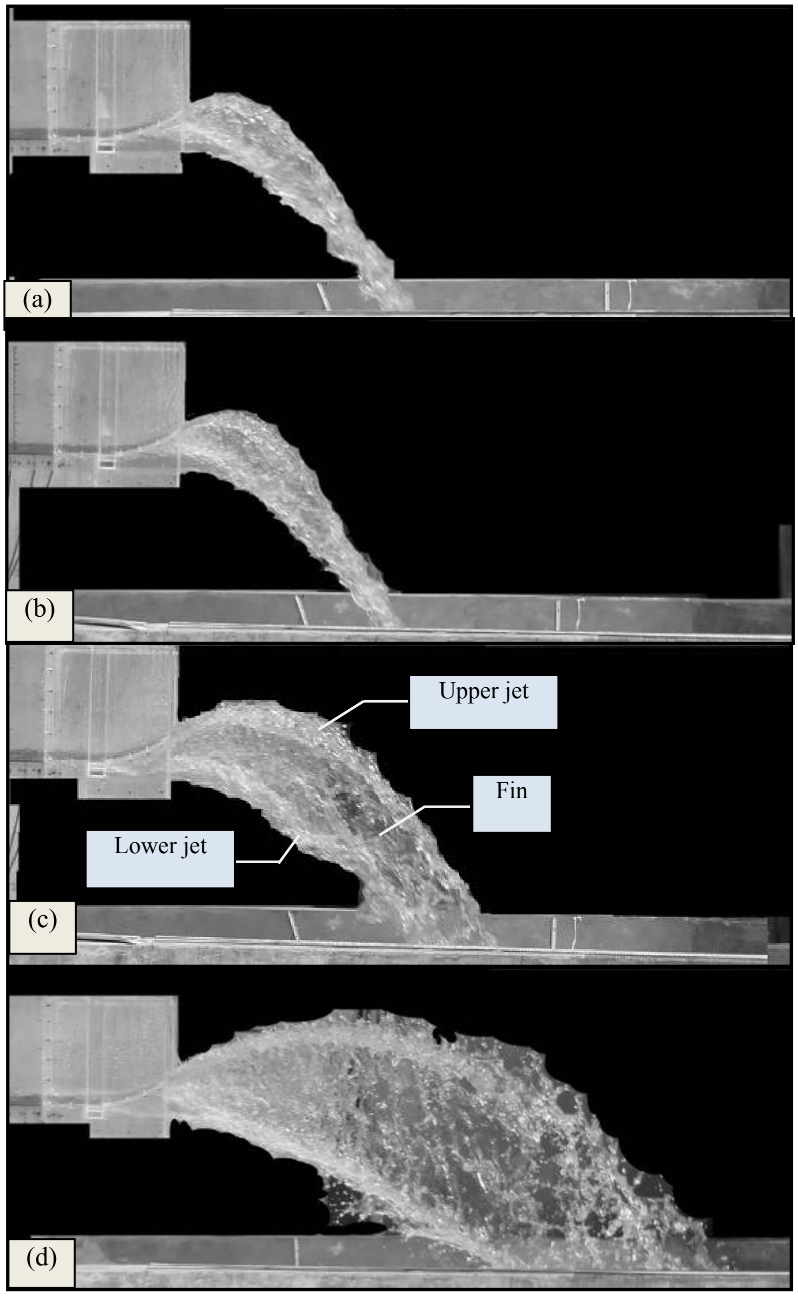

Figure 2. Flow regimes of jet (a-d) for M4: F_0 = 5.12, 5.73, 7.17, 10.49.

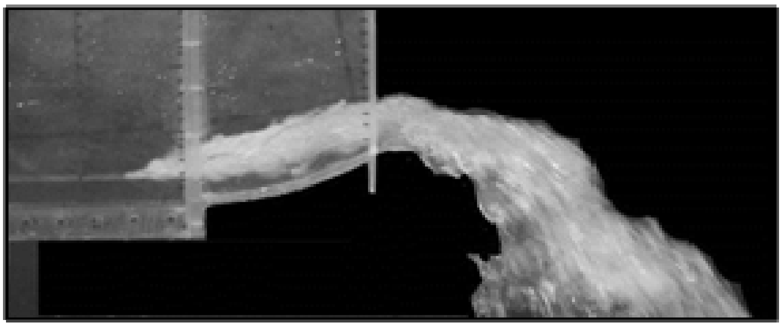

Figure 3. Flow choking（M1，h_0 = 0.030m, F_0 = 5.12.

3.2 Energy dissipation

As shown in Figure 4, the relative energy dissipation of flip buckets, from the approach flow location (section 1 - 1) to impact onto the tailwater channel (section 2 – 2) can be expressed as $\eta = (H_1 - H_2)/H_1$, where H_1 = s + h_0 +V_0 ^{2} /2g is the energy head of section 1 – 1 related to the tailwater channel elevation, $H_2 = h_2 + \frac{v_2^{\ 2}}{2g}$ is the energy head of section 2 – 2. h_0, h_2, h_3 - water depth of section1 – 1, 2 – 2 and 3 – 3. v_0, v_2 - flow velocity of section 1 – 1 and 2 – 2. As the flow at section 2 – 2 obviously fluctuate, a gate settled at the tailwater channel is used to control water depth for forming critical hydraulic jump, and thus h_2 can be calculated according to h_3.

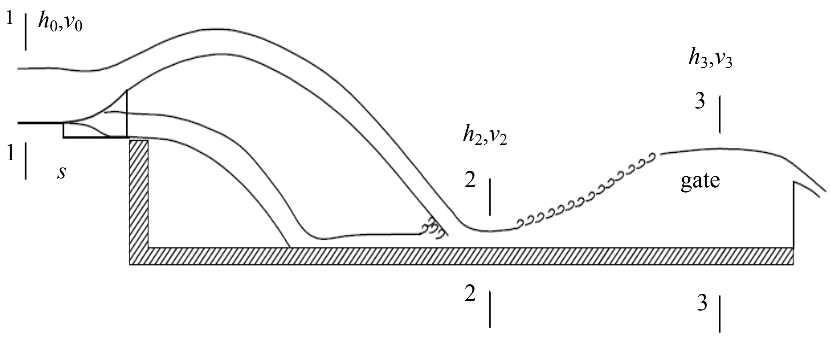

Figure 4. Sketch of energy dissipation calculation.

Figure 5 is the relationship between energy dissipation η and relative bucket height w/h_o. In Figure 5, data of M4 - M5 are dentate flip bucket used in this study, and data of M1 are traditional continues flip bucket in this study, whereas data of β = 10° - 40° are traditional continues flip bucket provided by previous researcher (Heller et al., 2005). It can be seen from Figure 5 that the energy dissipation of dentate flip bucket is remarkably higher than traditional continues flip bucket above 15%. Based on the regression analysis on data related to M2 - M4 in Figure 5, an expression for estimating energy dissipation for dentate flip bucket is given as Equation [1].

$$\eta = 0.083\frac{w}{h_0} + 0.352 \quad (1.76 < w/h_0 < 5.77) \qquad [1]$$

R^2 = 0.871

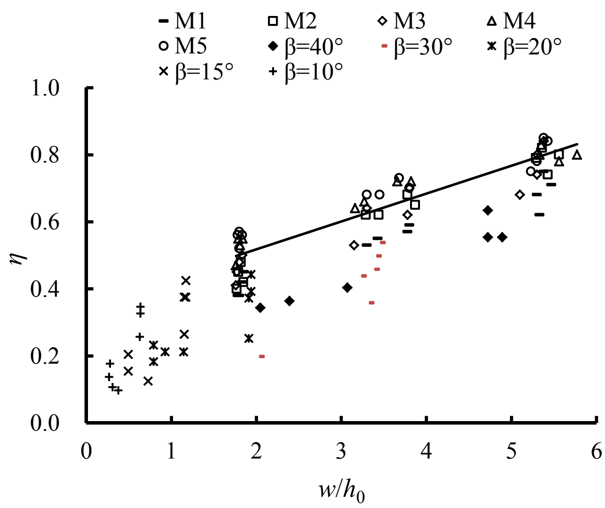

Figure 5. Variations of w/h_0 against η.

3.3 Cavity filling below aerator

The cavity filling below aerator usually leads to cavitation damage. Figure 6 shows the flow regime of cavity below aerator of M4. It can be seen that the cavity was filled by recirculation water as F_0 = 5.12, and with the increase of approach flow Froude number, the roller in cavity decreased gradually and even disappeared finally as F_0 = 8.40.

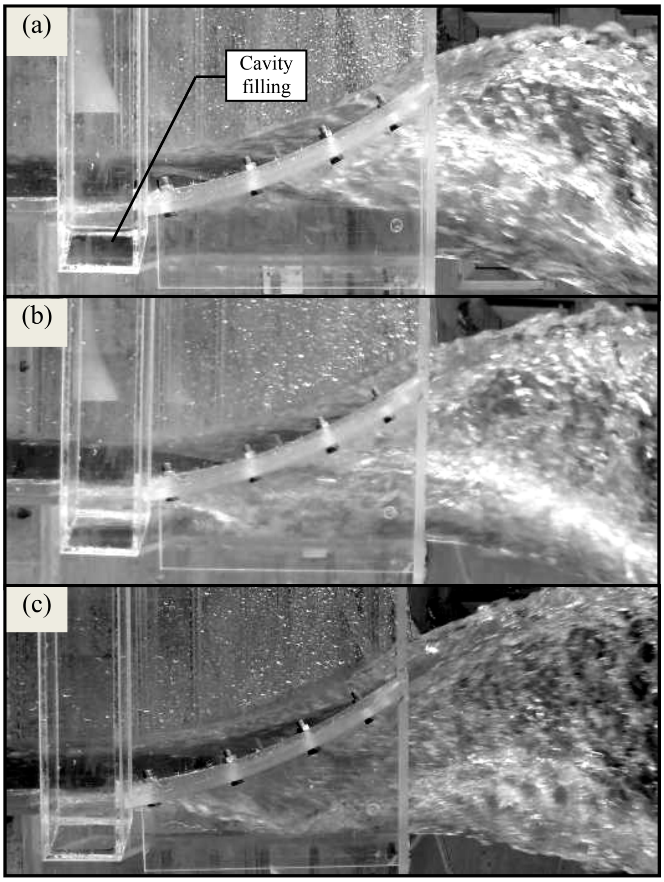

Figure 6. Flow regimes of cavity below aerator (a-c) for M4: F_0 = 5.12, 5.73, 8.40.

According to experimental observations, the cavity filling occurred in M3 and M4, whereas disappeared in M5. It demonstrated that the cavity filling is prone to occur at the horizontal gap bottom of dentate flip bucket. For estimating the cavity filling, F_c is defined as the critical approach flow Froude number when the cavity filling just occurs. Then, F_c is mainly influenced by h_0, b, and t for horizontal gap bottom of dentate flip bucket. Figure 7 presents the relationship of F_c and comprehensive coefficient $(h_0/b)^2(t/b)$ for M2 – M4. The empirical expression for predicting cavity filling for dentate flip bucket with horizontal bottom gap is given as Equation [2].

$$Fr_c = -1.509(h_0/b)(t/b) + 5.218 \quad (0.43 < h_0/b < 1.43;\ 0.29 < t/b < 0.57) \quad [2]$$
$$R^2 = 0.952$$

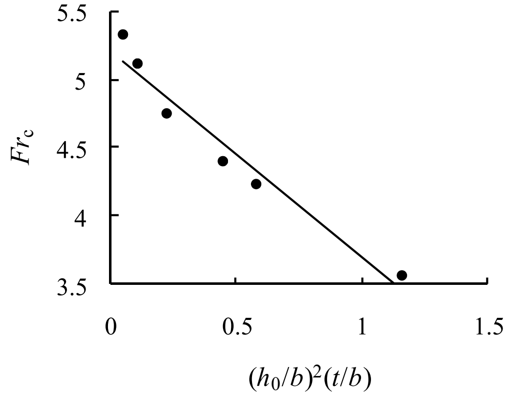

Figure 7. Variations of $(h_0/b)^2(t/b)$ against Fr_c.

4 CONCLUSIONS

The dentate flip bucket may separate the flow into two branches, and thus generate the jet stretched in longitudinal direction. Correspondingly, the average flow velocity of the jet is reduced, and the energy dissipation is increased too. Meantime, it is proved that the present flip bucket can avoid flow choking. Comparing with the traditional continues flip buckets, the energy dissipation is improved about 15% for flip bucket proposed in this work. Based on the regression analysis of test results, the expression of the energy dissipation rate and of prediction of cavity filling for dentate flip bucket are proposed in this paper. Air entrainment is an effective method to protect the dentate flip buckets from cavitation damage. However, cavity filling could not be ignored because it would lead to out of work for aerator. The paper presented an empirical expression for predicting cavity filling for dentate flip bucket.

ACKNOWLEDGEMENTS

The research reported herein was funded by the National Natural Science Foundation of China (Grant No. 51579076).

REFERENCES

Heller, V., Hager, W.H. & Minor, H. (2005). Ski Jump Hydraulics. *Journal of Hydraulic Engineering,* 131(5), 347-355.

Juon, R. & Hager, W.H. (2000). Flip Bucket without and with Deflectors. Journal of Hydraulic Engineering, 126(11), 837–845.

Khatsuria, R.M. (2005). *Hydraulics of Spillways and Energy Dissipators,* New York, USA.

Lucas, J., Hager, W.H. & Boes R.M. (2013). Deflector Effect on Chute Flow. *Journal of Hydraulic Engineering,* 139(4), 444-449.

Ma, F., Zhang, X. & Wu, J. (2016). Discussion of Trajectories and Air Flow features of Ski Jump Generated Jets. *Journal of Hydraulic Research,* 54(2), 245-247.

Ma, F., Xu, Z. & Wu. J. (2015). Flow Choking over Weir Flow Slit-Type Flip Buckets. *Journal of Hydrodynamics,* 27(6), 907-912.

Pfister, M. & Hager, W.H. (2009). Deflector-Generated Jets. *Journal of Hydraulic Research,* 47(4), 466–475.

Pfister, M., Hager, W.H. & Boes R.M. (2014). Trajectories and Air Flow features of Ski Jump Generated Jets. *Journal of Hydraulic Research,* 52(3), 336 – 346.

Schmocker, L., Pfister, M., Hager, W.H. & Minor, H.-E. (2008). Aeration Characteristics of Ski Jump Jets. *Journal of Hydraulic Engineering,* 134(1), 90-97.

Steiner, R., Heller, V., Hager, W.H. & Minor, H. (2008). Deflector Ski Jump Hydraulics. *Journal of Hydraulic Engineering,* 134(5), 562-571.

Wu, J., Wan, B., Ma, F. & Li, T. (2015). Flow Choking Characteristics of Slit-Type Energy Dissipaters. *Journal of Hydrodynamics,* 27(1), 159-162.

Wu, J., Yao, L. & Ma, F. (2014). Hydraulics of a Multiple Slit-Type Energy Dissipater. *Journal of Hydrodynamics,* 26(1), 86-93.

Proceedings of the 37th IAHR World Congress
August 13 – 18, 2017, Kuala Lumpur, Malaysia

FLOATING DEBRIS RETENTION RACKS AT DAM SPILLWAYS

LUKAS SCHMOCKER[(1)]

[(1)]Swiss Competence Center for Energy Research – Supply of Electricity SCCER-SoE, VAW, ETH Zurich, Zurich
schmocker@vaw.baug.ethz.ch

ABSTRACT

Flood events in mountainous areas may entrain and transport large amounts of floating woody debris or large wood (LW). LW may endanger the save operation of dam spillways, as it can result in blocking of the spillway cross section. Already partial blocking of the spillway can decrease the discharge capacity considerably. Due to the resulting backwater rise, the freeboard requirement may not be guaranteed and in an extreme case, uncontrolled overtopping of the dam may occur. The blocking of the Palagnedra spillway during the flood event in 1978 is a prime example demonstrating the hazard potential of transported LW. Two main measures handle LW at spillways and prevent blocking: (1) safe passage of the LW over the spillway; or (2) retention measures in the reservoir. If a spillway is prone to blocking and cannot be modified to guarantee safe passage, the floating debris must be retained in the reservoir. Given both the flow velocities and the reservoir water level variations are small, log or debris barriers may be suitable to retain LW in the reservoir. Otherwise, a rack placed in front of the spillway may prevent blocking of the spillway itself. The effect of such a rack on the reservoir level increase is systematically investigated using hydraulic model tests. According to the results, the rack considerably reduces the backwater rise, as the LW is retained upstream of the weir, where flow velocities are small. The rack must extend considerably below the open weir fields of the spillway to provide enough clear area below the rack for the flow to pass, even when the rack gets blocked. The backwater rise may consequently be reduced and the freeboard requirements can be met.

Keywords: Dam safety; floating woody debris; large wood blocking; retention racks; spillway.

1 INTRODUCTION

During flood events, large wood (LW) can be transported over long distances and reach reservoirs of hydropower plants. If the spillway is in operation during such flood events, the transported LW can endanger the safety of spillway operation (Figure 1(a)). Especially full or partial spillway blocking can decrease the discharge capacity significantly and lead to a rise of the reservoir water level. In the worst case scenario, this can lead to overtopping of the dam. Furthermore, already single logs can block the mechanics of e.g. gates and other movable parts and restrict their operation. Figure 1a shows the spillway of Palagnedradam, Italy, during the 1978 flood event, when the entire spillway got blocked by LW. This resulted in a major backwater rise that overtopped the dam, fortunately not leading to a dam failure.

Although LW transport during flood events is a major threat, limited knowledge is currently available on the interaction between the LW and the spillway and the magnitude of a possible backwater rise. Besides LW retention structures in the catchment area, mainly two measures to manage large wood at spillways are applied in practice: (1) guarantee safe spillway passage of the floating debris; or (2) retention measures in the reservoir. The present paper focuses on the possible retention of large wood in front of the spillway using a rack.

Figure 1. (a) Large wood at the spillway of Yarzagyo Reservoir in 2015 (Photo: M. Wieland, Pöyry Energy AG), (b) Blocking of spillway at Palagnedra Dam in 1978 (Photo: Ofima SA).

2 LARGE WOOD RETENTION IN RESERVOIRS USING RACKS

Racks in front of spillways should only be applied, if there are no possibilities to allow a safe passage of the wood (i.e. the adaption or reconstruction of the spillway is impossible) or the downstream transfer of wood is not permitted. Racks can prevent the blocking of movable spillway parts and therefore guarantee the safe operation. Furthermore, the complete blocking of the spillway can be prevented, if the LW gets retained upstream in the reservoir. However, if LW transport occurs, the rack itself gets blocked and a reservoir water level rise has to be expected nevertheless. To reduce the resulting backwater rise, the rack should therefore exhibit a large area and should be placed at a sufficient distance upstream of the spillway. This guarantees that water can flow below or around the rack to the spillway orifice, even if the rack is completely blocked by wood. Figure 2 shows two examples of racks placed upstream of the spillway.

Research on racks placed upstream of spillways is generally scarce. One reason for this is that most spillways did not yet exhibit extreme flood events with LW transport and the hazard awareness is consequently low. However, an evaluation of 52 power plants in Switzerland shows, that 90% of the spillways do not meet the necessary requirements to safely convey LW downstream in case of a flood event (Schmocker et al., 2016). There is consequently a need to investigate new and innovative measures for (1) upstream debris retention or (2) safe downstream conveyance. The rack at the Thurnberg reservoir (Figure 2(a)) was investigated and optimized with hydraulic model tests at the Technical University Graz, Austria (Schneider 1997). The results showed that the backwater rise due to a large wood accumulation considerably decreases when the rack is sinstalled. Hartlieb (2015) carried out hydraulic model test with an inclined rack placed in front of a spillway. The rack had an inclination of 15° to 30° and a pole spacing of half the weir width. The backwater rise could be reduced by ≈50% compared to the situation without the rack, where the wood accumulated directly at the spillway weir. Due to rack placement upstream of the spillway, the flow velocities were considerably smaller which resulted in a loose and more porous wood accumulation. The wood accumulated in a single-layer carpet and did not pile up, compared to the accumulation process directly at the spillway. Besides racks, floating barriers e.g. tuff booms are another element to retain large wood in the reservoir (Hartung and Knauss, 1976, Perham, 1987, 1988, Bradley et al., 2005). As no general conclusion on the effect of clogged spillway racks can be drawn from existing literature, the present study quantifies the reduction of backwater rise given a spillway rack is applied.

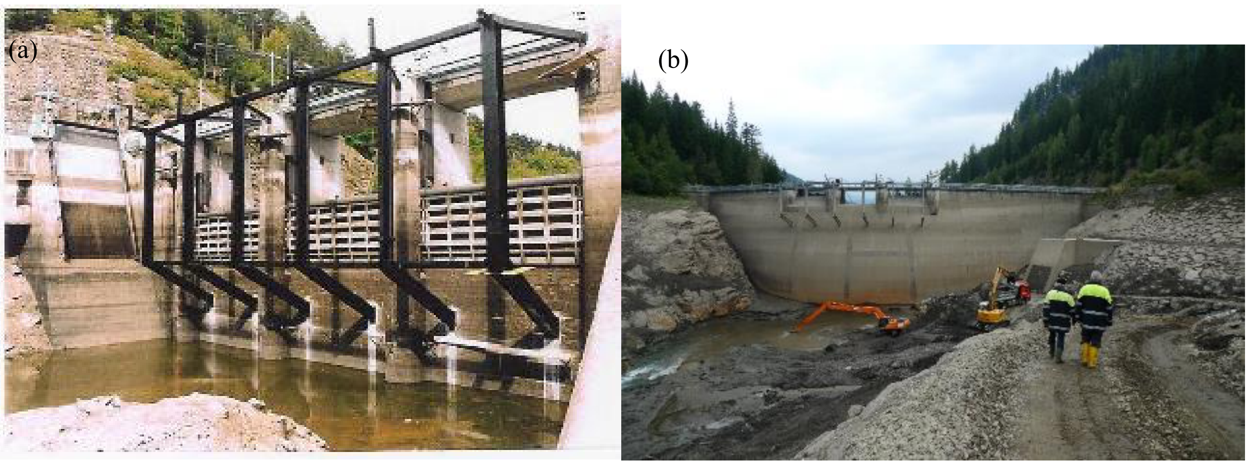

Figure 2. Rack placed upstream of the spillway at (a) Thurnberg reservoir, Austria and (b) Paalbach, Austria (Photo: Austrian Ministry for Agriculture, Forestry, Environment and Water Management).

3 HYDRAULIC MODEL TESTS

3.1 Model flume

The tests were conducted in a glass-sided flume at the Laboratory of Hydraulics, Hydrology and Glaciology (VAW) of ETH Zurich. It is equipped with a pump of 70 l/s maximum discharge capacity. The inflow discharge was regulated with a remote-controlled valve using a Personal Computer. The channel is 0.40 m wide, 0.70 m high and 8 m long. The intake is 0.66 m long and a flow straightener generates undisturbed inflow. The channel slope was horizontal for all tests. The hydraulics of the approach flow are characterized by the weir overflow depth h_o and the approach flow velocity $v_o = Q_o/(B(h_o+w))$, with Q_o = approach flow discharge, B = channel width, w = weir height and g = gravity acceleration. Figure 3 shows the test setup with notation.

A wooden board with two openings representing a spillway with two weir fields was placed 4 m downstream of the intake (Figure 3(d)). Both weir fields had a width of B_W = 0.18 m and a height of H_W = 0.10 m. They were located at a weir height of w = 0.20 m above the channel bottom. A rack consisting of five poles (diameter of 0.005 m) was inserted in 0.10 m distance to the weir fields. The clear pole spacing was c = 0.066 m. The rack height was H_R = 0.225 m (Figure 4(b)).

The water level h and thus the overflow depth h_o were continuously measured using 3 ultrasonic distant sensors (UDS) placed 0.40 m (UDS1), 1.0 m (UDS2) and 2.0 m (UDS3) upstream of the spillway. In addition, the flow depth was measured at arbitrary locations during the experiments using a manual point gauge.

The model large wood consisted of natural logs without branches with the following model log dimensions: log length L_L = 0.05-0.25 m and log diameter d_L = 0.010-0.020 m. The log length was chosen larger than the weir field width to increase the blocking probability. A total volume of 12 dm^3 of large wood (loosely placed volume) was added to the channel for each test run.

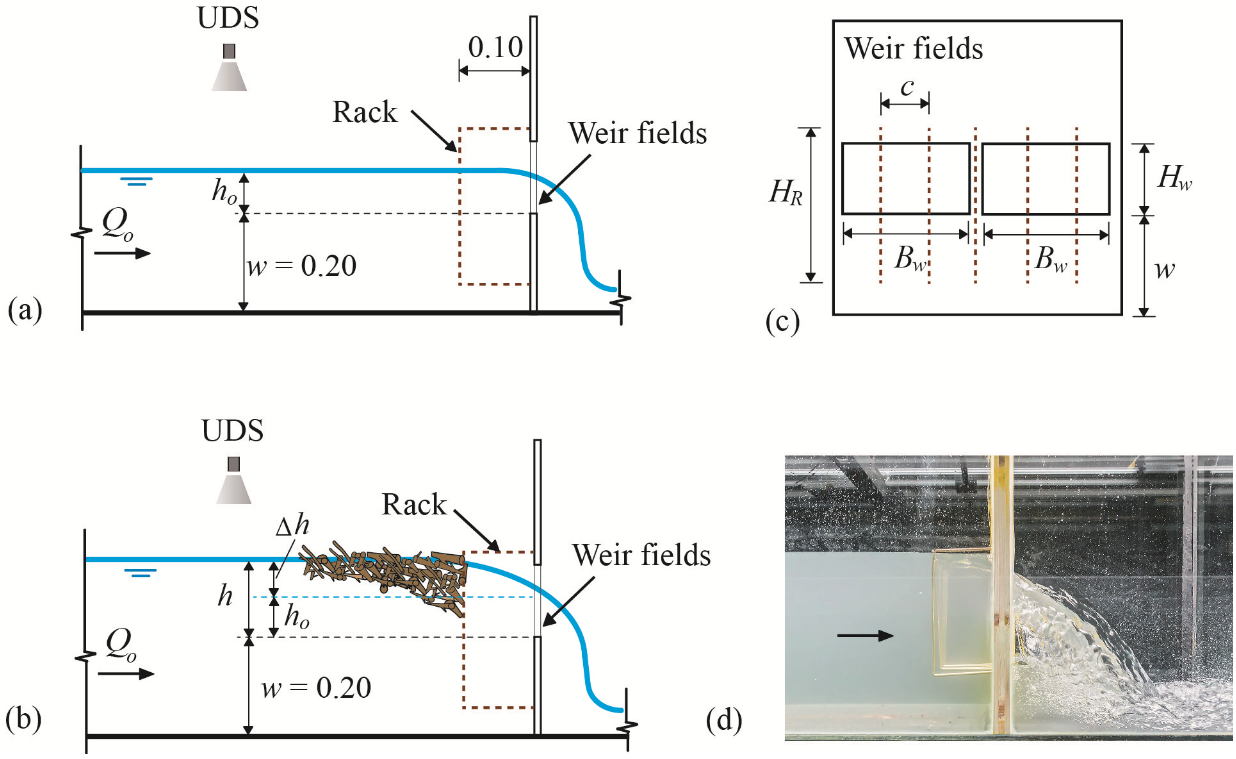

Figure 3. Test setup with notation for weir overflow including a rack (a) without and (b) with wood accumulation,(c) frontal view of weir fields; and (d) side view of model test with initial flow condition and Q_o = 25 l/s.

3.2 Test procedure and parameters

After establishing steady flow conditions for a selected inflow discharge Q_o, the loosely placed wood volume V_{LW} of 12 dm^3 was continuously added to the channel over the test duration of approximately 5 min. The logs were added in small clusters of five logs and not aligned in the flow direction. The wood was not watered prior to a test and was always fully floating. It was assumed that the wood moves at flow velocity (Braudrick and Grant, 2000). The wood having passed the weir was collected in a basket but not re-fed to the flow. The ultrasonic distance sensors recorded the overflow depth h over the entire test duration. The main parameters evaluated were the variation of the overflow depth $h(t)$ due to the debris addition and the backwater rise $\Delta h = h - h_o$. Each test was conducted with and without the rack. The test program is listed in Table 1.

Table 1. Test program.

Test	Q_o	Rack	Initial overflow depth h_o
A	10 l/s	No	61 mm
B	10 l/s	Yes	61 mm
C	20 l/s	No	98 mm
D	20 l/s	Yes	99 mm
E	25 l/s	No	111 mm
F	25 l/s	Yes	111 mm

4 RESULTS

4.1 Accumulation process at the weir

The test started when the first large wood was added to the flow. Due to the small flow velocity, not all logs were transported aligned with the flow and can therefore get blocked and spanned in front of the weir fields. Logs longer than the weir width may still pass the weir, if they are aligned in flow direction. The accumulation was initiated by blockage of one or two large logs at one of the weir fields. Especially small logs passed the weir prior to this initial blockage, however, following the initial blockage, almost all the additional large wood accumulated due to the small flow velocity, independent of its length. Wood transported at small flow velocities tends to get blocked if any of its parts touches an obstacle (Bocchiola et al., 2008). At the start of the accumulation process, only the top upper part of the weir field was blocked as the logs were still floating. Due to the momentum of flow and additional logs, the accumulation was compacted with time and finally expanded over the entire overflow depth and weir cross section. However, the wood was still very loosely accumulated and mainly formed a driftwood carpet. This is in agreement with observations of Rimböck (2003), that wood does not pile up for flow velocities of 0.8-1.0 m/s and is accumulated in a carpet.

The accumulated wood increased the flow resistance consequently resulting in a backwater rise. The flow depth upstream of the weir increased constantly overtime. Once the major portion of the weir fields was blocked, the upstream flow velocity decreased significantly. The incoming logs were then solely accumulated in a floating large wood carpet that continuously expanded upstream. Therefore, the large wood accumulation consisted of initial logs that spanned over the entire weir cross section and a subsequent debris carpet. The latter exhibits one or more layers, depending on the inflow velocity as the logs may get stacked on top of each other. The final accumulation at the weir without the rack is shown for all tested discharges in Figure 4(a) – (c).

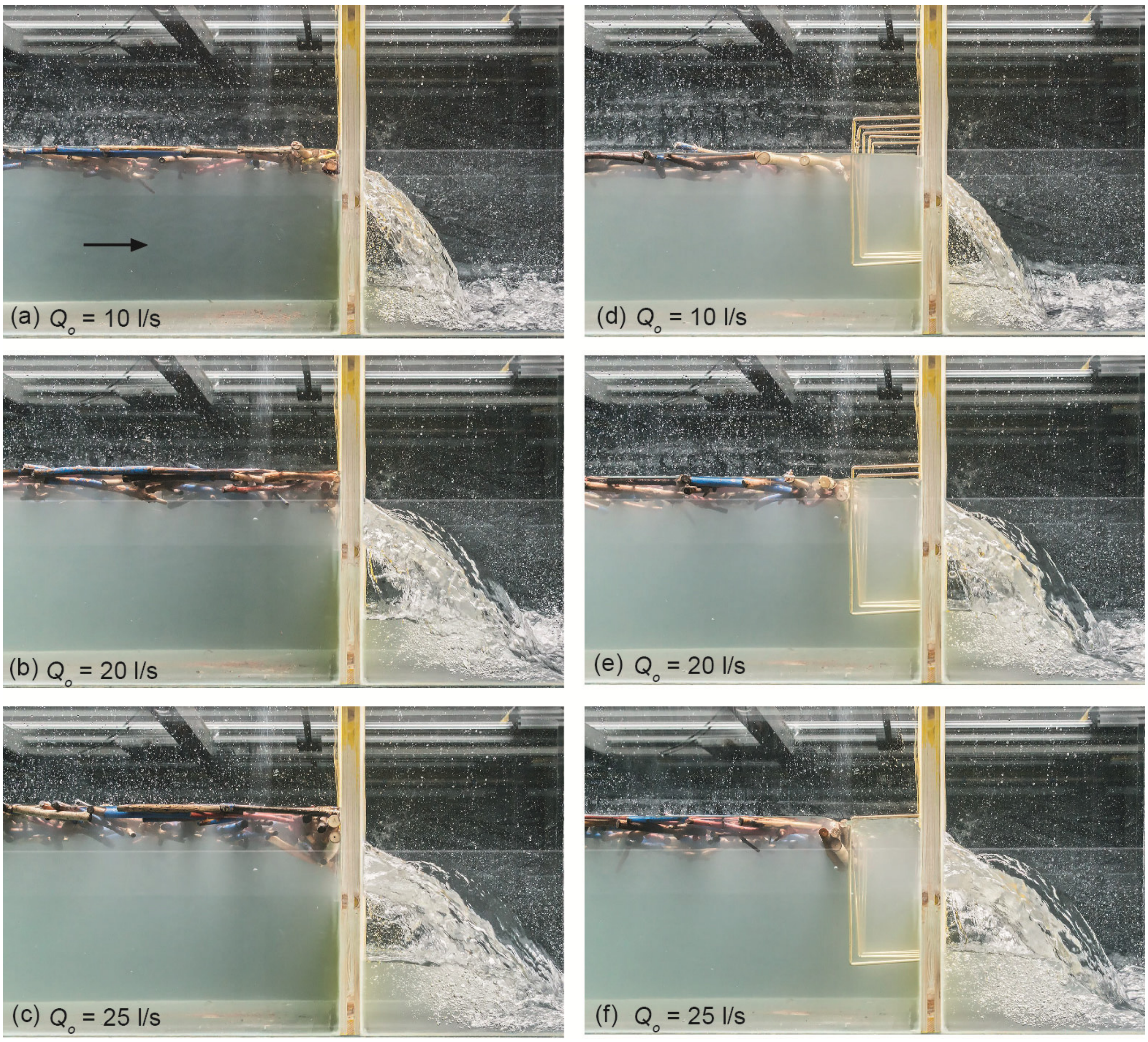

Figure 4. Side view of final large wood accumulation at the weir fields for various constant inflow discharges Q_o.(a-c) without and (d-f) with a rack located upstream of the weir fields.

4.2 Accumulation process at the rack

The accumulation process at the rack was similar to the one at the weir field (section 4.1). The test started when the first debris was added to the flow. The effect of the debris rack poles on the flow itself was negligible, such that the overflow depths were similar to the test setup without the rack (Tab. 1). The logs were mostly transported aligned with the flow, impacted a pole of the debris rack, got turned and spanned between two or more poles. No blocking of the weir field was observed in the model tests, as all logs directly accumulated at the rack. The flow velocity was too low to turn and drag logs through the rack to the weir field. After several logs were blocked at the rack itself, the large amount of the debris accumulated in a floating large wood carpet that continuously expanded upstream. The accumulation at the rack had a thickness of only 1-2 log layers, compared to the weir without the rack, where the logs were dragged down by the large flow velocities, such that the accumulation spanned over the entire overflow depth. The final accumulation at the weir field with the rack is shown for all tested discharges in Figure 4(d) – (f).

4.3 Backwater rise

The overflow depth h was continuously measured using ultrasonic distance sensors. Figure 5 shows the relative overflow depth h/h_o as a function of the added debris volume in percent V_{LW} at UDS1 and UDS2 for various discharges Q_o. All tests started at V_{LW} = 0% with h/h_o= 1.0. Due to the random accumulation process, h/h_o is characterized by a statistical variation. The UDS measurements are spuriously affected given the large wood carpet is located below the USD.

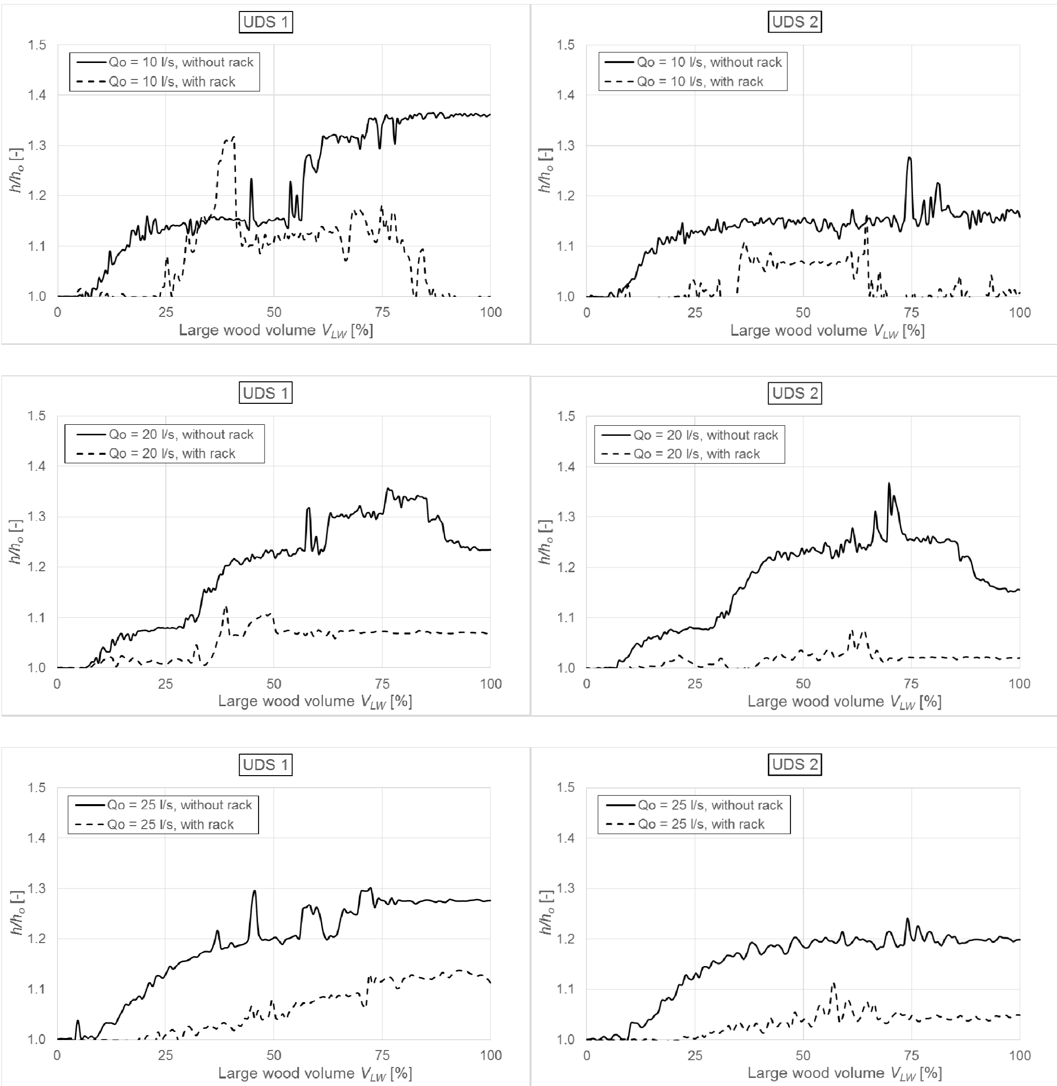

Figure 5. Relative overflow depth h/h_o measured at UDS1 and UDS2 as a function of added large wood volume V_{LW} for various constant inflow discharges Q_o.

For the tests without the rack, the debris accumulation resulted in a continuous increase of h/h_o for the first 75% of V_{LW} up to $h \approx 1.3 \cdot h_o$. At this stage, the relative overflow depth remained constant for Q_o = 10 and

25 l/s, whereas it decreased for Q_o = 20 l/s to $h \approx 1.22 \cdot h_o$. The reason for this decrease may be attributed to rearrangements in the blocked wood accumulation. However, no remobilization of blocked large wood was observed in the test. However, the backwater rise remained constant for $V_{LW} \geq 75\%$, as additional large wood mainly increases the carpet length with only a small effect on the backwater rise. The overflow depth consequently increased by ≈30% due to the large wood accumulation.

For the tests with the rack, the debris accumulation also resulted in a continuous increase of h/h_o with increasing V_{LW} up to $h \approx 1.08 \cdot h_o$ for Q_o = 20 l/s and $h \approx 1.1 \cdot h_o$ for Q_o = 25 l/s. The relative overflow depth h/h_o for Q_o = 10 l/s increased in the beginning but then decreased to $h \approx 1.0 \cdot h_o$ at test end, resulting in no backwater rise due to the large wood. Again, this may be explained with rearrangements of the large wood accumulation below the UDS. Overall, the overflow depth increased by≈10% due to the large wood accumulation.

Consequently, the backwater rise with the rack was considerably smaller compared to the backwater rise without the rack. The main reason for this is that the weir fields remain free of wood if the rack is applied. Moreover, the area for the flow to pass increases considerably with the rack as the water can pass below the accumulated wood. The flow area without the rack corresponded to the blocked weir field area i.e. $A = 2 \cdot (hB_w)$ and was further blocked by large wood. The flow area of the rack was about three times larger and the weir fields remained free of wood. A rack placed upstream of a weir is consequently a robust solution to keep the backwater rise due to a large wood accumulation at a minimum. This was also observed at the Thurnberg reservoir during the flood event 2002 (Figure 6). The rack located in front of the spillway prevented the weir field from blocking and consequently the dam from overtopping. The rack considerably increases the flow area (Figure 2(a)) and the water could pass below the accumulated debris.

Figure 6. Debris accumulation in front of the spillway of Thurnberg reservoir during the 2002 flood event (Photo: Austrian Ministry for Agriculture, Forestry, Environment and Water Management).

4.4 Maximum backwater rise for wood pile-up

For high flow velocities, the large wood might pile up in front of the weir or the rack. This was for example observed at the Palagnedra Dam in 1978 (Figure 1(b)), where the wood was transported by a fast flood wave and almost overtopped the spillway itself. To simulate this worst-case scenario, the total large wood volume was manually compacted in front of the weir field and the rack, respectively. Figure 7 shows the compacted large wood for a constant inflow discharge of Q_o = 25 l/s. It can be clearly seen that the backwater rise was considerably larger for the setup without the rack, as both weir fields were now completely blocked. With the rack in place, a major part of the rack is still free and the flow can pass under the accumulation and over the weir fields. For the tests without the rack, the piled up accumulation resulted in a relative overflow depth at USD1 of h/h_o = 1.4 i.e. a 40% increase of the overflow depth. With the rack, the increase was 10% and consequently equaled to Test 6 (Figure 4(f)), where the wood did not pile up.

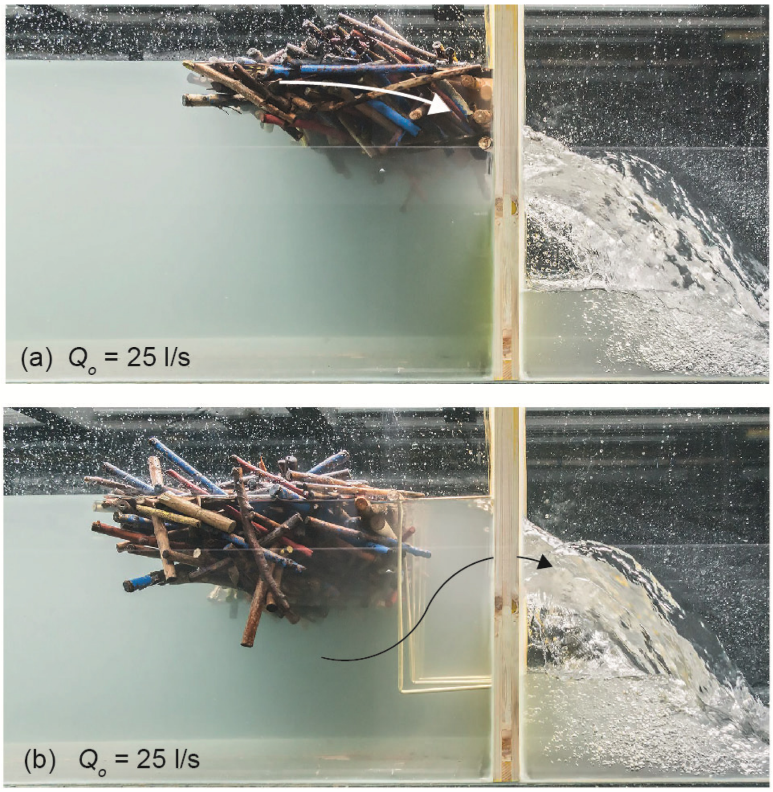

Figure 7. Piled up wood accumulation in front of the weir fields for (a) without and (b) with a rack.

5 CONCLUSIONS

Systematic hydraulic model tests are conducted to investigate the effect of a rack placed upstream of a spillway on the resulting backwater rise due to a large wood accumulation. The tests demonstrate that the backwater rise and consequently the overflow depth is considerably smaller if a rack is applied. Without the rack, the large wood accumulates directly at the weir fields and completely blocks the flow area. With a rack placed upstream, the backwater rise is considerably smaller. The main reason for this is that the weir fields remain free of wood and the area for the flow to pass increases considerably with the rack, as the water can pass below the accumulated wood. A maximum increase of the overflow depth of ≈40% is observed for the tests without the rack, compared to a maximum of ≈10% with the rack in place. So far these results are limited to the present test setup and large wood characteristics. The amount of large wood and especially fine materials like branches and leaves may considerably increase the backwater rise. However, the basic effect of the rack remains the same. As long as not the entire rack area gets blocked, the backwater rise remains comparatively small.

ACKNOWLEDGEMENTS

The author would like to thank all members of the STK working group “Floating debris at spillways” and Prof. Dr. Josef Schneider of TU Graz, Austria, for the fruitful discussions as well as Helmut Czerny of the Austrian Ministry for Agriculture, Forestry, Environment and Water Management for the photos and information on the Thurnberg reservoir.

REFERENCES

Bocchiola, D., Rulli, M.C. & Rosso, R. (2008). A Flume Experiment on the Formation of Wood Jams in Rivers. *Water Resources Research,* 44(2), 1-17.

Bradley, J.B., Richards, D.L. & Bahner, C.D. (2005). *Debris Control Structures, Evaluation and Countermeasures.* U.S. Department of Transportation, Federal Highway Administration FHWA, Salem, Oregon, Publication No. FHWA-IF-04-016.

Braudrick, C.A. & Grant, G.E. (2000). When Do Logs Move in Rivers? *Water Resources Research,* 36(2), 571-583.

Hartlieb, A. (2012). Modellversuche zur Verklausung von Hochwasserentlastungsanlagen mit Schwemmholz (Model tests on Spillway Clogging due to Drift Wood). *Wasserwirtschaft*, (6), 15–19. (In German)

Hartung, F. & Knauss, J. (1976). Considerations for Spillways Exposed to Dangerous Clogging Conditions. *Proceeding of 12th ICOLD Congress, Mexico,* 447.

Perham, R.E. (1987). *Floating Debris Control: A Literature Review,* Final Report REMR-HY-2. US Army Corps of Engineers, Washington, DC.

Perham, R.E. (1988). *Elements of Floating-Debris Control Systems,* Final report REMR-HY-3. US Army Cold Regions Research and Engineering, Hanover, New Hampshire.

Rimböck, A. (2003). Schwemmholzrückhalt in Wildbächen (Driftwood Retention in Mountain Torrents), *Doctoral Thesis*. TU Munich, Germany. (In German)

Schmocker, L., Boes, R., Bühlmann, M., Hochstrasser, H., Kolly J.-C., Lauber, G., Monney-Ueberl, J., Pfister, M., Radogna, R., Stucki, A. & Urso, F. (2016). Schwemmholz an Hochwasserentlastungsanlagen von Talsperren (Drift Wood at Dam Spillways). *Internationales Symposium: Wasserbau – mehr als Bauen im Wasser, Wallgau,* 263 – 274. (In German)

Schneider, J. (1997). Modellversuche KW Thurnberg (Model Tests on HPP Thurnberg). *Personal Communication* Josef Schneider,Technical University Graz (Unpublished).

REDUCING CALIBRATION DEPENDENCY IN RUNOFF ESTIMATION BY SYSTEMATIC DEVELOPMENT OF DISTRIBUTED HYDROLOGIC MODEL IN FLOOD MODELLING

ABD JALIL HASSAN[1], NORHAN ABD RAHMAN[2], SOBRI HARON[3] & TARMIZI ISMAIL[4]

[1,2,3,4] Department of Hydraulics and Hydrology, Faculty of Civil Engineering, Universiti Teknologi Malaysia, 81310 Skudai, Johor, Malaysia,
abdjalil.hassan @gmail.com, norhan@utm.my
[2] Centre of Tropical Geoengineering, Faculty of Civil Engineering, Universiti Teknologi Malaysia, 81310 Skudai, Johor, Malaysia,

ABSTRACT

Runoff estimation depends on many factors and parameters which requires calibration. However, majority of catchments are ungauged and cause calibration to bea difficult task to achieve. Calibration is always required as standard practise but can be abused only to show a good match between observed and simulation. One issue which requires attention is that calibration should only be applied on paramater that cannot be measured prior to all measured data had been input correctly. Development of computer model that enables the combination of hydrologic and hydraulics component in a single model have changed the way flood analysis is carried out. However, the unguided use of model development could lead to the wrong way of modelling the hydrologic component which then leads to wrong estimation of runoff from the catchment. The Lumped model is very much similar to a black box model as it simplifies many parameters when converting rainfall into runoff. Parameters such as time of concentration (T_c), rainfall spatial distribution and landuse are lumped together as one input. This paper is about the development of hydrologic model by adopting a distributed hydrodynamic model. In this situation, the component of hydraulic mainly river channel and flood plain are introduced to the hydrologic model which shall reduce the dependency to various hydrologic parameters. Sg Ketil is one of the tributaries of Sg Muda Basin, Kedah which was used for the distributed model development. Three levels of hydrologic models were built to represent the catchment from one single catchment to one hundred fifty one subcatchment representing the tributeries using the readily available data from Department of Survey and Mapping Malaysia and landuse information from Google Map. Four method of T_c were tested and the simulations results show that the level III model give very similar runoff estimation regardless of the T_c method used. The flood plain was introduced to capture the storage effect. This results conclude that the distributed model which deployed the dynamic wave equation is able to reduce errors of the hydrologic model for computing runoff from subcatchment.

Keywords: Runoff Estimation; distributed model; time of concentration; flood modelling.

1 INTRODUCTION

For the last 40 years, flood analysis had been evolved from simple hydrologic model and steady flow to complex catchment modelling involving two dimensional flood plain with the use of Geographical Information System (GIS) and Digital Elevation Model (DEM). Runoff from sub-catchment normally computed using lumped model but on the other hand, river model deployed the powerful St Venant equation which describes the flood flow in a river system more accurately and more realistic (Innovyze, 2016). Even though it is more accurate, the differential equation requires finite different comprehensive input, analysis method and sophisticated software. Many software in the market capable of developing river model which combine hydrologic and hydraulic component and the flood plain in the analysis using 2D technique. It makes the flow routing along a river more realistic. However, problem still arises when it comes to rainfall runoff modelling. The requirement of observed data for calibration makes the hydrologist to struggle in creating the hydrologic modelling.

With the availability of dynamic wave routing, a proper migration from hydrologic model to hydrodynamic of a catchment will increase the accuracy of the rainfall runoff model for the ungauged catchment. The research focuses on the approach to develop a reliable Distributed model by utilizing readily available elevation data from Department of Survey and Mapping Malaysia (JUPEM) and iFSAR with the aid from Google Map. At this present situation, there is no clear methodology in developing a reliable distributed rainfall runoff model. The objective of this study is to investigate an approach of good model development method for generating runoff from the catchment of Sg Ketil, Kedah, Malaysia using InfoWorks ICM.

1.1 Study Area

Sg Ketil, located at the north of Peninsular Malaysia was selected for the study area (Figure 1.). It is one of the tributaries of Sg Muda basin with total catchment area about 754 km2, measures upstream of Kuala

Pegang and the main river is about 60 km long. The river starts from elevation of 1100m from mean sea level (MSL) and joins Sg Muda at about 20m. The land-use of the catchment is mainly covered with forest and agriculture with small percentage of urban area. Flood occurs very frequently along the river which affects the town of Baling and Kupang and the flood prone area are shown in Figure 1.

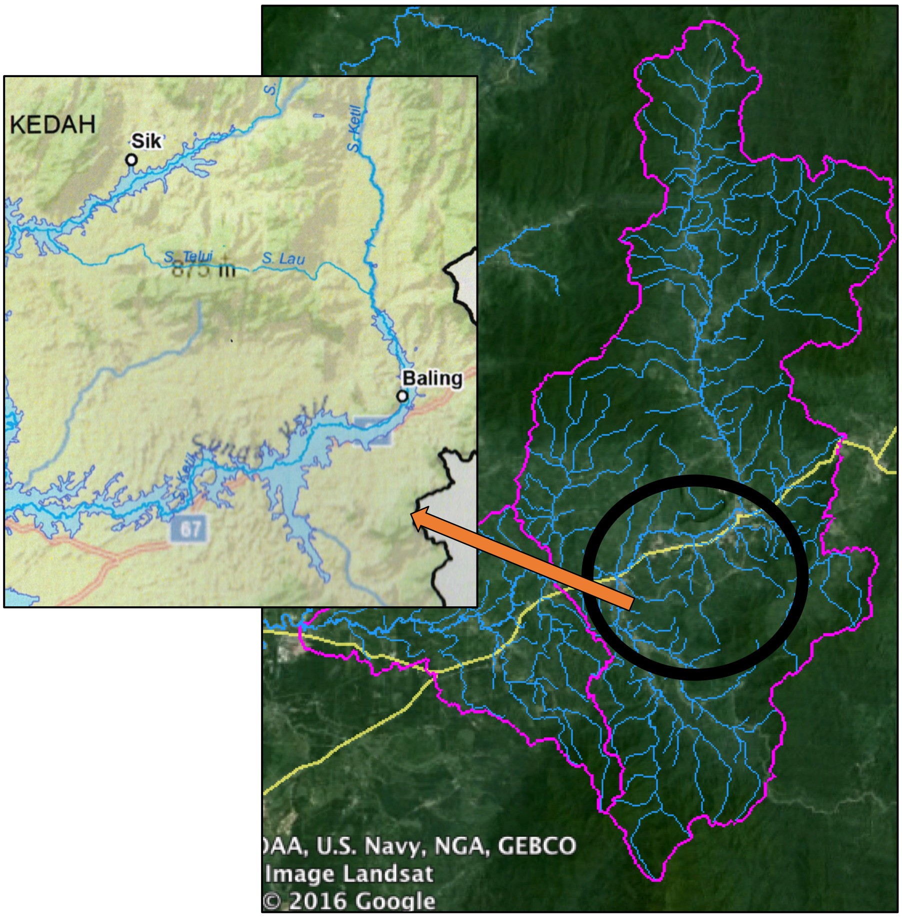

Figure 1. Sg Ketil catchment with flood prone area shown on the left

2 PROBLEM STATEMENT

Many factors contribute to the runoff from sub-catchment either the peak or volume. Among the most dominant factors are the catchment size, soil, land-use, time of concentration, flood plain storage and channel capacity. For large catchment located at the upstream of river system, catchment contributing area can be determined from contour map available from JUPEM. The soil and land use map are available from Department of Agriculture (DOA) and Department of Town and Country Planning (JPBD), respectively which are suitable for the infiltration estimation.

There are many methods available to estimate the time of concentration, mainly depend on slope and length of catchment (Chow et al., 1988). In Peninsular Malaysia, the approach to estimate T_c and runoff is recomendded in Hydrological Procedure No 11 (HP11) (DID, 1980). Each method above has a limitation for specific site condition, however, no clear explanation is given when it is used with comprehensive computer model. The uncertainties in modelling can be divided into five parameters which are precipitation, computation of runoff/volume, computation of direct runoff from excess precipitation, computation of base flow and modelling channel flow (Price, 2003)

Hydrologic model tend to used the lumped approach which tend to mixed all parameters and remove the effect of spatial. The Distributed model on the other hand will distribute the input spatially but without systematic method could lead to wrong approach and time consuming.

This research focuses on the catchment size which directly affect the time of concentration (t_c) during the development of distributed model.

3 METHODOLOGY

Four methods of estimating T_c were investigated, which included Velocity method, Kirpich, HP11and SCS lag. The stream slope was estimated from contour map and calculated based on weighted slope proposed in Hydrological Procedure No 11 (HP11) (DID, 1980). Rainfall was converted into runoff using Unit Hydrograph method (Bedient et al., 2008). As the sub-catchment is break down to smaller sub-catchment, the flow shall be taken by the river channel represented by the dynamic wave equation based on the St Venant equation.

The software used in the modelling was InfoWorks ICM which is capable of modelling rainfall runoff, open channel and flood plain. The main input in developing the distributed hydrologic model were river map and contour map from JUPEM and land-use map from Google Map. Design rainfall applied in this analysis was based on design storm from HP1. The key issue to develop a good distributed model is to ensure that all measurable data is added correctly and accurately. Based on Department of Survey and Mapping Malaysia (JUPEM) topographical data, some of the data can be used to build a reliable hydrodynamic model. The data are river map and contour map while Google can be used to determine the river width.

Unit hydrograph is normally used to represent a characteristic of a catchment in the computation of runoff. Time of concentration is the main input to the Unit Hydrograph method which describes that T_c is time for runoff to travel from the hydraulically most distant point of the watershed to the point of interest within the watershed. Factors affecting T_c and travel time are surface roughness, channel shape and flow pattern, slope, storage along the channel. (USDA, 1986). HP11 describes the step to estimate the Time to Peak for catchment in Peninsular Malaysia. This research investigates four methods as listed below:

- Velocity method – Based on manning equation of channel flow
- Kirpich – Developed from seven small rural basin in Tennessee
- HP11 - Developed from 19 catchments with less than 200 sq mile area.
- SCS lag - Developed based on several small urban basin

The infiltration of rain water to the soil will greatly influence the surface runoff. The behaviour depends on the type of soil, weather condition and surface cover (land use). Various methods to develop infiltration model are available, which included method of Green and Ampt, Horton and SCS (Bedient et al., 2008). However, SCS was used in this study and the Curve Number (CN) was determine from the (USDA, 1986) and (Chow et al., 1988). The value of CN ranging from 45 for forest area to 98 for urban and industrial.

Flood water travel from upstream to downstream in a well-defined channel is well represented by dynamic wave (Chow et al., 1988). InfoWorks ICM deployed the St Venant equation for open channel flow. All data requires in this study was digitized from JUPEM topographical map with projection of Rectified Skew Orthomorphic (RSO) as shown in Figure 2. The main data are river alignment and contour and design rainfall. Land use information was extracted from the latest Google Map as shown in Figure 3.

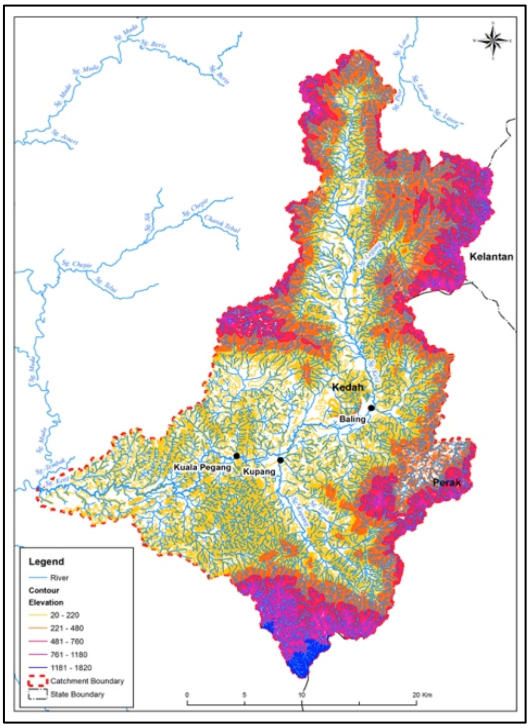

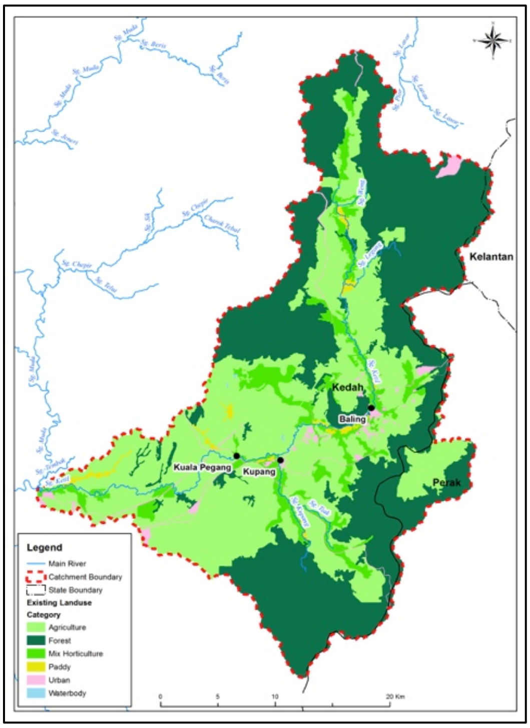

Figure 2. Left -River and contour map. **Figure 1**. Right - Land use map

Design rainfall applied in this analysis is based on design storm from HP1 (DID, 2015). The procedure provides design storm for the whole peninsular Malaysia based on the record of more than 30 years. The IDF curve for Station Bt. 61 Baling which was used in this study is shown in Figure 4. Figure 5 shows one of the temporal pattern of 3 hours which is available in the manual.

  / ISSN 1562-6865 (Online) - ISSN 1063-7710 (Print)

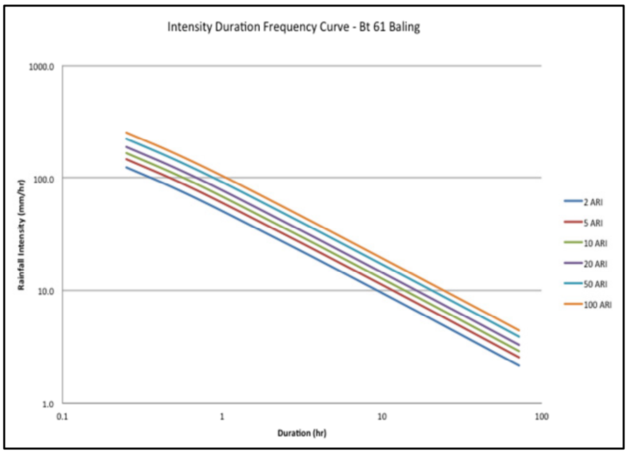

Figure 4. IDF for Station Bt 61 Baling.

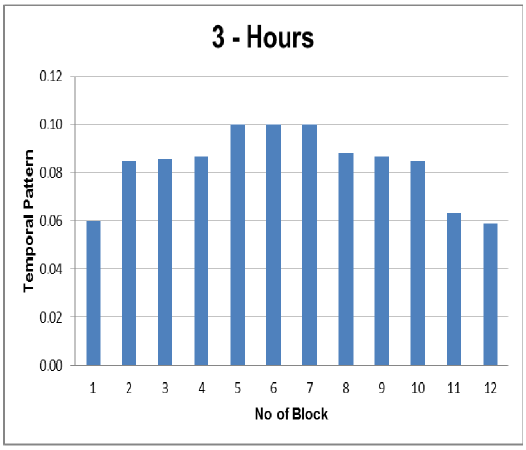

Figure 5. Temporal Pattern for North Peninsular

Three level of sub-catchment that had been developed for the hydrologic model are as listed below:

- Level I – One catchment representing the upstream of the observed point
- Level II – sub-catchments representing all main tributaries of the main river
- Level III – All sub-catchment in Level II which has river length exceeding 10% of the main river are further breakdown following the second tributaries.

Based on the classification of level above, the outcome is shown in Table 1. Figure 6 to 8 show the sub-catchment for each level.

Table 1. Sub-catchments for various level of catchment breakdown

Model Level	No of subcatchment	Area below 3% of total catchment	Total length of river channel (km)	Length below 10% of total length
I	1	*NR*	*NR*	*NR*
II	42	77	61.6	41 %
III	151	96	170.0	85 %

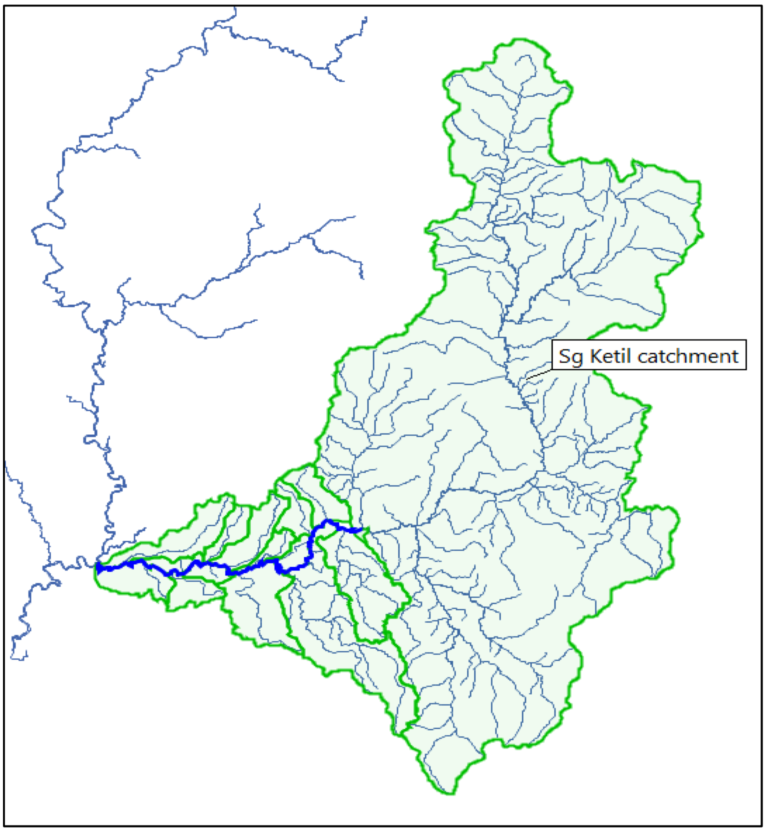

Figure 6. Level I model

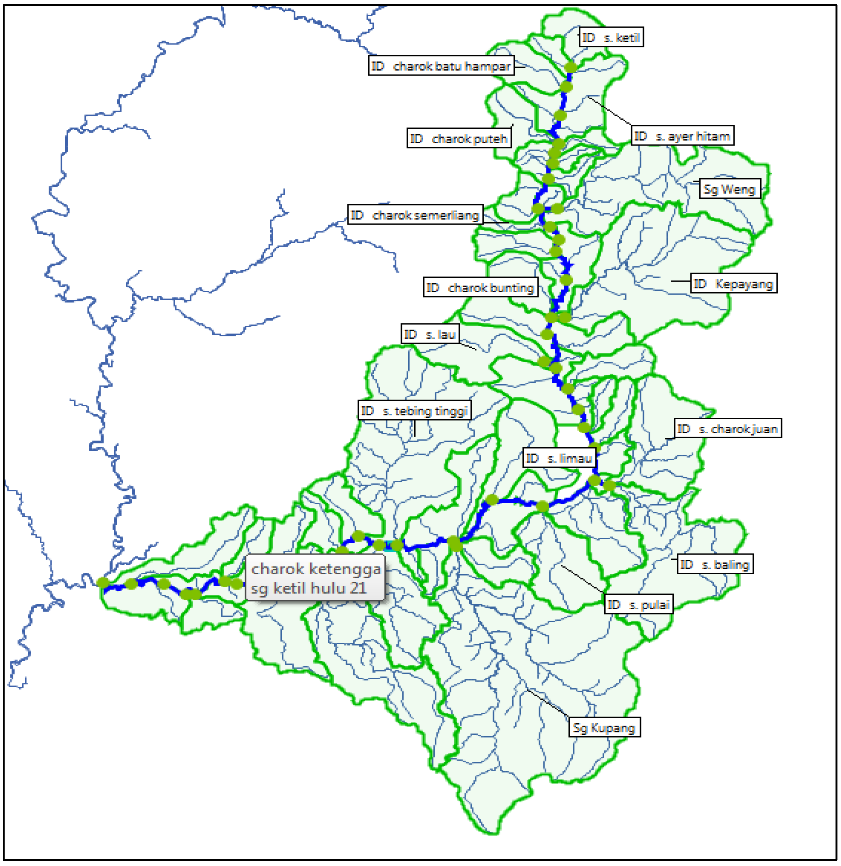

Figure 7. Level II model

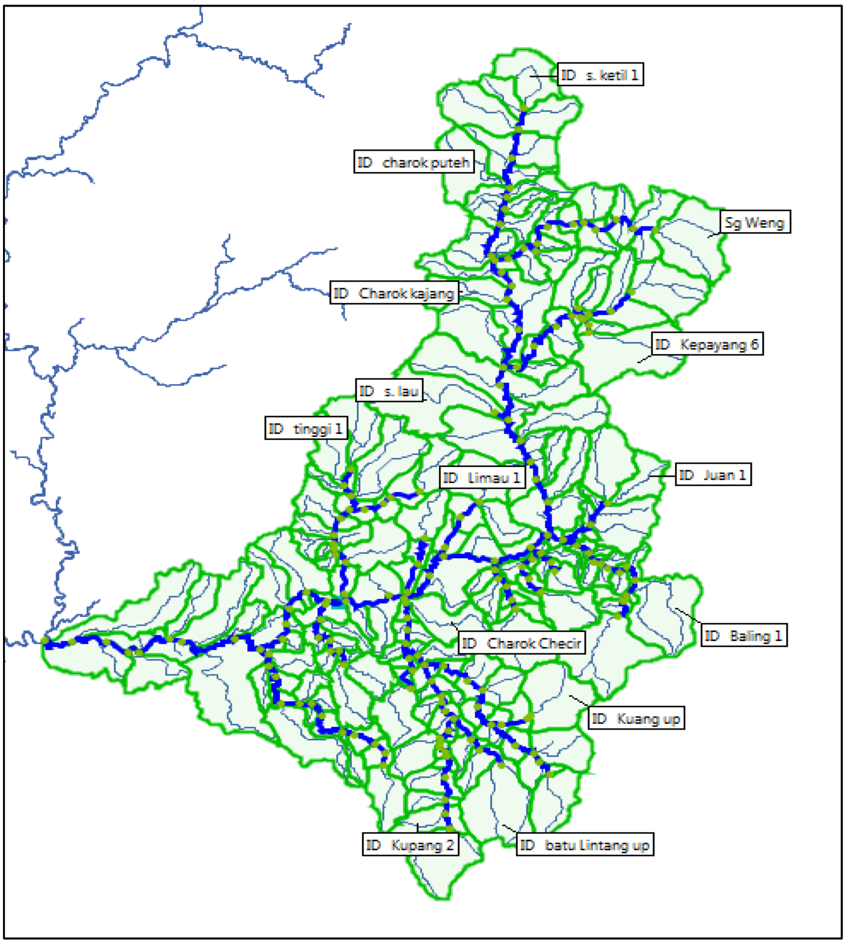

Figure 8. Level III model

3.1 Time of concentration

The time of concentration of the four methods for Level II and III were plotted as shown in Figure 9 and 10 and summary are shown in Table 2 and 3. The T_c for Level II model shown a wide difference between all four methods where the range of average is 241 Minutes. As for Level III model, the range of average is reduce to 102 minutes or about 42%. The best fit lines for all method of Level III model show closer agrement as compared to Level II model.

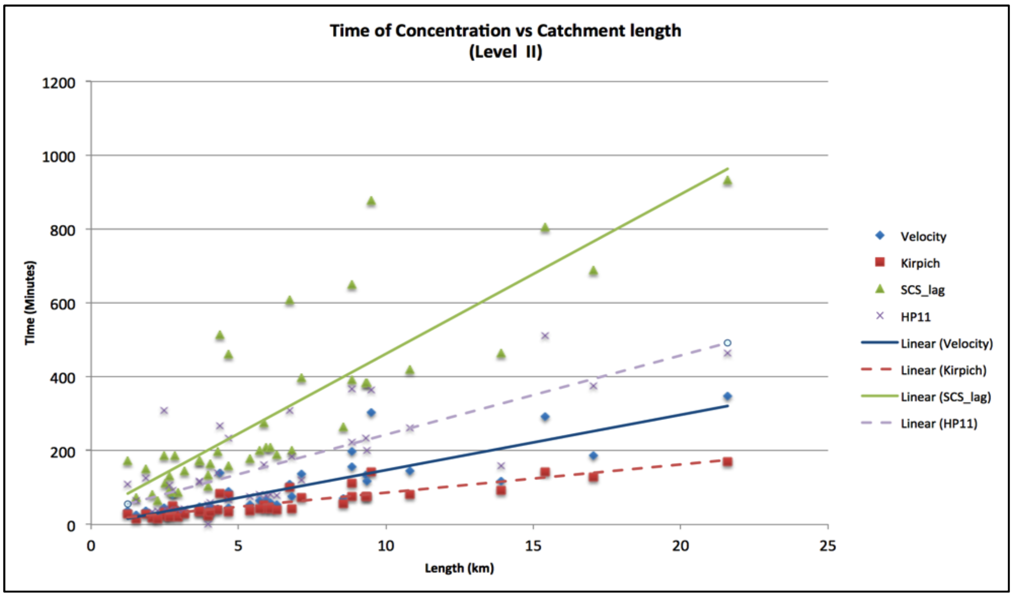

Figure 9. T_c distribution for various methods (Level II model)

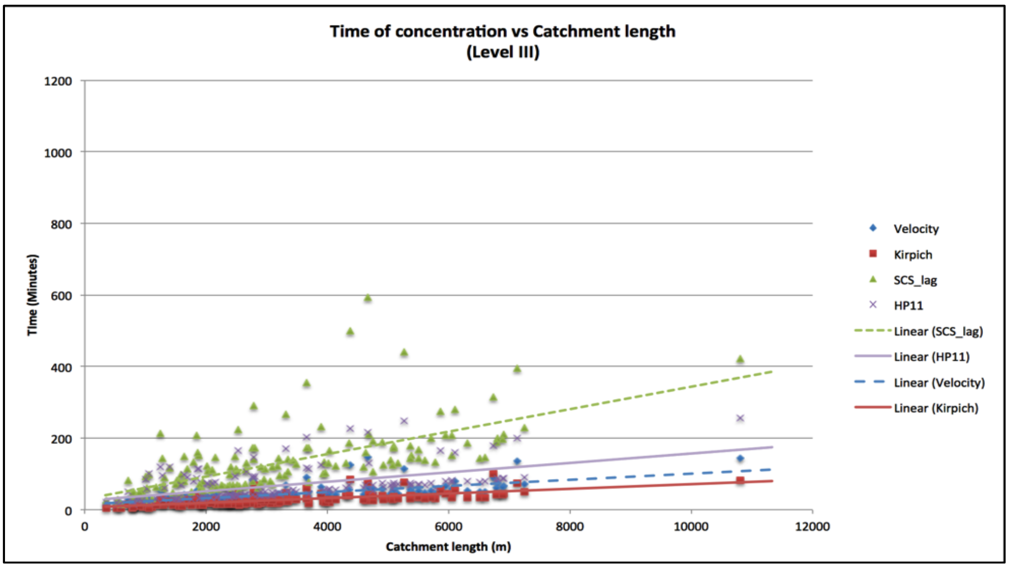

Figure 10. T_c distribution for various method (Level III model)

Table 2. T_c for various method (Level II)

	Time of Concentration (Minutes)				
	Velocity	Kirpich	SCS lag	HP 11	Range
Minimum	22	15	65	33	50
Average	91	57	299	162	241
Maximum	348	170	934	512	764
Std Dev	80	39	235	126	195

Table 3. T_c for various method (Level III)

	Time of Concentration (Minutes)				
	Velocity	Kirpich	SCS lag	HP 11	Range
Minimum	17	4	15	13	13
Average	42	27	129	67	102
Maximum	146	102	595	257	493
Std Dev	23	17	91	47	74

3.2 River Channel

River channels are introduced to Level II and Level III to represent rivers in the distributed model. By introducing the channel, the model shall deployed the dynamic wave equation and flow is routed through the system using the St. Venant equation. A total of 62km and 170 km of channel was added into the model II and III, respectively to represent the river system. These approach will allow each sub-catchment runoff to enter the river system at the appropriate locations. The time travel for each runoff hydrograph will depend on the channel characteristic such as slope, roughness and the water depth. To avoid other parameters affecting the computation, the channel is assumed to be wide enough as not to cause constriction. This condition normally occurs at the upstream of catchment where the channel is steep or river is canalized due to flood mitigation work. Under this condition, the flood plain will not have any influence on the flood volume. Longitudinal section for the main river is shown in Figure 11 with slope of the channel varies from upstream to downstream. Sample of longitudinal section for Sg Kupang is shown in Figure 12. This characteristic will allow the model to compute velocity of water to along the river reach.

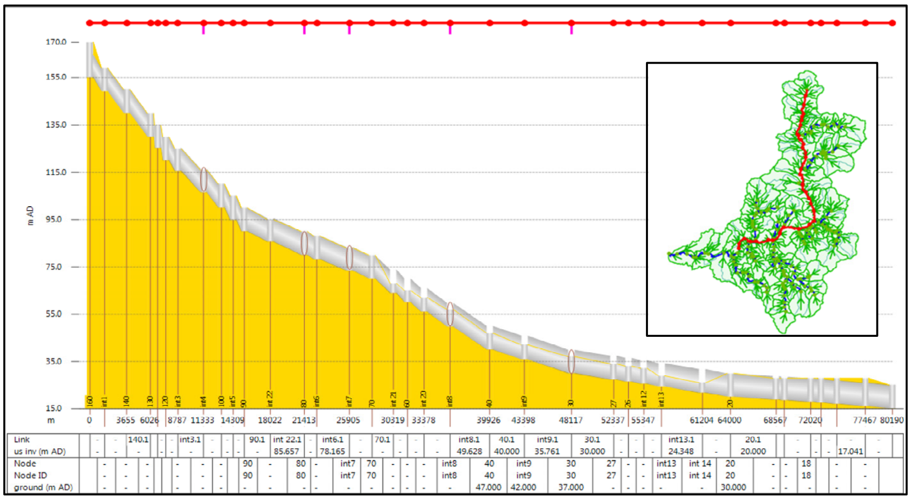

Figure 11. Longitudinal section of Sg Ketil from upstream to downstream

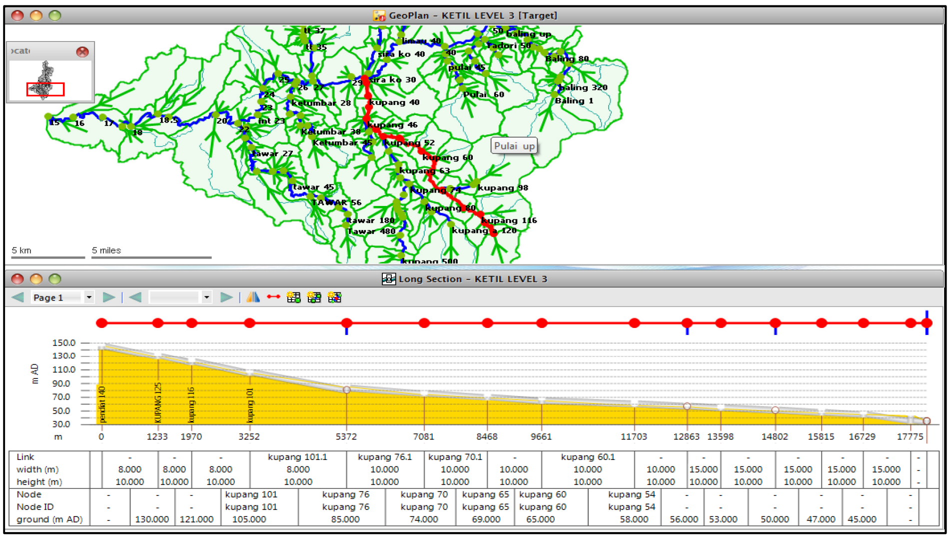

Figure 2. Longitudinal section of Sg Kupang (tributaries of Sg Ketil)

4 Results

Simulation for storm duration of 24 hours and 100 ARI were tested for all levels and different Tc methods. Figures 13 to 15 show the flood hydrographs for each method of Tc computation applied for different level of models. For each method of computation, all models show large difference of peak discharges for Level I as compared to Level II and III. The results indicate that model Level I does not give any good relationship between rainfall and runoff. However, when main channel is included to the model of Level II, all methods show close relationship. Finally, when the model is upgraded to Level III, the difference of runoff hydrograph tend to minimised. Summary of the differences between all the value of peak discharges and time to peak are listed in Tables 4 to 6.

Table 1. Summary of results Model level I

T_c method	Q (m^3/s)	Time to Peak (Hrs)	% Diff Q	% diff T
Velocity	485	34	0	0
Kirpich	601	30	24%	-12%
HP11	211	45	-56%	32%
SCS	160	72	-203%	53%

Table 2. Summary of results Model level II

T_c method	Q (m^3/s)	Time to Peak (Hrs)	% Diff Q	% diff T
Velocity	845	19	0	0
Kirpich	959	17	13%	-11%
HP11	733	22	-13%	16%
SCS	611	26	-38%	27%

Table 3. Summary of results Model level III

T_c method	Q (m^3/s)	Time to Peak (Hrs)	% Diff Q	% diff T
Velocity	904	18	0	0
Kirpich	911	17	1%	-6%
HP11	878	18.5	-3%	3%
SCS	832	21	-9%	14%

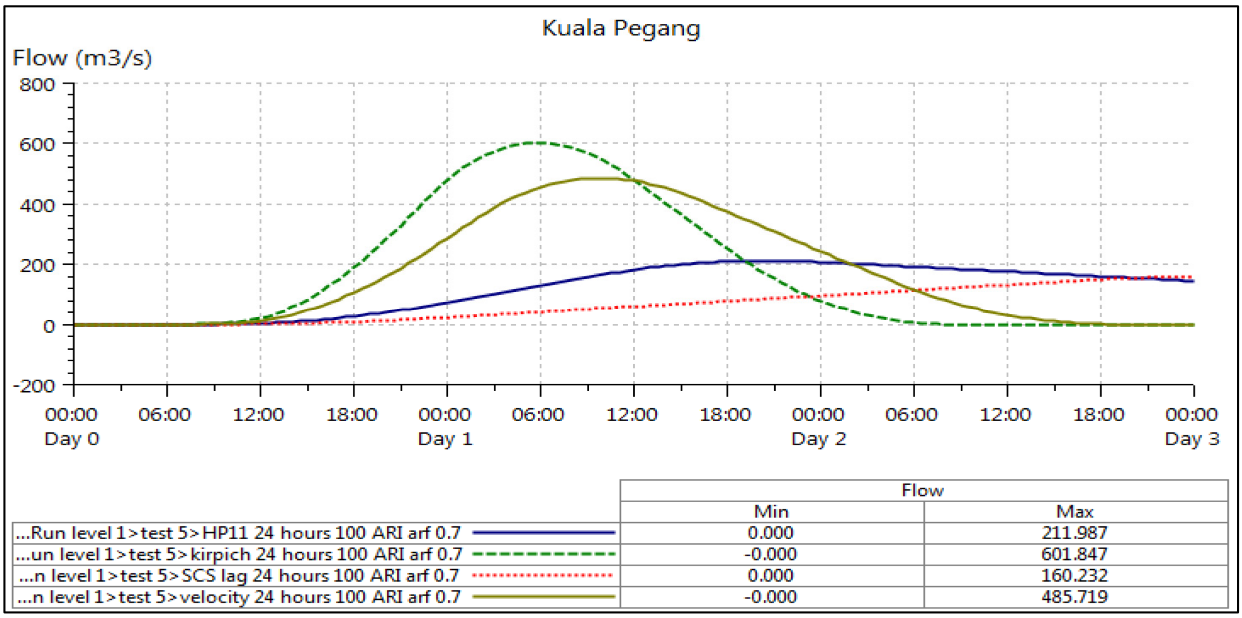

Figure 13. Runoff hydrograph using various T_c method for model Level I

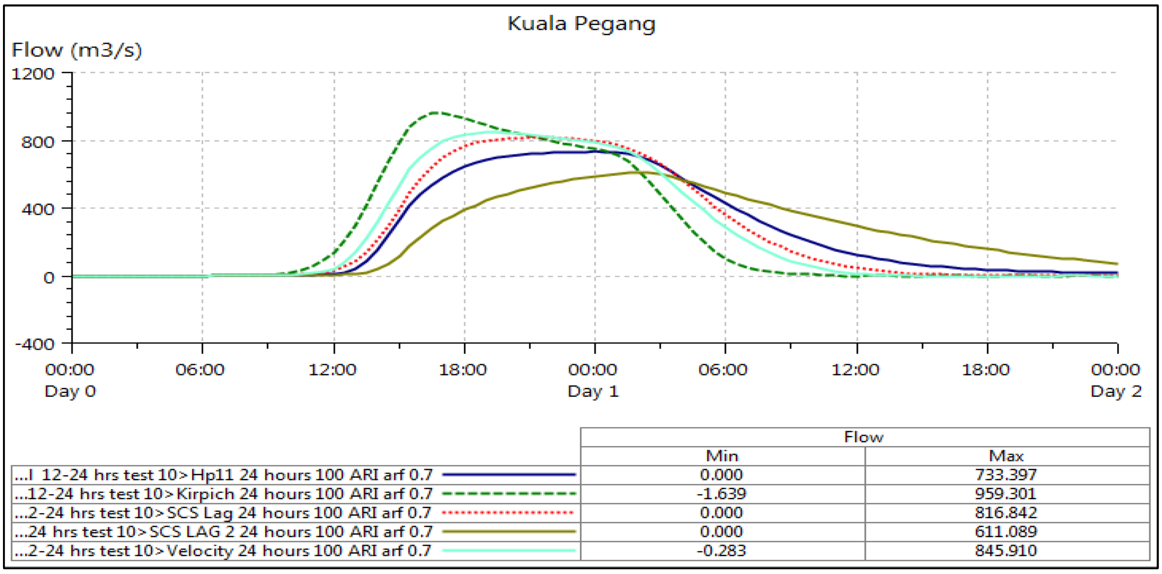

Figure 3. Runoff hydrograph using various T_c method for Level II model

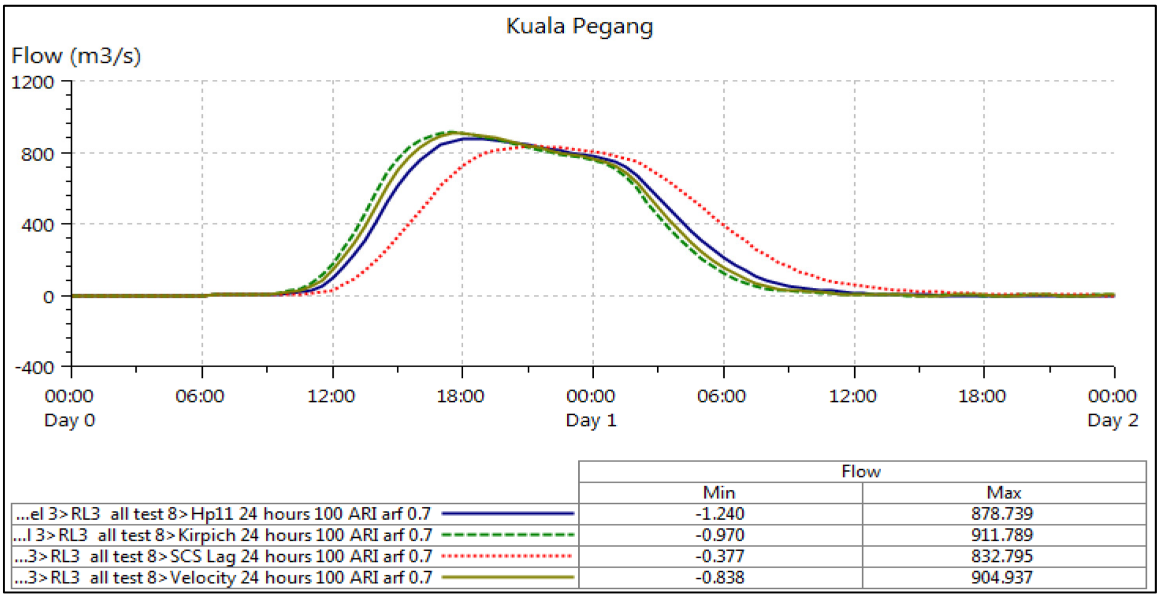

Figure 4. Runoff hydrograph using various T_c method for Level III model

5 Flood plain / Storage Effect

All analysis carried out earlier did not consider any storage in the flood plain i.e. the model is only controlled in the channel. To get the effect of the flood plain, the model is further extend to the flood plain with the support of digital terrain model available in IFSAR. Two dimensional flood plain model was developed by extending the 1D model along the flood plain as shown in Figure 16.a and 16.b. The mesh size for the 2-D model was set between 2000 m^2 to 4000 m^2 with Manning roughness of 0.1. This mesh setting produced about 48,000 mesh for an area of 12,000 ha. The August 1992 flood event was used for the comparison purposes. Simulation based on 6 days storm was carried out which took about 22 minutes on i7 laptop. Flood extent along the flood plain is shown in Figure 16c. Results of simulation for both situation with and without flood plain are shown in Figure 16c. Discharge for with and without flood plain was 393 m^3/s and 487 m^3/s, respectively, while the observed peak discharge was 383 m^3/s. The timing of the peak discharge for the hydrologic model is earlier by 12 hours but with the flood plain component, the peak discharge is delayed and match very well to the observed. This give the difference of discharge between the observed and simulation to a very good agreement.

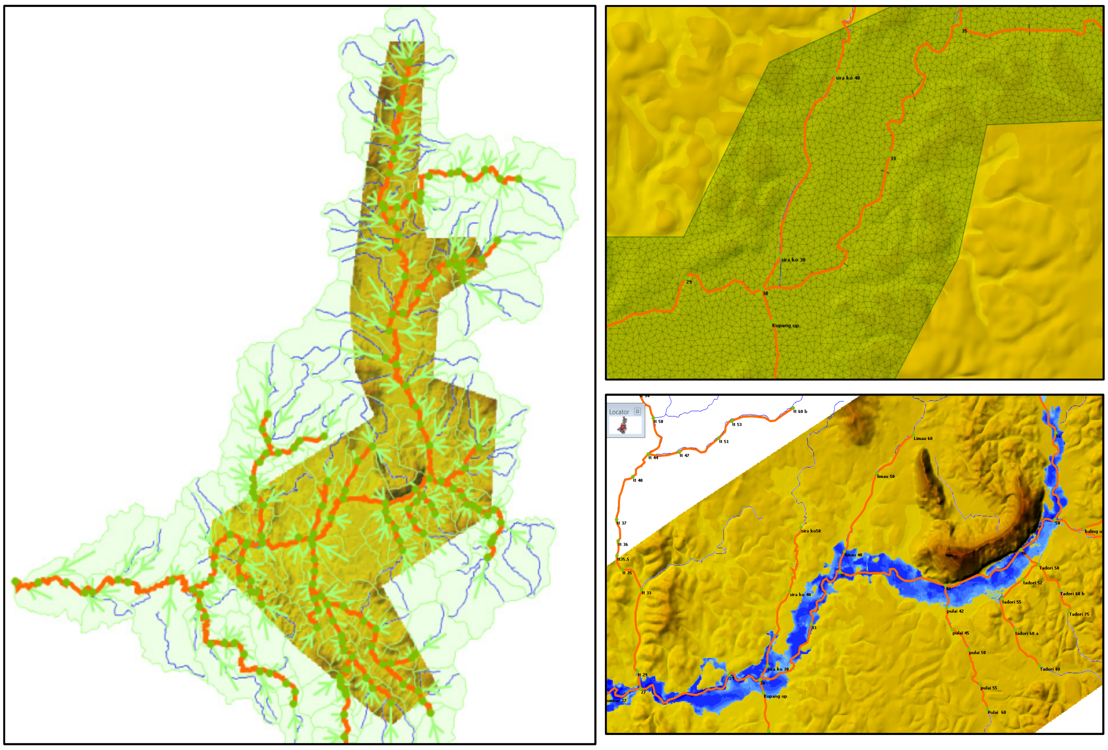

Figure 16. (a: Left - River model with DTM, b: Top Right – 2-D Mesh , c: Bottom - Flood extent)

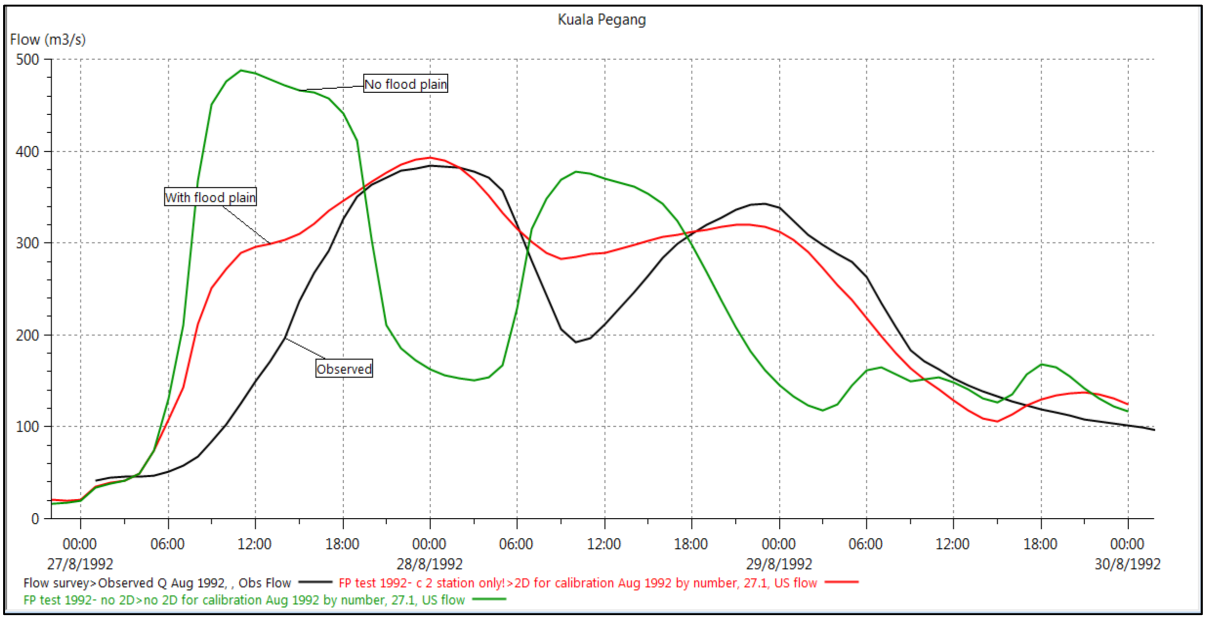

Figure 17. Flood hydrograph for 1992 event (with and without) flood plain compared to the observed discharge of Sg Ketil at Kuala Pegang.

6 CONCLUSION

The transformation of hydrologic model from Lumped to Distributed which is based on the river tributaries created up to 151 small subcatchments and about 170km of river channel length. The catchment size were break down to about 2% of whole catchment size. The length of each subcathment was breakdown to 10 % from the total length of the main river. The peak discharge differences for all T_c methods reduce from 203% to 9%. The differences of time to peak estimation also reduced from 53% to 14 %. It can be concluded that the used of river channel to represent the time of concentration had contribute to the consistency of the flow estimation. Model of Level III shown the consistent hydrograph for all method of T_c computation. This concludes that the distributed model based on hydrodynamic equation produces more consistence results regardless of the method to compute the T_c.

The impact of storage was included into the model using the 2D flood plain model and shows huge reduction to the peak flow. The results for the 1992 flood event shown a good agrement between observation and simulation once flood plain is included into the model. This results also indicate that the hydraulic component can be easily incorporated into hydrologic model to produce realistic flow estimation.

REFERENCES

Drainage and Irrigation Department (1980). *Reprinted 1994, Hydrological Procedure No 11. (HP11),* Design flood hydrograph estimation for rural catchment in Peninsular Malaysia.

Drainage and Irrigation Department (2012). *Updating of Condition of Flooding and Flood Assessment in Malaysia- Final Report – State Report for* Kedah, Volume 2.2: Figure No KDH_4.1a

Drainage and Irrigation Department (2015). *Revised and Updated the Hydrological Procedure No 1*, Estimation of Design Rainstorm in Peninsular Malaysia: 39-66.

Innovyze (2016) *Innoyyze Ltd* (http://innovyze.com) – 2016

Philip B Bedient, Wayne C. Huber, Baxter E. Vieux (2008). Hydrology and Flood Plain Analysis: Fourth Edition, Pearson International Edition: 115-139.

Price R.K (2003). *Short Course on Hydroinformatics for Flood and Urban Drainage Management*, IHE, DELFT: 9-10 of Lecture 12

Ven Te Chow, David R. Maidment, Larry W. Mays (1988). *Applied Hydrology*. McGraw-Hill, 500-501, 237-285

United States Department of Agriculture (USDA) (1986). *Natural Resources Conservation Services (NRCS)*, Urban Hydrology for Small Watershed, TR55, (June 1986): Chapter 3.

ESTIMATION OF FLASH FLOOD GUIDANCE USING GEOMORPHIC UNIT WITH HYDROGRAPH METHOD

DAWEI ZHANG(1), JIN QUAN(2), ZHIHAN YE(3) & GUANGYUAN KAN(4)

(1,2,4). China Institute of Water Resources and Hydropower Research, Beijing, 100038, China
zhangdw@iwhr.com; quanjin@iwhr.com; kangy@iwhr.com
(1,4). Research Center on Flood & Drought Reduction, Ministry of Water Resources, Beijing, 100038, China
(3). Beijing Water Science & Technology Institute, Beijing, 100048, China
zhihan79@163.com
(4). State Key Laboratory of Hydroscience and Engineering, Tsinghua University, Beijing, 100084, China

ABSTRACT

In this study, a novel conceptual hydrological model is presented to simulate flash flood process in un-gauged basins. The highlight of the new model is the utilization of the geomorphic unit with hydrograph method to simulate the overland flow process, which makes the model extremely valuable in un-gauged basins. The model was then tested in the Hongluogu headwater catchment in Beijing city and the results indicated that the new hydrological model performed well. Two villages of Beijing were selected as the research object for the FFG and they are Sihetang village in Sihetang catchment and Nanjiangou village in Nanjiangou catchment respectively. We carried on the FFG analysis as follows: First, we calculated the disaster-induced discharge (corresponding to FFG) of the two villages through the hydraulics method. Next, we assigned probabilistic rainfall by 1hr ,2hr and 3hr for the given return periods (2, 5, 10, 20, 50, and 100 year) by using Beijing Hydrology Handbook and then the hydrological model is used to calculate the design flash flood process of Sihetang and Nanjiangou respectively. Then we can generate the relationship curve between rainfall and the corresponding peak discharge for every return period. Finally, the FFG value can be interpolated from rainfall-discharge relationship curve based on the disaster-induced discharge. The new computed FFG values of Sihetang and Nanjinggou were tested in the “7.20” flash flood event occurred in Beijing on Jul 20th, 2016 and the result proved that the new FFG value is reasonable and reliable for real world applications.

Keywords: Flash Flood guidance (FFG); hydrological model; geomorphic unit hydrograph (GUH); un-gauged catchment; Beijing.

1 INTRODUCTION

The flash floods, which are characterized by a quick rise of water levels, often occur in mountainous areas after heavy rainfall with short duration. Due to the complexity of flash flood formation process and the limited available lead time for flood prediction, flash flood prevention has become a worldwide problem which poses great challenges. Furthermore, with the exacerbation of climate change, flash flood disasters have occurred more frequently than ever before and has caused huge number of casualties in China (Sun et al., 2013). For the purpose of constructing better flash flood prevention scheme, the Flash Flood Guidance (FFG) is adopted in China. The FFG is the threshold amount of rainfall that needed for flash flood disaster occurrence. The FFG is commonly calculated by using the rainfall-runoff (RR) model. However, the research on flash flood simulation is full of challenges as flash floods often occur in un-gauged basins. Many scholars have conducted studies on flash floods simulation and the geomorphological unit hydrographs have become one of the most popular methods for calculating hydrological processes when instrumental data cannot be obtained (Zhang et al., 2015; Diakakis, 2011; Du et al., 2009).

In this study, a novel hydrological model based on geomorphological unit hydrographs has been developed considering the velocity differences between the overland flow and channel flow. The model is then tested in the Hongluogu headwater catchment in Beijing city and the results indicated that the new hydrological model performed well. And then it was treated as a useful tool to estimate the FFG values of Sihetang and Nanjinggou village, and the new FFG values was proved reasonable when they were tested in “7.20” flash flood event occurred in Beijing on Jul 20th, 2016.

2 HYDROLOGIC METHOD

2.1 Model Formulation

The new conceptual hydrological model is based on the SCS-CN method and GUH method. SCS-CN (Soil Conservation Service Curve Number) method is one of the most popular methods for computing the volume of surface runoff for a given rainfall event especially in the un-gauged catchment (SCS, 1985; Shadeed and Almasri, 2010). For the flash flood, the surface flow is the main component of the runoff, so in this study, SCS-CN method was used to calculate the net rainfall process. In order to calculate the surface runoff efficiently, the GUH method was used. For the new hydrological model, the novelty lies in considering the velocity difference between the overland flow and channel flow in the geomorphic unit with hydrograph method.

(1) SCS-CN method

The standard SCS-CN method is based on the following relationship between rainfall *P* (mm) and runoff *Q* (mm) (Schulze et al., 1992):

$$Q = \begin{cases} \dfrac{(P-I_a)^2}{P-I_a+S} & p > I_a \\ 0 & P \le I_a \end{cases} \quad [1]$$

where, *S* (mm) is potential maximum retention and I_a (mm) is all loss before runoff begins. Variable I_a is generally correlated with soil and land cover parameters. For the convenience of calculation， a linear relationship between I_a and *S* was suggested by SCS(1985) as:

$$I_a = \lambda S \quad [2]$$

where, λ is an initial abstraction ratio. The values of λ vary in the range of 0 to 0.3. Generally, λ is set to be 0.2. Substituting I_a=0.2s gives:

$$Q = \frac{(\mathrm{P}-0.2\mathrm{S})^2}{P+0.8S} \quad [3]$$

Due to *S* value varying in large range, a non-dimensional catchment parameter CN is introduced to meet the needs of practical application .The variable *S* can be estimated as:

$$S = \frac{25400}{CN} - 254 \quad [4]$$

where, *CN* is a parameter ranging from 0 to 100. A high *CN* value means high runoff and low infiltration, whereas a low CN value means low runoff and high infiltration.

(2) GUH method

The presented GUH method was based on the DEM data and the first step is to obtain the travel time at each point in the catchment. Zhang et al (2014, 2015) proposed a method to calculate the velocity of runoff and the method cannot distinguish the difference between overland flow and channel flow. Actually, the moving path of most raindrops can be divided into two phases and the following Figure 1 shows how it works. In this study, a new method was used to calculate the overland flow and channel flow respectively.

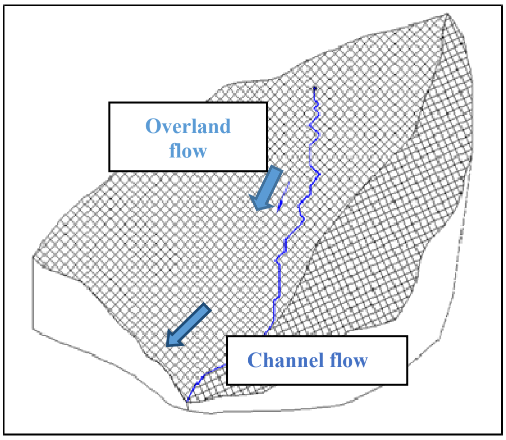

Figure 1. Moving path of raindrop in the catchment.

Generally, the velocity of overland flow and channel flow can be estimated using the following equation because the runoff flow of flash flood is driven mainly by gravity:

$$V = KS^{1/2} \quad [5]$$

where, V is the velocity of overland flow or channel flow, K is the velocity coefficient, and S is the average slope of the catchment. In theory, there are orders of magnitude difference between the overland flow velocity and channel flow velocity. Therefore, the values of K should be determined respectively and K_1, K_2 represents overland flow coefficient and channel flow coefficient respectively.
Any raindrop in the catchment has its own independent flow path to the outlet and water flows into the adjacent grid according to the maximum gradient based on the D8 algorithm. The concentration time of water in each grid can be determined according to the flow path and the runoff velocity.
If the time step of unit hydrographs was assumed to be DT, then by counting the grid numbers reaching the outlet in each period, it is possible to obtain the cumulative drainage areas in the duration DT. So according to the time–area curve method, the dimensionless unit hydrograph can be calculated using the S-hydrograph:

$$u(\Delta t, t) = S(t) - S(t\text{-}\Delta t) \quad [6]$$

where, $u(\Delta t, t)$ is the dimensionless unit hydrograph, $S(t)$ is the S-hydrograph, and Δt is the actual period of the unit hydrograph.
If the precipitation within Δt is given as i, the period unit hydrograph can be calculated according to dimensionless unit hydrograph:

$$q(\Delta t, t) = \frac{F}{\Delta t} u(\Delta t, t) i \quad [7]$$

where, $q(\Delta t, t)$ is the period unit hydrograph and F is the basin area.

To the catchment with large areas, the storage function of watershed should also be considered (Li, 2005). And the linear reservoir method is as follows:

$$Q_i = c(\frac{q_i + q_{i\text{-}1}}{2}) + (1-c)Q_{i-1} \quad [8]$$

where, Q is the final value of period unit hydrograph; c is the coefficient of linear reservoir.

2.2 Model Validation

The new presented hydrological model was used in the headwater catchment of Hongluogu in Beijing city, as seen in the Figure 2.

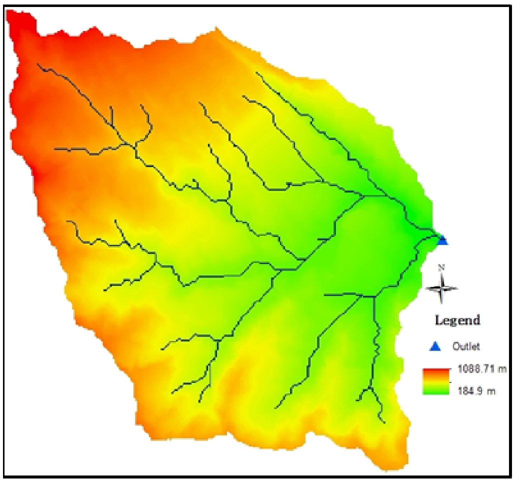

Figure 2. Hongluogu headwater catchment.

The study of headwater catchment covers an area of 5.94km^2. There is a rainfall station in the study area and maximum discharge in the outlet of this study area was also obtained. So we use the “7.20” flash flood event occurred in Beijing on Jul 20th, 2016 to validate the presented model.

The GUH of Hongluogu headwater catchment can be calculated based on the DEM data. In this study, the time interval was 5min and the overland velocity coefficient K_1 was taken as 0.5 and the runoff velocity coefficient K_2 was taken as 3.0. The GUH result is shown in Figure 3.

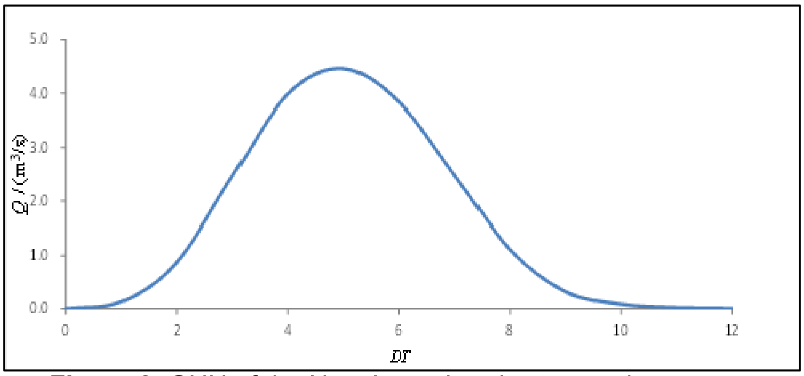

Figure 3. GUH of the Hongluogu headwater catchment.

The developed new hydrological model has been validated using the "7.20"flash flood of the study area. According to the existing research results (Fu et al., 2013), the CN value is set to be 65 and 75. The simulation result is shown in Figure 4. From the figure we can see when the CN is taken as 65, the calculated maximum discharge was 39 m^3/s and when the CN is taken as 75, the calculated maximum discharge was 45 m^3/s, which was close to the measured flood peak of 43 m^3/s. The results demonstrate that the computed peak discharge generally agrees well with the measured peak discharge and it can be treated as a useful tool for FFG estimation.

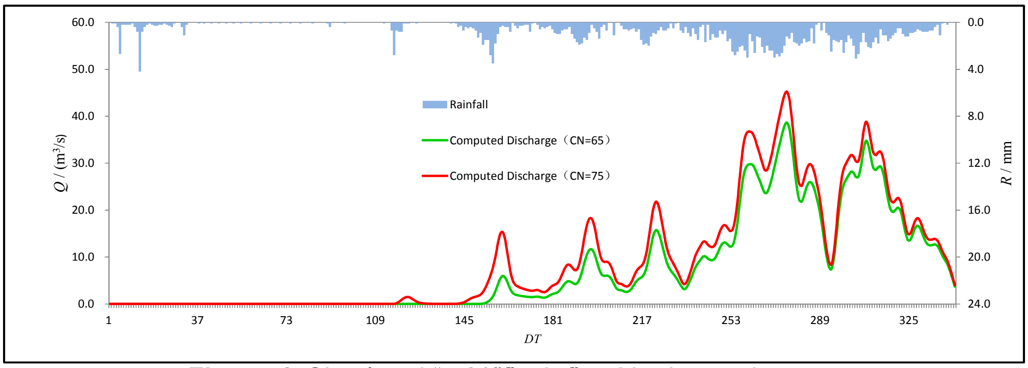

Figure 4. Simulated "7.20"flash flood hydrograph.

3 COMPUTATIONAL METHOD OF FFG

In this study, the computational method of FFG includes three main steps:

(1) Decision of critical discharge

Firstly, we should choose the typical control section near the village and then determine the critical water level of the typical control section. The critical water level mainly refers to the level corresponding to the lowest settlement (as shown in Figure 5). Critical discharge (corresponding to the critical water level) was also called disaster-induced discharge can usually be calculated by simple empirical hydraulics formula, such as Manning formula, Chezy formula, or according to the actual flash flood events stage-discharge relation, etc.

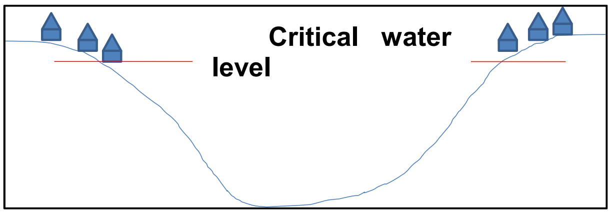

Figure 5. Scheme of critical water level.

(2) Decision of rainfall-discharge relationship curve

We assigned probabilistic rainfall by 1hr, 2h and 3hr for the given return periods (2, 5, 10, 20, 50, and 100 year) by using Hydrology Handbook. Assuming that uniform rainfall occurred in the study area, the new presented hydrological model can be used to calculate the different design of rainfall runoff process. Then we can generate the relationship curve between rainfall and the corresponding peak discharge for every return period and different rainfall duration.

(3) FFG calculation from rainfall-discharge relationship curve

FFG value can be interpolated from rainfall-discharge relationship curve based on the critical discharge of the control section (decided in step 1). It is important to note that the FFG value was calculated under a certain soil moisture conditions.

4 APPLICATION

4.1 Study areas

Two villages in Miyun county and Mentougou county of Beijing were selected as the research object for the FFG and they are Sihetang village in Sihetang catchment (seen in Figure 6) and Nanjiangou village in Nanjiangou catchment (seen in Figure 7), respectively. Sihetang catchment covers an area of 24km^2 and Nanjiangou catchment covers an area of 15km^2. The Sihetang village and Nanjiangou village are both located in the outlet of the catchments.

The two catchments belong to typical hilly areas and the average slope reached 0.73 in Sihetang catchment and 0.51 in Nanjiangou catchment with elevation values between 190m-1075.7m in Sihetang catchment and 180m-990m in Nanjiangou catchment. Because of their geographical location, the specific study areas have a general semiarid climate. In the summer period of June-October, intense downpours of short duration causes flash flood easily and the region's steep gradient help converge these precipitated volumes quickly. The flood is characterized by large flow rates and high transport ratios of alluvial matter can cause severe damage to the area. There are several land use types, mainly includes arable land, forest, and residential land, among which the forest land accounts for the major part. More than 300 people live in Sihetang village and 200 people live in Nanjiangou village.

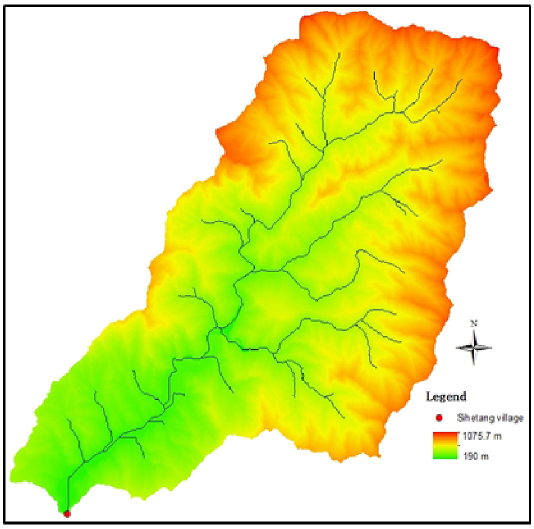

Figure 6. Sihetang catchment.

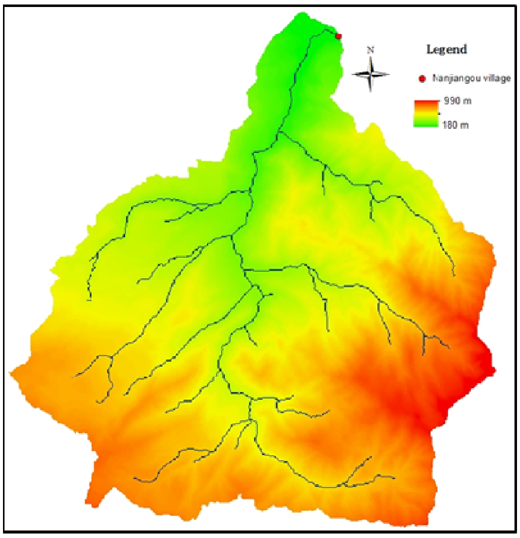

Figure 7. Nanjiangou catchment.

4.2 FFG estimation

First, we should calculate the critical discharge of the two villages. Figure 8 and Figure 9 are the control section and the critical water level of Sihetang village and Nanjiangou village. The channel slope is 1.2% and the critical water level is 205.97m in Sihetang village. The channel slope is 2.3% and the critical water level is 190.57 m in Nanjiangou village. The Manning equation was used to calculate the critical discharge and the Manning coefficient is set to be 0.055 considering the gravel riverbed in both channels. After calculation, the critical discharge of Sihetang village is 128 m^3/s and the critical discharge of Nanjiangou village is $32m^3/s$.

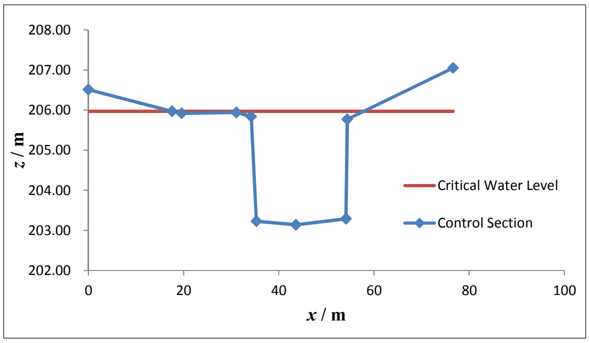

Figure 8. Critical water level of Sihetang village.

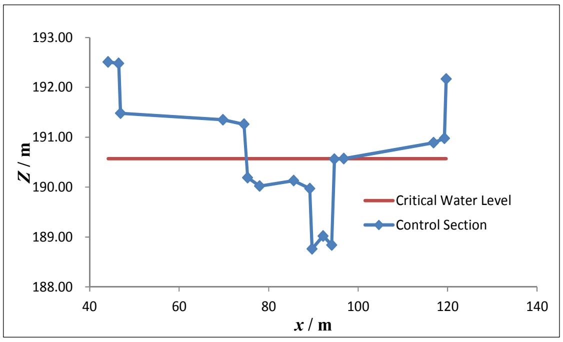

Figure 9. Critical water level of Nanjiangou village.

In this study, the time interval was set to be 5min and CN was set to be 75 in the two catchments. we got the probabilistic rainfall process by 1hr, 2hr and 3hr for the given return periods (2, 5, 10, 20, 50, and 100 year) using the Beijing Hydrology Handbook. And then the presented hydrological model was used to simulate the design flash flood process of Sihetang village and Nanjiangou village respectively using the probabilistic rainfall as the input condition. After the flood simulation, the relationship curve between rainfall and the corresponding peak discharge for every return period can be generated and the result is shown in Figure 10 (Sihetang village) and Figure 11 (Nanjiangou village).

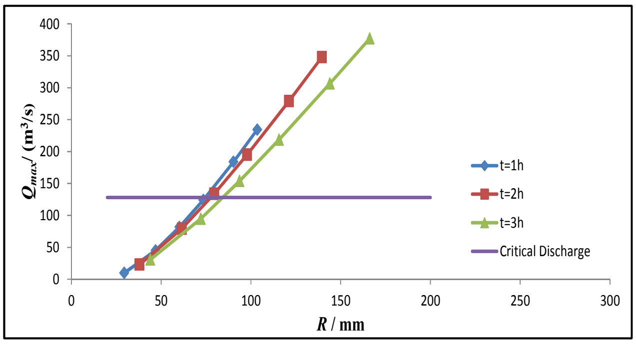

Figure 10. FFG estimation of Sihetang village.

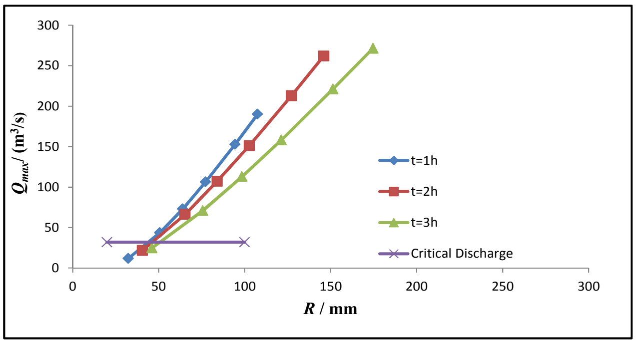

Figure 11. FFG estimation of Nanjiangou village.

The FFG value can be easily interpolated from rainfall-discharge relationship curve and the FFG values of the two villages are shown in the Table 1. The new FFG values were tested in the “7.20” flash flood event that occurred in Beijing on Jul 20th, 2016. The result showed that the FFG values are reasonable and can be used as the actual personnel transfer basis.

Table 1. FFG value of Sihetang and Nanjiangou.

Rainfall duration	T=1h	T=2h	T=3h
FFG of Sihetang village(mm)	75	78	84
FFG of Nanjiangou village(mm)	44	46	51

5 CONCLUSIONS

A new hydrological model for flash flood simulation has been presented and the novelty is that the geomorphic unit hydrograph is used to model surface runoff coupled with the velocity differences of the overland flow and channel flow are considered. The model is tested in the Hongluogu headwater catchment in Beijing city and the result shows that it can simulate flash flood well in un-gauged basins. After validation, the hydrological model is treated as a useful tool to estimate the FFG values in the Sihetang village in Sihetang catchment and Nanjiangou village in Nanjiangou catchment respectively. When we calculate the FFG value, the critical discharge should be determined firstly using the hydraulic equation, and then the relationship curve between probabilistic rainfall and the corresponding peak discharge for every return period can also be obtained by using the hydrological model. At last, the FFG value can be interpolated from rainfall-discharge relationship easily. In this study, the new FFG values of Sihetang village and Nanjiangou village are given and tested in the "7.20" flash flood event that occurred in Beijing on Jul 20th, 2016. The test results showed that the FFG values are reliable and can be used in the real world applications.

ACKNOWLEDGEMENTS

The research reported herein is funded by National Natural Science Foundation of China, "Numerical simulation technology of flash flood based on Godunov scheme and its mechanism study by experiment (No.51509263)" and the China Institute of Water Resources and Hydropower Research under the Project "Study on the key technology of the high practical hydrodynamic model based on Godunov scheme".

REFERENCES

Diakakis, M. (2011). A Method for Flood Hazard Mapping Based on Basin Morphometry: Application in Two Catchments in Greece. *Natural Hazards*, 56(3), 803-814.

Du, J.K., Xi, H., Hu, Y.J., Xu, Y.P. & Xu, C.Y. (2009). Development and Testing of a New Storm Runoff Routing Approach Based on Time Variant Spatially Distributed Travel Time Method. *Journal of Hydrology*, 369(1-2), 44-54.

Fu, S.H., Wang, H.Y., Wang, X.L., Yuan, A.P. & Lu, B.J. (2013). The Runoff Curve Number of SCS-CN Method in Beijing. *Geographical Research*, 32(5), 797-807.

Li, G.D. (2005). *Hydrology,* 1st edition. Wu-Nan Book Compang Ltd.

Schulze, R.E., Schmidt, E.J. & Smithers, J.C. (1992). *SCS-SA User Mannual PC Based SCS Design Flood Estimates for Small Catchments in Sourthern Africa*, Pietermaritzburg: Department of Agricultural Engineering, University of Natal.

Shadeed, S. & Almasri M. (2010). Application of GIS-Based SCS-CN Method in West Bank Catchment, Palestine. *Water Science and Engineering*, 3(1), 1-13.

Soil Conservation Service. (SCS). (1985). *Hydrology, National Engineering Handbook*. Washington, D.C:Soil Conservation Service, USDA.

Sun, D.Y., Zhang, D.W. & Cheng, X.T. (2012). Framework of National Non-Structural Measures for Flash Flood Disaster Prevention in China. *Water*, 4, 272-282.

Zhang, D.W., Quan, J., Wang, F. & He, X.Y. (2014). Flash Flood Simulation using Geomorphic Unit Hydrograph Method: Case Study of Headwater Catchment of Xiapu River basin, China. *11th International Conference on Hydroinformatics, HIC 2014*, New York City, USA.

Zhang, D.W.,Quan, J., Zhang, H.B., Wang, F., Wang,H. & He, X.Y. (2015). Flash Flood Hazard Mapping—A Pilot Case Study in The Xiapu River Basin, China. *Water Science and Engineering*, 8(3), 195-204.

Proceedings of the 37th IAHR World Congress
August 13 – 18, 2017, Kuala Lumpur, Malaysia

FLOOD FORECASTING AND WARNING FOR MUAR RIVER: NON-STRUCTURAL MEASURES FOR FLOOD MITIGATION

WAN HAZDY AZAD WAN ABDUL MAJID(1), EMMA BROWN(2), SAZALI OSMAN(3), GAPAR ASAN(4), AB QAHAR OSMAN(5), ROSHAM KADIMAN SAMSUDIN(6), LEONORE BOELEE(7) & FAIZAH AHMAD(8)

(1, 3, 4, 5) Jabatan Pengairan dan Saliran, Jalan Sultan Salahuddin, 50626 Kuala Lumpur, Malaysia,
wanhazdyazad@gmail.com; sazali@water.gov.my; gapar@water.gov.my; ab.qahar:water.gov.my
(2, 7, 8) HR Wallingford Asia Sdn Bhd, Block 3B, Level 5, Plaza Sentral, Jalan Stesen Sentral 5, 50470 Kuala Lumpur, Malaysia,
e.brown@hrwallingford.com; l.boelee@hrwallingford.com; faizah.ahmad@hrwallingford.com
(6) Pinnacle Engineering Consult, Medan Puteri, Bandar Tasik Puteri, 48020 Rawang, Selangor Darul Ehsan Country, Malaysia,
pinnacleurban@gmail.com

ABSTRACT

The Muar River catchment has repeatedly suffered prolonged, significant flood events which have caused widespread disruption and impacts to residents, businesses and infrastructure. The impacts have been exacerbated by considerable rapid development over the past decade, which has modified the flow regimes and flooding mechanisms. To help prepare for, and mitigate, the effects of future floods, the Malaysian government is implementing a range of flood management projects, which will provide an integrated approach based on structural and non-structural measures. The integrated Flood Forecasting and River Monitoring system (iFFRM) for the Muar River is a key non-structural measure that has been recently implemented. The government's Department of Irrigation and Drainage (DID) is responsible for providing a flood forecasting and warning service to the public where the iFFRM is a tool designed to enable effective decision support by DID. The iFFRM is a fully automated system that is driven by a combination of live, telemetered gauged data from DID's own InfoBanjir database, spatial rainfall radar data, and Numerical Weather Prediction (NWP) rainfall forecasts from the Malaysian Meteorological Department. Hourly simulations are carried out automatically, to forecast water levels and flows in the river channels, and to map the flood inundation process within the flood plains. Simulation results are used to warn DID staff so that immediate action can be taken to provide an effective and proactive emergency response. Results are also passed to the project website, and dedicated smartphone application, enabling forecasts to be disseminated more widely. A parallel analytical modelling network can take over the forecasting role should the primary iFFRM system fails. Ongoing structural measures for flood mitigation are captured through a flexible modelling approach that can incorporate model updates to reflect real changes in the catchment to complement the structural measures being implemented by DID in ensuring a sustainable solution.

Keywords: Flood forecasting; warning; decision support.

1 INTRODUCTION

Hydrological extremes, droughts and flooding, affect every generation and cause suffering, death and material losses (Kundzewicz and Kaczmarek, 2009). The latest data on natural disasters puts the size of historical flood disasters into context, illustrated through information on the impacts of the top ten flood disasters since 1900, through the numbers of people killed and the numbers affected are low (CRED, 2014). Strikingly, in the first half of the twentieth century, hundreds of thousands of people lost their lives to flood disasters; on the other hand, in the latter half of the period, hundreds of millions of people have been affected. This would imply that whilst the situation has improved in terms of reducing the numbers of people killed through flood disasters, there is still an enormous role for effective flood forecasting and warning to reduce the wider impacts of flood disasters. Significantly, the people affected in the greatest numbers, and the countries suffering the largest economic damages, are primarily found in east and south-east Asia. Flood records for peninsular Malaysia, as far back as 1886 and 1926, reported severe floods affecting large parts of the country and causing extensive damage to road systems, property, agricultural lands and crops (Wing, 2004). In recent decades, flooding has become more frequent; the main reasons include loss of flood storage due to development of floodplains, increased runoff due to urbanisation, inadequate drainage systems, flow constriction in river channels due to bridges, culverts and blockages, and siltation due to land clearing (Wing, 2004). In addition, climate change is expected to cause an increase in flood frequency in Malaysia towards the second half of the 21st century (Amin et al., 2017).

Hydrological forecasting is a non-structural measure which has proven to be efficient and cost effective in minimising the negative impacts of flooding and increasing drought preparedness and mitigation (WMO and GWP, 2013; Mishra and Singh, 2011). Effective flood forecasting has the potential to save significant numbers of human lives, as well as saving disruption to many times that figure, and has the ability to save enormous sums of money. A global survey of early warning systems carried out by the UN and the International Strategy for Disaster Reduction, (UN/ISDR, 2006), resulting from the assessment of progress towards Millennium Achievement Goals, concluded that to be effective, early warning systems must be people-centred and must integrate four elements:

- Risk knowledge;
- Monitoring and warning service;
- Dissemination and communication;
- Response capability.

The global survey notes that “a weakness or failure in any one part could result in failure of the whole system“ (UN/ISDR, 2006). Kundzewicz (2013) takes this description as the ‘Achilles heel’ of effective flood forecasting and warning systems one step further by pointing out that if “the observation system may fail, the forecast may be grossly in error, the warning message may be wrong, the communication of a warning may be deficient and the response may be inadequate. A single weak point in a system, which otherwise contains many excellent components, may render the overall system performance unsatisfactory”. Furthermore, to be successful, such a system requires sufficient integration of components and collaboration and coordination between multiple institutions. Flood forecasting and warning systems sit at the interface of meteorology, hydrology, hydraulics, information technology, and social science. Therefore, each component must be able to perform its role, and the links between them, their integration, must be working effectively too.

The Malaysian government’s Department of Irrigation and Drainage (DID) is responsible for providing a flood forecasting and warning service to the public. It is developing a programme based upon the phased implementation of systems for key river basins; the integrated Flood Forecasting and River Monitoring system (iFFRM) for the river Muar is one of the first flood forecasting systems to have become operational. The objectives of this system were to develop and maintain an effective and efficient integrated flood forecasting and river monitoring system, with flood warning dissemination, using national network data, telemetry data, radar data and rainfall forecasts; the iFFRM is a tool designed to enable effective decision support provided to DID.

The development of the iFFRM is described in this paper, from a description of the nature of flooding in the catchment, through the dataflow and modelling methodologies used, and the operational implementation of the end-to-end forecasting system. Lessons learnt are discussed, with suggestions for how these lessons will be integrated into the total framework of flood forecasting systems in Malaysia.

2 BACKGROUND

2.1 Catchment description

The river Muar lies on the west coast of peninsular Malaysia, straddling Negeri Sembilan and Pahang states (Figure 1). Its catchment has repeatedly suffered prolonged, significant flood events which have caused widespread disruption and impacts to residents, businesses and infrastructure (Asmara and Ludin, 2014). The impacts have been exacerbated by considerable rapid development over the past decade, which has modified the flow regimes and flooding mechanisms (Wing, 2004). Significant recent flood events occurred in 2006, 2007, 2011, and 2015 where these events led to the evacuation of tens of thousands of local residents in the Muar catchment alone. Across Malaysia, an estimated fifth of the population is at risk of flooding (DID, 2009).

The topography of the catchment is a mix of steep mountainous, hilly country and undulating low terrain (Hong and Hong, 2016). The climate in the Muar catchment is tropical, with the southwest monsoon occurring in April and May, and the northeast monsoon occurring in October to December. Dry periods dominate in January to March and June to September (Hong and Hong, 2016). The annual average rainfall in peninsular Malaysia is 2500 mm, with as much as 600 mm falling in 24 hours in extreme storm events (DID, 2009b).

The Muar catchment area is approximately 6600 km^2 and subdivides into 21 subcatchments. The total length of the main channel is 310 km, with an average annual discharge at the river mouth of approximately 140 m^3/s. High flows are recorded during the monsoon seasons, with the north-east monsoon (October to December) resulting in the highest flow conditions. The lowest flows are recorded during the dry period of July and August.

Land use in the Muar catchment is a combination of urban, primary rainforest, and agricultural plantations including rubber, oil palm, paddy, maize and vegetable cultivation. Land use has changed rapidly in recent decades. From the 1950s, increasing agricultural production had led to the loss of forested land to become agricultural land to rubber plantations and then palm oil (Abdullah and Nakagoshi, 2008). Malaysia has also seen a growth in manufacturing since the 1980s, which has led to rapid industrialisation and associated increases in urbanisation (Abdullah, 2003) and decreases in agricultural land (Erickson, 1995). Levels of urbanisation are expected to increase further due to allocated housing, commercial and industrial activities. The precise impacts of land use change on hydrology are difficult to predict accurately, but deforestation is generally associated with an increase in runoff (Siriwardena et al., 2006) and increased urbanisation is associated with increases in peak flows (Hundecha and Bardossy, 2004). In summary, the rapid urbanisation and associated land use change in the catchment has led to reduced permeability of runoff surfaces and thus higher, faster, rates of runoff, as well as reduced conveyance capacity in the river channels. These factors have led to increased flood risk, notably of flash flooding, in the catchment (DID, 2007).

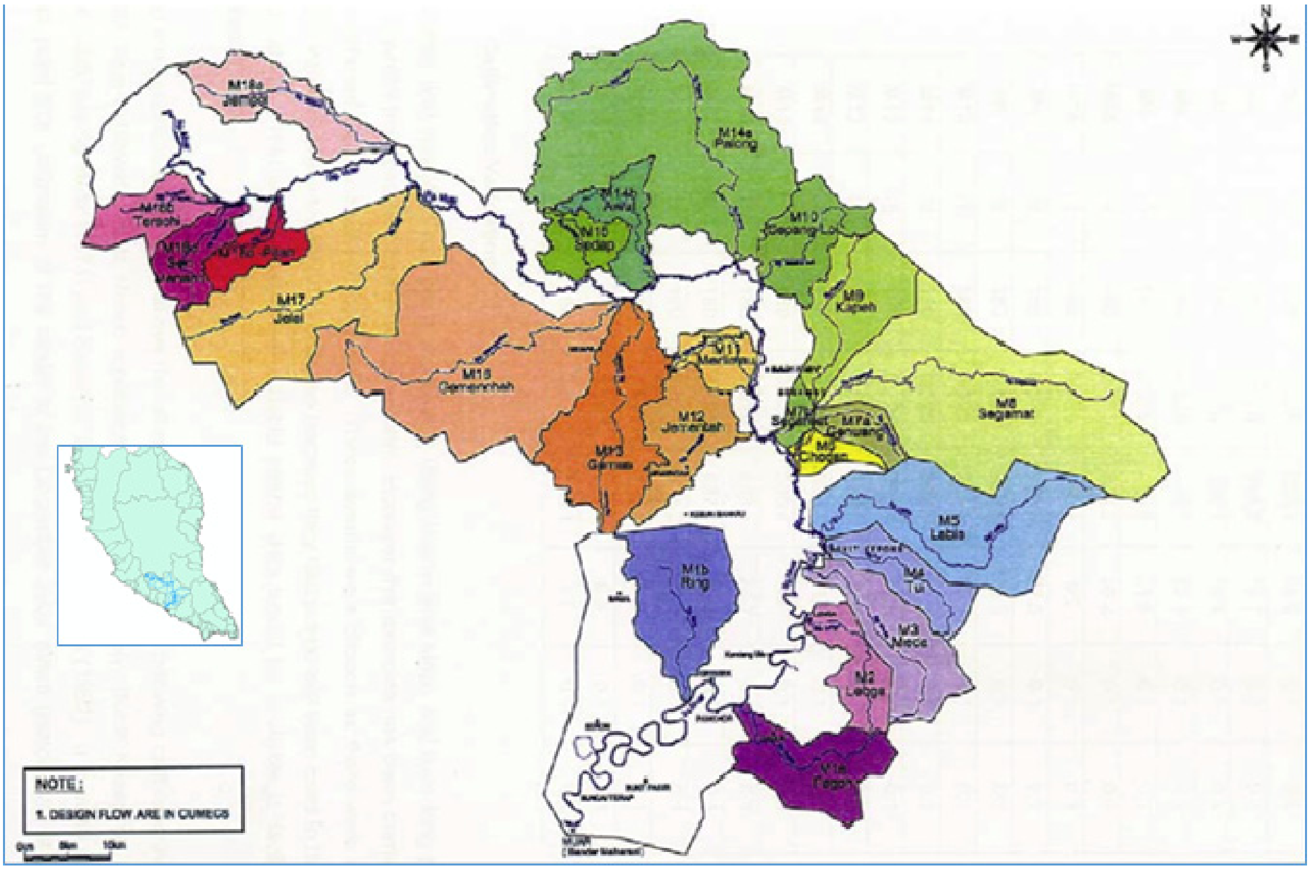

Figure 1. Map of the River Muar catchment, showing the location of the catchment in Peninsular Malaysia.

3 APPROACH TO SYSTEM DEVELOPMENT

The main goals of the iFFRM are to forecast river levels up to three days into the future and to issue warnings if threshold levels have been crossed, and to provide an indication of the likely flood extents on the floodplain.

The iFFRM is a fully automated system that is driven by a combination of live, telemetered gauged data from DID’s own InfoBanjir database, spatial rainfall radar data, and Numerical Weather Prediction (NWP) rainfall forecasts from the Malaysian Meteorological Department. Hourly simulations were carried out automatically, to forecast water levels and flows in the river channels, and to map the flood inundation process within the flood plains.

The catchment is represented by a series of models driven by live, observed and forecasted data feeds. These models broadly represent the processes of runoff generation from upstream subcatchments (rainfall-runoff models), feeding the boundaries of detailed hydrodynamic models of the main river channels.

3.1 Hydrological and hydrodynamic modelling

In selecting appropriate models for flood forecasting, the approach of Booij (2005) is sensibly taken: “find a model that is sufficiently detailed to capture the dominant process and natural variability, but not unnecessarily refined that computation time data is wasted or data availability is limited.”

Hydrodynamic modelling for the Muar catchment was carried out using InfoWorks RS. This tool was able to model river reaches using full hydrodynamic solution techniques, based upon the Saint Venant equations for shallow water waves in open channels. It can be used to model open channel and overbank flows in a network of channels. Any sensible looped or branched network can be modelled along with a wide range of hydraulic structures. It can be used to solve systems under both steady and unsteady flow conditions. For unsteady solutions, InfoWorks RS uses the governing hydraulic equations for each network object. These equations are a combination of empirical and theoretical equations, many of which are non-linear. The non-linear equations are first linearised and the solution to the linear version of the problem is then found via matrix inversion. An iterative procedure was used to account for the non-linearities (Innovyze, 2014). InfoWorks RS also includes flow routing methods. Flow routing determines the change in shape of a flow hydrograph as it moves along a channel without necessarily calculating water levels. It is a useful technique when detailed cross-section data are not available and a smaller range of results is required. The Muskingum method is a commonly used hydrologic routing method in situations requiring a variable storage-discharge relationship. The network object was based on the continuity equation and the Muskingum storage relationship. The representation of the main river channels of the Muar catchment is shown in Figure 2.

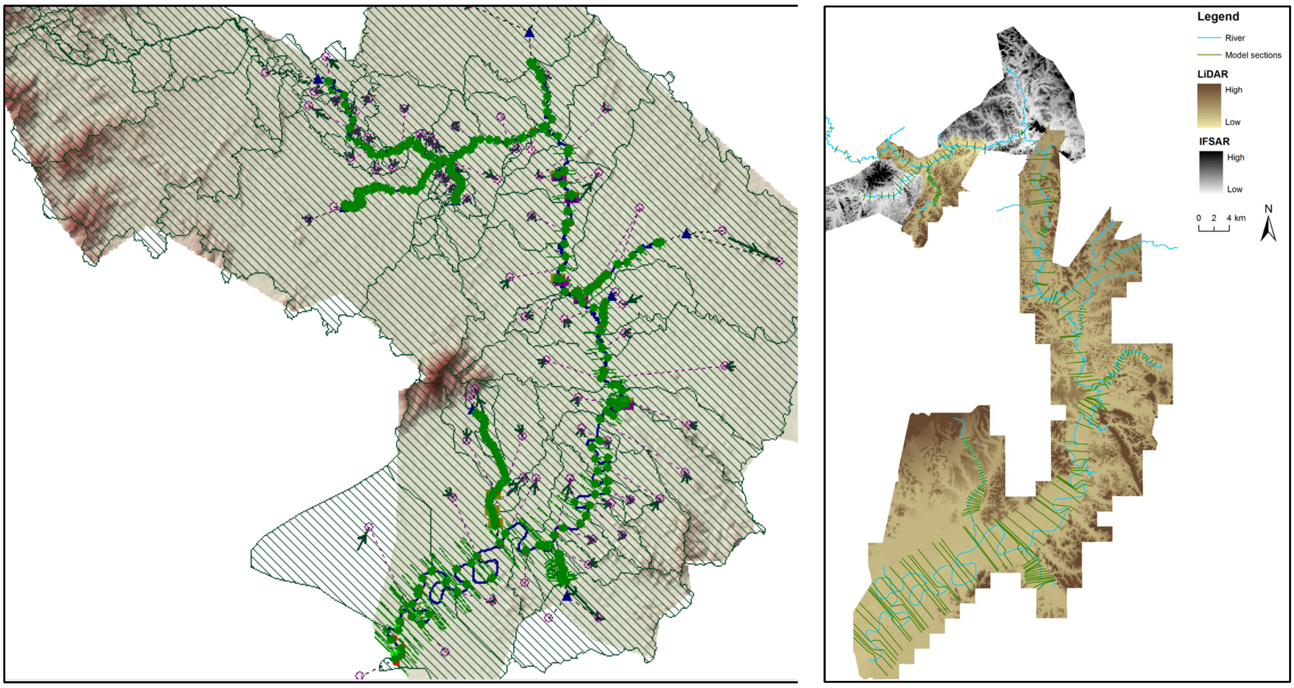

Figure 2. Map of the River Muar catchment, showing the modelled representation of the subcatchments (left), the main and flood plains as covered by the Digital Terrain Model (right).

3.1.1 Probability Distributed Model (PDM)

There are broadly two types of hydrological model to choose from: physically-based models and data-driven models. Both types of model have advantages and disadvantages, thus the reader is referred to Todini (2007) for a comprehensive overview. In the case of the Muar catchment there is limited historical data available which would limit the training sets that could be created for a data-driven approach. Using a physically-based model allows all *priori* knowledge of the hydrological processes to be used in setting up the model, with the aim of reducing the uncertainty of the *a posteriori* forecasts (Todini, 2007).

For gauged subcatchments, the Probability Distributed Model (PDM) provides a pragmatic approach between inherently complex, physically-based approaches, and simplified lumped modelling approaches. This probability-distributed approach considers the frequency of occurrence of certain hydrological variables used to derive algebraic expressions for the integrated flow response from the basin (Moore, 1985). The PDM is a fairly general conceptual rainfall-runoff model which transforms rainfall and evaporation data to flow at the catchment outlet and was developed with operational applications in mind (Moore, 1985). The PDM model essentially distributes rainfall between runoff and recharge according to a soil moisture store. The runoff and recharge are routed via stores to the catchment outlet. One of the main advantages of the model is the use of a probability distribution rather than a single value for the soil moisture store. This represents the spatial variability in soil storage across the catchment and prevents threshold-type behaviour. The model's short computational run time and continuous soil moisture accounting model makes it suited to continuous simulation using incoming telemetry data for flood forecasting. The model can also use observed flow data from telemetry to update its internal soil moisture values in a process known as state correction, which was important for maximising the accuracy of the model results.

3.1.2 Simple Runoff Model (SRM)

In the Muar catchment, not all of the subcatchments for which the rainfall-runoff process needs to be modelled are gauged. Setting up hydrological models for ungauged catchments remains a challenge (Bloschl, 2006). When no runoff data are available, keeping it simple is often the best solution. The Simple Runoff model (SRM) is useful for deployment in catchments without any calibration data, or in urban areas if the runoff response is thought not to follow a soil moisture response. Eq. [1] presents the SRM equation.

$$P_{eff} = P_c * RC * (1 - SMD) \quad [1]$$

where,

$$P_{eff} = Effective\ Precipitation$$

$$P_c = Catchment\ Precipitation$$
$$RC = Constant\ Runoff\ Coefficient\ (0-1)$$
$$SMD = Soil\ Moisture\ Deficit\ Fraction\ (0-1)$$

In this approach, catchment rainfall is multiplied by a runoff fraction which is determined by the user and by a soil moisture deficit (SMD) fraction. The SMD fraction may be fixed, but for rural catchments more accurate results are achieved if a time series of values is supplied. Observed soil moisture data are not available in this catchment. However, using the concept of hydrological similarity, it was assumed that catchments close to each other will behave hydrologically in a similar manner and this assumption is known as spatial proximity (Bloschl, 2006). Using these concepts the soil moisture deficit time series from the PDM models in the gauged catchments can applied to the ungauged catchments. Although this method will increase the uncertainty of the forecasts, using calibration parameters from similar catchments in the same region was preferable to for example using parameters from donor catchments (Bloschl, 2006).

3.2 Representation of the flood plain

An important feature of effective flood warning dissemination, particularly to the general public, is the use of flood inundation maps, ideally generated in real time from the hydrodynamic model rather than as offline look up tables. Offline, event-based hydrodynamic models typically use a linked 2D model of the floodplain to generate flood inundation maps. However, for operational purposes, the simulation time required for 2D flood inundation mapping can be prohibitive, so a 1D approach must be used. For the flood prone areas of the Muar catchment, the topography of the flood plain was represented by a Digital Terrain Model (DTM); a combination of Light Detection and Ranging (LiDAR) data at 10 metres spatial resolution, along with an Interferometric synthetic aperture radar (IFSAR) data set with a spatial resolution of 5 metres. A 1D flood inundation modelling approach was used, to generate flood compartments, at the nodes of which the model calculates water levels, then subtracts the ground elevation to obtain flood depths, and interpolates between them to achieve contoured flood inundation maps. An example of the operational flood map output from the Muar iFFRM is given in Figure 3.

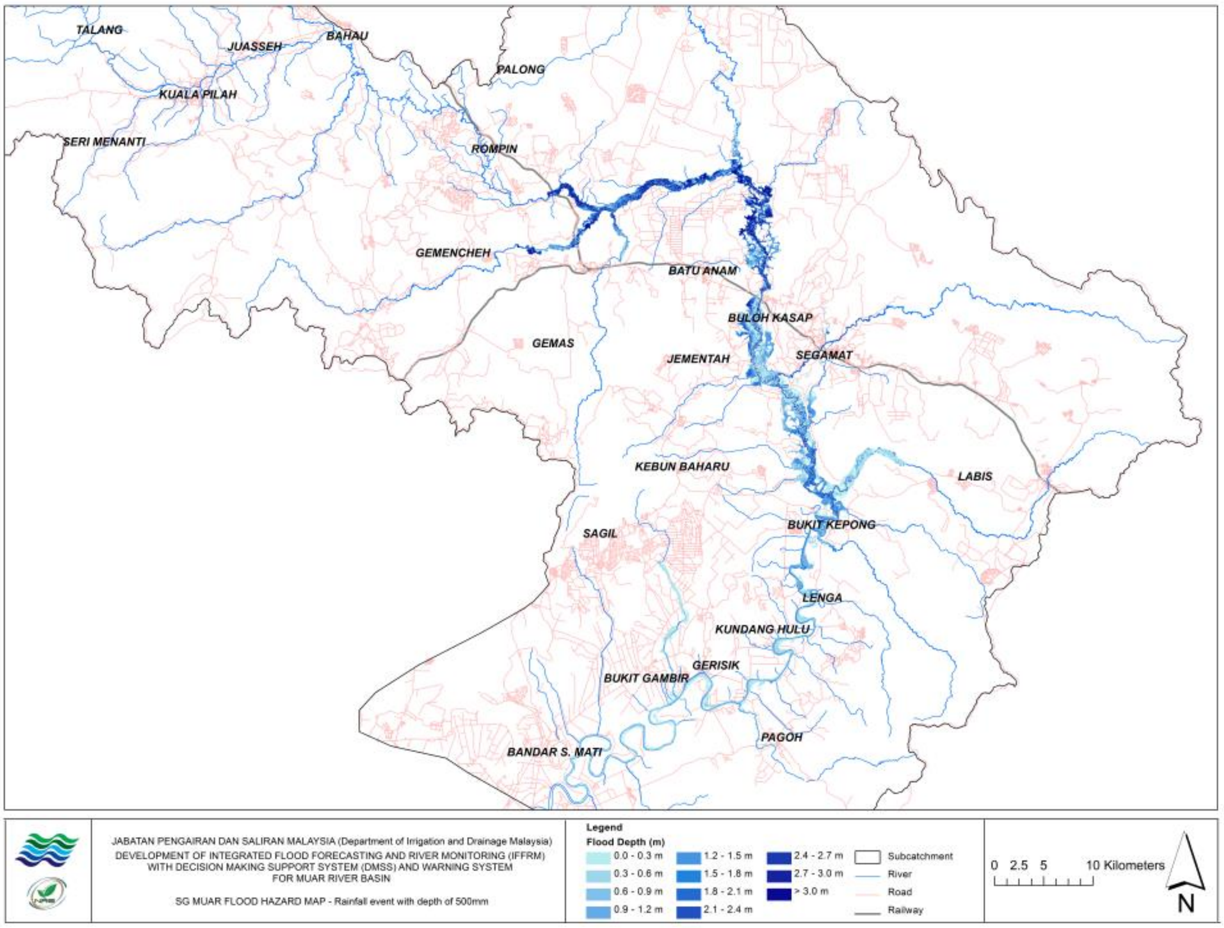

Figure 3. Example of the operational flood map output from the Muar iFFRM.

  / ISSN 1562-6865 (Online) - ISSN 1063-7710 (Print)

3.3 Observed data

As with any operational system, high quality input data of suitable coverage were required for calibration of the underlying models and for driving the operational models in real time. DID operates its own network of telemetered gauges, whose data are stored in the InfoBanjir telemetry database. InfoBanjir was first developed in 1999 as a centralised database system for the telemetry stations and was commissioned in the year 2000. The system receives real time rainfall and water level data from almost 200 telemetry stations throughout the country. Hydrological data from the stations are sent to the state server and further transmitted to InfoBanjir. Initially, InfoBanjir was developed to assist DID officers in monitoring current river water level and rainfall status remotely. More recently, a public portal for InfoBanjir has been developed, with a special focus on flood warning to the general public; a new initiative aims to update InfoBanjir, combining information from the two portals, improving the interface to ease public understanding, and to process the raw data more quickly.

DID operate 19 rain gauges (Figure 4) and 11 water level gauges (Figure 5) throughout the Muar catchment and DID plans to install further gauges to increase the network density. The data are made available through a live feed from InfoBanjir direct to the iFFRM server located at DID headquarters. In addition, rating equations for two of the water level data streams enable conversion to pseudo real time flow data for those locations. Telemetered water level (and flow) data were used in calibration of the underlying models, and were used operationally to raise warnings and for validation of the model results.

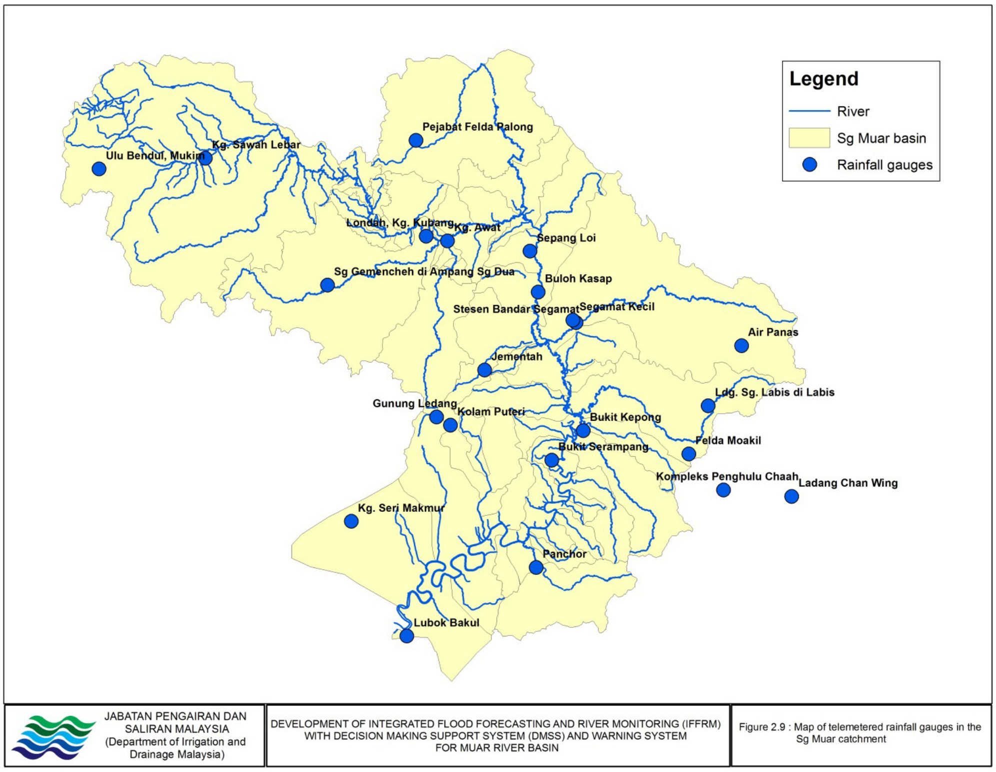

Figure 4. Map of the River Muar catchment, showing the location of the telemetered rain gauges.

3.4 Radar rainfall data

Spatial variability of rainfall is known to be high in peninsular Malaysia. Given the relatively low density of the telemetered rain gauge network in the Muar catchment, the use of radar rainfall observations, of a suitably high spatial and temporal resolution, was required. Through better understanding the localised nature of the rainfall events, a better representation of the runoff generation process could be achieved through rainfall-runoff modelling. Radar rainfall data were available in the GRIB file format. FloodWorks automatically finds and loads the radar rainfall data when they become available. Prioritisation can be given to either the gauged or the radar rainfall, as appropriate. The model will then use the prioritised rainfall to calculate the runoff. The iFFRM uses both telemetered rainfall data and radar rainfall images as inputs.

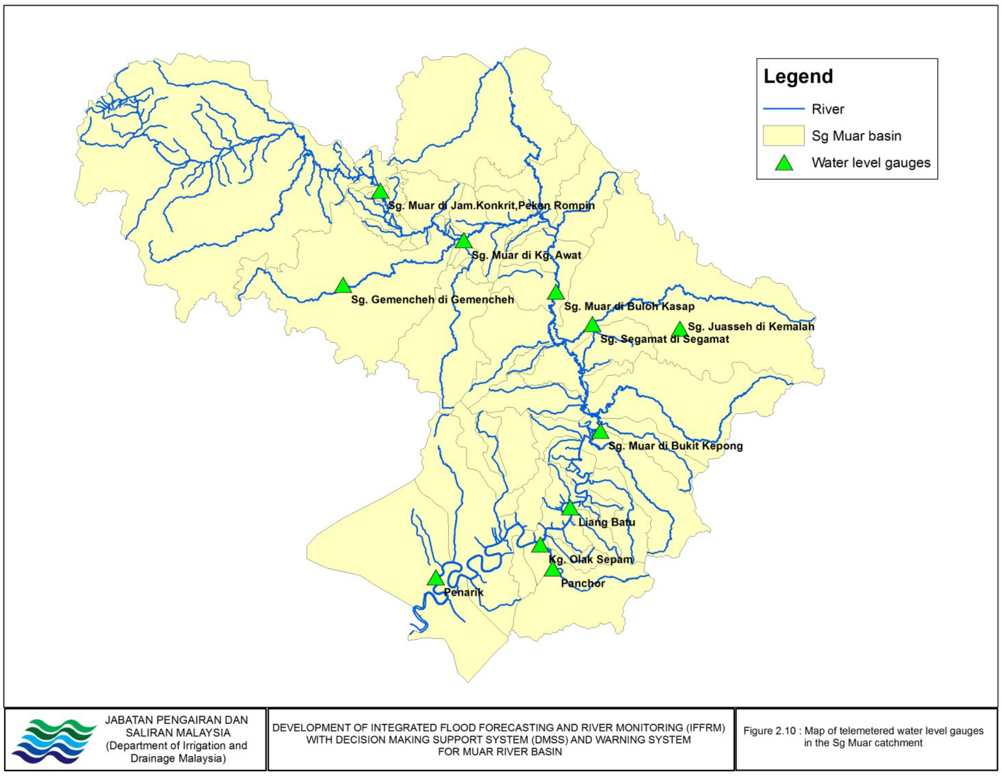

Figure 5. Map of the River Muar catchment, showing the location of the telemetered water level gauges.

3.5 Forecast data

In addition to observed rainfall data, rainfall forecasts were required to provide a Quantitative Precipitation Forecast (QPF) to drive the iFFRM into the forecast period. The Malaysian Meteorological Department (MMD) makes available rainfall forecasts from its Numerical Weather Prediction (NWP) model twice a day. Gridded ASCII files are made available twice per day at 00 hours and 12 hours. FloodWorks checks for new files and loads the new forecast data. The first three days of the precipitation forecast are used for the flood predictions.

The Malaysian Meteorological Department (MMD) operationally runs the Weather Research and Forecasting model (WRF) (NCAR et al., 2017). The WRF model was first released in 2004 with one of its main objectives being to advance the understanding and prediction of mesoscale weather systems including precipitation systems. The wide user community and dissemination of the WRF model has been successfully advanced since the release date. Currently the user group has over 30,000 registered users in 150 countries (NCAR et al., 2017). The MMD has extensively tested the forecast performance of the WRF model for precipitation forecasts in Malaysia, for more information the reader is referred to Ibadullah et al. (2013). Currently MMD are running WRF model version 2.2, a hydrostatic model at a horizontal resolution of 3km over a forecast time period of 5 days. The WRF model will be updated to a later version corresponding with the upgrade of the high performance computer (HPC). In preparation for this, extensive tests of the WRF model version and ensembles have been conducted (Subramaniam et al., 2010).

3.6 Flood warning dissemination and communication

The Office of U.S. Foreign Disaster Assistance (OFDA) experience in communication of forecasts, supports the need to strengthen the links between the early-warning systems (often managed by government institutions) and their intended beneficiaries at the local level, “thereby encouraging the development of truly end-to-end early warning systems that result in timely, well-understood warnings and effective response actions based on preparedness of the local communities. This link, often called the “last mile” of the system, has consistently been seen as both the most essential and the weakest aspect of early warning systems in developed and developing countries, alike” (USAID, 2013). The forecasting and warning strategy, including raising awareness of flood risk, and appropriate communication strategies, has a range of features that can be enhanced by effective system development.

Simulation results from iFFRM Muar are used to warn DID staff directly so that immediate action can be taken to provide an effective and proactive emergency response. A total of 137 Points of Interest have been configured to provide fast access to results for locations prone to flooding. Results are also passed to the project website, and to a dedicated smartphone application, enabling forecasted flooding to be disseminated more widely, to the public at large.

This system has been designed so that a parallel analytical modelling network can take over the forecasting role should the primary iFFRM system fail.

4 DISCUSSIONS

The paper presents the work undertaken to develop an end-to-end flood forecasting and warning system for the river Muar in Malaysia. Efforts have been made towards developing the system so that it is resilient to missing or poor quality input data, and a pragmatic approach has been taken towards system development for subcatchments with sparse data observation networks. Ongoing structural measures aimed at flood mitigation are captured through the use of a flexible modelling approach that can incorporate model updates to reflect real changes in the catchment. Continuous simulation maintains catchment states to ensure that the models at the core of the iFFRM, forms a realistic representation of catchment conditions. Updating applied algorithms at key locations around the catchment enable real time data to be used to correct model results and so improve model forecasts. In these ways, the iFFRM complements the structural measures being implemented by DID and ensures a sustainable solution.

5 CONCLUSION

This paper presents the work undertaken to develop an end-to-end flood forecasting and warning system for the river Muar in Malaysia. The iFFRM for Muar River has been developed to address the need of advance warning to population is Muar which has been repeatedly affected by significant flood events over the past decades. As part of flood forecasting system, an analytical/rule-based model has been developed that will utilize the combined rainfall information from InfoBanjir and MMD NWP data to replicate the historic and predicted hydrologic performance of the Sungai Muar river basin. The output has been shown to provide a realistic replication of the system against the detailed model. The system will provide an indication of potential flood levels based on the amount of flow generated by the rainfall falling on the catchment. In these ways, the iFFRM complements the structural measures being implemented by DID and ensures a sustainable solution.

REFERENCES

Abdullah, S.A. (2003). Fragmented Forest in Tropical Landscape - The Case of the State of Selangor, Malaysia. *J. Environ. Sci.*, 15(2), 267–270.

Abdullah, S.A. & Nakagoshi, N. (2008). Changes in Agricultural Landscape Pattern and Its Spatial Relationship with Forestland in the State of Selangor, Peninsular Malaysia. *Landsc. Urban Plan.*, 87(2), 147–155.

Amin, M.Z.M., Shaaban, A.J., Ercan, A., Ishida, K., Kavvas, M.L., Chen, Z.Q. & Jang, S. (2017). Future Climate Change Impact Assessment of Watershed Scale Hydrologic Processes in Peninsular Malaysia by a Regional Climate Model Coupled with a Physically-Based Hydrology Modelo. *Sci. Total Environ.*, 575, 12–22.

Asmara, T.A.T. & Ludin, A.N.M. (2014). Mapping Perception of Community Preparedness towards Flood in Muar River, Johor Malaysia, *IOP Conf. Series: Earth and Environmental Science, 18*. Presented at the 8th International Symposium of the Digital Earth.

Bloschl, G. (2006). *Encyclopedia of Hydrological Sciences*; *133 Rainfall-Runoff Modeling of Ungauged Catchments*. John Wiley and Sons, Ltd.

Booij, M.J. (2005). Impact of Climate Change on River Flooding Assessed with Different Spatial Model Resolutions. *J. Hydrol.*, 303(1), 176–198.

Centre for Research on the Epidemiology of Disasters (CRED). (2014). Data from EM-DAT, the OFDA (US Office of Foreign Disaster Assistance)/CRED International Disaster Database, www.em-dat.net, CRED, Université Catholique de Louvain, Brussels, Belgium.

Hussaini, H.A. (2007). Flood and Drought Management in Malaysia. Department of Irrigation and Drainage, keynote speech by the Chief Director. 21 June 2007.

Department of Irrigation and Drainage (DID). (2009). *DID Manual. Volume 1: Flood Management.*

Department of Irrigation and Drainage (DID). (2009b). *DID Manual. Volume 4: Hydrology and Water Resources*.

Department of Irrigation and Drainage (DID). (2011). http://www.water.gov.my/images/pdf/managing_flood.pdf

Erickson, D.L. (1995). Rural Land Use and Land Cover Change Implications for Local Planning in the River Raisin Watershed. *Land Use Policy,* 12(3), 223–236.

Hong, D. & Hong, K.A. (2016). Drought Identification, Monitoring and Forecasting for Selangor River Basin. *Int. J. U- E- Serv. Sci. Technol.*, 9(3), 53–66.

Hundecha, Y. & Bardossy, A. (2004). Modelling of the Effect of Land Use Changes on the Runoff Generation of a River Basin Through Parameter Regionalization of a Watershed Model. *J. Hydrol.*, 292(1), 281–295.

Ibadullah, W.M.W., Sammathuria, M.K. & Kwok, L.L. (2013). Comparison of Performance of NWP Models WRFV2.2 and WRFV3.4 during a Heavy Rainfall Episode in Northeast Monsoon Season 2011 (No. 2/2013). Malaysian Meteorological Department (MMD).

Innovzye (2014). InfoWorks RS Online Help System.

James, B., Rouhban, B., Papa, H. & Tovmasyan, K. (2007). *Disaster Preparedness and Mitigation* (No. SC/BES/NDR/2007/H/1). United Nations Educational, Scientific and Cultural Organization, Paris, France.

Kundzewicz, Z.W. (2013). *Late Lessons from Early Warnings: Science, Precaution, Innovation*. Published by European Environment Agency (EEA), Report No 1/2013, Chapter C15.

Kundzewicz, Z. & Kaczmarek, Z. (2009). Coping with Hydrological Extremes. *Water Int*., 25(1), 66–75.

Mishra, A.K. & Singh, V.P. (2011). Drought Modelling - A Review. *J. Hydrol.,* 403(1), 157–175.

Moore, R.J. (1985). The Probability-Distributed Principle and Runoff Production at Point and Basin Scales. *Hydrological Sciences Journal*, 30(2), 273-297.

NCAR, NCEP, FSL, AFWA, Naval Research Laboratory, University of Oklahoma & FAA. (2017). *The Weather Research and Forecasting Model* [WWW Document]. WRF Model. http://www.wrf-model.org/index.php (Accessed 30 January 2017).

Paiva, R.C.D., Collischonn, W. & Buarque, D.C. (2013). Validation of a Full Hydrodynamic Model for Large-Scale Hydrologic Modelling in the Amazon. *Hydrol. Process*., 27(3), 333–346.

Pappenberger, F., Beven, K.J., Horritt, M. & Blazova, S. (2005). Uncertainty in the Calibration of Effective Roughness Parameters in HEC-RAS using Inundation and Downstream Level Observations. *J. Hydrol*., 302(1), 46–69.

Siriwardena, L., Finlayson, B.L. & McMahon, T.A. (2006). The Impact of Land Use Change on Catchment Hydrology in Large Catchments: The Comet River, Central Queensland, Australia. *J. Hydrol*., 326(1), 199–214.

Subramaniam, K., Kwok, L.L. & Hassan, W.A.W. (2010). Performance of Ensemble Prediction for Malaysian Meteorological Department Numerical Weather Prediction Model (No. 13/2010). MMD.

Todini, E. (2007). Hydrological Catchment Modelling: Past, Present and Future. *Hydrol. Earth Syst. Sci*., 11(1), 468–482.

UN/ISDR (2006). *Global Survey of Early Warning Systems. An assessment of Capacities, Gaps and Opportunities towards Building a Comprehensive Global Early Warning System for All Natural Hazards*. A report prepared at the request of the Secretary-General of the United Nations, by the International Strategy for Disaster Reduction (ISDR) secretariat.

USAID (2013). USAID/DCHA/OFDA Annual Program Statement (APS) No. OFDA-FY-13-000003 APS for Innovative Partnerships for Enhancing End to End (E2E) Early Warning Systems (EWS) for Hydrometeorological Hazards in South Asia. U.S. Agency for International Development.

Proceedings of the 37th IAHR World Congress
August 13 – 18, 2017, Kuala Lumpur, Malaysia

EFFECT OF LINED CYLINDERS BEHIND EMBANKMENT ON THE ENERGY REDUCTION OF OVERFLOWING WATER

YOSHIYA IGARASHI[(1)], NORIO TANAKA[(2)] & TAKEHITO ZAHA[(3)]

[(1)] Graduate School of Science and Engineering, Saitama University, Saitama, Japan,
[(2)] International Institute for Resilient Society, Saitama University, Saitama, Japan,
tanaka01@mail.saitama-u.ac.jp
[(3)] Department of Civil and Environmental Engineering, Faculty of Engineering, Saitama University, Saitama, Japan,

ABSTRACT

The 2011 Great East Japan tsunami caused catastrophic damage to people and buildings in the Tohoku and Kanto districts of Japan and revealed the limit of using merely sea embankment as defense. After the tsunami, the importance of multiple defense systems for mitigating tsunamis has been recognized. This study was conducted to clarify the energy reduction of a tsunami due to a compound defense system by combination of a sea embankment and lined vertical piles by which tsunami energy of overflowing water is reduced through hydraulic jump and/or resistance of piles. This study investigates the relationship between flow structure and energy reduction with changing pile height and spacing. Even in the case of single embankment, energy reduction rates were approximately 38-81% because the overflowing water from embankment collided with the bed. In compound system, the flow structure after overtopping the embankment can be classified into ten types. The change of flow structure patterns was classified into two by pile spacing. The energy reduction rate was large with lined pile when the pile spacing was small. In some cases, due to resistance offered by lined piles, the standing wave was formed at immediately downstream of piles which resulted in decrease of energy loss. The energy reduction rate gradually decreased when the pile sank in water. However, the energy can be expected to reduce if the pile height is large and/or the pile spacing is small because of the large resistance of piles. Eddies are generated just behind the piles when the pile spacing is small and the water depth at the pile is larger than the pile height. This is due to the large difference of flow velocity inside the piles and over the piles. Therefore, the energy loss can also be expected in this case.

Keywords: Energy reduction; hydraulic jump; multiple defense; overflow from embankment.

1 INTRODUCTION

The 2011 Great East Japan tsunami caused catastrophic damage to people and buildings in the Tohoku and Kanto districts of Japan and revealed the limit of using merely sea embankment as defense. After the tsunami, the Ministry of Land, Infrastructure, Transport and Tourism, Japan (MLIT) classified tsunamis as level 1 and level 2. The return period of the magnitude for level 1 tsunamis is defined around 100 years interval, while for level 2 tsunamis is within hundreds to a thousand years. Thus, a compound defense system is proposed for level 2 tsunamis to mitigate damage. However, the optimum compound defense system for mitigating level 2 tsunami is still unknown. Recently, the number of studies of compound defense system using sea embankment with a coastal forest (Tanaka et al., 2014) and a second embankment (Tanaka & Igarashi, 2016) is increasing. Second embankment has the risk of being washed out by a tsunami if it is made of soil. Even in that case, the energy reduction for a tsunami can still be expected when piles set inside the second embankment appeared from the second embankment.

If the spacing of pile is small enough to affect upstream of piles, hydraulic jump can be generated. It is widely known that the hydraulic jump can dissipate tsunami energy (Mahmoud et al., 2014; Moussa et al., 2016). Besides, it is also known that the ski-jump type flow can dissipate energy (Wu et al., 2016). If a free nap flow like a ski-jump is generated around the pile, dissipation of tsunami energy can be expected due to collision with the downstream bed of piles although no hydraulic jump is generated.

Therefore, a flume study was conducted to clarify the relationship between the energy reduction rate and the flow structure when the tsunami passes through a compound defense system i.e., a combination of embankment and piles (lined cylinders) towards the land side.

2 MATERIALS AND METHODS

2.1 Experimental apparatus and procedures

Figure 1 shows the experimental setup. The compound system is proposed for reducing tsunami energy of overflowing water by hydraulic jump and/or resistance of pile. This study changed the pile height and spacing, and the relationship between the flow structure and energy reduction was investigated. As a first step, steady flow condition was set in a flume with the energy reduction ratio for various compound defense models on a physical scale of 1/100 as shown in Figure1. For hydraulic conditions, Froude similarity was used. The wooden embankment model of height 14.5 cm was set on the flume bottom. For the pile models, wooden circular cylinder of diameter 0.4 cm was used and the pile models were set in a single row at regular intervals along the embankment.

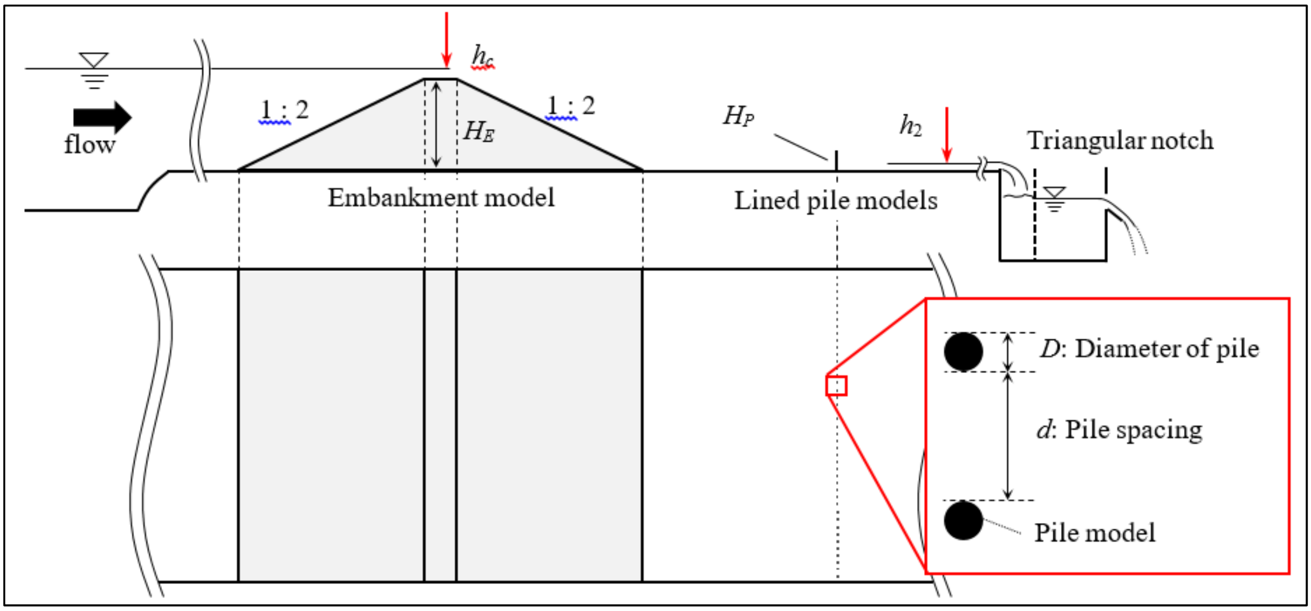

Figure 1. Experimental setup.

2.2 Parameters used in this study

Non-dimensional pile height (H_P^*) was defined as $H_P^* = H_P/H_E$; where H_P and H_E are the pile height and embankment height, respectively. H_P^* were set as 0.07, 0.14, and 0.28. d^* was defined as the non-dimensional pile spacing defined as $d^* = d/D$, where d and D are the spacing in between the piles and the diameter of pile, respectively. d^* were set as 0.75, 1.5, and 2.25. For comparing results, non-dimensional overflow water depth (h_c^*) was defined as $h_c^* = h_c / H_E$ where h_c is the critical depth. In all the cases, the flow structure was investigated in relation with h_c^* in the range of approximately 0.08 to 0.37. Moreover, only embankment case was tested for comparison with the compound system.

2.3 Methods for evaluating energy reduction of tsunami

The overflow water depth from embankment (h_c) and water depth behind the pile (h_2) was measured in all cases. In some cases, fluctuations in the water surface were observed behind the pile with time and space and hence maximum and minimum h_2 were measured. For estimating the tsunami mitigation effect by the pile, this study defined an energy reduction rate ΔE [%] as $\Delta E = (E_1 - E_2)/E_1$; where, E_1 and E_2 were the energies at which h_c and h_2 were measured respectively and were calculated from Bernoulli's theorem. For deciding the location of h_c on the embankment where Froude number equals to 1, the flow discharge was measured by using triangular notch.

3 RESULTS

3.1 Classification of the flow structure

In single embankment case, energy reduction rates were approximately 38-81% because the overflowing water from embankment collided with the bed. In compound system, the flow structure after overtopping the embankment can be classified into ten types according to d^*.

When d^* is small (0.75), the flow pattern can be classified into six types for h_c^* = 0.08-0.36 as shown in Figure 2. With the increase in non-dimensional over flow water depth (h_c^*), the type of flow structure changed from Type 1, 2, 3, 4, 5 to 6. When h_c^* is small (0.08), the flow can have the supercritical condition between embankment and piles while it becomes subcritical condition when the location of piles corresponds to Type 1. When h_c^* becomes even larger, a hydraulic jump occurred in front of piles (Type 2). By further increasing h_c^*, the retained water was washed away and Type 3 was generated. In this type, the flow jumped on the pile like a ski-jump, a free nap flow collided with the downstream bed of piles, and a hydraulic jump occurred in succession.

  / ISSN 1562-6865 (Online) - ISSN 1063-7710 (Print)

With further increasing h_c^*, the hydraulic jump downstream of piles was not generated (Type 4). With more increase in h_c^*, the water depth at the pile becomes larger than the pile height, which resulted in eddy formation instead of a free nap flow just behind the pile. This is because of a large difference of flow velocity inside the piles and over the piles (Type 5). By further increasing h_c^* , eddy is not generated and the effect of resistance of pile becomes smaller (Type 6).

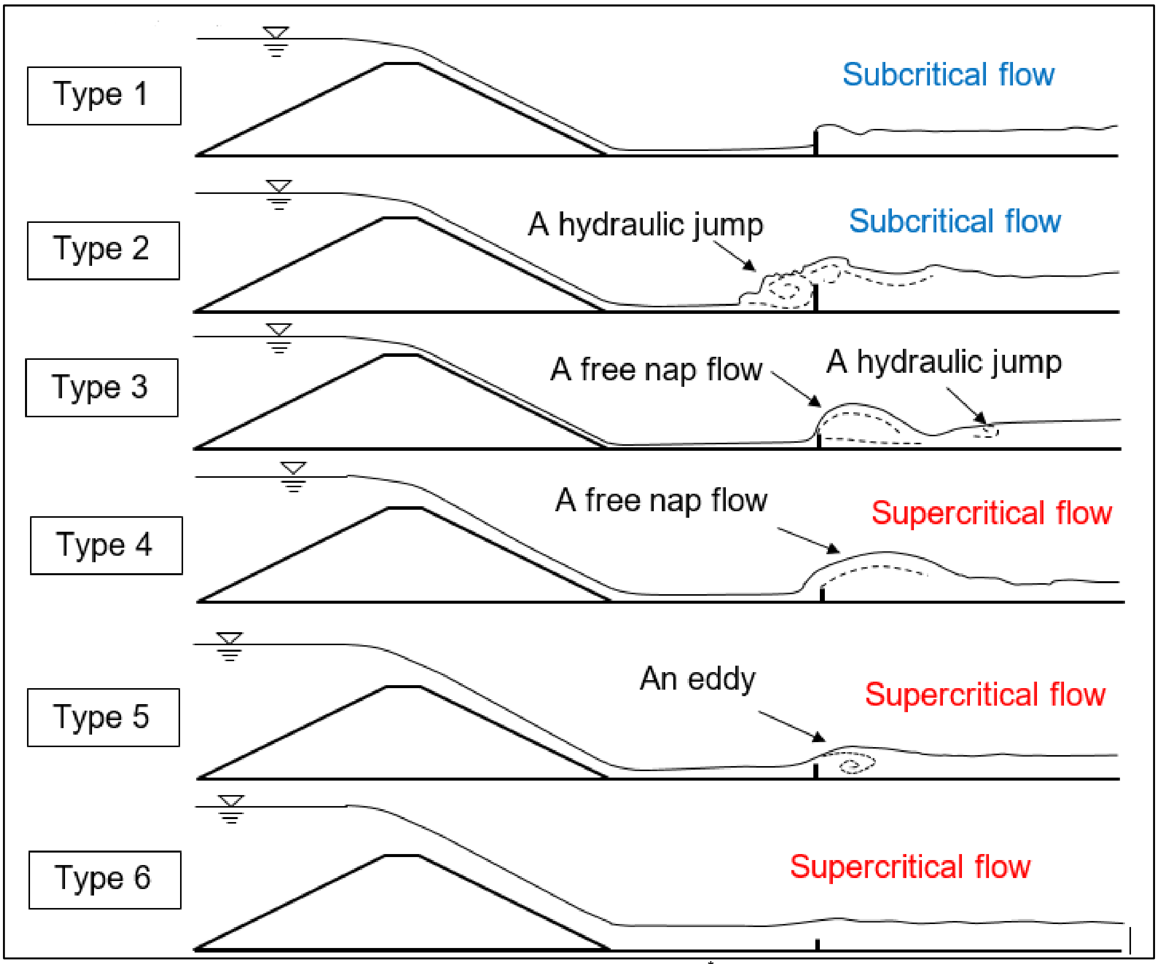

Figure 2. The flow structure (d^* = 0.75).

When d^* is large (1.5, 2.25), four flow pattern can be observed for h_c^*= 0.08 - 0.37 as shown in Figure 3. With the increase in non-dimensional over flow water depth (h_c^*), the type of flow structure changed from Type A to B to C, to D. When h_c^* is small (0.08), a hydraulic jump occurred behind pile models (Type A). With further increasing h_c^*, the hydraulic jump is not generated behind piles. In this case, when the flow passes through the piles in supercritical flow, oblique standing wave (Figure 3, Type B and D) is generated just behind the piles. Therefore, the water depth and water surface fluctuation becomes large. By further increasing h_c^*, the standing wave becomes like a free nap flow (Type C). Type C is similar to Type 4. By further increasing h_c^*, the water depth at the pile becomes larger than the pile height, and in this case just behind piles, neither the free nap flow is generated nor the eddy formation is observed because the difference of flow velocity inside the piles and over the piles is small (Type D).

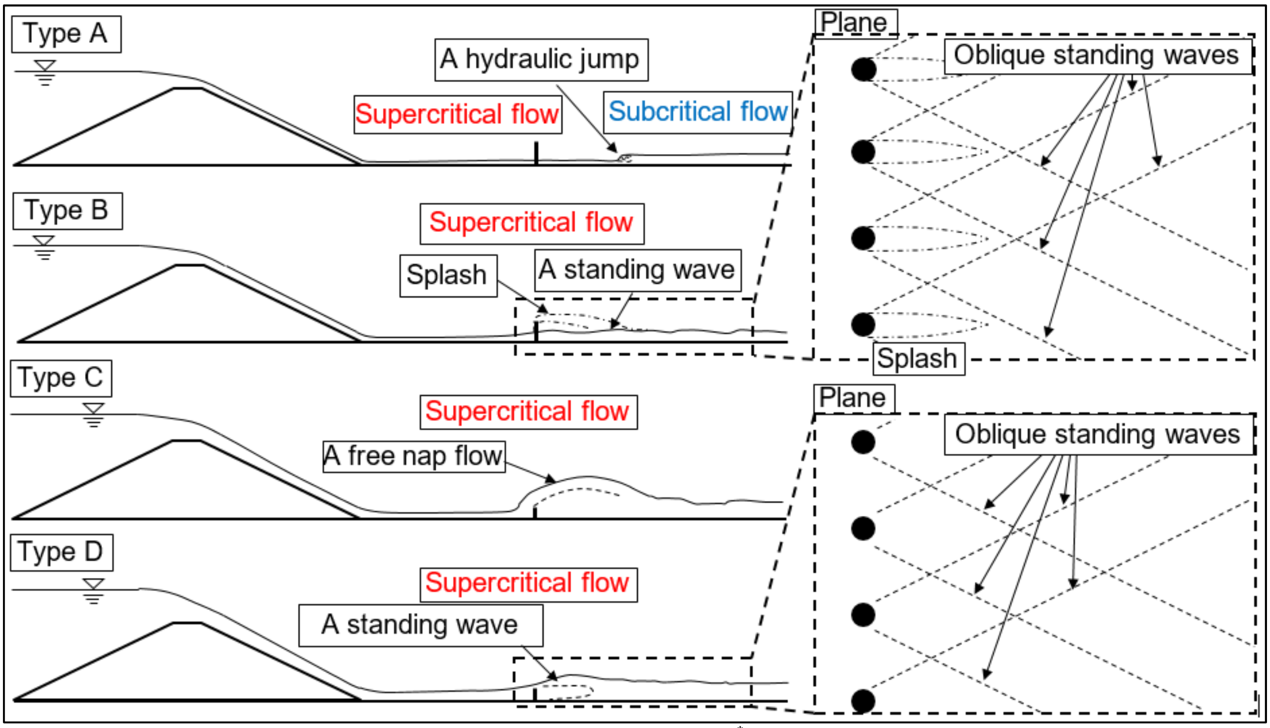

Figure 3. The flow structure (d^* = 1.5, 2.25).

3.2 Relationship between the flow structure and energy reduction rate

The figure of flow structure types which has h_c^* on vertical axis and H_P^* on the cross axle was plotted with a different color in each flow structure as shown in Fig. 4(a), (b) and (c) which are in d^* = 0.75, 1.5, and 2.25, respectively. The type of flow structure was judged from the animation of experiment. In the figure, the boundary lines are shown/drawn.

Figures 4(a), (b) and (c) show that, if h_c^* is larger than 0.2 and H_P^* is 0.07 or h_c^* is larger than 0.3 and H_P^* is 0.14, the water depth at the pile is higher than pile height even if d^* is 0.75, 1.5 or 2.25. Therefore, the type of flow structure becomes Type 5, 6 or D. It is shown that, the relationship between pile height and the water depth at the pile depend on the relationship between h_c^* and H_P^* but not d^*. Fig. 4(a) suggests that the pile height is important whether hydraulic jump occurs in front of lined pile. When the pile height is small (H_P^* = 0.75, 1.5), a free nap flow on the lined pile like a ski-jump is easy to occur although hydraulic jump is not generated in front of lined pile.

The figures of relationship between the non-dimensional overflow water depth (h_c^*) and energy reduction rate (ΔE) are shown in Figure 5(a), (b) and (c) where d^* = 0.75, 1.5, and 2.25, respectively. In some cases, the water level immediately behind the lined piles varied which resulted in wide range of energy reduction rate although non-dimensional overflow water depth was constant. Therefore, crossbars as a range of energy reduction rate were drawn in the fgures.

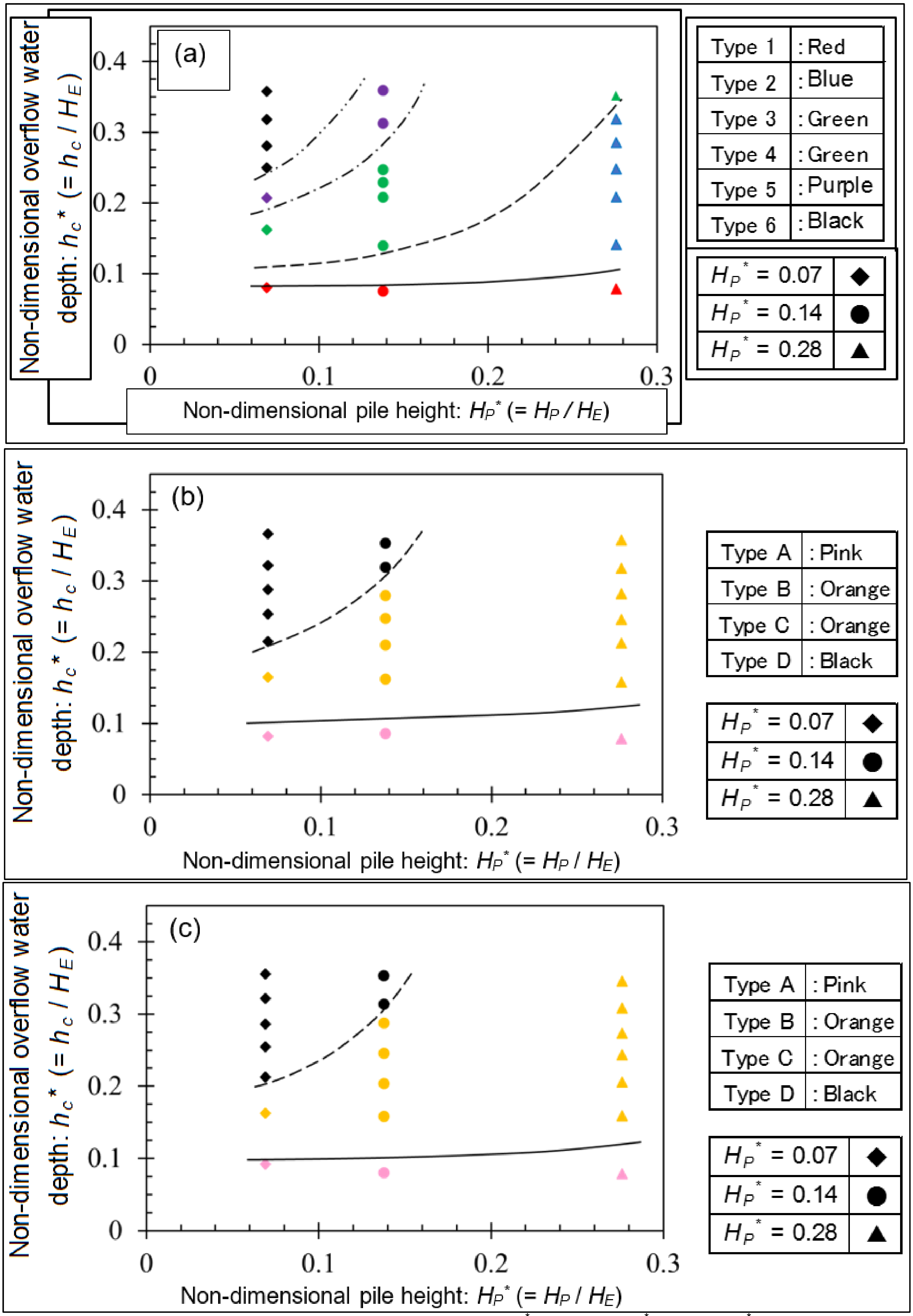

Figure 4. The classifications of flow structure ((a): d^* = 0.75, (b): d^* = 1.5, (c) d^* = 2.25).

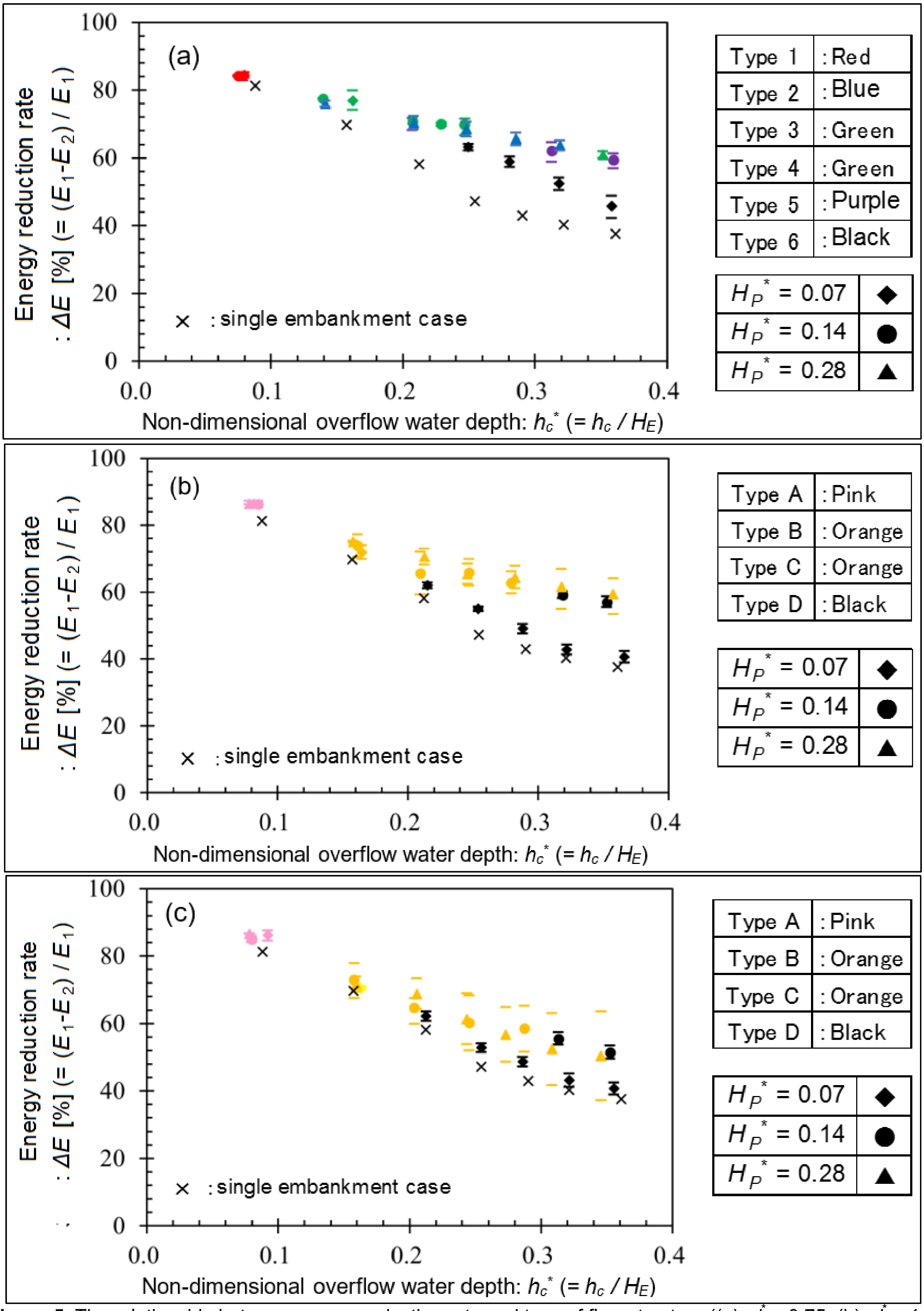

Figure 5. The relationship between energy reduction rate and type of flow structure ((a): d^* = 0.75, (b): d^* = 1.5, (c) d^* = 2.25). (All the symbols correspond to the symbols for classifying the flow type in Fig.4.)

When h_c^* is less than 0.15, single embankment case can dissipate tsunami energy and ΔE is large (70-81%) because the overflowing water from embankment collided with the bed. Therefore, the difference of ΔE between single embankment case and compound system is very small. Figures 4(a) and 5(a) show that, when d^* is 0.75 and h_c^* is less than 0.21, energy reduction rate was similar regardless of the type of flow structure in compound system. When h_c^* is larger than 0.21 and H_P^* is equal to 0.14 and 0.28, energy reduction rate was higher, up to 22% in maximum than that of single embankment case. However, when H_P^* is equal to 0.07 and type of flow structure becomes Type 6, energy reduction rate gradually decreased and almost equaled to that of single embankment case. The difference of energy reduction rate between the compound system in Type 6 and single embankment is only 8% at the minimum (Figure 5(a)).

Figures 4(b) and 5(b) show that, when d^* is 1.5 and h_c^* is less than 0.16, energy reduction rate was almost equal regardless of the type of flow structure in compound system. When h_c^* is larger than 0.16 and H_P^* is equal to 0.14 and 0.28, energy reduction rate was higher, up to 18% than that of single embankment case. When the type of flow structure becomes Type B, it formed a diamond shape in flow due to transverse crossing of oblique standing wave as shown in Figure 7. This diamond shaped flow varied the water level behind the piles, due to which the range of energy reduction rate increased to 12% and 26% at the most against d^*=1.5 and 2.25, respectively (Figures 5(b) and 5(c)). When the type of flow structure becomes Type D, the range of energy reduction rate became less i.e around 5%.

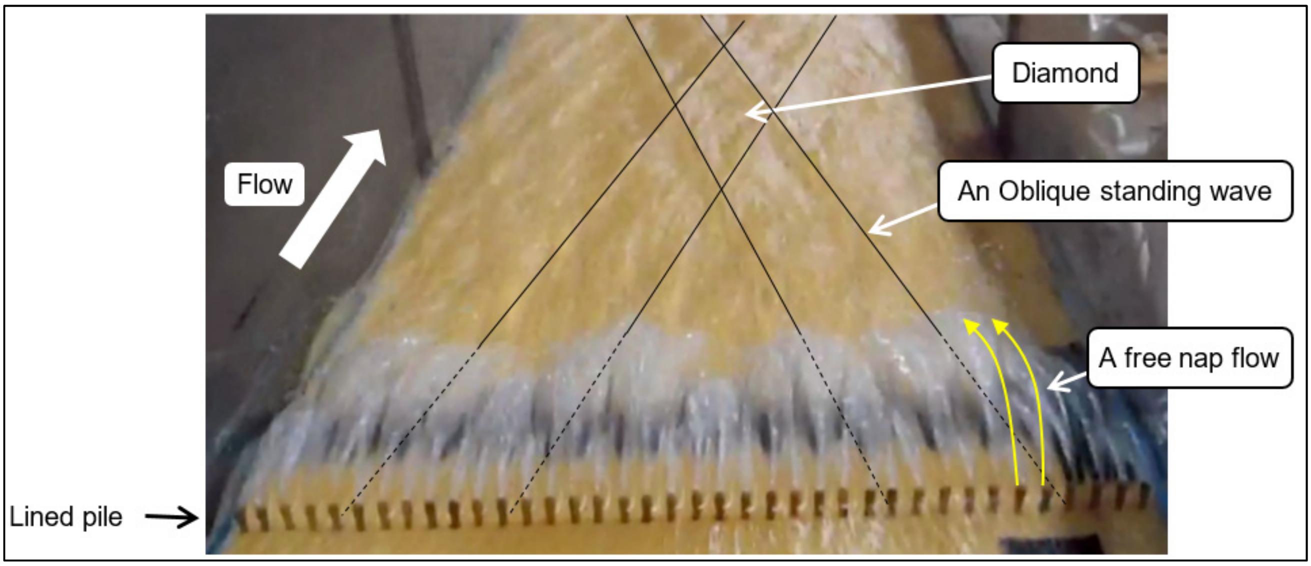

Figure 6. The image of a free nap flow and standing wave behind the lined pile.

When H_P^* is small (H_P^* = 0.07) and type of flow structure becomes Type D, energy reduction rate gradually decreases more than that of when H_P^* is equal to 0.14 or 0.28. When h_c^* is larger than 0.32, energy reduction rate is similar to that of single embankment case. However, energy reduction rate was higher, up to 19% than that of single embankment case although the flow structure is Type D. The reason seems to be the effect of drag force of piles. When H_P^* is small (H_P^* = 0.07) and h_c^* is large (h_c^* = 0.32), energy reduction rate is trivial because H_P is insignificant as compared to the water depth at the pile and the effect on flow of the drag force of pile is small. On the other hand, when H_P^* is large (H_P^* = 0.14) and h_c^* is also large (h_c^* = 0.32), energy reduction rate is quite large because H_P is similar to the water depth at the pile.

When Figure 4(b) is compared with Figure 4(c), the change of flow structure is similar. When d^* becomes larger, the average of energy reduction rate is slightly smaller as a whole and the range of energy reduction rate is larger (Figures 5(b) and 5(c)). When d^* is 2.25 and is H_P^* 0.28, the maximum range of energy reduction rate is 26%.

4 DISCUSSION

4.1 Energy dissipation

By comparing the compound system and single embankment system, increase of ΔE is affected only by the drag of lined pile in Type 6, B and D and hydraulic jump around the lined pile in Type 1, 2, 3 and A. Type 3, 4 and C affect the increase of ΔE because drag of lined pile and a free nap flow collide with the downstream bed of piles. In Type 5, the increase of ΔE is affected by drag of lined pile and an eddy just behind lined pile.

Fathi-Moghadam et al. (2011) conducted experiments on forced hydraulic jump in stilling basin and showed that the sill height and position affects the sequent depth ratio and shortening of the basin length. It also showed that the higher the height of the end sill, the more energy can be reduced at shorter distances. These results are closely related to Type 2 in which jumping occurs. In Type 2, the higher the piles height, the hydraulic jump can occur more easily, and also increase the energy dissipation rate.

In Type B, the area where the drag of pile has an effect on flow is the product of the water depth and the diameter of pile because the pile height is larger than the water depth at the pile. Therefore, the difference of ΔE between compound system and single embankment system becomes larger, up to 22% at the most with increase in h_c^*. On the other hand, in Type 6 and D, the area where the drag of pile has an effect on flow is the product of the pile height and diameter because the pile height is smaller than the water depth here. Therefore, the difference of ΔE between compound system and single embankment system becomes smaller to 1% in minimum with increase in h_c^*, because the effect of drag of pile is constant and the energy of flow increases.

In Type 1, 2, 3, and A, the maximum difference of ΔE between compound system and single embankment system is 23%, due to the occurrence of the hydraulic jump around the lined pile. Tanaka & Igarashi (2016) investigated the energy dissipation about double embankment system and suggested that the energy reduction rate in double embankment system is larger, up to around 20% in maximum than in single embankment system.

In Type 3, 4, and C, the maximum difference of ΔE between compound system and single embankment system is 22% because a free nap flow like a ski-jump collides with the downstream bed of piles. In Type 5, the maximum difference of ΔE between compound system and single embankment system is 22%, due to occurrence of an eddy just behind lined pile. Wu et al. (2016) showed that the energy reduction rate of flow due to ski-jump and a lot of steps is large in different structures.

4.2 Water surface fluctuation behind the lined pile

In Type 1, 2 and 3, water surface fluctuation behind the pile was small. On the other hand, in Type B, water surface fluctuation behind the pile was large because of transverse crossing of oblique standing wave which formed a diamond shape at top of flow. The range of energy reduction rate due to this difference of water level is bigger when the spacing of pile is greater. Therefore, if large spacing of pile is needed, the number of pile rows should be increased.

4.3 Control of scour length and depth behind an embankment

Hamidifar et al. (2017) investigated the influence of bed sill as a countermeasure against scour. The study showed that the maximum scour depth in front of and behind the sill was greater and smaller, respectively, than that without sill. Although our study didn't investigate the scour depth, the previous study indicates that the scour depth may also decrease behind the piles in our model. Furthermore, since the flow passes into the piles to the downstream side moderately, there is a possibility that the scour depth in front of the piles also decreases. From the point of decreasing the scour depth behind embankment, the piles may be effective. However, more study is needed on this point by conducting experiments on the mobile bed condition.

5 CONCLUSIONS

The following conclusions were derived from the flume study.

(1) Compound system dissipated 1-23% greater energy than single embankment system. The difference of the energy reduction between compound system and single embankment system was low for small overflow depths. In compound system, the flow structure after overtopping the embankment can be classified into ten types (Type 1, 2, 3, 4, 5, 6, A, B, C and D). In type 1, 2, 3, 4, 5 and A, the effect of tsunami mitigation is large.

(2) Although the pile sank in the water (Type D or 6) in compound embankment case, the energy reduction rate was still higher, (up to 19% in maximum against the same level of pile and water depth) than that of single embankment case, due to the drag force of piles. However, as the water depth at the pile increases, energy reduction rate gradually decreases and nears to that of a single embankment.

(3) In a Type B flow, transverse crossing of oblique standing wave formed a diamond shape at top of flow which resulted in variation in water level and consequently reduction of energy loss. The greater the spacing of piles, greater the range of an energy reduction rate. However, the range of an energy reduction rate can be reduced by increasing the numbers of rows of lined piles.

ACKNOWLEDGEMENTS

This study was partly funded by a JSPS Grant-in-Aid for Scientific Research (No. 15H02987) and Grant-in-Aid for Special Purpose (15H06923-01).

REFERENCES

Ahmed, Hossam Mohamed Ali, El Gendy, M.M., Mirdan, A.M.H., Ali, A.A.M. & Abdel Haleem, F.S.F., (2014). Effect of Corrugated Beds on Characteristics of Submerged Hydraulic Jump. *Ain Shams Engineering Journal,* 5(4), 1033-1042.

Fathi-Moghadam, M., Haghighipour, S., Lashkar-Ara, B. & Aghtouman, P. (2011). Reduction of Stilling Basin Length with Tall End Sill. *Journal of Hydrodynamics,* 23(4), 498-502.

Hamidifar, H., Nasrabadi, M. & Omid, M. H. (2017). Using a Bed Sill as a Scour Countermeasure Downstream of an Apron. *Ain Shams Engineering Journal*. (In Press)

Moussa, Y. A., Abde-lAzim, M. A., & Saleh, Y. K. (2016). Performance of Sills Over Aprons Under the Effect of Submerged Hydraulic Jump, (case study: Naga Hammadi Barrage). *Ain Shams Engineering Journal*.

Tanaka, N., Yasuda, S., Iimura, K., Yagisawa, J., (2014). Comparison of the Effects of Coastal Forest and Those of Sea Embankment on Reducing the Washout Region of Houses in the Tsunami caused by the Great East Japan Earthquake, *Journal of Hydro-environment Research*, 8(3), 270–280.

Tanaka, N. & Igarashi, Y., (2016). Multiple defense for tsunami inundation by two embankment system and prevention of oscillation by trees on embankment, *Proc. of 20th IAHR-APD,* Colombo, Sri Lanka

Wu, J. H., Qian, S. T., & Fei, M. A. (2016). A New Design of Ski-jump-step Spillway. *Journal of Hydrodynamics*, 28(5), 914-917.

Proceedings of the 37th IAHR World Congress
August 13 – 18, 2017, Kuala Lumpur, Malaysia

DATA ASSIMILATION IN A HYDRODYNAMIC-HYDROLOGICAL MODELLING SYSTEM

PETER GODIKSEN[1], MARC-ETIENNE RIDLER[2] & HENRIK MADSEN[3]

[1,2,3] DHI, Agern Allé 5, DK-2970 Hørsholm, Denmark,
png@dhigroup.com

ABSTRACT

Hydrodynamic-hydrological modelling is affected by various sources of uncertainty, which degrades its performance and predictive capabilities for use in different applications such as water resources management, flood forecasting, real time control and etc. Combining observations with model predictions using data assimilation can improve model prediction skills. State-of-the-art ensemble based Kalman filter algorithms are implemented for hydrodynamic-hydrological data assimilation in the MIKE HYDRO River modelling system. The focus of the paper is on data assimilation in the hydrological model, which is evaluated using a case study from Murrumbidgee River in New South Wales, Australia. It is demonstrated that the hydrological model states are updated consistently and the state updates benefit from the hydrological memory of the catchment for increasing forecast lead time. The rainfall-runoff is routed through a hydrodynamic river model and the combined improvement of rainfall-runoff estimates from upstream catchments leads to an improved estimate of the river discharge further downstream, and thus the predictive capabilities of the whole modelling system are increased.

Keywords: Data assimilation; ensemble transform Kalman filter; hydrological modelling; water management.

1 INTRODUCTION

Hydrodynamic-hydrological modelling systems are used in many different fields such as flood forecasting, water resources management, design and operation of water infrastructure and etc. In real-time systems, it is used for estimating the current state of a river basin as well as predicting future states, often integrating meteorological forecasts from numerical weather prediction models. The forecast capabilities and detailed information that can be obtained for a river basin makes the hydrodynamic-hydrological modelling system valuable. However, the usefulness of the modelling system largely depends on how accurate it estimates the quantities of interest to the end-user, and its value is therefore increased by improving its accuracy.

Model performance is degraded by various sources of uncertainty related to model forcing, model structure and model parameter estimation, and as a consequence the model estimates will differ from observations. Data assimilation techniques can be applied to improve the accuracy of the state estimate by combining information from observations and model predictions. Updating the model with observations does not only increase the model accuracy at the current time but also in the forecast period because of improved initial conditions at time of forecast.

Hydrodynamic model states such as discharge and water level are directly observable, whereas the hydrological states such as surface storage, root-zone storage, ground water storage, and etc. are difficult to measure. It is therefore challenging to perform data assimilation in a hydrological model as the information about the model state is scarce, and the model state itself might not resemble a measurable state as is the case for lumped, conceptual rainfall-runoff models.

It is beneficial to update the hydrological model and not only the hydrodynamic model because the effect of updating hydrological model states is more persistent in time due to hydrological memory and hence can increase forecast lead time. In the hydrodynamic model the effect of the model state update is quickly transferred downstream and has therefore a more limited effect on future states.

This paper describes the improved data assimilation capabilities that have been developed in the MIKE HYDRO River modelling system (successor of the MIKE 11 River modelling system) with support for both data assimilation in the NAM rainfall-runoff model and the 1D hydrodynamic models. The data assimilation is demonstrated on a case study from the Murrumbidgee River in New South Wales, Australia. Discharge observations are available for several catchments for assimilation in the NAM hydrological models. In addition, discharge data in the river are used for assimilation in the hydrodynamic model. Hydrological state updating at catchment level and its added benefit for forecasting in a hydrological-hydrodynamic modelling system are demonstrated.

2 METHODOLOGY

Data assimilation capabilities have been developed for the MIKE HYDRO River modelling system and supports data assimilation of both hydrodynamic and hydrological model states. It is based on the DHI data assimilation framework (Ridler et al., 2014).

2.1 DHI Data assimilation framework

The DHI Data assimilation framework supports different ensemble based Kalman filters, and it includes a range of functionalities for handling different types of observations, describing model and measurement of uncertainties, use of localization and other statistical regularization techniques. In addition, the framework includes procedures for joint state updating and parameter estimation, and bias-aware filtering. A general overview of the framework is shown in Figure 1.

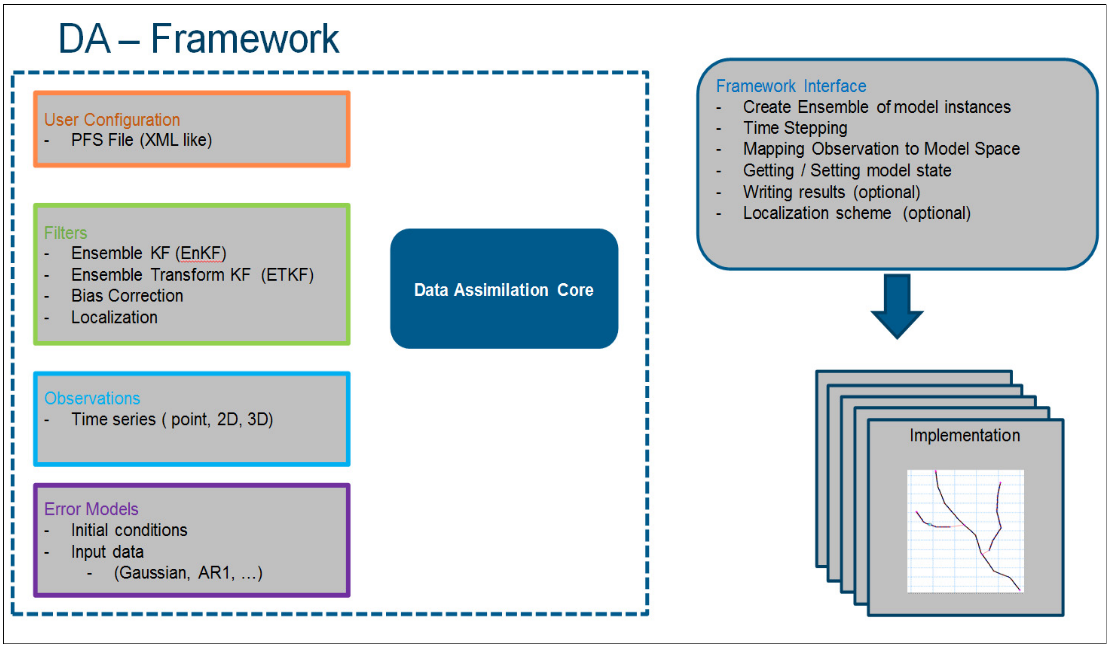

Figure 1. DHI data assimilation framework.

The framework is written in C# and includes an efficient interface for coupling with the MIKE HYDRO River modelling system with support for parallel propagation of ensembles.

2.2 Hydrodynamic-hydrological model description

The MIKE HYDRO River modelling system is a comprehensive one-dimensional hydrodynamic modelling system for river modelling. It is also capable of hydrological modelling through its rainfall-runoff module that supports a range of rainfall-runoff models that can be connected to the hydrodynamic model as lateral or point inflows.

Support has been added for data assimilation of the hydrodynamic model and for the NAM rainfall-runoff model, which is a lumped, conceptual model as in Figure 2. It models the hydrological cycle at catchment scale by accounting for the water content in different conceptual storages. Total catchment runoff includes overland flow, interflow and base flow components (Madsen, 2000).

Hydrodynamic model states include water levels and discharges at calculation points in the 1D river model. The NAM rainfall-runoff model includes different internal states corresponding to the water content in the conceptual storages cf. Figure 2: (1) surface storage, (2) overland flow reservoir 1, (3) Overland flow reservoir 2, (4) Interflow reservoir, (5) Lower zone (root zone) storage, and (6) groundwater storage. If snow modelling is included, the snow storage is added. By updating the storages the catchment conditions are updated and the resulting rainfall-runoff hydrograph is adjusted.

The NAM rainfall-runoff model forcing includes catchment average precipitation and potential evapotranspiration. If snow modelling is included, temperature is required. In the integrated modelling system catchment rainfall-runoff forces the hydrodynamic model together with other boundary conditions.

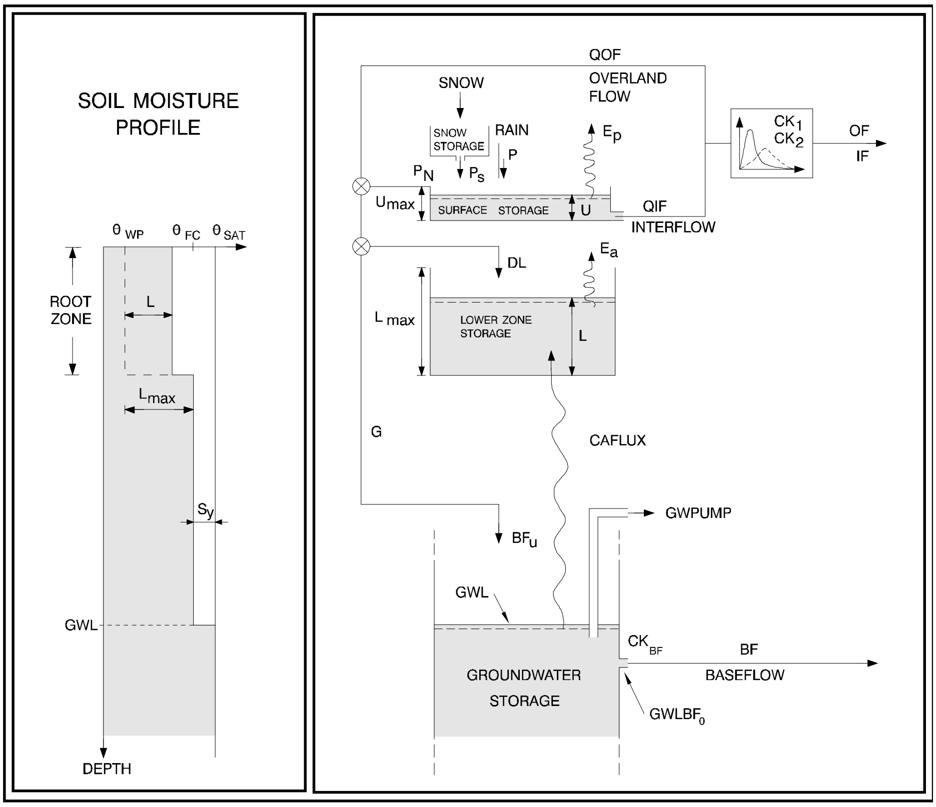

Figure 2. NAM rainfall-runoff model structure.

2.3 Data assimilation

Data assimilation combines observations and model estimates of the state of a system in an optimal way taking into account the uncertainty of the two estimates as well as the correlation between modelled and observed states. A selection of ensemble based Kalman filter formulations are available in the data assimilation framework but below has only described the Ensemble Transform Kalman Filter (ETKF) that was applied in the case study.

The state-based formulation for a numerical model without assimilation can be written as

$$\mathbf{x}_{\boldsymbol{k}} = \mathbf{M}(\mathbf{x}_{\boldsymbol{k-1}}, \mathbf{u}_{\mathbf{k}}, \boldsymbol{\theta}, \boldsymbol{\epsilon}_{\boldsymbol{k}}) \qquad [1]$$

where **M**(•) is the model operator that solves the mathematical equations from time step *k-1* to *k*, **x** is the state vector, **u** is the model forcing, $\boldsymbol{\theta}$ represents model parameters, and $\boldsymbol{\epsilon}_{\boldsymbol{k}}$ is the process noise term. When observations **y** are available, the model state can be related to the observation using a measurement operator **h**(•), such that

$$\mathbf{y}_{\mathbf{k}} = \mathbf{h}(\mathbf{x}_{\mathbf{k}}) + \boldsymbol{\eta}_{\mathbf{k}} \qquad [2]$$

with measurement error $\boldsymbol{\eta}_{\boldsymbol{k}}$**.** For a linear model to observation space mapping (for instance, when the model state is observed directly), the measurement operator is written as a matrix **H**.

In state-space formulation, a linear combination of equations (1) and (2) produces the model analysis (^{a}) by updating the back ground (^{f})

$$\mathbf{x}_{\mathbf{k}}^{\mathbf{a}} = \mathbf{x}_{\mathbf{k}}^{\mathbf{f}} + \mathbf{K}_{\mathbf{k}}\left(\mathbf{y}_{\mathbf{k}} - \mathbf{H}\left(\mathbf{x}_{\mathbf{k}}^{\mathbf{f}}\right)\right) \qquad [3]$$

where the gain matrix **K**, reflects how much emphasis should be placed on the observations or the model forecast (^{f}). The Kalman filter is the best linear unbiased estimator (Kalman, 1960). The gain matrix is calculated for time step *k*, as

$$\mathbf{K} = \mathbf{P}\boldsymbol{H}^{\boldsymbol{T}}(\boldsymbol{HPH}^{\boldsymbol{T}} + \boldsymbol{R})^{-\mathbf{1}} \qquad [4]$$

where **P** is the state error covariance matrix, a measure of the estimated accuracy of the state estimate, and **R** is the observation error covariance.

Ensemble based on Kalman filters are better suited than the standard or extended Kalman filter when dealing with non-linear evolution of the model error as the error covariance matrix **P** is propagated forward by the model itself. The ETKF is a square root filter variation of the Ensemble Kalman filter and has the advantage that perturbation of the observations is not needed (Bishop et al., 2000; Hunt et al. 2006).

The covariance matrix **P** is calculated from a model ensemble where each ensemble member was perturbed slightly different. The state matrix of *m* ensemble members can be written as

$$\mathbf{X} = [\mathbf{x}^{1}, \mathbf{x}^{2}, \dots, \mathbf{x}^{m}] \quad [5]$$

where each ensemble member **x** contains a complete set of model states included in the data assimilation. The forecast error covariance can be obtained from the sample covariance of the ensemble members

$$\mathbf{P}^{f} = (m-1)^{-1}\mathbf{A}^{f}\left(\mathbf{A}^{f}\right)^{\mathrm{T}} \quad [6]$$

where T denotes the matrix transpose. **A** is the matrix of ensemble anomalies defined as

$$\mathbf{A}^{f} = \left[\mathbf{x}^{f(1)} - \bar{\mathbf{x}}^{f},\ \mathbf{x}^{f(2)} - \bar{\mathbf{x}}^{f}, \dots,\ \mathbf{x}^{f(m)} - \bar{\mathbf{x}}^{f}\right] \quad [7]$$

where the background ensemble mean $\bar{\mathbf{x}}^{f}$ is subtracted from each ensemble member.

$$\bar{\mathbf{x}}^{f} = \frac{1}{m}\sum_{i=1}^{m}\mathbf{x}^{f(i)} \quad [8]$$

The ETKF updates the forecast covariance matrix $\mathbf{P}^{f}$ by updating the ensemble anomalies $\mathbf{A}^{f}$ deterministically through a transformation matrix **T** so the analysis error covariance $\mathbf{P}^{a}$ matches the theoretical value given by the Kalman filter. Both the ensemble mean and ensemble anomalies are updated based on **T**:

$$\bar{\mathbf{x}}^{a} = \bar{\mathbf{x}}^{f} + \mathbf{A}^{f}\mathbf{T}\left(\mathbf{H}\mathbf{A}^{f}\right)^{T}\mathbf{R}^{-1}\left(\boldsymbol{y} - \boldsymbol{H}\left(\bar{\mathbf{x}}^{f}\right)\right), \text{ and} \quad [9]$$

$$\mathbf{A}^{a} = \mathbf{A}^{f}\mathbf{T} \quad [10]$$

that must satisfy

$$\mathbf{T} = \mathbf{T}^{s}\mathbf{U}, \text{ and} \quad [11]$$

$$\mathbf{T}^{s} = \left[\mathbf{I} + \frac{1}{m-1}\left(\mathbf{H}\mathbf{A}^{f}\right)^{T}\mathbf{R}^{-1}\mathbf{H}\mathbf{A}^{f}\right]^{-1/2} \quad [12]$$

where **U** is an arbitrary orthonormal matrix $\mathbf{U}\mathbf{U}^{\mathrm{T}} = \mathbf{I}$, and the solution to $\mathbf{T}^{s}$ is symmetric.

A good description of the model error is crucial in the application of data assimilation as the model state update depends on the model and observation uncertainties described by the state error of covariance matrix **P** and the observation error covariance **R**. The model error is described through perturbation methods used to perturb the deterministic model and generate the model ensemble. It is therefore important that these methods are flexible enough to introduce error into the model system, replicating the major error sources of the model without being overly complex to configure. Perturbation methods that are based on relative errors (relative to the value being perturbed) have therefore been implemented to allow the perturbation magnitude to follow the dynamics of the system.

Main uncertainty sources are related to the model states, forcings and parameters. Currently only uncertainty in model state and forcing have been implemented, and parameters are considered calibrated and fixed in time.

Forcing perturbation

Precipitation is considered as the main contribution to the forcing uncertainty in the hydrological model. Two perturbation options are available, relative logarithmic and relative truncated Gaussian.
The relative logarithmic perturbation method can be described by:

$$\mathbf{u}_{perturbed} = \mathbf{u} \cdot \boldsymbol{\varepsilon}_{log} \quad [13]$$

where $\mathbf{u}$ is the forcing, and $\boldsymbol{\varepsilon}_{log} \in LN(1, \sigma^2)$ is the relative error sampled from a logarithmic distribution with mean 1 and standard deviation σ.

The truncated Gaussian perturbation method is described by:

$$\mathbf{u}_{perturbed} = \mathbf{u} + \mathbf{u} \cdot \boldsymbol{\varepsilon} \qquad [14]$$

where $\boldsymbol{\varepsilon} \in N(0, \sigma^2)$ is the relative error sampled from a normal distribution with standard deviation σ and truncated to the interval [-1 ; 1].

State perturbation

State perturbation can be applied to the different NAM model states and is defined relative to the change of state similar to the method described in Clark et. al (2008).

The state perturbation can be described by:

$$\mathbf{S}_{perturbed} = \mathbf{S} + (-\boldsymbol{\varepsilon}_\mathbf{s} + \mathbf{2} \cdot \mathbf{u}_s \boldsymbol{\varepsilon}_\mathbf{s}) \cdot \Delta\mathbf{S} \qquad [15]$$

where S is the current state, $\Delta\mathbf{S}$ the change of state since last perturbation time, $\mathbf{u_s}$ is sampled from the Q-function (one minus the cumulative distribution function of the standard normal distribution) with bounds [0 ; 1], and $\boldsymbol{\varepsilon}_s$ is the perturbation limits.

Time and space correlation

The forcing and state uncertainties cannot, in general, be assumed uncorrelated in time and space. Temporal correlations are described by a first order autoregressive process

$$\boldsymbol{\varepsilon}_\mathbf{t} = \boldsymbol{\varphi} \cdot \boldsymbol{\varepsilon}_{\mathbf{t-1}} + \boldsymbol{\gamma}_\mathbf{t} \qquad [16]$$

where ε_t and ε_{t-1} are the errors sampled on the current and previous time steps, φ is the first order autocorrelation coefficient, and γ_t the independent error component. The distribution of $\boldsymbol{\varepsilon}_{log}$ in [13] is logarithmic but the sampling of ε_t takes place in log space where the errors are normally distributed and [16] is valid. In [14] ε_t is normally distributed and [16] is used directly. In the state perturbation [15] is used in the sampling of u_s from the Q-function. Rather than defining φ directly, temporal correlation is defined in terms of the half time constant, $T_{1/2}$, that specifies the time it takes for the exponential decay of the error cf. Eq. [17] to reach half of its initial value, i.e.

$$\boldsymbol{\varphi} = \mathbf{exp}\left(-\frac{\Delta \boldsymbol{t} \cdot \mathbf{ln(2)}}{\boldsymbol{T}_{\frac{1}{2}}}\right), \qquad \boldsymbol{T}_{\frac{1}{2}} > 0 \qquad [17]$$

where $\Delta\boldsymbol{t}$ is the model time step. This provides a more consistent definition of the temporal correlation that is independent of the model time step used.

Localization

Localization was used to limit the influence a given measurement has on the state variables in order to reduce the problem of spurious correlation (Hunt et al. 2006). The hydrological model states of a catchment can be localized to the specific observation of the catchments rainfall-runoff. For the hydrodynamic model, states can be localized to within a distance of a river discharge observation in the upstream and downstream direction.

Advanced adaptive localization methods are available in the data assimilation framework but they have not been applied in this study (Ridler et al. 2014).

3 CASE STUDY

The Murrumbidgee River is situated in New South Wales (NSW), Australia and is one of the main tributaries of the Murray River in the Murray-Darling basin. It has a length of 1,600km and a catchment area of 86,000km^2.

The river system is highly complex with extensive agricultural areas, important ecosystems and urban developments. Average annual rainfall within the basin ranges from 1700mm in the mountain areas to as little as 350mm in the plains creating the need to efficiently manage the availability of water resource to meet the diverse ecological, irrigation and town water demands without releasing excess water from reservoirs in the region. (NSW Office of Water, 2011)

To improve the water management, Water NSW has implemented an operational forecasting and control system named Computer Aided River Management (CARM). It employs advanced hydrodynamic-hydrological modelling and optimization of dams and control structures to efficiently deliver water to its users (NSW Office of Water, 2017; Kalken et al. 2012).

For testing the data assimilation system at the upstream part of the CARM modelling system is used. It covers the area from Blowering Dam and Burrinjuck Dam and downstream to the city of Waggawagga as shown in **Figure 3**.

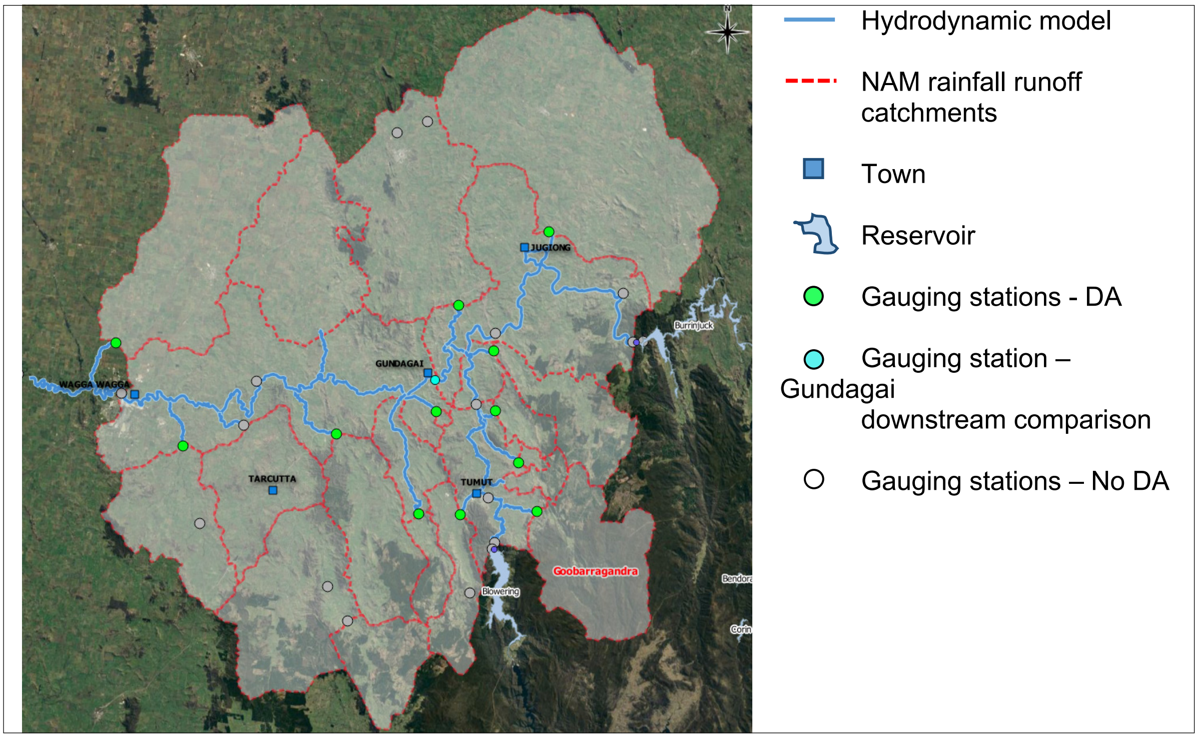

Figure 3. CARM sub-model and gauging stations. Green gauging stations are used in data assimilation.

The model has a total of 22 NAM rainfall-runoff catchments of which 12 are head catchments where the catchment runoff was measured and data assimilation can be applied in the hydrological model.

4 RESULTS AND DISCUSSIONS

Evaluation of the internal states of the hydrological model was difficult because they are unobservable, only the combined rainfall-runoff can be directly compared to observations. The filter updates of the model states are therefore expected visually to evaluate if the state updates are physically consistent with the expected rainfall-runoff processes.

In the following, the NAM rainfall-runoff model for the Goobarragandra catchment has been selected to demonstrate the data assimilation. Next, the combined effect from updating multiple rainfall-runoff models was assessed in the hydrodynamic model by comparing against a downstream flow gauge near Gundagai, located in the center of the modeling area (see Figure 3).

4.1 Data assimilation of Goobarragandra NAM rainfall-runoff model

The Goobarragandra catchment is located in the most south western part of the model area in the mountainous region receiving the highest annual rainfall in the area, see Figure 3. (NSW Office of Water, 2011).

Model uncertainty is included by perturbing the precipitation (relative logarithmic perturbation with 25% standard deviation and correlation half time of 4 hours) and the groundwater state (relative error of 35% and correlation half time of 5 days). The observation uncertainty has been defined as relative to the discharge magnitude with 10% standard deviation.

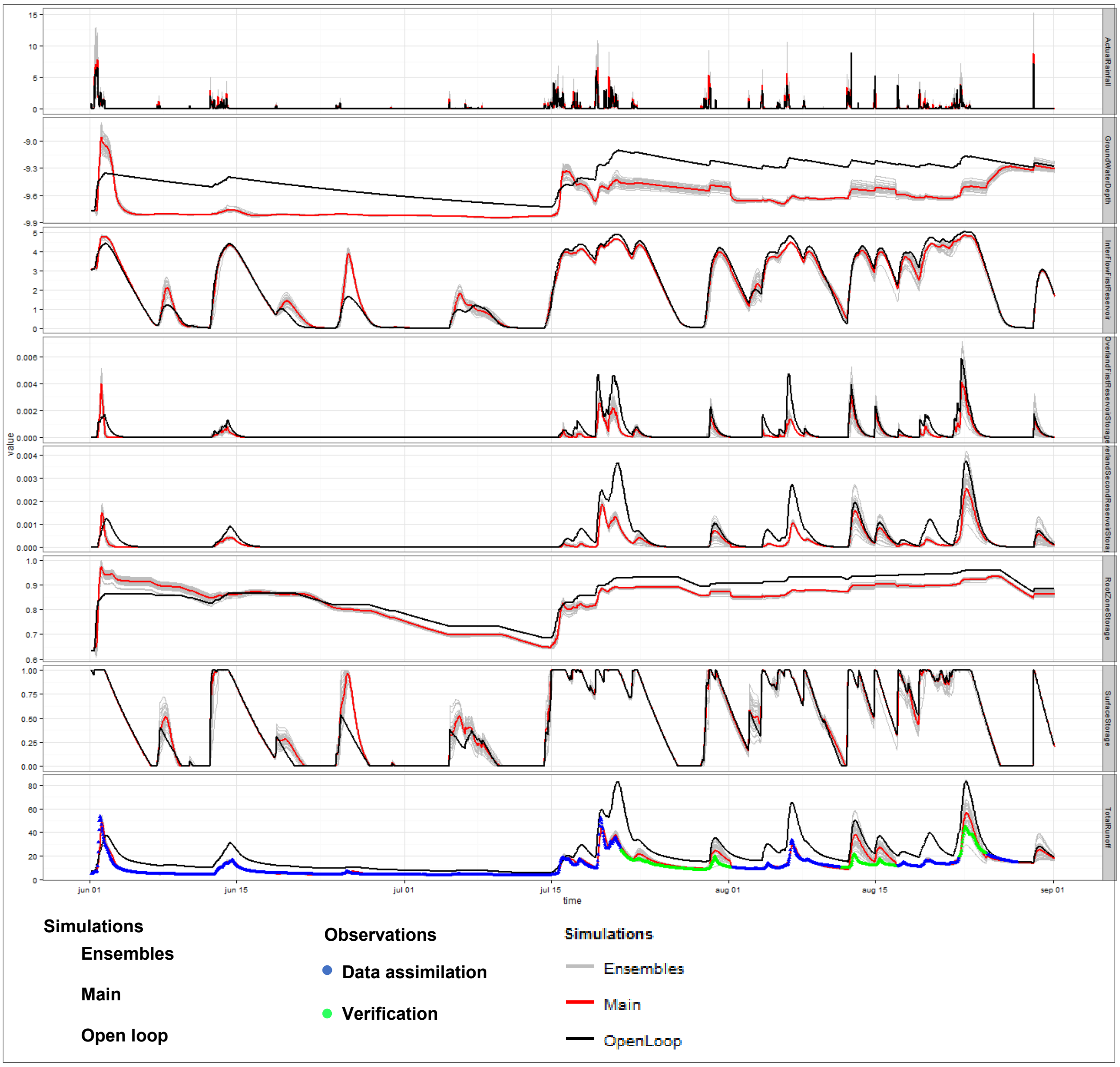

Figure 4. NAM data assimilation results for Goobarrangandra catchment. From the top is plotted rainfall forcing, groundwater depth, interflow reservoir, overland flow reservoir 1, overland flow reservoir 2, root zone storage, surface storage and catchment runoff. The data assimilated results in terms of the full ensemble and the ensemble mean (Main) are plotted together with the Open loop run (no data assimilation). Results include both periods where observations are assimilated (blue) and verification periods without data assimilation (green).

From Figure 4 and Figure 5 the effect of the data assimilation on the individual hydrological model states and the rainfall-runoff hydrograph can be seen. This includes both periods with (blue observations) and without (green observations) data assimilation. A good rainfall-runoff simulation in the sense that it resembles well the observed catchment runoff and is not a good evaluation criterion in it-self as this can be achieved through physically unrealistic rainfall-runoff process updates. For instance, peak flows are expected to primarily originate from overland flow processes, and in the long periods with no appreciable rainfall the runoff originates from ground water base flow. The state updates seem reasonable since the filter updates the overland flow reservoirs to correct the runoff peaks and the groundwater depth to update the recession parts of the hydrograph.

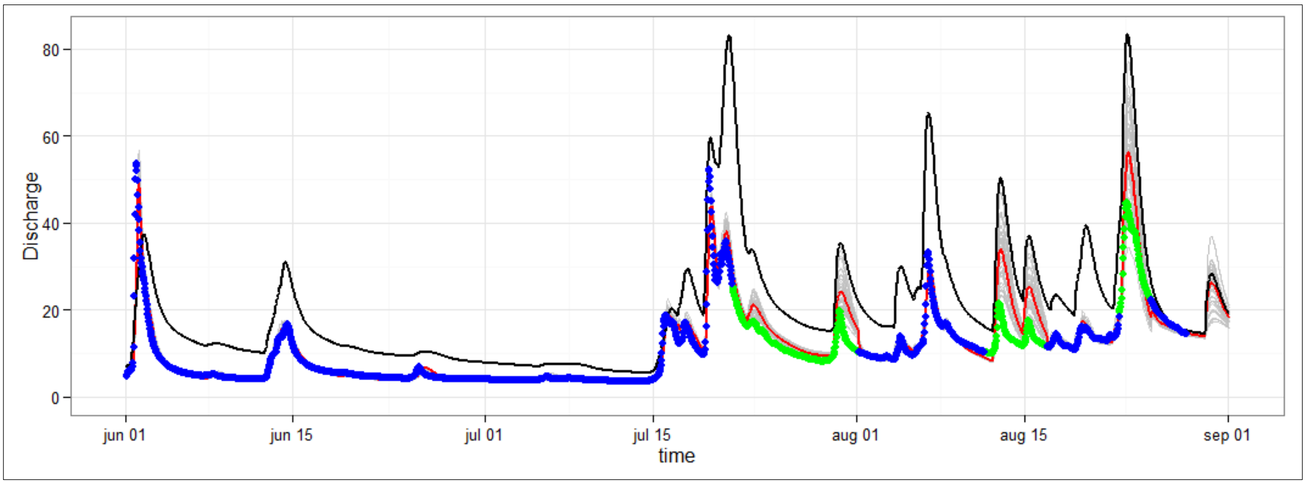

Figure 5. Goobarrangandra simulated catchment runoff as in Figure 4.

A large improvement in catchment runoff is achieved by data assimilation over the open loop simulation. The groundwater depth is lowered in June and July that would otherwise have caused an overestimation of the catchment runoff. In the verification period 20-31 July the updated groundwater depth causes a long lasting improvement on the hydrograph recession. Also the peak flow estimates are improved significantly in the verification periods by updating the model states up to the onset of the peak events. During peak flow events in the verification periods, the uncertainty increases due to the uncertainty in the precipitation forcing.

4.2 Impact of updated NAM rainfall-runoff catchment models on river simulation

A total of 11 catchments drain to the Murrumbidgee River upstream Gundagai and 7 of these catchments are head catchments with direct observations of the catchment runoff where data assimilation has been applied. To assess the combined effect of updating these catchments the simulated discharge at a downstream flow gauge situated near Gundagai was analysed. See Figure 3 for location of downstream flow gauge and catchment overview.

The data assimilation results of updating the river discharge in Gundagai alone (HD), updating the upstream catchments alone (RR) and updating both river discharge and catchments (RR + HD) are presented in Figure 7 together with the observed river discharge in Gundagai. By updating the upstream catchments alone, the error in simulated river discharge is reduced considerably over the open loop simulation but the rainfall-runoff errors from ungauged catchments still remains. When the observed river discharge in Gundagai is used to update the hydrodynamic model, the error was removed almost entirely but as seen from the figure the simulated discharge will return very quickly to the open loop simulation when forecasting (verification). The combined approach where both upstream catchments and the river discharge is updated gives the best result and illustrate that both can be applied simultaneously in the effort to improve the forecasting capabilities of the integrated hydrodynamic-hydrological modelling system.

Peak travel time from the most upstream end of the system and down to Gundagai is approximately 14 hours. In Figure 6 the three verification periods are about 10, 5 and 3 days, considerable longer than the travel times in the river model but the effect from the updated catchment states are seen to last throughout the verification periods showing a consistent improvement of the model forecast.

4.3 Remark on perturbation configuration improvement

The available perturbation methods have many degrees of freedom for defining the model uncertainty, and in this experiment it is likely that a more optimal set of configuration parameters exists that would lead to improved state updating. Investigation in how to optimize the configuration of the Kalman filter is ongoing, but even with suboptimal perturbation parameters significant improvement in the model forecast can be achieved.

Through the data assimilation framework it is possible to include the autoregressive error components in the state vector and update them together with model states, which could also lead to improvements in the filter updating.

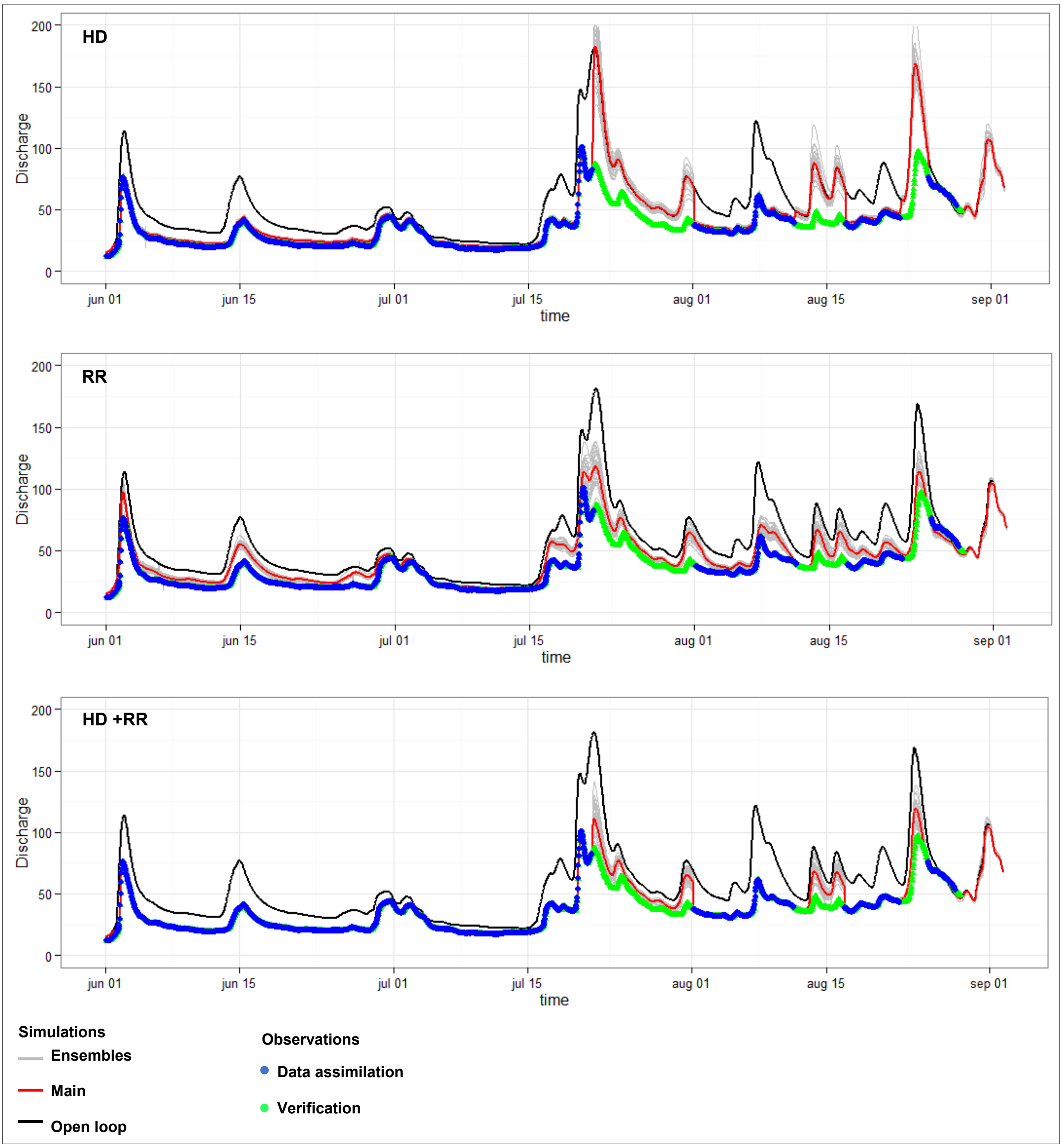

Figure 7. Comparison of modelled river discharge with observed flow at Gundagai. Data assimilation of observed flow at Gundagai for updating the hydrodynamic model states (**HD**), data assimilation of upstream NAM catchments (**RR**), and the two combined (**HD + RR**). The data assimilated results in terms of the full ensemble and the ensemble mean (Main) are plotted together with the Open loop run (no data assimilation). Results include both periods where observations are assimilated (blue) and verification periods without data assimilation (green).

5 CONCLUSIONS

Data assimilation of hydrological model states was demonstrated in a hydrodynamic-hydrologic modelling system resulting in consistent updates of the catchment rainfall-runoff processes. The effect of updating the hydrological states was shown to have long time persistence due to the hydrological memory of the catchments, and through routing of the updated rainfall-runoff the forecasted river discharge consequently improved downstream in the basin.

The increased forecast skills are important for improving water management, such as real-time control and optimization of water infrastructure, flood forecasting and early warning, etc.

REFERENCES

Bishop, C.H., Etherton, B.J. & Majumdar, S.J. (2001). Adaptive Sampling with the Ensemble Transform Kalman Filter. Part 1: Theoretical Aspects. *Monthly Weather Review*, 129(3), 420-436.

Clark, M.P., Rupp, D.E., Woords, R.A., Zheng, X, Ibbitt, R.P., Slater, A.G., Schmidt, J., Uddstrom, M.J. (2008). Hydrological Data Assimilation with the Ensemble Kalman Filter: Use of Streamflow Observations to Update States in a Distributed Hydrological Model. *Advances in Water Resources*, 31(10), 1309-1324.

Hunt, B.R., Kostelich, E.J. & Szunyogh, I. (2007). Efficient Data Assimilation for Spatiotemporal Chaos: A Local Ensemble Transform Kalman Filter. *Physica D: Nonlinear Phenomena*, 230(1-2), 112-126.

Kalman, R. (1960). A New Approach to Linear Filtering and Prediction Problems. *Journal of Basic Engineering*, 82(1), 35-45.

Madsen, H. (2000). Automatic Calibration of a Conceptual Rainfall-Runoff Model using Multiple Objectives. *Journal of Hydrology*, 235(3-4), 276-288.

Office of Water. (2011). *Water Resources and Management Overview. Murrumbidgee Catchment.* NSW.

Office of Water. (n.d.). WaterNSW. NSW Retrieved at 10 March 2017, from: //www.waternsw.com.au/projects/efficiency/CARM

Ridler, M.E., Madsen, H., Stisen, S., Bircher, S. & Fensholt, R. (2014). Assimilation of SMOS Derived Soil Moisture in a Fully Integrated Hydrological and Soil-Vegetation-Atmosphere Transfer Model in Western Denmark. *Water Resources Research*, 50(11), 8962-8981.

van K.T., Nachiappan, N., Berry, D. & Skinner, J. (2012). An Optimized, Real Time Water Delivery and Management System for the Murrumbidgee River. *In Hydrology and Water Reseources Symposium 2012,* 1374-1384.

Proceedings of the 37th IAHR World Congress
August 13 – 18, 2017, Kuala Lumpur, Malaysia

THE EFFECTIVENESS OF FLOOD DEFENSE FORESTS AS THE FLOOD CONTROL IN THE LOWER REACH OF GOUNOKAWA RIVER

KENTARO AOKI [(1)] & MASAHARU FUJITA [(2)]

[(1)] Department of Civil and Earth Resources Engineering, Graduate School of Engineering, Kyoto University
aoki@ideacon.co.jp
[(2)] Disaster Prevention Research Institute, Kyoto University
fujita.masaharu.5x@kyoto-u.ac.jp

ABSTRACT

The Gounokawa River has the maximum basin area in the Chugoku region, with its lower reaches located in the Shimane Prefecture in Japan. In the lower reaches of the Gounokawa River, many districts without dikes exist, and the degree of river improvement security is low. In addition, it is expected that the local population will decrease by more than 30% in the next 30 years. Therefore, it is difficult to construct dikes with a degree of progress similar to that in the past. However, bamboo trees planted as flood reduction measures still remain as flood defense forests. Therefore, in the lower reaches of the Gounokawa River, it is important to utilize the flood defense forests for river security improvement. Flood water depths are high, and early velocity acts on the flood defense forests, which may be lodged and washed away. However, these risks have not been considered for large-scale flooding. In this study, we built a numerical analysis model (2-D shallow-water flow model) capable of quantitatively calculate river improvement effects and lodging of flood defense forests. We evaluated the lodging of flood defense forests based on the bending moment acting on them at the time of flooding. We performed a quantitative evaluation of the river improvement effect of the flood defense forests in the lower reaches of the Gounokawa River and examined the maintenance policy utilized for river improvement effects. In addition, based on our assumptions about lodging flood defense forests at the time of large-scale flooding, we considered differences due to floodplain velocity.

Keywords: Flood defense forests; fooding water; food control effectiveness; lodging flood defense forests; velocity of floodplain.

1 INTRODUCTION

1.1 Flood defense forest

Flood defense forests are bamboo forests planted to alleviate flood damage before a dike is built; they reduce flood flow velocity and control bank erosion. However, over the recent years, flood defense forests have been cut down to expand river widths and increase embankments throughout Japan. In response to the growing interest in the environment, river environment preservation, as well as flood control, is becoming more important, and the original function of the flood defense forest is beginning to be reconsidered.

In addition to the Gounokawa River, other flood defense forests were planted along the Yoshino River (Tokushima Pref.), the Adogawa River (Shiga Pref.), and the Yuragawa River (Kyoto Pref.) They still exist throughout Japan and have long been maintained in anticipation of their flood controlling effects. Therefore, many studies have investigated flood defense forests and their flood control effects. It is a bamboo forest with a width of 30 m or more as a feature of flood defense forests which showed its effect at the time of large flood, it has been growing over a long range in the longitudinal direction and that the number of bamboo per 100 m^2 is 600 to 900 (Yoshino, 1978).

Bamboo forests that were planted as measures against flood damage as per the teachings of “Kobo Daishi” in the lower reaches of the Gounokawa River, still remain. However, in recent years, due to the withering of flood defense forests and expansion of the extent of proliferation, the water level rises during floods. Therefore, in the lower reaches of the Gounokawa River, it has become important to utilize the flood defense forest for river improvement.

1.2 Bamboo material properties

Currently, many bamboo groves in Japan are being neglected, which has led to their general devastation. At the same time, experiments to grasp the fundamental material properties of bamboo are being carried out to utilize bamboo as a building structure. Yoshida et al. (2008) have tested bending, compression shearing, tension and splitting using Mousou bamboo growing near Yokohama City. In the full-scale experiment, using unmodified bamboo test bodies, the bending stress, σ_b, was 6.1 to 7.7 kN/cm^2. In addition, these values were compared with experimental data from other laboratories. However, because the results shown in Table 1 differ in the location of specimen extraction and specimen shape, the data varies. In this study, the bending stress, σ_b from the bamboo material property test result was used as the threshold for judging lodging; the validity was examined by comparing the experimental results with the flood result from July, 1983.

Table 1. Bamboo bending test results

Testing institution		Bending stress (kN/cm^2)
Tokyo Univ.		12.2
Oita Univ		14.4
Washington State Univ.		10.5
Univ. Aachen		7.6
Polytechnic Univ.	Test piece experiment	19.0
	Full-scale experiment	6.1

2 Study Methods

2.1 The target area

The Gounokawa River has a maximum basin area in the Chugoku region, with the lower reaches located in Shimane Prefecture in Japan. This research targeted the Tazu district, an area with few dikes located on the left bank, approximately 21 to 23 km from the estuary. On the riverbank, there is a 90 m wide Mousouchiku flood defense forest, wherein the bamboos reach heights of approximately 15 m, a breast height diameter of 70 mm, and a density of 3 to 8 threads/m^2. On the right bank of Tazu district lies Onuki district, which is currently developing interim dikes. The flood defense forest in Tazu district both hinders flood flow and is a factor in rising upstream water levels. Therefore, from the viewpoint of the flood control plan, it is necessary to cut down the flood defense forest, but it is important to utilize the flood protection forest because the dikes are undeveloped.

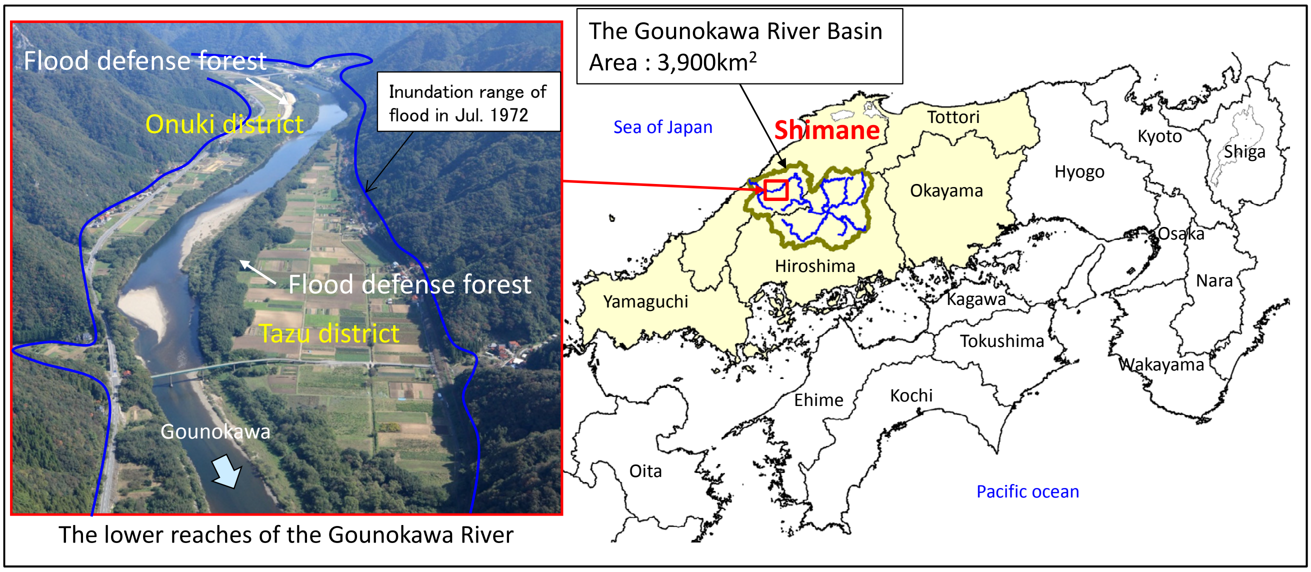

Figure 1. Position map of the lower reaches of the Gounokawa River

2.2 Outline of the numerical analysis model

In order to evaluate the flood effect of the flood defense forest and to examine the management of the flood defense forest, a 2-D shallow-water flow model was created.

$$\frac{\partial u}{\partial t}+u\frac{\partial u}{\partial s}+v\frac{\partial u}{\partial n}+\frac{uv}{r} = -g\frac{\partial H}{\partial s}-\frac{\tau_s}{\rho h}+2\frac{\partial}{\partial s}\left[\varepsilon\frac{\partial u}{\partial s}\right]+\frac{\partial}{\partial n}\left[\varepsilon\frac{\partial u}{\partial n}\right] \quad [1]$$

$$\frac{\partial v}{\partial t}+u\frac{\partial v}{\partial s}+v\frac{\partial v}{\partial n}-\frac{u^2}{r} = -g\frac{\partial H}{\partial n}-\frac{\tau_n}{\rho h}+\frac{\partial}{\partial s}\left[\varepsilon\frac{\partial v}{\partial s}\right]+2\frac{\partial}{\partial n}\left[\varepsilon\frac{\partial v}{\partial n}\right] \quad [2]$$

$$\frac{\partial H}{\partial t}+\frac{\partial (uh)}{\partial s}+\frac{\partial (vh)}{\partial n}+\frac{vh}{r}=0 \quad [3]$$

where, u is water depth average flow velocity in the s direction, v is water depth average flow velocity in the n direction, r is the curvature radius of the flow channel, g is gravitational acceleration, H is water level, h is water depth, ρ is fluid density, and t is time. τ_s, τ_n are the riverbed shear stress in the s and n directions and are given in Eq. [4] and [5]. Besides, n is the coefficient of roughness.

$$\frac{\tau_s}{\rho h}=\frac{gn^2}{h^{4/3}}u\sqrt{u^2+v^2} \quad [4]$$

$$\frac{\tau_n}{\rho h}=\frac{gn^2}{h^{4/3}}v\sqrt{u^2+v^2} \quad [5]$$

The coefficient of eddy viscosity, ε is provided, assuming logarithmic law in the water depth direction as shown in Eq. [6].

$$\varepsilon=\frac{\kappa}{6}u_*h \quad [6]$$

where, κ is the Karman constant, and u_* is the friction velocity.

2.3 The vegetation model

The vegetation model is treated as Eq. [7] and [8], assuming an equivalent roughness coefficient calculated from the characteristics of tree growth (diameter, denseness etc.). The vegetation transmission coefficient, K representing the tree propagation characteristic is expressed by Eq. [7].

$$K=(2\cdot g/a_w/C_d)^{0.5} \quad [7]$$

where, a_w=N*D_m, the drag coefficient C_d=1.2, and g is gravitational acceleration. n is the number of trees growing per unit area, and D_m is breast high diameter.

The roughness coefficient, considering the growth of the vegetation, is represented by Eq. [8] according to water depth.

$$\begin{array}{ll} h_m=0 & n=\infty \\ h_m>0\ and\ h\le h_m & n=\left(n_b^2+h^{4/3}/K^2\right)^{0.5} \\ h_m>0\ and\ h_m<h\le h_v & n=(h/h_m)^{5/3}\cdot\left(n_b^2+h_m^{4/3}/K^2\right)^{0.5} \\ h_m>0\ \ and\ h_v<h & n=(h_v/h_m)^{5/3}\cdot\left(n_b^2+h_m^{4/3}/K^2\right)^{0.5} \end{array} \quad [8]$$

where, h_m is the branch length, h_v is tree height, and n_b is the roughness coefficient of the surface of the high-water site within the range of tree group growth.

2.4 Confirmation of hydraulic analysis model reproducibility

We confirmed the validity of the hydrological analysis model for the flood in Jul, 2010, which was the largest flood in recent years (Kawahira St.: 5,817 m^3/s).

Figure 2 shows the flood mark at 20 km to 30 km, the target section of this study, and the observed water level in the Tanijugo water gauge station (right bank 14.8 km), in the vicinity of the target section. The average water level difference from the flood mark was 0.28 m, and the difference from peak water level at the observation station was 0.11 m. This confirmed that the flood can be reproduced on both the water surface shape and hydrograph.

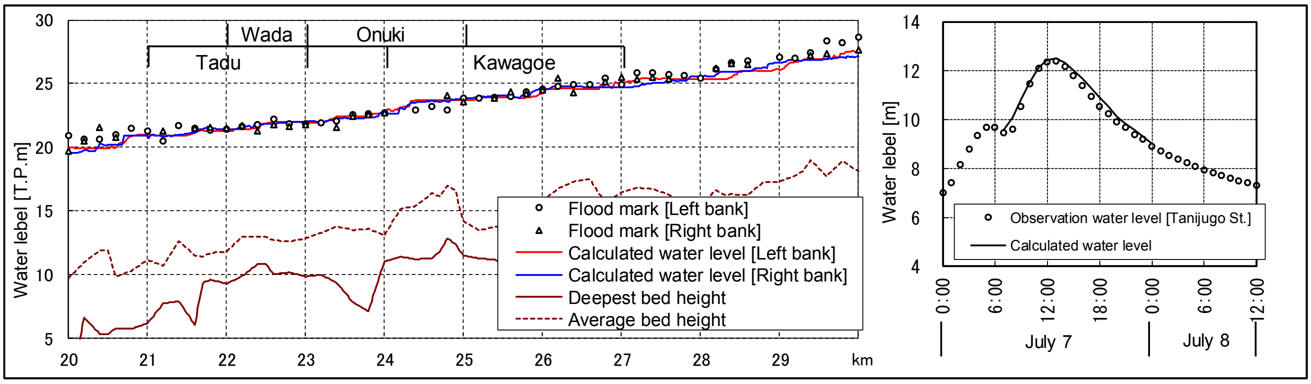

Figure 2. Flood mark longitudinal section and water level hydrograph

3 The management method for flood defense forests

3.1 Case setting

In order to examine the management method for flood defense forests, the following cases were set and the optimum management method was selected.

Table 2. Case settings for flood defense forest management

	State of flood defense forest	
	The down stream side	The up stream side
Case1	Remove	Remove
Case2	Leave	Remove
Case3	Remove	Leave
Case4	Leave at 20 m width	Leave at 20 m width

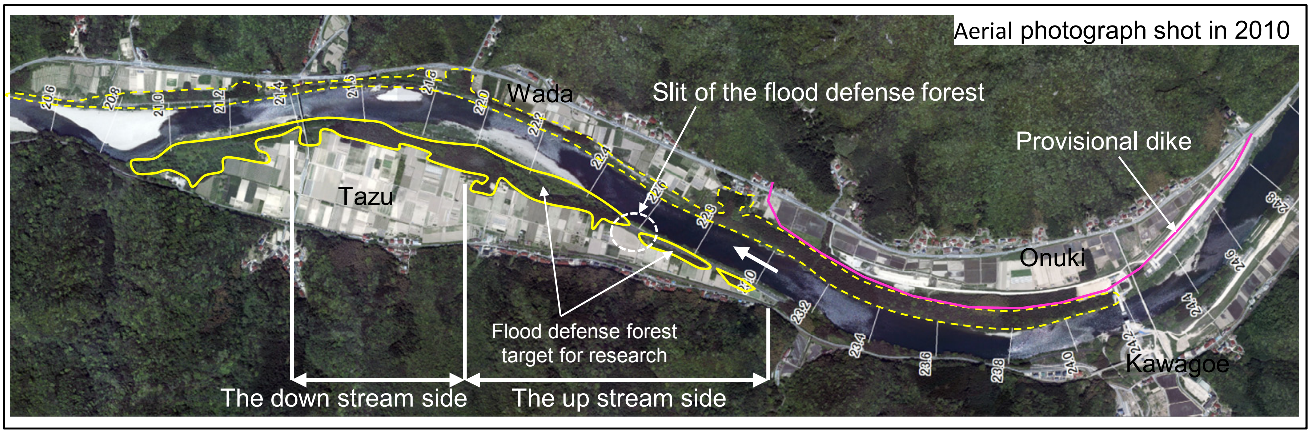

Figure 3. Position map of flood defense forest in the Tazu district

3.2 Numerical analysis results

Figure 4 shows the maximum flow velocity plan view for the flood in July, 1972; Figure 5 shows the maximum flow velocity plan view for the flood in July, 1983. The flood in July, 1972 had a large-scale water discharge (Gotsu St.: 10,400 m^3/s), while the flood in July, 1983 was a mid-scale water discharge (Gotsu St.: 7,800 m^3/s).

3.2.1 The Tazu district (Left bank 21 km to 23 km)

An overflowing flood occurred in the Tazu district because the dike was not well developed. In Case 1, because the flood defense forest is nonexistent, the mean value of flow velocity inside the flood plain rises to 1.2 m/s, and the effect of reduction in the velocity from the flood defense forest disappears.

In Case 2, the flood flow velocity increases from the upstream side, at the location of flood defense forest lodging, and flows into the inside of the flood plain; the velocity inside the flood plain rises compared with the current river channel. In addition, the flow velocity increases locally, immediately upstream of the flood defense forest outlet. This implies that the flow direction changed toward the inside of the flood plain due to the resistance of the flood defense forest, as the upstream end of the remaining flood defense forest is wide.

In Case 3, the downstream velocity of the flood plain where the flood defense forest was removed is not significantly different compared to the current river channel. However, the flow velocity in the vicinity of the small amount of the flood defense forest on the upstream side increases compared to the current river channel. It is hypothesized that this is due to the flood defense forest lodging on the downstream side, so that the flow on the flood plain is unimpeded downstream and the flow velocity is increased upstream.

In Case 4, the flow velocity in the flood plain remains unchanged compared with the current river channel. By maintaining the flood defense forest with a width of 20 m, it is possible to utilize the flood defense forest to reduce flow velocity.

3.2.2 The Onuki district (Right bank 23 km to 25 km)

Since the flood in July, 1974 was large-scale, overflowing flooding would occur in all cases due to flow capacity even if the provisional dike is constructed. Flooding in July, 1983 was at such a flow rate scale that it would flow below the dike level. Overflow flooding in Cases 1, 3, and 4 is eliminated.

3.1 Optimal management method

The advantages and disadvantages of removing sections of the flood defense forest were comprehensively evaluated and improvement methods for the flood defense forest in the Tazu district were selected. In Table 3, modifications that resulted in improvements compared to current river channels are indicated with ○ modifications that resulted in neither improvement or worsening are indicated with △ and modifications that deteriorate the existing conditions are indicated with ×. The evaluation results suggest that Case 4, maintaining a flood defense forest with 20 m width, is the best modification of the four cases.

Table 3. Comprehensive evaluation of flood defense forest management methods

	Tazu district		Onuki district		Comprehensive evaluation
	Flood in July, 1972	Flood in July, 1983	Flood in July, 1972	Flood in July, 1983	
Case1	×	×	○	○	×
Case2	×	×	△	△	×
Case3	×	×	△	○	×
Case4	△	△	○	○	○

4 Consideration on lodging situation of flood defense forest

4.1 Consideration lodging from the flood in July, 1987

In this chapter, a 2-D shallow-water flow model was constructed for flood mitigation in July, 1983, where lodging data from the flood protection forest after flooding is available. In order to reproduce the flow condition at the time of the flood in July, 1983, topography data was created using survey results immediately after the flood. The range of the flood defense forest was set from aerial photographs taken in 1987 after the flood. In the target section (20 km to 30 km) of this study, the dike was not developed in all the areas, so it became a unified flow with the floodplain, damages such as house flooding, erosion / sedimentation of flood plains, collapse of protection banks, and the flood defense forest lodged. Fig. 6 shows the aerial photographs after the flooding (shot in 1988) and the lodging situation of the flood defense forest at the flood in July, 1983 (March, 1984 survey).

Based on the model and flooding, the bending stressed acting on flood defense forest was calculated. The bending stress, σ_f acting on the flood defense forest and the bending stress, σ_b from the bamboo material property test result were compared and the threshold value for lodging was evaluated. The bending stress degree, σ_f acting on the flood defense forest is given by Eq. [9].

$$\sigma_f = \frac{M}{W} \qquad [9]$$

where, M is the external force moment and is given by Eq. [10] using water depth and flow rate obtained from hydraulic analysis. W is the section modulus, obtained from the bamboo diameter as shown in Eq. [11].

$$M = \frac{1}{2}\rho C_D S u^2 L \qquad [10]$$

where, ρ is water density, C_D is the drag coefficient of the tree, S is the area of action of drag, u is the flow velocity, and L is the length from the center of destruction to the drag center.

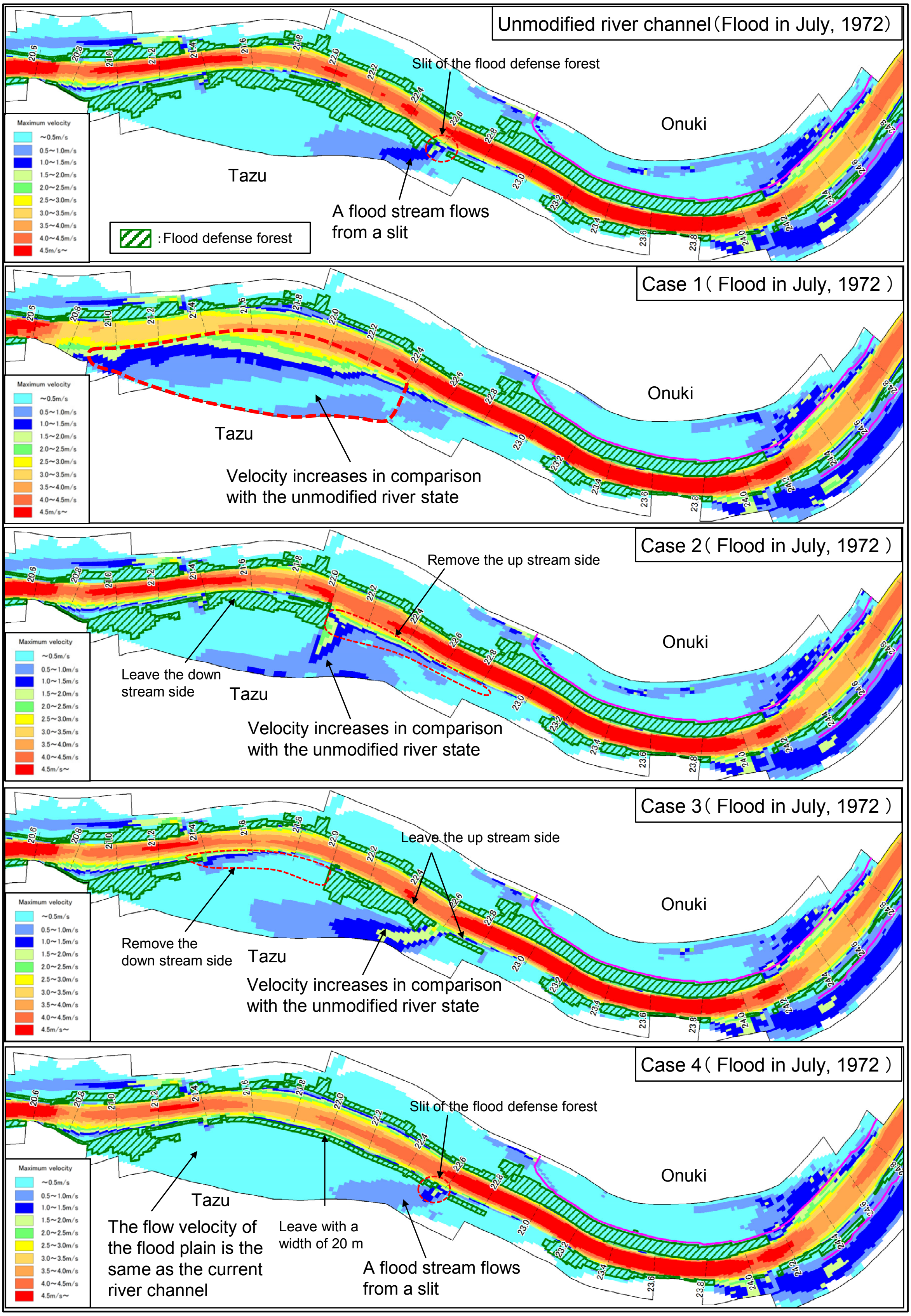

Figure 4. Velocity distribution map of the flood in July, 1972

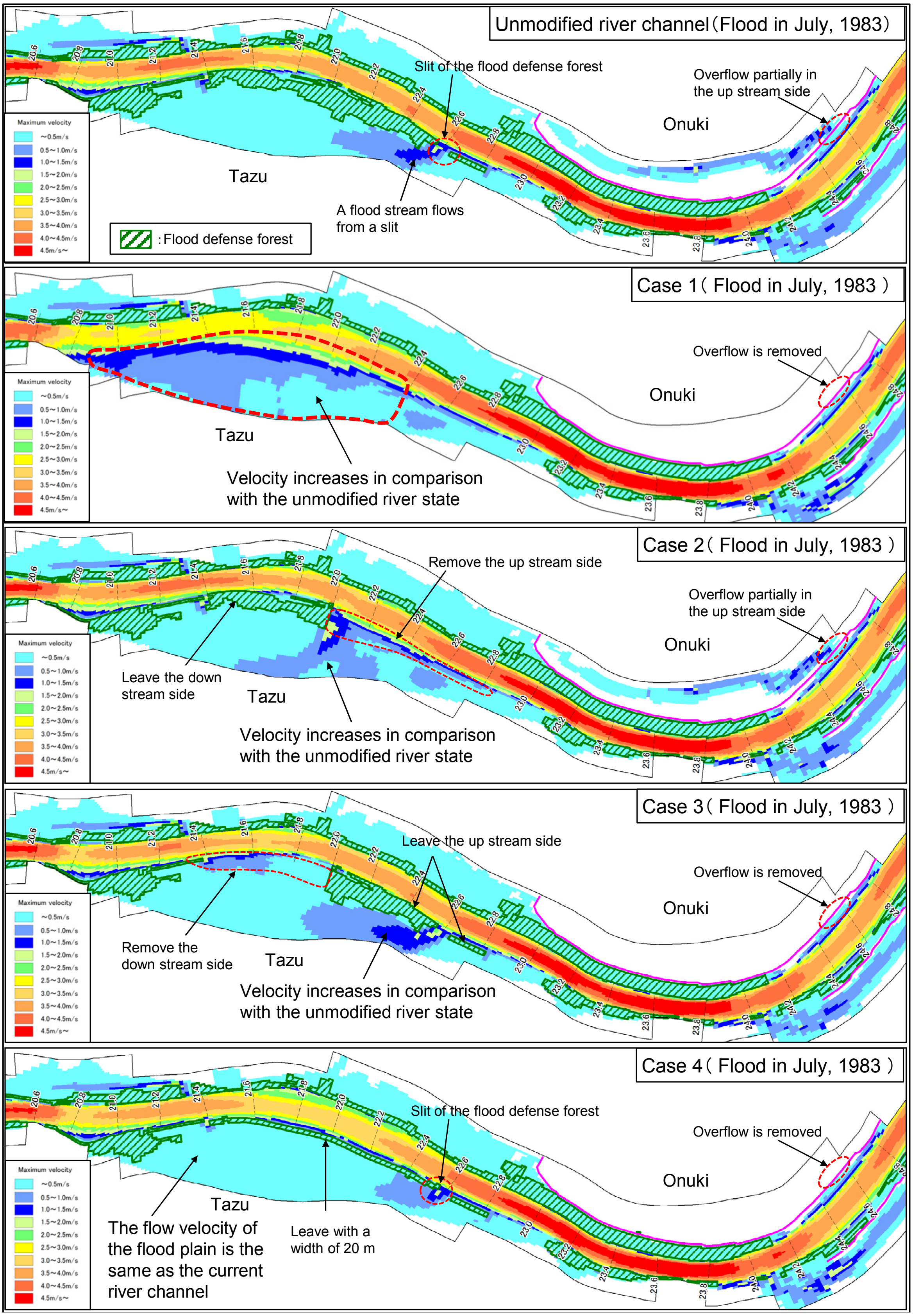

Figure 5. Velocity distribution map of the flood in July, 1983

$$W = \frac{\pi}{32}\frac{D^4 + d^4}{D} \qquad [11]$$

where, D is the bamboo diameter, and d is the bamboo thickness.

The degree of bending stress calculated from the hydraulic quantity for each mesh at the retention and lodging points (refer to Figure 6) of the flood defense forest is shown in Figure 7. The bending stress calculated from the average hydraulic quantity is shown in Table 4. In places where the flood defense forest was dislodged during the July, 1983 flood, the bending stress, σ_f acting on the flood defense forest is greater than the experimentally derived bending stress, σ_b, 6.1 kN/cm^2, of the bamboo. In the areas where trees were not lost during flooding, the bending stress, σ_f acting on the flood defense forest is less than 6.1 kN/cm^2, the stress necessary to bend, break or remove the bamboo. The comparison between flood results and experimental results confirm that 6.1 kN/cm^2 can be used as an index in determining flood defense forest lodging by floods.

4.2 Possibility of lodging the flood defense forest on the current river channel

We conducted a 2-D flow analysis using a probability scale (1/30 to 1/200) on the current river channel and evaluated the flood defense forest situation for the Tazu district, which is an undeveloped embankment area.

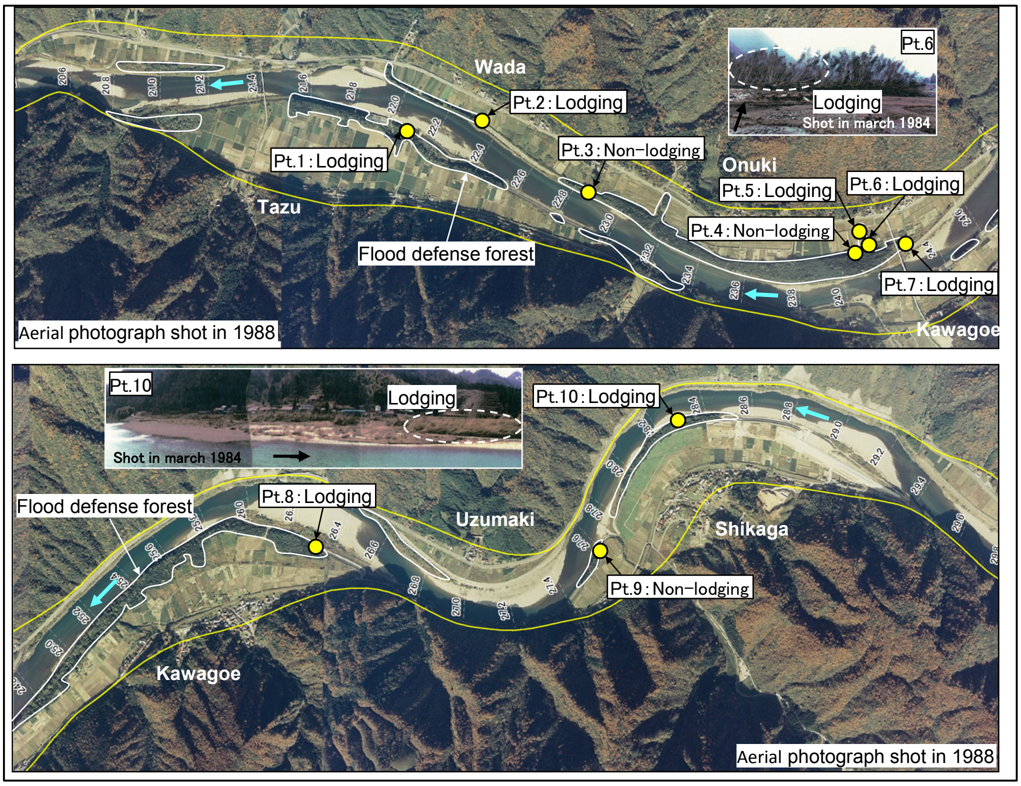

Figure 6. Aerial photograph after flood in July, 1988 and assessment of the flood defense forest after flood

4.2.1 Analysis conditions

For the topography analysis, we used survey results from 2010 and an analysis mesh subdivided to extract hydraulic quantity in the flood defense forest in more detail. For external forces, the water discharge was set using a probability scale (Table 5).

Table 5. Water discharge by probability scale

Return period	Water discharge (m^3/s)	
	Gotsu St.	Target section
1/30	8,300	7,800
1/50	9,300	8,700
1/100	10,700	10,000
1/200	12,500	11,800

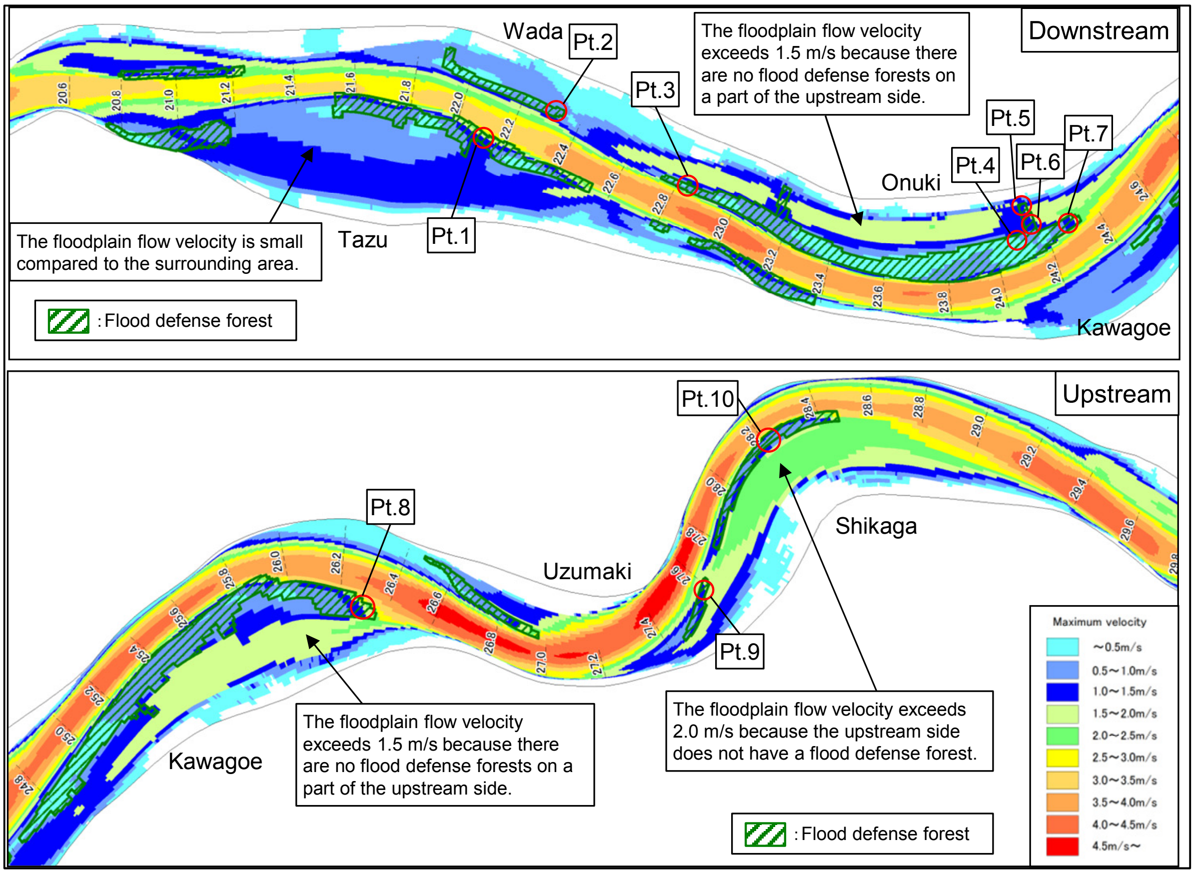

Figure 7. Maximum flow velocity plan from the flood reproduction calculation for July, 1983

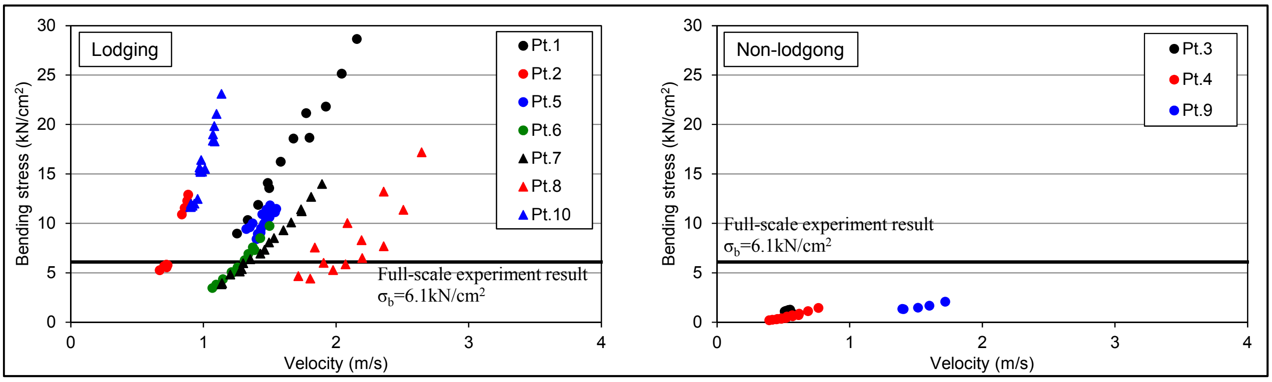

Figure 8. Bending stress level acting on the flood defense forest

Table 4. Bending stress calculated from average hydraulic quantity

Pt.	Position	Lodging situation	Diameter (cm)	Average hydraulic quantity		Bending stress (kN/cm^2)
				Velocity (m/s)	Water depth (m)	
1	Left bank 22.1 km	Lodging	12	1.66	13.04	16.9
2	Right bank 22.4 km	Lodging	6	0.78	9.55	8.0
3	Right bank 22.8 km	Non-lodging	6	0.54	4.81	1.0
4	Right bank 24.0 km	Non-lodging	6	0.54	3.53	0.5
5	Right bank 24.1 km	Lodging	6	1.45	5.80	10.2
6	Right bank 24.1 km	Lodging	6	1.28	5.02	5.9
7	Right bank 24.3 km	Lodging	6	1.48	4.92	7.6
8	Left bank 26.4 km	Lodging	9	2.13	5.22	7.9
9	Left bank 27.6 km	Non-lodging	12	1.53	4.31	1.6
10	Left bank 28.2 km	Lodging	6	1.00	15.54	15.5

4.2.1 Analysis results

In the probability scales of 1/30 and 1/50, the fluid force acting on the flood protection forest is small, so it is estimated that the flood defense forest will not be dislodged except for a part of the low flow channel side. Since the retention range of the flood defense forest continues in the longitudinal direction, it is possible to utilize the flow velocity reduction effect from the flood defense forest.

With a probability scale of 1/100, there is a possibility that the width of the slit upstream of the flood defense forest will expand due to forest lodging. One issue with the flood defense forest in the lower reach of the Gounokawa River is that the local flood plain flow velocity will increase due to the flow inundation from the slit on the upstream side. If the slit width expands due to the bamboo lodging, additional flood flows may increase the floodplain flow rate.

On the probability scale of 1/200, there is a possibility that the flood defense forest on the upstream side is totally lodged. In addition, because approximately 3/4 of the flood defense forest in the Tazu district is lodged, there is a possibility that the flow rate reduction effect from the flood defense forest will be lost.

When the flood defense forest is left with a width of 20 m, even if the same water discharge flows compared with the current width, it is considered that the lodging area ratio increases because the width of the flood defense forest is narrow.

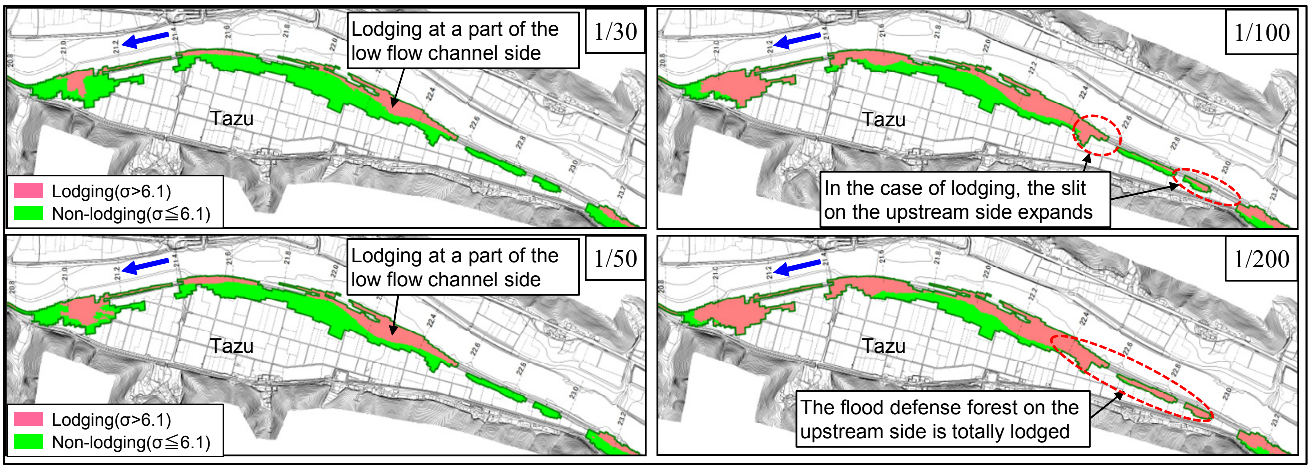

Figure 9. Plan view of lodging situation of flood defense forest (current width)

Table 6. Lodging area of flood defense forest

Return period	Area (ha)		Ratio	
	Lodging	Non-lodging	Lodging	Non-lodging
1/30	4.02	9.94	28.8%	71.2%
1/50	5.52	8.45	39.5%	60.5%
1/100	8.35	5.62	59.8%	40.2%
1/200	10.09	3.87	72.3%	27.7%

5 CONCLUSIONS

We were able to confirm the effectiveness of flood defense forests for cases where the forest widths are more than 20 m. The growth range and width are important factors in flood control and we examined the management policy that can be utilized to improve river protection and security.

In floods with high flood discharge, the numerical analysis results showed that more than half of flood defense forests are lodged, and the water velocity within the floodplain increases. When the flood defense forests are completely bent, damaged or removed, the water velocity in the floodplain is high enough to increase flood hazards. Therefore, it is necessary to manage flood risk assuming flood defense forests are rendered useless in large-scale floods.

We did not consider the influence of river bed fluctuations because we focused on the flow velocity in the floodplain in this study. In order to investigate the influence of the flood plain on sediment deposition in detail, it is necessary to calculate river bed variations.

We investigated flood defense forest lodging effects in the lower reaches of the Gounokawa River for the historical flood in July, 1983, but it is still necessary to investigate future flooding. In addition, gathering and analyzing information concerning flood defense forest behavior during flooding is also important for other rivers.

ACKNOWLEDGEMENTS

We would like to thank the members of the Hamada Office of Ministry of Land, Infrastructure and Transport, Japan for providing the flood data used in this study.

REFERENCES

Yoshino H. (1978). Evaluation of Flood Vontrol Function of Flood Defense Forest. *Civil Engineering Journal,* 20-2, 15-19.

Fukuoka, S., Igarashi, M. & Takahashi, H. (1995). Characteristics of Flood Defense Trees and It Effectiveness to the Flood Control. *Proceedings of Hydraulic Engineering*, 39, 501-506.

Yoshida K., Iizuka S. (2008). Material Characteristics of Bamboo in Yokohama City Area. *Polytechnic Univ. Tokyo School Research Report,* 23, 115-124.

Ministry of Land, Infrastructure and Transport, Japan (1984). *Report of the Gounokawa River Flood Flow Chart*. Ministry of Land, Infrastructure and Transport, Japan

EXPERIMENTAL STUDY OF HYDRAULIC JUMP CHARACTERISTICS IN DIVIDING FLOW OF URBAN STREETS

QI ZHOU [1], CHUNBO JIANG [2], JIAN LIU [3], WANGYANG YU [4] & ALBERT S. CHEN [5]

[1,2,3,4] Department of Hydraulic Engineering, Tsinghua University, Beijing, China,
gfjykldd@gmail.com; jcb@tsinghua.edu.cn; s21liujian@163.com; sea198719@126.com
[5] Center for Water System, University of Exeter, United Kingdom,
A.S.Chen@exeter.ac.uk

ABSTRACT

Urban flood is becoming more severe due to rapid urbanization and global climate change in past decades. High discharge in steep slope environment often causes supercritical flow, which leads to hydraulic jumps around the slope transition area. A simplified physical model was designed to investigate hydraulic jumps under various dividing flow conditions. A series of tests performed inside a circulation water flume, were completed, that covered a range of lateral outflow positions and Froude numbers. Four dividing streets controlled separately, were set on the two sides of the main street. The flow regimes and time averaged water depth profiles under various incoming discharge ratios were obtained. The hydraulic jump characteristics (jump toes, roller length, conjugate depth ratios, etc.), were different from the classical hydraulic jumps. The relationships between conjugate depth, discharge ratios, and dividing flow positions were determined. The obtained experiment data can be readily used for urban cities designs and flood protect policymaking, as well as validating or calibrating numerical models for urban flood simulations.

Keywords: Hydraulic jump; experiment model; dividing flow; urban streets; flood.

1 INTRODUCTION

With the rapid progress of urbanization and global climate change, urban flood events have been occurring more frequently all over the world in recent decades (Bazin et al., 2016). The destructive flood events often cause property losses and casualties (Bellos et al., 2015). Thus, many researchers have done considerable works related to urban flooding. Some of them used either T type or U type simplified physical open channel models (Van et al., 2012; Rivière et al., 2011; El et al., 2011; Mignot et al., 2008; Nanía et al., 2004; Schwalt et al., 1995), others develop 1D or 2D numerical models (Özgen et al., 2016; Bazin et al., 2016; Tsakiris et al., 2014; Huang et al., 2014; Van et al., 2012; Kao et al., 2012), or coupled 1D/2D modeling approaches (Rubinato et al., 2013; Prihoda et al., 2012; LaRocque et al., 2012; Mignot et al., 2008). In actual urban environment, steep streets are inevitable situations, which lead to occurrences of hydraulic jump once water flows into another horizontal street (Nanía et al., 2004). The flow patterns of hydraulic jumps always present three dimensional structure and highly turbulent flow structure which make it difficult to study the detailed characteristics (Bayon et al., 2016). Despite of the various results, researchers always treat the streets as equal depth open channels and rarely focus on the hydraulic jumps formed in streets. However, since urban design and streets distribution are often different from case to case, results from previous researches cannot apply to all cases. The present paper aims to investigate the flow characteristics of hydraulic jump under urban streets dividing flows. Jump pattern, toe position, roller length and discharge ratio are chosen as the specific parameters. The results obtained can be readily used to calibrate or validate numerical models and improve the accuracy of urban flood models as well.

2 Experiment setup

All test cases were conducted in laboratory of Hydraulic Engineering Department of Tsinghua University. Fig.1~Fig.3 show schematically the water recirculating flume which is 18m long, 0.8m wide and 0.8m high. Incoming flow driven by a centrifugal pump controlled by a varied frequency transducer from the water recirculation tank is recirculated in the flume system. The pump can provide a maximum discharge rate of 138L/s. Two continuous honeycomb steel plates were positioned ahead of the flume to make the incoming flow smoothly. Downstream water depth in main flume was controlled by a tailgate driven by an electrical motor.

A 3% slope bottom bed was designed to produce upstream supercritical flow. The slope section is 8m in length, which makes it long enough for the upstream flow to reach steady state and the flow can be treated as uniform flow at the slope changing point. Around test section area, 4 flow dividing gate (0.2m width) on each side of the flume were designed symmetrically to simulate the different position of perpendicular cross streets, and the flow in the main flume can be split by opening the gates to simulate the flow movement into side streets. The ratio of dividing streets width to main streets is 1/4.

There were 6 Ultrasonic Water Level Sensors (WL705-003) setting along the lead rails. Two sensors were fixed at specific point on the rail used to record upstream and downstream water depth, and the others were moveable along the rail and were used to record transient water depth at different centerline positions. The flow discharge in the main flume and each side flume were all recorded by real-time magnetic flow meters.

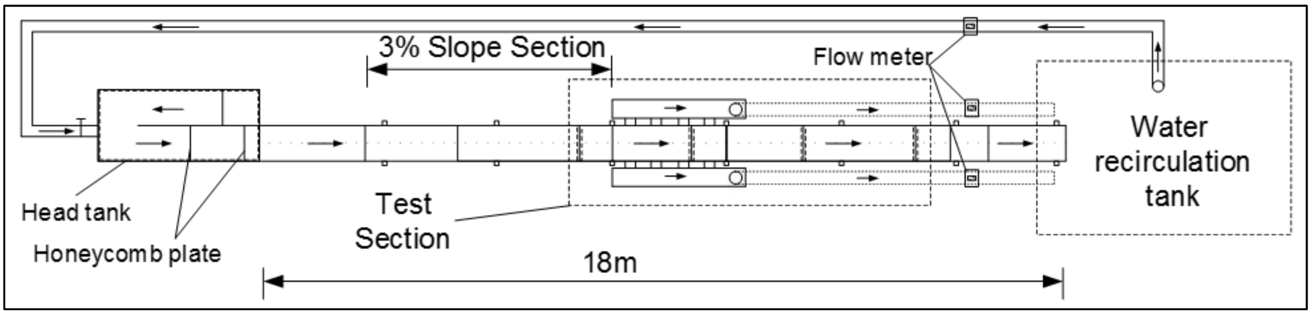

Figure 1. Flume control system

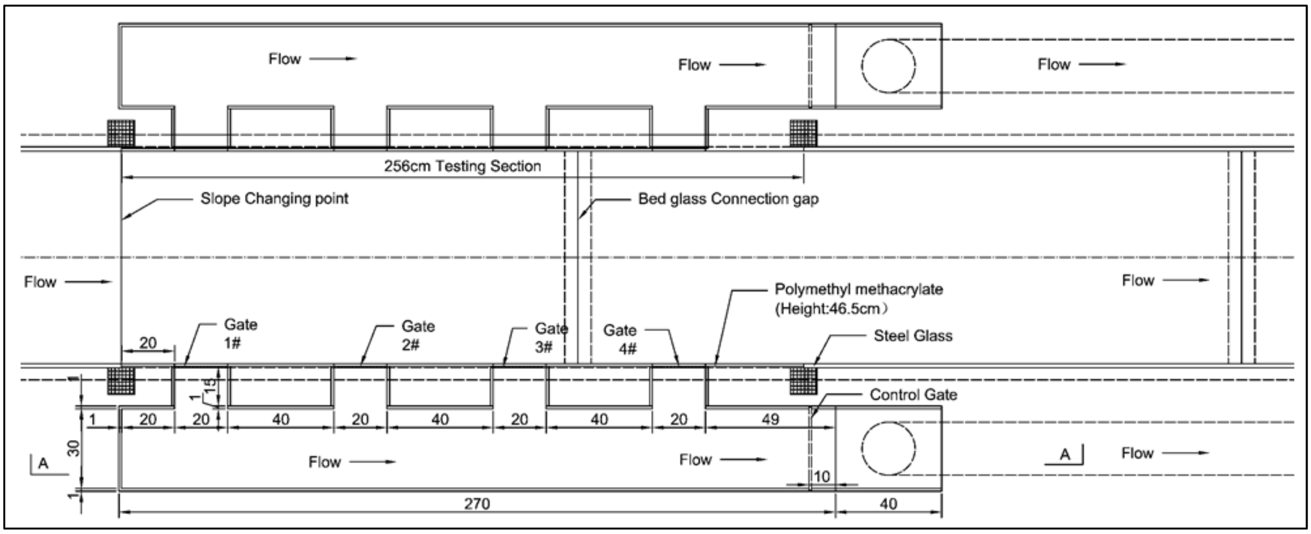

Figure 2. Side streets configuration (unit: cm)

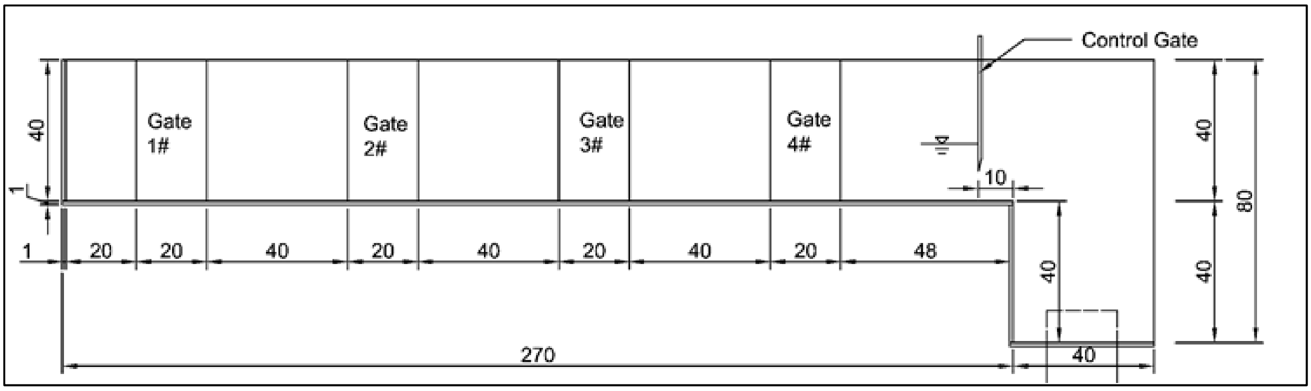

Figure 3. Side View of A-A (unit: cm)

The coordinate origin was set at the middle point of the bed slope changing line. Let x denote the flow direction along the center line of the main flume and y denote from right to left vertical the x in horizontal plane. The discharge, velocity, depth of incoming flow and the corresponding Froude Number are represented as Q, h_1, V_1, Fr_1, respectively. While C001, C002, C003, C004 indicate different dividing flow positions cases with no open gate, gates 1# open, gates 2# open gates 3# open and gates 4# open, respectively. Gates on both sides were controlled synchronously for each test case. In order to study the characteristics of hydraulic jumps in dividing flow, six upstream flow discharge cases were proposed. Table1 shows the detail incoming discharge ratio and corresponding flow parameters. Thus, there were 5×6=30 test scenarios in total.

Table 1 Incoming flow conditions

Test Index	**Q ($10^{-3}m^3/s$)**	**h_1 (cm)**	**V_1 (m/s)**	**Fr_1**
Q_1	1.5667	3.394	1.2282	3.1059
Q_2	2.1852	4.237	1.3986	3.1953
Q_3	2.8476	5.055	1.5498	3.2650
Q_4	3.3468	5.630	1.6495	3.3070
Q_5	4.2275	6.578	1.8044	3.3665
Q_6	5.2562	7.606	1.9610	3.4205

3 Results and Discussion

3.1 Time-Averaged Water depth profiles

Water depth plays a crucial role in the protection of people and properties under urban flooding events. Figure 4 to Figure 9 show the time averaged water depth profiles along the main flume center line. From the figures, it can be seen that the jump toes were almost vertical to the flow direction and the position of the hydraulic jump nearly depend on the dividing flow position except for few cases. It was found that under low incoming upstream discharge, such as Q_1 and Q_2, the jump did not occur at the open gates. For C003 and C004, the flow presented a deflect pattern with a large flow recirculation area following the jump. The dividing discharge on the side of the recirculation zone is much larger than the discharge on the other side. However, with the increasing of upstream discharge, the jumps occurred around the gate and presented two different roller pattern types under specific flow conditions, especially for C004.

Figure 10 illustrates both roller types. Roller type 1 is the same as classical hydraulic jump with highly air entrainment and gradually increasing depth, while the type 2 roller is similar to undular jump with a smooth crest and a following water impinging. The transition from type 1 to type 2 is related to the incoming flow discharge and the position of dividing flow. The determination of the specific transitional point needs further study and analysis. It was observed that there is no type 2 roller pattern that occurred for C001 and C002, while it is more likely to occur for C004, which means the occurring of type 2 roller pattern is related to the position of dividing flow.

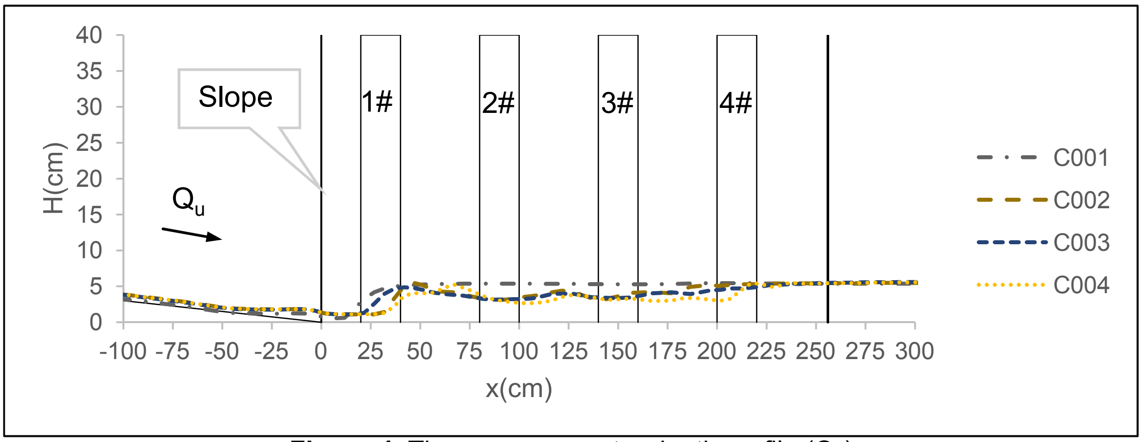

Figure 4. Time average water depth profile (Q_1)

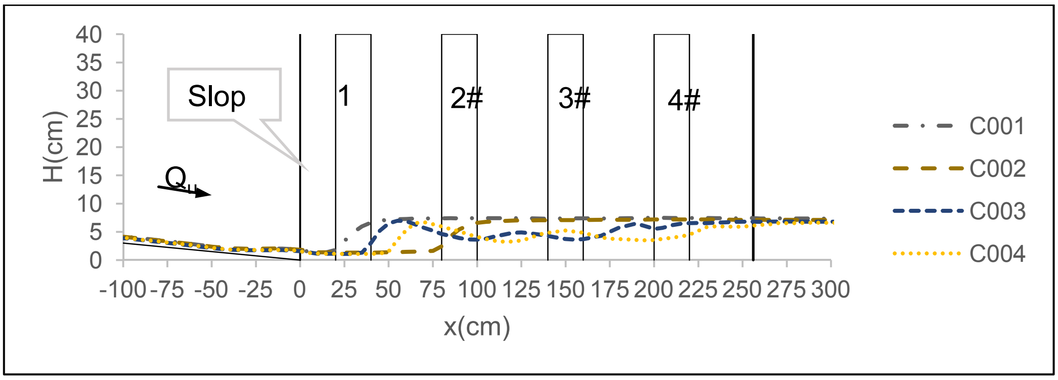

Figure 5. Time average water depth profile (Q_2)

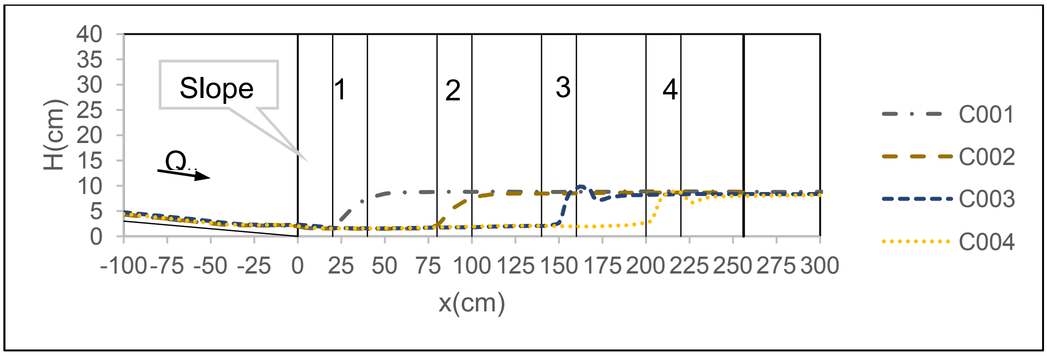

Figure 6. Time average water depth profile (Q_3)

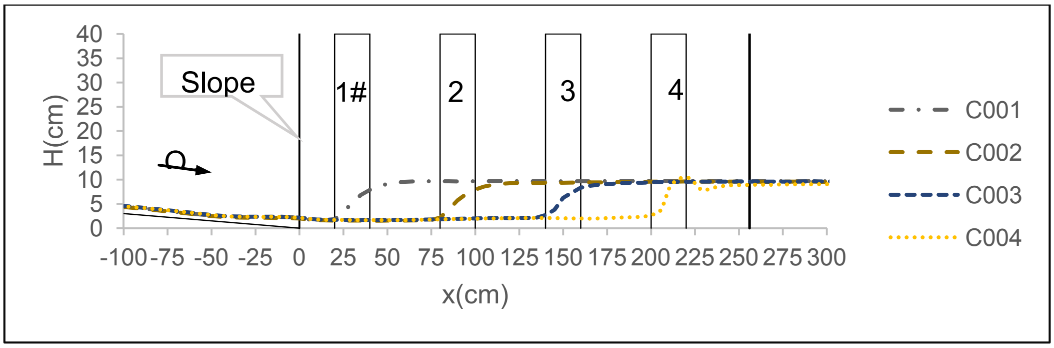

Figure 7. Time average water depth profile (Q_4)

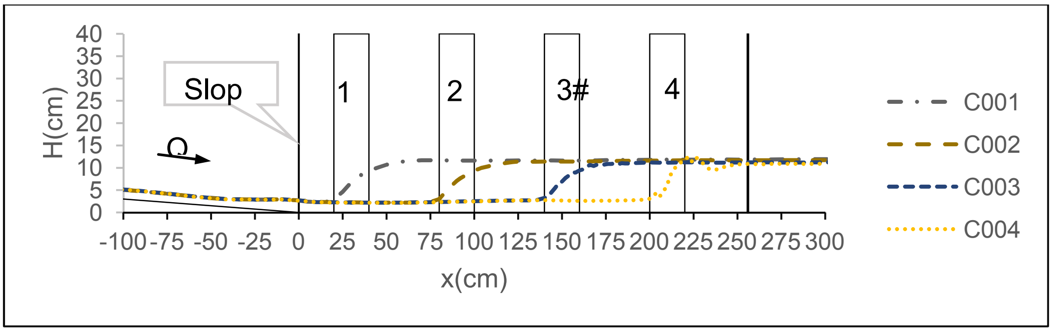

Figure 8. Time average water depth profile (Q_5)

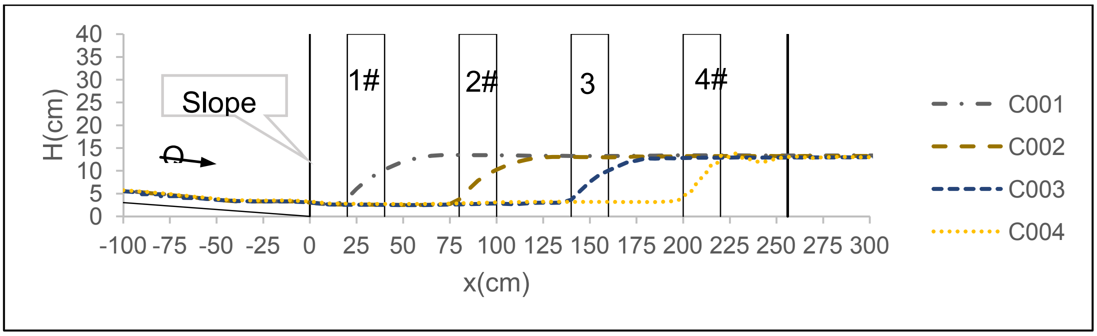

Figure 9. Time average water depth profile (Q_6)

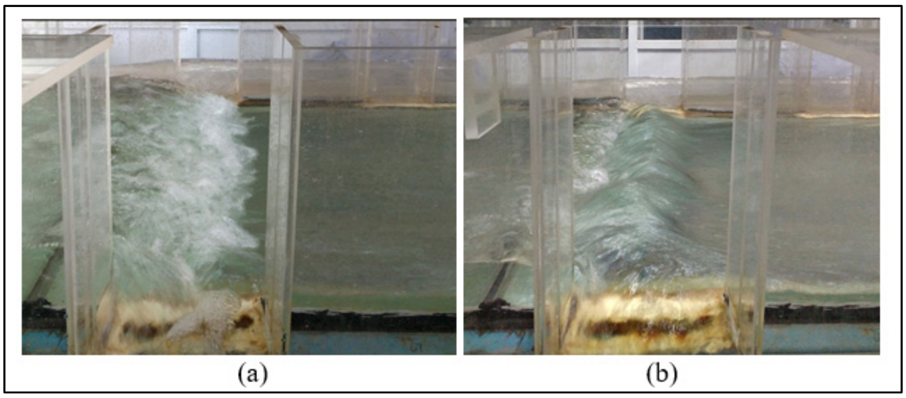

Figure 10. Roller types (a. type 1; b. type 2)

3.2 Roller length

The results of roller length are shown in Figure 11. The roller was almost confined in a unit side street width around each gate and larger length was kept with increasing upstream discharge for C003 and C004. The roller length under C003 and C004 was much more different from C001 and C002 for the occurring of type 2 roller pattern as stated in previous section. The roller length of type 2 roller pattern was relatively larger than type 1 under the same flow condition.

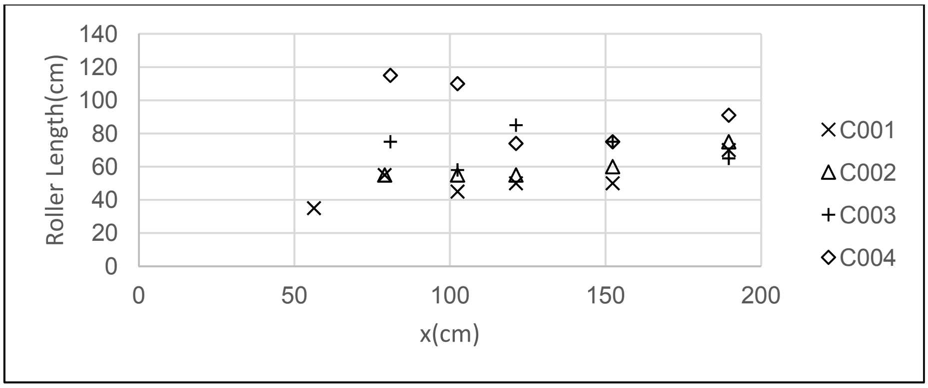

Figure 11. Roller length under different inflow discharge

3.3 Depth ratio

The depth ratio, □ was defined as downstream water depth to the depth at jump toe point. Figure 12 shows the results of depth ratio under all test cases. According to the figure, it is indicated that the four positions of dividing flow can be divided into 2 groups, C001 and C002 as group 1, C003 and C004 as group 2. The depth ratio for group 1 is about 5.5 when the incoming discharge is less than 125m^3/h and is almost the same for gate 1# and gate 2# when incoming discharge is above 125m^3/h. The same case is applied to group 2 except for the discharge 100m^3/h as the transition point. It can be concluded that depth ratio would be nearly steady with larger incoming discharge and dividing flow position farther from the slope changing point.

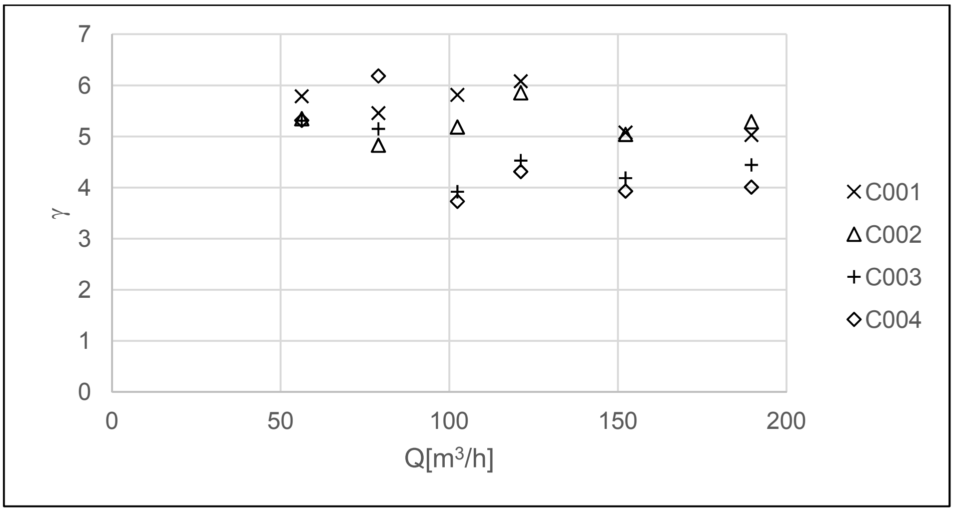

Figure 12. Depth ratio under different inflow discharge

3.4 Discharge ratio

Figure 13 shows the relationship between main discharge and dividing flow ratio for different side gate open scenarios. The discharge ratio, □ was defined as dividing discharge to upstream discharge. It can be seen that the discharge ratio is descending with larger upstream flow discharge despite of the dividing flow position. The relationship varied for specific dividing flow position. More test cases need to be done in order to determine the roller pattern transition position.

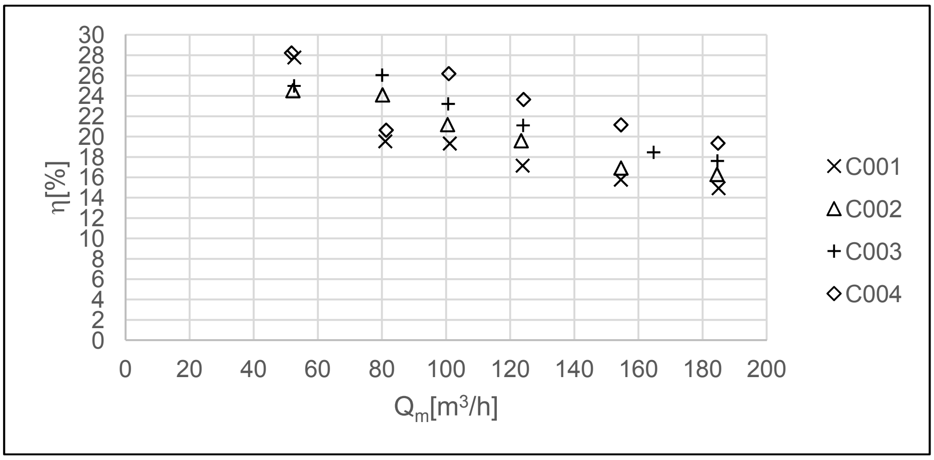

Figure 13. Discharge ratio under different side gate opening

4 CONCLUSIONS

A simplified physical urban streets model was designed to study the characteristics of hydraulic jump with dividing flow. A series of tests performed inside a flume were completed which covered a range of dividing flow positions and Froude numbers. Time averaged water depth, roller length, depth ratio and discharge ratios were obtained. Two types of roller patterns were found depend on the specific flow conditions. The obtained experimental data can be readily used for urban street designs and policy making for flood protection, as well as calibrating and validating numerical models for urban flood simulations.

Since the results were obtained under fixed tailgate opening, the relationship between downstream depth and tailgate opening may change with different tailgate opening. Thus, further study should take these aspects into consideration.

ACKNOWLEDGEMENTS

This research was supported by National Natural Science Foundation of China (Grant NO. 51679121) and the International Exchange Scheme co-funded by National Natural Science Foundation of China (Grant NO. 51511130073) and the Royal Society, UK (Ref IE140883).

REFERENCES

Bayon, A., Valero, D., García-Bartual, R. & López-Jiménez, P. A. (2016). Performance Assessment of Open FOAM and FLOW-3D in the Numerical Modeling of a Low Reynolds Number Hydraulic Jump. *Environmental Modelling & Software,* 80, 322-335.

Bazin, P. H., Mignot, E. & Paquier, A. (2016). Computing Flooding of Crossroads with Obstacles Using a 2D Numerical Model. *Journal of Hydraulic Research*, 1-13.

Bellos, V. & Tsakiris, G. (2015). Comparing Various Methods of Building Representation for 2D Flood Modelling in Built-up Areas. *Water Resources Management*, 29(2), 379-397.

El Kadi Abderrezzak, K., Lewicki, L., Paquier, A., Rivière, N. & Travin, G. (2011). Division of Critical Flow at Three-branch Open-channel Intersection. *Journal of Hydraulic Research*, 49(2), 231-238.

Huang, C. J., Hsu, M. H., Chen, A. S. & Chiu, C. H. (2014). Simulating the Storage and the Blockage Effects of Buildings in Urban Flood Modeling. *Terrestrial, Atmospheric & Oceanic Sciences*, 25(4), 591-604.

Kao, H. M. & Chang, T. J. (2012). Numerical Modeling of Dambreak-induced Flood and Inundation Using Smoothed Particle Hydrodynamics. *Journal of hydrology*, 448, 232-244.

LaRocque, L. A., Imran, J. & Chaudhry, M. H. (2012). Experimental and Numerical Investigations of Two-Dimensional Dam-break Flows. *Journal of Hydraulic Engineering*, 139(6), 569-579.

Mignot, E., Paquier, A. & Rivière, N. (2008). Experimental and Numerical Modeling of Symmetrical Four-branch Supercritical. *Journal of Hydraulic Research*, 46(6), 723-738.

Mignot, E., Rivière, N., Perkins, R. & Paquier, A. (2008). Flow Patterns in a Four-branch Junction with Supercritical Flow. *Journal of Hydraulic Engineering*, 134(6), 701-713.

Nanía, L. S., Gómez, M. & Dolz, J. (2004). Experimental Study of the Dividing Flow in Steep Street Crossings. *Journal of Hydraulic Research*, 42(4), 406-412.

Özgen, I., Liang, D. & Hinkelmann, R. (2016). Shallow Water Equations with Depth-dependent Anisotropic Porosity for Subgrid-scale Topography. *Applied Mathematical Modelling*, 40(17), 7447-7473.

Prihoda, J. & P. Zubik, et al. (2012). Experimental and Numerical Modelling of Turbulent Flow Over an Inclined Backward-facing Step in an Open Channel. *Komunikacie*, 14(4 A), 6-12.

Rivière, N., Travin, G. & Perkins, R. J. (2011). Subcritical Open Channel Flows in Four Branch Intersections. *Water Resources Research*, 47(10).

Rubinato, M., Shucksmith, J., Saul, A. J. & Shepherd, W. (2013). Comparison between InfoWorks Hydraulic Results and a Physical Model of an Urban Drainage System. *Water Science and Technology*, 68(2), 372-379.

Schwalt, M. & Hager, W. H. (1995). Experiments to Supercritical Junction Flow. *Experiments in Fluids*, 18(6), 429-437.

Tsakiris, G. & Bellos, V. (2014). A Numerical Model for Two-dimensional Flood Routing in Complex Terrains. *Water resources management*, 28(5), 1277-1291.

Van Emelen, S., Soares-Frazão, S., Riahi-Nezhad, C. K., Hanif Chaudhry, M., Imran, J. & Zech, Y. (2012). Simulations of the New Orleans 17th Street Canal Breach Flood. *Journal of Hydraulic Research*, 50(1), 70-81.

NUMERICAL MODELING OF LANDSLIDE AND LANDSLIDE GENERATED WAVES IN RESERVOIR

RADIANTA TRIATMADJA[(1)], NURUL AZIZAH[(2)] & BENAZIR[(3)]

[(1,2,3)] Department of Civil and Environmental Engineering, Faculty of Engineering and Tsunami Research Group, Universitas Gadjah Mada, Indonesia
radianta@ugm.ac.id, nururu.azizah@gmail.com:benazir_27iska@yahoo.com

ABSTRACT

Karalloe dam is in the progress of construction. It is located in the District of Gowa of South Sulawesi Province. The dam is intended to store water for irrigation and domestic water purposes. Visually there are three zones of potential landslides at the embankment of the reservoir especially during high water level (Wijaya, et al., 2016). The potential landslide volume was 2.53 million m^3 at Zone 1, 0.83 million m^3 at Zone 2, and 0.3 million m^3 at Zone 3. During rainy seasons when the water in the reservoir is high or even if it reaches the maximum allowable elevation, these areas of the reservoir slopes may slide down and enter the water creating tsunami like waves. Wijaya et al. (2016) indicated that the areas are nearly unstable during reservoir high water with the safety factor of less than 1.5 based on SLOPE/W software. This safety factor is considered insufficient especially with additional load due to rainstorm that makes the slope even less stable. Therefore, it is essential to carry out studies to identify the hazards that the landslide may create for necessary mitigation of the flood disaster. The aim of the research is to simulate the landslide and landslide generated wave in the Karalloe reservoir to observe its possible run-up and overtopping on the dam body. The landslide movement was modeled based on Wang and Sassa (2010). The movement of the landslide front followed the dry and wet scheme by Goto et al. (1997).

Keywords: Landslide modeling; landslide generated wave; flood mitigation; numerical method; dam safety.

1 INTRODUCTION

A number of landslides into reservoirs have caused disasters, especially in the downstream areas. The huge amount of rock or soil mass that entered the reservoirs has created giant waves that propagated towards and overtopped the dam crest. The overtopping flow of water caused severe flooding downstream. When the dam is an earth filled type, the overtopping may also endanger and break the dam body which may result in more catastrophic disasters. Even if the dam is not damaged by the overtopping such as that happened in Vaiont Valley reservoir in 1963, the flash flood with extremely high peak hydrograph was catastrophic and killed about 3000 people (Kiersch, 1964). There were mass materials of approximately 270 million m^3 that entered the Vaiont reservoir (Genevois & Ghirotti, 2005). The depth and the speed of the water that rush downstream may destroy everything in its path. A number of landslides generated waves in the reservoir have been conducted for example by Chaudry et al. (1983), Townson and Kaya (1988), Triatmadja (1990) and Wijaya et al. (2016). Although the last three authors have been able to simulate the resulted waves using numerical simulations, they have assumed the process of the landslide as the input of the simulation which could have significantly affected the resulting waves. Wang and Sassa (2010) proposed a numerical model of landslide movement. The model is based on momentum and continuity equations and the effect of mechanical and dynamical parameters of the landslides. The model output may be used as an input for the hydrodynamic model to simulate the resulting wave when the landslide enters the water.

Karalloe dam in the District of Gowa of South Sulawesi Province, Indonesia is under construction. The dam is aimed at storing water for irrigation and domestic water purposes. Based on the design plan, Karalloe dam is 396 m long and 8 m wide of dam crest at an elevation of +253 m above sea level. Visually there are three zones of potential landslides at the embankment of the reservoir especially during high water level (Wijaya, et al., 2016). The potential landslide volume was 2.53 million m^3 at Zone 1, 0.83 million m^3 at Zone 2, and 0.3 million m^3 at Zone 3 as shown in Figure 1. During rainy seasons when the water in the reservoir is high or even reach the maximum allowable elevation, these areas of the reservoir slopes may slide down and enter the water creating tsunami like waves. Wijaya et al. (2016) indicated that the areas are nearly unstable during reservoir high water with the safety factor of less than 1.5 based on SLOPE/W software calculation. This safety factor is considered insufficient especially with additional load due to rainstorm that makes the slope even less stable. Therefore, it is essential to carry out studies to identify the hazards that the landslide may create and how to mitigate the flood disaster.

Wijaya et al. (2016) have actually simulated the landslide generated wave at Karalloe reservoir. However, they have simplified the landslide where the landslide was straight along one direction as shown in Figure 1, which is not according to the natural topography of the dam area. They also have simplified and assumed the thickness, speed, and the extension of the slide while keeping the slide mass conserved. The simplification may have resulted in inaccurate prediction of landslide generated wave due to different landslide speed, thickness and the extent of the landslide. The aim of the research is to simulate the landslide and used the result as an input to simulate landslide generated wave in the Karalloe reservoir to observe its possible run-up and overtopping on the dam body.

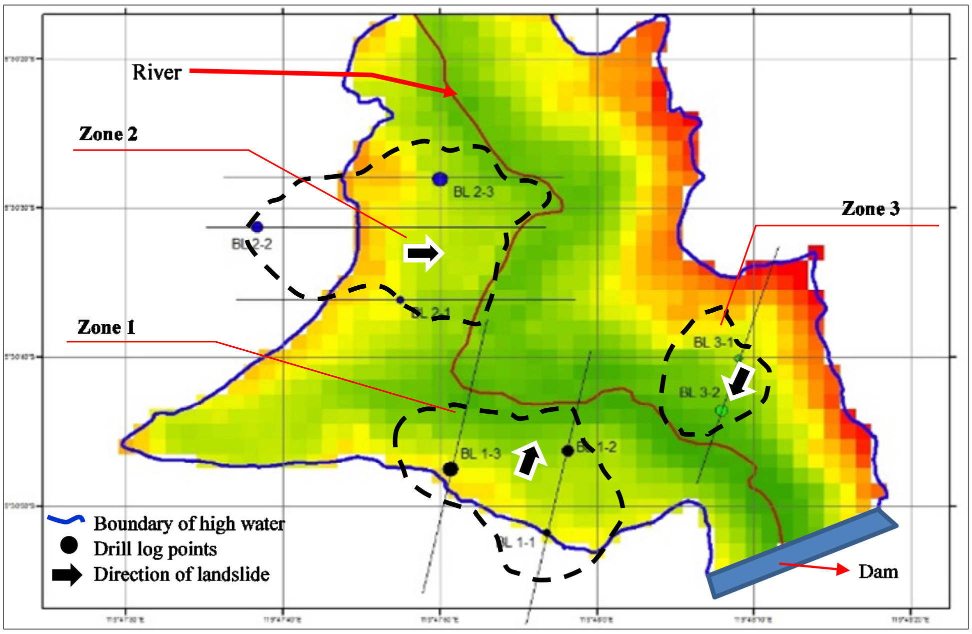

Figure 1. Karalloe reservoir and location of potential landslide zones (Wijaya et al., 2016).

2 RESEARCH METHOD

The landslide model was based on Wang & Sassa (2010) by using the following equations. In those equations, h_s is the thickness of the sliding mass, u, v, and w is the velocity in x, y, and z direction respectively, $M = uh_s$ and $N = vh_s$ where N and M are discharge in x and y direction per unit width. Then, k stands for lateral earth pressure coefficient, $\tan \emptyset_a$ is apparent friction coefficient of soil in the sliding zone, $\tan\alpha$ and $\tan\beta$ are inclination of the intersection between the original slope surface and the xy plane and yz plane, $q = \tan^2\alpha + \tan^2\beta$, and h_c as cohesion head.

$$\frac{\partial \eta}{\partial t} + \frac{\partial M}{\partial x} + \frac{\partial N}{\partial y} = 0 \qquad [1]$$

$$\frac{\partial M}{\partial t} + \frac{\partial}{\partial x}(uM) + \frac{\partial}{\partial y}(vM) = gh_s\frac{\tan\alpha}{q+1} - kgh_s\frac{\partial h_s}{\partial x} - \frac{g}{(q+1)^{1/2}}\frac{u}{(u^2+v^2+w^2)^{1/2}}\{h_c(q+1) + h_s\tan\emptyset_a\} \qquad [2]$$

$$\frac{\partial M}{\partial t} + \frac{\partial}{\partial x}(uN) + \frac{\partial}{\partial y}(vN) = gh_s\frac{\tan\beta}{q+1} - kgh_s\frac{\partial h_s}{\partial y} - \frac{g}{(q+1)^{1/2}}\frac{v}{(u^2+v^2+w^2)^{1/2}}\{h_c(q+1) + h_s\tan\emptyset_a\} \qquad [3]$$

Wave propagation in the reservoir was simulated using a set of nonlinear shallow water equation in the Cartesian coordinate system which usually used in tsunami model. This tsunami model was originally developed by Goto et al. (1997) and Imamura et al. (2006) and it is also known as TUNAMI Model and it is widely used in recent tsunami modeling topics.

$$\frac{\partial \eta}{\partial t} + \frac{\partial M}{\partial x} + \frac{\partial N}{\partial y} = 0 \qquad [4]$$

$$\frac{\partial M}{\partial t} + \frac{\partial}{\partial x}\left(\frac{M^2}{D}\right) + \frac{\partial}{\partial y}\left(\frac{MN}{D}\right) + gD\frac{\partial \eta}{\partial x} + \frac{1}{2}\frac{f}{D^2}M\sqrt{M^2+N^2} = 0 \qquad [5]$$

$$\frac{\partial M}{\partial t} + \frac{\partial}{\partial x}\left(\frac{MN}{D}\right) + \frac{\partial}{\partial y}\left(\frac{N^2}{D}\right) + gD\frac{\partial \eta}{\partial y} + \frac{1}{2}\frac{f}{D^2}N\sqrt{M^2+N^2} = 0 \qquad [6]$$

$D = h + \eta$ is the total water depth, where h is the still water depth and η is the sea surface elevation. M and N are the water velocity fluxes in the x and y directions, respectively.

$$M = \int_h^\eta udz = u(h+\eta) = uD \qquad [7]$$

$$N = \int_h^\eta v dz = v(h+\eta) = vD \quad [8]$$

Bottom friction in the x and y direction are respectively represented by last terms in Eq. [5] and [6] which are a function of friction coefficient$f$. This coefficient can be computed from Manning roughness n by the following relationship

$$n = \sqrt{\frac{fD^{1/3}}{2g}} \quad [9]$$

Eq. [9] describes that the friction coefficient increases when the total water depth decreases. Manning roughness was chosen as constant equals 0.01 for landslide above water and 0.10 for landslide underwater. In this study, the dynamic interaction between the sliding material and the water was not accurately simulated but instead, a larger Manning coefficient was employed to accommodate the friction between the landslide and the water.

The area of landslide followed that of Wijaya et al. (2016). Since they found that landslide at Zone 1 had created the largest landslide wave, therefore in this study Zone 1 was selected for simulation. The direction and the slope of the slide were approximated based on Wijaya et al. (2016). The sliding surface was depicted in Figure 2 with $R = 125$ m and was referred to as the Alternative 1.

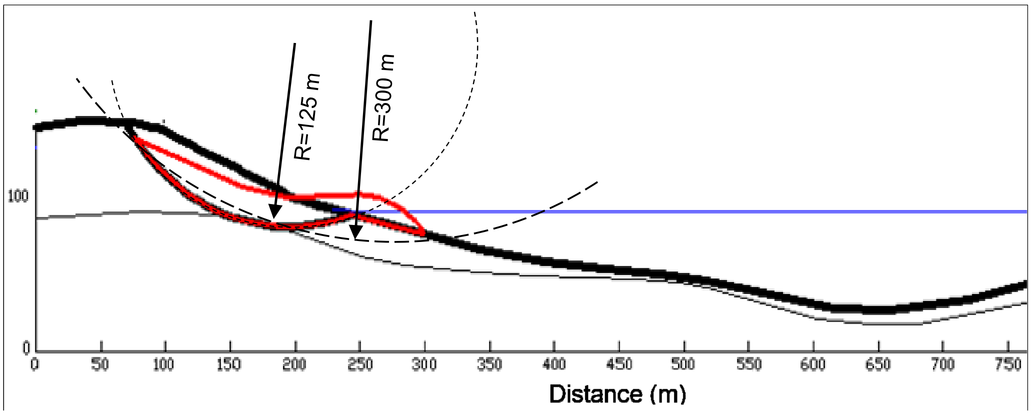

Figure 2. Sliding surface (Wijaya et al., 2016) with $R = 125$ m, and another alternative of possible land slide ($R = 300$ m).

The sliding surface of Figure 2 was based on soil data at one drill log location. It is possible that the position and the size of the landslide may vary when more data is available. Therefore, another possible sliding surface was assumed. This was sliding surface with $R = 300$ m as Alternative 2 and was given in Figure 2. There was not enough geotechnical data for the simulation and hence some of the data were assumed or approximated as follows.

Table 1. Soil properties used for landslide simulations.

$\boldsymbol{k = 0.5}$	$\boldsymbol{tan\,\phi = 0.5}$
$\boldsymbol{Bss = 1.0}$	$\rho = 2.0\ ton/m^3$
$\boldsymbol{\tau = 30\ kPa}$	$c = 3.0\ kPa$

The simulation of wave dynamic was carried out at a domain bounded by 1,880 m by 2,285 m (376 nodes × 457 nodes with the grid size of 5 m). The surface elevation data was obtained from DEM and SRTM 30 and to create more detail data (5 m of grid size) an interpolation was employed. The topography data was adapted to the input program where the elevation was initiated from 248.5 m above sea level (normal water level in the reservoir) to became 0 m and was applied to the entire topography data. The dam and spillway structures were included in the simulation as shown in Figure 3. To accommodate the bottom friction effect a typical value of 0.01 was employed. The time step was chosen as 0.05 sec to satisfy the CFD condition. The propagation of the wave in the reservoir with respect to the volume of slide materials was simulated over the computation domain.The initial condition was varied as follow. First, the elevation of the water was at the spillway crest (Case 1). In this case, the water body in the reservoir was assumed to stand still. The fluctuation of the reservoir bottom due to landslide was then used as an input to trigger the landslide generated waves. Six stations were monitored to observe the water level fluctuation. These were 3 stations along the spillway crest and 3 stations along the dam crest.

The second case was conducted by assuming that the water level at the reservoir was at the level of the maximum probable flood (252.5 m). At such situation, the flow within the reservoir was simulated for 6 minutes before landslide was simulated. At the upstream boundary, the water was made slightly higher (1.0 m) to keep the water close the (252.5 m) since the reservoir was drained through the spillway. With such relatively short time, the water within the reservoir may not be in exactly steady state condition but any fluctuation resulted from the initial condition within the reservoir was expected to be small enough and may be neglegible. In order to simulate the flow over the spillway, the water level at approximately 50 m downstream of the spillway crest was made zero.

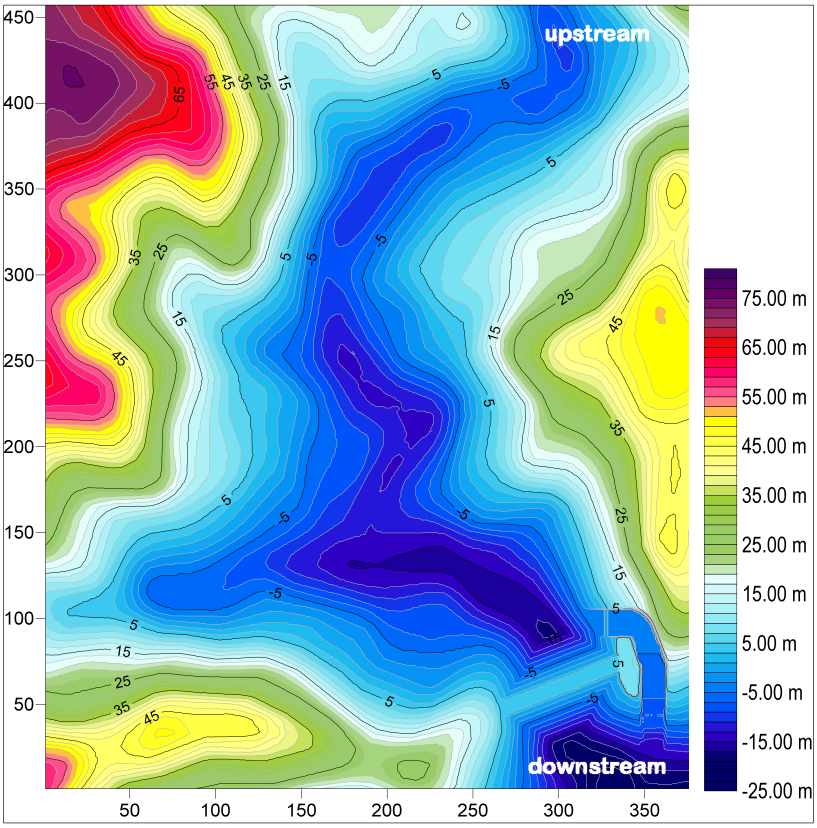

Figure 3. Topography data as simulation area in Cartesian coordinate system.

As describe in the preceding paragraph, there are three zones of potential landslide in the Karalloe dam but only Zone 1 was investigated.

3 RESULT AND DISCUSSION

3.1 Landslide Simulation

The result of the landslide simulation is given in Figure 4. It can be seen that the landslide thickness varied throughout the process of simulation where $R = 125$ m and $R = 300$ m are shown in Figure 4.a-c and Figure 4.d-f, respectively.

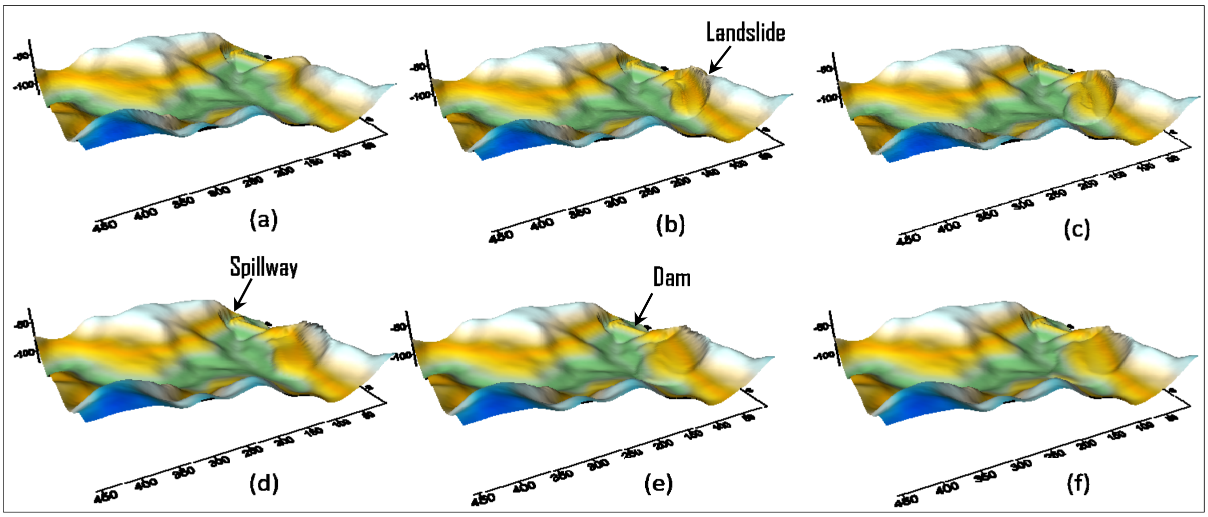

Figure 4. Simulated landslides of first alternative (a) prior to landslide, (b) after 20 seconds and (c) after 40 seconds, second alternative (d) after 20 seconds, (e) after 40 seconds and (f) after 60 seconds.

The sliding slope of Alternative 1 was significantly steeper than that of Alternative 2 as can be seen in both Figure 2 and Figure 4. After 40 seconds, the slide mass moves significantly slower where only those at the bottom of the reservoir can be observed visually. Such slow movement may not significantly contribute to landslide generated waves. The position of the landslide can be seen in Figure 5.

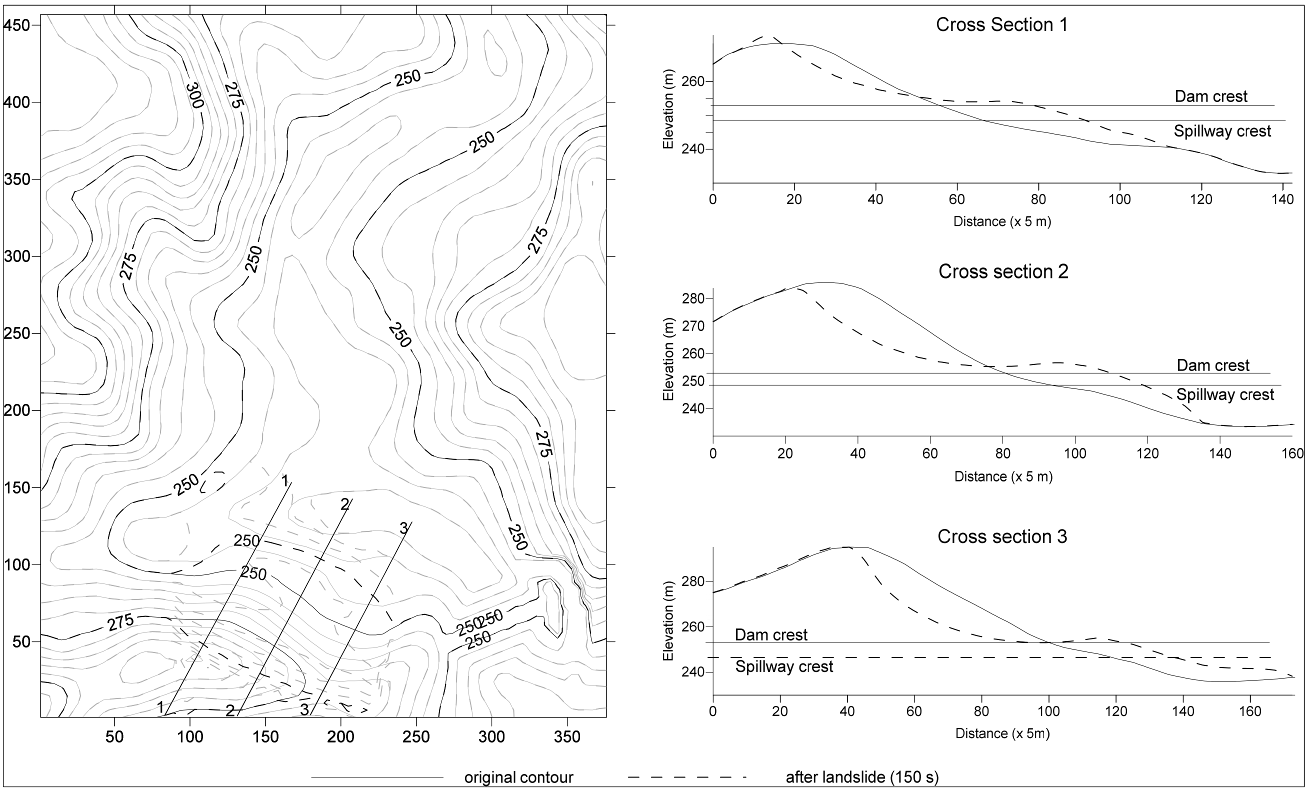

Figure 5. Landslide conditions after 60 seconds. (a) top view and (b) cross section 1, 2 and 3.

The top view of the landslide indicates that the landslide slightly spread to the left direction but mostly went straight down the slope as assumed by Wijaya et al. (2016). The cross section on the right shows that the landslide mass was more or less conserved. The contour of 248.5 m above sea level was the elevation of the spillway crest. Hence, during the simulation with water elevation at spillway crest level (Case 1), not all of the landslide went below the water and hence did not contribute to the landslide generated wave. During the simulation when water level in the reservoir was at 252.5 m, more landslide material was inside the water as indicated in Figure 5, which may generate higher wave. From the cross sections at Figure 5 the landslide move approximately 300 m within 60 seconds. This means that the average sliding velocity was 5 m/s similar to that assumed by Wijaya et al. (2016).

3.2 Wave Simulation

The wave simulation was carried out using the landslide as the input. The fluctuation of the bottom due to landslide was directly converted into additional water surface elevation or reduced water surface elevation depending on whether the bottom fluctuates upward or downward respectively. From the simulation of Case 1, the wave generated overtopped the spillway but was not high enough to overtop the dam crest. As can be seen in Figure 6, the maximum elevation at the spillway was 3 m. Even so, the discharge through the spillway was significantly high which may create flash flood downstream. The discharge through the spillway was approximately based on the flow over a dam crest as in Equation 10.

$$Q = C_d b\, h^{3/2} \qquad [10]$$

where Q (m^3/s)is discharge, C_d is discharge coefficient, b (m) is the width of the weir and h (m) is the water depth above the weir crest. The value of C_d was assumed to be equal to 2.0.

The flash flood in this case should be acceptable in term of discharge since the spillway was designed to flow more than the flash flood (Figure 7). However, it was expected that there will be no warning regarding the flash flood. Such sudden flood, therefore, may result in disaster at downstream.

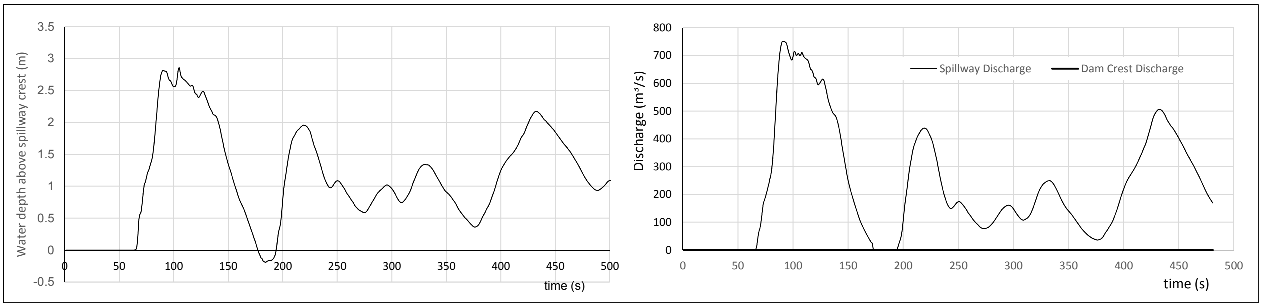

Figure 6. (a) Water depth fluctuations above spillway crest and discharge over spillway crest of Case 1 of Alternative 1.

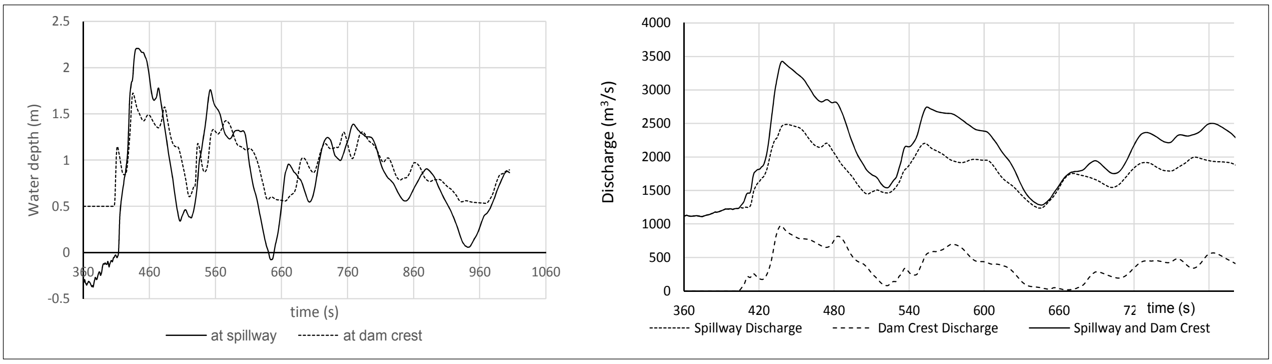

Figure 7. Water depths and discharges through the spillway and over dam crest at Case 2 of Alternative 1.

During the maximum flood (Case 2), wave induced landslide resulted in significantly higher water level as shown in Figure 8. The dam crest was overtopped which creates flooding downstream. There was water fluctuation at the dam crest and the spillway which diminished with time since the displaced water was drained downstream. The spillway discharge was much higher compared to the discharge over the dam crest. The maximum total discharge through the dam and the spillway was more than 4000 m^3/s. The flash flood that was higher than the designed for maximum flood through the spillway lasted for 90 seconds or 1.5 minutes, followed by another flash flood of another 1.5 minutes at lesser discharge and followed by another flash flood of slightly longer duration but at significantly lower discharge.

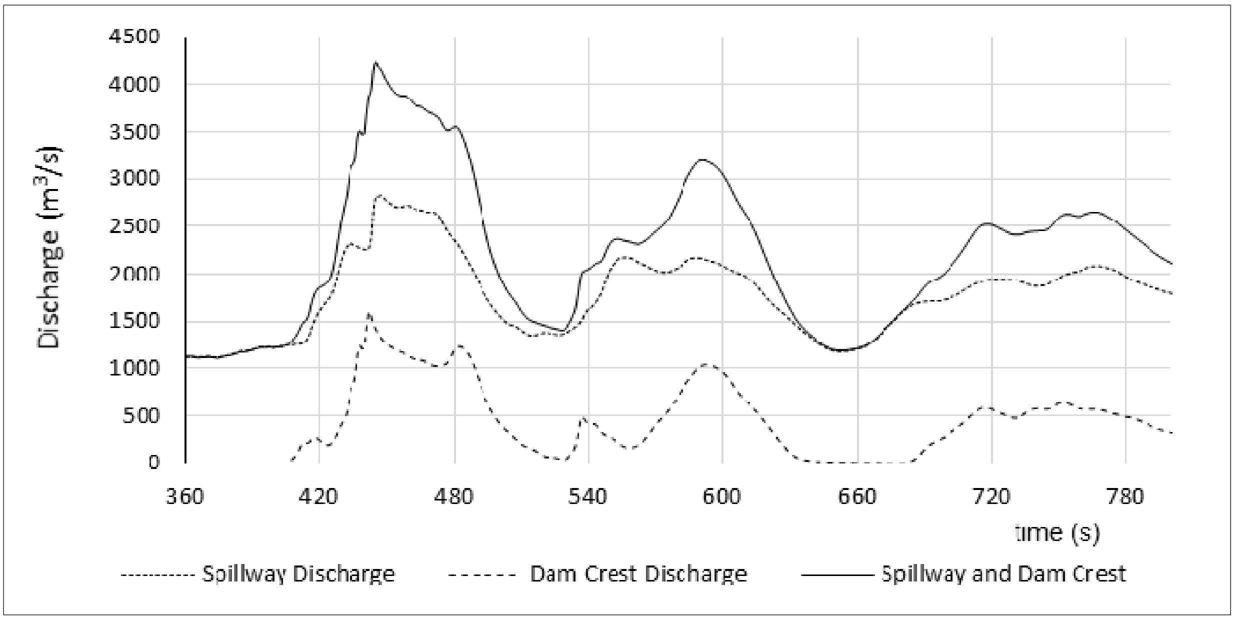

Figure 8. Discharges through the spillway and over dam crest of Case 2 of Alternative 2.

Such fluctuation may continue until all the displaced water due to landslide was drained downstream. The effect of the overtopping of the dam crest may endanger the stability of the dam's earth. This suggests that the dam's earth structure should be strengthened. More importantly is the mitigation to reduce the risk of landslide.

The snapshots of wave propagation during Case 2 of Alternative 2 in the reservoir are illustrated in Figure 9. The wave direction initially depended on the path of landslide material. The figures show that the wave fronts propagated upstream and downstream of the slide location. It can be observed in the figures that the highest run-up occurred at the slope directly in front of the slide location. Such situation was similar to that of landslide generated wave run up in Lituya Bay in 1958. Further information about Lituya Bay landslide generated wave is available in Miller (1960).

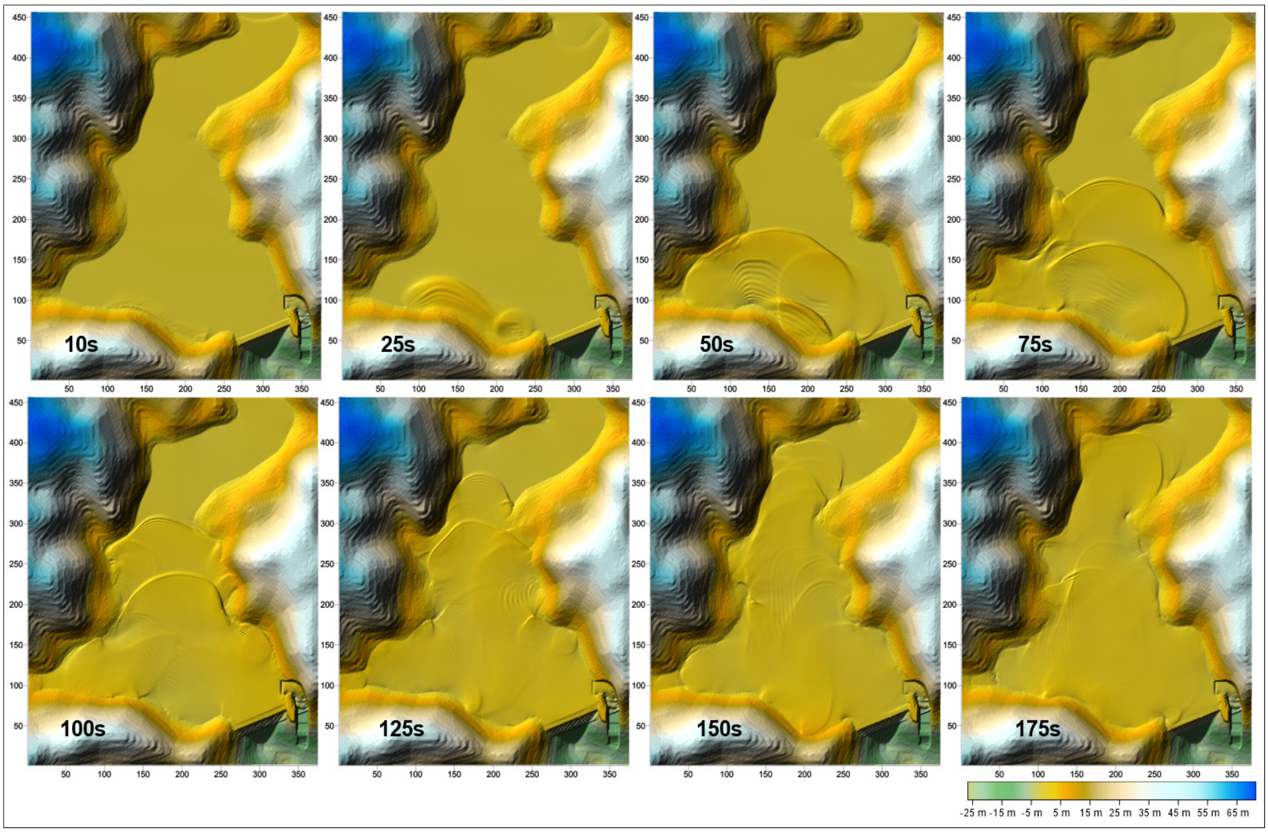

Figure 9. Snapshots of wave propagations in the computation domain for Case 2 of Alternative 2.

It was interesting to compare the result of the present simulation with that of Wijaya et al. (2016). The present simulation yields maximum landslide generated wave of 1.7 m during Case 1 of Alternative 2, whilst Wijaya et al. simulation was 0.9 m. Other than that the shape of the water fluctuation above the dam crest was different where the present simulation indicated longer landslide generated waves. This difference could have been caused by the size and the duration of the landslide where Wijaya et al. (2016) based their simulation on assumed landslide size and volume.

4 CONCLUSIONS

The study shows that the probable landslide at Zone 1 may create disaster downstream of the dam. The situation becomes worst when the landslide occurs simultaneously with peak discharge of the spillway. At this case, the dam crest would be overtopped and the total discharge at downstream could create disaster. The relatively long duration of overtopping (more than 5 minutes) may endanger the dam body where the failure of the dam body may create further fatal disaster. This suggests that this preliminary study should be followed by a more serious study to determine the probable landslide occurrence.

The present study resulted in higher and longer landslide generated wave that overtopped the dam crest compared to that of Wijaya et al. (2016).

REFERENCES

Chaudhry, M. H., Mercer, A. G. & Cass, D. (1983). Modelling of Slide-Generated Wave in Reservoir. *Journal of Hydraulic Engineering,* 109(11),1505-1520.

Genevois, R. & Ghirotti, M. (2005). The 1963 Vaiont Landslide. *Giornale di Geologia Applicata,* 1, 41-52.

Goto, C., Ogawa, Y., Shuto, N. & Imamura, F. (1997). *Numerical Method of Tsunami Simulation with Leap-Frog Scheme,* IOC Manual: IUGG/IOC Time Project, UNESCO.

Imamura, F., Yalciner, A. C. & Ozyurt, G. (2006). *Tsunami Modelling Manual (TUNAMI Model).* Sendai: Disaster Control Research Center, Tohoku University.

Kiersch, G. A. (1964). Vaiont Reservoir Disaster. *Civil Engineering,* 34(3),32-39.

Miller, D. J. (1960). Giant Waves in Lituya Bay Alaska. *Geological Survey Professional Paper, 354C,*51-83.

Townson, J. M. & Kaya, Y. (1988). Simulation of the Waves in Lake Botnen Created by the Rissa Landslide. *Proceeding Institution of Civil Engineers,* 85(Part 2), 145-160.

Triatmadja, R. (1990). *Numerical and Physical Studies of Shallow Water Waves with Special Reference to Landslide Generated Waves and the Method of Characteristics, Ph.D Thesis* ed. Glasgow, UK: University of Strathclyde.

Wang, F. & Sassa, K. (2010). Landslide Simulation by a Geotechnical Model Combined with a Model for Apparent Friction Change. *Physics and Chemistry of the Earth,* 35, 149-161.

Wijaya, Y., Benazir, Rifa'i, A. & Triatmadja, R. (2016). Simulation of Hypothetical Landslide Generated Wave in Karalloe Reservoir, South Sulawesi, Indonesia. *Malaysia, 4rd Regional Conference on Natural Disaster*.

Proceedings of the 37th IAHR World Congress
August 13 – 18, 2017, Kuala Lumpur, Malaysia

PERFORMANCE ON INFLOW FORECASTING INTO TEMENGOR DAM USING INTEGRATED FLOOD ANALYSIS SYSTEM

MOHD IDHAM NAJID(1), LARIYAH MOHD SIDEK(2), HIDAYAH BASRI(3), AZWIN RAZAD(4) & MAZLAN MOHD SOM(5)

(1,2,3) Sustainable Technology & Environment Group, Institute for Energy Infrastructure, Universiti Tenaga Nasional, Selangor, Malaysia
idham2521@gmail.com
(4) Tenaga Nasional Berhad Research, Kajang, Selangor,
azwinzailti.arazad@tnbr.com.my
(5) Stesen-stesen Janakuasa Sg. Perak, Generation Division, Gerik, Perak,
mazlans2@tnb.com.my

ABSTRACT

Nowadays, natural disaster like flood is of main concern for dam conservation as it can result in property damage and endanger lives. The prediction of flood is one of the keys in understanding its frequency of occurrence. This can be obtained using real-time rainfall, water level data of telemetry stations network and real-time forecasting. The selection of appropriate flood forecasting model needs to be based on systematic approach for flood mitigation and dam operation decision support system. The objective of this study is to optimize the flood preparation and flow response measure for dam reservoir. Inflow forecasting analysis and determination of hydrograph are carried out using Integrated Flood Analysis System (IFAS) and Hydrologic Engineering Centre-Hydrologic Modeling System (HEC-HMS). The comparison of IFAS and HEC-HMS shows that IFAS hydrograph is lower than that of HEC-HMS. The flow discharges generated by IFAS and HEC-HMS are found to be 505.77 m^3/s and 515.2 m^3/s, respectively. Similar location is used to compare each of the hydrograph and the hydrograph generated from modeling helps in determining the inflow that enters into the reservoir. It also provides lag time for the inflow before it enters into the outlet of the dam. Thus, this research finding helps in understanding that if a higher value is noticed for flow due to flooding, it can be reduced by early releasing of flow from the operational dam based on the information obtained from the values of hydrograph and lag time.

Keywords: Hydrograph; integrated flood analysis system; hydrologic engineering centre-hydrologic modeling system; flood forecasting.

1 INTRODUCTION

Inflow forecasts are one of the key inputs in the short-term scheduling of hydroelectric generation. Therefore, an inflow forecast module is an essential part of an operational Decision Support System (DSS) for hydro scheduling for dam operation management. In order to optimize the hydropower system for maximizing the value of water resources, flow forecasting can be implemented in one of Tenaga Nasional Berhad (TNB) hydropower plants for better production and optimization.

These operational operation flow forecasting modules are implemented by Stesen-Stesen Janakuasa (SSJ) TNB Sg. Perak which is at Temengor Dam. Moreover, for the ungauged catchment like Temengor, the selection of an appropriate flood forecasting model is important. The Integrated Flood Analysis System (IFAS) which is a deterministic model, founded by ICHARM (International Centre for Water Hazard and Risk Management) of Japan is used for analysis of flood in the river basin.

In brief, IFAS provides prompt and efficient implementation of flood analysis and forecasting system even in poorly-gauged rivers and step by step improvement of accuracy with the enhancement of in-situ hydrological observation network. In essence, IFAS is a distributed hydrological model (PWRI-DHM) developed by Public Works Research Institute of Japan in the 1990s.

Integrated Flood Analysis System (IFAS) is developed by International Centre for Water and Hazard and Risk Management (ICHARM) under the auspices of UNESCO to develop flood-runoff analysis system. IFAS uses both satellite and ground bases rainfall data as an input in the design concept, regardless of whether availability of ground rainfall stations is limited. IFAS effectively uses the satellite-based rainfall which comprises interfaces as the input and suitable to the catchment. It can also implement runoff analysis engine; model creation and parameter estimation function; visualization of flood result and free distribution.

It has been applied mainly in large-scale river basin in Japan. In order to evaluate the performance of the model, mathematical model from Hydrologic Modeling System (HEC-HMS) is implemented to make comparison on the hydrograph and calibration of the model by using the same rainfall data from ground and satellite observation. At this point, the performance of both models can be estimated for this poorly-gauged catchment.

2 STUDY AREA

Sg. Perak River is the main river in Perak, which comprises a catchment area of 3504 km^2 and river length of approximately 400 km, flowing from Hulu Sg. Perak at upper of Temengor catchment through Bagan Datoh until Straits of Malacca. Sg. Perak is the second largest river in Peninsular Malaysia after Sg. Pahang. Figure 1 shows the overall Temengor catchment river basin. Figure 2 shows the upper and lower parts of the catchment.

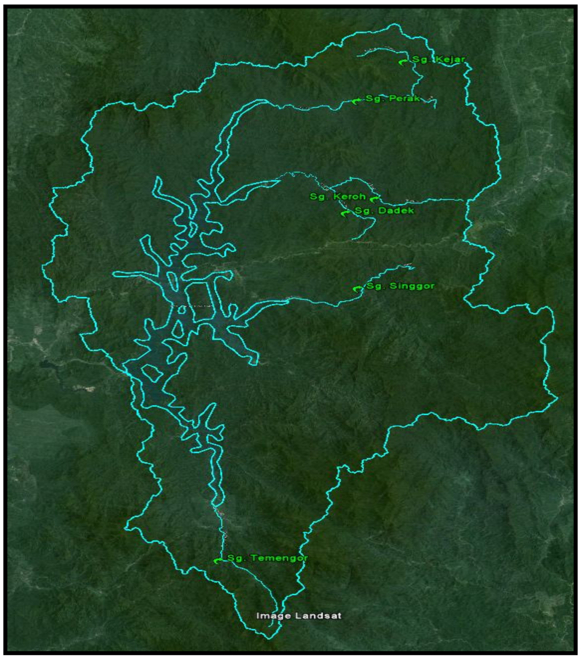

Figure 1. Temengor River Basin

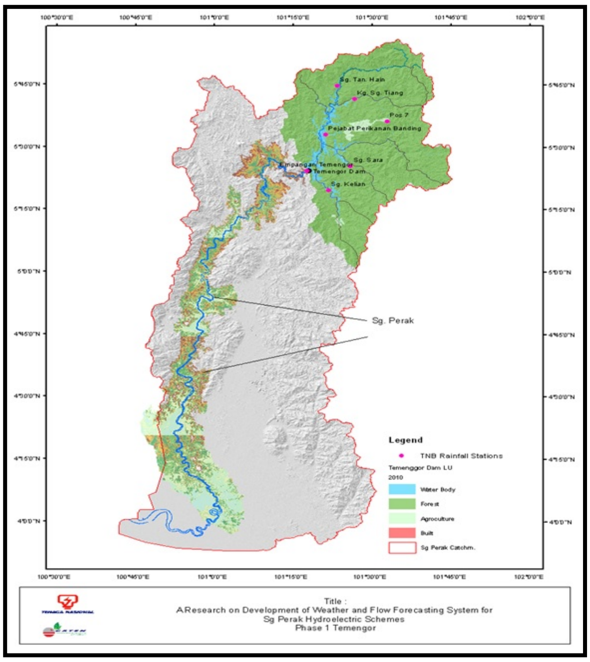

Figure 2. Upper and Lower parts of the Catchment

3 MODEL SETUP

3.1 Model Setting

The catchment boundaries (Figure 3) of the study area were determined by Digital Elevation Model (DEM) and the landuse data from the Global Data (USGS). Global Data set can give relevant data set for flood analysis, by which it creates run-off analysis model and estimates parameters.

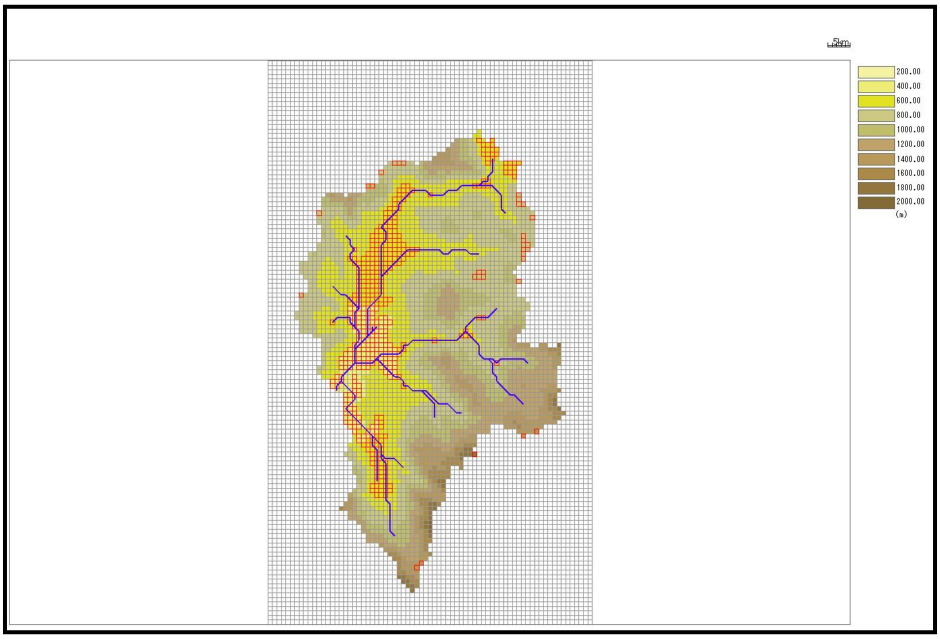

Figure 3. IFAS Catchment Boundary

3.2 Rainfall Input

There were altogether eight ground rainfall stations in the catchment area being used as input data to the IFAS model as listed in Table 1.

Table 1. Ground-Based Rainfall

StationName	StationNo	DataTransmission
EmpanganTemengor	9061	Manual
Sg Tan Hain	9119	Telemetry
Kg Sg. Tiang	9120	Telemetry
Pos 7	9132	Telemetry
Sg Sara	9138	Manual
SgKelian	9139	Manual
PejabatPerikanan Banding	9187	Manual
Tasik Banding	5513001	Telemetry

3.3 Catchment Parameter

The three parameters used in the calibration process were surface, groundwater and river course parameters. The calculated simulated discharge produced by IFAS was compared to the HEC-HMS simulated discharge because there was still no observed discharge data from the Temengor reservoir. Figure 4 shows the simulated hydrograph with IFAS and HEC-HMS in November 2009 rainfall event.

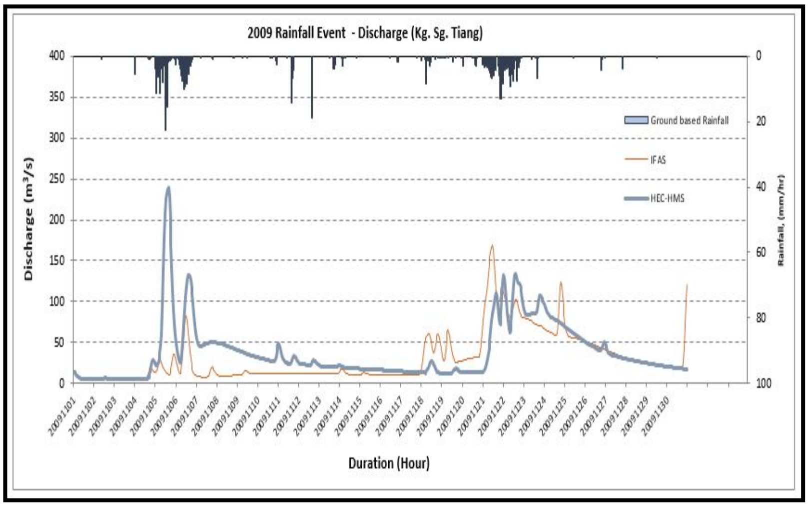

Figure 4. Simulated hydrograph with IFAS and HEC-HMS models

3.4 Result

The simulated hydrographs from both models considered several rainfall events and the summary of the results are shown in Table 2

Table 1. Result Discharge of IFAS and HEC-HMS

Rainfall Event	IFAS	HEC-HMS
Nov 2009	505.77 m^3/s	515.2 m^3/s
Nov 2010	244.93 m^3/s	336 m^3/s

4 CONCLUSIONS

The simulated discharges produced by IFAS for all the events are compared to those of HEC-HMS. These are done on the study area as they are limited to observed discharge data. The actual calibrations are impossible to make because there are no observed data to represent actual flow. Results from both models give roughly the idea for fine tuning the parameters for each model before the installation of flow measurement can be done at site.

ACKNOWLEDGEMENTS

The authors would like to acknowledge International Centre for Water Hazard and Risk Management (ICHARM), Tenaga Nasional Berhad Research (TNBR) and Stesen-stesen Janakuasa Sg. Perak Generation Division TNB for their support and collaboration in making this project successful.

REFERENCES

Hafiz, I., Nor, N. D. M., Sidek, L. M., Basri, H., Hanapi, M. N. & Livia, L. (2013). Application of Integrated Flood Analysis System (IFAS) for Dungun River Basin. *IOP Conference Series: Earth and Environmental Science*, 16(1), 012128

Najid, M. I., Sidek, L. M., Hidayah, B. & Roseli, Z. A. (2016). Hydrological Analysis for Inflow Forecasting into Temengor Dam. *IOP Conference Series: Earth and Environmental Science*, 32(1), 012067.

Sugiura T, Fukami K, Fujiwara N, Hamaguchi N, Nakamura S, Hironaka S, Nakamura K, Wada T, Ishikawa M, Shimizu T, Inomata H. & Itou K (2009). *Development of Integrated Flood Analysis System (IFAS) And Its Applications,*Conference of 7th ISE & 8th HIC, Chile.

Sugiura, T., Fukami, K. & Inomata, H. (2008). Development of Integrated Flood Analysis System (IFAS) and its Applications. *World Environmental and Water Resources Congress 2008: Ahupua'A*, 1-10.

Fukami, K., Sugiura, T., Magome, J. & Kawakami, T. (2009). User Manual Integrated Flood Analysis System (IFAS Version 1.2), 88-89. ISSN 0386-5878

Government of Malaysia Department of Irrigation and Drainage (DID Malaysia) (2009). *DID Manual*, Volume 4 – Hydrology and Water Resources

World Meteorological Organization (2011). *Manual on Flood Forecasting and Warning,* World Meteorological Organization (WMO-No. 1072)

Proceedings of the 37th IAHR World Congress
August 13 – 18, 2017, Kuala Lumpur, Malaysia

FLOOD MITIGATION MEASURES TOWARDS ACHIEVING ZERO FLOOD FOR SUNGAI KERAYONG CATCHMENT, SUNGAI KLANG RIVER BASIN

YUK SAN LIEW[(1)], NURFARESYA ZAINURIN[(2)], NORSYAMIRA HASSAN[(3)], AZMAN MAT JUSOH[(4),]
NASEHIR KHAN E. M. YAHAYA[(5)], JAZURI ABDULLAH[(6)], MOHD FOZI ALI[(7)] & AZMI IBRAHIM[(8)]

[(1,2,3,4,5)] National Hydraulic Research Institute of Malaysia (NAHRIM), Seri Kembangan, Selangor, Malaysia,
ysliew@nahrim.gov.my; nurfaresyaelya@gmail.com; syamirahassan@gmail.com; azman@nahrim.gov.my; nasehir@nahrim.gov.my
[(6,7,8)] University Teknologi Mara (UiTM), Shah Alam, Selangor, Malaysia,
jazuri9170@salam.uitm.edu.my; mohdfozi@salam.uitm.edu.my; azmii716@yahoo.com

ABSTRACT

Flash floods have caused a lot of distress to the people living in Klang River Basin; from long hours of traffic jam congestion, damages of cars, to the destruction of homes and business properties. Comprehensive flood mitigation measures have been implemented by the authority. However, the effectiveness of the flood mitigation measures is still being questioned since floods still occurs. Thus, this research aims to analyse, evaluate, predict and provide recommendations for flood mitigation measures towards achieving zero floods for Sg Kerayong river basin, a subcatchment of Klang River Basin. This research covers the development of a hydrodynamic model which is capable to simulate the integrated hydrologic and hydrodynamic analysis, production of flood forecasting maps in real-time simulation which in later stage to serve as an important data for flood relief operations as well as to propose environmental-friendly soft-structures with appropriate flood mitigation system. Flood maps for three different rainfall designs (50-year, 100-year and Probable Maximum Precipitation (PMP) events) are produced using river modelling - TREX. This study found that Kerayong River Basin has undergone quite comprehensive flood mitigation measures which include ponds and river rehabilitation. The model simulations indicate that the mitigation measures are satisfactory to cater for the 50-year and 100-year design rainfall. However, about 7% of the catchment areas are predicted to be flooded if PMP storm events occur. If rainwater harvesting is implemented in these areas, then peak discharge can be reduced by 39% and a reduction of 50% in peak discharge can be achieved if new materials such as porous rock matrix filters are used for open spaces such as parking or pavement.

Keywords: Flood; river modellin; flood mitigation; rainwater harvesting; porous pavement.

1 INTRODUCTION

Flooding is the most frequent and disastrous weather phenomenon for Malaysia ever since long time ago. The main cause of severe flooding in Malaysia is the heavy monsoon or convective rainfall. Flash floods have caused a lot of distress to the people living in Klang River Basin; from long hours of traffic jam congestion, damages of cars, to the destruction of homes and business properties. Comprehensive flood mitigation measures have been implemented by the authority including enforcing storage ponds for construction sites, improving river channel sections and building the SMART tunnel. However, the effectiveness of the flood mitigation measures is still being questioned since floods still occurs. A thorough investigation with accurate and up-to-date analysis and hydrodynamic modelling will help to gauge how effective are the flood mitigation measures at Klang River Basin and to provide recommendation towards achieving zero flood. This research focuses on implementation, types, maintenance and effectiveness of flood mitigation structures in Sg Kerayong river basin by developing a hydrodynamic model to simulate the integrated hydrologic and hydrodynamic analysis. Flood maps for three different rainfall designs (50-year, 100-year and Probable Maximum Precipitation (PMP) events) are produced using river modelling –Two-Dimensional Runoff Erosion and Export (TREX).

2 STUDY AREA

Sg Kerayong river basin is located at the Federal Territory of Kuala Lumpur and is considered to be one of the important branches of the main Klang River. Figure 1 shows the location of Sungai Kerayong river basin and its land use details. Most of the areas have been developed as residential and industrial areas. The width and length of the river are 20m and 30km, respectively. The catchment area is approximately 55km^2. The lowest and highest elevation is 33m and 400m, respectively.

The study site experiences the tropical rainforest climate, which is warm and sunny throughout the year. It receives more rainfall especially during northeast monsoon season between October to March. The average annual rainfall ranges from 2,500mm to 3,000mm. The maximum recorded rainfall for 1-hour duration is

94.5mm on June 1, 2010 according to the Department of Irrigation and Drainage (DID) (2014) based on the recorded data from 2007 to 2010 (DID, 2014).

Several factors had been analyzed by choosing Sg Kerayong as case study area. For instance, it was recorded some of the worst flooding events at Sg Kerayong in the past few years and the impervious surface of the area had increased by more than 95%.

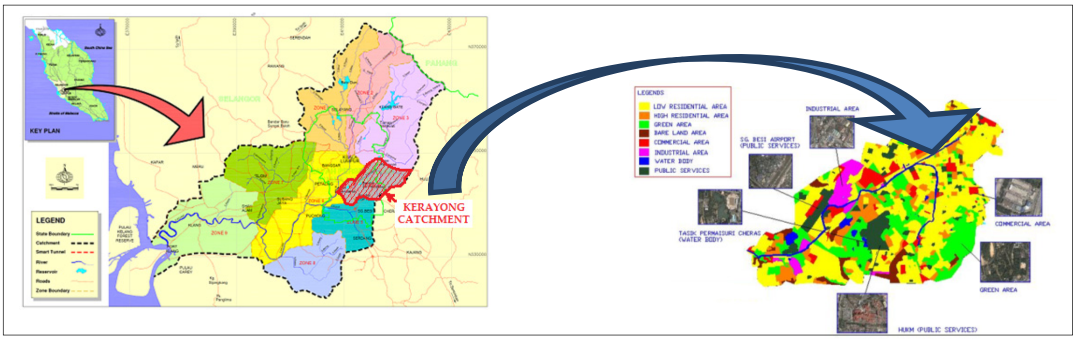

Figure 1. The location of Sg. Kerayong catchment area and landuse details.

3 METHODOLOGY OF STUDY

3.1 Data collection and analysis

The overall methodology of this research included the desktop study, data collection from the relevant agencies and the development of hydrodynamic modelling and flood forecasting mapping. Figure 2 shows the overall methodology.

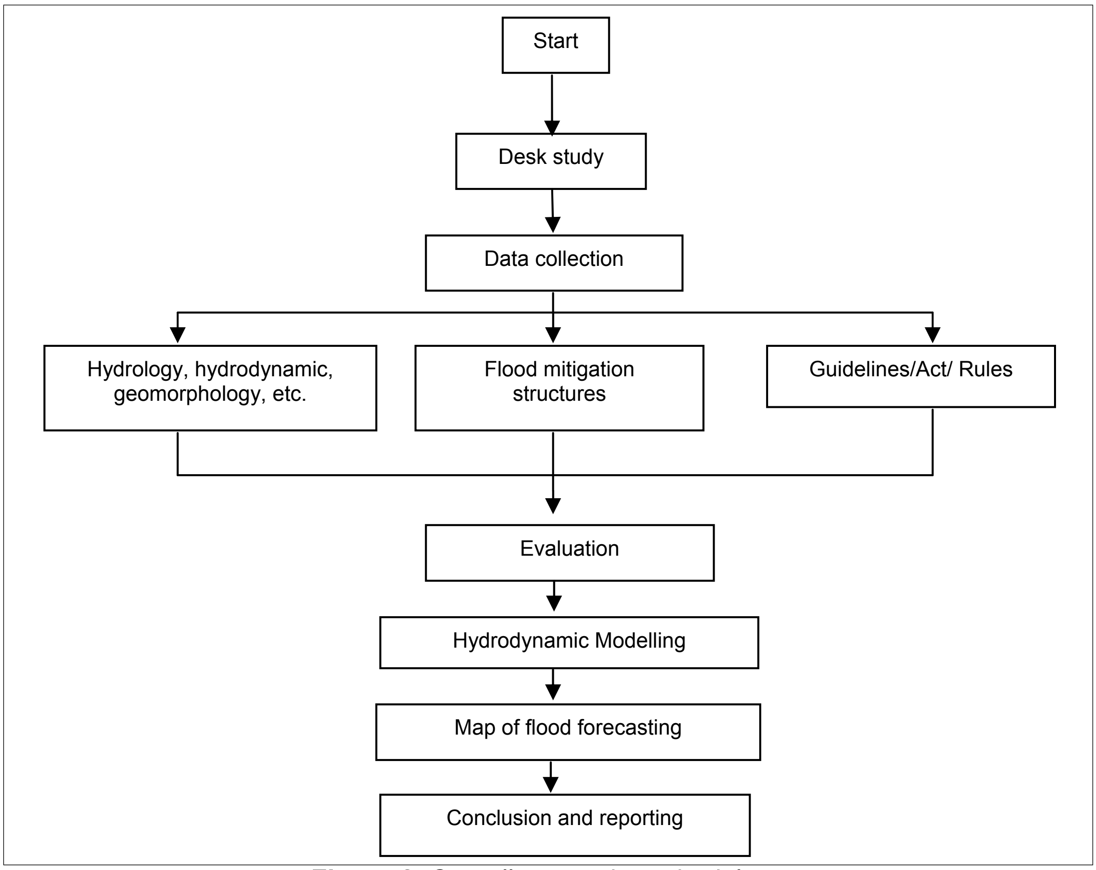

Figure 2. Overall research methodology.

3.2 Model set-up

3.2.1 TREX hydrodynamic modelling

Two-dimensional spatially distributed TREX model was used to simulate the relationship between rainfall and runoff. There were four (4) main hydrologic processes included in the TREX model: (1) rainfall and interception; (2) infiltration and transmission loss; (3) storage; and (4) overland and channel flows.

There were eleven (11) layers prepared using ArcGIS software. These layers had been prepared from four (4) basic data, *i.e*. Digital Elevation Model (DEM), soil type, land use and river flow direction. Figure 3 shows TREX hydrodynamic modelling for Kerayong River basin. The DEM was obtained from the DID with a resolution of 50m. Data for the channel flow and land use were obtained from DID and Department of Agriculture (DOA), respectively. The soil type was assumed to be limestone based on the geological map available from SMARTwebsite (DID, 2014).

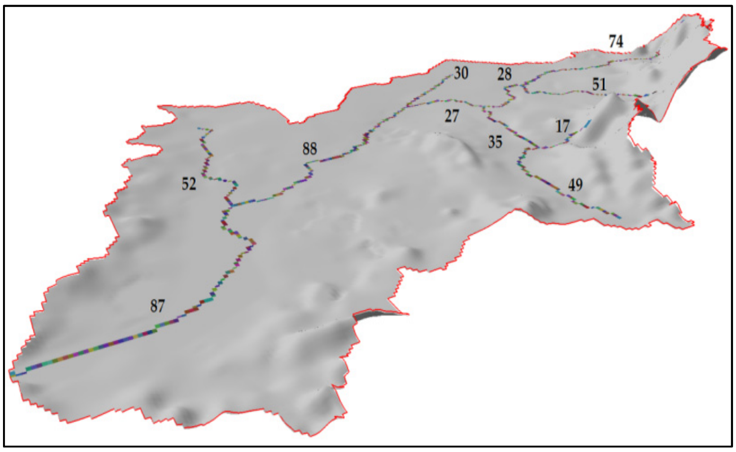

Figure 3. TREX hydrodynamic modelling.

The input data had to be tested by applying the impervious condition. The hydraulic conductivity value of soil was set to zero. The rainfall intensity of 50mm/hr was chosen. The rational method with runoff coefficient (C) equal to one (1) was used to compare the discrepancy between these two values (*i.e.* rational method and TREX model). The application of rational method is valid provided the hydrological simulations are: (1) the peak flow is reached when the entire watershed is contributing to the runoff and (2) the rainfall intensity is assumed to be uniform across the watershed and over the duration of rainfall.

The Relative Percentage Difference (RPD) and Percent BIAS (PBIAS) methods were used for the statistical analysis to check on the model performance. The RPD is the simplest statistical method among others used to calculate the differences between observed and simulated peak discharge, total volume and time to peak (Singh et al., 2005; Fernandez et al., 2005), while the PBIAS method is a statistical error analysis that measures the average tendency of the simulated results to underestimate or overestimate the observed data (Gupta et al., 1999). The summary of model performance evaluation for RPD and PBIAS methods is tabulated and shown in Table 1.

Table 1. General performance ratings to classify the performance of the model.

Performance Rating	RPD and PBIAS
Very Good	RPD, PBIAS $\leq \pm 10\%$
Good	±10%<RPD,PBIAS≤±15%
Fair / Satisfactory	$\pm 15\% < RPD, PBIAS \leq \pm 25\%$

3.3 Calibration and validation

The calibration and validation procedure focused on the accuracy of simulated peak discharge, total volume and time to peak at the main outlet (*i.e*., at the point-end-downstream of the river/channel). After the calibration process, another storm event was used for the validation purpose.

Based on the study conducted by Abdullah (2013), Velleux et al. (2006) and Velleux et al. (2008), the typical hydrologic sub model parameters subjected to be calibrated are hydraulic conductivity (K_h) and flow resistance coefficient (Manning's *n*). They also added that other hydrologic sub model parameters, such as interception, hydraulic suction head and dead storage are less significant in affecting the discharge magnitude.

During the validation processes, the rainfall-runoff relationship was simulated using calibrated parameters (Kh and n) without any changes. Before the validation process was made, the grid size analysis was conducted (this process was parallelly conducted during calibration). The main purpose of this process was to determine the most suitable grid size that can be used for further analyses. Four (4) different grid sizes were used; 90m, 150m, 210m and 270m. Storm event on April 2, 2008 was used for the calibration and grid size analysis purposes. Total rainfall for this event is 113mm which occurs for 3-hour of rainfall duration. This is the highest recorded rainfall and discharge. The calibration and validation procedure focused on the accuracy of simulated peak discharge and time to peak at the main outlet (*i.e.*, at the point-end-downstream of the channel).

Tables 2 and 3 show the summary of the calibration (and validation) and grid sizes analysis, respectively. From the calibration analysis, the goodness-of-fit-test (GoFT) indicated that all grid sizes can reproduce the storm event on April 2, 2008 with an error of less than 10% based on the RPD matric. The time to peaks were estimated with the highest lag time of 15 minutes. The lag value, for small catchment (definition of small catchment is less than 100km^2 as described by Singh (1995) and used by Abdullah (2013)), is still acceptable.

Table 2. Performance of the TREX model during calibration and validation processes.

CALIBRATION							
Grid Size (m)	Storm event	Q_{peak} (m^3/s)			T_{peak} (Hour)		
		Obs.	Sim.	RPD (%)	Obs.	Sim.	Lag
90	02-Apr-08	184.4	175.9	4.6	19:00	19:06	0:06
150			201.3	-9.1		19:15	0:15
210			203.7	-10.4		18:48	0:12
270			164.8	10.6		18:51	0:09

VALIDATION							
Grid Size (m)	Storm event	Q_{peak} (m^3/s)			T_{peak} (Hour)		
		Obs.	Sim.	RPD (%)	Obs.	Sim.	Lag
90	16-Apr-08	68.9	55.0	20.1	17:00	17:15	0:15
150			56.9	17.4		18:45	1:45
210			41.8	39.3		18:45	1:45
270			72.3	-5.0		17:09	0:09
90	27-Aug-08	97.2	61.9	36.3	19:00	20:12	1:12
150			73.2	24.7		21:00	2:00
210			95.8	1.4		18:00	1:00
270			87.9	9.5		18:06	0:54
90	14-Dec-08	36.1	42.1	-16.5	15:00	15:48	0:48
150			37.7	-4.4		16:15	1:15
210			21.6	40.2		17:06	2:06
270			55.8	-54.5		15:09	0:09
90	26-Feb-09	91.4	78.7	13.9	16:00	16:02	0:02
150			86.5	5.3		16:06	0:06
210			68.7	24.8		17:12	1:12
270			120.0	-31.3		16:00	0:00
90	24-Mar-09	54.1	74.4	-37.6	09:00	09:02	0:02
150			80.2	-48.3		10:02	1:02
210			71.6	-32.4		09:32	0:32
270			104.2	-92.7		09:00	0:00

Table 3. Grid size analysis for Kerayong River Basin for storm event on April 2, 2008.

GRID SIZE (m)	Simulation Time		Q_{peak} (m^3/s)			Time to Peak (Hrs.)			Volume (m^3)		
	Secs.	Mins.	Sim.	Obs.	RPD(%)	Sim.	Obs.	Lag time	Sim.	Obs.	PBIAS
90	3,708	60	176	184	-4.4	20:06	19:00	0:06	669,879	731,985	8.5
150	160	2.68	201		9.4	20:15		0:15	765,120		-4.5
210	222	3.7	204		10.7	19:48		0:12	752,017		-2.7
270	45	0.75	165		-10.4	19:51		0:09	1,048,352		-43.2

Table 3 shows the simulation time for smallest grid size was about an hour and decreasing for coarser grid sizes. The simulation time for the calibration was less than five minutes for grid size more than 150m. Most of the grid sizes overestimated the volume of water except for smallest grid size, which was underestimated by 8%. However, the simulated volume using 270m grid size was unacceptable by which the difference between simulated and observed was more than satisfactory criteria, *i.e.* 25%. From this study, a conclusion can be made that the 90m grid size was suitable for flood map and 150m can be used for real time simulation. The model performance reached at least the satisfactory criteria in replicating these storm events (*i.e.* peak discharge and time to peak) when 90m grid size was used. For the 150m grid size, the model estimated time to peak with 1 hour lag time after the observed. Overestimating the peak discharge can be found for 270m grid size. Similar conclusion was also made by Abdullah and Julien (2014). They concluded that for a small watershed (less than $100km^2$), the appropriate grid that can be used to represent the water depth distribution is less than 90m of grid. Figure 4 shows the distribution of water depth for storm event on April 2, 2008 at different grid sizes.

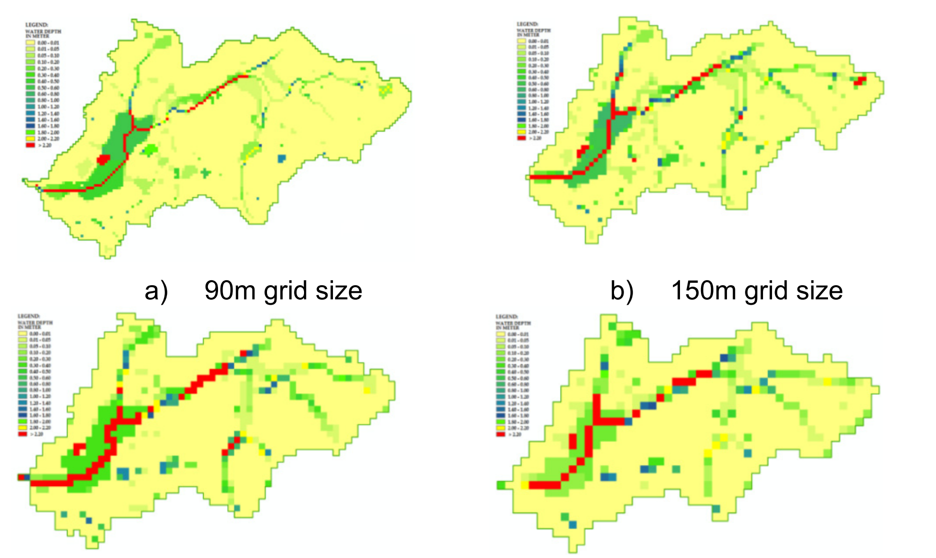

a) 90m grid size
b) 150m grid size
c) 210m grid size
d) 270m grid size

Figure 4. Distribution of water depth for storm event on April 2, 2008 at different grid sizes.

4 RESULTS AND DISCUSSIONS

4.1 Flood map

The flood maps were produced based on the 50-year, 100-year and Probable Maximum Precipitation (PMP) data. The objective was to produce flood forecasting map using real-time simulation that can evaluate and assess the flood damage caused by flooding. These rainfall events occurred for two (2) hours duration. The rainfall intensities for 50- and 100-year were obtained from DID (2012) and PMP was obtained from NAHRIM (2008). Kirpich's formula was used to calculate the rainfall duration.

Table 4. Rainfall intensity for 50-, 100-year and PMP.

	Rainfall Intensity (mm/hr)	Maximum discharge(m^3/s)
50-year	56	185
100-year	62	238
PMP	288	3,786

According to Abdullah (2013), the discharge magnitude of PMP event is between 6 and 15 times larger than discharge for 100-year Average Recurrence Interval (ARI). From this study, the estimated PMP peak discharge was 15 times larger than peak discharge for 100-year ARI. The maximum water depth was 0.3 meter which recorded for 50- and 100-year ARI. The water depth more than 1.0 meter can be found only in the channels.

The 50-year ARI storm event was similar to the calibration storm event (refer to Table 2). An additional of total rainfall by 10mm did not change much on the water depth distribution. The existence of two ponds gives a lot of advantage in ponding excess water from overtopping the channel. The flood prone area was increased when high rainfall intensity was used. The 288mm/hr of rainfall intensity was simulated to estimate any possible flood area for the PMP storm event. Low-lying areas which had an elevation less than 35m were found prone to be flooded (Figure 5c). The grid size less than 150m is recommended for flood mapping purpose so as more accurate representation of the actual scenario can be obtained.

For the purpose of real time simulation to obtain faster result, to be used for flood forecasting for example, grid size between 150 and 210m is recommended. Most of the low-lying areas are covered by houses and business center. Using the design rainfall of 50- and 100-year return period as the input to the model, the flood maps produced were analyzed and were found that none of the area was seriously inundated. It can be concluded that the existing flood mitigation system (*i.e.* Taman Seri Desa and Sri Johor Ponds) are reliable to reduce the magnitude of flood. The maximum rainfall intensity of these cases was

  / ISSN 1562-6865 (Online) - ISSN 1063-7710 (Print)

62mm/hr. However, the overland water depth estimated had reached beyond 2.2m when the rainfall intensity was increased by 5 times from 62mm/hr to 288mm/hr (PMP storm event). The flooded area was estimated to be 7% (approximately 4.0km^2) which occurred at low land as shown in Figure 5(c). The flood map can be used to assess flood damages knowing the values of the infrastructure and properties in the inundated areas.

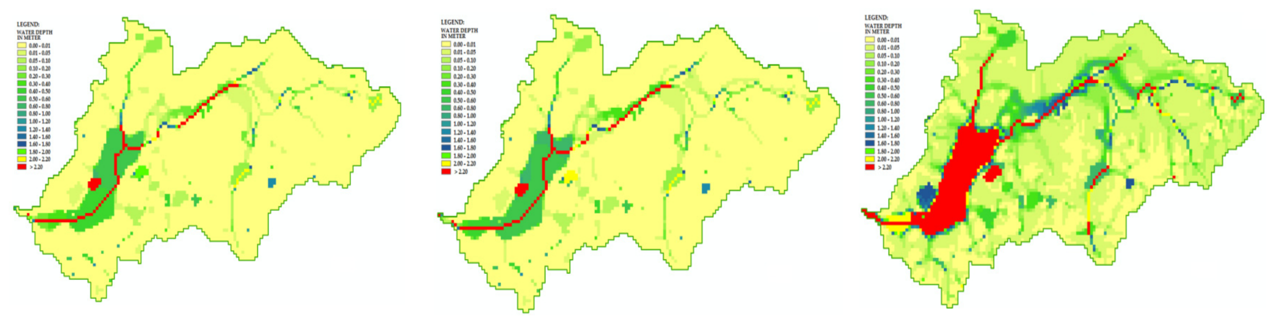

a) 50-year ARI | b) 100-year ARI | c) PMP event

Figure 5. Water depth distribution for 50-, 100-year and PMP event.

4.2 Environmental-friendly soft structures for flood mitigation system

Flood protection measures can be structural or non-structural (soft) such as source control, zoning, flood proofing, insurance and flood forecasting system (Menzel and Kundzewicz, 2003). Watershed management which focuses on the source control is a concept used in minimizing the surface runoff, erosion and sediment transport. It includes vegetation cover management in which the concept of 'catching water where it falls' by enhancing storage of water on the land surface, is applied.

Another method used is green infrastructure such as installations of distributed stormwater controls such as porous pavement, bio-retention structures, green and blue roofs, infiltration systems and rain water harvesting system.

There were two different approaches considered in this study: 1) introducing more pervious and higher roughness surface materials and 2) installing rainwater harvesting system at residential and businesses areas. For the first approach, the 100-year storm event was used to study the effectiveness of this approach. A selected area which covers around 7% of Kerayong Catchment located at the flood prone area was replaced with more pervious surfaces with high roughness values. The simulated value of peak discharges was found to be reduced to 117m^3/s from the original value of 283m^3/s. The results show that the peak discharge can be decreased by 50% from the existing condition if there are more pervious surfaces with higher infiltration rate installed, especially at the upstream of the catchment. For the second approach, the alternative to reduce runoff was by storing the rainwater through rainwater harvesting concept. Figure 6 shows the potential residential and businesses areas for installation of rainwater harvesting system.

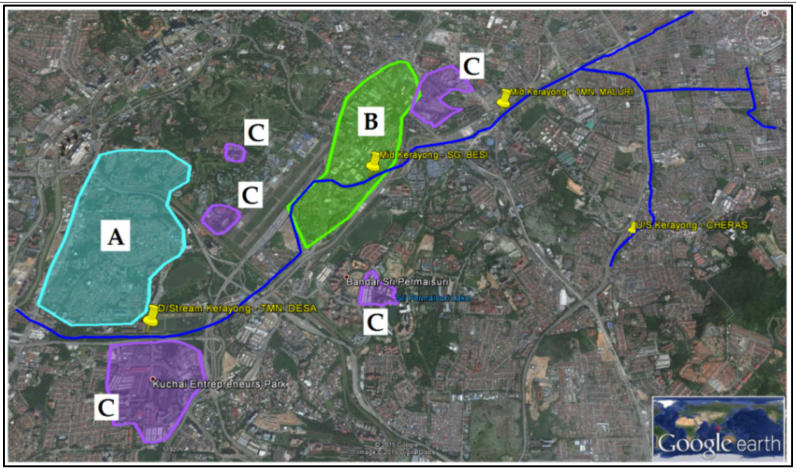

Polygon	Area (km^2)
A (Residential Area)	3.163
B (Residential and Industrial Areas)	2.158
C (Industrial Area)	0.45+0.13+1.04+0.14+0.06=1.82

Figure 6. Potential locations for installation of rainwater harvesting.

Table 5 shows the estimation of harvested water based on four scenarios for the location of rainwater harvesting. The simulation showed that 39% of peak discharge can be reduced if a rainwater harvesting system was installed at various selected residential and businesses areas.

Table 5. Estimation of harvested water for rainwater harvesting.

No	Scenario	Harvested area (km^2)	Harvested water (m^3/s)	Percent of reduction for peak discharge (%)
1	Installing rainwater harvesting at area A only	3.16	41	17
2	Installing rainwater harvesting at area B only	2.16	28	12
3	Installing rainwater harvesting at area C only	1.82	24	10
4	Installing rainwater harvesting at area A, B and C	7.14	92	39

5 CONCLUSIONS

It can be concluded that, as long as the flood mitigation measures at Sg Kerayong such as concrete channelization, rehabilitation with good floodplain, retention ponds are well maintained, there will be a reduction in flood risk. Many curative actions have been taken by related agencies in reducing the impact of flood in Kerayong River Basin. Hydrodynamic modelling using TREX is able to simulate the relationship between rainfall and runoff, and to further produce flood maps. Soft structures such as introducing pervious surfaces with higher roughness materials are installed in upstream of catchment, which could help in reducing peak discharges up to 50%. On the other hand, through installation of rainwater harvesting at all the residential and businesses areas, approximately 39% of peak discharge can be reduced. All these measures are suggested to be implemented especially in urban and flood prone areas like Kerayong River Basin which could help in achieving towards zero floods.

ACKNOWLEDGEMENTS

NAHRIM are glad that this project towards zero floods for Kerayong River Basin is successfully completed within a year. The successful completion of this project is made possible with the commitment and cooperation by various parties. NAHRIM are also thankful to those who are involved and have commented for the improvement of the overall projects output.

REFERENCES

Abdullah, J. (2013). Distributed Runoff Simulation of Extreme Monsoon Rainstorm in Malaysia using TREX, *PhD Thesis*. Department of Civil and Environmental Engineering, Colorado State University, CO.

Abdullah, J. & Julien, P.Y. (2014). Distributed Flood Simulations on a Small Tropical Watershed with the TREX Model. *Journal of Flood Engineering,* 5(1-2), 17-37.

Department of Irrigation and Drainage (DID). (2012). *Urban Stormwater Management Manual (MSMA Manual),* Chapter C13-3.

Department of Irrigation and Drainage (DID). (2014). Digital Maps from JUPEM. http://www.water.gov.my/programme-aamp-activities-our-services-382/37. [Accessed on 5 October 2014].

Fernandez, G.P., Chesheir, G.M., Skaggs, R.W. & Amatya, D.M. (2005). Development and Testing Watershed-Scale Models for Purely Drained Soils. *American Society of Agricultural Engineers*, 48(2), 639-652.

Gupta, H.V., Sorooshian, S. & Yapo, P.O. (1999). Status of Automatic Calibration for Hydrologic Models: Comparison with Multilevel Expect Calibration. *Journal Hydro. Eng.*, 4(2), 135-143.

Menzel, L. & Kundzewicz, Z.W. (2003). Non-Structural Flood Protection – A Challenge, *International Conference 'Towards Natural Flood Reduction Strategies'*, Warsaw, 6-13.

National Hydraulic Research Institute of Malaysia (NAHRIM). (2008). Technical Guideline for Estimating Probable Maximum Precipitation for Design Floods in Malaysia. *NAHRIM Technical Research Publication No. 1(TRP1).*

Singh, J., Knapp, H.V., Arnold, J.G. & Demissie, M. (2005). Hydrological Modelling of the Iroquois River Watershed using HSPF and SWAT. *Journal of the American Water Resources Association*, 41(2), 343-360.

Singh, V.P. (1995). *Computer Models of Watershed Hydrology*. Water Resources Publication.

Velleux, M., Julien, P.Y., Rojas-Sanchez, R., Clements, W. & England, J. (2006). Simulation of Metals Transport and Toxicity at a Mine-Impacted Watershed: California Gulch, Colorado. *Environmental Science and Technology*, 40(22), 6996-7004.

Velleux, M., England, J. & Julien, P.Y. (2008). TREX: Spatially Distributed Model to assess Watershed Contaminant Transport and Fate. *Science of the Total Environment,* 404(1), 113-128.

THE ABILITY OF MULTI-LINEAR REGRESSION MODELS TO FORECAST WATER LEVELS AT CALAMAR, COLOMBIA

TJEERD DRIESSEN[1], BART-JAN VAN DER SPEK[2] & MARIUS SOKOLEWICZ[3]

[1,3] Royal HaskoningDHV, Rivers & Coasts, Nijmegen, The Netherlands,
tjeerd.driessen@rhdhv.com; marius.sokolewicz@rhdhv.com
[2] CDR International, Amersfoort, The Netherlands
bj.vanderspek@cdr-international.nl

ABSTRACT

The Canal del Dique (CDD) is a man-made connection between the Río Magdalena near Calamar and the Caribbean Sea near Cartagena in Colombia. The Environmental Restoration of Canal del Dique project was initiated after a large flooding event that occurred in December 2010. A solution is chosen in which the inlet of water from the Río Magdalena is regulated by a water control structure near Calamar. This provides a controlled dynamics of water levels necessary for environmental purposes while maintaining the bi-annual peak flows in the Canal system. For operational control of this water control structure, a forecasted water level on the Rio Magdalena near Calamar is required. This paper describes the development of multi-linear regression (MLR) forecasting models that predict water levels for different time horizons using 10 water level stations upstream. Stepwise regression is used to systematically add and remove input variables (predictors) such that the total regression model improves. A challenge in the selection of input variables is the presence of multicollinearity which refers to the (mutual) correlation between input variables. Stepwise regression is performed using time series from 1990-2010 (calibration). As expected, the accuracy is decreasing for larger time lags, but is considered very acceptable given the time lag: RMSE (Root Mean Square Error) of 2.0 cm and 10.3 cm for respectively the 1-day and the 5-day forecast models. Validation is done using the time series from 1980-1990 and provides even lower RMSE values which has led to the conclusion that the forecasting power of the models is fairly good. Quantile regression is used for probabilistic forecasting and provides the uncertainty of the prediction. These quantitative uncertainty bands are useful for risk assessments and robust decision-making and provide, in combination with the MLR models, a useful tool for the operation of the Canal del Dique system.

Keywords: Rio Magdalena; multiple linear regression; probabilistic forecasting models; quantile regression; water control.

1 INTRODUCTION

The Rio Magdalena River is the primary river in Colombia. The river basin has a length of approximately 1,600km and an area of 257,000km^2 including the area of its main tributary, the Cauca River, that joins the Rio Magdalena near Magangué. On average the River drains 7,200m^3/s into the Caribbean Sea at Barranquilla (Restrepe and Kjerfve, 2000). The river basin's climate contains two dry seasons and two rainny seasons which are heavily influenced by the El Niño-Southern Oscillation (ENSO) conditions of El Niño and La Niña. This climatic variation is often the driver of droughts and floods in the area.

The Canal del Dique (CDD) is a man-made connection between the Río Magdalena and the Caribbean Sea near Cartagena in Colombia. The area consists of system of interconnected water bodies (lakes and swamps known as ciénagas) that drain into the main canal via small canals (known as caños). In December 2010, the dike on the right bank of the Canal breached resulting in an inundation of 35,000ha of land and rendering thousands of people homeless.

In 2013 the Environmental Restoration of Canal del Dique project was started with the aim to develop and implement an integral solution to the problems related to the Canal, balancing the interests of flood protection, environment, navigation, agriculture and drinking water supply (Fondo Adaptación, 2017). Three alternatives have been evaluated that finally led to a solution in which the inlet of water from the Río Magdalena is regulated by a water control structure near Calamar. This provides a controlled dynamics of water levels necessary for environmental and navigational purposes while maintaining (and controlling) the bi-annual peak flows in the Canal system.

1.1 Water control system

The water control system is a combination of telemetry, complex decision-making schemes, a SCADA system and forecasting information safeguarding correct operation of the water control structures. The three vertical lift gates at Calamar are considered the most important structures to govern the water management in the CDD system. These gates control the amount of water entering the CDD system.

During the majority of the year a base flow of 60 to 70m^3/s is allowed to enter the canal. In general two flood waves occur on the Río Magdalena every year; around June and July as well as around November and December. These flood waves are allowed into the Canal system if the water reservoir Guájaro can be filled and/or ciénagas can be flushed. The water level on the Rio Magdalena is therefore an important variable that drives the operation of these gates. Opening of the gates is initiated when the required water level threshold at Calamar is expected to be exceeded and takes two to five days depending on the water level on the Rio Magdalena. This amount of time is required, since the maximum flood wave discharge into the CDD system may vary between 600 and 1,000m^3/s while the rate at which the water level in Canal del Dique is allowed to increase is limited due to safety and ecological reasons.

If real-time measurements were used for water control, the Calamar gates would open once the water level threshold is reached. The disadvantage of this approach is that the first couple of days of the flood wave cannot be used to flush the ciénagas and/or fill Guájaro, since the complete opening of the Calamar gates can take up to 5 days. A more reliable method, based on multiple linear regressions, is presented in this paper.

1.2 Water level forecast

The gates at Calamar need to be opened as early as possible once exceedance of the water level threshold at Calamar is expected, since the flood wave duration is uncertain which necessitates maximum use of each flood wave. However, early opening of the gates introduces the uncertainty of future water levels. This increases the chance of an ineffective opening event: a flood wave entering the CDD system that is not able to exceed the water level threshold and thus cannot fill Guajaro reservoir and/or flush the ciénagas. Thus, the water control of the gates at Calamar needs to optimize maximum use of flood waves while remaining effective.

Forecasting the water level at Calamar would provide information that helps decision-making to open the Calamar gates before the water level threshold is actually reached on the Río Magdalena. It allows maximum use of the flood wave while preserving the effectiveness of the opening events. At present there is no forecasting model available for Calamar. The objective of this paper is to describe the development process and performance of models that forecast the water level at Calamar for different forecast time horizons using multiple linear regression (MLR) and data of 10 water level stations upstream of Calamar. The available data and used methodologies are discussed after which the results were presented and discussed.

2 DATA COLLECTION

The availability of sufficient historical time series of water level, discharge and/or precipitation is of great importance in the development of MLR models. The objective is to obtain a qualitatively good forecast with a small number of predictors. Three criteria have been used in the selection of measurement stations that have the potential to be in the MLR models:

- The locations should be well-spread and represent different parts of the river basin. This makes sure that there is sufficient independence between the observations at different locations;
- The stations should have sufficient historical observations, so that calibration and validation can be executed during model development and to ensure that different flow conditions are captured in the model behavior;
- The stations should preferably be automated stations, since it is expected that these can have better data availability in the future.

Table 1. Overview of selected, operational measurement stations for the development of MLR models.

MEASUREMENT STATION	OBSERVATION TYPE	PROVIDES INFORMATION ON
PUERTO SALGAR	Automatic	Upstream part Rio Magdalena
PUERTO BERRIO	Automatic	Upstream part Rio Magdalena
BARRANCABERMEJA	Automatic	Upstream part Rio Magdalena
LA COQUERA	Automatic	Cauca River
LAS VARAS	Automatic	Cauca and Nechi River
EL BANCO	Automatic	Upstream part Rio Magdalena and Cesar River basin
SAN ROGUE	Manual	Storage in wetland area
MAGANGUE	Manual	Storage in wetland area
PLATO	Automatic	Routing between wetland area and Calamar
CALAMAR	Automatic	Historical data at Calamar

Based on the above criteria 10 measurement stations have been selected: Puerto Salgar, Puerto Berrio, Barrancabermeja, La Coquera, Las Varas, El Banco, San Rogue, Magangue, Plato and Calamar. Long time series are available for these stations. In Table 1 it can be seen that 8 out of 10 stations are automated and that each location provides different type of information to the MLR models. Furthermore, all stations and their measurements, except for San Rogue, are visualized in the FEWS Colombia platform[b] which allows easy access to the information from these stations. It should be noted that the station of Calamar is also selected, since it gives valuable information on the historical state at Calamar. Figure 1 shows the selected water level stations.

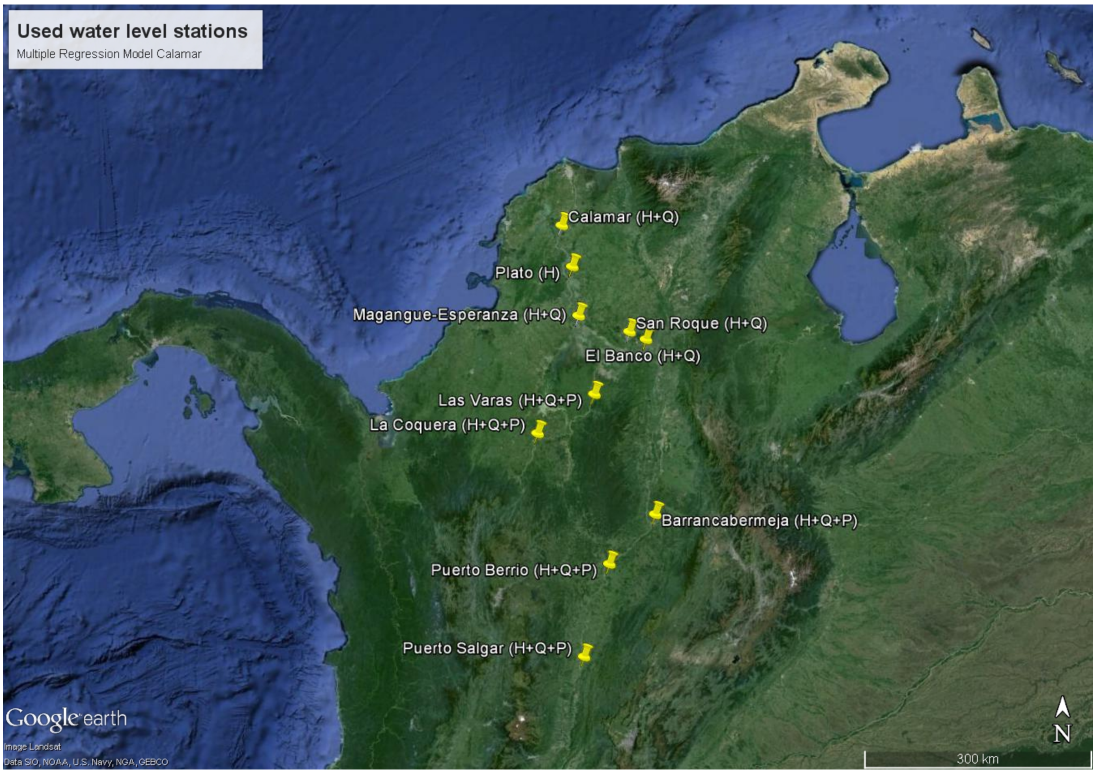

Figure 1. Overview of selected measurement stations (source: Google Earth).

Following the conservation of mass it follows that the water system will be more linear when using discharge, while this is not the case when water level is used. This would advocate the use of discharge measurements. Nevertheless, water level, rather than discharge, was used as the predictive variable in this study. The water level is found through direct measurement in the field while discharge is a derivative from water level measurements and the relationship between discharge and water level. This introduces a potential error, because the relationship is only an approximation and should be updated on a regular basis for all measurement stations. During the development of the MLR models there was no evidence found that the regression models were performing better when discharge was used as parameter.

The IDEAM - Instituto de Hidrología, Meteorología y Estudios Ambientales has provided long historical time series of daily discharge and water level which allowed the MLR models to be developed. In Figure 2 an overview is given of the data availability of the ten water level stations for the period 1980 to 2010. The average data availability is 93.6%. Especially the period of 2000 to 2010 is characterized by high data availability (99.4%). As regression is sensitive to outliers, all the input time series have been pre-processed by removing the outliers. In this study an outlier is defined based on the gradient of the water level in time. After some iteration it became apparent that removing daily water level data points with a daily water level difference of more than 90cm provides the best pre-processing for using the time series in developing the models.

Stations	23037010 PTO SALGAR	23097030 PTO BERRIO	23157030 BARRANCABERMEJA	25027020 ELBANCO	25027200 LAS VARAS	25027320 SAN ROQUE	25027450 PLATO	25027680 MAGANGUE-ESPERANZA	26247020 LA COQUERA	29037020 CALAMAR	Total
1980	0.0	100.0	44.3	97.8	100.0	99.7	70.8	24.9	79.0	98.9	71.5
1981	100.0	100.0	91.8	100.0	100.0	100.0	89.3	52.1	100.0	100.0	93.3
1982	100.0	100.0	100.0	100.0	100.0	99.7	90.1	63.6	96.7	100.0	95.0
1983	100.0	100.0	100.0	99.7	100.0	80.3	56.2	63.8	100.0	100.0	90.0
1984	100.0	100.0	100.0	100.0	99.2	100.0	86.9	99.2	96.7	100.0	98.2
1985	100.0	90.7	42.2	100.0	100.0	100.0	89.9	100.0	100.0	100.0	92.3
1986	100.0	100.0	0.0	100.0	91.5	98.1	93.4	42.5	100.0	100.0	82.5
1987	100.0	78.1	100.0	100.0	96.4	94.5	97.5	79.7	100.0	100.0	94.6
1988	100.0	100.0	100.0	100.0	100.0	75.7	78.7	25.1	100.0	100.0	88.0
1989	100.0	47.4	37.8	100.0	100.0	96.2	99.2	79.2	100.0	100.0	86.0
1990	100.0	83.8	61.1	0.0	100.0	91.5	83.6	69.9	100.0	91.5	78.1
1991	100.0	100.0	83.0	100.0	100.0	98.1	90.4	40.8	100.0	99.7	91.2
1992	100.0	100.0	91.0	100.0	100.0	91.5	41.8	76.2	100.0	100.0	90.1
1993	100.0	100.0	87.7	100.0	100.0	87.9	50.4	94.5	100.0	100.0	92.1
1994	100.0	100.0	32.9	100.0	100.0	52.6	100.0	91.0	100.0	100.0	87.6
1995	100.0	97.3	81.9	100.0	100.0	20.0	82.2	83.6	100.0	95.9	86.1
1996	100.0	100.0	100.0	100.0	100.0	98.1	94.0	100.0	100.0	100.0	99.2
1997	100.0	55.9	100.0	100.0	100.0	100.0	100.0	100.0	100.0	100.0	95.6
1998	100.0	99.7	100.0	100.0	100.0	100.0	64.1	100.0	100.0	100.0	96.4
1999	100.0	100.0	97.3	100.0	100.0	100.0	100.0	100.0	100.0	100.0	99.7
2000	100.0	100.0	100.0	100.0	100.0	100.0	100.0	96.2	100.0	100.0	99.6
2001	100.0	100.0	100.0	100.0	100.0	100.0	100.0	83.3	100.0	100.0	98.3
2002	100.0	100.0	100.0	100.0	100.0	100.0	92.3	96.7	100.0	100.0	98.9
2003	100.0	99.7	100.0	100.0	100.0	100.0	100.0	100.0	100.0	99.2	99.9
2004	100.0	100.0	100.0	100.0	100.0	100.0	100.0	100.0	99.7	100.0	100.0
2005	100.0	100.0	98.4	100.0	100.0	100.0	100.0	89.0	100.0	100.0	98.7
2006	100.0	100.0	100.0	99.7	100.0	100.0	100.0	100.0	99.5	100.0	99.9
2007	100.0	100.0	100.0	100.0	100.0	100.0	100.0	91.0	100.0	100.0	99.1
2008	98.9	100.0	100.0	100.0	100.0	100.0	100.0	100.0	100.0	100.0	99.9
2009	100.0	100.0	100.0	100.0	100.0	100.0	100.0	100.0	100.0	100.0	100.0
2010	100.0	100.0	100.0	100.0	100.0	100.0	96.2	100.0	96.7	100.0	99.3
Total	96.7	95.2	85.5	96.7	99.6	93.0	88.6	82.0	99.0	99.5	93.6

Figure 2. Data availability of selected water level stations.

3 METHODOLOGY

3.1 Multiple linear regression

The models that forecast the water level at Calamar are developed using multiple linear regressions which is a statistical, black-box method to estimate a regressor using multiple predictors and linear regression. The multiple linear regression function is written in the following form:

$$y_i = \beta_0 + \beta_1 x_{1i} + \beta_2 x_{2i} + \ldots + \beta_p x_{pi} + e_i, \qquad [1]$$

where y_i denotes the regressor; in this case the water level at Calamar at a certain (future) moment in time, x_{pi} denotes the pth predictor, in this case the water level at an upstream water level station at different (past) moments (lags) in time, $ß_p$ denotes the regression coefficient of the pth predictor and e_i denotes the residuals of the model.

  / ISSN 1562-6865 (Online) - ISSN 1063-7710 (Print)

Hence, this method can also linearly relate present or historical water levels of upstream measurement stations with future water levels at Calamar by which the regression model becomes a forecasting model. The MLR method has been used earlier for streamflow forecasting applications worldwide. For example, for a long period the water level of the River Rhine entering The Netherlands at Lobith was forecasted using an MLR model (Parmet and Sprokkereef, 1997). When using of the MLR method for forecasting purposes it is important that there are no important water control structures present in the river that significantly affect the streamflow and thus introduce noise in the regression model. In this Rio Magdalena application there are no large water control structures that are having a significant effect on the outcome of the model results.

For the purpose of this study the daily water levels at the present moment (T_0) down to five days back (T_{-5}) are taken into account for each measurement stations. This results in six time stamps that can potentially be used for the purpose of the regression model. Figure 3 shows the time line that is used for this study. The blue area shows the time stamps that are used as input data (predictors) which are used to create regression models for the 10 time stamps in the future (red area). With 10 measurement stations, this leads to a total of 60 different input parameters and potential predictors for the regression models.

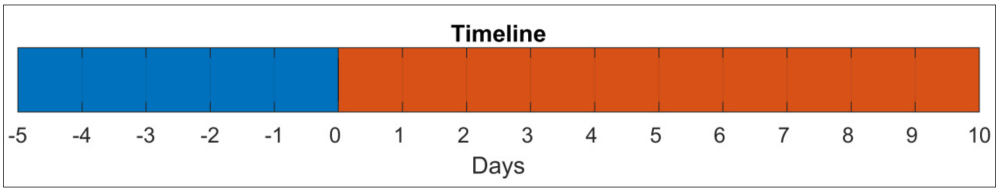

Figure 3. Time line of regression models, blue area is used as input for regression model; red are different output variables for consecutive models.

Multiple linear regressions assume that there is a linear relationship between the regressor and the predictors, that the predictors are normally distributed, that there is no multicollinearity and that the data is homoscedastic. The linear relationship and normal distribution assumptions are easily satisfied in, while the absence of multicollinearity and homoscedasticy are more difficult to realize. Since all the input variables (predictors) are (physically) correlated, the regression models will suffer from multicollinearity. That means that certainly using all available input variables with multiple time lags as predictors in the regression model will not be the best model as multicollinearity will increase when adding more variables. This is not preferred, since the error of the regression coefficients may become too large and it may result in overfitting of the model to the calibration dataset (thus making the model less generic).

Instead of using all 60 predictors a subset of the input variables is therefore required that will lead to the most optimal forecast model. The goal of the regression exercise is to find a model that best fits the data with fewest predictors and smallest predictor errors. As the number of possible subsets is enormous (i.e. 2^{60} subsets), the stepwise regression technique was used for a smart selection of input variables. Stepwise regression is a systematic method for adding and removing terms (predictors) from a multilinear model based on their statistical significance in a regression. The method begins with an initial model and then compares the explanatory power of incrementally larger and smaller models. The method first checks if any terms not yet present in the model have p-values of an F-statistic less than the entrance tolerance. So if it is unlikely that terms would have a zero coefficient if added to the model, the term with the smallest p value is added after which this step is repeated. Then, the method checks if any terms in the model have p-values of an F-statistic greater than the exit tolerance. So if it is unlikely that the hypothesis of a zero coefficient can be rejected, the term with the largest p value is removed. The entrance and exit coefficients (p-values) used in this study are respectively 0.02 and 0.03

3.2 Calibration

The MLR models are developed using stepwise regression and use water level time series from 1990 to 2010 to calibrate the regression coefficients. The predictors Calamar, Magangue and El Banco have the biggest contribution in the MLR models. The amount of significant predictors that are found by stepwise regression ranges between 23 and 31 in the 10 models and is considered large which, given their mutual dependency, consequently suggests that multicollinearity is surely present between the predictors. However, the small Root Mean Square Errors (RMSE) of the validation shows that this is not something of a big concern. As expected, the RMSE values are increasing for larger time lags, but are considered very acceptable given their time lag (e.g. 2.1cm for 1-day forecast (T_{+1}) and 10.3cm for 5-day forecast (T_{+5})). In Table 2 all calibration results can be seen. Figure 4 shows the results of the regression model for forecast time horizon T+1. Clearly the results are very good given the relatively low RMSE of 2.1cm for the complete calibration time series. Note that for some periods the data availability was not sufficient to predict a water level at Calamar.

Table 2. Summary of calibration and validation results for all ten MLR models.

TIME STAMP	T_{+1}	T_{+2}	T_{+3}	T_{+4}	T_{+5}	T_{+6}	T_{+7}	T_{+8}	T_{+9}	T_{+10}
NUMBER OF PREDICTORS	24	26	28	31	28	27	27	25	25	23
R^2 CALIBRATION	1.00	1.00	1.00	1.00	1.00	0.99	0.99	0.98	0.98	0.97
RMSE CALIBRATION (CM)	2.0	3.5	5.3	7.6	10.3	13.1	16.0	18.9	21.8	24.5
R^2 VALIDATION	1.00	1.00	1.00	1.00	1.00	0.99	0.99	0.99	0.98	0.97
RMSE VALIDATION (CM)	1.8	3.3	5.0	6.7	9.2	11.7	14.0	16.8	19.8	22.6

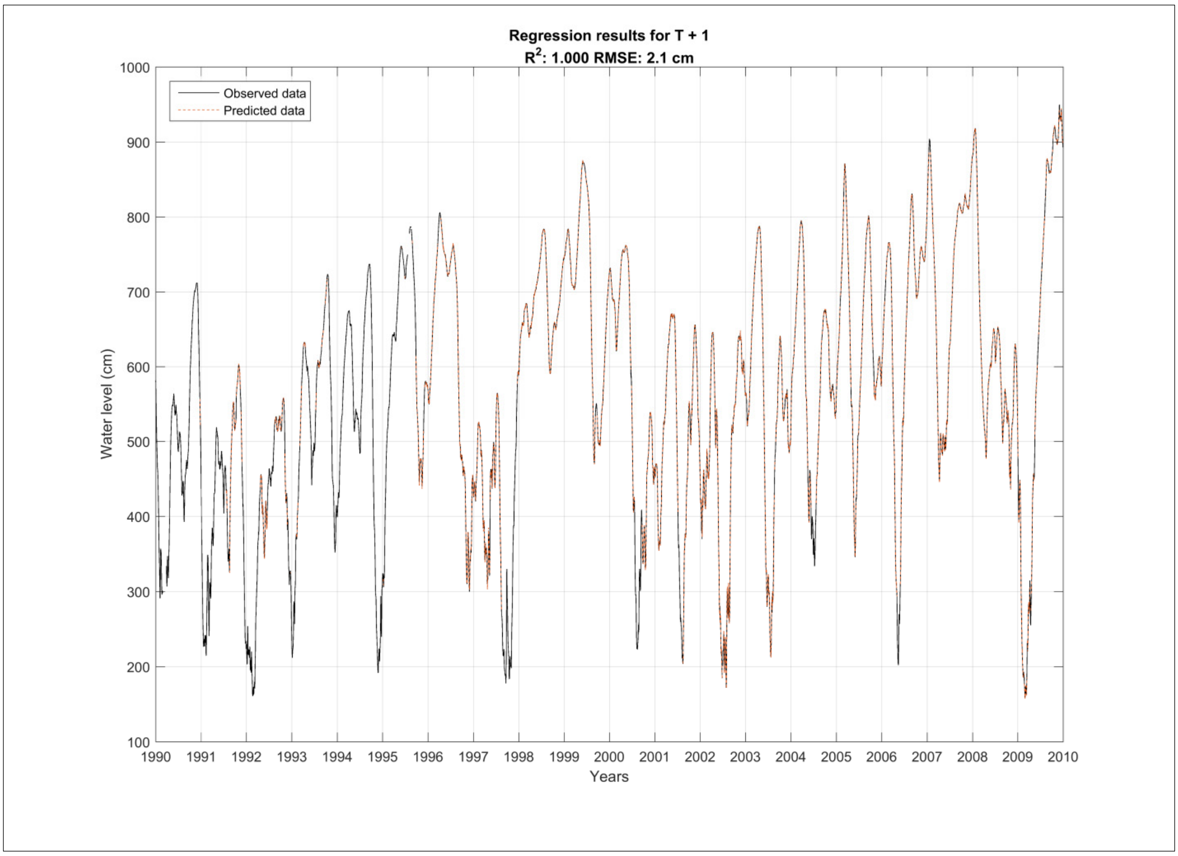

Figure 4. Regression results for forecast time horizon T+1 on calibration data.

3.3 Validation

Validation of the MLR models is important to check if the calibrated regression coefficients are representing the water system correctly. Since there is always some collinearity between the predictors it is important to establish if there is some false accuracy present due to overfitting. To establish if this false accuracy is present, the generated MLR models are validated on the time period from 1980 to 1990. It is important that the validation was executed using other time series than for calibration to ensure that overfitting of the models (due to multicollinearity) is detected. There should be a balance in the amount of data used for calibration and validation, since the model performance increases when longer calibration time series are used for calibration (Parmet and Sprokkereef, 1997). Figure 5 shows the prediction of water levels at Calamar using the generated regression model for the validation time period compared to the observed water levels. The validation provides even lower RMSE values than the calibration which leads to the conclusion that the forecasting power of the models is fairly good (see Table 2). Note that for some periods, the data availability was not sufficient to predict a water level at Calamar.

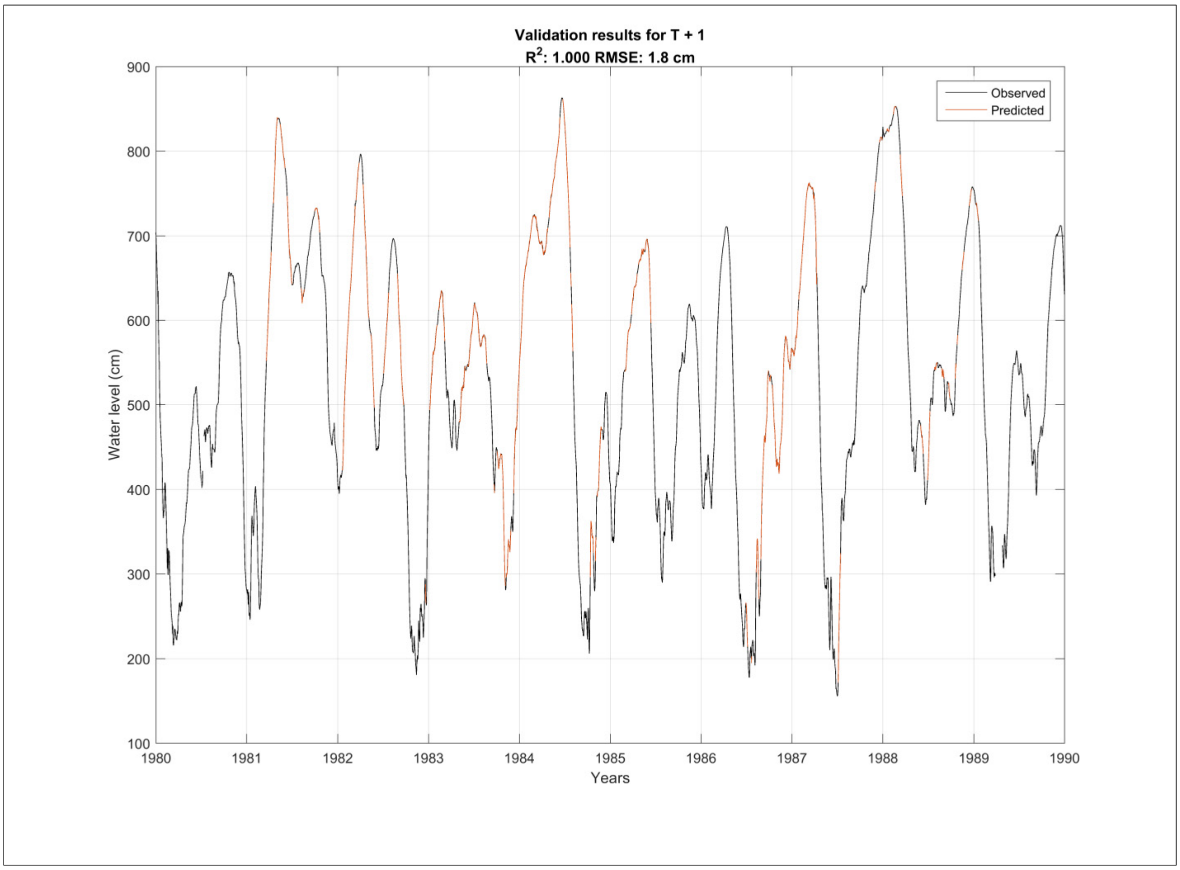

Figure 5. Validation results for forecast time horizon T+1.

3.4 Quantile regression

The presented regression models are deterministic, statistical forecasting models as they only provide a single prediction of the water level for a certain moment in time using statistical relationships. Combined they form a toolbox which enables a complete forecast for ten consecutive days. Since the models are used for forecasting a better insight in the uncertainty of the forecast values is of great importance. Fortunately, with the use of some post-processing techniques it is possible to determine the uncertainty of the prediction, which in turn can be used for probabilistic forecasting. In this study quantile regression was used to determine the uncertainty of the forecast. The quantitative uncertainty bands that were created by quantile regression are useful for risk assessments and robust decision-making as they can provide the probability of exceedance or undershooting of specified water levels.

Quantile regression finds the percentiles of the model residuals. Normal regression is based on minimizing the squared error, while quantile regression is based on minimizing the absolute error. It yields the sample median, rather than the sample mean like for normal regression. With use of error weights the sample percentiles can be found. The percentiles (i) can be written in the form

$$p_i = a_i + b_1 Y_{pred}, \qquad [2]$$

where p_i denotes the percentile, a_i denotes the intercept and b_i denotes the regression coefficients found using quantile regression. The linear relationships that are found are used to create the confidence bound on the forecasted values. It is noted that this method provides a linear estimate of the percentiles. Locally the real uncertainty may be different as the spreading of the residuals are not always fully linear related with the predicted water level. Figure 6 shows the quantile regression for the T+4 model for several percentiles (left) as well as the percentiles imposed on the residuals (right). So the percentiles are (linear) dependent on the predicted water level. From Figure 6 it becomes clear that the uncertainty for low water levels is higher than for high water levels. This heteroscedastic trend is found for every regression model.

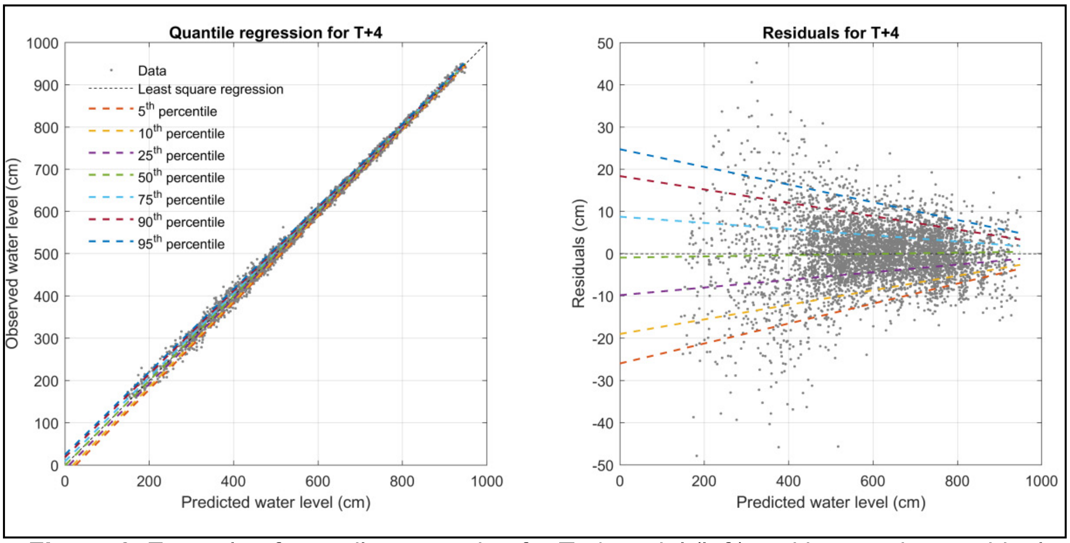

Figure 6. Example of quantile regression for T+4 model (left) and imposed on residuals (right).

4 RESULTS

The presented methods of stepwise regression, calibration, validation and quantile regression lead to a probabilistic forecast model of 10 days when the results of all 10 models are combined. It is clear that in general the forecasts provide a very good prediction for the first couple of forecast in time horizons. For example, the RMSE value of the forecast for the first five days is lower than 10cm. Forecasts for six days ahead or longer show a general trend that deviates more from the actual water levels than the forecast for the first five days. This is in line with the confidence bounds that show that the prediction logically becomes more uncertain for increasing time horizons. Figure 7 shows an example of a 10-day water level forecast at 10 November 2005 which is a composite using 10 MLR models (yellow/orange/red circles). The blue, dashed line indicates the truth line for validation of the forecast, the black line indicates the median forecast and the grey bounds indicate different confidence intervals using the quantile regression output. The confidence bounds can be used for risk assessments. For example; the top of the 90% confidence bounds defines the water level that is exceeded with a probability of 5%, while the bottom of the 90% confidence bounds defines the water level that is undershot with a probability of 5%.

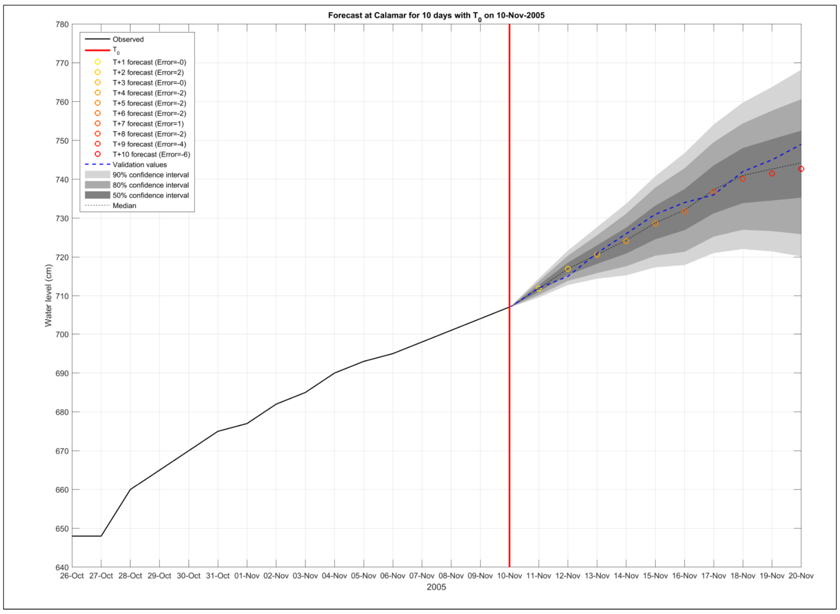

Figure 7. Example of 10-day water level forecast at 10 November 2005.

It is important to realize that the MLR models are trained by historical events and that no physical behavior is present herein. Also, it is likely that the average discharge regime is better represented than the extreme discharge events, since their frequency and thus contribution in the regression is higher. This corresponds with the objective of the MLR-models, since the forecasts are used for correcting timing of opening of the Calamar gates. Most opening events occur in the average discharge regime when water levels at Calamar vary between +4 and +7 m.s.n.m. Nevertheless, the MLR models also perform reasonably well for peak water levels. Figure 7 already showed that the residuals are smaller for higher water levels and in Figure 8 example forecasts is shown for the 2008 flood wave for the rising and falling limb of the hydrograph. In this example the peak water level at Calamar is +9.18 m.s.n.m.

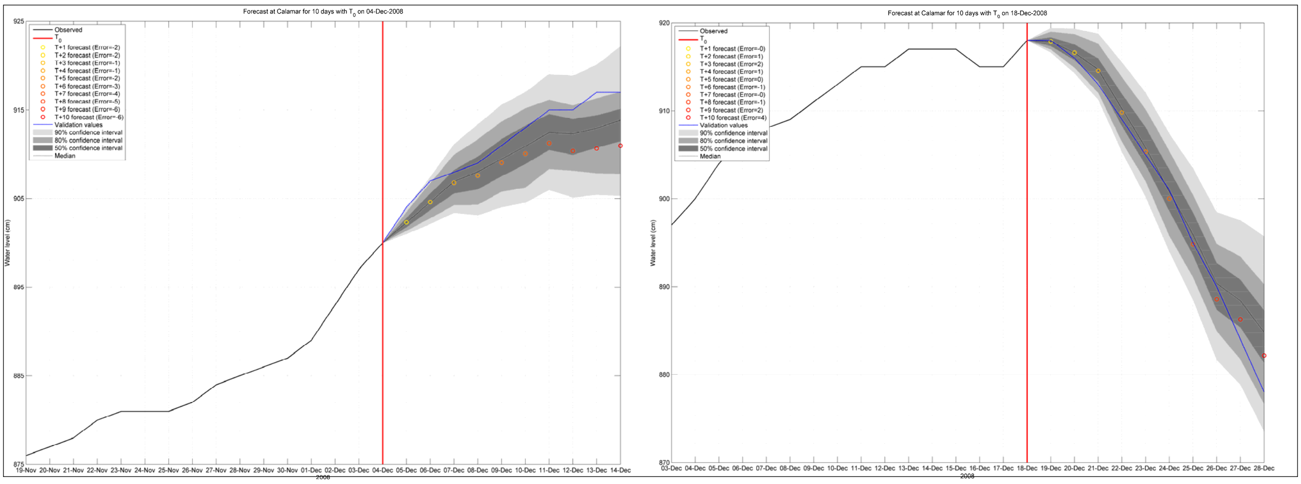

Figure 8. Example of 10-day water level forecast for rising (left) and falling (right) hydrograph for the December 2008 event.

5 CONCLUSIONS

From the Environmental Restoration of Canal del Dique project arise the necessity to develop a model that forecasts water levels in the Rio Magdalena at Calamar for correct water control of the gates at Calamar which determines the volume of water entering Canal del Dique. Multiple linear regressions was used to create 10 models for 10 different time horizons using 10 upstream water level stations and six time stamps. The calibration and validation was performed on respectively 20 and 10 years of data and proved that the black-box models could forecast the water levels at Calamar reasonably well with forecasting errors below 10 cm for the first five days. The use of quantile regression quantified the uncertainty of the forecast models by applying regression on the residuals. This enabled the use of confidence intervals and provided the ability to create probabilistic forecasts. Hereby, the developed tool meets the objective to assist robust decision-making in the water control system of Canal del Dique system and improved control of the gates at Calamar.

ACKNOWLEDGEMENTS

The authors would like to thank the staff of IDEAM - Instituto de Hidrología, Meteorología y Estudios Ambientales in Colombia for their contribution and their effort to provide the historical water level data that was used in this study.

REFERENCES

Fondo Adaptación (2017). Canal del Dique. website: http://sitio.fondoadaptacion.gov.co/index.php/el-fondo/macroproyectos/canal-del-dique [Accessed on 2017-01-29].

Parmet, B.W.A.H. and Sprokkereef, E. (1997). *Hercalibratie Model Lobith – Onderzoek naar mogelijke verbeteringen van de voorspellingen met het Meervoudig Lineaire Regressie Model Lobith na de hoogwaters van 1993 en 1995*, RIZA Rijksinstituut vaar Integraal Zoetwaterbeheer en Afvalwaterbehandeling, RIZA rapport 97.061.

Restrepe, J.D. & Kjerfve, B. (2000). Magdalena River: Interannual Variability (1975–1995) and Revised Water Discharge and Sediment Load Estimates. *Journal of Hydrology*, 235(1-2), 137-149.

Proceedings of the 37th IAHR World Congress
August 13 – 18, 2017, Kuala Lumpur, Malaysia

STUDY ON THE DECISION-MAKING METHOD FOR RESERVOIR OPERATION SCHEME BASED ON BAYESIAN MODEL

MINGLEI REN (1), XIAOYAN HE (2) , HUI LI (3) & XIAOMING JIANG (4)

(1,2,3,4) China Institute of Water Resources and Hydropower Research, Beijing 100038, China
mingleiren@163.com

ABSTRACT

Based on the theory of Bayesian model, and combined with the feature and requirement of decision-making method for reservoir operation scheme, a new decision-making method for reservoir operation scheme based on Bayesian model is proposed in this paper and applied for Zhangze reservoir in Shanxi province, China. The instance application shows that: the new decision-making method based on Bayesian model could provide a scientific, reasonable, and accurate decision-making method for reservoir operation scheme. This method not only could improve the reservoir management level of safe operation, but could also improve the utility ratio of water resources and hydro-energy resources.

Keywords: Bayesian model; reservoir operation scheme; decision-making.

1 INTRODUCTION

Reservoir operation is closely related to nature, society, economy, ecology, environment and other aspects. Under the condition of meeting principle of reservoir operation (Chen, 2001), real-time operation study provides a number of feasible operation options for decision makers to choose. In order to solve the current or future problems of reservoir and its upstream and downstream areas, decision-makers need to select the best solution among the several operation schemes. Therefore, the decision-making of reservoir operation scheme belongs to multi-objective, multi-attribute and multi-stage complex decision-making process, meanwhile, the choice of the operation scheme is an unrepeatable real-time process. The correctness of decision is significant, which is related to reservoir and it's upstream and downstream of the economic benefits or flood losses.

At present, there are many research results of multi-objective decision-making for reservoir. For example: Li (2000) has studied the multi-objective optimization issue of the hydro-electric system by using fuzzy optimization theory； Liang (2001) has studied the flood operation decision-making research for the particularity of flood operation quality by adopting the multi-objective fuzzy decision-making method; Fang (2001) has solved the problem of multi-objective optimization operation issue of water resources system by using genetic algorithm； Wang (2003) has proposed a multi-objective optimization operation theory of reservoir based on Markov single-chain elastic correlation theory, and carried out applied research and others. The Bayesian model was developed in the process of dealing with uncertainties issues in the study of artificial intelligence, and is now widely applied to solve decision-making and evaluation problems that has uncertainties. Reviewing the research trends at home and abroad, the relevant theories relating Bayesian model are becoming more and more perfect, the development level is continuously improved, and the application scope is continuously expanded. The Bayesian model is a key research project topic in the field of reservoir operation decision-making.

The Bayesian decision-making model is a method of statistical decision model (Gao, 2006), which takes the decision that supposed to be taken depending on a certain natural state as the starting point. Through the judgment and sampling, this model obtains the prior information about natural state first, then transforms posterior probability by using Bayesian formula, corrects the prior information, thereby analyzes and makes decision according to the posterior probability to make the information based on decision close to reality.

In view of the reservoir operation scheme, decision-making is classified as advance decision-making and risk decision-making, under the incomplete information, this paper use Bayesian decision-making model to estimate partial unknown state by subjective probability, and correct the probability of occurrence by using Bayesian formula, the optimal membership degree of each feasible reservoir operation scheme is deduced by statistics with respect to the optimal operation scheme, and finally, the decision of the optimal reservoir operation scheme is selected according to the principle of maximum optimal membership degree. Taking the Zhangze reservoir in Shanxi Province as an example, this paper use reservoir operation scheme based on the Bayesian model to judge the decision-making scheme, and make the final decision.

2 RESERVOIR OPERATION DECISION-MAKING BASED ON BAYESIAN MODEL

2.1 Theory of operation decision-making scheme based on Bayesian model

Reservoir operation scheme is one kind of decision making, which compares each operation schemes and make the final decision by using various information (Ni et al., 2004). The reason for choosing Bayesian model to make decision on reservoir operation scheme is: (1) Bayesian model exactly use the known information to analyze reasons, and obtain the probability of occurrence of the event (probability inference); (2) This method is intuitive and simple, with clear principles, few calculations and is convenient. Therefore, the Bayesian model provides a new technological approach and method for reservoir decision-making.

The operation decision-making method based on Bayesian model is defined as follows (Yu, 2008), suppose that the sample space of the feasible operation scheme is Ω, $A \in \Omega$, $B_i (i = 1, 2, ..., s)$ is a finite division of Ω, and $P(B_i) > 0$, when $P(A) > 0$, then

$$P(B_i / A) = \frac{P(B_i) P(A / B_i)}{\sum_{i=1}^{s} P(B_i) P(A / B_i)} \quad [1]$$

where, B_i represents the operation scheme level I (superior), II (relatively superior), III(general), IV (relatively poor), and V (poor));

A represents each operation index in the operation scheme;

$P(B_i)$ is the priori probability of event B_i, which estimate the operation scheme to be the possibility of program level through the experience of intuition and judgment.

$P(A / B_i)$ is the conditional probability, which measure the possibility of corresponding indicators in a certain operation scheme when the operation schemes belong to different levels.

$P(B_i / A)$ is the posterior probability, which indicates the possibility that the operation scheme belongs to the level i under the condition when the information A is obtained.

$P(B_i)$ is one kind of priori probability, a prior estimation of S kinds of possibility (Qi, 2009). Generally, the evaluation and decision of the reservoir operation scheme (the level of inferred scheme) need to be based on the characteristic information of each index in the operation scheme, however, in absence of information, people usually use the experience intuition and judgment to estimate the operation scheme possibility of belonging to a scheme level that is to estimate $P(B_i)$. $P(B_i)$ is called priori probability since is generally predicated before characteristic index information, $P(A / B_i)$ can be seen as a likelihood probability, which represents the size of each characteristic index in the operation scheme, and is closely related to its scheme level. The probability of occurrence of poor characteristic index is relatively small when the operation scheme is superior or relative superior, on the contrary, the probability is also small when the operation scheme is poor or relatively poor. $P(A / B_i)$ measures the possibility that a certain characteristic index appears when the operation scheme belongs to different levels. $P(B_i / A)$ is posterior probability, which indicates the possibility that the operation scheme belongs to the level under the condition that the information A is obtained. Therefore, since this probability is obtained after the information appears, it is called posterior probability.

The operation scheme evaluation is usually based on posterior probability $P(B_i / A)$ to make quantitative assessment, and then to make decisions. Thus, how the posterior probability is estimated from accumulated experience and acquired new information becomes the key problem. Bayesian model established is the exact method to solve the key problem. Type (1) display, $P(B_i / A)$ is estimated from $P(B_i)$ (depending on prior knowledge) and $P(A / B_i)$ (depending on new obtained information). Therefore, its essential meaning is: the Bayesian method provides a simple and convenient mechanism for transforming prior probabilities into posterior probabilities under the condition of acquiring new information. In this paper, we used this mechanism, according to the information obtained, calculate the posterior probability, and in accordance with this logic judgment, to evaluate the operation scheme and achieve the purpose of making final decision.

According to the situation of reservoir operation scheme evaluation and decision and the characteristics of operation scheme characteristic index data, in this paper, the parameters in (1) are defined as follows: B_i is level of operation scheme, which value is denoted by y_{ji}, A is each characteristic index data, that value is denoted by x_j; i is the number of levels of operation scheme, $i=1,2,3...,s$; j is the number of selected characteristic index, $j=1,2,...,m$. Since this paper is a different level of evaluation of the operation scheme (there are five levels in scheme from I to V which include superior, relatively superior, general, relatively poor, and poor), so you can judge $s=5$. Therefore, the formula (1) can be rewritten as (2). Therefore, this is the Bayesian evaluation method which is used as the evaluation and decision basis of the operation scheme.

$$P(y_{ji}/x_j)=\frac{P(y_{ji})P(x_j/y_{ji})}{\sum_{i=1}^{s}P(y_{ji})P(x_j/y_{ji})} \qquad [2]$$

where, x_j is the j-th characteristic index value of the operation scheme.

y_{ji} is the j-th characteristic index standard value of the operation scheme, when the operation scheme level is i.

2.2 Implementation steps of operation decision method based on Bayesian model

According to formula (2), the basic steps to evaluate a operation scheme are as follows:

(1) To calculate $P(y_{ji})$, under the condition of without any priori information, it is difficult to determine which level the operation scheme belongs to. The most accepted principle is that the operation scheme belong to the level with the same probability under the condition of the non-characteristic index value of the operation scheme. This is to take

$$P(y_{j1})=P(y_{j2})=P(y_{j3})=P(y_{j4})=P(y_{j5})=1/5 \qquad [3]$$

(2) To calculate $P(x_j/y_{ji})$, in the Bayesian model for operation scheme evaluation and decision-making, the rational determination of $P(x_j/y_{ji})$ is the most critical. This paper adopt the most commonly used distance methods, because it is intuitive and simple, clear principle. Based on the concept of geometric probability, the distance method can be expressed as: the reciprocal of distance absolute value which is between the characteristic index value of a specific operation scheme and standard value of operation level index is calculated (see figure, 4).

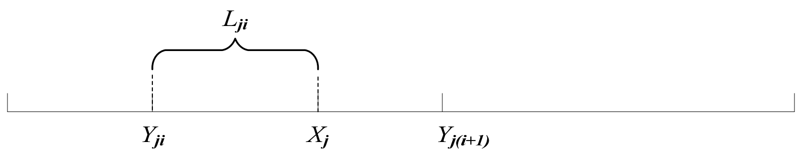

Figure 1. Schematic of distance between characteristic index of operation scheme and operation level.

$$P(x_j/y_{ji})=\frac{\frac{1}{L_{ji}}}{\sum_{i=1}^{5}\frac{1}{L_{ji}}} \qquad [4]$$

where, $L_{ji}=\left|x_j-y_{ji}\right|$, $j=1,2,...,m$; $i=1,2,...,5$. y_{ji} represents the j-th characteristic index standard value, when the operation scheme level is i. x_j is the actual j-th characteristic index value of the operation scheme. L_{ji} indicates that the actual value of the j-th characteristic index of the operation scheme is farther from the standard value y_{ji}, then the probability of the level of the operation scheme belonging to i is smaller. It is worth to say that the summation $\sum(1/L_{ji})$

located denominator to the right of the equation is used to ensure that $P(x_j / y_{ji})$ is significant, $0 < P < 1$.

(3) To calculate $P(y_{ji} / x_j)$, the meaning is: in the case of knowing the j–th characteristic index value x_j in the operation scheme, the calculation of probability which the index belongs to the i-level. It is important to note that the specific values of characteristic index for each feasible operation scheme are calculated for the probability of each operation level (there are five levels in scheme from I to V which include superior, relatively superior, general, relatively poor, and poor). It can also be understood as to calculate the probability that each single characteristic index value of each operation scheme belongs to a different operation scheme level.

(4) To calculate posterior probability, P_i respectively under multi-index synthesis when the operation scheme level is i.

$$P_i = \sum_{j=1}^{m} w_j P(y_{ji} / x_j) \qquad [5]$$

where, x_j is the actual j-th index value of the operation scheme, y_{ji} is the j-th index standard value when the operation scheme level is i; w_j is the impact weight of the j-th index on the operation scheme. P_i is the posterior probability which integrate m indexes, that is the probability of which level is i of the operation scheme after considering the information of m indexes.

(5) The final level h is inferred from the principle of maximum probability.

$$P_h = \max_{i=1\wedge 5} P_i \qquad [6]$$

According to this step, we can evaluate the feasible operation scheme and make the final decision.

3 APPLICATIONS

Zhangze reservoir dam site is located in the northern suburb of Changzhi city, Shanxi Province, is a control engineering in the zhuozhanghe south source stream of upstream zhanghe of Haihe basin, and reservoir basin diagram is shown in figure2 (IWHR, 2012). The reservoir is a comprehensive utilization of large type (Ⅱ) reservoir project with flood control, irrigation, industrial and urban water supply as the mainstay, fish and tourism supplemented. The control drainage area of this reservoir is 3176 km^3, and the capacity of reservoir is 4.27 million m^3. The reservoir is designed with once-in-a-century flood, and calibrated with 2000-year flood. The normal pool level is 902.4m, the design flood level is 903.61m, and the flood level is 908.45m. Flood season is from July to September, of which the flood limit water level in main (July15-August15) is 901.0m, limit water level is 901.5m before flood season (June1-July14) and after the flood season (August16-September30). The floods above the Zhangze reservoir are mainly caused by heavy rains, mostly in mid-July to mid-August, and the storm flood occur less frequently, usually only once or twice every year, especially since 2007, there has been no flood. Therefore, the Office of State Flood Control & Drought Relief Headquarters take Zhangze reservoir to be the second batch of pilot reservoir of the dynamic control of limited level, to carry out the research work on dynamic control of limited level by relevant units, put forward a dynamic operation plans including storage and drain in advance for Zhangze reservoir.

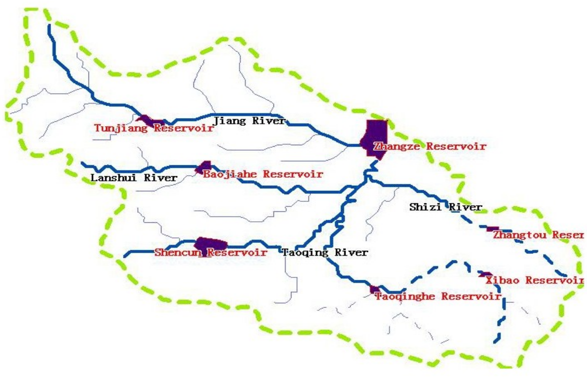

Figure 2. Basin diagram of Zhangze reservoir.

According to the characteristics and experiences of Zhangze reservoir operation, three goals are generally considered in the decision-making of the operation scheme: During the process of reservoir regulation a flood, the highest water level as low as possible, this goal is equivalent to the occupation of the flood storage capacity of the smaller the better; the closer to the ideal water level, the better the end of reservoir flood water level is, this goal is equivalent to the end of flood storage capacity of the ideal reservoir capacity as possible. In the regulation of a flood process, the smaller the maximum discharge flow of the reservoir, or the largest combination flow through the flood control points as possible. Obviously, the first goal is to reflect the flood security of the reservoir and upstream. The second goal is to consider the convergence of the two floods and take into account the benefits of water storage. The third goal is the downstream flood protection of the reservoir.

On the basis of the research results and operation goals of the 《dynamic control research report on flood control level of Zhangze reservoir》, the characteristics of the original design operation scheme of the reservoir and the characteristics of the dynamic operation scheme including storage and drain in advance with different fluctuating limitation level are shown in Table 1 below.

Table 1. Characteristic index value in original operation scheme of Zhangze Reservoir.

Scheme number	Fluctuating limitation level (m)	The highest flood water level(m)	The end of flood water level(m)	The maximum discharge flow of reservoir(m^3/s)
1(Regular operation)	901	904.2	902.73	1365
2(Dynamic operation)	901.75	903.57	901.49	1249
3(Dynamic operation)	902	903.59	901.51	1252

According to the reservoir operation scheme decision-making method based on Bayesian model, each variable calculation results in the Bayesian model are as follows:

(1) Priori probability $P(y_{ji})$. The probability of the operation scheme belong to a certain level is equal in the case that the characteristic values of each index of the operation scheme are unknown. That is:

$$P(y_{j1}) = P(y_{j2}) = P(y_{j3}) = P(y_{j4}) = P(y_{j5}) = 1/5$$

(2) To calculate conditional probability $P(x_j / y_{ji})$, that is, when the operation scheme belong to different levels, the probability of index in the operation scheme.

The standard values of characteristic index corresponding to each level scheme are shown in Table 2.

Table 2. The standard values of evaluation characteristic index corresponding to each level scheme.

Scheme level		Ⅰ	Ⅱ	Ⅲ	Ⅳ	Ⅴ
The standard value of characteristic index	The maximum flood water level(m)	903.55	903.6	903.65	903.7	903.75
	The difference between the end of flood water and fluctuating limitation level (m)	0	0.1	0.2	0.3	0.4
	The maximum discharge flow of reservoir(m^3/s)	1250	1300	1350	1400	1450

For each operation scheme, $P(x_j / y_{ji})$ is calculated respectively. To take operation scheme 1 as an example, the characteristic index of operation scheme: $X = \left(x_j\right) = \left[904.2 \quad 1.73 \quad 1365\right]$, the conditional probabilities $P(x_j / y_{ji})$ for characteristic index x_1, x_2, and x_3 are calculated according to Eq. (4).

(3) To calculate posterior probability $P(x_j / y_{ji})$,

In the case of knowing the j–th characteristic index value x_j in the operation scheme, calculate the probability which the index belongs to i-level. Still taking operation scheme 1 as an example, according to formula (2) and the above step (2) conditional probability calculation results, then:

For the characteristic index x_1, the probability that the index belongs to the i –th level is as follows:

$$P(y_{11} / x_1) = 0.166$$

$$P(y_{12} / x_1) = 0.181$$

$$P(y_{13} / x_1) = 0.197$$

$$P(y_{14} / x_1) = 0.216$$
$$P(y_{15} / x_1) = 0.24$$

In the same way, we can get the posterior probability of characteristic index x_2 、 x_3, which belongs to the level i.

(4) To calculate posterior probability, P_i respectively under multi-index synthesis when the operation scheme level is i.

$$P_i = \sum_{j=1}^{m} w_j P(y_{ji} / x_j) = w_1 P(y_{1i} / x_1) + w_2 P(y_{2i} / x_2) + w_3 P(y_{3i} / x_3)$$

The operation scheme 1 is still used as an example, which can be calculated by Eq. (5)

P_1=0.148； P_2=0.169； P_3=0.260； P_4=0.216； P_5=0.212

Similarly, the posterior probability for each scheme level in operation scheme 2 can be obtained as follows:

P_1=0.479； P_2=0.208； P_3=0.127； P_4=0.13； P_5=0.056

the posterior probability for each scheme level in operation scheme 3 can be obtained as follows:

P_1=0.289； P_2=0.402； P_3=0.083； P_4=0.151； P_5=0.076

(5) The final level h is inferred from the principle of maximum probability.

$$P_h = \max_{i=1\wedge 5} P_i$$

Under this principle, according to the decision-making operation scheme result of Zhangze Reservoir which is determined by reservoir operation scheme decision method based on the Bayesian model, the final level P_h of operation scheme 1 is level III, the normal scheme; Operation scheme 2 is level I , the superior scheme; Operation scheme 3 is level II, the relative superior scheme. Therefore, it is suggested that the reservoir management department or the relevant decision-making department choose the operation scheme 2 as the final operation scheme.

4 CONCLUSIONS

In this paper, the decision-making method for reservoir operation based on Bayesian was applied to the decision-making of Zhangze reservoir. This decision-making method provides a method of how to find a satisfactory decision-making scheme from several feasible operation schemes for the real-time operation of Zhangze reservoir, and achieve the quantitative analysis of the feasible reservoir operation scheme, then provides a scientific, reasonable, practical and accurate decision analysis method for reservoir real-time operation decision-making. It plays an important role on effectively preventing the flood losses of reservoirs and their upstream and downstream caused by operation scheme, and has great realistic significance to effectively utilize and give full control to flood control and irrigation projects and benefits of reservoirs. Compared with other decision-making methods, the Bayesian model can quantitatively evaluate the decision-making results and combine the prior knowledge with the subjective probability. The decision-making method has good reference significance for the decision-making of flood control scheme of reservoirs with outstanding contradictions between flood control and benefit.

REFERENCES

Chen, S. (2001). Semi-Structural Decision-Making Theory and Approach for Flood Control and Dispatching System. *Journal of Hydraulic Engineering,* 11, 26-33.

Gao, R. (2006). Study on Bayesian Decision Making Theory and Methods, *Master Thesis.* Shandong University of Science and Technology, 55-80.

Ni, J., Xu, L., Li, C. & Wang, J. (2004). Review and Research on Reservoir Operation Decision Making. *Advance in Science and Technology of Water Resources,* 24(6), 63-66.

Yu, Z. (2008). Research on Water Quality Assessment of the Three Georges Reservoir based on Bayesian, *Master Thesis.* Shandong University, 20-34.

Qi, P. (2009). Evaluation and Prediction of Water Quality based on Bayesian Network, *Master Thesis,* Wuhan University of Technology, 65-95.

The China Institute of Water Resources and Hydropower Research. (2012). *Research on Dynamic Control of Flood Limited Water Level in Zhangze Reservoir,* Annual Report, IWHR, 50-124.

ASSESSING THE FLOOD DYNAMICS OF THE SOMERSET LEVELS USING TELEMAC-2D

DAVID GLOVER(1) & SHUNQI PAN(2)

(1, 2)Hydro-environmental Research Centre, Cardiff University, Cardiff, UK, CF24 3AA
GloverDM@cardiff.ac.uk; PanS2@cardiff.ac.uk

ABSTRACT

This paper describes the development of 2-Dimensional (2D) computer models with algorithms, suitable for High Performance Computing (HPC), to study the flood dynamics in the flood prone regions, such as the Somerset Levels in the United Kingdom (UK). This study uses the open-sources code TELEMAC-2D as the modelling tool, by implementing various control devices into the model with the high-resolution unstructured mesh, so that the flood dynamics linking to the coastal and fluvial processes can be better understood and more accurately predicted. The model results are expected to be integrated into a decision support system for better coastal zone management in the UK. The development of different unstructured mesh designs and the comparison of initial results with Environment Agency (EA) flood maps is discussed. This study aims to meet and improve approaches towards EU Floods Directive 2007/60/EC regarding coastal flood risk and planning.

Keywords: Flood Dynamics; TELEMAC; somerset levels; storm; computer modelling.

1 INTRODUCTION

Each year, approximately 76,000 people in the UK are at risk of being flooded. Under a business-as-normal scenario, this could also lead to damages of £1bn for urban areas which could again double by 2030 (Marshall, 2015). In the winter of 2013/14, low atmospheric pressure brought persistent heavy rainfall and high tides which led to the extensive flooding in many areas of the UK, causing flooding to over 17,000 acres of agricultural land (Morris, 2014). One of the areas severely affected by the extreme storm conditions is the Somerset Levels. The Somerset Levels is a coastal plain and wetland area situated between the Mendip and Blackdown Hills (see Figures 1 and 2). The River Parrett drains the land to the south whilst the rivers Axe and Brue drain the northernmost parts. The Somerset Levels consist of marine clay "levels" along the coast, and inland (often peat-based) "moors"; agriculturally, about 70% of the area is used as grassland and the rest is arable. The Levels are about 6m above Ordnance Datum (O.D.). The general elevation of the inland moors is around 3 ~ 4m above O.D., which are prone to flooding from upstream fresh water and occasional downstream salt water inundations. The area contains 12 Sites of Special Scientific Interest because of the wetland nature of the Moors and Levels (Environment Agency, undated).

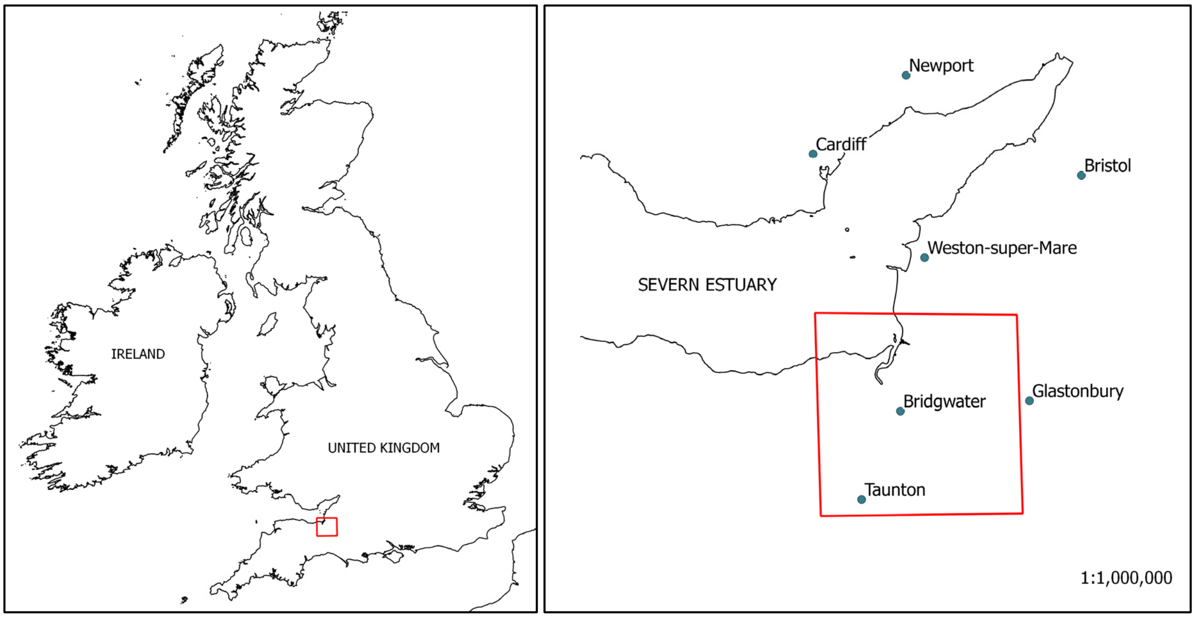

Figure 1. Domain Area (Source Data: European Environment Agency)

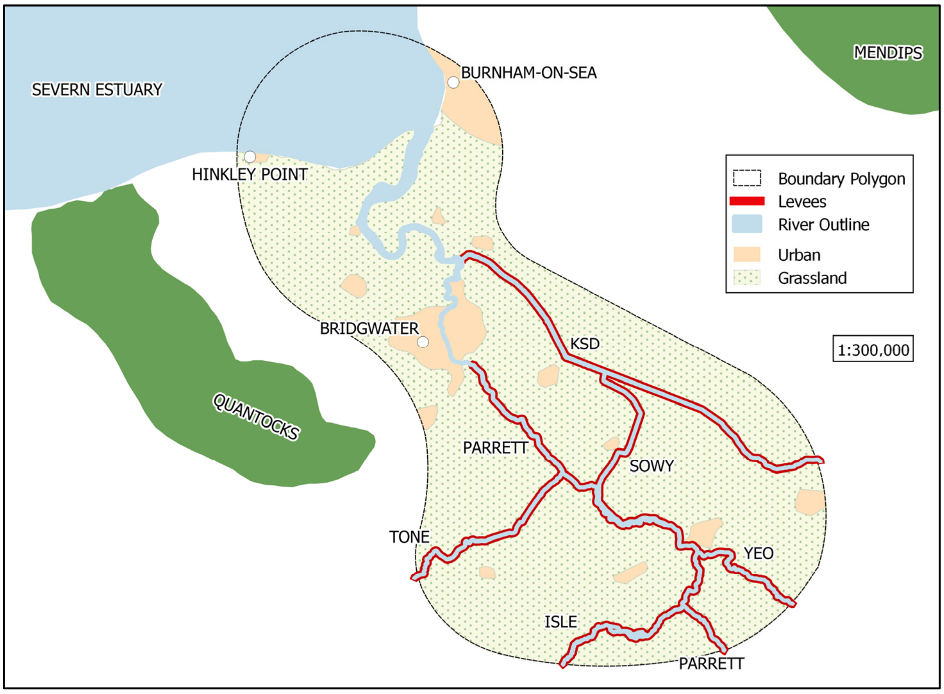

Figure 2. Somerset Levels (Source: Ordnance Survey Open Data)

In this study, the open-source code TELEMAC-2D was used as the modelling tools to assess the flood risk in the study site – the Somerset Levels for the extreme events occurred in the winter of 2013/2014. The TELEMAC modelling framework allows the following advanced features: unstructured mesh for better representation of topography without losing the desired high resolution in the areas of high significance; finite-volume algorithm for mass conservation; TDV schemes for rapidly varying flows; and full parallelization for HPC facilities. The flexibility of user-defined functions and direct access to the source codes allow the improvement of the dynamic friction due to the land use, and implementation of the mitigating engineering measures. By integrating TELEMAC-2D results and QGIS, a robust flood-forecasting system can be designed to assess future flood management strategies effectively. As suggested in Anderson and Bates (2002) and later by Bates (2012), this study utilizes the following approaches to achieve the proposed research aims: using LiDAR data to develop the computational domain for TELEMAC-2D with sufficient high spatial resolution to represent the complex geographic features in the study site; assessing and evaluating the flood mitigation schemes as proposed by DEFRA et al, (2014); and improving the land use management through creating a flood forecasting system and better understanding of the flood dynamics of the Levels.

2 METHODOLOGY

In building the computer model for the study site, the UK 2015 LiDAR data was used to create a computational mesh with varying resolution from 800 m at the offshore area to 5 m in the nearshore and fluvial areas, see Figure 2. Savage et al. (2016) state that above 50 m, probabilistic flood inundation is unreliable due to changes in flow pathways and below 50 m, there is little gain in performance. QGIS was used to supplement this LiDAR date with river bathymetry. Elevation data was interpolated between known elevation points i.e. river gauge stations. The model domain uses OSGB1936 for greater accuracy and compatibility for integrating the results in the QGIS system.

One important feature of the Somerset Levels is the perched rivers which elevate the river beds above the floodplains. If water overflows into the surrounding moors; Curry and Hay Moors etc. it is pumped back into the river as the levees prevent the water receding back into the river at lower flows. The pumping network in the study site is shown in Figure 4. Whilst the integration of pumping functionality into the model is ongoing, the topography of the levees has already been collected through the UK 2015 LiDAR data. Various site visits have been undertaken to gain an understanding of the flood management systems in place but also to supplement the author's knowledge of modelling this domain.

One of the important aspects in flood modelling is that the levees of the river network must be accurately represented in the bathymetry to ensure the river banks ability of containing river flows around populated areas. In TELEMAC, it is suggested that 5 points are used to model levees/dikes to properly handle the flow behaviour. The discretization that is recommended is shown in Figure 5.

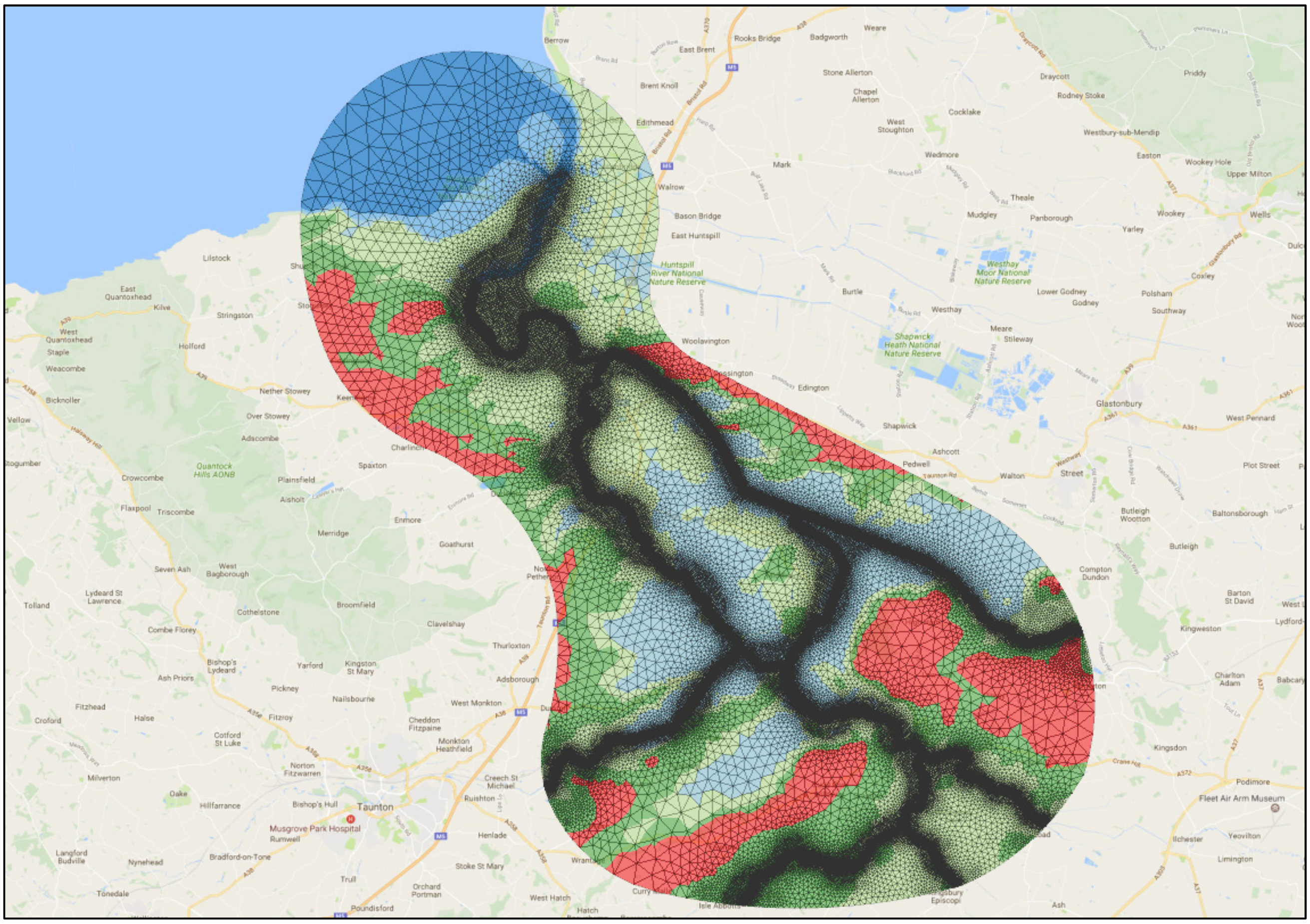

Figure 3. Computational domain and mesh for the Somerset Levels

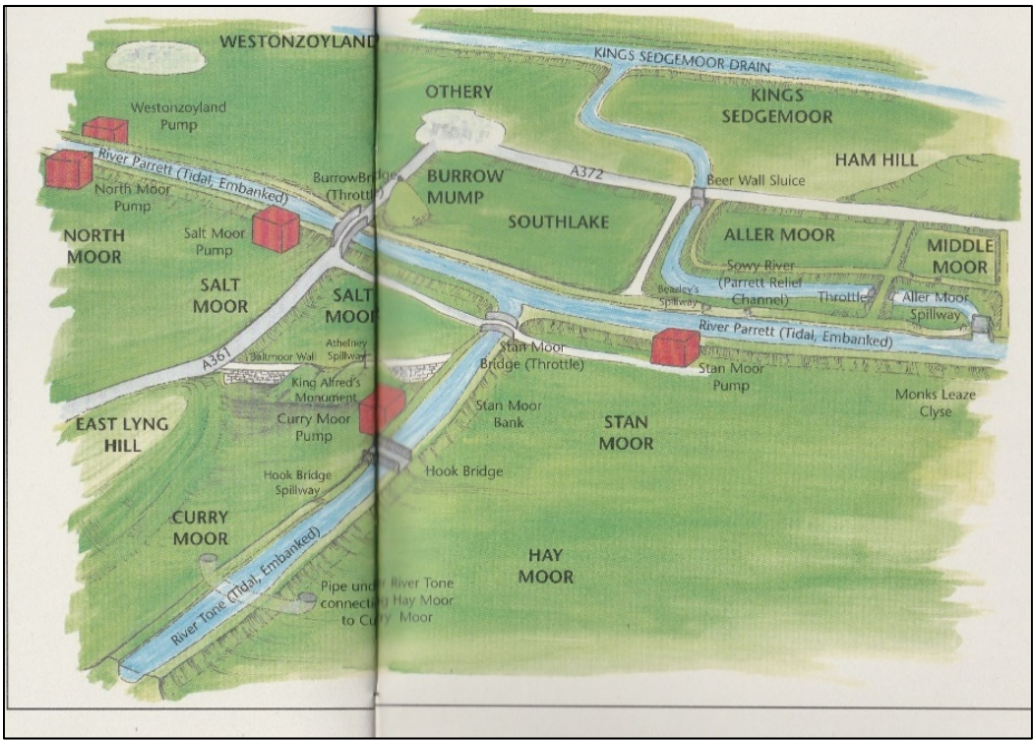

Figure 4. Schematic diagram of the pump network at Salt Moor (Source: Environment Agency)

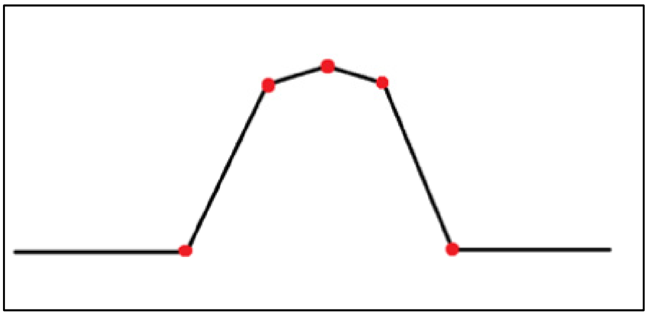

Figure 5. Levee Modelling in TELEMAC (Source: Lang and Desombre, 2013)

The levees and dykes in the Somerset Levels are often less than 10m in width; it was found that finer resolution may be needed to accurately model these features. A more 'detailed' model was created; 2m grid cells formed 'high-resolution belts' either side of the river (Figure 6) to better model these smaller levees. However, this resulted in higher computational times and 850,000 nodes.

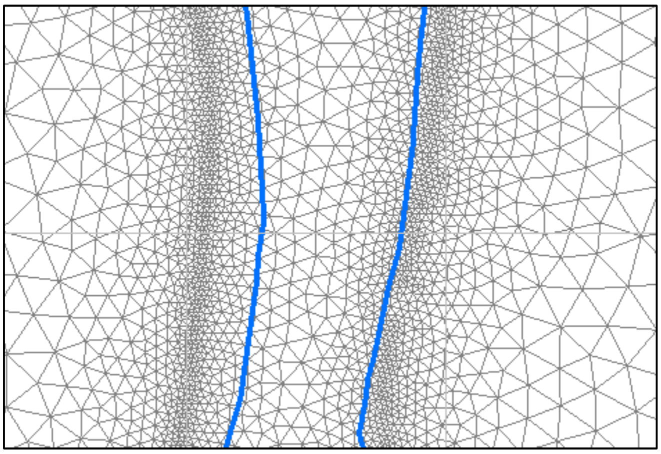

Figure 6. 2m resolution belts around River Levees (in blue)

The operational computational mesh uses a minimum 5m resolution. The contour data was adapted and widened so that each levee cover multiple nodes. More precise grid resolution would show changes in the bank gradient itself whereas the adopted 5m resolution leads to 'smoothed' levees with less points (Figure 7). This mesh has a significantly better running time using <300,000 nodes, making it more suitable for initial model runs with an awareness that this slightly poorer levee representation returns substantial computational savings.

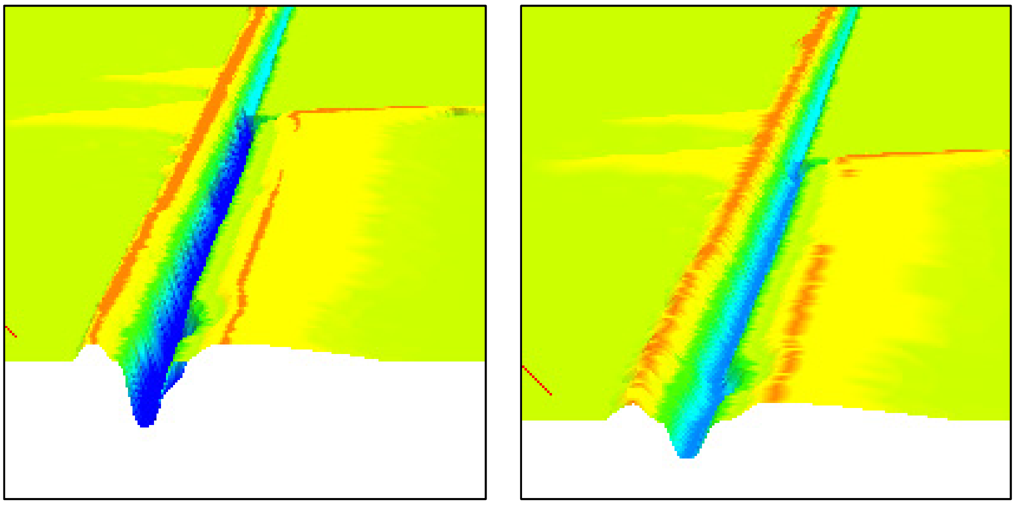

(a) (b)

Figure 7. (a) Detailed and (b) simplified levees on the KSD

Another modification was made to the levees as they are not continuous, there are many small-scale rhines which segment them. Since these small-scale rhines are too small to model this led to large gaps within the levees themselves which have been 'closed' manually through manipulating the contours in QGIS. This guideline was met with the 'detailed' model but not with the 'simplified' model. Many cross-sections were taken for each of the rivers Parrett, KSD, Sowy, Tone, Yeo, and Isle to evaluate how the levees were being represented. Figure 8 shows an example cross-section for the KSD comparing the 5m 'simplified' mesh, KSD 5, with the 2m 'detailed' mesh, KSD 2. There was no such an improvement in the levee modelling to warrant that much of an increase in the computational time. However, it is something that is now apparent and can be simulated in greater detail later in the study.

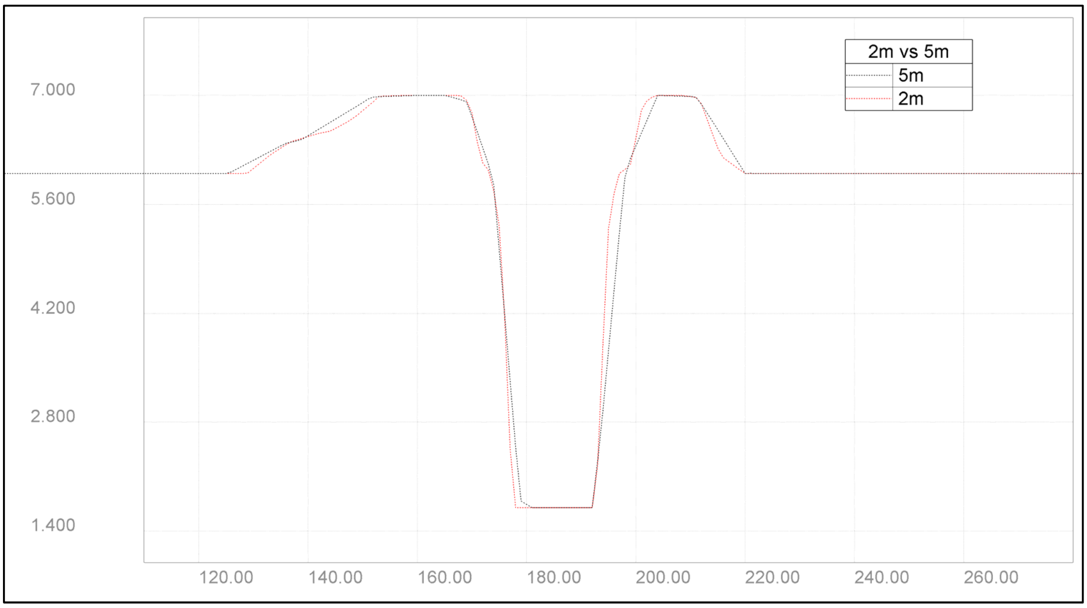

Figure 8. Cross-sectional representation of the River Parrett using 5m and 2m mesh design

This can be implemented as "soft lines" in the post-process software – BlueKenue, for manipulating the positioning of the mesh nodes to capture those areas of higher interest. In a third 'soft' mesh design, soft lines were used to identify the center of the levees with the intention that these nodes plus the surrounding nodes would create those 5 discretization points needed to accurately model a levee (Lang and Desombre, 2013). However, issues arose with the construction of the mesh as to get a suitable result that the mesh resolution had to be increased again, making the simulations too computationally expensive for initial results.

Assigning different friction parameters within a flood inundation model is very important according to Savage et al. (2016b). Their investigation into flood extent; during the drying phase, floodplain friction was the most influential input factor whereas during peak flood the channel friction was more influential. We have applied the following Manning's n values to model friction: urban area (0.015); farming/grassland (0.02) and river channels (0.03). Due to the detail of the land use survey used, this data was dissolved into coarser areas of land use (Figure 2). Savage et al. (2016) also concluded that the spatial resolution is important in assessing the water depths which we should continue to study in detail if we are to produce dynamic flood maps capable of showing depth and time. In Savage et al. (2016b), the friction parameters were separated into two values only: floodplain, 0.025-0.05 and 0.025-0.04 for the channel as justified by Werner *et al.* (2005). In future work, we will vary the Manning's friction within the domain to model changes to land-use and compare the sensitivity of this value when compared to upland catchments.

3 MODEL CONDITIONS

The tide conditions, measured at the Hinkley Point in the Bristol Channel, are used at the downstream end of the computational domain with an averaged surge level during Dec 2013 and Jan 2014 added on. At the upstream end, the multi-year average flowrates for 4 Rivers: Tone, Yeo, Isle, and Parrett, were used. Figure 9 shows the spring and neap tides at Hinkley Point, reproduced from the constituents provide by the British Oceanographic Data Centre (BODC, 2016). The tide ranges were 10.8 m for spring tides and 4.9 m for neap tides, which are near-identical to the Environment Agency (EA) (2013) data with the spring and neap tides being 10.7 m and 4.8 m, respectively. Chart Datums were converted to Ordnance Datum using a conversion of -5.90m specified by National Oceanographic Centre ((NOC, 2017). The mean sea level (MSL) at the Hinkley Point Gauge station was 0.335 mAOD.

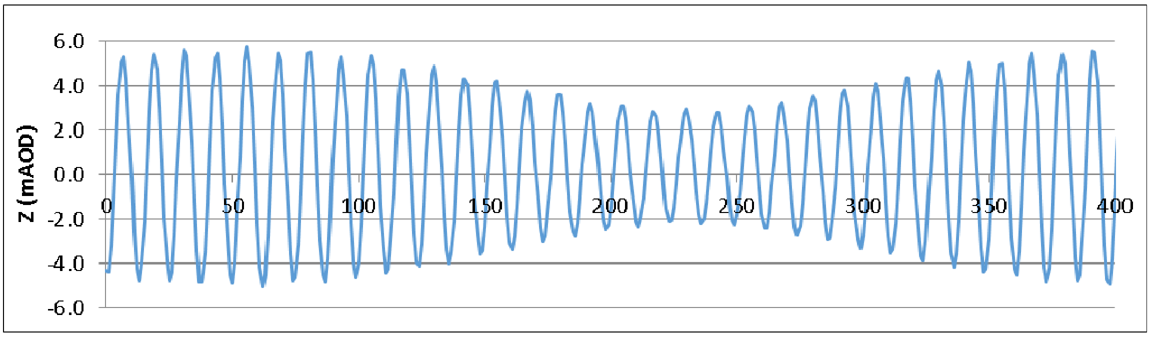

Figure 9. Tide levels at Hinkley Point Tidal Gauge over 400 hours

For surge level at the study area, an average value of 0.4 m was extracted from the BODC data base as shown in Figure 10 for both December 2013 and January 2014. This surge level was added to the total tide level for the downstream boundary conditions.

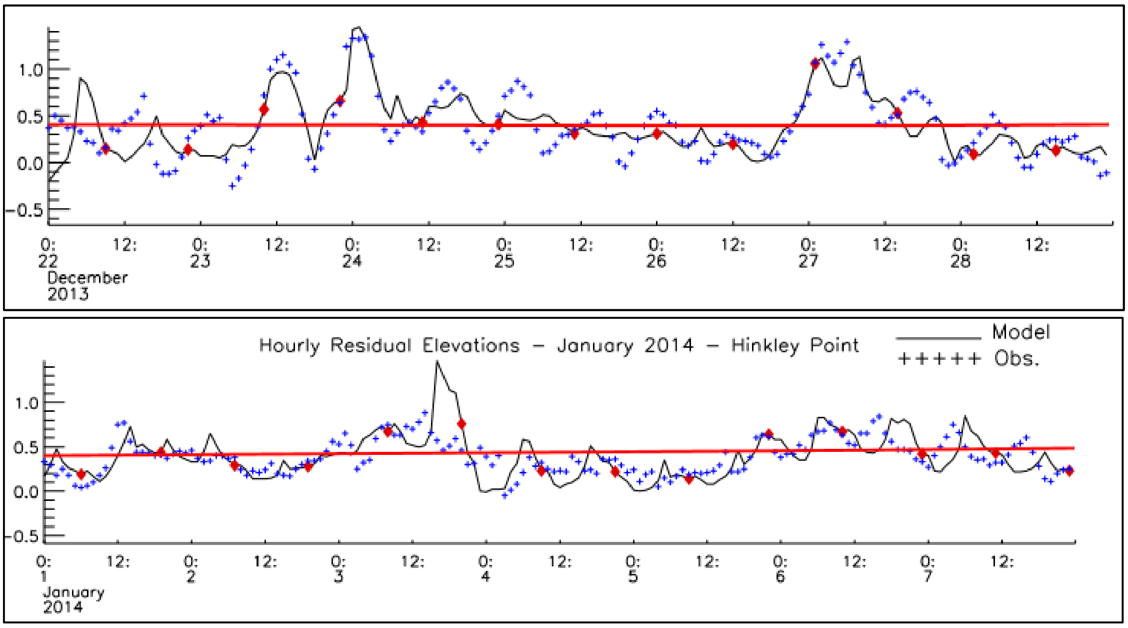

Figure 10. Measured storm surge values between Dec 2013 & Jan 2014 at Hinkley Point (Obs) compared with the UK operational storm surge model (Model). (Source: NOC, 2017b)

Table 1. River discharges in the Somerset Levels

River	Tone	Isle	Parratt	Yeo
Multi-Year average (m^3/s)	3.02	0.83	1.19	2.61
100-Year Return Period (m^3/s)	61.37	16.36	34.25	72.80

4 RESULTS

Figure 11 shows the flood map produced from the model results, which is compared with a typical EA's flood map. The results show that the flood map matches well with the EA's flood map in terms of the extent of the flooded area. The flooded areas between M5 motorway and A39 road, south to the Bridgewater, are correctly reproduced. At the upstream of the River Parratt, the flooded area also agrees well with that shown in the EA's flood map. The results indicate that the model has been correctly set up and the resolution of the computational mesh is adequate. The results also reveal more detailed information on flood water depth in the affected areas in addition to the flood extent, which is extremely useful for effective mitigation measures to be managed.

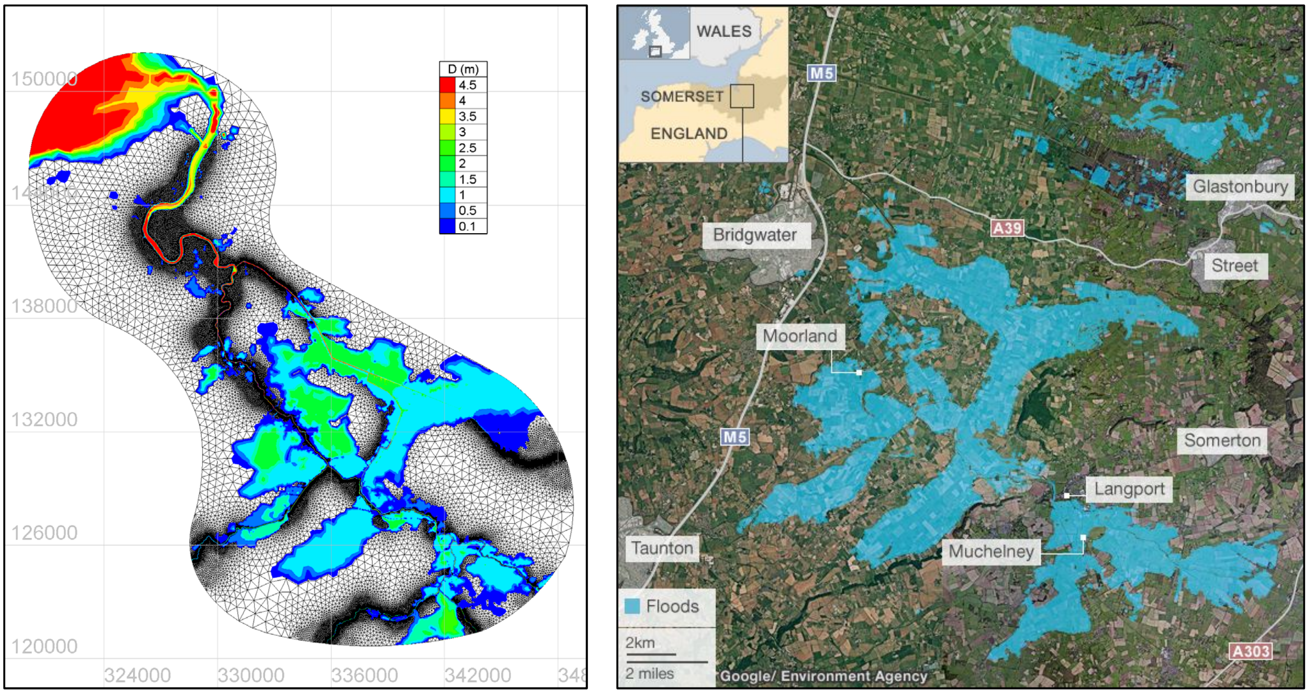

(a) (b)

Figure 11. Flood maps for the Winter Flood 2013/14 from: (a) Model; (b) EA

Figure 12 shows the flood extent and flood water depth when the river discharges with 100-year return period (see Table 1) were used. In comparison with Figure 11(a), it is clear that the flooded areas are extended further, particularly in the area near Moorland (Fig 11b). The flood water depth also increases in places, up to over 3 m. However, the increase of the river discharge mainly affects the upstream reaches of the rivers and has little impact on the land north to Bridgewater, as evidenced from the EA flood map.

5 DISCUSSION

From the 5 m resolution model, the preliminary results show the similarity of the flood extent when comparing the flood maps from model and the EA, see Figure 10, although further refinement is required for better levees of the rivers. However, the overall topography in the model appeared in general is well represented. During the simulation, the undesired leakages of the water from the misrepresented levees of some parts of the rivers due to the interpolation of the bathymetry are found to cause some areas being unrealistically or overly flooded. This highlights the need for more accurate river bathymetry to be used and interpolated to the finer mesh size. Some bathymetric data, in particularly, the depth to channels, is sparse and less accurate, which resulted in the formation of the v-shaped channels, thus, the overall cross-sectional area is reduced. The work is on-going to refine the upstream narrow channels to be as u-shaped channels. Further work also include the implementation of varying friction based on the land use, the weirs and pumping stations in the study site, so that more realistic flood maps can be reproduced and detailed information to be gathered for effective management and mitigation of the floods in this site. The results are also to be integrated with QGIS for stakeholders to view the results especially when coupled with background imagery in real time.

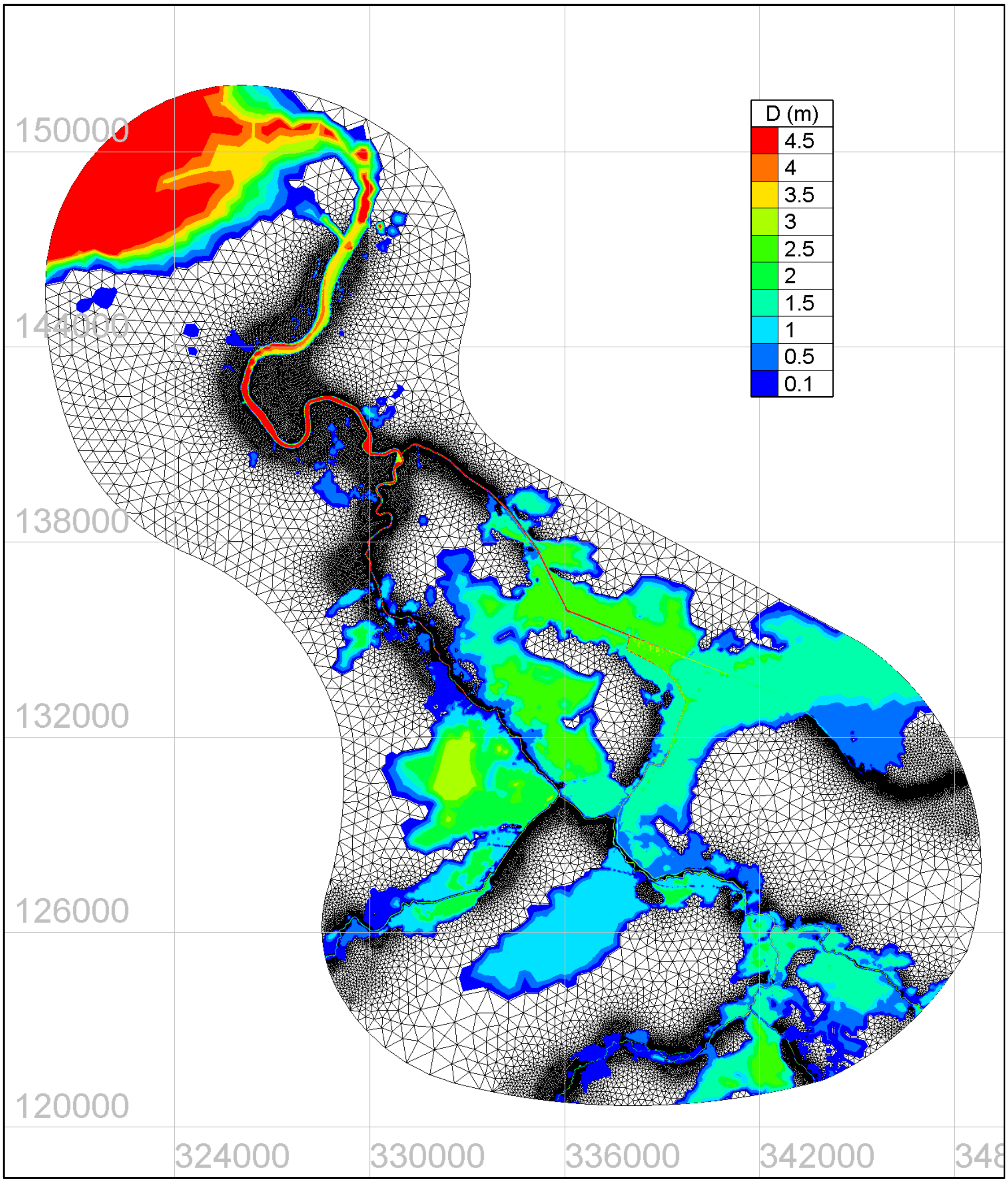

Figure 12. Computed flood extent with 100-Year return period river discharges

6 CONCLUSIONS

A flood model at the Somerset Levels based on the TELEMAC-2D is presented. The preliminary results show similarities of the simulated flood maps with those from the EA's flood, but the flood extent in some areas are unrealistic due to the inaccurate representation of the river levees. More work is required to refine the levees for a better representation. Pumps and other flood management schemes are also to be integrated as this is an important part of the flood management programme in the area especially if the model is to be adopted by industry. If extra data can be collected for the river bathymetry, this would give greater confidence in the results and in the representation of the channel morphology. The LiDAR data has however facilitated the flood inundation study in this area. Flood management schemes can now be experimented and evaluated in a coarser aspect whereas smaller scale studies for the Tone and the Parrett would be beneficial.

ACKNOWLEDGEMENTS

The research reported herein was funded by the Engineering and Physical Sciences Research Council (EPSRC) under the Centre for Doctoral Training in Water Informatics: Science and Engineering (WISE CDT) Program (Grant Number: EP/L016214/1).

REFERENCES

Anderson M.G. & Bates, P.D. (2002). *Evaluating 1D and 2D Dimensional Models for Floodplain Inundation Mapping*. Interim Report 007, US Army. European Research Office of the US Army.

Bates, P. D. (2012) Integrating Remote Sensing Data with Flood Inundation Models: How Far Have We Got?. *Hydrological Processes*, 26(16), 2515-2521.

British Oceanographic Data Centre, BODC (2016). BODC Database [Online] Available from: https://www.bodc.ac.uk/data/ [Accessed: 06/03/2016].

DEFRA, DCLG, DFT, Paterson O & EA (2014). "New action plan to protect Somerset from flooding". [Online] UK Government. Available from: https://www.gov.uk/government/news/new-action-plan-to-protect-somerset-from-flooding. [Accessed: 06/03/2016]

Environment Agency (2013). Hinkley Point C Appropriate Assessment for related Environment Agency permissions. [Online Report] Environment Agency [Accessed: 06/03/2016] Available from: https://www.gov.uk/government/uploads/system/uploads/attachment_data/file/291300/LIT_7887_b828d6.pdf

Environment Agency (2016). *Safeguarding the Somerset Levels and Moors. [Leaflet].* Bridgwater: Rivers House.

Lang, P. and Desombre, L. (2013) TELEMAC-2D Software Release 6.2, Operating Manual [Online Manual] EDF-R&D [Accessed: 06/03/2016] Available from: http://www.opentelemac.org/index.php/manuals/ summary/13-telemac-2d/1058-telemac-2d-user-manual-en-v7p0.

Marshall, C. (2015) Global flood toll to triple by 2030. BBC [Online]. 05 March 2015 [Accessed: 05/02/2017] Available from: http://www.bbc.co.uk/news/science-environment-31738394

Morris, S. (2014). UK floods: council declares major incident on Somerset Levels. The Guardian. [Online]. 24 January 2015 [Accessed: 05/02/2017] Available from: https://www.theguardian.com/environment/2014/jan/24/uk-floods-major-incident-somerset-levels

National Oceanographic Centre (2017). Chart datum & ordnance datum. [Online] Available from: http://www.ntslf.org/tides/datum [Accessed: 18/04/2017]

National Oceanographic Centre, (2017b). Surge model archive for Hinkley Point [Online] Available from: http://www.ntslf.org/storm-surges/monthly-surge-plots [Accessed: 06/03/2016]

Savage, J.T.S., P. Bates, J. Freer, Neal, J. & G. Aronica (2016). When does Spatial Resolution become Spurious in Probabilistic Flood Inundation Predictions?. *Hydrological Processes*, 30, 2014-2032.

Savage, J.T.S., F. Pianosi, P. Bates, J. Freer & T. Wagener (2016b). Quantifying the Importance of Spatial Resolution and Other Factors through Global Sensitivity Analysis of a Flood Inundation Model. *Water Resources Research,* 52(11), 9146-9163.

Werner, M., S. Blazkova, & J. Petr (2005). Spatially Distributed Observations in Constraining Inundation Modelling Uncertainties. *Hydrological Processes*, 19(16), 3081-3096.

Proceedings of the 37th IAHR World Congress
August 13 – 18, 2017, Kuala Lumpur, Malaysia

ASSESSMENT OF DEBRIS ISSUES IMPACTING DESIGN OF A FLOOD DIVERSION PROJECT IN A LARGE SCALE PHYSICAL MODEL

ANDREW CORNETT[(1)], PAUL KNOX[(2)], JOHN MENNINGER[(3)], RICK LUX[(4)] & MITCHEL PROVAN[(5)]

[(1,2,3,5)] Ocean Coastal and River Engineering, National Research Council, Ottawa, Canada
Andrew.Cornett@nrc-cnrc.gc.ca, Paul.Knox@nrc-cnrc.gc.ca, Mitchel.Provan@nrc-cnrc.gc.ca
[(3,4)] Stantec, Cincinnati, USA
John.Menninger@stantec.com; Rick.Lux@stantec.com

ABSTRACT

A large scale physical model study has been conducted to support the design of the Springbank off-stream storage project being planned to protect the city of Calgary, Canada, from catastrophic flooding. The main focus of the physical model study is the behaviour of sediments and the effects of woody debris conveyed downstream during flood events with proposed diversion inlet and sluiceway/spillway structures. This paper introduces the physical model and describes how it is used to assess the performance of the proposed structures and their ability to accommodate large woody debris. The physical model proves to be a very useful tool for assessing and improving the design of new flood control structures to mitigate adverse impacts due to water-borne woody debris.

Keywords: River hydraulics; physical modelling; flood control; debris; diversion inlet.

1 INTRODUCTION

The Elbow River originates at Elbow Lake in the eastern slopes of the Rocky Mountains and flows eastward for roughly 120 km before joining the Bow River in the city of Calgary, Alberta, Canada. The watershed area is 1,238 km^2 at elevations between 1,030 m and 2,100 m above sea level, and has an average grade of 8.8%. The river is susceptible to flooding with catastrophic results. During the flooding event of June 2013, the peak flow rate of the Elbow River entering the Glenmore Reservoir (just west of Calgary) reached approximately 1,240 m^3/s, while the natural capacity of the river, without taking any precautions against flooding, is just 180 m^3/s. The losses experienced during the June 2013 flood were valued in excess of $5 billion. As part of a subsequent flood mitigation study, the Springbank Off-stream Storage Project was conceived to divert the excess flows of the Elbow River during flood events into an off-stream storage reservoir where the flood water could be stored and released gradually back into the Elbow River after the flood peak has passed. The $250+ million project includes design, permitting and construction of a new diversion inlet structure that intersects the Elbow River west of Calgary, a diversion channel excavated through the adjacent land to transport the flow to the off-stream storage reservoir, a new earth dam to impound flood waters in the reservoir, and a new service spillway and sluiceway to control the flow through the Elbow River at the diversion junction, see Figure 1. Figure 2 shows an artist's impression of the diversion inlet and sluiceway/spillway structures based on a preliminary conceptual design.

A physical model study was subsequently commissioned to assist in assessing the performance of the initial designs for the diversion inlet, spillway and sluiceway structures, optimize them as necessary, and verify that these structures would perform well under flood conditions. Of particular concern was the behavior of sediments and the potential for sediment deposition, as well as the impact of woody debris transported downstream on the flood. Hence, the main objectives for the physical model study were to:

- Determine the hydraulic performance of various key elements of the new diversion inlet, service sluiceway/spillway and emergency spillway for a range of operational and extreme flow conditions;
- Assess the behaviour of sediments and the potential for sediment deposition within and around the diversion inlet, sluiceway, and service spillway;
- Assess the impact of debris on the performance of the diversion, sluiceway and service spillway;
- Help optimize the proposed designs to improve conveyance, reduce the risk of erosion and sedimentation, reduce the risk of blockage by debris, improve constructability, and reduce costs where possible; and
- Determine rating curves for the optimized hydraulic structures.

A relatively large length scale of 1:16 was adopted for the physical model study to ensure that distortions due to scale effects would be minimized as much as possible.

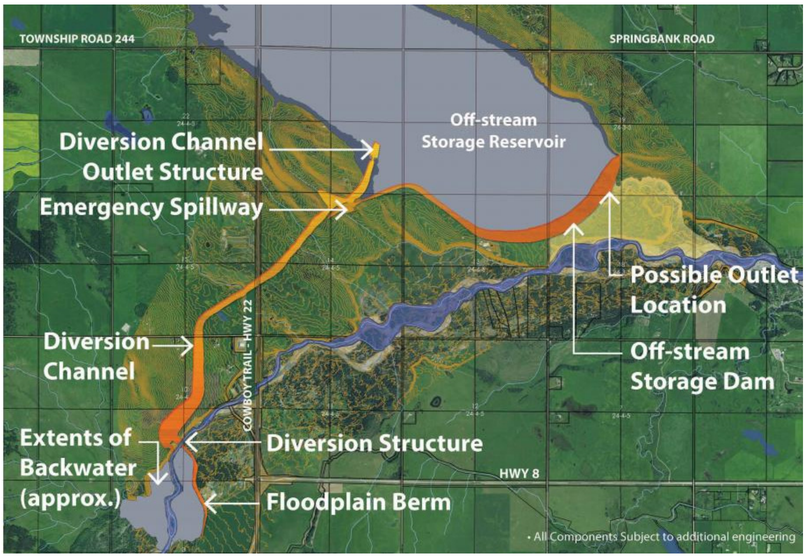

Figure 1. Overview of the Springbank Off-stream Storage Project (Government of Alberta, 2016).

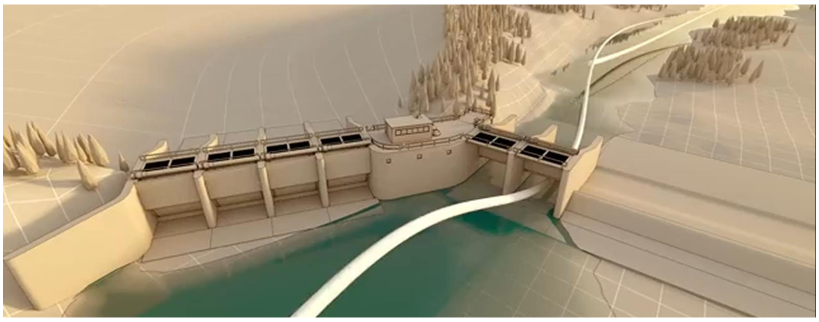

Figure 2. Artist's impression of conceptual designs for the diversion inlet (left) and sluiceway/spillway (right) structures (Government of Alberta, 2016).

The current paper provides an overview of the physical model and its role in assessing the interaction of floating debris with the proposed diversion inlet and sluiceway/spillway structures. While several different structure design alternatives were modelled and assessed in the study, this paper will focus on the initial design considered in the first part of the study. Alternative designs that offered improved performance were considered in the second half of the study, but these are not discussed in this paper.

The Elbow River watershed extends into the Rocky Mountains west of Calgary, and large portions of the watershed are densely forested with mature conifers (Hemlock, Spruce, Lodgepole Pine and other similar species). The floodplain near the project site is littered with large clumps of old woody debris, see Figure 3, clear evidence of the many trees uprooted and transported downstream during previous flood events. Any future flooding will feature downstream transport of new and old woody debris, both as individual trees and clumps or rafts comprised of many pieces interlocked together. It is clear that any new flood control structures need to be designed to accommodate this debris load to the extent possible.

Figure 3. Photos showing bottom sediments and woody debris on the Elbow River floodplain.

Field surveys were conducted (by others) to collect information on the sediments in the riverbed near the site and the type of woody debris to be expected during flood events. The field surveys found that:

- 63% of logs had root wads;
- The mean log length was 16.5 m (standard deviation of 4 m);
- Mean diameter of the large end was 0.44 m (standard deviation of 0.09 m); and
- Mean diameter of the slender end was 0.14 m (standard deviation of 0.09 m).

The diversion inlet and sluiceway/spillway structures were designed primarily to regulate the volume of water passing downstream through the diversion channel and natural river channel for various flood events, up to an including events with a peak discharge of 1,240 m^3/s. The desired flow split for several design flood discharges is summarized in Table 1. A 48/52 flow split was desired for the 1,240 m^3/s design event (600 m^3/s through diversion inlet and 640 m^3/s through the sluiceway/spillway) whereas a 80/20 flow split (600 m^3/s into the diversion and 160 m^3/s into the downstream river channel) was desired during the 760 m^3/s flood. The control structures were equipped with gates that could be raised and lowered to achieve the desired regulation.

The initial structure designs modelled in the first part of the study are shown in Figure 4 and Figure 5. The diversion inlet has a 46 m wide opening divided by three 2 m wide piers into four 10 m wide sub-channels. Each diversion inlet sub-channel is equipped with a raised sill and radial lift gate. The 10 m wide sluiceway is located on the left riverbank (looking downstream) and is fitted with a lift gate. The service spillway has a 31 m wide opening, a single small central pier, and is fitted with a set of adjustable hinged Obermeyer-type crest gates.

Table 1. Target discharges (m^3/s).

Combined discharge	Diversion discharge	Downstream river discharge
160	0	160
320	160	160
760	600	160
1,240	600	640

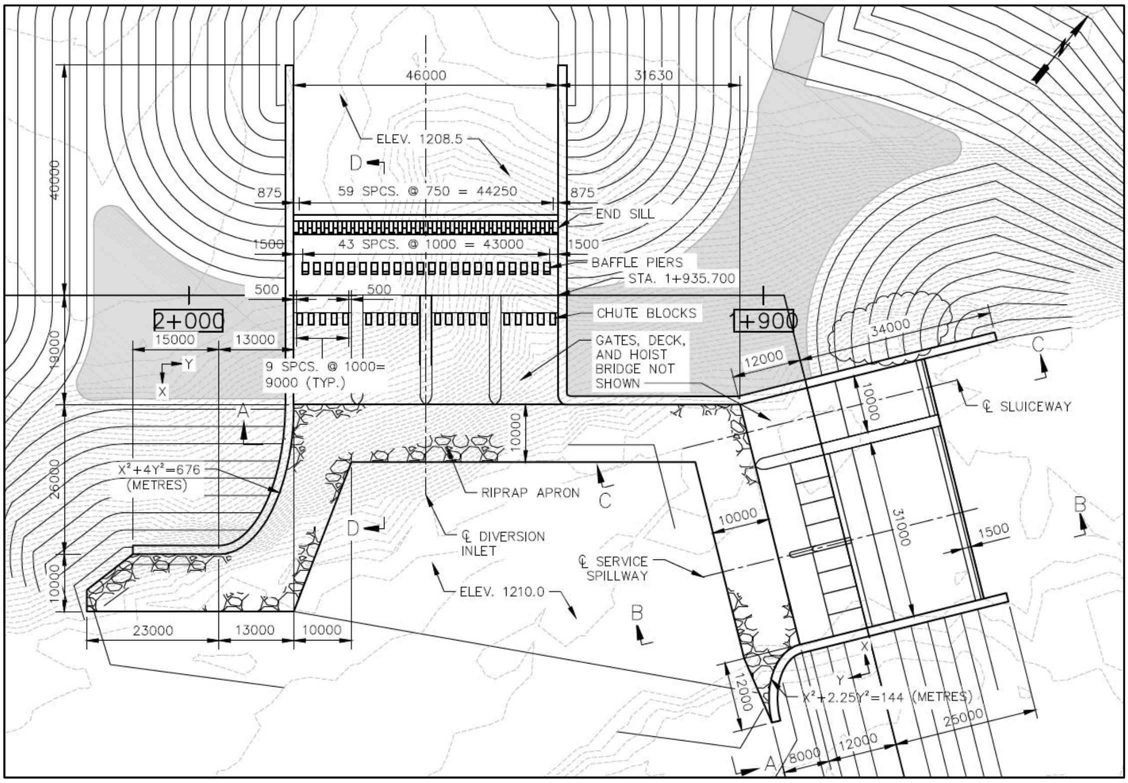

Figure 4. General arrangement of initial designs for the diversion inlet and sluiceway/spillway structures (by Stantec).

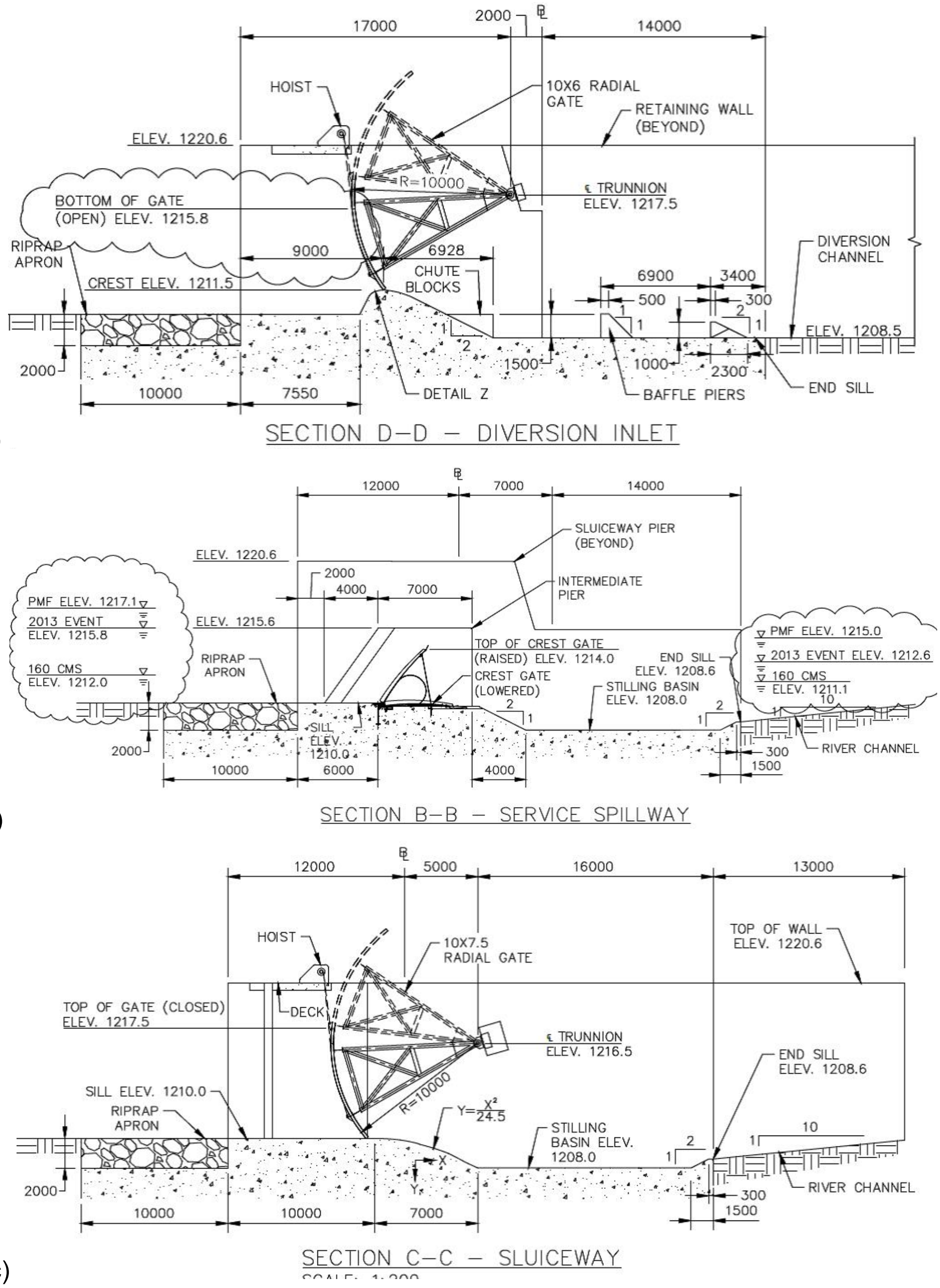

a) b) c)

Figure 5. Cross-section views of: a) diversion inlet, b) service spillway and c) sluiceway structures (by Stantec).

Physical modelling has been used on many previous occasions to investigate the interaction of woody debris with bridges, river flow control structures and its behaviour in braided channels. Reports of previous studies include Baraudrick et al. (1997; 2001), Bocchiola et al. (2006), Gschnitzer et al. (2013), Lyn et al. (2003) and Welber et al. (2013). While the present study was informed by this previous work, it is believed to be innovative and unique in several respects:

- The use of a relatively large 1:16 length scale and the large size of the model.
- The realistic manner in which the woody debris was modelled, i.e. harvesting appropriately sized tree branches from the forest rather than using smooth wooden dowels.
- Realistic manner in which the trees growing on the floodplain were modelled.
- Investigation of the relative behaviour of debris with and without root wads.
- Investigation of the relative behaviour of natural debris (tree branches) and artificial debris (smooth wooden dowel).

2 THE PHYSICAL MODEL

The selection of a suitable geometric scale is a key element in the design of any physical model. Mobile-bed models are especially sensitive in this regard. Although many factors are considered, the decision hinges on establishing a compromise between two important and conflicting requirements:

- minimizing scale effects, particularly with respect to the simulation of sediment transport processes, by selecting the largest model scale possible; and
- working within constraints related to the dimensions and capabilities of key equipment such as the test facility, the pumps used to generate flows, and the sensors used to monitor conditions in the model.

For models with mobile, erodible beds, these erodible materials must be carefully selected to ensure that they provide a reasonable representation of prototype behaviour. While large scale models are generally more realistic, they are also more expensive to build and operate.

An undistorted three-dimensional physical model of the proposed diversion inlet and sluiceway structures was designed and constructed at a length scale of 1:16. This scale represents a reasonable compromise between minimizing scaling and boundary effects, while maximizing the extent of the model domain and the accuracy of processes under investigation. This large scale physical model occupied a footprint of 50 m by 30 m and included realistic reproductions of the bathymetry and topography around the location of the diversion inlet, including the existing river channel and adjacent floodplain and proposed diversion channel as well as the diversion inlet and sluiceway/spillway structures. The physical model layout is sketched in Figure 6, while Figure 7 provides a general overview of the model during testing. All aspects of the model, except for the mobile-bed sediment, were designed using Froude scaling criterion which assumes that gravitational and inertial forces are dominant in comparison to viscous forces.

The bathymetry and topography were modelled as a rigid surface formed in grout. Where appropriate, the concrete grout was given a stiff broom finish to roughen the bottom of the river channel, diversion channel and floodplain to approximate the hydraulic roughness of the prototype channels. Also, where the prototype floodplain was tree-covered, tree branches harvested from the forest were cast into the wet grout with a placement density similar to prototype conditions. A variable-pitch pump drawing from a large sump was used to supply a steady (adjustable) discharge into the upstream end of the model, and a pair of adjustable weirs were used to control the water level at the downstream end of both the river and diversion channels. Various flood flows up to the 1,240 m^3/s event were simulated by regulating the inflow discharge via the pump controller, while using the adjustable sharp-crested weirs to control the downstream water levels. The model was outfitted with instruments for measuring water levels and flow velocities in multiple locations. The discharge passing through the diversion and downstream river channels was estimated by measuring the water levels above the two sharp crested weirs and applying a well-known relationship between head and discharge.

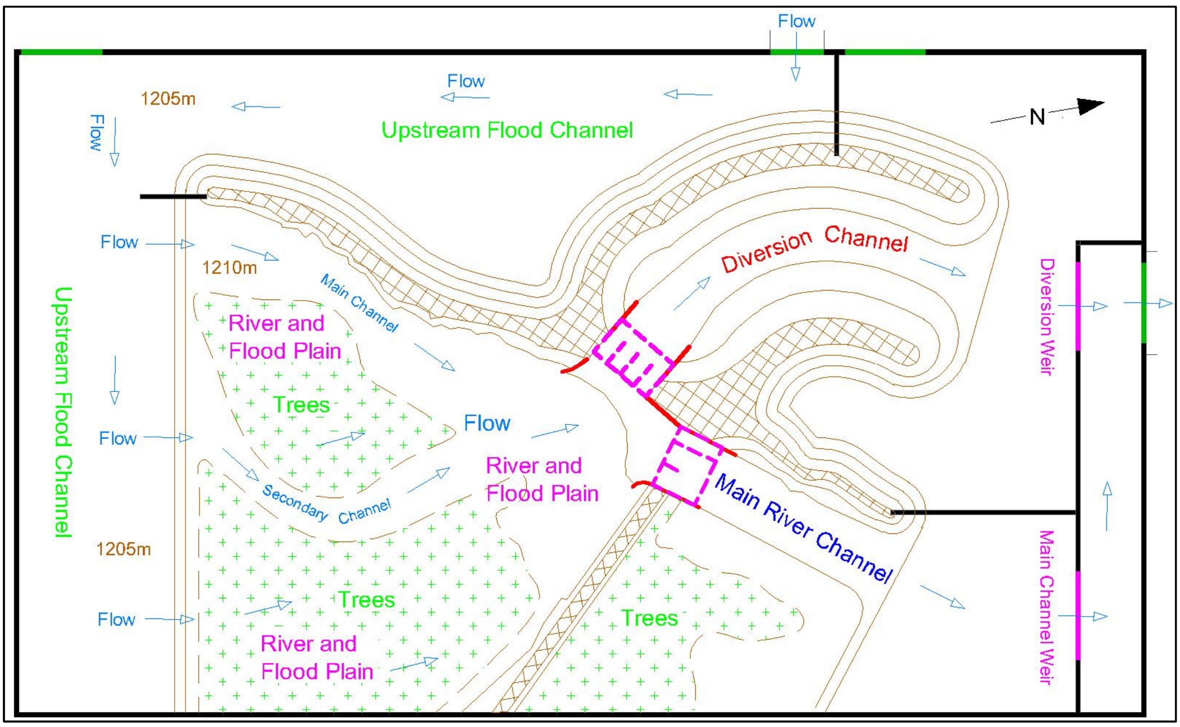

Figure 6. General layout of the 1:16 scale physical model.

Figure 7. Overview of the 1:16 scale physical model looking upstream.

Faithful scaled reproductions of the diversion inlet structure, the sluiceway and the service spillway were designed and constructed, see Figure 8. The diversion inlet gates were not required and where therefore not modelled; however, the model sluiceway was equipped with an adjustable lift gate, while the model service spillway had adjustable bottom-mounted Obermeyer-type crest gates. These gates were adjusted as needed to control the water level in the “headpond” area immediately upstream of the structures, and the portion of the incoming flow that was diverted into the diversion channel.

a)

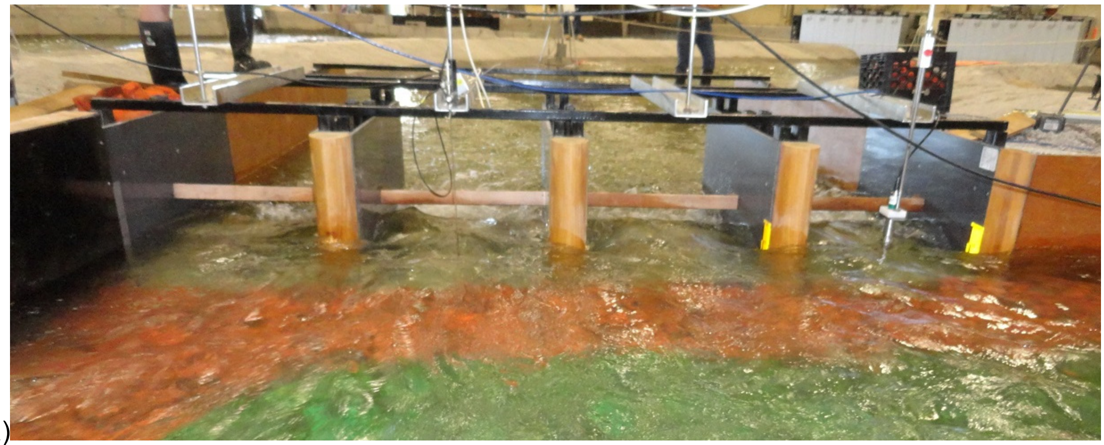

b)

Figure 8. Physical model of: a) diversion inlet and b) sluiceway and service spillway, looking downstream.

A fine granular material was selected, based on equivalent mobility, and used in some tests to represent the coarser sediments observed on the riverbed and floodplain at the site. For these tests, a large portion of the upstream riverbed was preloaded with sediment, and additional sediment was delivered during testing at prescribed rates using three mechanical spreaders fed from large sediment hoppers. Three-dimensional laser scanning was used to map the initial and final geometry of the mobile bed before and after a test, and identify the changes in bed morphology caused by specific flood flows. In other tests where sedimentary processes were not being investigated, the riverbed was lined with a coarser granular material that was non-erodible.

Over 300 pieces of woody debris were prepared for use in the physical model to simulate mature conifer trees that had been uprooted and transported downstream by previous floods and observed near the project site. It was decided to focus on modelling large woody debris, as the larger debris was expected to be more problematic. The model debris was prepared from tree branches with mean diameters from 0.025 to 0.031 m (0.4 m to 0.5 m full scale) harvested in the forest and then cut to random lengths between 1.0 and 1.3 m (16 m to 21 m full scale). A small (~0.1 m) "X" shape made of timber was secured to one end of ~60% of the branches to simulate a root wad (or root ball). It is noted that the length of the model trees was greater than the 10 m open distance between adjacent piers of the diversion inlet structure and the 10 m width of the sluiceway.

3 ASSESSMENT OF DEBRIS ISSUES

Streamlines were identified by tracking, with overhead cameras, the pathways followed by neutrally buoyant drogues introduced in several upstream locations. Examples of the flow pathways identified for the 320 m^3/s and 760 m^3/s flow conditions are shown in Figure 9. For the 320 m^3/s condition, 50% of the upstream flow passes through the diversion inlet, with the remainder passing through the sluiceway and service spillway. For the 760 m^3/s flow condition, 80% passes through the diversion inlet and 20% passes through the sluiceway/spillway. The flowlines and the position of the flow split line for each case reflect these differences.

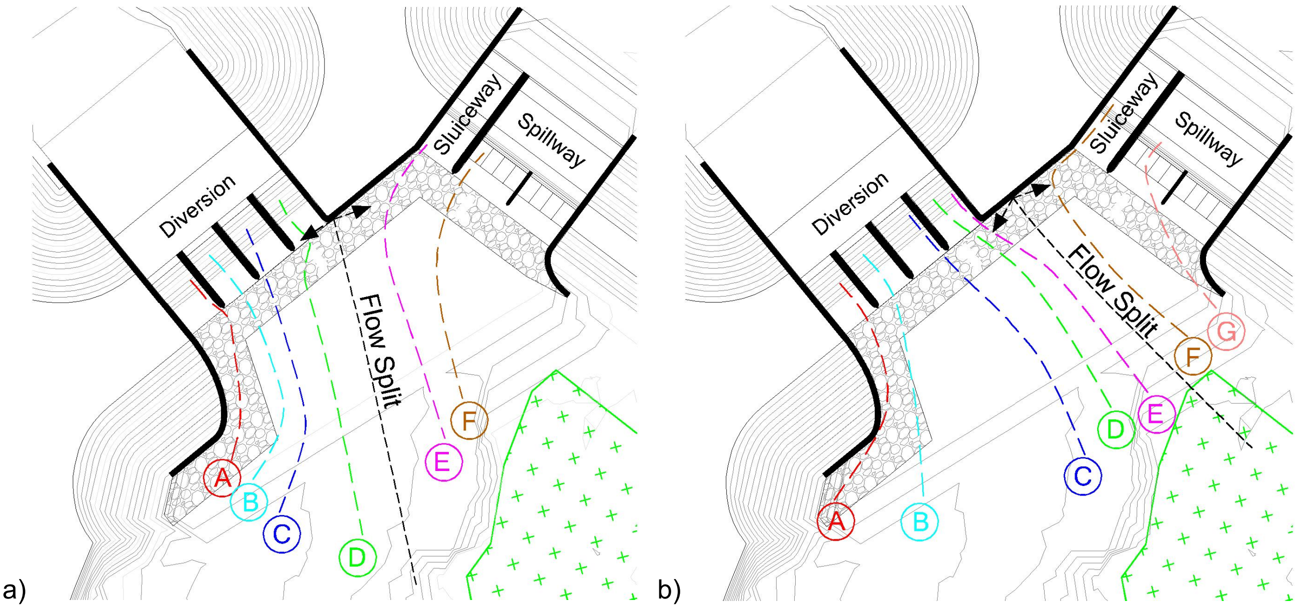

Figure 9. Flow pathways for the a) 320 m^3/s and b) 760 m^3/s flow conditions.

The behaviour of individual debris pieces as well as debris rafts of various sizes was investigated in the model. Once stable flow conditions were achieved, the debris was added to the flow in various upstream locations and allowed to travel downstream, propelled only by the flow. Individual trees were typically studied first, followed by a series of debris rafts comprised of four, ten and forty trees. Some of the model trees passed through the diversion inlet and were retrieved from the diversion channel. Others passed through the sluiceway and/or service spillway and were retrieved from the downstream river channel. For higher flows, some trees passing through the service spillway became trapped in the roller that formed immediately downstream of the Obermeyer-type crest gates.

Many model trees were snagged on the upstream side of the diversion inlet and sluiceway/spillway structures and did not pass downstream, see Figure 10. Individual trees oriented roughly parallel to the flow were able to pass through the 10 m wide sub-channels of the diversion inlet. However, trees oriented perpendicular to the flow often become snagged on the upstream face of the inlet piers. In order to simulate conditions expected at the peak of the flood, the trees that became snagged were generally left in place while additional debris was added upstream. Once the first tree was snagged, other trees released in the same upstream location were more likely to become snagged as well. The number of trees trapped at the upstream face of the diversion inlet grew over time, as did the size of the debris raft that formed there. Eventually, the size of the snagged debris raft became large enough to affect the discharge passing through the diversion inlet and the flow split between the diversion channel and the downstream river channel. Flow reductions on the order of 10% were observed for very large debris rafts comprised of ~150 model trees.

  / ISSN 1562-6865 (Online) - ISSN 1063-7710 (Print)

a) 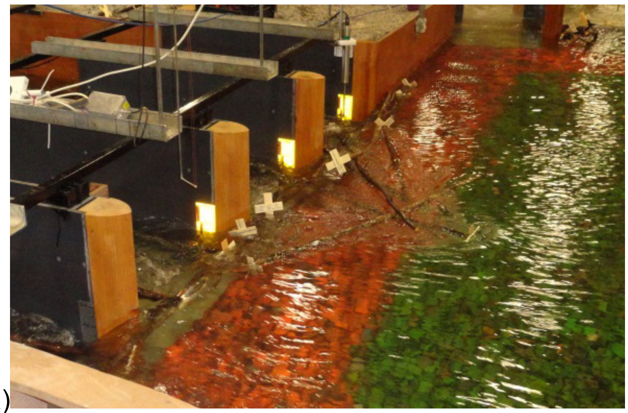 b) 

Figure 10. Single trees (a) and a 40-tree raft (b) snagged on the diversion inlet piers.

Debris interaction with the sluiceway was highly dependent on the flow condition and gate settings. Trees were unlikely to pass through the 10 m wide sluiceway whenever the sluiceway gate was lowered below the upstream water level. Even when the sluiceway gate was fully open, some trees became snagged on the adjacent pier and bridged across to the left abutment, see Figure 11.

The likelihood of trees passing through the service spillway was strongly dependent on the depth of water above the crest of the Obermeyer-type gates. Trees were routinely snagged on the gate crest and/or central pier when the water depth was low, and passed more frequently when the depth was greater, see Figure 11. For moderate freeboard conditions, model trees with a root wad, were far more likely to become snagged on the gate crest than those without, due to their greater draft when floating.

Figure 11. Woody debris trapped on the upstream side of the sluiceway (left) and service spillway (right).

Individual trees with a root wad were consistently more likely to become snagged than equivalent trees without a root wad. The snagging and accumulation of trees was slower when trees with root wads were excluded, and was accelerated by including trees with root wads. These experiments showed that the presence of a root wad has an important influence on the debris-structure interaction process. The root wads increase the probability of snagging, and they also improve the degree of interlocking within a debris raft. This increased interlocking makes it more difficult to break apart a debris raft once it has formed. Given that much of the woody debris observed near the project site includes either stub-branches and/or a root wad of some sort (see Figure 3), the use of model debris with simulated root wads is believed to provide an improved simulation of true prototype behaviour.

The natural woody debris used in the physical model study was comprised of branches cut from the forest which had small irregularities and greater surface roughness than equivalent "artificial" debris comprised of lengths of smooth wooden dowel. To investigate the influence of the irregularities and surface roughness, a series of tests were conducted in which the behavior of the natural woody debris was compared with the behavior of equivalent artificial debris (equivalent lengths of smooth wooden dowel with equal diameter). The results showed that the natural debris was more likely to become snagged in the model. Thus, the surface roughness and irregularity of the natural debris was found to be an important factor influencing the debris-structure interaction process. The use of model debris derived from natural sources having realistic surface roughness and irregularities is believed to provide a more realistic simulation of prototype conditions.

Based on the results discussed above, alternative structure designs with fewer piers and wider openings were developed, modelled and assessed in the second part of the study. The new diversion inlet featured two 20 m wide sub-channels instead of four 10 m wide sub-channels. The 10 m wide sluiceway was eliminated and the location of the service spillway was moved upstream closer to the diversion inlet. Four different types of pier noses were also modelled and their relative ability of shedding debris was assessed. The revised designs were much better adapted to accommodating the downstream transport of large woody debris and avoiding the formation of debris jams during flood events.

4 CONCLUSIONS

An undistorted physical model with a length scale of 1:16 was designed, constructed and operated to support the design of diversion inlet, sluiceway and service spillway structures proposed as part of the Springbank off-stream storage flood control project. The physical model generated valuable information on the hydraulic conditions around these structures for a range of flood flows; information that was useful for calibration and validation of a numerical model of the flood hydraulics. In addition, the physical model was used to assess the behaviour of sediments and large woody debris transported downstream during flood events; important processes that were difficult to investigate numerically. The large woody debris observed on the floodplain at the site was represented in the physical model using real tree branches with realistic surface roughness and irregularities; an approach that is believed to provide a realistic simulation of prototype conditions. Tests were conducted in which the behaviour of individual trees, a series of individual trees, and debris rafts comprised of 4, 10 and 40 overlapping pieces was investigated for several flood scenarios. This approach proved to be an efficient method for assessing debris-related issues, such as the tendency for large woody debris to accumulate on the upstream side of the structures.

Results from the first phase of the model study were used to inform the development of alternative structure designs that would improve the hydraulic conditions and the conveyance of large woody debris and reduce the tendency for woody debris to snag and accumulate at the upstream side of the structures. The revised structure designs were subsequently implemented, assessed and validated in the physical model. The physical model proved to be a very useful tool for assessing the performance of the proposed flood control structures, informing the development of refined structure designs, and confirming the performance of new structure designs that delivered improved downstream conveyance of large water-borne woody debris during flood events.

REFERENCES

Baraudrick, C.A., Grant, G.E., Ishikawa, Y. & Ikeda, H. (1997). Dynamics of Wood Transport in Streams: A Flume Experiment. *Earth Surface Processes and Landforms*, 22(7), 669-683.

Baraudrick, C.A. & Grant, G.E., (2001). Transport and Deposition of Large Woody Debris in Streams: A Flume Experiment. *Journal of Geomorphology*, 41(4), 263-283.

Bocchiola, D., Ruili, M.C. & Rosso, R. (2006). Transport of Large Woody Debris in the Presence of Obstacles. *Journal of Geomorphology*, 76(1-2), 166-178.

Government of Alberta. (2016). Springbank Off-stream Reservoir Project. <http://aep.alberta.ca/water/programs-and-services/flood-mitigation/flood-mitigation projects/springbank-road.aspx>. [Accessed on December 20, 2016].

Gschnitzer, T., Gems, B., Aufleger, M., Mazzorana, B. & Comiti, F. (2013). Physical Scale Model Test on Bridge Clogging. In *35th IAHR World Congress, Chengdu*.

Lyn, D., Cooper, T., Yi, Y., Sinha, R. & Rao, A. (2003). *Debris Accumulation at Bridge Crossings: Laboratory and Field Studies*, School of Civil Engineering, Purdue University, Joint Transportation Research Program, 48, 1-61.

Welber, M., Bertoldi, W. & Tubino, M. (2013). Wood Dispersal in Braided Streams: Results from Physical Modeling. *Water Resources Research,* 49, 7388–7400.

OPTIMIZATION OF OPERATING AGRICURTUAL DIVERSION WEIRS TO MITIGATE FLOOD

MITSUMASA ANAN[(1)], KOZUE YUGE[(2)] & KOSUKE HAMADA[(3)]

[(1,2)] Faculty of Agriculture, Saga University, Saga, Japan
anan@cc.saga-u.ac.jp, yuge@cc.saga-u.ac.jp
[(3)] Graduate School of Bioresource and Bioenvironmental Sciences, Kyushu University, Fukuoka, Japan
hama.suke1204@gmail.com

ABSTRACT

Prompt gate control of diversion weirs is required to flow the excess water under the flood condition. It is also important for gate opening method of diversion weir to ensure safety and simplicity to prevent the water accidents and human errors. The aims of this study are evaluating the effect of gate opening of a series of diversion weirs on the temporal and spatial fluctuations of river water level and optimizing the gate opening operation for disaster prevention under the flood condition. A simulation model describing one dimensional unsteady flow is introduced to evaluate the effect of the gate opening of multiple diversion weirs on the downstream current in the Onga River. Using this model, the spatial and temporal variations of the river water level are clarified under the different patterns of gate opening operation. To evaluate the influence that the fall dawn time for weir affects the change of water level, river water level simulations are calculated for six observed floods. As the result of river water level calculated using unsteady flow model, it is recognized that the fall down time for the weir are related to the change of the river water level closely. In particular, the fluctuation of water level and extent of impact by gate opening varies with the speed of the gate opening. The appropriate speed of the gate opening is clarified to reduce the fluctuation of water level by gate opening under the flood condition. The method introduced in this study is effective to develop the optimal gate control method of the diversion weirs for not only prompt flood protection but also safety.

Keywords: Flood control; irrigation facility; surface water track; river modeling; unsteady flow.

1 INTRODUCTION

When constructing the agricultural diversion weir, it is also important to pay attention to flood control function so that it may not become the obstruction of flowing water or the cause of overflow at the time of flood occurring, in addition to planning so that irrigation water can be taken appropriately. However, the proper control of maintenance of agricultural water facilities is becoming a difficult situation from advance of aging of the farmer, or decrease in population of a rural area of these days.

Agricultural water facilities in Japan have multiple functions for water environment or habitat. In order to exhibit those functions, the techniques of continuous maintenance and management of facilities are very important (Yuge et al., 2008). Furthermore, the drowning accidents in a river under water management work at the time of flood have also occurred in various places, and improvement and simplification of the agricultural water management system are also required. Therefore, while maintaining the safety on structure, it will be important to estimate the application of facilities that agricultural diversion weirs are appropriately operated at the time of flood, and to aim at an improvement of the operation method.

The aims of this study are evaluating the effect of gate opening of a series of diversion weirs and spatial fluctuations of river water level and optimizing the gate opening operation for disaster prevention under the flood condition. A simulation model describing one dimensional unsteady flow was introduced to evaluate the effect of the gate opening of multiple diversion weirs on the downstream current in the Onga River, Japan. Construction of the simulation model was performed using MIKE11 (DHI, 2009) which is used all over the world as an analysis tool of hydrology. MIKE11 is used for the water surface tracking and runoff analysis in consideration of water management facilities in various rivers, and is very accurate, and its reproducibility is good (Kamel, 2008; Timbadiya et al., 2014; Wijesekara et al., 2014).

Furthermore, optimal gate operation method that collateralize both the safety and efficiently at the time of a flood by setting up the diversion weir gate operation conditions variously within the simulation model are looked for in this study.

2 STUDY SITE

Onga river which extends for 61km and its basin is 1,026km^2 is located in Fukuoka Prefecture (west of Japan). A simulation model was performed to the about 15km section from the upstream water level observation point 'Ookuma' to the downstream observation point 'Kawashima'. Figure 1 shows the map of

 / ISSN 1562-6865 (Online) - ISSN 1063-7710 (Print)

study site and Figure 2 shows a longitudinal section of the object river with the positions of agricultural diversion weirs.

The vertical difference of the object section is about 35m, and the stream bed slope is 1/400.And the agricultural diversion weir is located at eight places of the object section. In addition, the DW1 was demolished by the flood from the heavy rain (224mm d^{-1}) generated in the summer of 2010. In most of these floodgates, deterioration is progressing so they will be repaired in the near future. At that situation, it is necessary to examine a design condition of the weir, taking the influence of gate operation of other weirs into consideration.

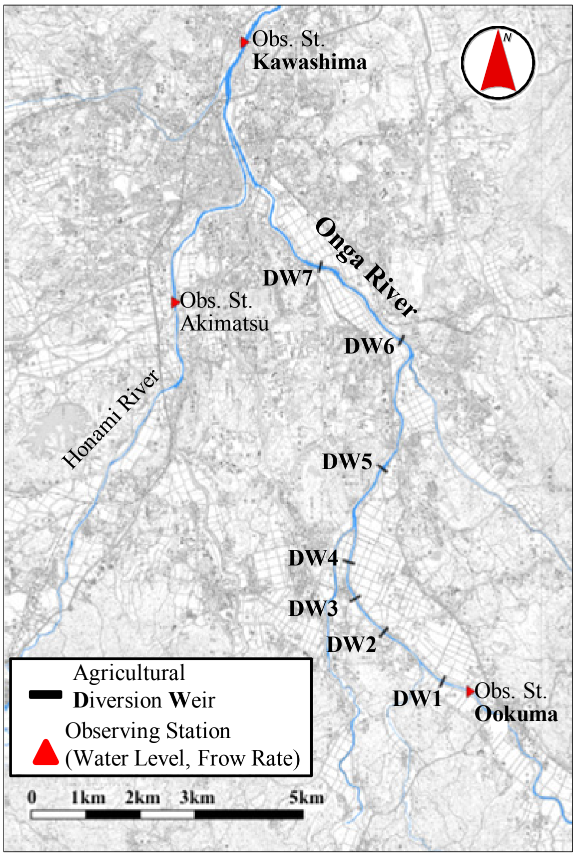

Figure 1. Study river and location of the agricultural diversion weirs.

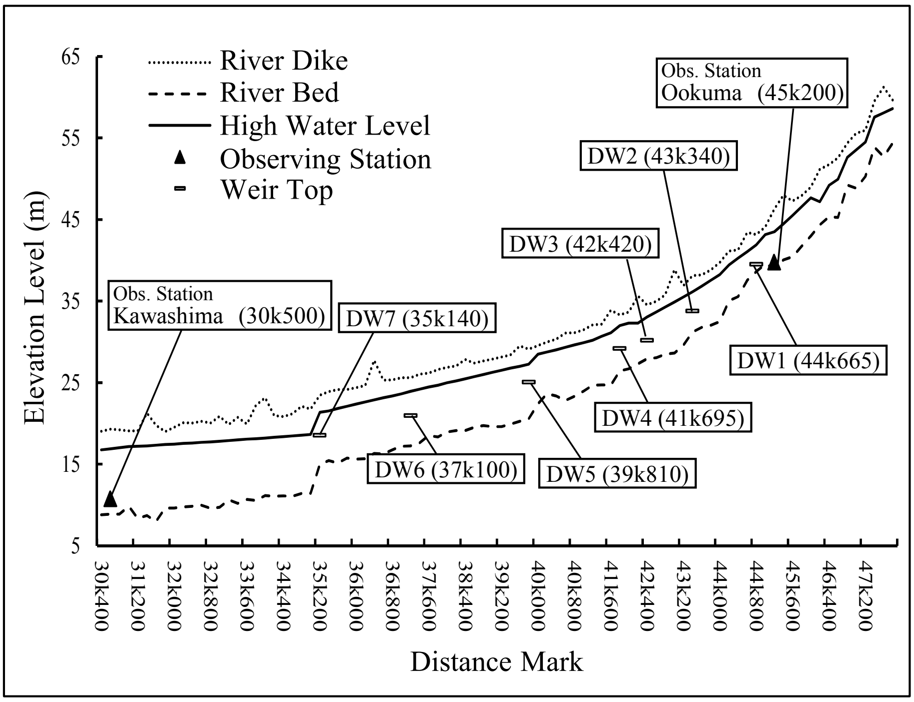

Figure 2. Elevations of the river bed and bank, and high water level.

  / ISSN 1562-6865 (Online) - ISSN 1063-7710 (Print)

3 MATERIALS AND METHODS

3.1 Governing Equation

In this study, a simulation model describing one dimensional unsteady flow using MIKE11 was introduced to evaluate the effect of the gate opening of multiple diversion weirs. In this code, unsteady flow can be described with following motion equation and equation of continuity.

$$\frac{1}{g}\left[\frac{\partial v}{\partial t}\right]+\frac{1}{g}\frac{\partial}{\partial x}\left[\frac{v^2}{2}\right]-S+\frac{\partial h}{\partial x}+\frac{n^2|v|}{R^{4/3}}v=0 \qquad [1]$$

$$\frac{\partial A}{\partial t}+\frac{\partial Q}{\partial x}-q=0 \qquad [2]$$

Where, g: gravitational acceleration(m s^{-2})
v:average flow velocity (m s^{-1})
S:river bed slope (-)
h:water depth (m)
n: roughness coefficient (-)
x:segment length (m)
t:time (s)
R: hydraulic mean depth(m)
A: cross-sectional area of water flow (m)
Q:water flow rate(m^3 s^{-1})
q:cross direction flow rate (m^3 s^{-1} m^{-1})

In this model, the depth of water of the main lattice position shown in Figure 3 was calculated with the finite difference method proposed by Abbott and Ionescu (1967). The water depth of the point of the diversion weir was calculated using Villemonte (1947) formula shown in the following equation.

$$Q=Qc\left\{1-\left(\frac{h_2}{h_1}\right)^{1.5}\right\}^{0.385} \qquad [3]$$

$$Qc=1.8Bh_1^{\;1.5} \qquad [4]$$

where, h_1: water depth by the side of the upper stream of the gate(m)
h_2: water depth by the side of the downstream of the gate (m)
B: width of the overflow weir (m)

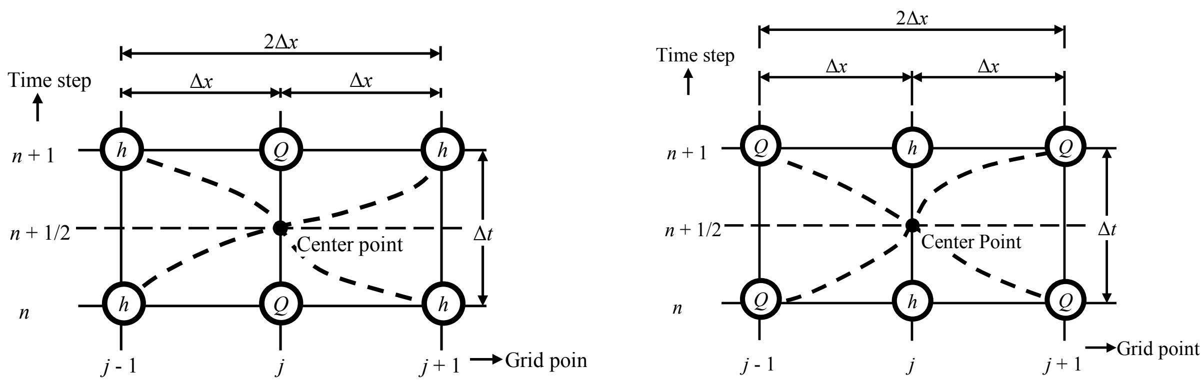

(a) Motion equation (b) Equation of continuity

Figure 3. Numerical schemes of governing equations.

3.2 Modeling of falling down operation of diversion weir

At the point of diversion weir, flow rate and water depth of the overflow were calculated using the water depth of the water level calculation grid point (in Figure 3). When a diversion weir begins to fall down, the water level before and behind a weir would change gradually. When the calculation water level of the diversion weir point reaches a fall water level, the weir starts to fall down at fixed speed. Since the fall down time of a weir was modeled, the following equation was defined.

$$v_w = \frac{H_w}{t_w} \qquad [5]$$

where, v_w: fall down speed of a weir (m s^{-1})
H_w: height of a weir (m)
t_w: time taken to complete fall down of a weir (s)

By setting up t_w variously, the fall down speed of the weir was changed and the water level was calculated.

3.3 Boundary conditions

As an analysis period, six floods by which the remarkable rise of the river water level was observed in recent years were chosen. Figure 4 shows the flow rate of the downstream end at the flood.

In order to calculate change of a water level, the water gauge data which were in the upstream and downstream point of the object section were given as a boundary condition. Further, water budget calculation was performed using the flow rate observational data of the downstream point, and the flow rate Q of the branch junction were set up.

Under these conditions, the spatial and temporal variations of the river water level were clarified under the different patterns of diversion weir operation.

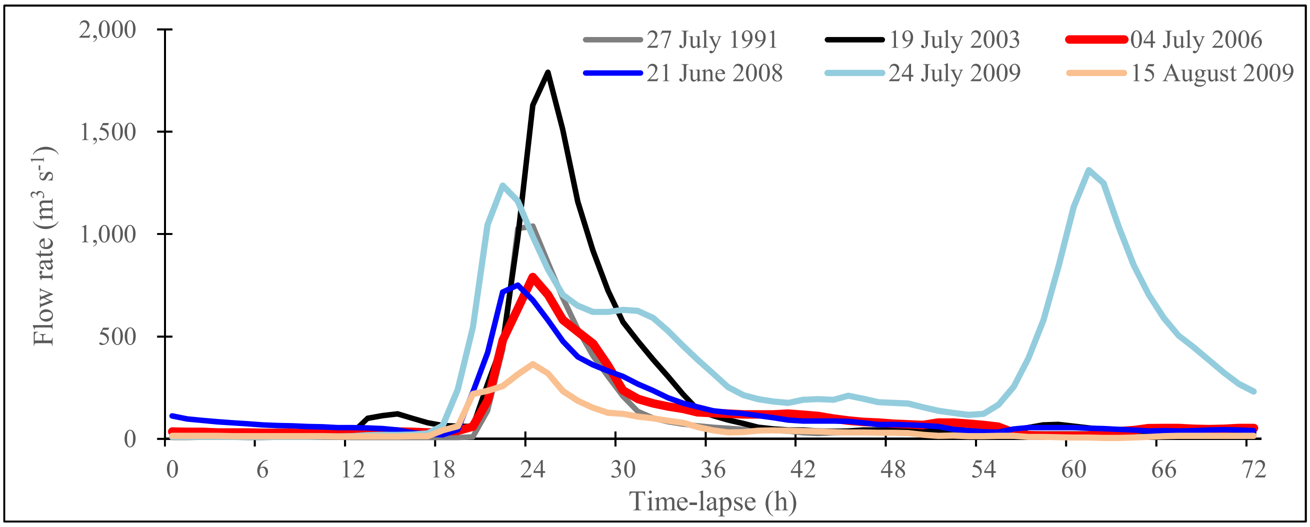

Figure 4. Hydrograph of the downstream end as boundary condition for simulation.

4 RESULTS AND DISCUSSION

4.1 Surface water tracking in consideration of operation of diversion weir

Figure 5 shows a part of the calculation result for the flood occurred on July 4, 2006. The target flood peaks at 22:00, but, after the peak of the flood arrival, water level begins to decline from the upstream, and, on the other hand, the water level of the downstream side continues rising. The model calculations reproduce the situation the diversion weirs are falling down sequentially from the side of upstream to downstream.

By this calculation result, when the upstream diversion weir (DW1) started to invert, downstream side water level of DW1 rose 5cm. The precipitation of this flood was a peak before this water level rise, it seems that sudden increase in river flow rate and the fall down time for the weir are related to the change of the river water level closely.

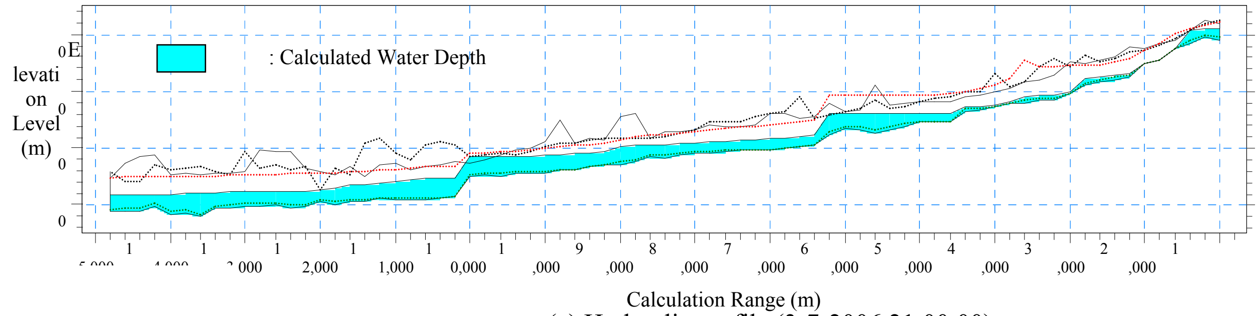

(a) Hydraulic profile (3-7-2006 21:00:00)

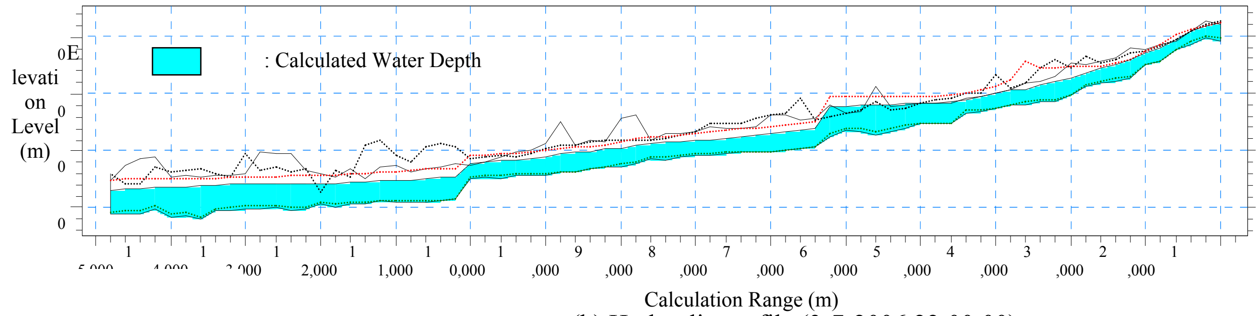

(b) Hydraulic profile (3-7-2006 22:00:00)

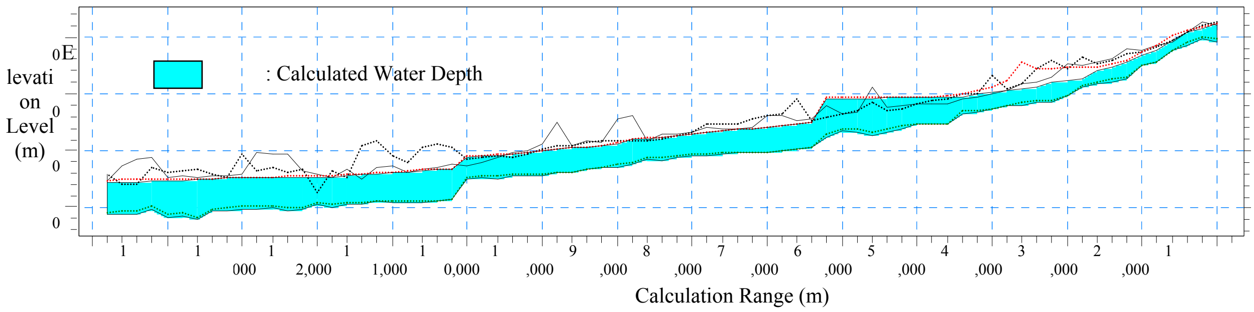

(c) Hydraulic profile (3-7-2006 23:00:00)

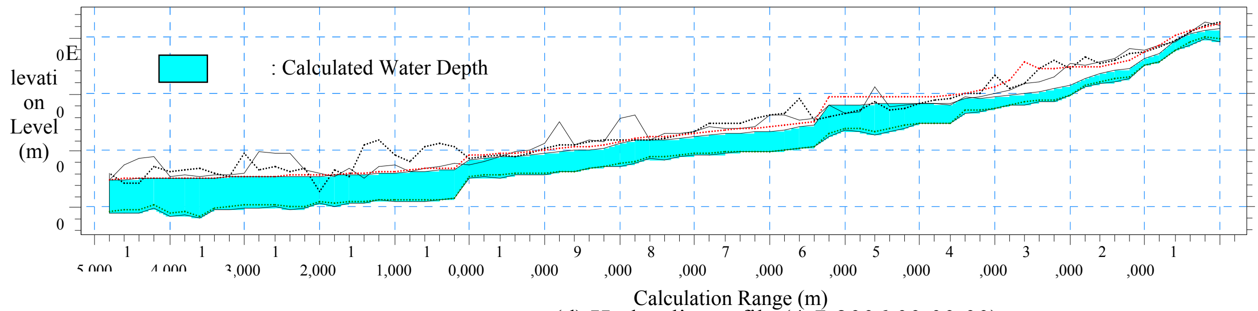

(d) Hydraulic profile (4-7-2006 00:00:00)

Figure 5. Temporal and spatial fluctuations of the river water level calculated as unsteady flow.

4.2 Effect on the change of river water level under diversion weir control

To evaluate the influence that the fall dawn time for weir affects the change of water level, river water level simulations were calculated for six observed floods. As the simulation conditions, three cases of fall down time for weir (for 20 minutes, 30 minutes and 40 minutes) were set, and the water level change of the downstream side was confirmed.

Figure 6 shows the water level change of the downstream side of DW1 which located upstream and start to fall down first at the time of flood. From Figure 6, it was clear that influence extends to the water level change of the approximately 800m downstream by the fall dawn of DW1. In addition, it was shown that a downstream water level change was remarkable so that fall down time was short. As distance left the dam, the water level change tended to be reduced. From these simulation results, it may be said that 40 minutes are appropriate as for the fall dawn time for DW1 at the time of the flood.

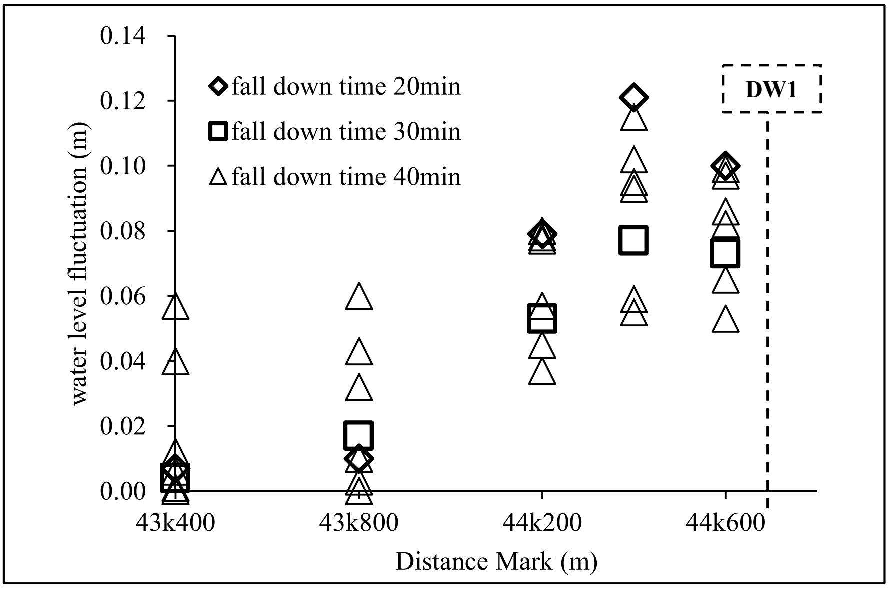

Figure 6. Spatial fluctuation of the river water level with operation of diversion weir.

5 CONCLUSIONS

To evaluate the effect of gate opening of a series of diversion weirs and spatial fluctuations of river water level, a simulation model describing one dimensional unsteady flow was introduced.

As the result of river water level calculated using unsteady flow model, it was recognized that the fall down time for the weir are related to the change of the river water level closely. From these analyses, it was revealed that the change of river water level occurred to 800m downstream part by operating diversion wear (DW1). As the conclusion of this result, it was proper to set fall dawn time of DW1 for 40 minutes in order to control a water level change in the downstream part.

Generally, when a flood occurred, prompt gate operation is demanded to flow down quickly. However, it was proven that flowing down sometimes might cause remarkable rise of the water level and overflow of the downstream side. The operation of the agricultural diversion weir in flood has to establish the fall down conditions based on mutual influence carefully to have an influence on the downstream part complicatedly.

REFERENCES

Abbott, M.B. & Lonescu, F. (1967). On the Numerical Computation of Nearly Horizontal Flows, *Journal of Hydraulic Research*, 5(2), 97-117.

DHI (2009). *MIKE 11, A Modelling System for Rivers and Chanels, Reference Manual*, Danish Hydraulic Institute.

Kamel, A.H. (2008). Application of a Hydrodynamic MIKE 11 Model for the Euphrates River in Iraq. *Slovak Journal of Civil Engineering*, 2008(2), 1-7.

Timbadiya, P.V., Patel, P.L. & Porey, P.D. (2014). One- Dimensional Hydrodynamic Modelling of Flooding and Stage Hydrographs in the Lower Tapi River in India. *Current science*, 106(5), 708-716.

Villemonte, J.R. (1947). Submerged Weir Discharge Studies. *Engineer News Record*, 139, 54-56.

Wijesekara, G.N., Farjad, B., Gupta, A., Qiao, Y., Delaney, P. & Marceau, D.J. (2014). A Comprehensive Land-Use/Hydrological Modeling System for Scenario Simulations in the Elbow River Watershed, Alberta, Canada. *Environmental Management*, 53(2), 357-381.

Yuge, K., Anan, M. & Nakano, Y. (2008). Historical Development of Rice Paddy Irrigation System and Problems on Water Management in Recent Years: Yamada Diversion Dam Command Area in Japan. *Journal of the Faculty of Agriculture,* Kyushu University, 53(1), 215-220.

THE IMPACT OF FLOODPLAIN DEGRADATION ON FLOODING IN THE UK

GEORGE HERITAGE[1] & NEIL ENTWISTLE[2]

[1] AECOM Exchange Court 1 Dale Street, Liverpool L2 2ET
George.Heritage@AECOM.com
[2] University of Salford, Peel Building, University of Salford, Salford M5 4WT, UK

ABSTRACT

A review of floodplain functioning in the north of England following the winter storms of 2015 is conducted using high resolution aerial imagery of the events captured using drone and helicopter survey during and immediately after the flooding. This reveals that for the most part, 100% of the floodplain area is inundated. Sediment left across floodplains from the 2015 flood events areas suggests high floodplain velocities (> 1.5 m/s). GIS analysis of land use mapping for valley bottom areas across England reveals part of the cause for these unnaturally high velocities is the near complete loss of natural rough floodplain surfaces, having been replaced by a hydraulically smoother managed arable/grassland mix. The review has revealed extensive and severe degradation of floodplain systems in England and it is highly likely that similar results would be found for floodplains across the rest of the UK, both upland and lowland areas are equally impacted and the result is an almost complete loss of natural floodplain functioning. River restoration remains concentrated on in-channel activity, however, the push for natural flood management offers an opportunity to restore our floodplains with an associated improvement in ecological value and flood driven functionality. The research presented here suggests that it is not lack of floodplain storage space in the upper catchment, rather the decreased efficiency of floodplain areas to retard flow which is leading to increased downstream flood risk. Floodplain reconnection, vegetative naturalization and selective grazing reduction are required to begin to restore upstream floodplain flood function to alleviate flooding pressure downstream.

Keywords: Floodplains; flooding; land management; natural flood risk management.

1 INTRODUCTION

Natural floodplains have been shown to be among the most biologically productive and diverse ecosystems on Earth (Tockner and Stanford, 2002). This is in a large part due to their dynamic nature forming the transitional ecotone between aquatic and terrestrial environments. Natural fluvial dynamics result in flood-controlled disturbances, encouraging geomorphic processes and successional patterns (Amoros and Roux, 1988; Junk et al., 1989). As a result, floodplains in their natural state exhibit complex dynamic spatial mosaics controlled by the surface and subsurface hydrological regime (Thoms, 2003). These features also reflect past and present geomorphological activity associated with the fluvial system (Nanson and Croke, 1992) with features developing ecologically as connectivity with the main river alters over time.

Mitsch and Gosselink (2000) estimated that globally floodplains cover between $0.8x10^6$ km^2 to $2x10^6$ km^2, approximately 1.4% of the land surface, however they contribute around 25% of all terrestrial ecosystem services (Tockner and Stanford, 2002). Recent figures on floodplain state are not known to the authors, however the situation is unlikely to have improved on the status levels reported at the turn of the century when it was estimated that some 80%-90% of Europe's river floodplains are now cultivated intensively compared to figures of 46% for North America (excluding northern Canada and Alaska) and 11% for African Rivers (Tockner and Stanford, 2002). As such, floodplain condition and functionality have been reported as being in a critical situation across Europe (Wenger et al., 1990; Klimo and Hager, 2001).

Longitudinal and lateral fragmentation of large river systems, linked principally to human activities have led to severe and widespread floodplain degradation and this is fundamentally threatening the integrity of running water ecosystems (Dynesius and Nisson, 1994; Schiemer, 1999). This degradation is closely linked to the rapid decline in freshwater biodiversity, linked principally to habitat alteration through altered land use and flow, flood control, pollution and also to invasive species. Tockner and Sanford (2002) provided the stark statistics that in Europe and North America, up to 90% of floodplains are already 'cultivated' and therefore functionally extinct.

In England and Wales, watercourse and to a lesser degree floodplain alteration and degradation has been quantified as part of the European Water Framework Directive (WFD) with water bodies classified based on their degree of alteration; labeled as artificial, heavily modified and near natural (non-designated). Statistics provided by the Department for Environment Food and Rural Affairs (Figure 1) illustrate the generally poor state of UK rivers with only around 30% of water bodies achieving the required good ecological status/potential. Seager et al. (2012) conducted a stratified random sample of 4,849 River Habitat Survey sites sampled in 1995-1996 and 2007-2008 across England and Wales to assess the general physical character of rivers and streams. From these data, they estimated that 11% of river length had a 'near-natural' channel form with a further 14% classed as predominantly unmodified. Bentley et al. (2016) found a similar picture of hydromorphic diversity reduction along an engineered reach of the River Wharfe and their findings suggested that engineering driven changes to morphology, which are common on UK watercourses, have severely degraded system form and function.

Further insight into wider modification to floodplain areas was reported by Heritage et al., (2016), who analyzed floodplain connectivity and land use on eight SSSI rivers in England and Wales. They found that even these high value watercourses have been significantly impacted by current and former engineering and management of the river and valley bottom with intense use of the floodplain along all of the watercourses resulting in a loss of natural habitat to farming. This study extends their analysis further, quantifying land use patterns across all floodplain areas in England with respect to their natural function. The study utilizes GIS based land use data cropped to the 100 year flood zone mapping for the country to reveal the extent and pattern of floodplain degradation.

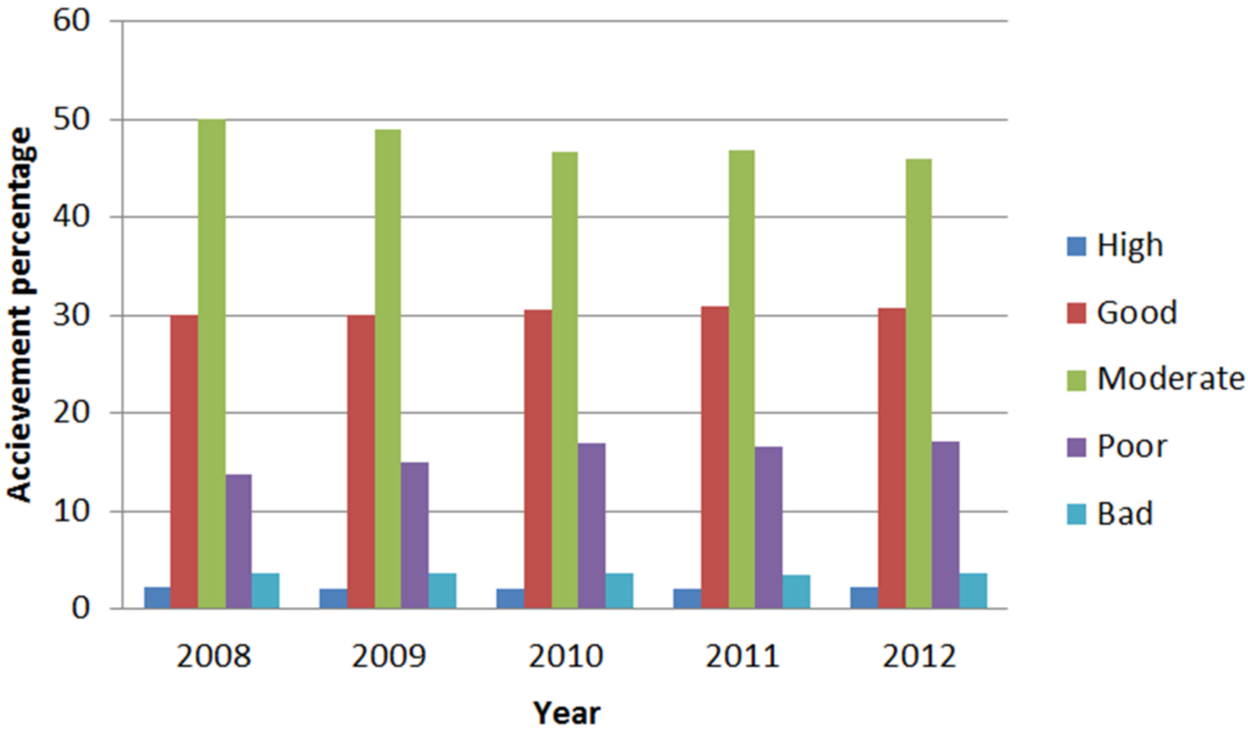

Figure 1. Water Framework Directive status summary for UK Rivers (2008-2012).

2 PROJECT METHOD

Initially, the Environment Agency Digital River Network was used to delineate river units across England by main river name; this included all associated tributary units (Figure 2(a)). Next, the Environment Agency Flood zone 2 polygons (equivalent to the 100-year return period flood) were associated with river network (Figure 2(b)). Each new river floodplain polygon was then intersected with the national land cover map of Great Britain (Centre for Ecology and Hydrology (CEH), 2007) (Figure 3). Areas of each land use type were then extracted and converted to percentage cover by dividing by the total floodplain area for each watercourse network.

This analysis generated data on a total of 555 main river units across England covering just over 6600 km^2 of floodplain area.

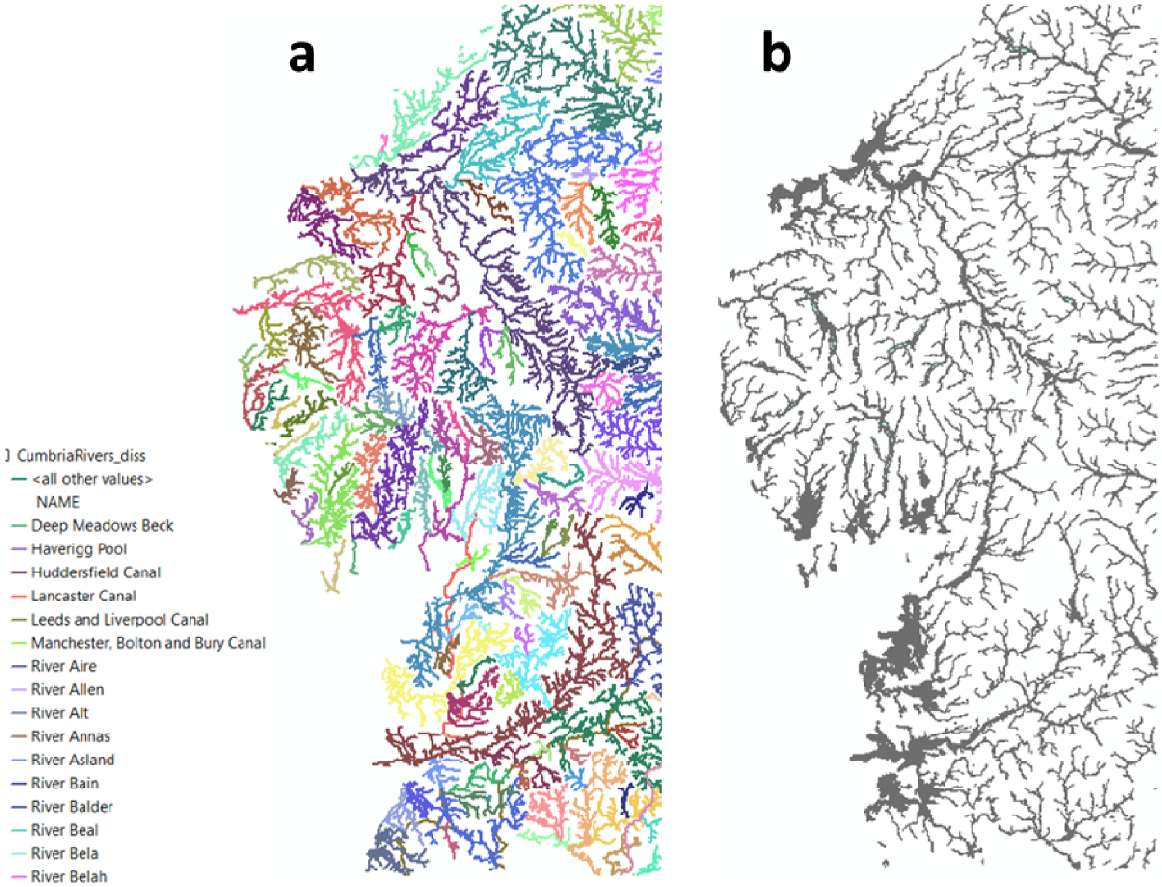

Figure 2. Example area of the river network in England (a), and the associated floodplain areas (b).

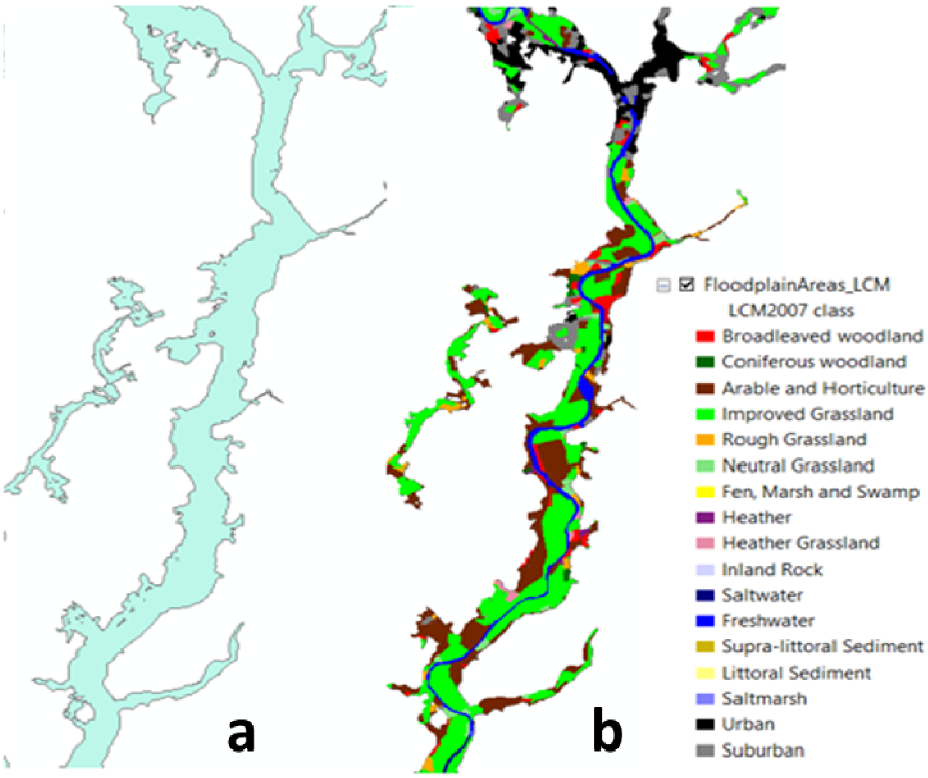

Figure 3. GIS process to define and segment floodplain area and assign land use categories on a river by river basis.

3 RESULTS

A review of the gross area coverage figures for all floodplain in England (Figure 4) revealed that around 65% had been modified extensively due to agriculture with arable, horticulture and improved grazing activities all severely impacting the natural floodplain ecology and functioning. A further 9% had been lost to urban and suburban development. Of the remaining 25%, 4% was occupied by open water. Semi-natural woodland and rough grassland together occupied only 6% of floodplains, whilst natural fen, marsh and swamp were reduced to less than half a percent of the total floodplain area.

The spatial patterning of these land use types had been mapped (Figure 5 and 6) using areal dominance classes to reveal both the distribution and dominance of each category across England. Natural fen, marsh and swamp was an extremely sparse land cover type across the country and was at a low level across all sites where it was present (Figure 5(a)). Broadleaved woodland showed a better distribution (Figure 5(c)) with a strong presence in the West Country, even here, however, coverage was generally below 10% of total floodplain area. Conifereous woodland (Figure 5(b)) was concentrated across higher topography in the north of England at generally low levels. The distribution of floodplain under arable use was strongly confined to the area around the Wash, Lincolnshire & Humberside, where coverage levels were generally in excess of 75%.

Floodplain rough grassland (Figure 6(a)) was distributed largely in the north and west of England but was most likely locally patchy with overall coverage levels below 25% of the available floodplain. Urban and suburban cover (Figure 6(b)) was as expected concentrated around towns and cities, whilst improved grassland (Figure 6(c)) displayed a near ubiquitous distribution exhibiting moderate to high levels of cover (20-50%). Areas of heather and heather grassland (Figure 6(d)) were both rare and at very low concentrations.

A count of the presence of a particular land use type each of the 555 river floodplain systems analyzed (Table 1) backed up the distribution statements made previously. Of note was the very low occurrence of the natural fen, marsh and swamp habitat, which was now seen on only 71 watercourse floodplains, less than 13% of the total present.

Table 1. Floodplain presence statistics of the 555 river floodplain systems analyzed for key land use types for England on a river basis.

Land use category	Occurrence	% rivers
Arable and horticulture	534	96.2
Broad leaved, mixed and yew woodland	541	97.5
Built up areas and gardens	523	94.2
Coniferous woodland	417	75.1
Dwarf shrub heath	335	60.4
Fen marsh and swamp	71	12.8
Improved grassland	545	98.2
Rough low-productivity grassland	501	90.3

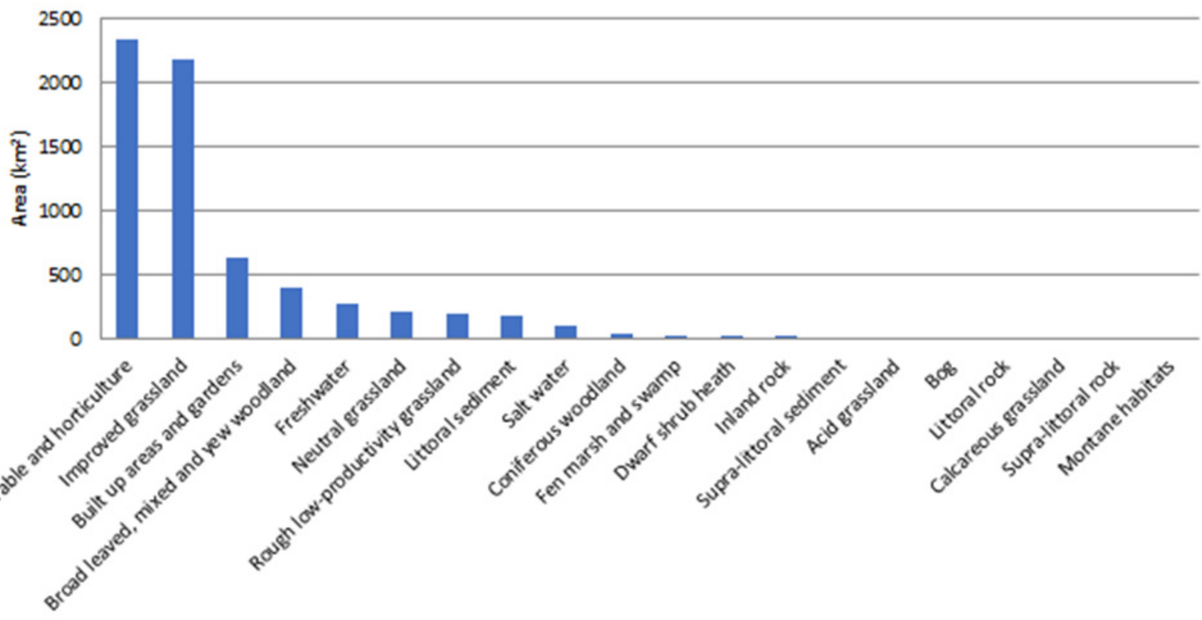

Figure 4. Land use area cover for all river floodplain in England.

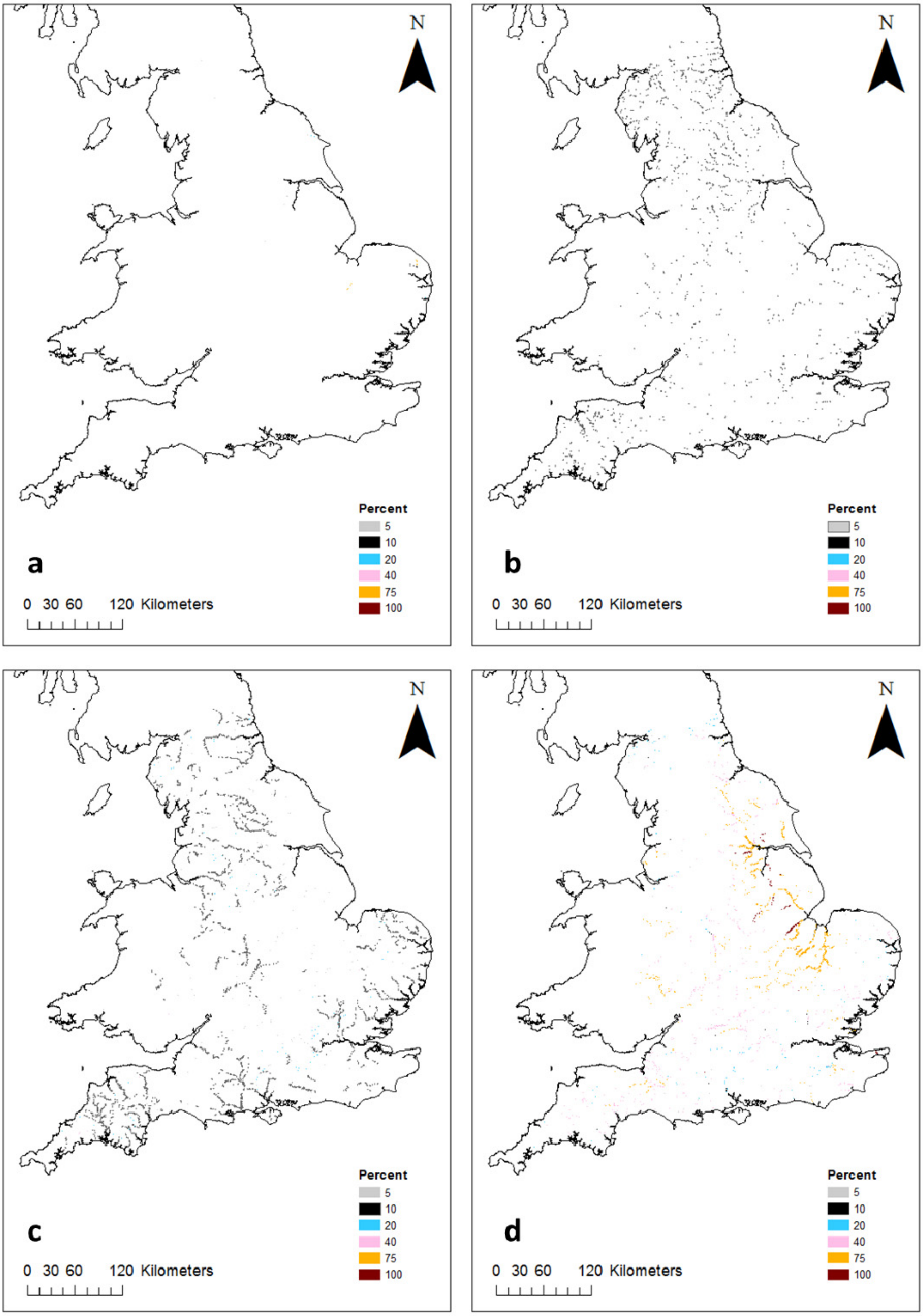

Figure 5. Floodplain land-use maps for England (a) Fen, marsh and swamp, (b) coniferous woodland, (c) Broadleaf woodland, (d) arable and horticulture (Source, CEH, 2007).

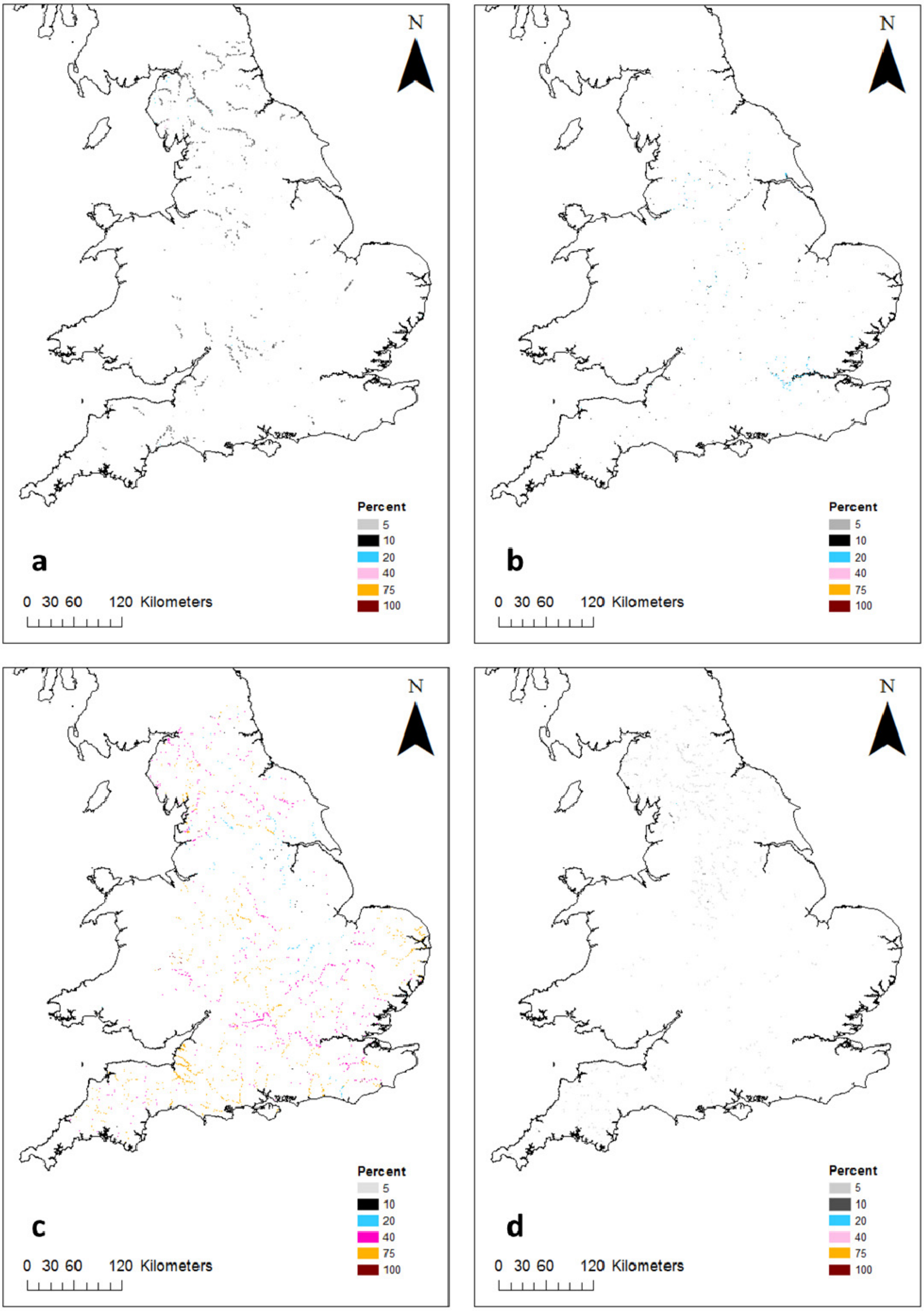

Figure 6. Floodplain land-use maps for England (a) Rough grassland, (b) Urban/suburban, (c) Improved grassland, (d) Heather/heather grassland (Source, CEH, 2007).

The local dominance of a particular land use type was further examined by extracting the frequency of areal coverage categories across all rivers (Figure 7). It was immediately clear that the majority of fen, marsh and swamp were present at coverage of less than 1% of the overall river floodplain area. Rough grassland was also only generally present at low levels of cover of between 5 and 10%. These figures contrasted starkly with the strong dominance of improved grassland and to a slightly lesser degree, arable usage which generally occupied 50% to 75% of any floodplain area where they were present.

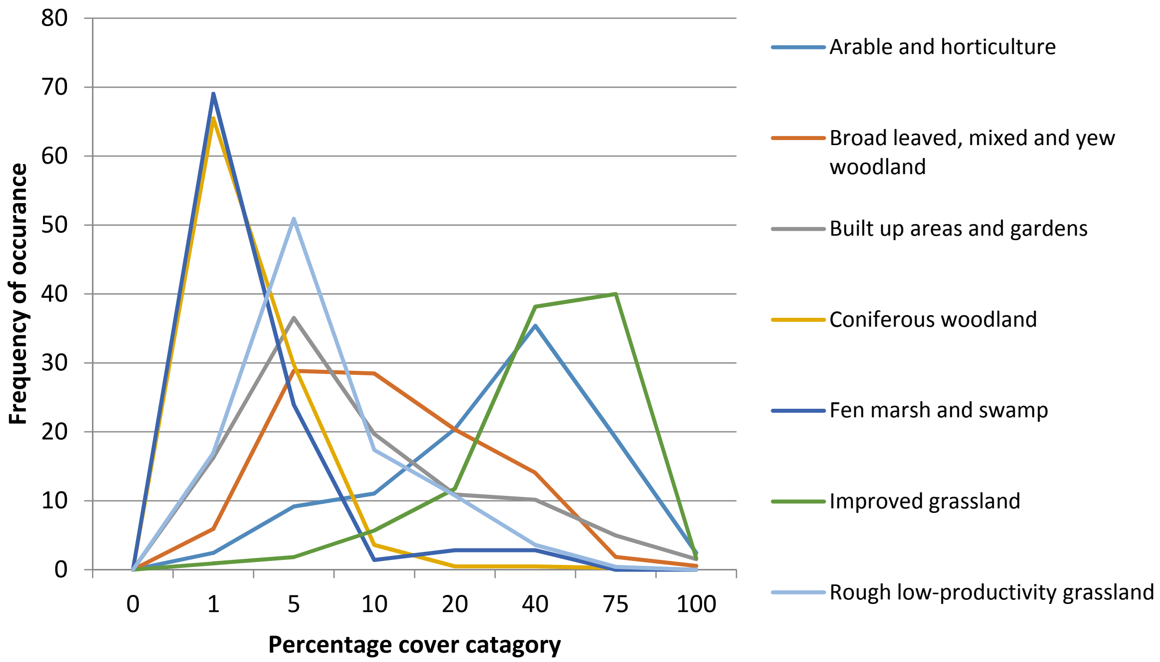

Figure 7. Variation in percentage area for key land use types.

4 DISCUSSION AND CONCLUSIONS

This paper presents the first nationwide assessment of floodplain condition for England. It has used land use and floodplain area information together to build a clear picture of the magnitude of change to floodplains away from their natural fen, marsh and swamp habitat towards a uniform, heavily managed improved grassland and arable use. It has revealed the near complete destruction of fen, marsh and swamp habitat with only small, isolated remnant areas remaining on less than 15% of watercourses. When this level of natural habitat destruction is linked to earlier studies demonstrating the severe loss of floodplain functionality resulting from anthropogenic modification of the watercourse (Heritage et al., 2016; Seager et al., 2012), the true extent of the destruction of floodplains in England becomes apparent. It is interesting to review this stark reality against the measure of river health currently being used across Europe. The Water Framework Directive standards being used in England largely fail to consider the floodplain at all in any assessment as such rivers water bodies are being classified at good ecological status when almost certainly their floodplain condition and functionality remain degraded. Whilst it is most probably too late to change the assessment criteria being used, it should be recognized that efforts must be made to improve the connectivity between floodplain and watercourse and where possible to begin restoring floodplain hydromorphic units to once again see truly functional river and floodplain systems in England with the consequent ecological and downstream. The advantages of taking such action can also be seen in terms of flood benefit. The high floodplain flow velocities approaching 1.5 m/s witnessed on the River Eden, Cumbria during the Storm Desmond extreme event (estimated at a 1 in 200-year return period by the Environment Agency) could be slowed significantly by reintroducing lost rough grassland, fen, marsh and swamp and scrub habitats. This may be simply illustrated by inverting the manning equation to derive average flow velocity from flow depth valley slope and water depth characteristics. Figure 8 illustrates this effect for a typical floodplain surface with a slope of 0.001 under three vegetation scenarios (improved grassland, rough grassland/swamp and scrub with Mannings '*n*' roughness values of 0.025, 0.04 and 0.06, respectively (values from Chow (1959)). It is clear that significant velocity reductions are likely with consequent flood wave attenuation and downstream flood risk reduction.

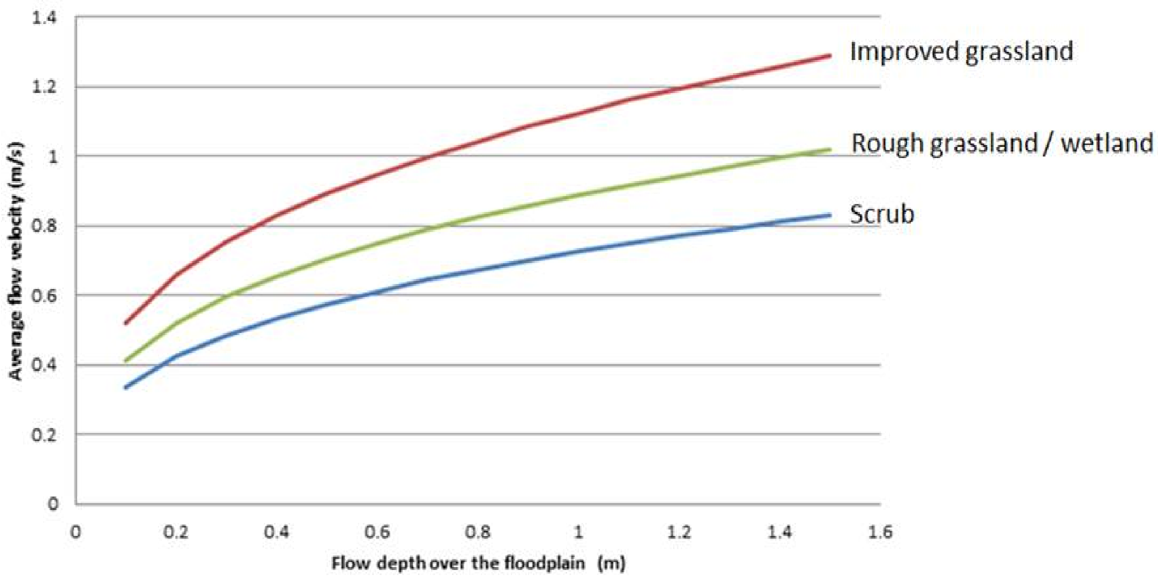

Figure 8. Variation in percentage area for key land use types.

ACKNOWLEDGEMENTS

The authors would like to acknowledge the financial support provided by Co-op Insurance, GIS assistance by Dr. Robert Williamson and Dr. Lucy Schofield and raw data by the UK Environment Agency and the Centre for Ecology and Hydrology.

REFERENCES

Amoros, C. & Roux, A.L. (1988). Interaction between Water Bodies within the Floodplains of Large Rivers: Function and Development of Connectivity. *münsterschegeographischeArbeiten,* 29, 125-130.

Bentley, S.G., England, J., Heritage, G.L., Reid, H., Mould, D. & Bithell, C. (2016). Long-reach Biotope Mapping: Deriving Low Flow Hydraulic Habitat from Aerial Imagery. *River Research and Applications,* 32(7), 1597-1608.

CEH. (2007). *Center for Ecology and Hydrology Land Cover Map,* www.ceh.ac.uk

Chow, V.T. (1959). *Open-Channel Hydraulics: New York.* McGraw-Hill Book Co., 680.

Dynesius, M. & Nilsson, C. (1994). Fragmentation and Flow Regulation of River Systems in the Northern Third of the World. *Science,* 266, 753-762.

Heritage, G.L. & Hetherington, D. (2007). Towards a Protocol for Laser Scanning in Fluvial. *Geomorphology, Earth Surface Processes and Landforms,* 32(1), 66-74.

Heritage, G.L., Entwistle, N.S. & Bentley, S. (2016). Floodplains: The Forgotten and Abused Component of the Fluvial System. *Flood Risk 2016 3rd European Conference on Flood Risk Management Innovation, Implementation, Integration.*

Junk, W.J., Bayley, P.B. & Sparks, R.E. (1989). The Flood Pulse Concept in River Floodplain. *The Floodplain Forests in Europe,* 106(1), 110-127.

Klimo, E. & Hager, H. (2001). *The Floodplain Forests in Europe: Current Situations and Perspectives.* Brill, 10.

Mitsch, W.J. & Gosselink, J.G. (2000). *Wetlands. New York.* USA: Wiley.

Nanson, G.C. & Croke, J.C. (1992). A Genetic Classification of Floodplains. *Geomorphology,* 4(6), 459-486.

Schiemer, F. (1999). Conservation of Biodiversity in Floodplain Rivers. Archiv für Hydrobiologie, Supplementband Large Rivers, 115(3), 423-438.

Seager, K., Baker, L., Parsons, H., Raven, P.J. & Vaughan, I.P. (2012). *The Rivers and Streams of England and Wales: An Overview of their Physical Character in 2007-2008 and Changes Since 1995-1996. In: River Conservation and Management.* Chichester, Wiley, 29-43.

Thoms, M.C. (2003). Floodplain–River Ecosystems: Lateral Connections and the Implications of Human Interference. *Geomorphology,* 56(3), 335-349.

Tockner, K. & Stanford, J.A. (2002). Review of: Riverine Flood Plains: Present State and Future Trends. *Environmental Conservation,* 29, 308-330.

HEC-RAS FLOW ANALYSIS IN THE RIVER TAPI

DARSHAN J. MEHTA(1), SANJAY M. YADAV(2) & SAHITA I. WAIKHOM(3)

(1,2)National Institute of Technology, Surat, Gujarat, India
darshanmehta2490@gmail.com; shivnam27@gmail.com
(3)Ghandhy Government Engineering College, Surat, Gujarat, India
siwgecs@gmail.com

ABSTRACT

Floods are natural disaster where they cause losses and damages to lives, properties and nature. The main objective of this study is to integrate science of meteorology, hydrology and hydraulics by using an appropriate and effective method in flood management. 1-D Hydrodynamic model is used to evaluate geomorphic effectiveness of floods on lower Tapi River basin. In this present study, geometry of lower Tapi River, flood plain of Surat City and past observed flood data have been used to develop 1-D integrated hydrodynamic model of the lower Tapi River, India. After collecting the entire data using 1-D hydrodynamic model to simulate the flood of year 1944, 1945, 1968, 2006, 2007, 2012 and 2013. As Surat city has been facing many floods from the year 1883 to 2013. The carrying capacity of river is approximately about 450000 cusecs (12753 cumecs) at present. The river network and cross sections for the present study are extracted from the field surveyed contour map of the river Tapi River. In this, stability of a segment of lower reach of Tapi River approximately 9 km length between Weir cum causeway and Kapodra (Uttran Bridge) is evaluated for its carrying capacity and geomorphic effectiveness. The study reach consists of 36 cross-sections. The model is used to evaluate steady flow analysis, flood conveyance performance and uniform flow analysis. The study area selected is highly affected by the flood and it is necessary to develop flood reduction plan for the study area which will helps to control a big disaster in future. The recommendations are done based on this study either to increase height of the retaining wall or construct a retaining wall at certain sections along study reach. The present study also recommends improving carrying capacity of Tapi River so that it will minimize the flood in surrounding area of Surat City.

Keywords: Flood event; HEC-RAS; steady flow; Tapi River; uniform flow computations.

1 INTRODUCTION

Rivers play a major role in the human civilization as they are the major source of fresh water, transportation, and resources. However, sometimes this relationship is often “troubled” because change in river discharge which leads to flood or drought. Floods has been considered as one of the most devastating natural hazards/disasters causing huge immediate damage and long term loss on human activity, economic development of a society as well as on the environment. River Tapi is originates from a Multai Hills (Gavilgadh hill ranges of Satpura) and flowing through three states Maharastra, Madya Pradesh and Gujarat having length of 725 km. The flow of water and water level in the river Tapi is controlled at Ukai dam which is 100 kms away from Surat city. The foundation of dam is resting on Dolerite dykes (Basalt). It is constructed for irrigation purposes mainly and also for flood control, generation of hydropower and supply of industrial and drinking water. The average rainfall in the catchment area is about 785 mm and average yearly run off is 17,226 MCM. The area of Surat city river is 326.51 sq.km which is situated at delta stage and population is about 4 million. The city has 60,000 shops and establishments engaged in trading activity. The city is also famous for diamond industry. The Major industries like Essar Steel, Reliance, ONGC, L & T, Gail, Kribhco, Shell, NTPC, GSPC, Torrent Power etc. are also situated in the city.

A flood is an unusually high stage in a river at which the river overflows its banks and inundates the adjoining area. As Surat city has faced many floods since long back. Major flood event occurred in the year 1883, 1884, 1942, 1944, 1945, 1949, 1959, 1968, 1978, 1979, 1990, 1994, 1998, 2002, 2006, 2007, 2012 and 2013. With rapid advancement in computer technology and research in numerical techniques, various 1-D hydrodynamic models, based on hydraulic routing, are developed in the past for flood forecasting and inundation mapping. In this study, one dimensional hydrodynamic model HEC-RAS is developed using geometric and past flood data of the lower Tapi River. The discharge (past flood data) and river stage (stations and elevations) were chosen as the variables in practical application of flood warning.

The developed model is used to simulate the flood of year 1959, 1968 and 2006 for uniform flow computation. Many practicing Engineers already have established HEC-RAS models for floodplain analysis. Thus, this single terrain is usable for both hydrologic and hydraulic modeling. Tapi is main source of water in Surat and other region surrounded it. In Tapi River, floods mostly occur due to upstream raining and therefore it is necessary to forecast flood and prepare for flood mitigation plan.

With rapid advancement in computational technology and research in numerical techniques, various one dimensional (1D) hydrodynamic models, based on hydraulic routing, are developed, calibrated, validated and successfully applied for flood forecasting and inundation mapping. Hydrodynamic models that reproduce the hydraulic behavior of river channels are proven to be effective tools in floodplain management (Timbadiya et. al, 2001). Floods are occurring in river Tapi frequently, due to which major portion of the city is submerged creating a lot of damage in residential as well as industrial areas. There is a need of reducing the effect of flood. In this paper, the flood water levels along the Tapi River in Surat were simulated using the HEC-RAS 1-D hydrodynamic model to prepare the people to survive during floods with minimum damages

2 OBJECTIVES

The flood affects human lives, destroying their home and livelihood, moreover affecting the country's business, economy and industry. As the research and development continues to overcome this vulnerability, the study made in this project tries to focus on use of HEC- RAS. The objectives of the study is to analyze the stability of a segment of lower Tapi river reach between Weir cum causeway and Kapodra (Uttran Bridge) by evaluating its carrying capacity in response to peak discharge and slopes.

3 STUDY AREA

Surat is situated between latitude 21° 06' to 21°15' N and longitude 72°45' to 72°54' E, on the bank of river Tapi and having coastline of Arabian Sea on its west. Surat falls in Survey of India map number 46C/15, 16. The Tapi River receives several tributaries on both the banks and there are 14 major tributaries having length more than 50 km. On the right bank, 4 tributaries namely Vaki, Gomai, Arunavati and Aner join the Tapi River. On the left bank, 10 important tributaries namely the Nesu, Amaravati, Buray, Panjhra, Bori, Girna, Waghur, Purna, Mona and Sipna drain into the main river channel. The drainage system on the left bank of the river Tapi is, therefore, more extensive as compared to the right bank area. The Purna and Girna, the two important left bank tributaries, together account for nearly 45 % of the total catchment area of the Tapi River. The river Tapi, the second largest west flowing river in India, originates from Multai (Betul district) in Madhya Pradesh (M.P.) at an elevation of 752 m having length of 724 km and falls in to the Arabian Sea at little beyond the Surat city. The total drainage area of Tapi is 65,145 km^2 out of which 9804 km^2 lies in Madhya Pradesh, 51,504 km^2 lies in Maharastra and 3837 km^2 lies in Gujarat.

The Tapi river basin is divided in three sub-basins namely, upper Tapi basin (up to Hathnur), middle Tapi basin (Hathnur to Gighade) and lower Tapi basin (Gighade to the sea). The Surat city is located at the delta region of the Tapi river. Surat city lies at a bend of the river Tapi, where its course swerves suddenly from the south-east to south-west. From the right bank of the river, ground rises slightly towards the north but the height above Mean Sea Level (MSL) is 13 m.

River Tapi flows through the city and meets the Arabian Sea at about 16 km from Surat. Surat is 90 km downstream of Ukai Dam over river Tapi. At present the most challenging problem the city faces, is the frequently occurring floods in the river of Tapi. The city of Surat and its economy have been hit by a number of floods over the past few decades which were mainly during 1944, 1945, 1949, 1959, 1968, 1979, 1990, 1994, 1998, 2006, 2007, 2012 and 2013. Floods are occurring in river Tapi time to time, due to which major portion of the city is submerged creating lot of damage in residential as well as industrial areas. There is a need of reducing the effect of flood. In this paper the aspects of river channel modification are also considered for enhancing the carrying capacity and reducing the effect of flood in the city.

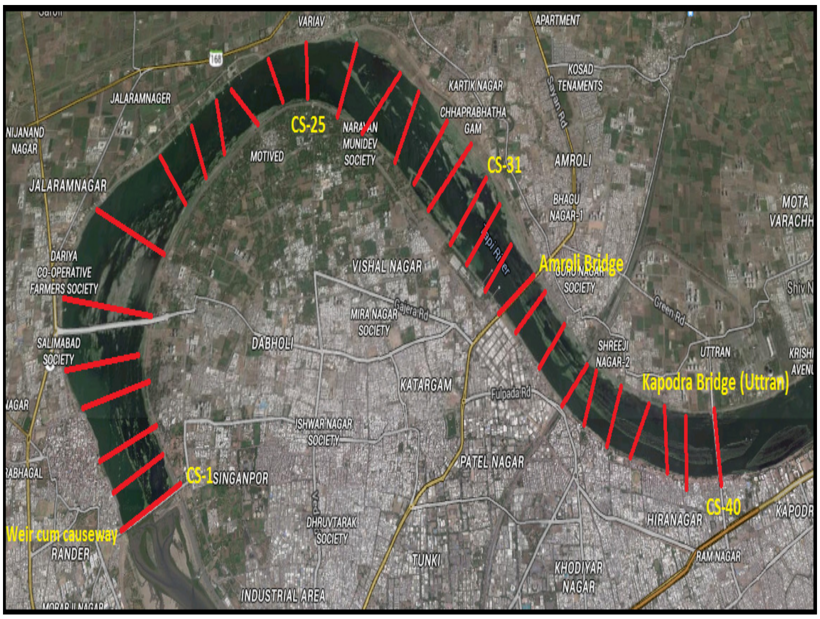

Figure 1 - Study area with cross-sectional details

Due to encroachment, silting and scouring, depth and width are reducing day by day. By reducing carrying capacity on adjoining areas and modifying the channel it will helpful in the preparation of flood mitigation plan for Surat city as a curative measure for the control of flood in the river Tapi. Thus, the modification of river channel is done to increase the carrying capacity of river Tapi and thus reducing the effect of flood in Surat city and surrounding region. Figure 1 shows the study area from Weir cum Causeway to Kapodra Bridge. The details of the study reach includes total numbers of cross-sections are 36 (CS-1 to CS-36), river reach length is 9 km, red line indicates cross-sections in river reach, average interval between cross-sections to cross-sections is 250 metres and upstream is the Weir cum causeway while downstream is Kapodra Bridge.

4 HEC-RAS OVERVIEW

Originally designed in 1995, the United States Army Corps of Engineers Hydraulic Engineering Center's River Analysis System (HEC-RAS) is "software that allows you to perform one-dimensional steady and unsteady flow river hydraulics calculations, sediment transport-mobile bed modeling, and water temperature analysis." The program solves the mass conservation and momentum conservation equations with an implicit linearized system of equations using Preissmann's second order box finite difference scheme (Subramanya et. al., 2006). In a cross-section, the overbank and channel are assumed to have the same water surface, though the overbank volume and conveyance are separate from the channel volume and conveyance in the implementation of the conservation of mass and momentum equations (Hong et. al., 2011). HEC-RAS was first released in 1995 and since that time there have been several major versions of HEC-RAS of which 4.1 is the latest version released in 2010. In this paper, version 4.1 of HEC-RAS was used. The development of the program (HEC-RAS) was done at the Hydrologic Engineering Centre (HEC), which is a part of the Institute for Water Resources (IWR), U.S. Army Corps of Engineers. HEC-RAS has the ability to make the calculations of water surface profiles for steady and gradually varied flow as well as for subcritical, super critical, and mixed flow regime. In addition to this, HEC-RAS is capable to do modeling for sediment transport, which is notoriously difficult. Therefore, modeling sediment transport is based on assumptions and empirical theory that is sensitive to several physical variables (Beaver, 2004).

5 DATA REQUIRED IN HEC-RAS

The data's required for carrying out 1-D hydrodynamic modeling using HEC-RAS are Manning 'n' value, slope of a river bed, detailed cross sections of river (geometric data), map of study area, past flood data or peak discharge data (Table 1), R.L of both banks that is left side and right side bank of the study.

Table 1 Flood History of Surat City

Sr. No.	Year	Discharge at Kakrapar weir (Cumecs)	Discharge at Kakrapar weir (Hundred Thousand Cusecs)
1	1876	20530	07.25
2	1883	28456	10.05
3	1894	22682	08.01
4	1942	24352	08.60
5	1944	33552	11.85
6	1945	29018	10.25
7	1949	23843	08.42
8	1959	36670	12.95
9	1968	43924	15.51
10	1969	24239	08.56
11	1998	19017	06.73
12	2006	25788	09.10
13	2012	9508	03.35
14	2013	13092	04.62

5.1 Geometric Data

The basic geometric data consists of establishing how the various river reaches are connected (river system schematic) which includes cross section data, reach lengths, energy loss coefficients (friction losses, contraction and expansion losses) and stream junction information (John et. al., 2009). Surat Municipal Corporation (SMC) has provided the geometric data of the reach for present study as contour map in Auto CAD (.dwg file) format. The cross-section data at different locations were extracted from aforesaid map for the river under consideration. The effect of meandering has been neglected as there is no reasonable curvature seen in study reach by providing expansion and contraction coefficient as 0.3 and 0.1 respectively. Total 36 cross-sections at various important locations on the river were used. The detailed configuration of study reach was respectively collected from Surat Municipal Corporation (SMC) and Surat Irrigation Circle (SIC), Govt. of Gujarat, India in the hard map format. All stations should be entered from left to right looking upstream. Data such as Manning's n values, bank stations, reach lengths, and expansion/contraction coefficients are required for each cross-section. Manning's n values are used primarily for calibration purposes.

5.2 Cross sectional Data

Usually, the average cross section of a channel does not change under natural conditions over a period of years. Boundary geometry for the analysis of flow in natural streams is specified in terms of ground surface profiles (cross sections) and the measured distances between them (reach lengths). Cross sections should be perpendicular to the anticipated flow lines and extend across the entire flood plain. Cross sections are required at locations where changes occur in discharge, slope, shape or roughness and at locations where levees begin or end and at bridges or control structures such as weirs. Each cross section is identified by a Reach and River Station label. (Agnihotri et. al., 2011). The cross section is described by entering the station and elevations (x-y data) from left to right, with respect to looking in the downstream direction.

5.3 Reach Length

The reach length (distance between cross sections) should be measured along the anticipated path of the center of mass of the left and right over bank and the center of the channel (these distances may be curved).

6 FLOOD CONVEYANCE PERFORMANCE

For evaluation of flood performance, past flood data collected from the Surat Irrigation Circle, Surat and also Flood Cell, Surat were used. The flood frequency analysis results were based on data which coincides with the upstream limit of the project reach. Major flood events took place in the year 1883, 1884, 1942, 1944, 1945, 1949, 1959, 1968, 1994, 1998, 2002, 2006, 2007 and 2013. The summary of the floods is given in the Table 1.

7 METHODOLOGY

The input data require for 1-D analysis for carrying capacity of study reach, data collected from Surat Municipal Corporation are entered in HEC-RAS software. The study reach consists of 36 cross sections. The details like station number, elevation, Manning's roughness coefficient (Garde et. al., 2000) were entered in geometric data window of HEC-RAS software. After entering geometric data the necessary steady flow data can be entered. Steady flow data consists of number of profiles to be computed, flow data and the river system boundary conditions. To access the carrying capacity of particular section using hydraulic design function and uniform flow condition, input discharge of specific year in the software. Additionally, discharge can be changed at any location within the river system. Discharge must be entered for all profiles. A boundary condition must be established at the most downstream cross section for a subcritical flow profile and at the most upstream cross section for a supercritical flow profile. Based on this input data HEC RAS will compute section. The computed section is sufficient to carry input discharge if F.S.L is within the bank heights. If computed section is insufficient to carry input discharge software will develop levees on that bank which is overtopped by the input discharge. The above procedure is repeated for all the 36 sections.

8 RESULT AND RESULT DISCUSSIONS

In this study sufficiency of existing sections are accessed using two major historical flood events. The section were classified as highly critical (where depth of water above existing bank is more than 0.7m), moderately critical (where depth of water above existing bank is between 0.4 to 0.7m) and critical (where depth of water above existing bank is up to 0.4m). Figures presents computed sections using HEC-RAS software and past flood data. Figure shows the graph between station (Chainage in m) and elevation (Bed level in m). Fig. 2 to Fig. 9 shows the critical sections computed using flood discharge of 25788 cumecs (2006), 33552 cumecs (1944), 43294 cumecs (1968) and 36670 cumecs (1959). Table 2 shows the summary result of flood events 1968, 2006, 1959 and 1944 year.

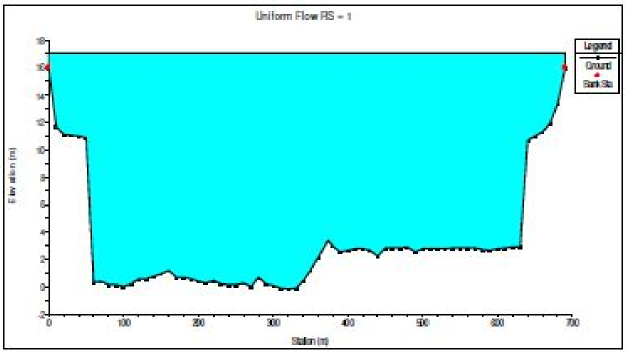

Figure 2 - Detail of Computed CS - 1

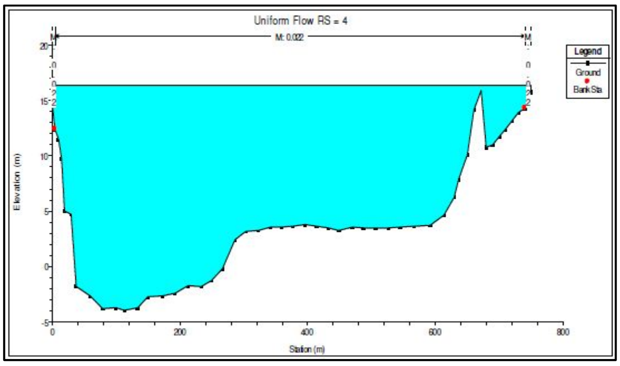

Figure 3 - Detail of Computed CS - 4

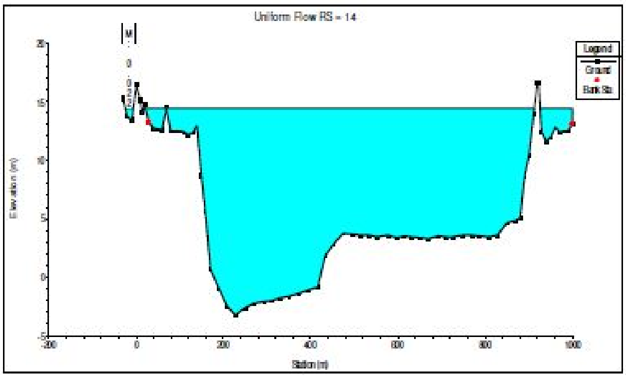

Figure 4 - Detail of Computed CS - 14

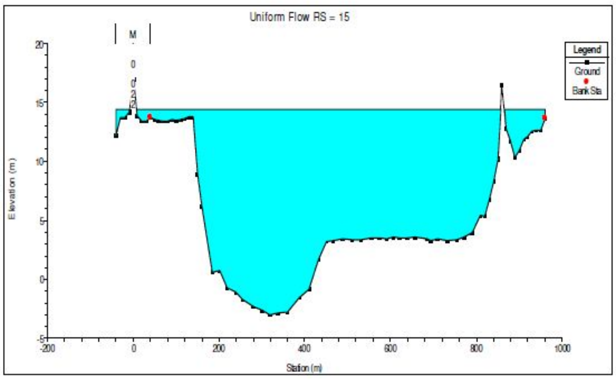

Figure 5 - Detail of Computed CS - 15

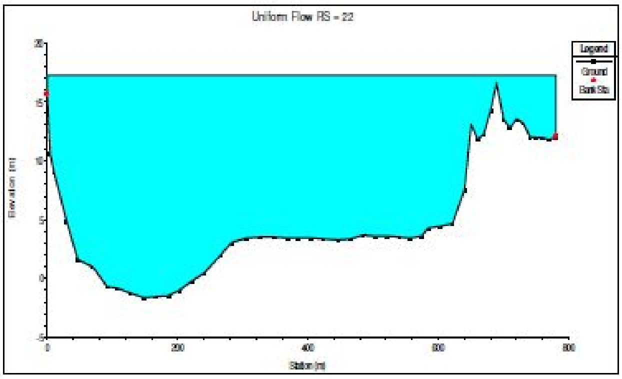

Figure 6 - Detail of Computed CS - 22

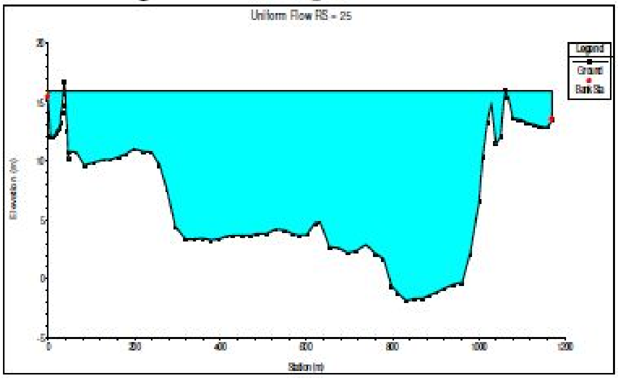

Figure 7 - Detail of Computed CS - 25

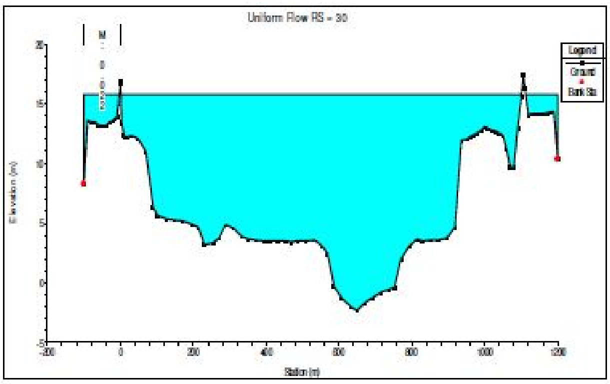

Figure 8 - Detail of Computed CS - 30

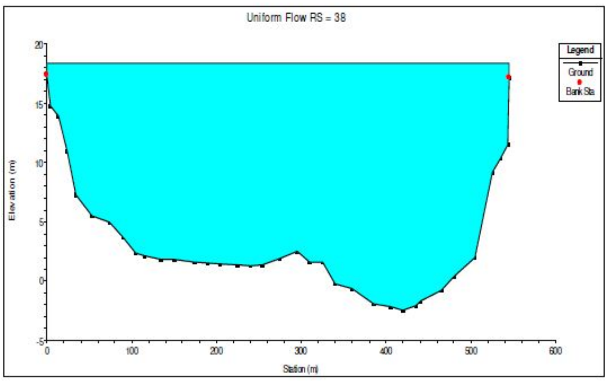

Figure 9 - Detailed of Computed CS - 36

In flood event 1968 having discharge 43924 cumecs, 9 sections are highly critical, 19 sections are moderately critical and 8 sections are critical thus it is strongly recommended to construct levees or retaining wall on the particular cross sections. In flood event 2006 having discharge 25788cumecs, 8 sections are highly critical, 10 sections are moderately critical and 18 sections are critical in which 18 sections are common as that in flood event of 1968, thus it is strongly recommended to raise the level of levees or retaining wall at particular cross sections and also suggest to construct the retaining wall or levees at particular sections. In flood event 1959 having discharge 36670cumecs, 8 sections are highly critical, 9 sections are moderately critical and 19 sections are critical. In flood event 1944 having discharge 33552cumecs, 4 sections are highly critical, 13 sections are moderately critical and 19 sections are critical.

Table 2 Classification of study reaches cross sections based on HEC RAS analysis

Sr. No.	Flood Event	Highly Critical	Moderately Critical	Critical
1	1968 (43924 cumecs)	CS-10, CS-13, CS-14, CS-15, CS-24, CS-32, CS-33, CS-34, CS - 36	CS-2, CS-3, CS-4, CS-5, CS-6, CS-7, CS-8, CS-9, CS-12, CS-18, CS-20, CS-21, CS-22, CS-23, CS-26, CS-28, CS-29, CS-30, CS-31	CS-1, CS-11, CS-16, CS-17, CS-19, CS-25, CS-27, CS-35
2	2006 (25788 cumecs)	CS-11, CS-13, CS-14, CS-15, CS-24, CS-32, CS-33, CS-34	CS-6, CS-8, CS-9, CS-10, CS-18, CS-20, CS-21, CS-25, CS-26, CS-27	CS-1, CS-2, CS-3, CS-4, CS-5, CS-7, CS-12, CS-16, CS-17, CS-19, CS-22, CS-23, CS-28, CS-29, CS-30, CS-31 CS-35, CS-36
3	1959 (36670 cumecs)	CS-2, CS-3, CS-10, CS-11, CS-13, CS-14, CS-15, CS-24	CS-5, CS-7, CS-9, CS-12, CS-20, CS-21, CS-32, CS-33, CS - 34	CS-1, CS-4, CS-6, CS-8, CS-16, CS-17, CS-18, CS-19, CS-22, CS-23, CS- 25, CS-26, CS- 27, CS-28, CS-29, CS-30, CS-31, CS-35, CS-36
4	1944 (33552 cumecs)	CS-2, CS-3, CS-10, CS-24	CS-5, CS-7, CS-9, CS-12, CS-11, CS-13, CS-14, CS-15, CS-20, CS-21, CS-32, CS-33, CS - 34	CS-1, CS-4, CS-6, CS-8, CS-16, CS-17, CS-18, CS-19, CS-22, CS-23, CS- 25, CS-26, CS- 27, CS-28, CS-29, CS-30, CS-31, CS-35, CS-36

9 CONCLUSIONS

It is strongly recommended that the sections, at which water overtop the existing level, embankment or retaining wall need to be raised. It is recommended that the storm drain outlets should be provided with flood gates to prevent entry of flood water in the study area. It is strongly recommended that the width of the river in no case be encroached as already sections are sensitive to high floods, encroachment will result in flooding of study region. It is strongly recommended that no new construction be allowed in flood plain area.

REFERENCES

Agnihotri, P.G. & Patel, J.N. (2011). Modification of Channel of Surat City Over Tapi River Using HEC- RAS Software. *International Journal of Advanced Engineering Technology*, 2, 231-238.

Anthony, L.F., Chester, W. & Brian, P.B. (2000). Stable Channel Design for Mobile Gravel Bed Rivers. *Journal of Water Resource and Protection*, 10, 1-9.

Beaver (1994). *Hydraulic Modelling of River Channels Using GIS Based Tools Named HEC*, 2, 45-55.

Frantisek, K. (2007). On the Determination of the Stable Bed Slope of a Channel Using Mathematical Model. *Journal of Soil and Water Resource,* 3, 104-111.

Garde, R.J. & Raju R.K. (2000). Mechanics of Sediment Transportation and Alluvial Stream's Problems. *New Age International Publishers (P) Ltd*., New Delhi, India.

Hong, IL., Joongu, K., Hongkoo, Y. & Yonguk, R. (2011). Channel Response Prediction for Abandoned Channel Restoration and Applicability Analysis. *Journal of Engineering*, 3, 461-469.

John, S. & Parr, D.A. (2009). Hydraulic Design Functions for Geomorphic Channel Design and Analysis Using HEC-RAS. *Journal of World Environmental and Water Resources Congress*, 2, 41-50.

Lan, E.W. (1995). Design of Stable Channels. Trans. *American society of Civil Engineering*. 120, 191-197.

Subramanya K. (2006). *Flow in Open Channels*. Tata McGraw-Hill Publishing Company Limited. New Delhi, India.

Jensen, M. (2002). Using HEC-RAS to model canal systems. *Journal of Engineering*, 2, 607-616.

Vincent, N.S. & Korte, N. (2001). Preliminary Channel Design of Blue River Reach Enhancement in Kansas City. *American Society of Civil Engineering*, 1, 31-42.

Richard, H.M., Colin, R.T. & Aff, M. (1984). Stable Channels with Mobile Gravel Bed. *Journal of American society of Civil Engineering*, 112(8), 671-689.

Timbadiya, P.V., Patel, P.L. & Porey, P.D. (2001). Calibration of HEC-RAS Model on Prediction of Flood for Lower Tapi River India. *Journal of Water Resource and Protection*, 3, 805-811.

A REVIEW OF THE UNDERSTANDING OF UNCERTAINTY IN A FLOOD FORECASTING SYSTEM AND THE AVAILABLE METHODS OF DEALING WITH IT

LEONORE BOELEE(1) , DARREN LUMBROSO(2), PAUL SAMUELS(3), ELISABETH STEPHENS(4) & HANNAH CLOKE(5)

(1,2,3) HR Wallingford, Wallingford, United Kingdom,
l.boelee@hrwallingford.com; d.lumbroso@hrwallingford.com; p.samuels@hrwallingford.com
(4,5) University of Reading, Reading, United Kingdom
h.l.cloke@reading.ac.uk; elisabeth.stephens@reading.ac.uk

ABSTRACT

The increased availability and application of probabilistic weather forecasts in flood forecasting means that the uncertainty arising from the precipitation forecast can be assessed. This has led to a wider interest in how uncertainty is affecting flood forecast systems. In literature, there are general techniques and principles available on how to deal with uncertainty. However, there are no well-accepted guidelines on the implementation of these principles and techniques. There is neither coherent terminology nor a systematic approach, which means that it is difficult and perhaps even impossible to assess the characteristics and limitations of uncertainty quantification methods. Selecting the most appropriate method to match a specific flood forecasting system is therefore a challenge. The main findings of this review are that there is remaining mathematical and theoretical challenges in uncertainty quantification methods and that this leads to the use of assumptions which in turn could lead to a misrepresentation of the predictive uncertainty.

Keywords: Ensembles; flood forecasting; hydrological modelling; hydraulic modelling; uncertainty.

1 INTRODUCTION

Flooding affects an average of 520 million people a year and is one of the most frequently occurring and deadly natural phenomena (James et al., 2007). Flood warning is a non-structural measure which has proved to be efficient and cost effective in minimizing negative impacts of flooding (WMO and GWP, 2013;Mishra and Singh, 2011; Pappenberger et al., 2015). Flood forecasting systems rely on a combination of historical observed data, in-situ measurements and models to produce forecasts. This paper focusses on fluvial flood forecasting systems. Operational flood forecasting systems, or real-time flood forecasting systems, are continuously running systems that forecast at a point in real time (defined as the forecast time origin) for a future time (WMO and GWP, 2013). They consist of four main components (Zappa et al., 2011):

i. **Numerical Weather Predictions (NWP)** can be deterministic or probabilistic; atmospheric observations are assimilated into NWP systems to produce forecasts (Rossa et al., 2011). Although this is highlighted by Zappa et al. (2011) as a main component of a flood forecasting system, not all systems have a NWP component, for example, basic flood forecasting systems can use a river level to river level correlation between an upstream gauge and downstream point(s) of interest. For more details on NWP prediction systems, the reader is referred to Palmer (2000).

ii. **Hydrological initial conditions** from observations or models for a flood forecasting system represent soil moisture, snow cover, the river and other waterbodies (Li et al., 2009 and Madsen and Skotner, 2005). Initial conditions can be either observed or estimated using models. If observations are available, data assimilation can be used to update the model. The subject of data assimilation is outside of the scope of this paper, for more information on this, the reader is referred to (Liu et al., 2012).

iii. **Flood prediction systems** use models to predict the state of the river; often a combination of model types is used. Available models for flood prediction include physically based models, conceptual models and data-driven techniques (Mure-Ravaud et al., 2016). At the end of the modelling chain the flood prediction system will predict the variable (e.g. simulated discharge, water level) at the point(s) of interest.

iv. **Warnings for end users**; the communication of uncertainty is beyond the scope of this paper and the reader is referred to Kreibich et al. (2016).

Historically, many flood forecasting systems produced deterministic forecasts. Ensembles of Numerical Weather Predictions (NWPs) are being increasingly used in flood forecasting systems. This allows the uncertainty of the meteorological forecast input data to be assessed, examples of this development include The Hydrological Ensemble Prediction Experiment (HEPEX, 2017) initiative (Cloke and Pappenberger, 2009).

Recently, there has been more emphasis on the presence of uncertainty in all components of the forecasting system (Krzysztofowicz, 2002; Pappenberger et al., 2005). Research with end-users has found that there is an appetite for uncertainty information if improvements in accuracy and lead time can be achieved (Lumbroso et al., 2009). Powerful techniques are becoming more widely available within flood forecasting systems and these allow the quantification of uncertainty, sensitivity analysis, risk analysis and decision analysis. However, there are no guidelines on how to implement these principles and techniques in complex flood forecasting systems where there are multiple sources of uncertainty to consider (Zappa et al., 2010; Liu and Gupta, 2007). There is a lack of coherent terminology and systematic approaches which leads to difficulty in assessing characteristics and limitations of individual methods. This makes the selection of the most appropriate method for practical problems difficult and perhaps impossible (Montanari, 2007). Within flood forecasting systems Liu and Gupta (2007) highlight four areas that need to be addressed:

i. Understanding of uncertainty
ii. Quantifying uncertainty
iii. Reducing uncertainty
iv. Communication of uncertainty.

This paper focusses on areas one and two: the understanding and quantification of uncertainty. More explicitly, the aim of this paper is to provide a review of the understanding of uncertainty in flood forecasting systems and the available methods of dealing with it. Furthermore, this paper identifies gaps and limitations with regards to the understanding and quantification of uncertainty.

2 UNDERSTANDING UNCERTAINTY

2.1 Definitions of uncertainty

Uncertainty indicates that something is not able to be relied on, is not known or not definite (Oxford English Dictionary, 2017). Two well-known types of uncertainty are: aleatory and epistemic. Aleatory uncertainty is uncertainty resulting from natural variability and randomness and epistemic uncertainty is uncertainty due to lack of knowledge (Li et al., 2013). In flood forecasting systems, uncertainty can be referred to in terms of 'predictive uncertainty' or 'predicting the uncertainty', (Todini, 2008; Weerts et al., 2011; Palmer, 2000; Van Steenbergen and Willems, 2015; Zappa et al., 2011), which is defined by Todini, (2008) as "the probability of any future (real) value, conditional upon all the knowledge and information, available up to the present.".

2.2 The sources of uncertainty

Sources of uncertainty in a flood forecasting system are linked to the elements that are included in the chain of models and will vary for different forecast setups. For example, the inclusion of a hydraulic model to estimate the levels and extent of flooding would add additional sources of uncertainty to a forecasting system which are only relevant if this element is part of the model chain. Krysztofowicz (1999) identifies input uncertainty and all other uncertainties in the aggregate (e.g. hydrological uncertainty). Table 1 shows the varying sources of uncertainty that can affect a flood forecasting system.

Table 1. Varying sources of uncertainty that can affect a flood forecasting system

Sources of uncertainty according to (Pappenberger et al., 2005)	**Sources of uncertainty according to** (Cloke and Pappenberger, 2009)	**Sources of uncertainty according to** (Zappa et al., 2011)	**Sources of uncertainty according to** (Klein et al., 2016)
Rainfall forecast	Correction and downscaling	Forecast data	NWP
Runoff model	Spatial and temporal owing to initial conditions and data assimilation	Initial conditions	Initial and boundary conditions of hydrological and hydraulic models
Hydraulic model	Model unable to fully represent processes	Model unable to represent processes	Meteorological observations
	Infrastructure failure	Observed data	Model parameters
	Model parameters		
	Geometry of the system		

Being explicit in naming sources of uncertainty is challenging owing to the wide variety of flood forecasting systems. The most prevalent sources of uncertainty affecting flood forecasting systems have been identified as: uncertainty resulting from NWP forecasts, uncertainty from issues with measurements and observations, uncertainty due to initial conditions, uncertainty due to the model being unable to fully represent processes and uncertainty due to parameters. In this paper, NWP forecasts are classified as input data and the uncertainties are treated as a single source of uncertainty. The authors are aware that NWP originates from atmospheric prediction models and uncertainty sources can be separated out in more detail; however, this is outside the scope of this paper.

2.2.1 Uncertainty due to using NWP forecasts

Atmospheric variables that are used in flood forecasting systems include precipitation, temperature and evaporation. Precipitation is considered to be the variable that has most effect on a flood forecasting systems outputs (e.g. water level, flow) (Strauch et al., 2012). Excluding seasonal forecasts, there are three types of precipitation forecasts that are typically applied to flood forecasting systems:

i. Short to mid-range precipitation forecasts for NWP.
ii. Short term rainfall forecasts and nowcasts (e.g. 0 to 9 hours) from extrapolation from weather radar rainfall estimations (Liguori and Rico-Ramirez, 2014).
iii. Merged NWP with radar products have been developed which combine the high spatial temporal resolution of radar nowcasting with the longer lead times of NWP forecasts.

Significant uncertainty is associated with forecasting precipitation (Bauer, et al., 2015). In radar nowcasting, uncertainty is due to a combination of uncertainty in the observations of the radar data and uncertainty in estimations in modelling the movement of the precipitation field in space and time (Liguori and Rico-Ramirez, 2014). In the NWP predictions uncertainty is due to model uncertainty, boundary and initial conditions. These uncertainties can be assessed using an ensemble (Palmer, 2000). A mismatch between the scale of the atmospheric model outputs and the required scale of the hydrological model can be solved by using downscaling techniques (Rodriquez-Rincon et al., 2015). However, these techniques lead to uncertainties and have limitations (Fowler and Wilby, 2007).

2.2.2 Uncertainty due to measurement and observations

Observations are essential to the calibration and validation of flood forecasting systems but are uncertain themselves (Gotzinger and Bardossy, 2007). Observed data are affected by both random and systematic errors varying over time. Frequently occurring uncertainties relating to the difference between the spatial and temporal characteristics of the observations compared to the model include:

i. Uncertainty due to the interpolation techniques used for applying a point measurement to areal or volumetric model inputs (Gotzinger and Bardossy, 2007).
ii. Uncertainty due to using a rating curve to convert water level into a discharge, for more details, the reader is referred to McMillan et al.(2012) and Di Baldassarre and Montanari (2009).
iii. Uncertainty in remote sensing data due to the sensing and retrieval techniques used (Li et al., 2016).
iv. Uncertainty in radar rainfall observations due to the difficulties in distinguishing solid precipitation (e.g. snowflakes and hailstones), the effect of terrain blocking and inaccuracies in the reflectivity-rain rate relationship (McMillan et al., 2012).

The reader is referred to (McMillan et al., 2012) and (Li et al., 2016) for a comprehensive review of uncertainty in measurements.

2.2.3 Uncertainty due to initial conditions

The initial conditions in flood forecasting systems include the soil moisture, snow cover, initial state of the rivers and other waterbodies in the catchment (Li et al., 2009; Madsen and Skotner, 2005). Not all initial conditions can be observed or will have data available. As a solution, these conditions are estimated using models, which lead to uncertainty. The continuous simulation of a flood forecast system will also inherit state uncertainty from preceding time steps (Gotzinger and Bardossy, 2007). Initial conditions that are especially associated with large uncertainty are soil moisture and snow cover (Li et al., 2009).

2.2.4 Uncertainty owing to the model unable to fully represent processes

The inherent simplifications of the model to represent the more complex real system lead to uncertainty. For example, distributed hydrological models use polygons or grids to represent the catchment, this will lead to uncertainty, as the physical processes (e.g. related to soil structure) often occur on smaller scales than the model elements (Gotzinger and Bardossy, 2007). An overview of different models in hydrology is provided by Todini (2007) for hydrological models and (Knight, 2013). An example of the range of uncertainty in hydrological models is presented by Haddeland et al. (2011) where 11 global models were forced with the same data. The results had significantly different results ranging from 290 to 457 mm/year depending upon the partitioning of evaporation and runoff year.

2.2.5 Uncertainty due to model parameters

Model parameters are related to the input data (Matott et al., 2009) but are not necessarily actual physical variables or are not directly measurable, which means they need to be calibrated to find values that are able to match the input-output behaviour of the model to the real system (Vrugt et al., 2003). The estimation or calibration processes inevitably leads to uncertainty. Parameter uncertainty will be different due to using different types of models available, e.g. conceptual, physical and black box. The parameters of a hydrological model (conceptual model) relate to catchment characteristics such as soil type, vegetation, antecedent moisture conditions. Variation in catchment characteristics leads to variation of the parameters. These local spatial heterogeneities and non-stationarities in the catchments affect the parameters, making them difficult to be estimated effectively (Gupta et al., 2003). This leads to a lack of transferability of the parameters across the catchment, which will inevitably lead to uncertainty of the runoff prediction (Pappenberger et al., 2005). In the case of hydraulic models (physically based) local heterogeneities in the channel and floodplain geometry and cover will affect the parameters. Local parameters will need to be calibrated using observed data, of which are often limited. As a result, there will be uncertainty with respect to the hydraulic model outputs, which can include flood inundation and the flood wave propagation (Pappenberger et al., 2005). Apparently, the parameters themselves can never represent reality which brings additional uncertainty due to e.g. equifinality (Beven and Freer, 2001).

3 QUANTIFYING UNCERTAINTY

To understand, analyse and compare different types of uncertainty, quantification methods are helpful to classify them into different categories. Montanari (2007) distinguishes four types of uncertainty quantification methods:

i. Approximate analytical methods; deriving uncertainty using known statistical properties of the system and input data.
ii. Approximate numerical methods/sensitivity analysis; define the system space as a collection of all possible modelling solutions that can be obtained by varying the parameters and model structure. Multiple runs can then be performed randomly to sample the system and input data space; the uncertainty can be derived from the collection of outputs.
iii. Techniques based on the statistical analysis of model error; statistical analysis of the model residuals of the forecast value compared to the observed values.
iv. Non-probabilistic methods; based on random set theory, evidence theory, fuzzy set theory or possibility theory which provide possibilistic information.

Methods from the first category are limited in flood forecasting due to the statistical properties of the input space being mostly unknown (Van Steenbergen et al., 2012). The fourth category is mostly relevant to situations with very limited data availability where human reasoning (possibilistic information) is used to assess the likelihood of a scenario taking place. The most common methods in flood forecasting to quantify uncertainty fall into categories two and three. Methods do not necessarily fall into a single category, but can fall across several categories (Montanari, 2007).

3.1 Approximate numerical methods and sensitivity analysis

The approximate numerical methods and sensitivity analysis aims to move away from the principle of a single optimum model setup, in which the model setup includes both model structure and model parameters. The philosophy behind this is that there are multiple model structures and parameters within these structure, that will provide an equally acceptable representation of the complex environment (Beven and Freer, 2001). The defined system and input space should cover all model parameters, structure and input uncertainty. Random sampling over the space was applied, allowing multiple model runs to take place (Van Steenbergen and Willems, 2015) . Observed data are not required as a direct input in this method. The multiple model runs that are part of this method will require additional computational power and data management resources compared to traditional deterministic methods of forecasting.

The main challenge when applying this method is the defining of the input and system space so that it will cover all aspects of uncertainty. Two approaches are available to this: 1) importance sampling (Kuczera and Parent, 1998); and 2) using a response surface with weights, the most common method to do this is the generalised likelihood uncertainty estimator GLUE (Beven and Freer, 2001).

Box 1 Uncertainty in the European Flood Awareness system
Operating Authority: European Flood Alert system (EFAS)
Models used: LISFLOOD, a GIS based distributed hydrological rainfall runoff routing model on a 5km grid with six hourly time steps. (Van Der Knijff et al., 2010)
Forecast rainfall: Deterministic forecast rainfall from the Deutsche Wetterdienst, ECMWF deterministic and ensembles (VAREPS) and Ensembles from Consortium for Small-scale Modelling (COSMO).
Uncertainty method: The uncertainty method is based on the atmospheric uncertainty which is quantified using ensembles and weather prediction from different models. The weather predictions from the different models and the ensembles are push through the hydrological model (LISFLOOD). Warnings are probabilistic based on return period threshold exceedance.
Example output – Probabilistic threshold exceedance warnings. (ECMWF, 2016; Smith et al., 2016) More information available: https://www.efas.eu/user-information.html and Thielen 2009

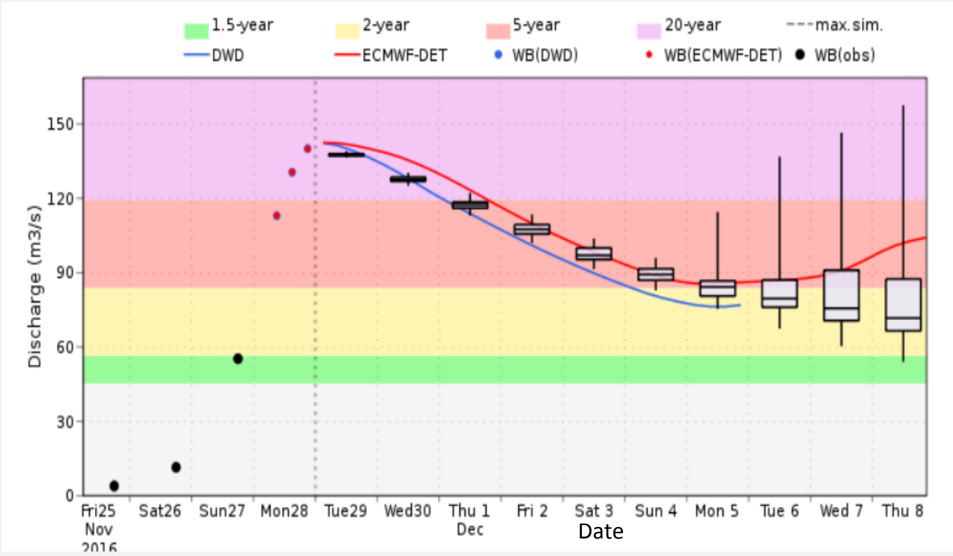

Figure 1. Uncertainty in the European Flood Awareness system

An example of using resampling and multiple model runs is where the uncertainty of all model components of the flood forecasting chain were quantified (Pappenberger et al., 2005); a probabilistic weather forecast containing 50 members and one control was used. The parameter uncertainty of the rainfall-runoff model was quantified using GLUE. GLUE was also applied to the flood inundation model in order to get ten different sets of roughness coefficients. This uncertainty analysis was applied to the European Flood Awareness System (EFAS); more details about EFAS are provided in Box 1.

3.2 Techniques based on the statistical analysis of model error

Techniques based on the statistical analysis of model uncertainty use statistics derived from comparing the forecast values to observed values. An example of this is the probability distribution of model residuals which can be derived by comparing, for example, forecast value of river discharge to observations (Montanari and Brath, 2004). This method assumes that the future uncertainty can be represented using the model residuals of past forecasts. This method is attractive due to the low requirements with regards to computational power and data management, because multiple model runs are not required. When dealing with data scarce locations, the application of this method is limited, due to observed data being directly used. From the perspective of observed data being in itself uncertain, this method has a limited ability to quantify uncertainty correctly (Montanari and Brath, 2004). Assumptions regarding stationarity and ergodicity of the model residuals are often required, but remain disputed for different systems and for different states of a system.

An example of the application of this method is given by Weerts et al. (2011) when they aim to quantify the predictive uncertainty of the rainfall-runoff and hydraulic forecasts. A retrospective quantile regression is applied to the hindcast water level. Independent sources of uncertainty are not considered, instead the effective uncertainty of the forecast process is considered, which can be a result of input or output uncertainty, model structural uncertainty or parameter uncertainty. The method has been tested for robustness on catchments across England and Wales of different sizes and hydrological characteristics (Weerts et al., 2011).

3.3 Combining the methods

These two methods represent two different approaches to quantifying uncertainty in flood forecast systems. However, due to the fact that flood forecasting systems consist of multiple components, there are forecasting systems that use a combination of these two methods. An example is described by Krzysztofwicz and Herr (2001), where a Bayesian formulation of a Hydrological Uncertainty Processor (HUP) was used in combination with probabilistic precipitation forecast. The HUP aims to quantify the aggregate of all uncertainties arising from sources other than those quantified by the probabilistic precipitation forecast. This system has been applied to the National Weather Service for a 1,430km^2 catchment in Pennsylvania, USA. The probabilistic precipitation forecast was generated using the first method, but the HUP is part of the second method.

4 CONCLUSIONS

Two main challenges have been identified as part of this review on the understanding and quantification of uncertainty for flood forecasting systems. The first challenge is that there is a lack of coherent terminology around uncertainty in flood forecasting. Calls for a more coherent terminology, for example by Montanari (2007), have thus far proven difficult to achieve. It could be that the difficulty lies in finding terminology around uncertainty that will be applicable to the wide variety of systems within flood forecasting. Another difficulty lies in the fact that flood forecasting brings together a wide variety of different disciplines, including meteorologists, hydrologists, geographers, mathematicians, engineers and social scientists.

The second challenge that has been identified is that the remaining mathematical and theoretical challenges in the quantification of uncertainty require assumptions to be made that could be leading to a misrepresentation of the predictive uncertainty. More specifically for approximate numerical methods and sensitivity analysis creating a usable ensemble that covers the input and system space remains a challenge. In the case of techniques based on the statistical analysis of model uncertainty, the questions about how representative the historical model residuals are for the future uncertainty remains unanswered.

Opportunities to improve uncertainty quantification methods can be found, for example, in the field of data assimilation and in many cases the coming together of research form different disciplines can be instrumental in developing better methods.

ACKNOWLEDGEMENTS

This work was funded by the in-house research programme of HR Wallingford. The first author is registered for a PhD with the Open University through the Affiliated Research Centre programme at HR Wallingford.

REFERENCES

Bauer, P., Thorpe, A. & Brunet, G. (2015). The Quiet Revolution of Numerical Weather Prediction. *Nature*, 525(7567), 47–55.

Beven, K. & Freer, J. (2001). Equifinality, Data Assimilation, and Uncertainty Estimation in Mechanistic Modelling of Complex Environmental Systems Using the GLUE Methodology. *Journal of Hydrology*, 249(1), 11–19.

Cloke, H. L. & Pappenberger, F. (2009). Ensemble Flood Forecasting: A Review. *Journal of Hydrology*, 375(3), 613–626.

Di Baldassarre, G. & Montanari, A. (2009). Uncertainty in River Discharge Observations: A Quantitative Analysis. *Hydrology and Earth System Sciences*, 13(6), 913–921.

ECMWF (2016) *EFAS Bulletin.* 6. Reading.

EFAS (2017) EFAS - User Information, *European Flood Awareness System*. Available at: www.efas.eu/user-information.html.

Fowler, H. J. & Wilby, R. L. (2007). Beyond the Downscaling Comparison Study. *International Journal of Climatology*, 27(12), 1543–1545.

Gotzinger, J. & Bardossy, A. (2007). Generic Error Model for Calibration and Uncertainty Estimation of Hydrolocial Models. *Water Resouces Research*, 44(12), W00B07.

Gupta, H. V., Sorooshian, S., Hogue, S. & Boyle, D. P. (2003). Advances in Automatic Calibration of Watershed Models. *Calibration of watershed models*, 9–28.

Haddeland, I., Clark, D. B., Franssen, W., Ludwig, F., Voß, F. R. A. N. K., Arnell, N. W. & Gomes, S. (2011). Multimodel Estimate of the Global Terrestrial Water Balance: Setup and First Results. *Journal of Hydrometeorology*, 12(5), 869-884.

HEPEX (2017) *HEPEX - Implementation Plan for The Hydrological Ensemble Prediction Experiment*, *A community of reasearch and practice to advance hydrologic ensemble prediction*. Available at: http://hepex.irstea.fr/science-and-implementation-plan/ (Accessed: 9 August 2016).

James, B., Rouhban, B., Papa, H. & Tovmasyan, K. (2007) *Disaster preparedness and Mitigation*. SC/BES/NDR/2007/H/1. Paris, France: United Nations Educational, Scientific and Cultural Organization.

Klein, B., Meissner, D., Kobialka, H.-U. & Reggiani, P. (2016). Predictive Uncertainty Estimation of Hydrological Multi-Model Ensembles Using Pair-Couple Construction. *Water*, 8(4), 125.

Knight, D. W. (2013). River Hydraulics a View from Midstream. *Journal of Hydraulic Research*, 51(1), 2-18.

Kreibich, H., Pech, I., Schroter, K., Muller, M. & Thieken, A. H. (2016). New Insights into Flood Warning and Emergency Response from the Perspective of Affected Parties. *EGU General Assembly Conferences Abstract,* 18.

Krzysztofowicz, R. (2002). Bayesian System for Probabilistic River Stage Forecasting. *Journal of Hydrology*, 268(1), 16–40.

Krzysztofwicz, R. & Herr, H. D. (2001). Hydrologic Uncertainty Processor for Probabilistic River Stage Forecasting: Precipitation-Dependent Model. *Journal of Hydrology*, 249(1), 46–68.

Krzysztofowicz, R. (1999). Bayesian theory of probabilistic forecasting via deterministic hydrologic model, *Water Resources Research*, 35(9), pp. 2739–2750.

Kuczera, G. & Parent, E. (1998). Monte Carlo Assessment of Parameter Uncertainty in Conceptual Catchment Models: The Metropolis Algorithm. *Journal of Hydrology*, 211(1), 69–85.

Li, H., Luo, L., Wood, E. F. & Schaake, J. (2009). The Role of Initial Conditions and Forecing Uncertainties in Seasonal Hydrologic Forecasting. *Journal of Geophysical Research*, 114(D4), D04114.

Li, Y., Chen, J. & Feng, L. (2013). Dealing with Uncertainty: A Survey of Theories and Practices. *IEEE Transactions on Knowledge and Data Engineering*, 25(11), 2463–2482.

Li, Y., Grimaldi, S., Walker, J. P. & Pauwels, V. R. N. (2016). Application of Remote Sensing Data to Constrain Operational Rainfall-Driven Flood forecasting: A Review. *Remote Sensing*, 8,(6), 456.

Liguori, S. & Rico-Ramirez, M. A. (2014). A Review of Current Approaches to Radar-Based Quantitative Precipitation Forecasts. *International Journal of River Basin Management*, 12(4), 391–402.

Liu, Y. & Gupta, H. V. (2007). Uncertainty in Hydrologic Modeling: Toward an Intergrated Data Assimilation Framework. *Water Resouces Research*, 43(7), W07401.

Liu, Y., Weerts, A., Clark, M., Hendricks Franssen, H. J., Kumar, S., Moradkhani, H. & Van Velzen, N. (2012). Advancing Data Assimilation in Operational Hydrologic Forecasting: Progresses, Challenges, and Emerging Opportunities. *Hydrology and Earth System Sciences*, 16, 3863–3887.

Lumbroso, D. M., Twigger-Ross, C., Orr, P., Kashefi, E. L. H. A. M., Walker, G. O. R. D. O. N. & Cotton, J. A. C. Q. U. I. (2009). Probabilistic Flood Warnings–Do Eight Out of then People Prefer Them?. *44th Defra Flood and Coastal Management Conference*.

Madsen, H. & Skotner, C. (2005). Adaptive State Updating in Real-Time River Flow Forecasting - A Combined Filtering and Error Forecasting Procedure. *Journal of Hydrology*, 308(1), 302–312.

Matott, L. S., Babendreier, J. E. & Purucker, S. T. (2009). Evaluating Uncertainty in Integrated Environmental Models: A Review of Concepts and Tools. *Water Resouces Research*, 45(6), W06421.

McMillan, H., Krueger, T. & Freer, J. (2012). Benchmarking Observational Uncertainties for Hydrology: Rainfall, River Sicharge and Water Quality. *Hydrological Processes*, 26(26), 4078–4111.

Mishra, A. K. and Singh, V. P. (2011). Drought modeling - A review, *Journal of Hydrology*, 403, pp. 157–175.

Montanari, A. (2007). What do We Mean by “Uncertainty”? The Need for a Consistent Wording about Uncertainty Assesment in Hydrology. *Hydrological Processes*, 21(6), 841–845.

Montanari, A. & Brath, A. (2004). A Stochastic Approach for Assessing the Uncertainty of Rainfall-Runoff Simulations. *Water Resouces Research*, 40(1), W01106.

Mure-Ravaud, M., Binet, G., Bacq, M., Perarnaud, J.-J., Fradin, A. & Litrico, X. (2016). A Web Based Tool for Opertaional Real-Time Flood Forecasting Using Data Assimilation to Update Hydraulic States. *Environmental Modelling & Software*, 84, 35–49.

Palmer, T. N. (2000). Predicting Uncertainty in Forecasts of Weather and Climate. *Reports on Progress in Physics*, 63(2), 71–116.

Pappenberger, F., Beven, K. J., Hunter, N. M., Bates, P. D., Gouweleeuw, B. T., Thielen, J. & De Roo, A. P. J. (2005). Cascading Model Uncertainty from Medium Range Weather Forecasts (10 Days) Through a Rainfall-Runoff Model to Flood Inundation Predictions within the European Flood Forecasting System (EFFS). *Hydrology and Earth System Sciences Discussions*, 9(4), 381-393.

Pappenberger, F., Cloke, H. L., Parker, D. J., Wetterhall, F., Richardson, D. S. & Thielen, J. (2015). The Monetary Benefit of Early Flood Warnings in Europe. *Environmental Science and Policy*, 51, 278–291.

Rodriquez-Rincon, J. P., Pedrozo-Acuna, A. & Brena-Naranjo, J. A. (2015). Propoagation of Hydro-Meteorological Uncertainty in a Model Cascade Framework to Inundatio Prediction. *Hydrology and Earth System Sciences*, 19(7), 2981–2998.

Rossa, A., Liechti, K., Zappa, M., Bruen, M., Germann, U., Haase, G., Keil, C. & Krahe, P. (2011). The COST 731 Action: A Review on Uncertainty Propagation in Advanced Hydro-Meteorological Forecast System. *Atmospheric Research*, 100(2), 150–167.

Smith, P., Pappenberger, F., Wetterhall, F., Thielen, J., Krzeminski, B., Salamon, P., Muraro, D., Kalas, M. & Baugh, C. (2016). On the Operational Implementation of the European Flood Awareness System (EFAS). *Flood Forecasting: A Global Perspective*, 313.

Strauch, M., Bernhofer, C., Koide, S., Volk, M., Lorz, C. & Makeschin, F. (2012). Using Precipitation Data Ensemble for Uncertainty Analysis in SWAT Streamflow Simulation. *Journal of Hydrology*, 414, 413–415.

Thielen, J., Bartholmes, J., Ramos, M. H., & Roo, A. D. (2009). The European Flood Alert System–Part 1: Concept and Development. *Hydrology and Earth System Sciences*, 13(2), 125-140.

Todini, E. (2007). Hydrological Catchment Modelling: Past, Present and Future. *Hydrology and Earth System Sciences*, 11(1), 468–482.

Todini, E. (2008). A Model Conditional Processor to Assess Predictive Uncertainty in Flood Forecasting. *International Journal of River Basin Management*, 6(2), 123–137.

Van Steenbergen, N., Ronsyn, J. & Willems, P. (2012). A Non-Parametric Data-Based Approach for Probabilistic Flood Forecasting in Support of Uncertainty Communication. *Environmental Modelling & Software*, 33, 92–105.

Van Steenbergen, N. & Willems, P. (2015). Uncertainty Decomposition and Reduction in River Flood Forecasting: Belgian Case Study. *Journal of Flood Risk Management*, 8(3), 263–275.

Vrugt, J. A., Gupta, H. V., Bouten, W. & Sorooshian, S. (2003). Shuffled Complex Evolution Metropolis Algorithm for Optimization and Uncertainty Assessmetn of Hydrologic Model Parameters. *Water Resouces Research*, 39(8), 1201.

Weerts, A. H., Winsemius, H. C. & Verkade, J. . (2011). Estimation of Predictive Hydrological Uncertainty Using Quantile Regression: Esmaples from the National Flood Forecasting System (England And Wales). *Hydrology and Earth System Sciences*, 15(1), 255–265.

WMO & GWP (2013). *Flood Forecasting and Early Warning*. 19. World Meteorological Organization & Global Water Partnership.

Zappa, M., Beven, K. J., Bruen, M., Cofino, A. S., Kok, K., Martin, E., Nurmi, P., Orfila, B., Roulin, E., Schroter, K., Seed, A. & Szturc, J. (2010). Propagation of Uncertainty from Observing Systems and NWP Into Hydrological Models: COST-731 Working Group 2. *Atmospheric science letters*, 11(2), 83–91.

Zappa, M., Juan, S., Germann, U., Walser, A. & Fundel, F. (2011). Superposition of Three Sources of Uncertainties in Operational Flood Forecasting Chains. *Atmospheric Research*, 100(2), 246–262.

UNCERTAINTY IN DEBRIS FLOW HAZARD ESTIMATION USING X-MP RADAR RAINFALL FORECAST

RATIH INDRI HAPSARI(1), SATORU OISHI(2), MAGFIRA SYARIFUDDIN(3) & ROSA ANDRIE ASMARA(4)

(1,4)Department of Civil Engineering, State Polytechnic of Malang, Malang, Indonesia
ratih@polinema.ac.id; rosa.andrie@polinema.ac.id
(2,3)Research Center for Urban Safety and Security, Kobe University, Kobe, Japan
tetsu@phoenix.kobe-u.ac.jp; magfira@stu.kobe-u.ac.jp

ABSTRACT

Debris flow, which is the most serious secondary impact of volcanic disaster, is highly triggered by rainfall. Limited access to the area of active volcano slope as well as the risk of measurement gages damage due to disaster motivate to the use of X-band weather radars for observing the rainfall. However, the use of radar-rain prediction in sediment-related disaster involves high amount of uncertainties. In this study, debris flow disaster mitigation system by utilizing the high-resolution nowcasting products from X-band multiparameter compact (X-MP) and the assessment of its uncertainty are presented. The ensemble rain prediction by perturbing the advection vector is introduced aiming to gain the knowledge of uncertainties inherent in the system. The study area is the rivers on Mount Merapi that is historically the most active volcano in Indonesia. The benefits of ensemble forecasting over the single deterministic forecast are demonstrated, particularly to reduce missing of severe events. By evaluating five ensemble rainfall spatial distributions at once, the basin or village that is most likely to be hit by the debris flow is analyzed through hazard zoning. Rainfall critical line diagram is applied as a basis for judging the occurrence of debris flow. In order to evaluate the uncertainty of predicted rainfall temporal variation, snake lines development of hourly and working rainfall from the radar ensemble nowcasting products is drawn. The uncertainty assessment in the rainfall prediction system provides important information regarding the potential of disastrous debris flow. Verified with past occurrences, the integration of ensemble forecast product could provide a plausible range of the prediction possibility. This framework could be applied in disaster mitigation efforts for partially help to gage a confidence in the warning system.

Keywords: Debris flow; X-MP radar; uncertainty, critical rainfall; hazard.

1 INTRODUCTION

Volcanic eruptions cause many direct and indirect hazards. Debris flow has been recognized as among the worst indirect hazards of volcanic ejection disaster. Thousands of people in the world have been affected by rapidly flowing mixture of rock debris and water from a volcano and their deposit, with solid fractions greater than that of normal stream flow, which is known as debris (Lavigne et al., 1988). Debris flow of Mount Pinatubo Philippine in 1991 has killed 1500 people within two years. In 2010, Mount Merapi Indonesia ejection has also caused the severe impacts on people, livelihood, and properties. High rainfall with long duration is highly associated with debris flow (Lavigne and Thouret, 2003). Therefore, estimation of rain event characteristic in small scale and short duration in the future is indispensable for mitigating volcanic disaster.

Limited access to the area of active volcano slope as well as risk of measurement gages damage due to disaster lead to the difficulty of observing the rainfall in the high elevation of a catchment. Weather radars are appealing instruments for observing rainfall over large spatial domains within fine time resolutions. Unlike single-polarization radar, multiparameter radar has ability to observe rain with high accuracy. X-band multiparameter (X-MP) radar observation, whereby 0.5 km resolution can be achieved every two minutes, provides more detail rainfall information than conventional radars. Recent studies confirmed the significance of rainfall spatial structure in hydrological application (Kato and Maki, 2009). Debris floods are distinguished from other event types by the small time and spatial scales. With short lead times, short-term prediction is required for the forecasting rain-induced debris flow.

The use of radar in debris flow disaster mitigation is subjected to high uncertainties. First, as a part of weather system, precipitation is an uncertain system. Second, the uncertainty emerges from the of quantitative precipitation forecast (QPF) model. Until recently, ensemble approaches have been increasingly used for QPF for building reliable probabilistic forecast (Burlando et al., 1993; Ebert, 2001; Fujita et al., 2008; Cloke and Pappenberger, 2009; Kim et al., 2009). The use of ensemble prediction allows the development of probabilistic forecast. Particularly, in the decision making situation, the ensemble prediction system considerably has higher value, instead of traditional approaches using single deterministic forecasts (Pierce et al., 2005). The reviews found that the implementation of ensemble method is primarily focused on hydro-meteorological prediction.

Merapi volcano is historically the most active volcano in Indonesia. The significant eruption events were in the years of 1872, 1953, 2006, and 2010. Rivers on this mountain flank are vulnerable from debris. The adverse impacts tend to be more critical as most rivers pass through highly populated region of Yogyakarta Special Province. Since 2015, X-MP radar is installed in Mount Merapi. As compared to the number of available rain gauges in this area, the radar has a wider coverage with high resolution. There have been some past researches on Merapi debris flow (Lavigne et al., 1988; Lavigne and Thouret, 2003). However, none of them studied the susceptibility analysis of debris by using radar for disaster mitigation.

Critical rainfall threshold for triggering flood and earth material movement is broadly used as the standard to predict the disaster occurrence (Neary et al., 1987; Georgakakos, 2006). In general, hourly rainfall intensity and accumulative rainfall are the main parameters considered in sediment transport critical line (Shieh et al., 2009). Japan government includes soil water index obtained through lump modeling as a criterion (MLIT, 2004). The use rainfall intensity duration curve described with a power formula is initially introduced by Caine (1980). In order to judge the timing of disaster occurrence, a draw of real-time motion of rainfall index is plotted on the chart called snake line. This method is officially applied in Japan (MLIT, 2004). Yet, few studies concerned on the inaccuracies of the critical line as well as snake line uncertainties arising from the quantitative precipitation estimation and prediction.

In this research, the predictive uncertainty in the nowcasting of localized rainfall and its effect to the debris flow hazard information is studied in Merapi Rivers. Debris mitigation system integrates the use of hazard map information to identify the vulnerable river and rainfall snake line to issue the warning. Uncertainty in high-resolution nowcasting products from X-band multiparameter compact (X-MP) radar is assessed by developing ensemble. Instead of using single deterministic prediction, five ensemble rainfall spatial distributions are evaluated at once with respect to the critical line exceedance. In the real time scheme, temporal variation of hourly and working rainfall from radar nowcasting products is drawn along with critical line to judge the most likely debris flow occurring in terms of time and location. The effect of prediction errors in the variation of the judgment lines is discussed. The reliability of the prediction approach which considers the uncertainty is examined through the verification with control prediction and observation. The finding of this paper is expected to be of some use for advancing the research on decision support system for debris disaster response.

2 STUDY AREA

The study area is the rivers on Mount Merapi, Yogyakarta Special Province, Indonesia (7.5407°S, 110.4457°E), which is historically the most active volcano in Indonesia. With the high Merapi volcanic activities, the rivers in this area have been affected greatly by the ejection of volcanic material. There are 12 rivers that are vulnerable for debris, *e.g.,* Pabelan River, Boyong River, Putih River, Kuning River, Gendol River, Krasak River (Figure 1). As many as 70,000 people are living in the first danger zone over the Merapi flank. The aftermath of 2010 eruption has caused 55 event of debris flow in Putih River. In October 2010, debris disaster at Gendol River has reached 20 km and buried 21 houses. In this study, Putih River and Gendol River are selected as case study.

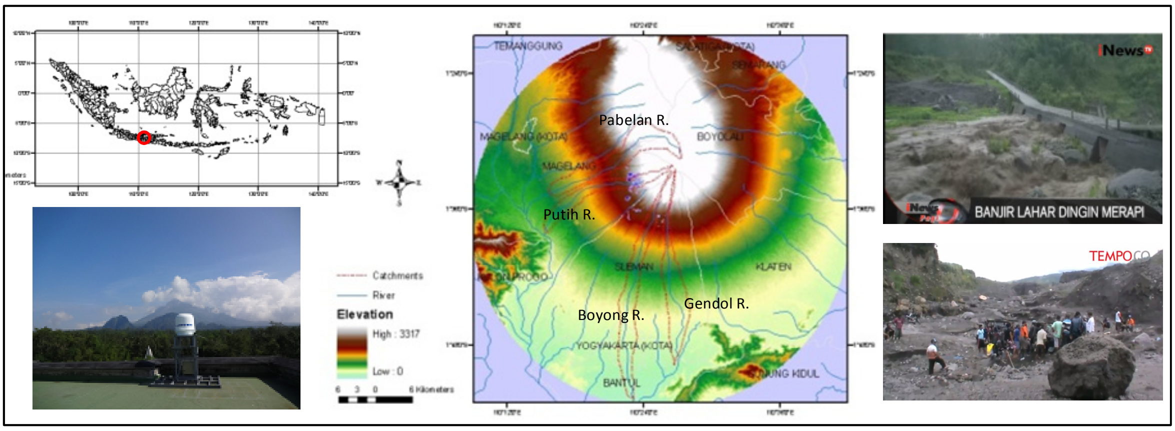

Figure 1. Study area, X-MP radar, radar range, topography, catchments area, and photos of February 17, 2016 debris flood.

In January 2015, X-MP radar was installed in Merapi Museum in the altitude of 755 MSL as shown in Figure 1. The purpose of installing this radar is to provide high precision monitoring and forecasting of short local meteorological phenomenon to contribute to better society safety from meteorological disasters, which includes vertical structure of cumulonimbus, nimbus movement, raindrops, multi-directional rain intensity, rain echo motion, and even volcanic ash. This radar provides rainfall measurement with 0.5 km spatial resolution

  / ISSN 1562-6865 (Online) - ISSN 1063-7710 (Print)

and two minutes temporal resolution. Rainfall events during the observation campaign in the rainy season between October 2015 and March 2016 are used in this study.

During the campaign period, there was at least one recorded event of debris attack. It occurred at Pabelan River and Gendol River on February 17, 2016. By using real time information of rainfall spatial distributions from X-MP radar, the high-localized rainfall, which leads to the debris flow, can be observed in detail. The rainfall as high as 70 mm/hr was detected in the upstream of the rivers between 16.30 to 17.00 LST. The length of the heavy rain events was three hours. This event highly contributed to the occurrence of the debris disaster along the river stream.

3 RESEARCH METHODOLOGY

3.1 Quantitative precipitation estimates

Radar echo extrapolation model is widely used for very short-term rainfall prediction with 1 – 3 hour lead time (Reyniers, 2008). The rainfall short term prediction used in this study is radar echo extrapolation model or translation model proposed by Shiiba et al. (1984). The dynamic of the horizontal rainfall intensity distribution r(x,y,t) with the spatial coordinate (x,y) at time t is described as follows:

$$\frac{\partial r}{\partial t} + m\frac{\partial r}{\partial x} + n\frac{\partial r}{\partial y} = w \qquad [1]$$

$$m = \frac{dx}{dt}, n = \frac{dy}{dt}, w = \frac{dz}{dt} \qquad [2]$$

where m and n are the advection vectors by which the horizontal rainfall distribution is assumed to be translated, and w is the growth/decay rate of rainfall intensity. The m, n, and w formations are specified on each grid linearly in the manner of:

$$m(x,y) = c_1x + c_2y + c_3 \qquad [3]$$

$$n(x,y) = c_4x + c_5y + c_6 \qquad [4]$$

$$w(x,y) = c_7x + c_8y + c_9 \qquad [5]$$

where c_1 to c_9 are the parameters being optimized by linear least square using past observed radar-rainfall. This model is powerful for predicting short events within three hours lead time.

3.2 Judgment of the hazard and warning issuance

Critical line is a threshold that specifies the rainfall amount for a specific duration that potentially causes critical debris movement. Empirically, the critical lines for Putih River and Gendol are shown by relationship of working rainfall (mm) and hourly rainfall (mm/h). These thresholds are used to distinguish the hazardous and non-hazardous area at grid mesh units based on the rainfall forecast product. Critical lines of debris flow disaster in Putih River and Gendol River (Mananoma and Wardoyo, 2009; Sutikno et al., 2013) are as follows:

$$Rh = -0.25\ Rw + 50 \qquad [6]$$

$$Rh = -0.3478\ Rw + 80 \qquad [7]$$

where Rh and Rw are the hourly rainfall and working rainfall, respectively.

Working rainfall is calculated by summing the cumulative rainfall from the start of a series of rain to the occurrence of the debris flow and the antecedent working rainfall (MLIT, 2004). In order to provide more specific real-time warning information in localized scale, snake line or temporal variation of hourly and working rainfall from radar nowcasting products is drawn on the graph to judge the occurrence of debris flow. Predicted rainfall events are plotted in the graph with hourly rainfall in the ordinate and working rainfall in the abscissa for each river basin.

3.3 Predictive uncertainty estimation

Issue regarding predictability of quantitative precipitation forecasts is still among the most difficult topics in meteorology. Moreover, due to the simplicity of prediction model, the field evolution is failed rapidly with advancing lead time. Ensemble forecasting could help to gain a feel for the possibilities of the pattern evolution. Here, the predictive uncertainty is analyzed through five ensemble members obtained by perturbing the rain advection vector with its Eigen values (see Hapsari et al., 2011 for detail). This model is used to predict the rain echo motion observed by X-MP radar with lead time of 2 to 5 hours.

The proposed scheme employs hazard map of rainfall-induced debris flow and rainfall snake line to judge the occurrence. In the system, there is a cascade of uncertainty started with the rainfall prediction and ended with the warning judgment with snake line. Ensemble considerably has higher value, instead of deterministic forecasts in the decision making situation. In this study, the ensemble is displayed by developing probability map of precipitation exceeding the critical threshold to pinpoint the greatest risk. The method of Islam and Sado (1999) using frequency analysis of flood affected is employed to determine the area with high risk. Afterward, the effect of predictive uncertainty to the variation of snake lines debris flow hazard information is studied. The spaghetti plot of the development of precipitation system in terms of hourly rain and working rain is built to help determining the most likely debris flow occurring. The reliability of the prediction approach that considers the uncertainty is examined through the verification with control prediction and observation.

4 RESULTS AND DISCUSSIONS

4.1 Hazard level from radar-rain observation

Rainfall spatial average observed by X-MP radar from February 17, 2016 event is illustrated in Figure 2. It can be seen from the hyetograph that the rainfall ranged from 1 mm/hr to 130 mm/hr. The rainfall spatial distribution indicates that the rainfall as high as 70 mm/hr was detected in the upstream of the river between 16.00 to 17.00 LST. The length of the heavy rain events was three hours. This event highly contributed to the occurrence of the debris disaster along the river stream.

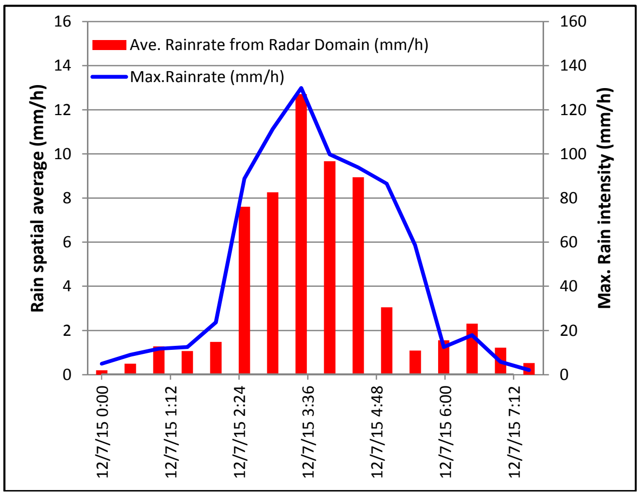

Figure 2. Observed rainfall intensity of February 17, 2016 case.

The hazardous area information given in Figure 3 observed by radar observation in conjunction with the rain-induced debris threshold is confirmed with real condition of debris occurrences. Due to the lack of established critical line, rainfall on Pabelan River catchment is analyzed by using the critical line of Putih River, while that on Gendol River is done by using critical line of Boyong River as they are located in close proximity. High debris flow has been reported by the authority along the stream of Pabelan, Putih, and Boyong River. The analysis reveals that the area with causing rainfall indicated by red area exists around the middle of these three streams, which is the most prone area for debris flow. This result demonstrates the conformity with the potential debris disaster provided by the hazard map using the currently applied critical line.

The rainfall growth in the debris susceptible area identified from hazard mapping is subsequently developed. The result is shown in Figure 4. The rain increases significantly from 15.00 to 16.30 and decay from 18.00. The snake line obtained from this analysis in the Putih and Pabelan Rivers did not reach the critical line, however the debris flow is observed in these areas. In Gendol River case, the local people reported that the disastrous flow occurred at 16.00 LST in Gendol River. This situation is confirmed by the snake line that grows extremely and surpasses the critical line. Yet, some uncertainties still exist, particularly in the case of Boyong River. In fact, there is no reported damage along this river during the event. These errors are attributable to critical line accuracy, graph representation to current physical condition of whole sub-basins, and radar observation itself. This result suggests that the uncertainty exists in the observations. Moreover, according to MLIT (2004), the judgment using this method is subjective. Yet, debris flow hazard mitigation mostly established based on distinguishing occurrence and non-occurrence events.

  / ISSN 1562-6865 (Online) - ISSN 1063-7710 (Print)

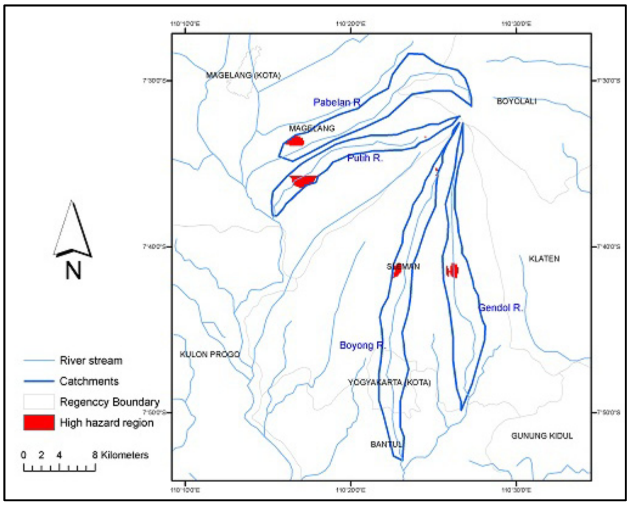

Figure 3. Estimated hazard level from radar observation.

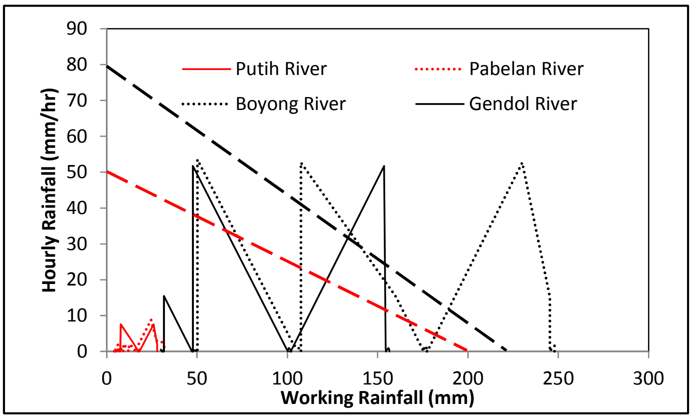

Figure 4. Observed rainfall growth shown by hourly rainfall against working rainfall. Red and black dashed lines are the critical lines for Putih River and Gendol River respectively.

4.2 Deterministic prediction of rainfall-induced debris flow

While the main concern of this study is mainly on obtaining the probable rainfall and flood, rather than accuracy itself, it is still necessary to evaluate the behavior and performance of the model. Figure 5 demonstrates qualitative forecast verification of translation model of one example taken from rainfall event with initial prediction time of 15.30 LST. The prediction uses three past rainfall observation sheets with six minutes interval. The rain is assumed to have rotation motion with growth/decay. By qualitative instant skill assessment through visual comparison, it can be inferred that prediction with lead times shorter than 30 minutes gives promising degree of accuracy. However, in a longer term, it showed widely decreasing contrasting skill. This condition hence strongly motivated the necessity of providing ensemble prediction system.

4.3 Probabilistic hazard zonation

In order to remedy the disadvantages of the judgment method, the ensemble rainfall prediction is developed, as given in Figure 6. While the control prediction gives slightly wrong direction of prediction, the ensemble members provides better results. One member that is closer to the observed data is given by member 3. All ensemble members could help to encompass the uncertainty of rain prediction. In terms of the rainfall temporal variation, the ensemble members could better reproduce the rain. However, as regards of the rainfall amount, the intensity of peak rainfall cannot be predicted accurately. All members overestimate the rain intensity. Also, there is still considerable uncertainty for the lead time longer than one hour. Much of this uncertainty is resulted from rapid changing of advection vector that cannot be identified by extrapolation model due to its simplicity (Reyniers, 2008).

Figure 7 shows the example of spaghetti ensemble rainfall short-term prediction with initial time of 15.30 LST for 5 hours lead time or the final is at 20.30 LST. This result shows the reliability and benefit of the ensemble. Among the five members, there is one member that is closer to the observation, *e.g.,* Pabelan case is served by member with purple color. The five ensemble members could help to eliminate the errors of rain prediction. Except for Putih River, all control predictions are covered by the members, indicating the reliability.

The members could better reproduce the rain in terms of the rainfall amount. However, as for the temporal variation, the timing of peak rainfall is slightly predicted inaccurately.

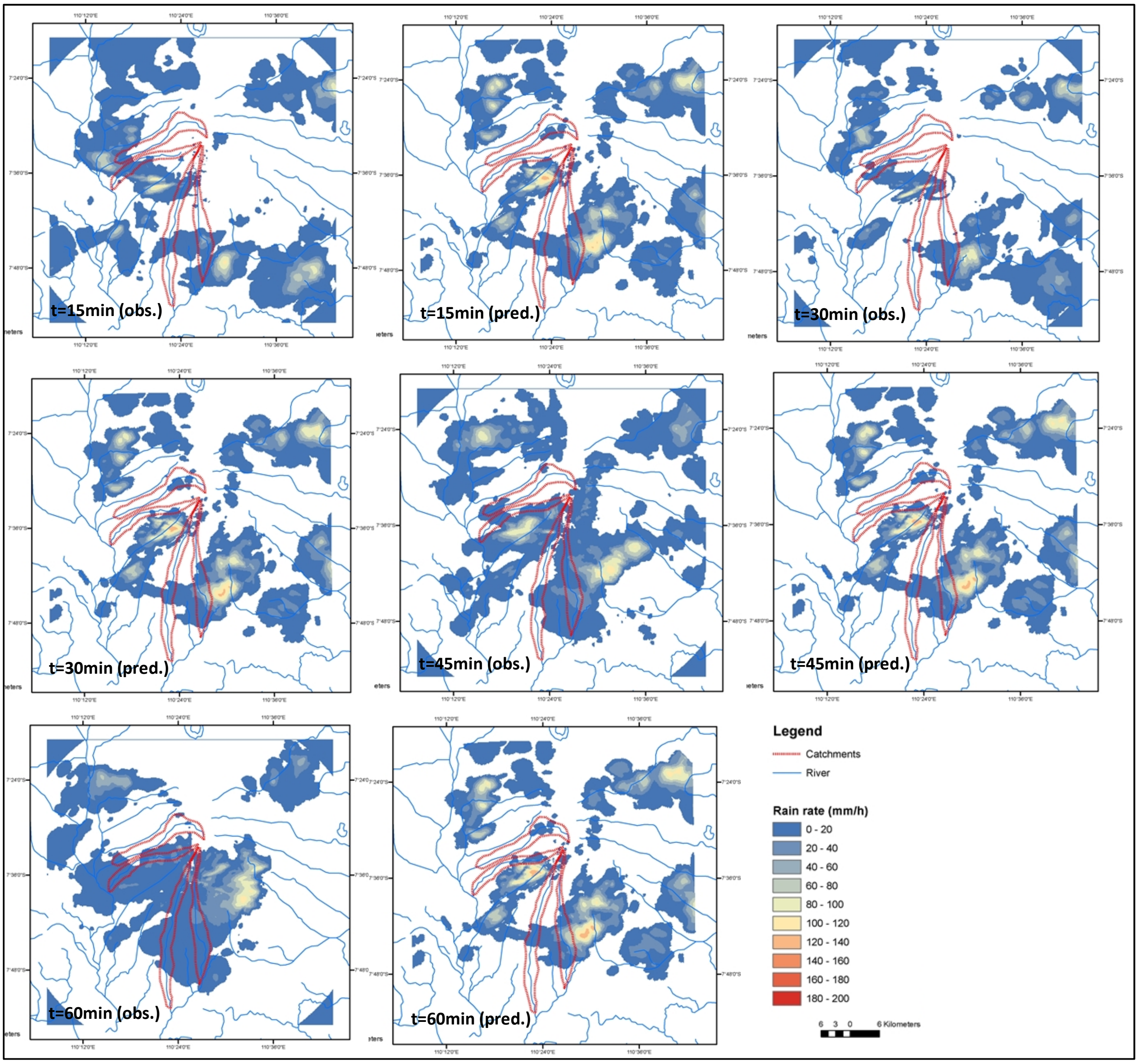

Figure 5. Example of single nowcasting stamp maps of rainfall intensity spatial distribution (mm/h) comparing observation and prediction at at 15.45, 16.00, 16.15, and 16.30 JST.

The map showing the area with rainfall exceeding the critical line for one hour lead time is demonstrated on Figure 8. As compared to the critical line exceedance in the observed rain on Putih River and Boyong River, the deterministic predictions give the similar pattern. It implies that the ensemble could help to gain the confidence in uncertain situation. However, in the case of Pabelan River and Gendol River, the better performance is given by other members. These results suggest that generally the observations are encompassed by the ensemble prediction indicating well predictability of the model.

Figure 9 shows the probability of exceeding critical level map resulted from frequency analysis integrating all members. By using this visualization, informing the level of probability of exceedance that will be useful for further decision making is made possible. Different colors indicate different rain-affected frequency. Meanwhile, in the above deterministic prediction, implementation of ensemble method is primarily focused on the case of only exceeding and non-exceeding critical level status. The analysis indicates that generally all over the sub-basin region Boyong River has lower risk than Gendol River. This result confirms the observation at the event occurrence that reports that Gendol River experienced severe debris flow.

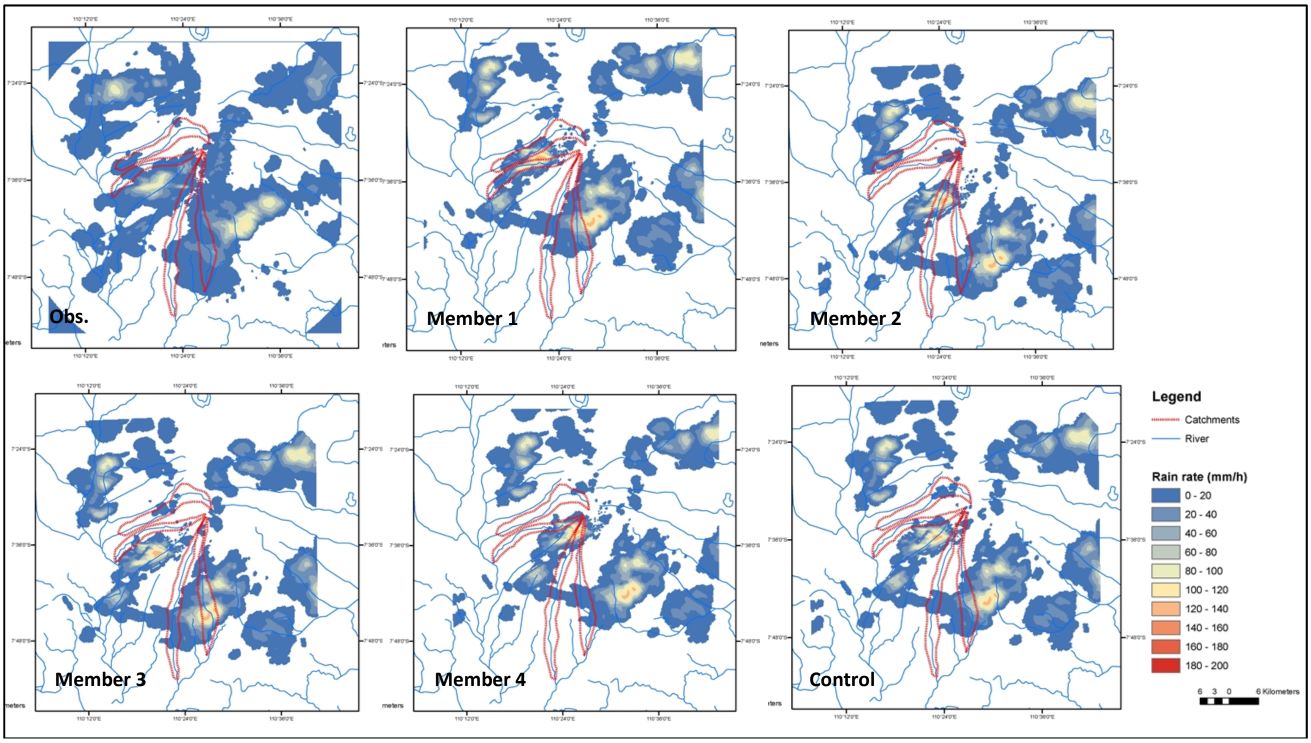

Figure 6. Stamp maps of ensemble rainfall intensity distribution (mm/h) at 45 minutes prediction.

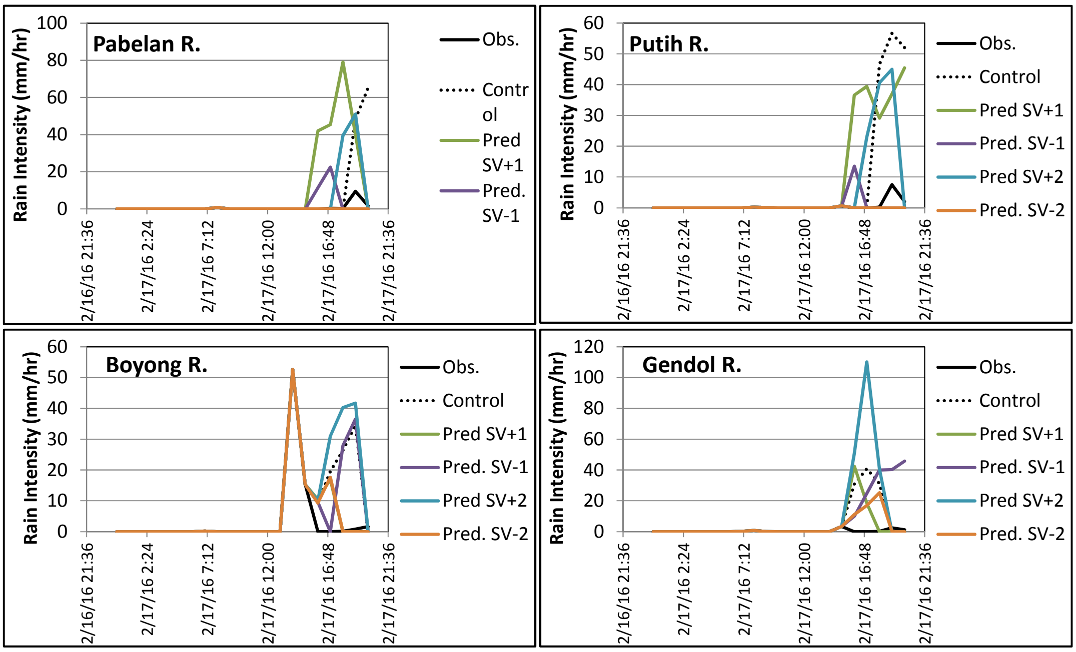

Figure 7. Spaghetti plot of rainfall hyetograph comparing observation, single prediction and ensemble prediction.

4.4 Uncertainty of snake line progression

Figure 10 shows the snake line development from five slightly different model runs from an ensemble taken at river sections with very high and high level hazard. Especially for Boyong River, the snake line members tend to grow in the same pattern. As for Gendol River, the snake lines of the members increase highly. This is to confirm that the past recorded debris disaster occurred severely at Gendol River. The good skill of the model is indicated by the fact that the band brackets most of the control. Also, the observed snake line is laid between the maximum and minimum band of the ensemble members for almost all time. This fact is in line with the finding in the hyetograph ensemble illustration, which demonstrates that the model could be performed reliably. At least a member tends to reproduce the same pattern as observation. By using this method, the amount of the uncertainties can be shown by the ensemble spread. This information will be useful to judge the most occurrence of rainfall onset that will be a trigger of debris flow.

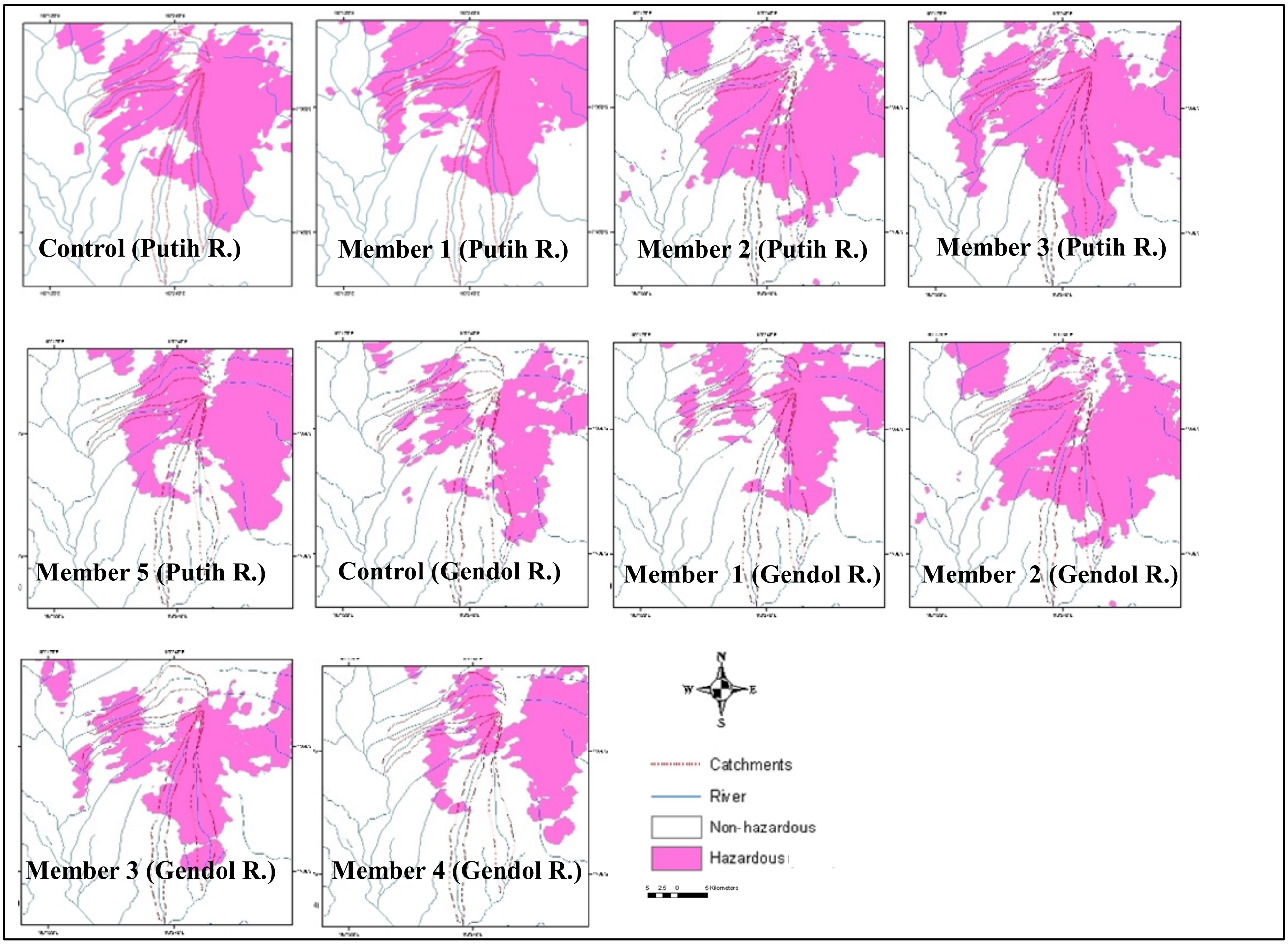

Figure 8. Area with rain that exceeds the critical level for 5 ensemble members with 1 hour prediction lead time using critical lines of Putih River and Gendol River.

The extent of the ensemble is a good indicator of forecast error. Small band shows a more predictable event, and should have narrower error range. On the other hand, the band should not be over-dispersive to guarantee the predictability. Regardless of some shortcomings particularly the remaining uncertainties, this method allows for better approach to deal with uncertainties in the whole system comprising of rainfall observation by using X-MP radar, rainfall nowcasting, critical line establishment, hazard map analysis, snake line generation, and finally decision of warning issuance. Each stage of cascade has to deal with non-linearity and the uncertainty will grow through such a cascade. By including the uncertainty consideration, the authority could have more confident to decide the issuance of warning.

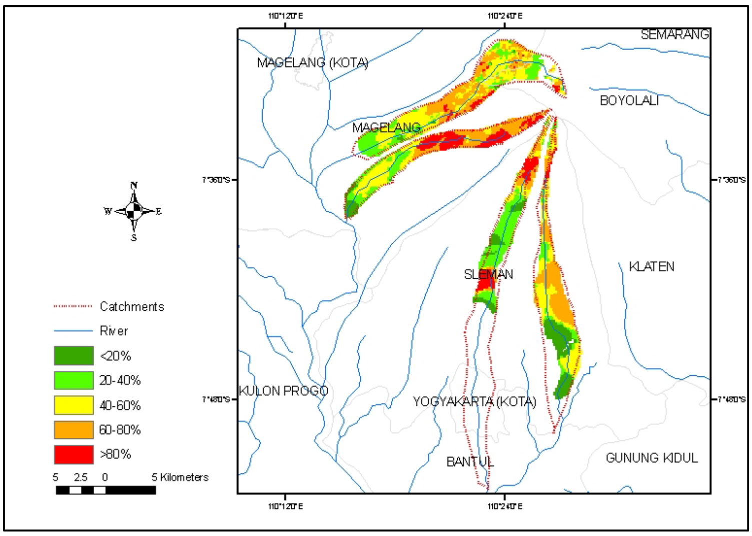

Figure 9. Debris-flow estimated hazard map with 1 hour prediction lead time.

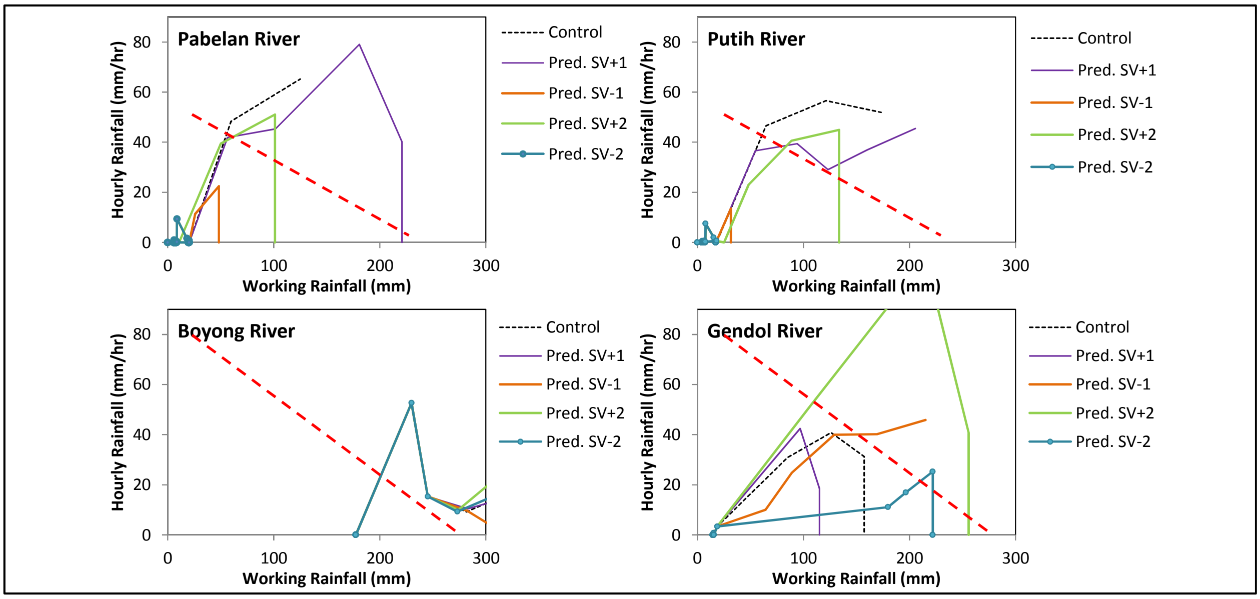

Figure 10. Ensemble predicted snake line shown by hourly rainfall against working rainfall for Feb 10 – 17 20.00 LST (top) and Feb 17 00.00 - 20.00 LST (bottom). Red line is the critical line.

5 CONCLUSIONS

The predictive uncertainty in the nowcasting of localized rainfall by using X-MP radar and its effect to the debris flow hazard information has been studied in Merapi Rivers. Debris mitigation system integrates the use of hazard map information to identify the vulnerable river and rainfall snake line to issue the warning under the basis of critical line. Uncertainty in high-resolution nowcasting products from X-band multiparameter compact (X-MP) is assessed by developing ensemble. The probabilistic hazard map obtained by frequency analysis of five ensemble members could show the basin or village that is most likely to be hit by the debris flow. The reliability is proven by the fact that five different hyteographs and snake line plots could embrace the control and observation. As compared to the traditional approaches using single deterministic prediction, this scheme could show the amount of uncertainties in the system. The finding of this paper is expected to be useful for the authority as decision support system for debris disaster response under emergency situation. Further studies will be primarily focused on the development of the current critical line by using radar observation and evaluation of its uncertainties.

ACKNOWLEDGEMENTS

The authors would like to send the greatest grateful to SATREPS Project, Integrated Study on Mitigation of Multimodal disasters caused by Ejection of Volcanic Products in giving a helpful channel for discussing and providing data for the completion of this paper.

REFERENCES

Burlando, P., Rosso, R., Cadavid, L.G. & Salas, J.D. (1993). Forecasting of Short-Term Rainfall Using ARMA Models. *Journal of Hydrology*, 144(1-4), 193-211.

Caine, N. (1980). The Rainfall-Intensity-Duration Control of Shallow Landslides and Debris Flows. *Geog rafiska Annaler Series*, 62(1), 23-27.

Cloke, H.L. & Pappenberger, F. (2009). Ensemble Flood Forecasting: A Review, *Journal of Hydrology*, 375(3-4), 613-626.

Ebert, E.. (2001). Ability of a Poor Man's Ensemble to Predict the Probability and Distribution of Precipitation. *Monthly Weather Review*. 129(10), 2461-2480.

Fujita, T., Stensrud, D.J. & Dowell, D.C. (2006). Surface Data Assimilation Using an Ensemble Kalman Filter Approach with Initial Condition and Model Physics Uncertainties. *Monthly Weather Review*, 135(5), 1846-1868.

Georgakakos, K.P. (2006). Analytical Results for Operational Flash Flood Guidance. *Journal of Hydrology*, 317(1-2), 81-103.

Hapsari, R.I., Oishi, S., Sunada, K., Nakakita, E. & Sano, T. (2011). Singular Vector Method on Short-Term Rainfall Prediction Using Radar for Hydrologic Ensemble Prediction. *Journal of Japan Society of Civil Engineers, Ser. B1 (Hydraulic Engineering)*, 67(4), 1_1091-1_114.

Hardjosuwarno, S., Sukatja, C.B. & Yunita, F.T. (2013). *Early warning system for lahar in Merapi*. Ministry of Public Works, Indonesia.

Islam M. & Sado K. (2000). Development of Flood Hazard Map of Bangladesh Using NOAA-AVHRR Images with GIS. *Hydrological Sciences*, 45(3), 337-355.

Kato, A., Maki, M. (2009). Localized Heavy Rainfall Near Zoshigaya, Tokyo, Japan On 5 August 2008 Observed by X-Band Polarimetric Radar - Preliminary Analysis. *Scientific Online Letters on the Atmosphere*, 5, 89-92.

Kim, S., Tachikawa, Y., Sayama T., Takara K. (2009). Ensemble Flood Forecasting with Stochastic Radar Image Extrapolation and a Distributed Hydrologic Model, *Hydrological Processes*, 23(4), 597-611.

Lavigne, F. & Thouret, J.C. (1988). Lahars in Java: Initiations, Dynamics, Hazard Assessment and Deposition Processes. *Forum Geografi*, 21(1), 17-32.

Lavigne, F. & Thouret, J.C. (2003). Sediment Transportation and Deposition by Rain-Triggered Lahars at Merapi Volcano, Central Java, Indonesia. *Geomorphology*, 49(1), 45-69.

Mananoma, T. & Wardoyo W. (2009). The Influence of Rainfall Characteristics Change on Sediment Migration Pattern after Merapi Eruption 2006. *Proceeding of International Seminar on "Climate Change Impacts on Water Resources and Coastal Management in Developing Countries*.

MLIT. (2011). *Guidelines for development of warning and evacuation system against sediment disasters in developing countries,* Ministry of Land, Infrastructure, Transport and Tourism, Japan.

Neary, D.G. & Swift, L.W. (1987). Rainfall Thresholds for Triggering a Debris Flow Avalanching Event in the Southern Appalachian Mountains. *Reviews in Engineering Geology*, 7, 81-95.

Pierce, C., Bowler, N., Seed, A., Jones, A., Jones, D. & Moore, R. (2005). Use of a Stochastic Precipitation Nowcast Scheme for Fluvial Flood Forecasting and Warning. *Atmospheric Science Letter*, 6(1), 78-83.

Reyniers, M. (2008). *Quantitative Precipitation Forecasts based on Radar Observations*. Royal Meteorological Institute of Belgium.

Shieh, C.L., Chen, Y.S., Tsai, Y.J. & Wu, J.H. (2009). Variability in Rainfall Threshold for Debris Flow after the Chi-Chi Earthquake in Central Taiwan, China. *International Journal of Sediment Res*earch, 24(2), 177-188.

Shiiba, M., Takasao, T. & Nakakita, E. (1984). Investigation of Short-Term Rainfall Prediction Method by a Translation Model. *Proceeding of Japan Conference on Hydraulic Engineering,* 28th, 423-428.

FLOOD RISK MANAGEMENT IN PANAWA, SRI LANKA USING FLOOD MODELLING

B.S.K. DE SILVA (1), P. S. D. ALUWIHARE (2) & J. CHANDIMALA (3

(1,2) Faulty of Engineering Technology, The Open University of Sri Lanka, Kandy Regional Centre, Kandy, Sri Lanka,
psalu@ou.ac.lk
(3) Water Supply and Drainage Board, Greater Kandy Water Supply Project, Kandy, Sri Lanka
janakiya@yahoo.com

ABSTRACT

Floods have become a major hazard to lives and infrastructure in Sri Lanka, but the management techniques adopted are extremely limited. This limitation is mainly due to the lack of knowledge in identification and assessment of flood risk in respective areas. The lower Deduru Oya basin in Sri Lanka is frequently affected by floods. A major flood disaster occurred in December 2014 and the damages were catastrophic in the lower reach of the Deduru Oya basin. This study focuses on introducing a flood management system for the Panawa area in Rasnayakapura DS division, situated at the lower reach of Deduru Oya river. The objective is achieved by developing a flood model for the study area using HEC-HMS hydrological model, HEC-RAS hydraulic model and HEC-GeoRAS in ArcGIS interface. The model has been calibrated and verified using actual flood levels observed during extreme flood events in 2014 and 2015 respectively. The water levels obtained as the output data of HEC-RAS were then exported to HEC-GeoRAS in ArcGIS interface, where the results of the hydraulic modelling could be visualized in the form of flood maps. The maximum flood map was subsequently superimposed on a Google Earth map which enabled the identification of flood vulnerable zones and safe zones in the study area. A comprehensive non-structural solution including a flood forecasting method, an early warning system and evacuation procedures has been proposed as the most sustainable solution to the flood problem in the selected study area.

Keywords: Deduru oya; flood model; flood maps; GIS; non–structural solution.

1 INTRODUCTION

Floods have become one of the most devastating natural hazards in Sri Lanka, affecting the geomorphologic, economic and social aspects (Wanniarachchi and Wijesekera, 2012) and claiming lives as well. Frequency of occurrence of floods and their magnitude in Sri Lanka has become variable (IPCC, 2001), which may be attributed mainly to climatic changes, unplanned development, environmental degradation and human intervention, etc. The increase in population and subsequent need for land have forced more and more people to live and work in areas that are vulnerable for floods, thereby intensifying the risk to life and property in the event of major floods. Although the catastrophic nature of flood events are understood, the management techniques adopted in Sri Lanka are extremely limited (de Silva et al., 2015). This limitation is mainly due to the lack of knowledge in identification and assessment of flood risk in respective areas.

Identification of the depth of flooding and extent of flood water inundation in flood prone areas will enable decision makers to make choices about the most suitable flood management plans and strategies. Flood models can be very useful in producing flood inundation maps and are capable of providing time series inundation information about the onset, duration and passing of a flood event (Nandalal and Ratnayake, 2011). Such information is crucial in strategic planning of flood mitigation measures and effective flood risk management.

Inundation assessment through flood models are carried out through four main components (Ahmed et al., 2010); the hydrological model, which converts a historic storm event to runoff, the hydraulic model, which routes the runoff to determine water surface profiles at the respective locations along the stream network, flood plain mapping and visualization using a prescribed tool and the extraction of geospatial data for the use in the models. The above integration provides valuable basis for assessment of flood prone area and modelling of flood hazard phenomenon. Generation of flood maps is one of the most important steps towards introducing a non–structural form of flood control. Conventionally, in Sri Lanka, the flood is mainly controlled by structural based solutions, such as floodwalls, levees, storage reservoirs, etc. maps (de Silva, 2015). But in recent decades, non-structural control methods have been tested to be very effective and economical in decreasing flood damages (comprehensive study on disaster management in Sri Lanka-final report, 2009). This approach adopts an effective method where basically a timely warning is given to the people to move out of the area before the breach of floods.

The lower Deduru Oya basin in Sri Lanka is frequently affected by floods (Wickramaarachchi, 2004). Prolonged floods disrupt daily activities and cause huge socio-economic damage almost every year for District Secretarial (DS) Divisions, such as Chilaw, Rasnayakapura, Kobeigane, Nikaweratiya and Wariapola. A major flood disaster occurred in December 2014 and the damages were catastrophic in the lower reach of the Deduru Oya basin. Several studies have been carried out for the Deduru Oya basin (Wickramaarachchi, 2004). However, research on the flood hazard assessment, mapping and subsequent introduction of a proper flood management system have not been done in the area.

This study focuses on introducing a non–structural form of flood management system for the Panawa area in Rasnayakapura DS division, situated at the lower reach of Deduru Oya River. The objective is achieved by developing a flood model for the study area using HEC-HMS hydrological model, HEC-RAS hydraulic model and HEC-GeoRAS in ArcGIS interface. The developed flood model will facilitate in determining the high flood levels and preparation of flood inundation maps. Final results of the numerical analysis will be used in proposing a suitable non-structural flood management system for the lower reach of Deduru Oya.

2 MATERIALS AND METHODS

2.1 Study area

2.1.1 Deduru Oya Basin

The Deduru Oya is the fourth largest river basin in Sri Lanka flowing through Matale, Kurunegala and Puththalam Districts, draining a total area of 2620 km^2 before entering the Indian Ocean, 2 km North of Chilaw on the west coast of Sri Lanka. The river originates from the mountainous area of the Matale district. The major tributaries of Deduru Oya are Ratwila Ela and Dik Oya in the upper reaches and Maguru Oya and Kimbulwana Oya in the middle reaches. The hydrometric network in the basin consists of several meteorological stations, namely Chilaw, Kurunegala, Millawana estate, Nikaweratiya, Polonthalawa, Wariyapola, Ridibediela and Bathalagoda tank and two stream gauge stations where only the Chilaw Gauge station situated at the west coast of Sri Lanka is in function. To effectively use the high amount of water that flows into the sea annually through Deduru Oya, the Dedu Oya reservoir has been built. The main objectives to be achieved by the commissioning of the dam and the reservoir are to increase cropping intensity of existing Ridi Bendi Ela scheme, trans-basin diversion of water to the adjoining Mee Oya basin, flood mitigation downstream of the dam, etc. Though flood mitigation is a major objective of the dam, it failed to prevent the major flood occurred in December 2014, nearly a month after commissioning the dam.

2.1.2 Rainfall

The rainfall pattern in the basin follows the bimodal pattern where the two peaks are in the months of April/ May and October/November and the minima in January/February and August, as illustrated in Figure 1 (Wickramaarachchi, 2004). The mean annual rainfall for the basin is 1650 mm and the runoff to the sea amounts to an average of 451 mm with a runoff factor of 27%. Converting this into volumetric figures, with a total catchment area of 2620 km^2, the rainfall amounts is about 4310 MCM while the runoff volume to sea is about 1180 MCM. The runoff to the sea is equivalent to an average discharge of 37.4 m^3/sec.

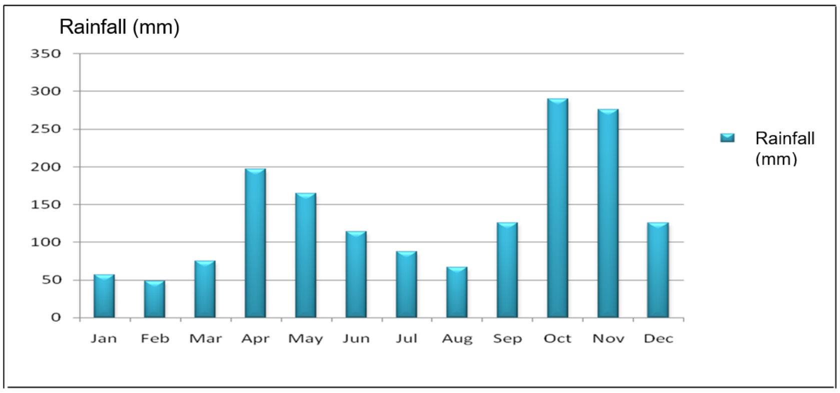

Figure 1. Bimodal pattern of the rainfall in Deduru Oya

2.1.3 Climate

About 90% of the Deduru Oya catchment area comes under the intermediate zone of Sri lanka and the remaining area in mountainous region falls under the mid country wet zone. The annual precipitation in the basin varies from 1100 mm in the coastal region to 2600 mm in the mountainous region. At the Kurunegala Weather Station in Deduru Oya catchment, the mean annual temperature is recorded as 27°C and the monthly mean annual relative humidity of 81% where the highest occurring during November (85%) and lowest in February/March (78%). Diurnal variation in relative humidity is about 20%. The daily wind run as measured at Puttalam is 290 km/day (Deduru Oya and Mee Oya Basins Development Project- Pre-Feasibility Report, 2001).

2.1.4 Selected study area in the Deduru Oya basin

Considering the severity of flood damages in the Deduru Oya basin, Panawa area in Rasnayakapura DS division has been selected as the study area. The study area and the dam location are shown in Figure 2.

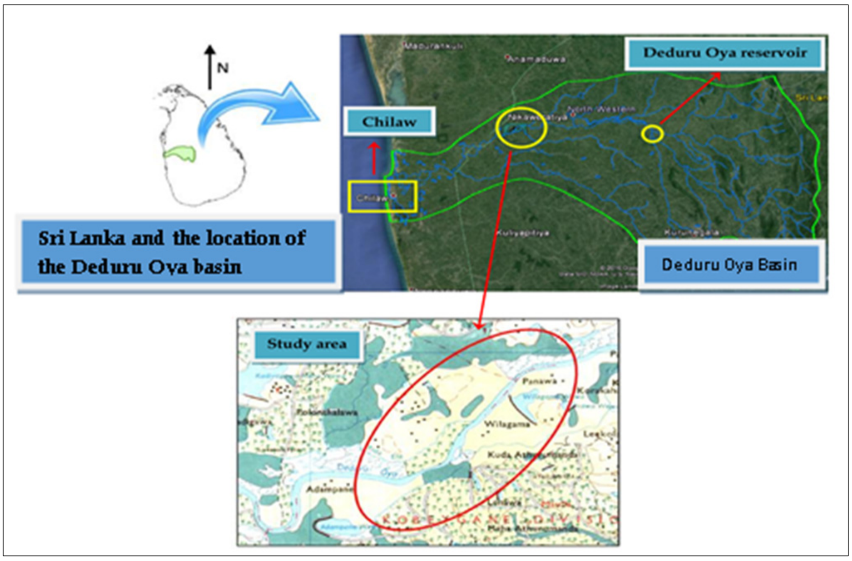

Figure 2. Selected study area – Panawa, Rasnayakapura DS Division.

2.2 Data Collection

The study utilized a number of spatial and hydrological data as given in the following subsections.

2.2.1 Questionnaire survey

A questionnaire survey was carried out to obtain details about historical flood events in the selected area, the operation of Deduru Oya dam and personal details of affected people in Rasnayakapura DS division. A special attention was also given to the mobile phone coverage and the contact details of the residents of the area were recorded during the questionnaire survey.

2.2.2 Field Measurements in the selected river reach

River cross sections were obtained at 11 locations in the selected river reach in order to improve the accuracy of the cross sections generated using the TIN (Triangular Irregular Network) of the area. Velocity profiles were also taken at two cross sections. Vegetation patterns, permeable and impermeable areas, conditions of the channel bed were recorded carefully to obtain the most suitable roughness coefficients of the floodplain.

2.2.3 Spatial and hydrological data

The spatial and hydrological data collected during the study and their sources are given in Table 1. Although there are several rain gauge stations in the basin, most of them record daily rainfall. Only the Kurunegala rain gauge station (Longitude 7^0 28' Latitude 80^0 22' and Altitude 116 m) was found to record hourly rainfall, which is mandatory for this type of flood study.

2.3 Flood model development

The Flood model was developed using HEC-HMS hydrological model, HEC-RAS hydraulic model and HEC-GeoRAS in ArcGIS interface.

2.3.1 Hydrologic Model

Hydrological model is developed for the lower reach of Deduru Oya using HEC-HMS (User's Manual- Hydrologic Modeling System HEC-HMS, Version 3.5, 2012). All sub-basins, network junctions and also the newly constructed Deduru Oya reservoir were included in the stream network. The watershed stream network was created manually in HEC-HMS. The sub-basins, network junctions, sinks and source were entered into the HEC-HMS model as "elements". The network consisted of seven sub basins, five reaches, four junctions, a sink and a reservoir. The selected elements were connected in a dendritic network to simulate runoff process, as shown in Figure 3.

Table 1. Spatial and hydrologic data and source.

No	Spatial data	Source
1	Topographic Map of the area (Scale 1:50,000 and 1:10000 in digital form)	Department of Surveys, Sri Lanka
2	Deduru Oya sub-basin areas	Digital Basin map and shape file from Department of Surveys, Sri Lanka
3	Land Use Maps of the area	Department of Surveys, Sri Lanka
4	Historical flood depths	Measured during field survey
No	Hydrological data	Department of Irrigation Sri Lanka
1	Climatic Data	Department of Meteorology, Sri Lanka
2	Discharges	Department of Irrigation Sri Lanka
3	River Cross-Sections	TIN created from contour map and measured for 2 km length
4	Stream lengths and slope of the main stream	From Digital Elevation Model

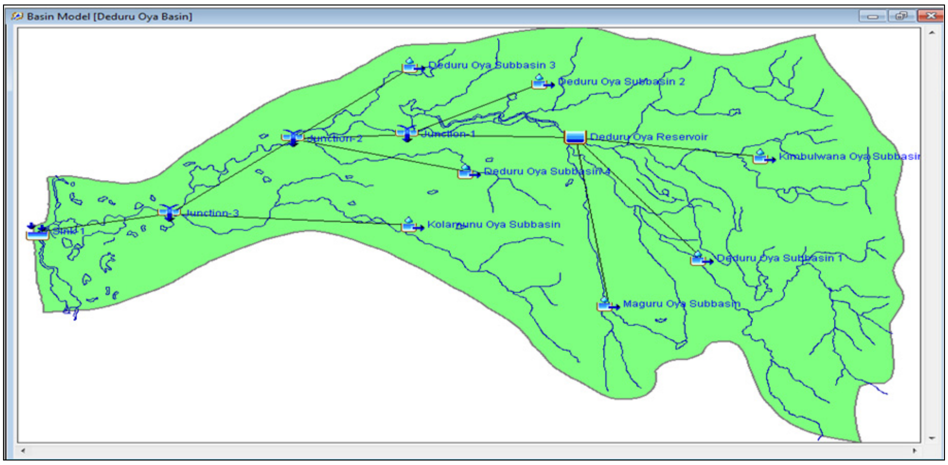

Figure 3. Dendritic stream network created in HEC-HMS interface.

Among the assortment of different methods to simulate infiltration losses, transform excess precipitation into surface runoff, base flow condition and routing in HEC-HMS, the following methods have been selected for the current model execution.

Table 2. Theories or methods used in hydrological model execution,

Input process Parameter	Theory or Method	Data required
Loss method	Initial and Constant	Initial loss (mm) Constant rate (mm/hr) Impervious area (%)
Transform method	SCS Unit Hydrograph	Lag time (min)
Base flow method	Constant Monthly	Base flow in all 12 months
Routing method	Kinematic Wave	Reach lengths Slope, Manning's Coefficients

All the other reservoirs and tanks are small compared to the newly constructed Deduru Oya reservoir. Therefore, it is assumed that all of the small reservoirs and tanks are at full supply level when the simulation starts. To account the Deduru Oya reservoir, a reservoir element has been added to the stream network.

2.3.2 Hydraulic Model

Hydraulic model for the lower reach of Deduru Oya was developed using HEC-RAS (Hydraulic Reference Manual-HEC-RAS River Analysis System 2010). Cross section details of the selected reach obtained from the TIN of the area (Triangular Irregular Network), measured cross sections details and suitable Manning's n value chosen according to the flood plain conditions were used as the main geometric data for executing the hydraulic model. The unit hydrograph generated from HEC-HMS model was used as the upstream boundary condition and a normal depth as downstream boundary condition. A set of flood levels were obtained at respective cross sections as the output of the hydraulic model.

2.3.3 Model Calibration and Verification

Model was calibrated considering the extreme flood event occurred in Deduru Oya basin in December 2014. Simulation results corresponding to different parameter values were visually compared with the observed data, and the parameter set, which matched observed values and simulated data, the best was selected as the calibrated parameter set. The minor flood which occurred in May, 2015 was used in the verification process.

2.3.4 Flood Mapping in the study area

1:10,000 digital maps in shape file format containing contours, stream lines, land use, spot heights, etc., of the selected study area of Deduru Oya basin were collected from the Department of Surveys. A Triangular Irregular Network (TIN) for the selected area was created using the contour shape file. The TIN is presented as a map in Figure 4, which can be used to obtain 3D data of the terrain. A RAS layer was created from HEC-GeoRAS in Arc GIS interface by digitizing the river centre line, river banks, flow paths and cross section cut lines. All three-dimensional data of the cross section cut lines and the river centre line were extracted from the TIN. The data was then exported to HEC-RAS as RAS data. These exported cross sections were modified in HEC-RAS using the bathymetric cross section data obtained from field measurement along Deduru Oya for a distance of 2.0 km in the selected study area. After the simulation run with the calibrated parameter set, the output data (containing cross sections and water levels) were exported back to HEC-GeoRAS (User's Manual-HEC-GeoRAS, GIS (2012) and the inundation maps were generated. The inundation map generated for the maximum flood, which occurred in December 2014, is shown in Figure 5.

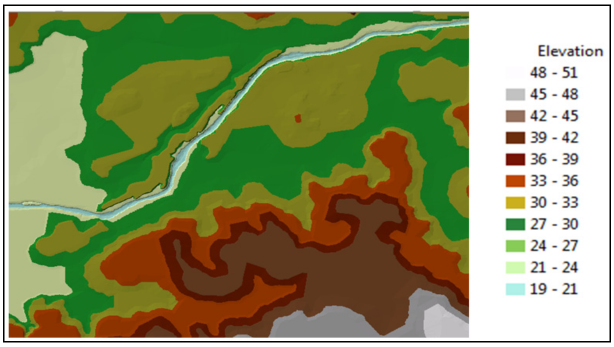

Figure 4. TIN created from the contour map.

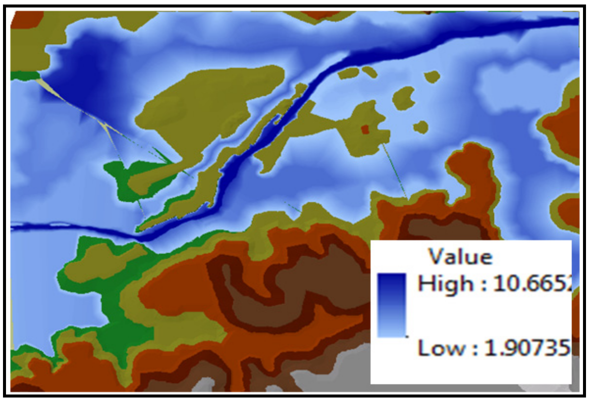

Figure 5. Flood map with flood extent in HEC-GeoRAS in ArcGIS interface.

2.3.5 Identification of flood vulnerable areas and safe zones

The maximum inundation map, which was obtained using HEC Geo-RAS in Arc GIS interface, was superimposed on a Google Earth map after changing the coordinates from Kadawala Sri Lanka Grid to WGS

1984 Web Mercator Auxiliary Sphere. Using the view from Google Earth, flood vulnerable zones and safe zones were identified.

3 RESULTS & DISCUSSION

3.1 HEC-HMS Model Output for the Extreme Flood Event in December 2014

The selected study area is located between junction-2 and junction-4 of the stream network given in Figure 3.

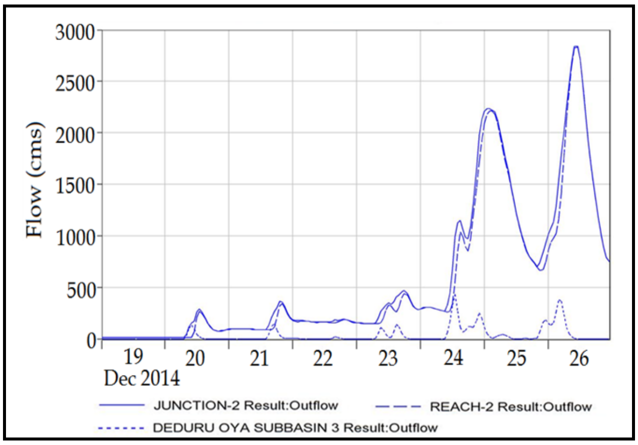

Figure 6. Hydrograph at the junction-2.

Figure 8 shows the flow hydrograph derived at the junction-2. The outflow hydrograph at juntion-2 was used as the upstream boundary condition in executing HEC-RAS model. It can be clearly observed that the maximum peak discharge is around 2800 m^3/s, which occurred in the early hours of 26^{th} December 2014.

3.2 Model Calibration and Verification

Figure 7 illustrates the model calibration curve to the flood event occurred in December 2014. The Mean Ratio Absolute Error (MRAE) between the actual and the simulated curves was calculated to be 2.38%. Model verification was carried out for the flood event that occurred in May 2015 where the duration of the storm was shorter thus making the event less catastrophic. MRAE for the verification process was calculated to be 2.61%, which is an indication of a successful verification. The verification curve is illustrated in Figure 8.

3.3 Generated flood maps during flood progression

The inundation maps obtained using HEC-GeoRAS and the corresponding views obtained by superimposing the flood maps on a Google Earth map are illustrated in Figure 9 for the study area. Inundation of the land with flood water (area in blue) is clearly visible through these figures.

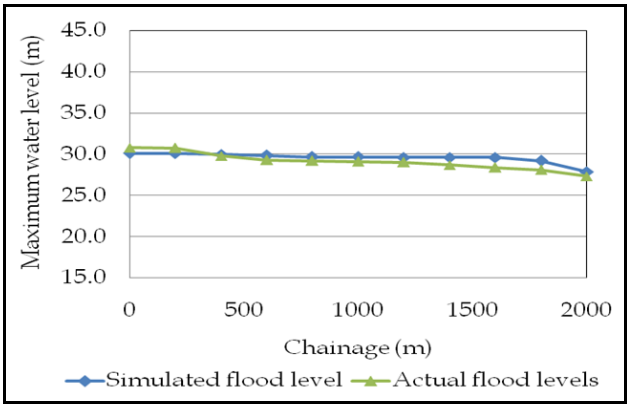

Figure 7. Model calibration curve.

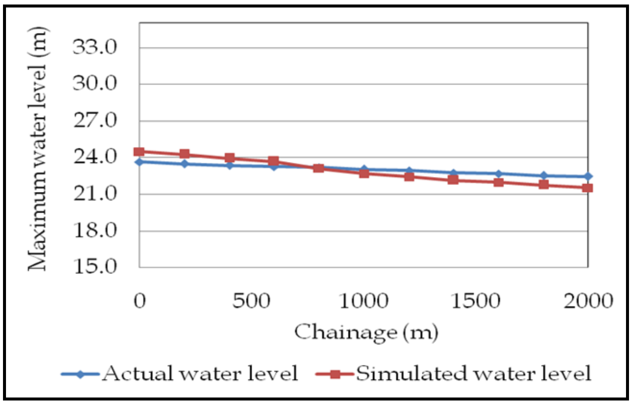

Figure 8. HEC-RAS model verification curve.

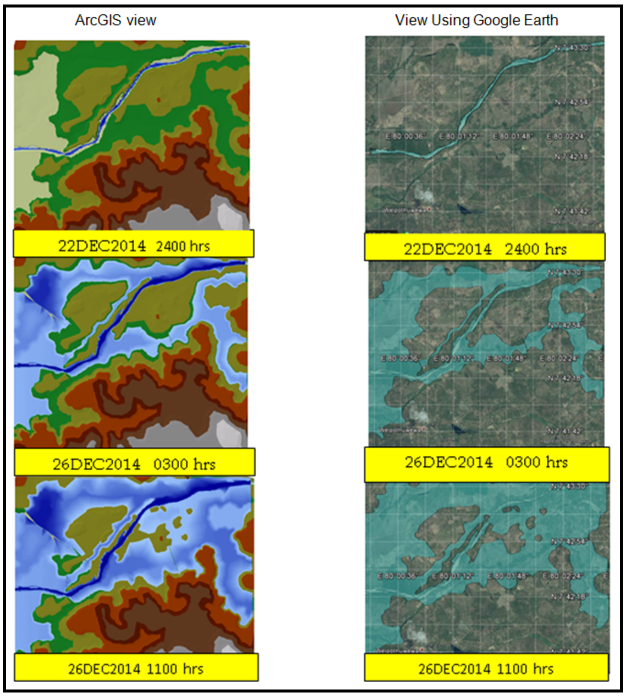

Figure 9. Inundation maps - Time series ArcGIS view and Google Earth view.

4 PROPOSED NON –STRUCTURAL SOLUTION

4.1 Suitability of a Non-Structural flood management system

A non-structural solution for the flood problem was found to be appealing for managing flood in the selected area due the low investment costs, less maintenance cost and negligible impact to the natural environment. The flood problem in Kelani Ganga, the fourth longest river in Sri Lanka was managed by adopting a non-structural flood management system in 2011, where the number of families affected has been drastically reduced (Comprehensive study on disaster management in Sri Lanka-final report, 2009).

4.2 Identification of safe and vulnerable zones for the affected people

As the first step of the solution, the maximum inundation map, which was obtained from HEC-GeoRAS in ArcGIS interface, was superimposed on a Google Earth map and flood vulnerable zones and safe zones were identified. All the houses and other buildings in the danger zone were identified from the Google Earth view, as illustrated in Figure 10.

4.3 Flood Forecasting Method

Since there is no stream gauge station between the study area and Deduru Oya reservoir, it was decided to forecast flood by using the discharge of the Deduru Oya reservoir. In this study, Deduru Oya reservoir has been considered as a control point of the flood forecasting system, because it discharges a large volume, which is frequently regulated and the discharge can be calculated using the predetermined discharge rating curve of the dam. From the model developed, it was found that water discharged from the reservoir takes

about two hours to reach the study area. Two hour time is adequate to carry out the emergency evacuation of the families who are in the danger zones to evacuation centers in the safe zones.
Considering flood event in December 2014, it was found that when the dam discharge exceeds a value of 243.6 m^3/s, flood occurs in the study area. This discharge value was considered as the critical discharge value of the dam before flooding. Important discharge ranges identified during the flood event occurred in December 2014 are tabulated in Table 3.

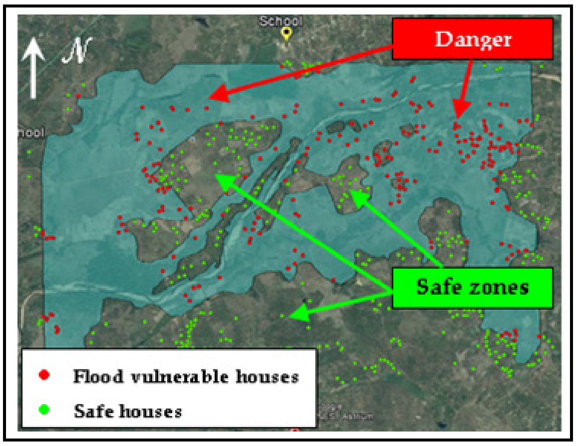

Figure 10. Identification of danger zone, safe zones etc.

Table 3. Critical discharge ranges.

Date and time of discharge of Deduru Oya dam	Date and time at which the discharge reach the study area	Discharge from the dam (m^3/s)	Description
22nd DEC2014 at 2400 hrs	23rd DEC2014 at 0200 hrs	150.5	No flooding
24th DEC2014 at 0800 hrs	24th DEC2014 at 1000 hrs	243.6	Maximum discharge before flooding
25th DEC2014 at 2100 hrs	25th DEC2014 at 2300 hrs	569.2	Flooding
26th DEC2014 at 0100 hrs	26th DEC2014 at 0300 hrs	645.7	Flooding
26th DEC2014 at 0300 hrs	26th DEC2014 at 0500 hrs	789.0	Flooding
26th DEC2014 at 0400 hrs	26th DEC2014 at 0600 hrs	1042.6	Flooding
26th DEC2014 at 0500 hrs	26th DEC2014 at 0700 hrs	1359.0	Flooding
26th DEC2014 at 0600 hrs	26th DEC2014 at 0800 hrs	1711.3	Flooding
26th DEC2014 at 0900 hrs	26th DEC2014 at 1100 hrs	2646.4	Maximum flooding

From the above table, the houses inundated from a particular discharge range can be easily identified before two hours and each house can be informed individually using a fast communication system. The study area has good mobile phone coverage and from the questionnaire survey it was found that more than 95% of the community in the study area uses mobile phones. Short Message Service (SMS) can be used as a fast communication system to inform individual houses in the danger zone to take necessary precautions.

4.4 Safe Evacuation Centers

Public buildings are considered as the most suitable locations to use as evacuation centers. Unfortunately, public buildings in the study area that can be used as safe evacuation centers are limited. Therefore, it is decided to establish four units of New Evacuation Centers (NEC) to accommodate people affected by the flood. The location of the four evacuation centers were selected in the safe zones in such a way that it can be safely, easily and quickly accessed by the evacuating people. Three schools in the area were also selected as the evacuation centers. The NECs' can be used as community buildings known as 'Praja shalawa's, when there are no floods.

4.5 Database of flood vulnerable houses and affected people

A database has been developed, including details of all the houses in the flood vulnerable zones with their coordinates, discharge range in which the house is situated, mobile phone numbers, house owner details, evacuation routes and the evacuation centers. Information will be sent to each house via a SMS according to the developed database.

4.6 Proposed Evacuation Method

4.6.1 Alarm System

An alarm system will be installed in the NEC 1 and 2 to alert the people in the danger zones by using speakers, which can be controlled from the dam location. The alarm system will send a warning sound to the area when the dam discharges the critical value of 243.6 m^3/s. This is the maximum value that the dam can safely discharge without causing any flood in the study area. When the dam discharge exceeds the critical value, the study area will be definitely affected by flood.

4.6.2 Informing Individual Houses

After the dam exceeds the critical discharge value, the warning alarm will be sent off from the dam location and further updates about the flood will be informed by means of a SMS system. As for a particular discharge value from the dam, the inundation zones and the houses inside the zones have been already identified. It is a matter of sending a SMS to the house owners informing that their houses will be inundated in less than two hours. After that the house owners can use the specified evacuation paths and proceed to a safe evacuation center.

4.6.3 Evacuation Paths for Safe Areas

The evacuation paths have been determined in such a way that every individual house gets its own evacuation path. The shortest and safest paths to the nearest evacuation centers have been obtained by using Google Earth, as illustrated in Figure11. The destination details and evacuation paths are mapped in the same figure.

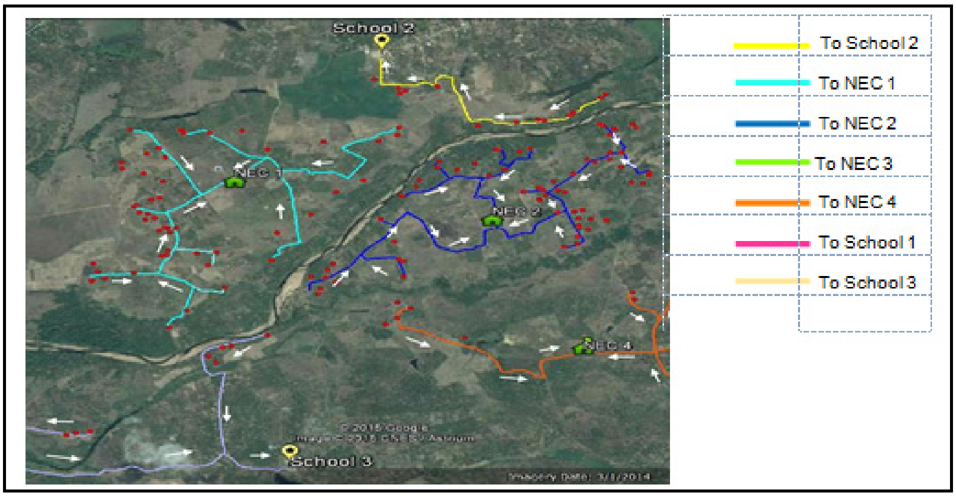

Figure 11. Evacuation paths.

The proposed non-structural solution can be explained well using Figure 12.

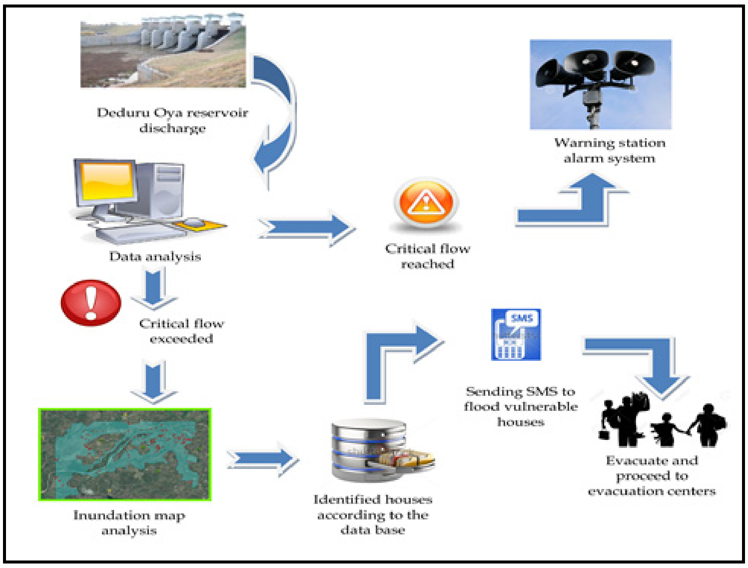

Figure 12. Flow diagram of the suggested nonstructural solution.

4.7 Details of the houses to be evacuated for different dam discharges

Inundation maps and evacuation paths for selected different dam discharge values can be presented for different discharge values given in Table 3. Details of the houses to be evacuated and the safe paths and evacuation centers are also subsequently tabulated. A single case where the dam discharge is 243.6 m^3/s is given in Table 4. In this case, house numbers 1 – 9 are in the danger zone and the respective house owners are instructed to take the Route A as the safest evacuation path to reach the respective evacuation center, School 2.

Table 4. Details of houses to be evacuated.

Discharge from Deduru Oya = 243.6 m^3/s			
House No.	**Latitude**	**Longitude**	**Evacuation path and Evacuation center**
1	7°43'31.33"N	80° 2'13.18"E	Route A To School 2
2	7°43'30.29"N	80° 2'12.40"E	
3	7°43'26.04"N	80° 2'7.06"E	
4	7°43'26.49"N	80° 2'7.16"E	
5	7°43'25.56"N	80° 2'6.43"E	
6	7°43'24.04"N	80° 2'1.57"E	
7	7°43'24.23"N	80° 2'0.52"E	
8	7°43'23.60"N	80° 1'56.34"E	
9	7°43'22.53"N	80° 1'49.03"E	

7 CONCLUSIONS

A flood model has been developed to determine the water levels and inundation areas in the Panawa area using tools, such as HEC-HMS, HEC-RAS, HEC-GeoRAS in ArcGIS interface and Google Earth. The model was calibrated and verified using the extreme flood events in December 2014 and May 2015 with MRAE values of 2.38% and 2.61%, respectively. Accordingly, the model is capable of preparing inundation maps for floods that occur in the Deduru Oya study area. A comprehensive non-structural solution including a flood forecasting method, an early warning system and evacuation procedures has been proposed as the most sustainable solution to the flood problem in Panawa area in Deduru Oya basin.

REFERENCES

Ahmed, B., Kaleem, M.S., Butt, M.J. & Dahri, Z.H. (2010). Hydrological Modelling and Flood Hazard Mapping of Nullah Lai. *Proc. Pakistan Acad. Sci,* 47(4), 215-226.

Comprehensive study on disaster management in Sri Lanka (2009). *Comprehensive study on disaster management in Sri Lanka final report,* Japan International Cooperation Agency, Department of Irrigation of the Ministry of Irrigation and Water Management, Sri Lanka.

Deduru Oya and Mee Oya Basins Development Project, Pre-Feasibility Report (2001). Planning Branch, Department of Irrigation, Sri Lanka.

De Silva Shammi, Aluwihare Shriyangi and Chandimala Janaki (2015). Trends of Floods in Sri Lanka, *E-Proceedings of the 36th IAHR world congress*, Delft, The Hague, Netherlands (28th June -3rd July), 4935.

Hydraulic Reference Manual-HEC-RAS River Analysis System, Version 4.1 (2010). Hydrologic Engineering Center, US Army Corps of Engineers.

IPCC (TAR) (2001). Third Assessment Report of the Inter-Governmental Panel on Climate Change, Synthesis Report and Policy Makers' Summaries, Cambridge University Press.

Nandalal, H.K., and Rathnayake, U.R. (2011). Flood Risk Management Incorporating Stake Holder and Climatic Variability. Thesis Submitted in Partial Fulfillment of Doctor of Philosophy, Department of Civil Engineering, Faculty of Engineering, University of Peradeniya, Sri Lanka.

User's Manual-HEC-GeoRAS, GIS Tools for Support of HEC-RAS using ArcGIS 10, Version 10 (2012). Hydrologic Engineering Center, US Army Corps of Engineers.

User's Manual-Hydrologic Modeling System HEC-HMS, Version 3.5 (2012). Hydrologic Engineering Center, US Army Corps of Engineers.

Wanniarachchi, S.S. & Wijesekara, N.T.S. (2012). Using SMMW as a Tool for Floodplain Management in Ungauged Urban Watershed. *Engineer: Journal of the Institution of Engineer, Sri Lanka*, 45(1).

Wickramaarachchi T.N. (2004). Preliminary Assessment of Surface Water Resources – A Study from Deduru Oya Basin of Sri Lanka, *Proceedings of the 2nd International Conference on Hydrology and Water Resources in Asia and Pacific Region (APHW 2004)*, 5th – 9th July 2004, Singapore.

INTERACTION OF TORRENTIAL AND URBAN CATCHMENTS - PROS AND CONS OF STORM SEWER RETENTIONS

STEFAN ACHLEITNER[1], BENJAMIN KAMMERECK[2], BERNHARD KOHL[3], LEOPOLD STEPANEK[4] & ROBERT SITZENFREI[5]

[1,2] Unit of Hydraulic Engineering; Institute of Infrastructure, Faculty of Engineering Science, University of Innsbruck, Austria, stefan.achleitner@uibk.ac.at; b.kammereck@gmail.com

[2,5] Unit of Environmental Engineering; Institute of Infrastructure, Faculty of Engineering Science, University of Innsbruck, Austria, b.kammereck@gmail.com; robert.sitzenfrei@uibk.ac.at

[3] BFW-Federal Research and Training Centre for Forests, Natural Hazards and Landscape; Department of Natural Hazards and Alpine Timberline, Unit of Torrent Processes & Hydrology, Innsbruck, Austria, Bernhard.Kohl@bfw.gv.at

[4] Gebietsbauleitung Mittleres Inntal; Austrian Service for Torrent and Avalanche Control (WLV), Innsbruck, Austria, leopold.stepanek@die–wildbach.at

ABSTRACT

The design of retention measures in urban sewer systems is well known, but only aspect of the sewer system itself is considered, with regard of the hydraulic design of retention basins. Runoff from urban and natural catchment parts is often considered independent due to the faster response from urbanized areas in many cases. To reduce the peak flows from the urban area at an economically feasible level is the main goal. In general, this argument does not lack logic but is far from being evidenced. Situations, where the urban peak discharge is reduced (which is positive) but as well delayed bear the risk that peak discharges (urban and torrent) superposition to an increased total discharge in the torrent. Purpose of this work is to investigate the dynamic interaction between an urban and torrential catchment. The aim is to test if reducing the urban peak discharge leads to an overall reduction of the peak flow for different situations. Two models describing the rainfall runoff generation from Torrent and Urban catchment parts were coupled and ran sequentially. A systematic variation of spatial rainfall distributions and simulation allowed evaluating the situation in a generalized way. Simulations were made with and without the retention basin installed. Although the urban catchment part, which is retained via the basin was small compared to the overall catchment, a clearly visible increase of peak flows was found in some cases. Combinations of rainfall situation in the different catchment parts led to increased peak discharges were identified. The magnitudes of increases found for this catchment situation were small. Still, for cases with smaller torrential catchments as compared to the urban parts, increases can be more significant. Thus, future steps include the assessment of different catchment configurations.

Keywords: Design rainfall; hydrograph superposition; retention basin; torrent hydrology; urban hydrology.

1 INTRODUCTION

Urban areas located in or in close proximity to torrent watersheds may impact the torrential design. Usually, the higher imperviousness of the urban areas can lead to a substantial contribution to the natural torrential discharges. Future population growth and associated land use change further and intensify the impact. Increasing usage claims in alpine space come along with a continuously dwindling acceptance of potentially affects the downstream inhabitants due to the subject of an additional surface runoff input.

Status quo is that retention basins are constructed to retain urban discharges, focusing exclusively on the urban area and the decrease of resulting peak flows. Often, the concept of "the bigger the better" rules. The actual interaction with the downstream receiving torrents is hardly addressed. It is assumed that discharges from natural systems are temporally decoupled, at least for the occurrence of peak discharges. This led historically to very different levels of applied design rainfalls. For the design of system components in urban hydrology, return periods for design rainfall events between 1 and 10 years are usually mandatory, based on economic and risk considerations as well as from fresh water-ecological aspects. For the design of rural flood control, design events with return periods between 20 and 100 years are used. For torrent engineering even higher return periods between 100 to 150 years are specified. Due to these different design approaches the effects of retention basins at the interface between urban and torrent flood control are indeterminate and uniform design criteria are not directly derivable.

In this context, there is a common argument that due to the faster response peak discharges from urbanized areas shall have passed prior the maximum flows from torrent catchments arrive. In general, this argument does not lack logic but is far from being evidenced.

Here, the present work intends to test these assumptions for alpine situations. The aim is to take a first step towards the development of a holistic design approach considering the interaction between torrential and urban runoff simultaneously. Situations where the urban peak discharge is reduced (which is positive) but as well delayed bear the risk that peak discharges (urban and torrent) superposition to an increased total runoff. Thus, the focus is the assessment of resulting peak discharges, considering situations with or without a retention basin (throttled discharge and overflow) installed downstream urban catchments. The interaction of torrential and urban runoff is investigated using a case study located in Tyrol, Austria. Besides using standard design conditions, the storm intensity and duration are varied to mimic systemically the effects of real rainfall events with specific spatial distribution of precipitation influencing the discharge dynamics in the catchments. Other catchment properties, such as the catchment sizes, scales, slopes, imperviousness, etc., play an important role as well, but are not investigated here.

2 CASE STUDY AREA AND CATCHMENT DECRIPTION

Here, parts of the municipality of Götzens (Tyrol, Austria) together with the torrential catchment Geroldsbach are used as case study. The catchment is located near Innsbruck, Austria, in south-west direction with an expansion of 47°11'32.53"N to 47°14'28.12"N latitude and 11°18'16.58"E to 11°20'25.92"E longitude. Until now, the population has grown up to 3951 (01. Jan. 2016) and an overall area of 9.72 square kilometer. The urban catchment comprises of the torrential catchments Geroldsbach (12km^2) and Marbach (1.2km^2) with two urban catchment parts (Götzens and Neu-Götzens) located in the downstream part (see Figure 1). Neu-Götzens is part of the municipality of Götzens with partly industrial and partly new settlement area. For the urban catchment Neu-Götzens (22 hectare) the existing drainage network is planned to be renewed, changing from a combined to a separate sewer system. Runoffs interact with the receiving water of both torrent watersheds. Current design proposes the retention of the urban runoff with a basin of 1,600 cubic meters.

The torrential catchment Geroldsbach is located above the village Götzens (~868m.a.s.l.). Its river spring is at an elevation of ~1920m.a.s.l. near the mountain Birgitzköpfl and is enclosed at the top by the mountain peaks Nockspitze (Saile; ~2404m.a.s.l.) and Birgitzköpfl (~1982m.a.s.l.). Total length of the torrent main catchment is 8km, whereas after 9.4 km the Geroldsbach joins the river Inn. Along its pathway, the river merges with several small side rivers and tributaries, like Gehrbach, Grosser Blaikenbach, Tödersbach, Kirchbach, Horachbach and Marchbach and some other (nameless) tributaries. The rural (torrential) area is defined as the total catchment area of the river.

The mean annual precipitation in the catchment is between 820 - 900mm (1981 – 2010). The design rainfall applied for the case study is presented in section 3.4. A weighted mean of the two datasets for the lower and bound design values available in Austria (Lorenz and Skoda, 2001) was used.

3 METHODS

3.1 Software

3.1.1 ZEMOKOST

The software is used to simulate rainfall runoff from small to medium rural and torrential catchments. The model is developed at the BFW - (Bundesamt und Forschungszentrum für Wald) by Kohl (2011) and is designed for mainly being applied to ungauged torrential basins. Basis is the numerical description of runoff processes on the surface and in torrents including runoff generation and concentration processes. The parameterization of the underlying equations relies strongly on the simultaneously developed methods to assess surface runoff coefficients for alpine soil-vegetation units (Markart et al., 2004). The developed methods and classifications are based on over 800 rainfall experiments in the field, describing the runoff processes with regard to initial and continuous losses as well as routing process. The methods are specifically designed to be applied in ungauged basins in absence of gauge measurements. Technically, the software is based on Visual Basic and is embedded in EXCEL. Worksheets are used to store input and output data.

3.1.2 Storm Water Management Model (SWMM)

For modelling of the urban runoff including sewers, the software SWMM 5.1 (Rossman, 2016) is used. The well-known software for assessment of Storm Water Management Model (SWMM) is developed by the US-EPA since 1969. Until today, SWMM plays an important role in hydrodynamic modelling and allows the simulation of water quantity and quality. It is used for planning, analysis and design of storm water runoff, combined and sanitary sewers (Rossman, 2015). It can be briefly described as hydrological-hydraulic water quality simulation model with either event based or long-term observations. The hydrological components are represented by rain gages and subcatchments (also aquifers, snow packs, unit hydrographs, LIDs) (Rossman, 2016). The runoff generated in a subcatchment is routed via hydraulic components using a network based system of nodes and links. Nodes definitions are therein junctions, outfalls, dividers and storage units.

Conduits, pumps, orifices, weirs and outlets are realized as linkages in between the nodes. The resulting hydraulic processes are solved for the one dimensional Saint Venant flow equations.

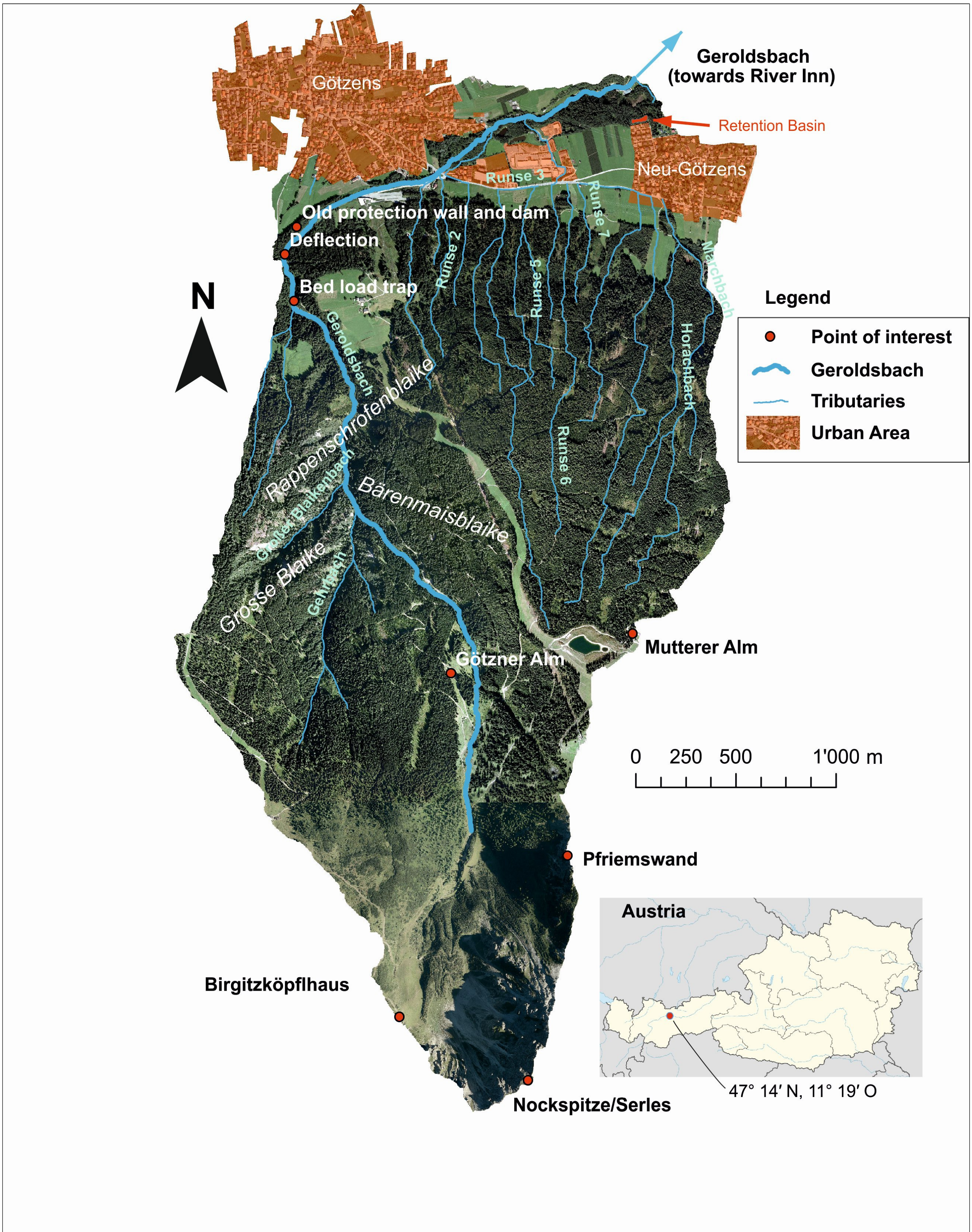

Figure 1. Overview on torrential and urban catchments in Götzens, Austria.

3.2 Model structure and coupling

Flooding situations with different probability of occurrence are simulated with and without retention basin. The modelling approach comprises of (a) hydrodynamic modelling of the urban drainage network, (b) hydrological modelling of the entire torrent catchment, and (c) different hydraulic designs for the retention basin.

The catchment parts are subjected to varying design rainfalls representing a coarse spatially variation of precipitation. The systematic analysis of temporal and spatial rainfall varied scenarios aims to assess the effect of the planned retention measure on the urban, torrent and combined discharges. Thus, the models used are run in a sequential coupled mode (see Figures 2).

The model setup considers discharges from the urban catchments entering the receiving stream Geroldsbach via (a) the sewer system or (b) surface runoff in the urban parts. Within (a), flows entering via the throttle or the overflow weir of the retention basin are covered. Surface flows in the urban area are triggered by overflows generated within the sewer system at manholes. The surface runoff is routed and delayed via the ZEMOKOST model and superpositioned with runoff generated in the torrent model itself. Another part of the flooding nodes is discarded, due to their opposite flow direction. If all necessary data is handed over, the rural model is ran twice to achieve results with and without a retention basin.

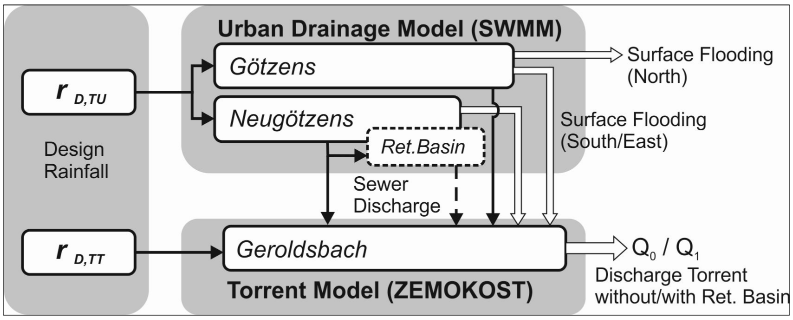

Figure 2. Schematic overview on rainfall variation and model links between urban and torrent runoff models. ($r_{D,TU}$ and $r_{D,TT}$ - design rainfall with Duration D and recurrence interval TU/TT for urban and torrent catchment respectively; Q_0 and Q_1 - discharge generated for scenarios without and with installed retention basin)

3.3 Model setups and calibration

3.3.1 Torrent modell (ZEMOKOST)

The setup of a model requires different parameters, which describe the catchment behavior.

Table 1. Table of the parameter set for a ZEMOKOST model.

PRECIPITATION	T	Recurrence time	[a]
	t_r	Rain duration	[min]
	I_t	Precipitation intensity	[mm/h]
RUNOFF: SURFACE AND INTERFLOW	A	Area of subbasin	[km²]
	L	Projected surface runoff	[m]
	J	Slope	[-]
	RCL	Discharge coeffeicient	[ha or %]
	R	Roughness coefficient	[ha or %]
	SZI	System status index	[min]
CHANNEL ROUTING	L_C	Channel length	[m]
	J_C	Channel slope	[º]
	d_{90}	Channel roughness	[m]

The quantification of these parameters is done with a combination of ArcGIS analysis and intense fieldwork. The majority of the parameters are assessed by delineation with the proven watershed toolbox by ArcGIS. As data base aerial photographs and a DTM with a resolution of 1m is provided by the Administration Office of the Tyrolean Region Government (AdTLR). In case of the most distinguished parameters, such as surface runoff and roughness coefficient, the field survey is indispensable. The catchment area is divided into several sub-basins and connected with inlet and outlet nodes. The nodes are set on important side characteristics and branches of the streamline. The division of the watershed depends on the observed area and the required accuracy. In view of the catchment area size and the model task, a fine resolution of the sub-basin was chosen. The watershed includes 105 sub-basins to cover all homogenous hydrological units and distinguished points.

In the beginning, the aerial photo is used to basically identify hydrological units with the same runoff behavior. These units were delimited with polygons in ArcMap. The definition of the listed vegetation units follows the structure adopted by Markart et al. (2011). A more accurate subdivision is enabled throughout the use of a forest map, provided by the Administration Office of the Tyrolean Region Government

3.3.2 Urban modelling (SWMM)

The Götzens' drainage system is a mix of combined and separate sewer system, collecting wastewater from households and rainwater in different channel systems. The model of the Götzens' sewer system (Figure 3) includes 160 subcatchments, 495 nodes and 497 links. The water is transported depending on the location of the subcatchments towards one of the three outlets towards the receiving water where one is a combined sewer overflow simulated in SWMM as a weir.

The sewer system of Neu-Götzens is based on *ca.* 60 year old conduits, which were built by private persons. In the course of renewal the whole drainage system is refurbished. Hereby, the drainage is upgraded to a source separation system, which means different discharge routes for waste and rainwater. A retention basin is planned for the discharge amount of the rainwater at the outlet of the sewer system. The basin comprises around 1,600 cubic meters at the current planning stage and restricts the water output in the receiving pre-flooder. The whole system includes 235 nodes, 236 conduits and 38 subcatchments.

For the calibration of the Götzens's SWMM model, a measuring campaign was performed in Götzens by the Institute of Environmental Engineering, the University of Innsbruck. The obtained dataset includes time series from a mobile rain gauge and discharge measurements and was used for calibration. The evaluation of the data is presented in the report by Kinzel (2015). Simulated and observed after calibration matched very well with Nash-Sutcliff efficiency coefficient (NSE) up to 0.951 for single events. Time series tests for several months show a good agreement with NSE values of 0.926.

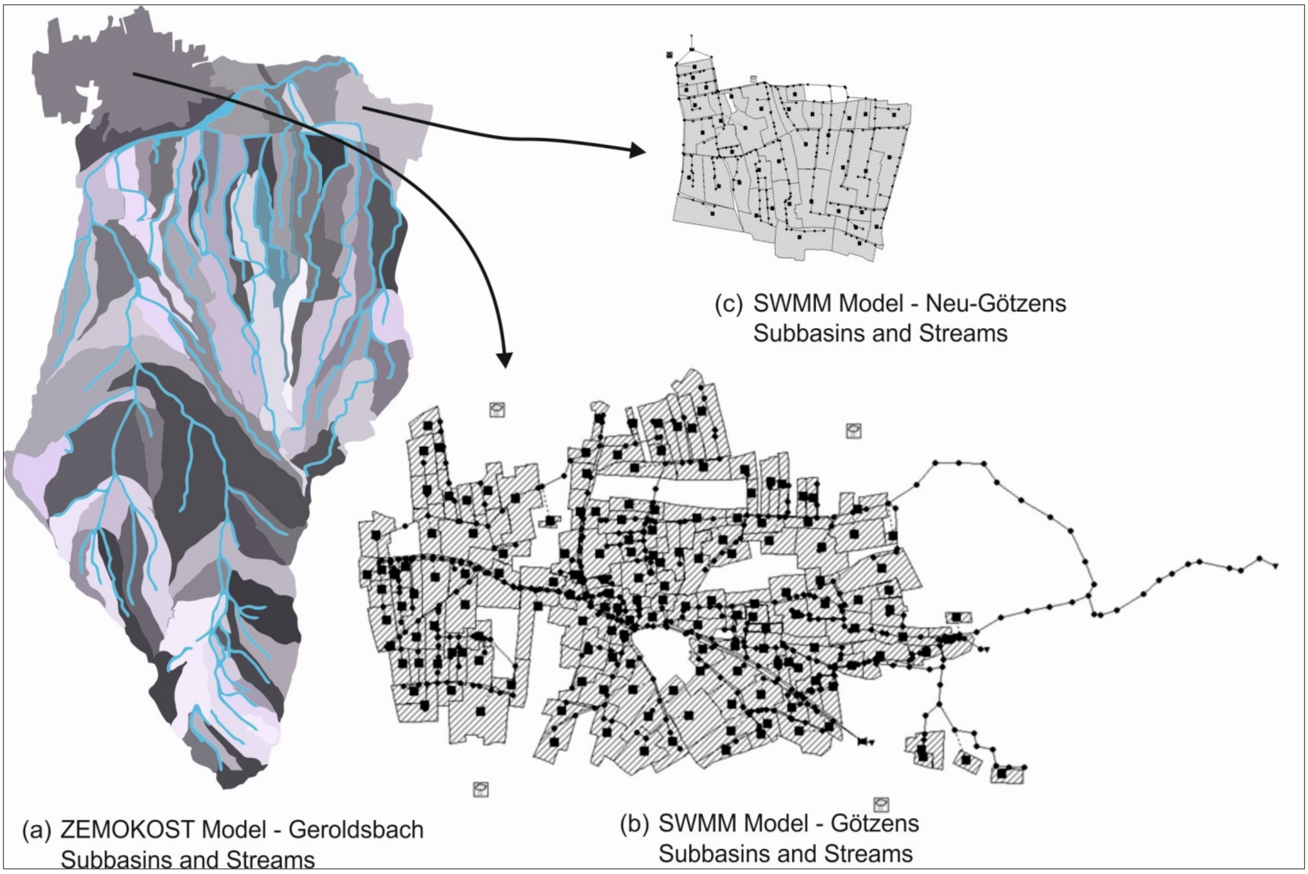

Figure 3. Model setup and discretization of the (a) Torrent-ZEMOKOST Model and urban SWMM Models for (b) Götzens and (c) Neu-Götzens (both SWMM).

3.4 Spatial variation or rainfall

In Austria, the Austrian Federal Ministry of Agriculture, Forestry, Environment and Water Management (BMLFUW) Administration provides design rainfall for planning purpose. These datasets consists of three different precipitation datasets for duration times from five minutes up to six days with varying return periods. The two main datasets, MaxModN and Ökostra (Lorenz and Skoda 2001), set the upper and lower limits based on different methods used when they were derived. For design purpose, the weighted mean value of both is recommended and is therefore used as well in this work. In Table 2, design value precipitation sum (P [mm]) are shown for different recurrence intervals (T [a]) and durations (D [min]).

Table 2. Design rainfall applied catchment Geroldsbach/Götzens.

T [a]	1	10	30	100	150
D[min]	P [mm]	P [mm]	P [mm]	P [mm]	P [mm]
30	14.7	39.4	51.0	63.6	67.9
60	18.2	47.7	61.6	76.5	81.6
120	22.3	55.2	70.5	87.1	92.8
180	25.1	59.6	75.9	93.4	99.4
240	27.4	63.2	80.2	98.7	105.0

With regard to the temporal distribution, block rainfall is used in this study. Further no areal reduction of the rainfall intensity is applied.

4 RESULTS

The model setup of the coupled ZEMOKOST-SWMM was subjected to systematic combinations of design rainfalls. For different durations (D), which are kept the same in all catchment parts, the intensities of the rainfall was varied. In overall, recurrence intervals between 1 and 150 years are run and combined in both catchments. For one fixed duration (D), sampling of return period results in 18 x 18 (324) combinations. Figure 4 shows selected results at duration D = 30, 60, 120 and 180 minutes. The chosen examples combined rainfall intensities in the torrent and the urban areas at which the peak discharge increase in case the retention basin is installed. Q_0 and Q_1 are therein the discharge hydrograph for a setup without and with a retention basin installed.

The differences in the respective peak flows ($Q_{0,P}$ and $Q_{1,P}$) are calculated for all scenarios to test if the total peak discharge increases or not, regardless of its time of occurrence. Figure 5 comprises the results from simulations using duration (D) for the design rainfalls of 60 and 120 minutes. Continuous and dashed lines are contour plots of peak discharges resulting at combinations of different rainfall intensities applied in the urban and torrent catchment respectively. The simulations were made using the model setup with and without retention basin installed downstream the urban catchment Neu-Götzens. The shift in between contour lines visualizes the increase or decrease of peak flows with the installed basin. In case that the contour line from simulation with retention basin is shifted to the upper right side compared to the case without a retention basin installed, an increase in peak discharge occurs. The red dashed curve separates cases of negative and positive developed peak discharges. The cases located above in the gray shaded area are found to have an increase of peak discharges.

It can be seen that the positive hydraulic effects in reducing the peak flows is given for a number of combinations for rainfall durations D = 60min. The positive offsets for lower recurrence intervals in the torrent and urban catchment are larger than for higher recurrence intervals. In comparison, the negative offsets above the red separation line ($\Delta Q = 0$) in Figure 5a, are less pronounced. Considering a larger duration D = 120 minutes, there is no more a continuous break line ($\Delta Q = 0$) for the whole spectrum of recurrence intervals. The combination at which an increase of the peak flow occurs is getting larger. Still, the absolute magnitudes of shifts are small as compared to the absolute peak discharges. In Figures 6a and 6b, the absolute differences between the peak discharges are plotted for various recurrence intervals of the rainfall applied in the urban and torrent catchment. The scenarios with D = 120 minutes, peak discharges increase by $0.6 m^3/s$ at the most.

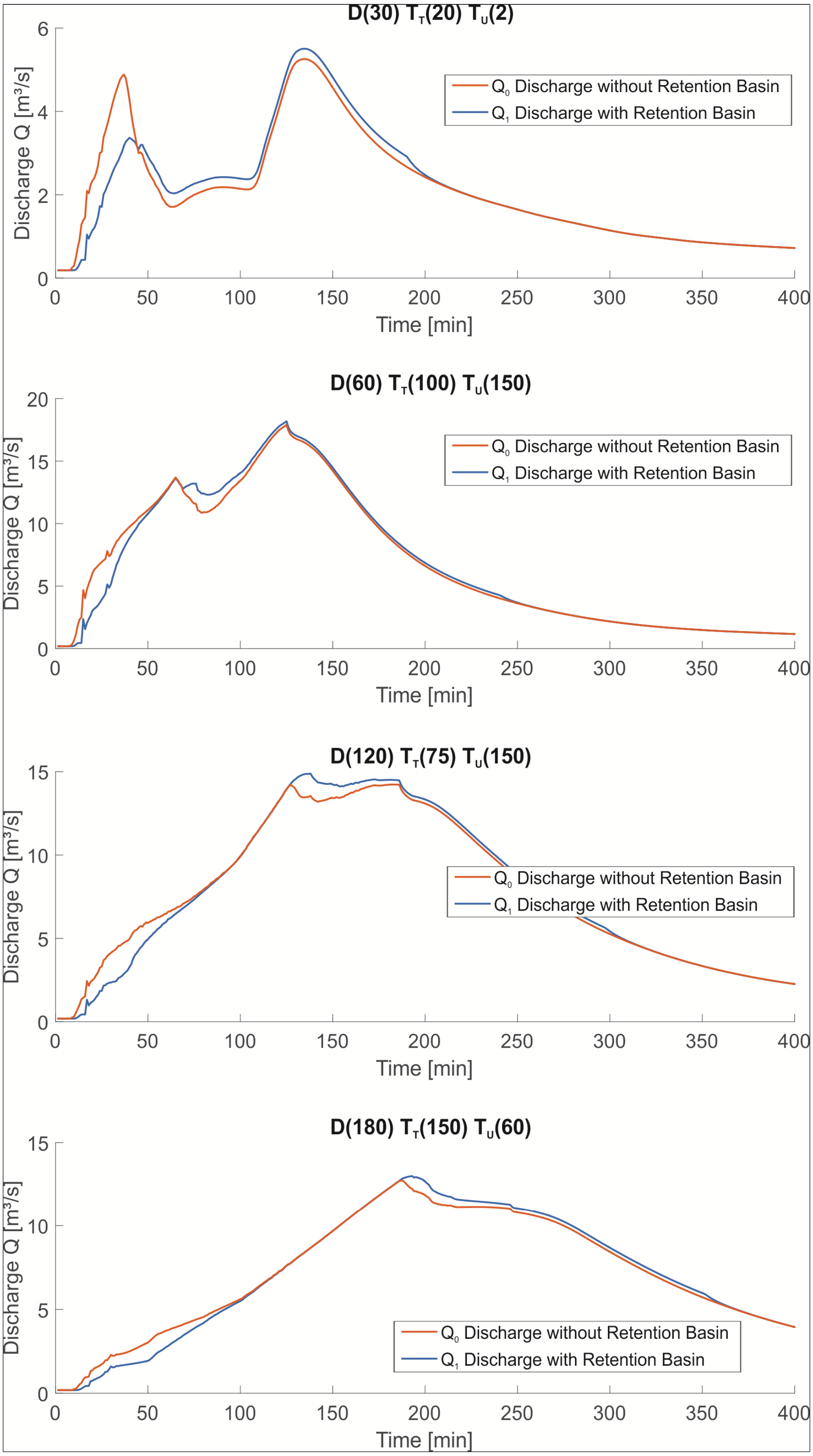

Figure 4. Hydrograph of the total discharge in the torrent Geroldsbach for Durations D = 30, 60, 120 and 180 minutes; the given scenarios of combined recurrence interval represent adverse combination, increasing the peak discharge in case of an installed retention basin.

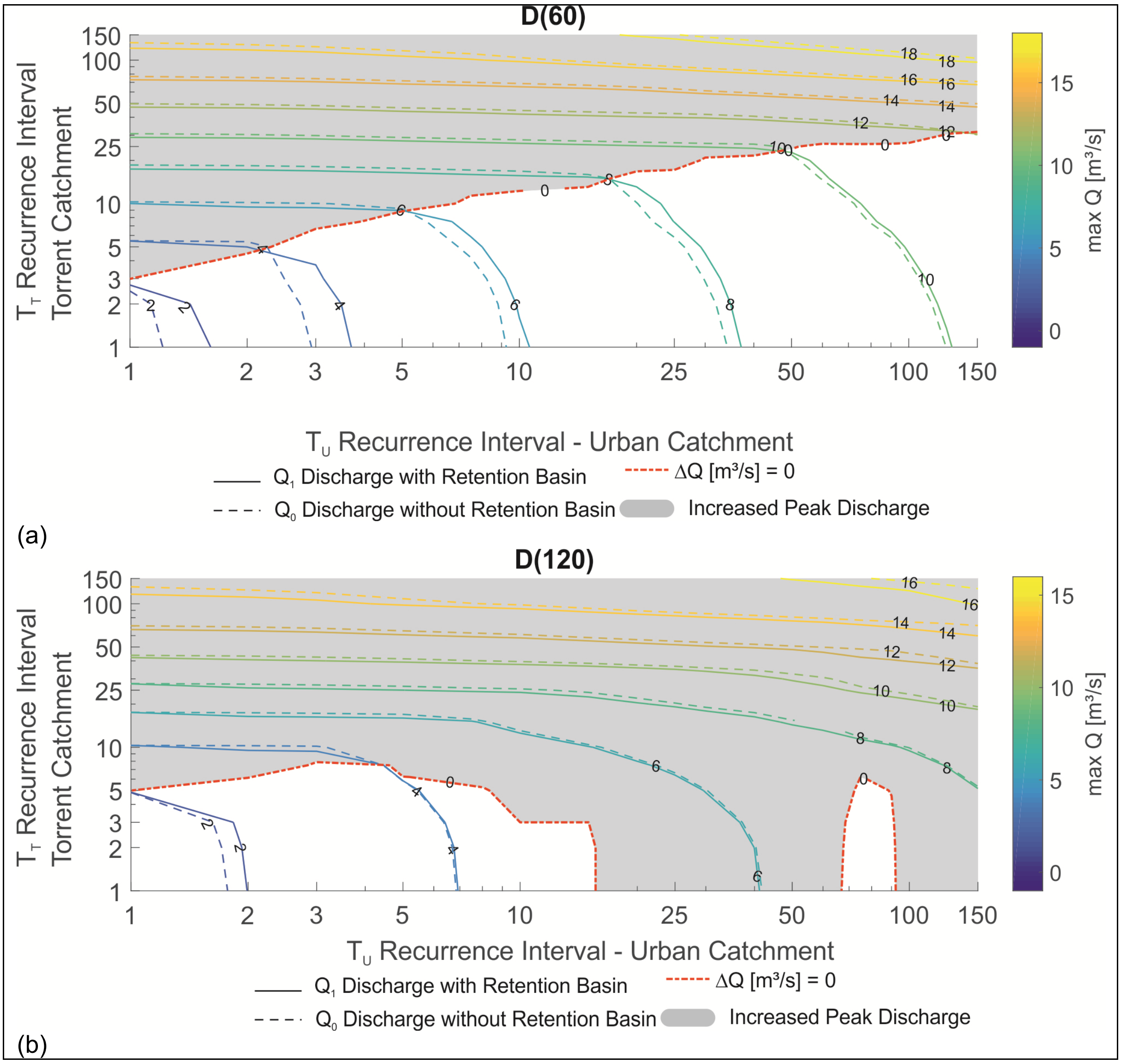

Figure 5. Contour plot of peak discharges for a duration of (a) D = 60 min and D = 120min obtained from simulation with and without a retention basin installed (Q_1 and Q_0). X and Y Axis mark the different combinations of the recurrence interval of the design rainfall applied in the urban and torrent catchment respectively.

Table 3. Peak flows Q with minimum and maximum reduction ΔQ at different event durations D.

D [min]	$Q_{1,P}$ [m^3/s]	$Q_{0,P}$ [m^3/s]	$\Delta Q_{P,MAX}$ [m^3/s]	T_T [a]	T_U [a]	$\Delta Q/Q_{0,P}$ [%]	$Q_{1,P}$ [m^3/s]	$Q_{0,P}$ [m^3/s]	$\Delta Q_{P,MIN}$ [m^3/s]	T_T [a]	T_U [a]	$\Delta Q/Q_{0,P}$ [%]
15	4.17	7.93	3.77	5	7.5	47	3.48	3.47	-0.01	150	1	0
30	4.22	5.94	1.71	1	5	29	5.50	5.26	-0.25	20	2	-5
60	2.44	3.12	0.68	1	2	22	18.18	17.90	-0.28	100	150	-2
90	2.30	2.65	0.36	1	2	13	9.61	9.28	-0.34	20	50	-4
120	2.01	2.24	0.23	1	2	10	14.89	14.23	-0.66	75	150	-5
180	1.52	1.71	0.19	1	2	11	12.99	12.73	-0.26	150	60	-2
240	1.21	1.39	0.17	1	2	13	5.81	5.56	-0.25	90	2	-4
360	1.20	1.30	0.10	1	3	8	5.48	5.44	-0.04	150	25	-1

$Q_{0,P}$ ... Peak discharge without Retention Basin
$Q_{1,P}$... Peak discharge with Retention Basin
ΔQ_P... Increase/Decrease in peak discharge
T_T... Recurrence Interval Precip. (Torrent Catchment)
T_U... Recurrence Interval Precip. (Urban Catchment)
D... Duration of the design rainfall

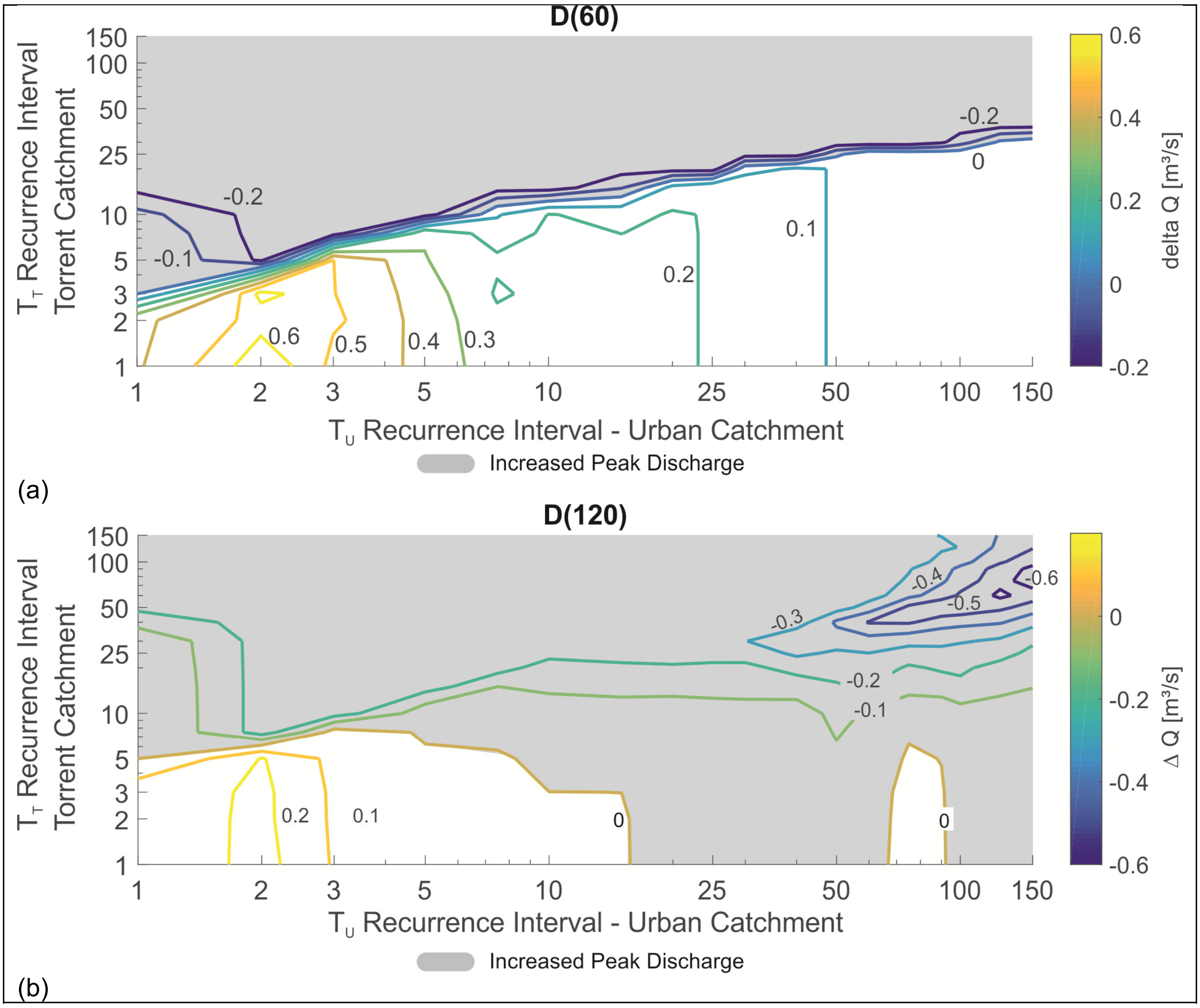

Figure 6. Hydrograph of the total discharge in the torrent Geroldsbach for Durations D = 30, 60, 120 and 180 minutes; the given scenarios of combined recurrence interval represent adverse combination, increasing the peak discharge in case of an installed retention basin.

Table 3 comprises scenarios, at which the minimum and maximum values of peak flow changes (ΔQ) occur. Maximum relative changes are found are found at D = 120 minutes. In this case, flow durations and delayed peak discharge due to the retention results in a 5% increase of the peak flow.

5 DISCUSSIONS

The common argument that retaining discharges is a general positive measure to reduce peak flows has been investigated. It is assumed that the faster response of peak discharges from urbanized areas shall have passed prior the maximum flow from the torrent catchment arrives. Hence, the flood peak in the torrent basin should not be increased by the urban catchment area. Although the argumentation is logical in a way, this does not apply at all cases. Retaining discharges and taking the dynamics of a retention basin into account makes the situation more complex. Besides using standard design conditions, the storm intensity and duration are varied to mimic systemically the effects of real rainfall events with specific spatial distribution of precipitation influencing the discharge dynamics in the catchments.

Without doubt the retention basin reduces the peak flow of the urban catchment area. At the same time, the catchment delays the hydrograph. When peak discharges from the torrent and urban catchment meet, the overall discharge increases compared to the situation without retention. In this case study it is proven that such a negative retention effect on the receiving river torrent can appear in special cases.

Still, for this case study the effects found were small having a maximum increase of 5%. Knowing that only a small area (22 hectare) compared to the total catchment (8 square kilometer) was retained, the found increases are still notable.

Although the work provides the basic tools for investigating the cost effectiveness of the design of the retention basin (size, throttle, etc.), the focus is put exclusively on the comparison between the setups with and without retention of urban runoff. Similar other catchment properties, such as catchment sizes (torrent and urban), scales, slopes, imperviousness, etc., play an important role as well and are to be tested further.

Here, the results reveal that other constellations, such as lower ratios between the torrent and urban catchment sizes, lead to even higher increases of the peak flow. Adaptations in the design criteria of retention basin could make sense. Additionally, effects due to the real rainfall situations, such as temporal and spatial distributed rainfall input, are to be accounted for.

6 CONCLUSIONS

The paper investigated the hydraulic interaction of urban and rural parts of an alpine catchment considering design options with or without urban retention basin installed. In the given case study, adverse effects with regard to the peak discharge in the receiving water are found. Although the magnitude of the increases was small, the effects occurred for combinations of high storm intensities. It is reasonable that the magnitude of the adverse effects increases for other catchment configurations, especially when the ratio of torrential vs. urban area reduces. For such cases, the retention of flood flow in the urban part bears a potential to lead to a more severe overall situation compared to without retention.

REFERENCES

Kinzel, C. (2015). *Messkampagne ABA Götzens*, report, Unit of Environmental Engineering, Institute of Infrastructure, Faculty of Engineering Science, University of Innsbruck.

Kohl, B. (2011). Das Niederschlags-/Abflussmodell ZEMOKOST. Entwicklung eines Praktikablen Modells zur Ermittlung von Hochwasserabflüssen in Wildbacheinzugsgebieten unter Einbeziehung Verbesserter Felddaten, *PhD Thesis.* University of Innsbruck.

Lorenz, P. & Skoda, G. (2001). *Bemessungsniederschläge auf der Fläche für Kurze Dauerstufen (D ≤ 12 Stunden) mit Inadäquaten Daten*. Wiener Mitteilungen, Band 164: Niederschlag-Abfluss Modellierung - Simulation und Prognose, 179-200.

Markart, G., Kohl, B., Sotier, B., Schauer, T., Bunza, G. & Stern, R. (2004). Provisorische Geländeanleitung zur Abschätzung des Oberflächenabflussbeiwertes auf alpinen Boden-/Vegetationseinheiten bei konvektiven Starkregen (Version 1.0); A Simple Code of Practice for the Assessment of Surface Runoff Coefficients for Alpine Soil- Vegetation Units in Torrential Rain (Version 1.0), *Report BFW-Dokumentation; Schriftenreihe des Bundesamtes und Forschungszentrums für Wald*, Wien, 2004, 3(88).

Rossman, L. (2015). *Storm Water Management Model User's Manual Version 5.1 - Manual*. US EPA Office of Research and Development.

Rossman, L. (2016). *Storm Water Management Model, Reference Manual, Volume I – Hydrology (Revised).* US EPA Office of Research and Development.

EXPERIMENTAL STUDY OF THE FLOOD SUPERPOSITION EFFECT DUE TO CASCADE DAM BREAK

HUO JIAN LIU(1), YUN LI(2), XIAO GANG WANG(3), GUO XIANG XUAN(4) & LONG ZHU(5)

(1)Hydraulics Department, Changjiang River Scientific Research Institute (Crsri), Wuhan, China,
huojian_smile@126.com
(2,3,4,5) Hydraulic Engineering Department, Nanjing Hydraulic Research Institute (NHRI), Nanjing, China,
xgwang@nhri.cn

ABSTRACT

Dam break could cause a significant disaster in the downstream, especially, cascade dam break would aggravate the disaster extent. This article presents an experimental study of the flood reinforcement due to cascade dam break in the glass flume, and opening speed of the gate is controlled for simulating different flood discharge hydrograph due to upstream dam break. In this article, the cascade dam break is divided into no-relationship type and relationship type. The experiment assumed that the downstream dam is suddenly broken due to overtopping in the relationship of cascade dam break, and the downstream dam is suddenly broken in a few seconds after the upstream dam break in the no-relationship of cascade dam break. The experimental results show that, the flood hydrograph induced by cascade dam break has some marked features at the downstream channel of the second dam compared to that induced by single dam break, such as higher peak water depth, fluctuated violently, multiple-peak, long duration. Also, there are some obvious differences on flood hydrograph between different cascade dam break types. The results can provide technical support for flood control management and flood control design of cascade dams.

Keywords: Cascade dam; dam break; superposition effect; overtopping break; experimental study.

1 INTRODUCTION

Reservoir and dam can bring great economic and social benefits to human, but also has the risk of breaking. Natural factors such as earthquake, extreme climate, the excessive flood and human factors such as improper design flaws, improper construction management, terrorist attacks are likely to result in dam break. A large volume of water discharges sharply downstream from the reservoir after the dam break, and the dam break floods in downstream channel have large flow rate and velocity. Compared with general storm floods, the features of dam floods that were burst strongly are high water level and large flow characteristics. So collapsing force of dam break is extremely huge, and it is a serious threat to people's life and property safety, sustainable economic and social development. Especially, cascade dam break would aggravate the disaster.

Scholars at home and abroad have carried out a large amount of experimental study on cascade dam break in recent years (Yue, 2010; Xue, 2011; Yang, 2011; Zhu, 2012; Cui, 2013; Zhou, 2013; Zhou, 2015; Chen, 2015; Evangelista, 2015; Niu, 2015). From the existing experimental studies on cascade dam break we can found that: (1) most of the existing experiments consider gradually break in cascade dams, and the main types of cascade dams are weir dams or embankment dams. The process of cascade dam break is that, upstream dam break gradually firstly, and water level of the downstream reservoir rise gradually, downstream dam overtopping, and downstream dam break gradually. Dam break floods from upstream reservoir evolve slowly to the downstream reservoir, so the impact force on the dam and the wave run-up before the dam is smaller. (2) Stefania had carried out the study on cascade dam break (Evangelista, (2015), and considered the upstream dam break instantaneously, the downstream dam break gradually. But the upstream dam flood energy is small because of the lower water level of the upstream dam, shorter distance between the cascade dams, and flat bottom of the water channel, so the impact force on the dam and the wave run-up before the dam is smaller. (3) The study on cascade dam break considering the upstream and downstream dam break instantaneously has been carried by Xue yang (Xue, 2011; Niu, 2015). But the way of controlling the bearing capacity of the downstream dam to simulate the break process has certain uncertainty, because there are two effect models which dam break floods impact to the downstream dam, one is non-breaking wave and other is break wave. The distribution and value of the impact face on the downstream dam have essential differences. Based on the above shortcomings, the paper carried out the experimental study on the superposition of cascade dam break, and considering the downstream dam break instantaneously by overtopping. The experimental results has the important significance on cascade dam risk evaluation and emergency plan preparation.

2 TEST MODEL DESIGN

The experimental apparatus include upstream reservoir and dam, the downstream reservoir and dam, the river channel and other parts. The rectangular sink is 14m long, 0.8m high and 0.4 m wide. Channel slope is 1:12.5, the width of the upstream and downstream reservoir are 0.8m respectively, the length between upstream and downstream reservoirs are 5m, and the length of channel at the back of downstream dam is 5m. Experimental model layout can be shown in figure 1 and figure 2. The sink was constructed by organic glass for observing the flow regime. The dams used at upstream and downstream dam is 0.02m thick, 0.6m high, 0.42m wide. Lifting speed of the gate is controlled for simulating different flood discharge hydrograph due to upstream dam break, and the speed is 1cm/s in this article. The downstream dam break instantaneously which collapses to downstream channel.

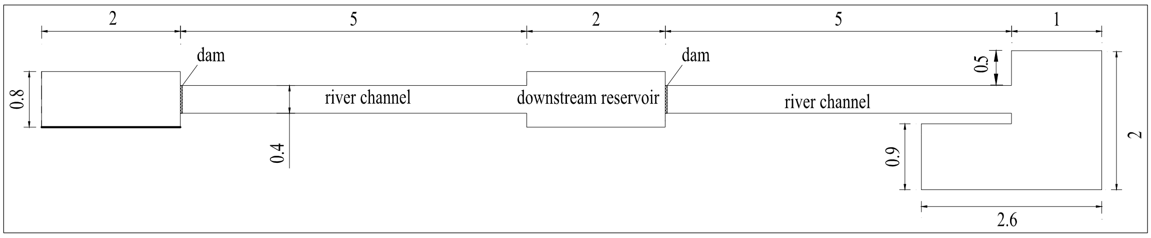

Figure 1. Plan form of the test model arrangement (unit is meter).

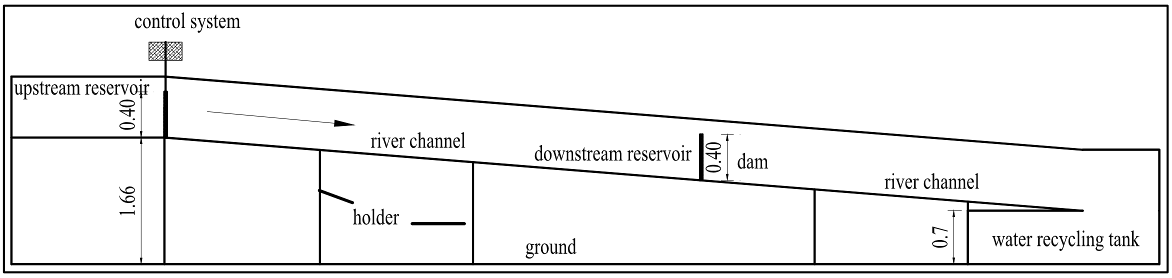

Figure 2. Side view of the experimental model arrangement (unit is meter).

Ultrasonic sensors are used to measure the water-depth variation in the reservoir and river channel in this test, and arrangement of the sensor points are shown in figure 3. All the sensors were decorated along the central axis. Kb1 and kb2 points are located in downstream reservoir, and kb3-kb6 points are located at downstream channel. The distance between kb2 and dam site is 0.12m, and the distance between kb1 and kb2 points is 0.5m. The distance between kb3 and dam site is 1.2m, and the distance between kb3, kb4, kb5, kb6 is 1.0m respectively, and the specific arrangement can be seen figure 3. Test parameters in article include H_1, H_2, b, v, H_d, which represent water level of the upstream and downstream reservoir, channel width, the lifting speed of the upstream dam, and the dam crest elevation of the downstream dam. The value of b, H_d are 0.4m, 0.42m respectively.

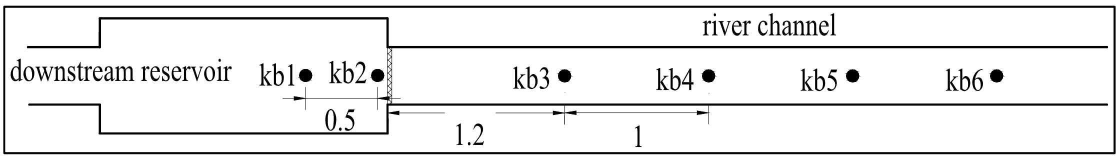

Figure 3. Arrangement diagram of the measuring points at the downstream reservoir and river channel (met).

3 EXPERIMENT RESULT ANALYSIS

3.1 Result analysis of the no-relationship cascade dam break

If downstream dam break has nothing to do with the upstream dam break, cascade dam break can be considered as mutually independent. Here the time difference between downstream and upstream dam break was taken as an example to study the superposition effect of dam break flood in cascade dam break of mutual independence, and the schematic diagram can be seen in Figure 4. Figure 5 shows varying curve of the water depth at the measuring points in cascade dam break at different time difference (H_1/b=0.75, H_2/b=0.75, v=2cm/s), and the arrangement of the measuring points is shown in figure 3, where t_0 is the time difference between downstream and upstream dam break. The figure also includes the water depth varying curve of the measuring points only the downstream dam break for comparison. The change rule of the water depth at the measuring points is as follows:

  / ISSN 1562-6865 (Online) - ISSN 1063-7710 (Print)

Kb1 and kb2 points are in the downstream reservoir. When only the downstream dam break, water in the downstream reservoir discharge into the channel at the back downstream dam in a short time. Water level of the reservoir decreases with time, and varying curve of the water level is a smooth descending curve. When the upstream and downstream dam break occurred in a few seconds, floods from the upstream reservoir do not evolve into the downstream reservoir in the beginning, and varying curve of the water level in downstream reservoir is a smooth descending curve as the same with the only downstream dam break. Water in the upstream and downstream reservoir are superimposed after the upstream floods evolve into the downstream reservoir, and water level of the downstream reservoir has a steep rise process, when t_0 is 0s, 2s, 4s, the water level of kb1 point steep rise 0.04m, 0.047m, 0.048m, and kb2 point steep rise 0.067m, 0.125m and 0.135m respectively, which show that the height of steep rise increases with t_0. After the steep rise, upstream floods evolve into the downstream reservoir continuously, and the downstream reservoir water evolve into the downstream channel continuously. The two parts water collide with each other in downstream reservoir. Water surface of the downstream reservoir fiercely fluctuate and appearing multiple jagged peaks. As time passed, water level of the downstream dam fell slightly, when t_0 is 0s, 2s, 4s, fluctuation time of kb1 point is 1s, 1.5s, 2.2s respectively, and fluctuation time of kb2 point is 0.7s ,1.3s, 2s respectively. After the upstream flood decreased significantly, water level of the downstream reservoir has a steep fall process, water level of kb1 point steep fall 0.048m, 0.075m, 0.065m, and kb2 point steep fall 0.032m, 0.054m and 0.082m respectively. Original water in the downstream reservoir completely evolve into downstream channel at this moment. As the upstream flood slowly evolve into downstream reservoir, water level of the downstream reservoir drop slowly until the end of cascade dam break.

Kb3 point is in the downstream channel. When only the downstream dam break, water level of the point rapidly increase, slowly decline after the peak value, varying curve of the water level is a smooth parabola curve. When the upstream and downstream dam break occurred in a few seconds, floods from the upstream reservoir do not evolve into the downstream reservoir in the beginning, and varying curve of the water level at kb3 point is a smooth rising curve which is similar with the only downstream dam break. Peak value of the water depth is in keeping with the only downstream dam break at different t_0. The upstream flood and the downstream reservoir water superimposed after the upstream flood evolve into the downstream reservoir, and water level in downstream channel has a steep rise process, when t_0 is 0s, 2s, 4s, the peak value of kb3 point is 0.114m, 0.185m, 0.183m respectively. The upstream flood evolve into the downstream reservoir continuously, and the downstream reservoir water evolve into the downstream channel continuously. The two parts water collide with each other in downstream reservoir, and the turbulence water evolve into the downstream channel, so water level of kb3 point near the dam site fluctuate fiercely and multiple significant peak appeared. As time passed, floods from the upstream reservoir decrease gradually, and the water level at the downstream channel decline gradually. Original water in the downstream reservoir completely evolve into downstream channel at this moment. As the upstream flood slowly evolve into downstream reservoir, water level of the downstream reservoir drop slowly until the end of cascade dam break. Variation rule of the water level at kb3 point is in keeping with kb4~kb6, but the water level of kb3 points fluctuate more fiercely compared with kb4~kb6 point, because the distance between kb3 point and downstream dam is nearest. The flood hydrograph induced by no-response cascade dam break had some marked features at the downstream channel compared to that induced by single dam break, such as higher peak value, fluctuated violently, multiple-peak, long duration.

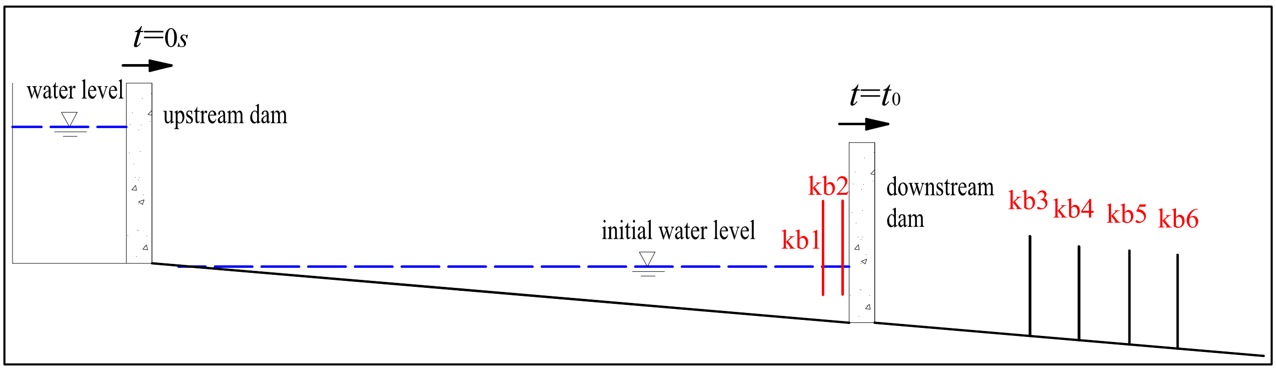

Figure 4. Schematic diagram of the cascade dam break at different time difference.

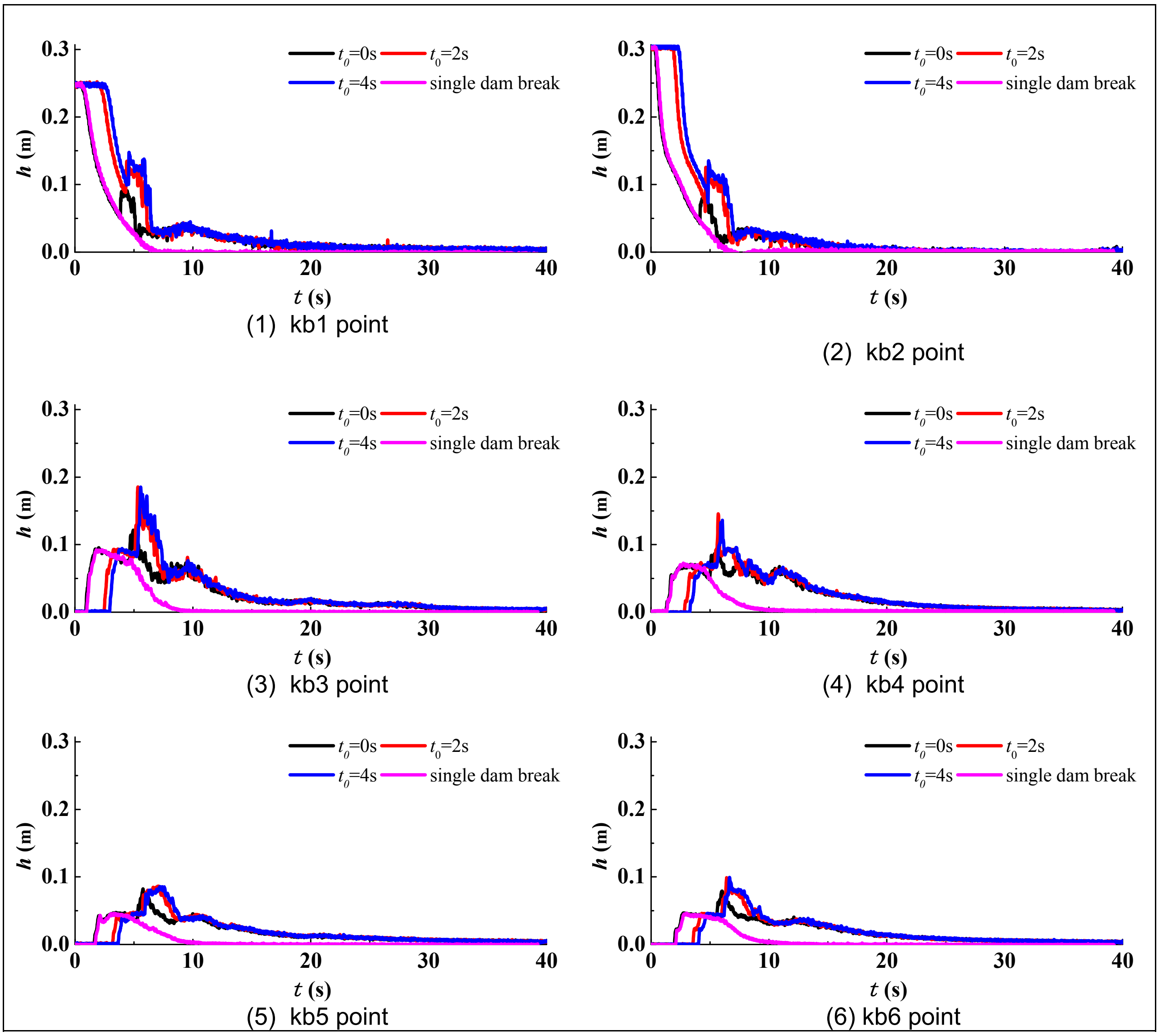

Figure 5. Water level change process of the measuring points at different time difference.

3.2 Result analysis of the relationship cascade dam break

If downstream dam break caused by upstream dam break, cascade dam break can be considered as causal relationship. Under the premise of downstream dam break instantaneously by overtopping, the cause of cascade dam break can be divided into initial surge climb and water level rise in downstream reservoir.

3.2.1 Result analysis of the cascade dam break caused by initial wave run-up

Cascade dam break caused by initial surge climb means that the initial surge climb caused by the initial flood from upstream reservoir evolve into downstream reservoir exceed the dam crest elevation, and the downstream dam break instantaneously by overtopping. The time point when downstream dam break instantaneously can be seen in figure 6.

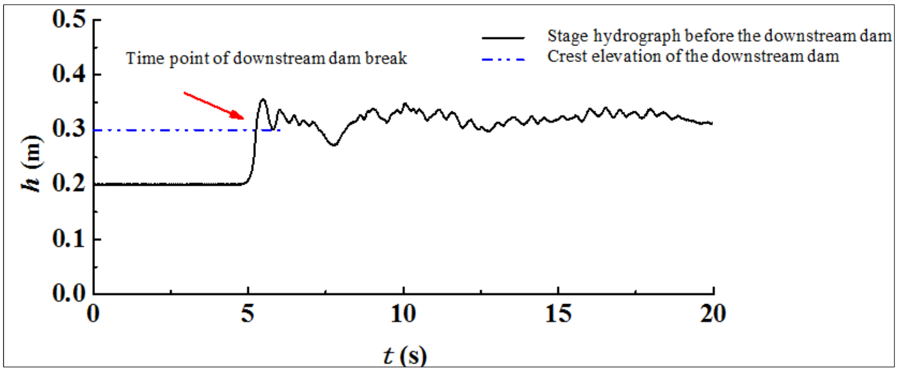

Figure 6. Schematic diagram of downstream dam break time caused by initial wave run-up.

Figure 7 shows varying curve of the water depth at the measuring points in cascade dam break caused by initial surge climb (v=2cm/s, H_1/b=0.50, H_2/b=0.50). The figure also includes the varying curve of the water depth at the measuring points only the downstream dam break for comparison. The change rule of the water depth at the measuring points is as follows:

Kb1 and kb2 points are in the downstream reservoir. When the initial surge climb caused by the initial flood from upstream reservoir drop into downstream reservoir evolve into dam site, water level of the downstream reservoir has a steep rise process, then the water level drop rapidly when the downstream dam break instantaneously by overtopping after the initial surge climb exceed the dam crest elevation. Kb1 point is close to the downstream dam site, so after the initial surge, peak value of the water depth appears once again when the upstream flood overlap with the reflection wave caused by swell climb. Upstream flood evolve into the downstream reservoir continuously, and downstream reservoir water evolve into the downstream channel continuously. The two parts water collide with each other in downstream reservoir, and water surface of the downstream reservoir fiercely fluctuate. As time passed, floods from the upstream reservoir decrease gradually, and the water level at downstream channel decline gradually. Original water in the downstream reservoir completely evolve into downstream channel at this moment. As upstream flood slowly evolve into downstream reservoir, water level of the downstream reservoir drop slowly until the end of cascade dam break.

Kb3 point is in the downstream channel. When cascade dam break caused by initial surge climb occurred, the water level at kb3 point appeared multiple peak values. The first peak value appeared at the beginning of downstream dam break, and water level of the downstream channel rise abruptly. The peak value is greater than single downstream dam break, because when the downstream dam break instantaneously by overtopping, the water level at the front of the downstream dam is sum of the initial water level and wave run-up. The upstream flood evolve into the downstream reservoir continuously, and the downstream reservoir water evolve into the downstream channel continuously. The two parts water collide with each other in downstream reservoir, and the turbulence water evolve into the downstream channel. Along with the increase of flow from upstream reservoir, water level of the downstream channel rise abruptly, the two parts water collide with each other in downstream reservoir, and the turbulence water evolve into the downstream channel, so water level of kb3 point near the dam site fluctuate fiercely and multiple significant peak appeared. As time passed, floods from the upstream reservoir decrease gradually, and the water level at downstream channel decline gradually. Original water in the downstream reservoir completely evolve into downstream channel at this moment. As the upstream flood slowly evolve into downstream reservoir, water level of the downstream reservoir drop slowly until the end of cascade dam break. Variation rule of the water level at kb3 point is in keeping with kb4~kb6, but the water level of kb3 points fluctuate more fiercely compared with kb4~kb6 point, because the distance between kb3 point and downstream dam is nearest. The flood hydrograph induced by cascade dam break caused by initial surge climb has some marked features at the downstream channel compared to that induced by single dam break, such as higher peak value, fluctuated violently, multiple-peak, long duration.

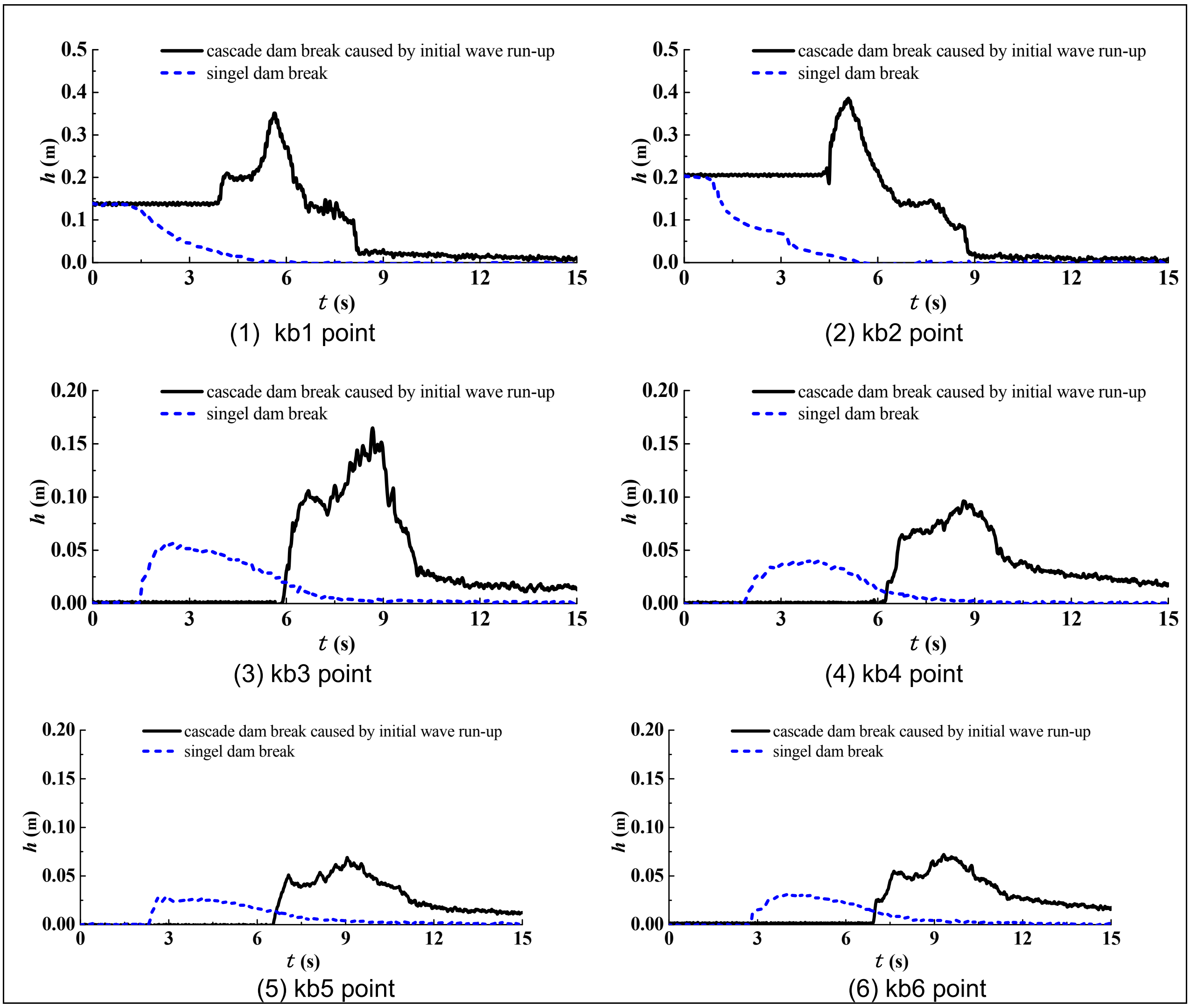

Figure 7. Water level change process of the measuring points caused by initial wave run-up.

3.2.2 Result analysis of the cascade dam break caused by water level rise

When the initial surge climb caused by the initial flood from upstream reservoir evolve into downstream reservoir do not exceed the dam crest elevation, the downstream dam is safety. As time passed, upstream floods evolve into the downstream reservoir continuously, and water level of the downstream reservoir rise gradually. The downstream dam break instantaneously by overtopping. This dam break model can be called cascade dam break caused by water level rise in downstream reservoir. The time point when downstream dam break instantaneously can be seen in figure 8. The break mechanism of cascade dam is different between initial surge climb and water level rise in downstream reservoir, and the superposition effect exists obvious difference, therefore it is necessary to discuss respectively.

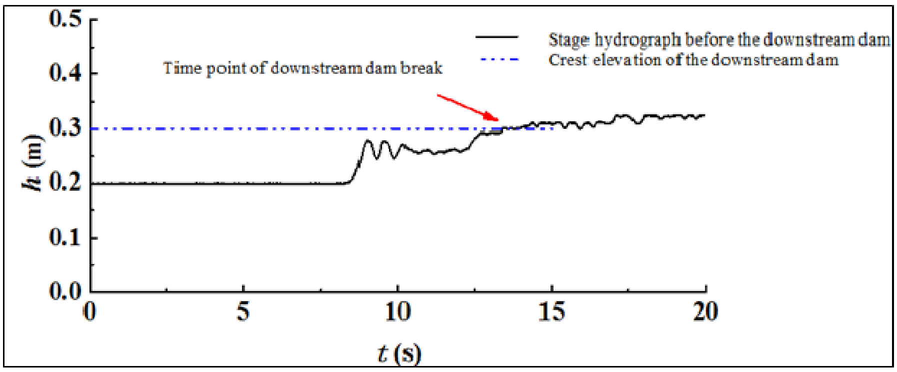

Figure 8. Schematic diagram of the downstream dam break time caused by water level rise.

  / ISSN 1562-6865 (Online) - ISSN 1063-7710 (Print)

Figure 9 shows varying curve of the water depth at the measuring points in cascade dam break caused by water level rise in downstream reservoir (v=0.5cm/s, H_1/b=0.50,H_2/b=0.50). The figure also includes varying curve of the water depth at the measuring points only downstream dam break for comparison. The change rule of the water depth at the measuring points is as follows.

Kb1 and kb2 points are in the downstream reservoir. When the initial surge climb caused by the initial flood from upstream reservoir drop into downstream reservoir evolve into dam site, water level of the downstream reservoir has a steep rise process. When the initial surge climb caused by the initial flood from upstream reservoir evolve into downstream reservoir do not exceed the dam crest elevation, the downstream dam is safety. As time passed, upstream floods evolve into the downstream reservoir continuously, and water level of the downstream reservoir wavelike rise continually until the downstream dam break instantaneously by overtopping. The characteristics of water level change rule at kb1 point are violently fluctuate and rising gradually before the downstream dam break. The added value of water level was caused by the surge and the flood from upstream reservoir. Changing process of the water level at kb2 point is rise abruptly, gradually smooth, and rise slowly before downstream dam break. When the downstream dam break, water in the downstream reservoir discharge into downstream channel in a short time. Water level of the reservoir decreases with time, and varying curve of the water level is a smooth descending curve.

Kb3-kb6 points are in the downstream channel. When only the downstream dam break, water level of the points rapidly increase, slowly decline after the peak value, varying curve of the water level is a smooth parabola curve. When cascade dam break occurred caused by water level rise in downstream reservoir, water level of the points rise abruptly, reach a peak value, and gradual decline. Varying curve of the water level in the downstream channel is similar with signal dam break, but the peak value is even bigger because of the higher water level of the downstream dam break. Changing process of the water level at kb3-kb6 points is bigger peak value and fiercely fluctuate. The flood hydrograph induced by cascade dam break caused by water level rising in downstream reservoir has some marked features at the downstream channel compared to that induced by single dam break, such as higher peak value, fluctuated violently, multiple-peak, long duration.

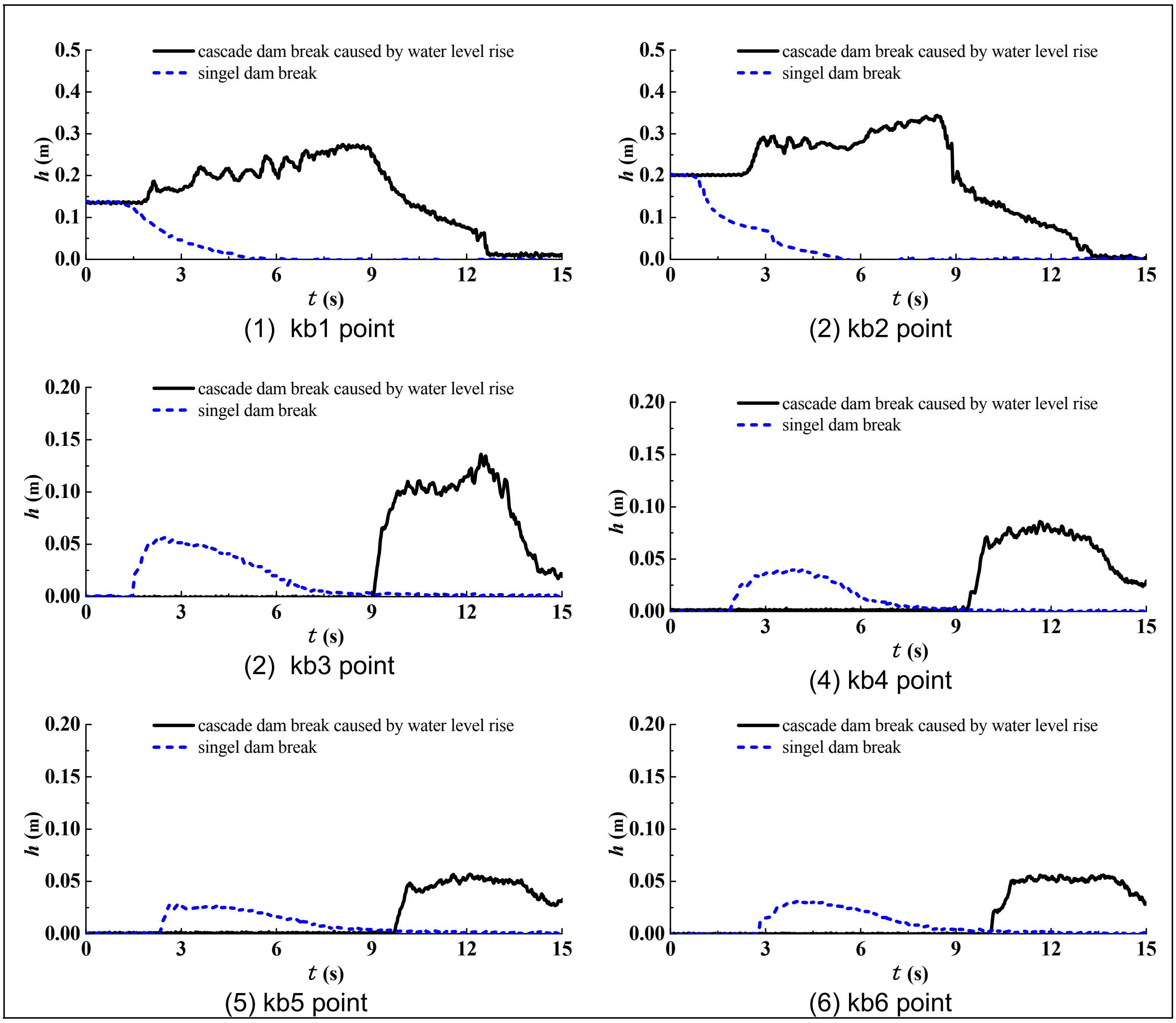

Figure 9. Water level change process of the measuring points caused by water level rise.

4 CONCLUSIONS

The article defines the model of cascade dam break considering the initial wave run-up, water level of the downstream reservoir and crest elevation, and get the change rule of the key parameters, such as the initial time of downstream dam break, water-level fluctuation, peak value and so on. The experimental results show that, the flood hydrograph induced by cascade dam break had some marked features at the downstream channel of the second dam compared to that induced by single dam break, such as higher peak water depth, fluctuated violently, multiple-peak, long duration. Also, there were some obvious differences on flood hydrograph between different cascade dam break types. The results can provide a technical support for flood control management and flood control design of cascade dams.

ACKNOWLEDGEMENTS

The study is financially supported by Non-profit Industry Financial Program of MWR (No.201401027), National Natural Science Foundation of China (No.51409173) and Financial Program of NHRI (No.Y114004, No.Y116009).

REFERENCES

Chen, S.C., Feng, Z.Y., Wang, C. & Hsu, T.Y. (2015). A Large-Scale Test on Overtopping Failure of Two Artificial Dams in Taiwan. In *Engineering Geology for Society and Territory-Volume* 2, 1177-1181. Springer International Publishing.

Chen, S.C., An, S.P. & Hsu, T.Y. (2015). High Precision and Adjusted Discharge Sediment- the Experimental Station in Landao Creek, Huisun Forest. *Chinese Journal of soil and water conservation*, 46(1), 1-6.

Cui, P., Zhou, G.G., Zhu, X.H. & Zhang, J.Q. (2013). Scale Amplification of Natural Debris Flows Caused by Cascading Landslide Dam Failures. *Geomorphology*, 182, 173-189.

Evangelista, S. (2015). Experiments and Numerical Simulations of Dike Erosion due to a Wave Impact. *Water*, 7(10), 5831-5848.

Niu, Z.P., Xu, W.L., Li, N.W., Yang, X.U.E. & Chen, H.Y. (2015). Experimental Investigation of the Failure of Cascade Landslide Dams. *Journal of Hydrodynamics,* 24(03), 430-441.

Xue, Y. (2011*). Dam-Break Flow Propagation in Cascade Reservoirs*, Sichuan University.

Yang, X.U.E., Xu, W.L., Luo, S.J., Chen, H.Y., Li, N.W. & Xu, L.J. (2011). Experimental Study of Dam-Break Flow in Cascade Reservoirs with Steep Bottom Slope. *Journal of Hydr*odynamics, Ser. B, 23(4), 491-497.

Yue, Z.Y. (2010). Mechanism and Hydrodynamic Processes of Natural Dam Failure-Experiments and Coupled Mathematical Modelling, Doctoral dissertation, *PhD Dissertation*. Wuhan University.

Zhou, G.G., Cui, P., Chen, H.Y., Zhu, X.H., Tang, J.B. & Sun, Q.C. (2013). Experimental Study on Cascading Landslide Dam Failures by Upstream Flows. *Landslides*, 10(5), 633-643.

Zhou, G.G., Cui, P., Zhu, X., Tang, J., Chen, H. & Sun, Q. (2015). A preliminary study of the failure mechanisms of cascading landslide dams. *International Journal of Sediment Research*, 30(3), 223-234.

Zhu, X.H., Cui, P. & Chen, H.Y. (2012). Effects of Cascade Failure of Dammed Lakes on the Evolution of Rivers in Wenchuan Earthquake Region. *Journal of Sichuan University (Engineering Science Edition),* 04, 4-69.

HYDRAULICS OF A HYDRAULIC JUMP AERATION BASIN

YU ZHOU[1] & JIANHUA WU[2]

[1,2] College of Water Conservancy and Hydropower Engineering, Hohai University, Nanjing 210098, China,
869272170@qq.com; jhwu@hhu.edu.cn

ABSTRACT

For a conventional stepped spillway, cavitation damage may occur on the vertical or horizontal surface of the steps of the spillway when the unit discharge is larger than some limit (such as 60m^3/(s·m)) due to the increasing flow depth and less air entrainment to the flow of the spillway. In the present work, a kind of hydraulic-jump-stepped spillway is developed and air is efficiently entrained into the flow in order to prevent cavitation damage by means of hydraulic jump aeration basin (HJAB), which is an aeration element of this stepped spillway. The physical models with different lengths and sill heights of the HJAB were designed, and the hydraulic characteristics were theoretically and experimentally investigated, including the effects of the approach flow condition, the length and sill height of HJAB on both the flow regimes and aeration effect. The results show that the flow regimes of the hydraulic jump in the HJAB significantly affect the performance of the aerated flow, and the submerged hydraulic jump should be chosen in the designs of the HJAB. Also, those flow regimes are strongly dominated by the geometry of the HJAB and the approach flow conditions and the submerged hydraulic jump could be formed even though the unit discharge reaches 110m^3/(s·m) at the present conditions.

Keywords: Aeration; air concentration; flow regimes; hydraulic jump; stepped spillway.

1 INTRODUCTION

Stepped spillways have been widely used in hydropower projects over the past two decades owing to their simple structure, significant energy dissipation and weak atomization (Chanson, 1994; Chinnarasri and Wongwises, 2004; Guo and Liu, 2002).

For a given stepped spillway, the flow regimes may be either nappe, transition, or skimming flow for increasing discharge (Boes and Hager, 2003). The skimming flow is characterized by the appearance of a non-aerated region between the first step and incipient point of air entrainment and this non-aerated region increases with increasing discharge. Under a large unit discharge, sub-pressure generated on step faces is reached. Therefore, the negative pressure faces may cause cavitation damage due to insufficient air content (Xu et al., 2015). The energy dissipation also decreases because of the reduced effect of steps for large flow depths relative to the step size (Chen et al., 2003).

To alleviate cavitation damage and increase energy dissipation, recent investigations have focused mainly on the means of introducing air into the flow to make the incipient point of air entrainment move upstream, thus reducing or eliminating the non-aerated region. Pfister et al. (2006) and Wu et al. (2008) mounted an aerator upstream of the first step, and Zamora et al. (2008) added an aerator at the first vertical step face. Their aerators were efficient at introducing air into the flow, but the effectiveness of the preaerator decreases significantly and cannot meet the needs of engineering safety because the air cavity of the preaerator is filled with water immediately at the downstream at low Froude numbers (Chanson, 1995). Lin et al. (2002) and Zheng et al. (2002) proposed joint energy dissipations, which efficiently increase the amount of entrained air if flare gate piers or aerated piers are installed. However, high fins are induced by piers. Qian et al. (2016) proposed a totally new type of energy dissipater, called ski-jump-step energy dissipater, which combines the advantages of the jet generated by ski-jumps and stepped spillways. The roller and aeration in the ski-jump basin preaerate the flow. However, the flow regimes and the type of structure are relatively complex.

In this study, a hydraulic-jump-stepped spillway was introduced for the purpose of preventing cavitation damage and enhancing energy dissipation under large unit discharges. Figure 1 shows the sketch of the structure, which is composed of a WES weir, a hydraulic jump aeration basin (HJAB) and stepped spillway. The WES weir is located in the front of the structure, which makes the flow supercritical so that a hydraulic jump can occur. The HJAB begins from the toe of the weir and ends at the upstream face of the sill, which is chosen to supply air to the flow by means of hydraulic jump. While macro-scale vortices develop in the jump roller, air entrainment occurs in the form of air bubbles and air packets are entrapped at the impingement of the upstream jet flow with the roller (Chanson and Brattberg, 2000). As a result, when the flow passes over the HJAB, the preaeration is achieved. The objectives of this paper are to theoretically and experimentally investigate the hydraulics of the HJAB, including the flow regimes and aeration effect.

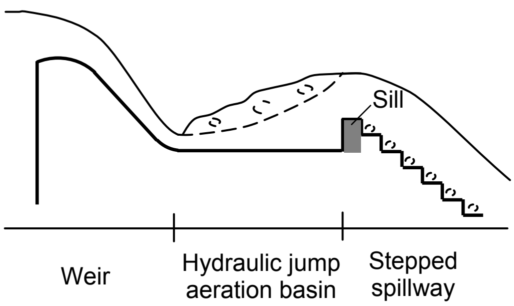

Figure 1. Sketch of a hydraulic-jump-stepped spillway.

2 THEORETICAL CONSIDERATION

Figure 2 shows the sketch of the flow through the HJAB. The whole structure includes an upstream reservoir, a WES crest weir, an HJAB with a sill and outflow channel. In this figure, h_0 and v_o are the flow depth and velocity at the weir crest section, respectively, h_c and v_c are the flow depth and velocity at the contraction section, respectively, and calculated from:

$$h_c = E_o - \frac{q^2}{2g\varphi^2 h_c^2} \quad [1]$$

$$v_c = \frac{q}{h_c} \quad [2]$$

where E_0 is the total energy at the weir crest section, q is the unit discharge, g is the acceleration of gravity, and φ is the coefficient of velocity, which is caused by the weir type.

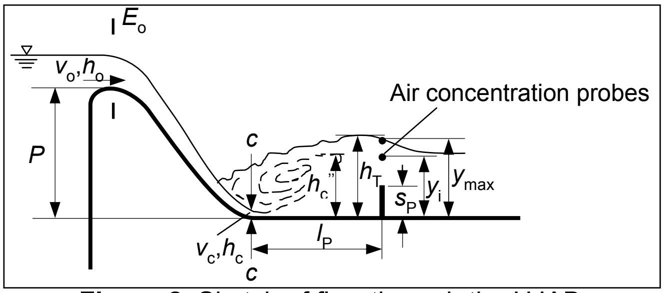

Figure 2. Sketch of flow through the HJAB.

h_c'' is the conjugate depth of the h_c, which is generally obtained by:

$$h_c^{"} = \frac{1}{2} \times h_c \left(\sqrt{1 + 8\frac{q^2}{gh_c^3}} - 1 \right) \quad [3]$$

h_T is the maximum flow depth near the sill of the HJAB, P is the height between the weir crest and the bottom of the HJAB, l_P and s_P are the length and sill height of the HJAB, respectively. In this study, the hydraulic and geometric parameters mentioned above affect the flow regimes and then affect the air concentration.

Based on its location and submergence degree ($\sigma = h_T / h_c$''), a hydraulic jump can be classified into three types: the critical hydraulic jump ($\sigma = 1$), the repelled downstream hydraulic jump ($0 < \sigma < 1$) and the submerged hydraulic jump ($\sigma = 1$) (Wu, 2003).

Thus, the flow regimes of the HJAB can be described by the submergence degree of the hydraulic jump. Furthermore, the air concentration (C) of the outflow over the sill shows the aeration effect of the HJAB. Neglecting the effect of the weir type, σ and C could be constructed as:

  / ISSN 1562-6865 (Online) - ISSN 1063-7710 (Print)

$$\sigma, C = f(v_o, h_o, P, s_P, l_P, g) \qquad [4]$$

Eq. [4] could be rewritten in view of dimensional analysis as:

$$\sigma, C = f(Fr_o, \frac{P}{h_o}, \frac{s_P}{h_o}, \frac{l_P}{h_o}) \qquad [5]$$

where $Fr_0 = v_0 / (gh_0)^{0.5}$, is the Froude number at the weir crest section. Substituting the Froude number (Fr_c) at the contraction section into Fr_0 in Eq. [5], by using continuity equation and P is equal to a constant. Thus, Eq. [5] could be simplified as:

$$\sigma, C = f(Fr_c, \frac{s_P}{h_o}, \frac{l_P}{h_o}) \qquad [6]$$

Eq. [6] implies that both submergence degree (σ) of the hydraulic jump and air concentration (C) of the outflow over the sill is a function of Fr_c, s_P/h_0 and l_P/h_0. The experimental cases are designed according to Eq. [6].

3 EXPERIMENTAL SETUP AND METHODOLOGY

3.1 Experimental setup

The experiments were conducted in the High-Speed Flow Laboratory at Hohai University in Nanjing, China. The experimental setup (Figure 3) consisted of a large feeding basin, a pump, an approach conduit, a rectangular channel, a test model, and a flow return system with electric discharge measurement. The discharge (Q) was measured with a permanent magnetic flowmeter (± 0.002m^3/s) and the maximum discharge was 115.00L s^{-1}. The rectangular sink is 25.00m in length, 0.50m in width and 0.55m in height. In the rectangular sink, the test mode made of Perspex was designed at a scale of 1:70 on the basis of the Froude number criteria, including a weir and an HJAB with a sill. P = 36.0cm is the height between the weir crest and the HJAB bottom. The design head above the weir is 22.0cm and the standard weir crest profile is described by the equation y = 11$x^{1.85}$. The sill was restricted to 1.0cm in consideration of neglecting the effect of its thickness.

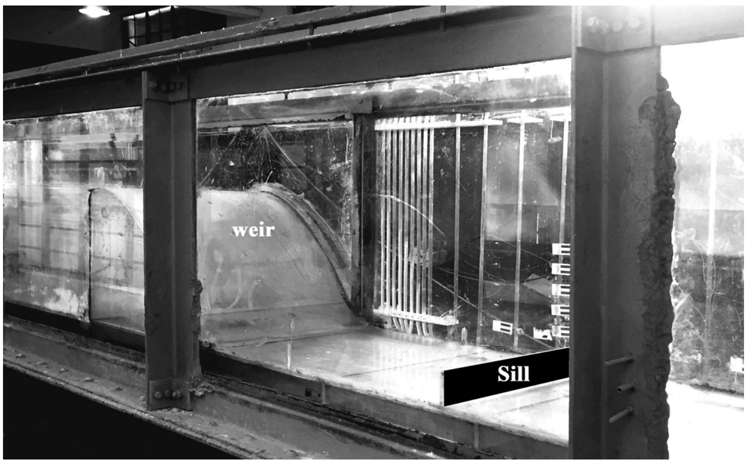

Figure 3. Experimental set-up.

3.2 Experimental methodology

Table 1 lists the experimental cases and geometric parameters of the model HJAB. The parameters were designed to investigate the effects on σ and C. Cases M12, M22 and M32 serve as the effect of l_P, while cases are for the effect of s_P. All experimental cases were carried out in unit discharges ranging between 102.40 and 230.00 L/(s·m). In the experiment, Fr_0 varied from 0.92 to 1.04 and the corresponding Fr_c varied from 4.85 to 3.43. The parameters of h_0 and h_T were measured by a steel ruler of 1 mm reading accuracy. The air concentration probes were plastered on the side wall and then connected to the air concentration measuring instrument (Type CQ6-2005). For different locations of the sill of the HJAB, there were six probes above the sill, with the lowest and highest probes at 7.0 cm and 28.0 cm from the bottom, correspondingly. The highest probe is just for the case whose sill height equals to 8 cm.

Table 1. Geometric parameters of hydraulic jump aeration basin.

	l_P (×10^{-2}m)	s_P (×10^{-2}m)
M12	50.00	6.50
M22	60.00	6.50
M32	70.00	6.50
M31	70.00	5.00
M33	70.00	8.00

4 RESULTS AND DISCUSSIONS

4.1 Flow regimes

Figure 4 shows the flow regimes under different approach flow conditions for case M31. With the increase in the unit discharge q, Fr_c decreases from 4.85 to 3.43 and the flow regimes of the hydraulic jump change from the submerged hydraulic jump to the repelled downstream hydraulic jump. For Fr_c = 4.85 and Fr_c = 4.08 (Figures 4(a) and 4(b)), it is evidenced that the entire flow becomes aerated and the hydraulic jump occurs upstream of contraction section; however, for the latter, the location of the hydraulic jump slightly moves downstream and there is more clear water near the bottom of the basin. For Fr_c = 3.76 (Figure 4(c)), the hydraulic jump becomes a critical one that starts roughly at the contraction section, and the clear water region expands at the bottom while the area of the roller is reduced. For Fr_c = 3.61 and Fr_c = 3.43 (Figures 4(d) and 4(e)), entrapping air bubbles within the lower part of the flow is difficult, resulting in the presence of clear water near the sill. As Fr_c decreases, the location of the hydraulic jump moves downstream rapidly, especially for the repelled downstream hydraulic jump.

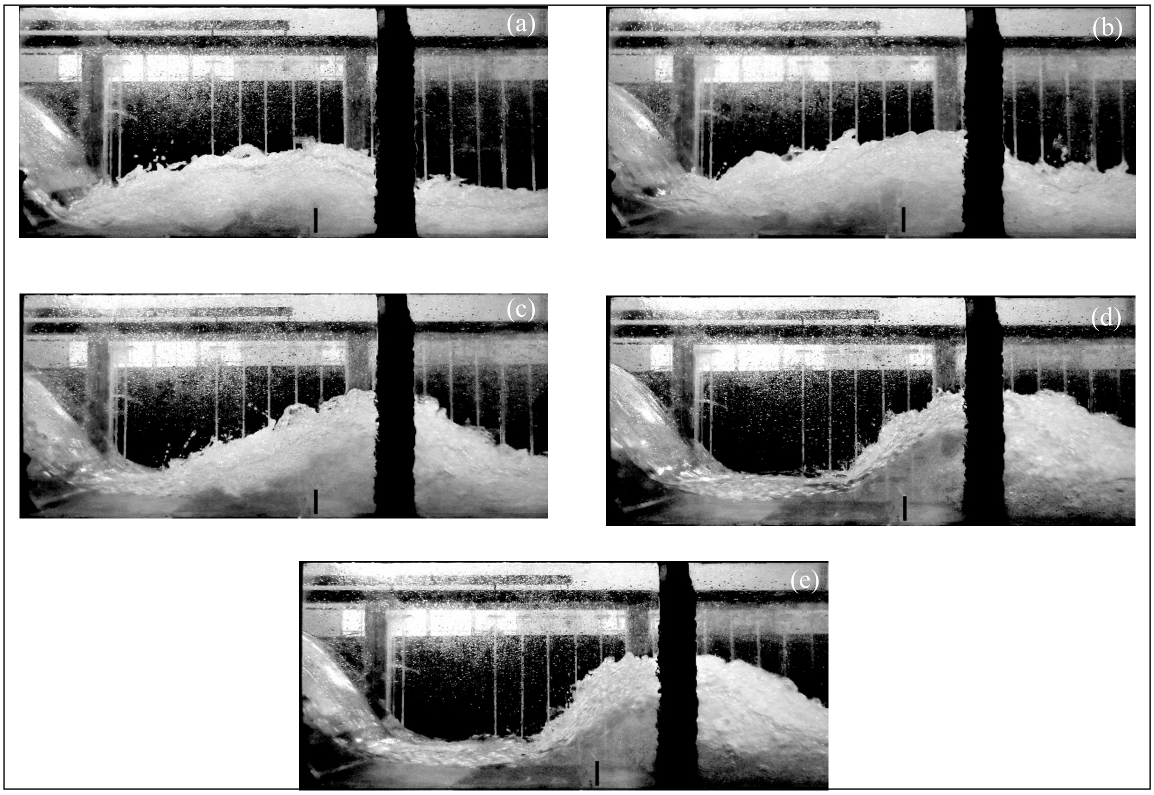

Figure 4. Flow regimes of the HJAB (M32): (a) Fr_c = 4.85; (b) Fr_c = 4.08; (c) Fr_c = 3.76; (d) Fr_c = 3.61; (e) Fr_c = 3.43.

Since similar changes in flow regimes were also observed in other cases, it is important to investigate the relationship between σ and the geometry of the HJAB for different Fr_c. Figure 5 shows the variations of σ with Fr_c at different l_P and s_P = 6.5cm. Obviously, σ is in a good linear relationship with Fr_c and decreases with the increasing l_P. Figure 6 shows the variations of σ with Fr_c at different s_P and l_P = 70.0cm. σ is still well linear with Fr_c, and increases with the increase of s_P.

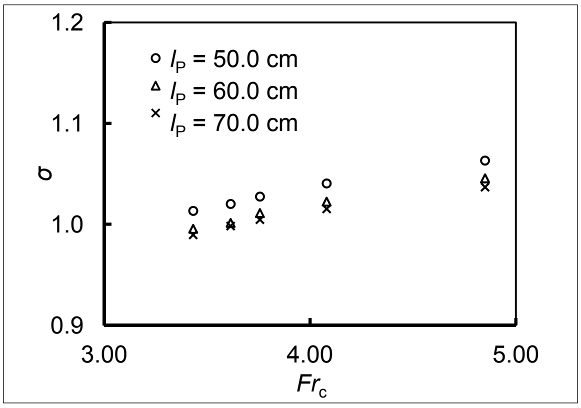

Figure 5. Variations of σ with Fr_c at different l_P and s_P = 6.5cm.

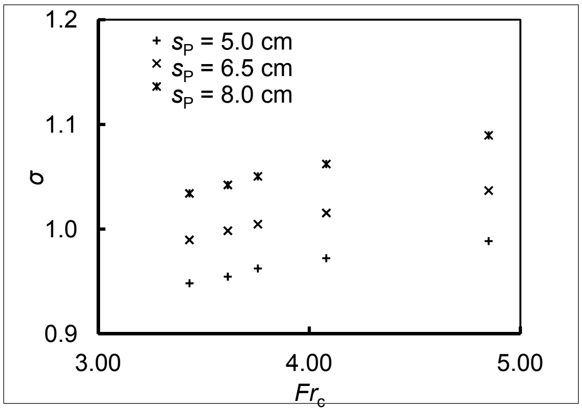

Figure 6. Variations of σ with Fr_c at different s_P and l_P = 70.0cm.

Figure 7 presents the relationship between σ and its influencing factors, and the best fit is:

$$\sigma = 0.71 Fr_c^{0.20} \left(s_P / h_o\right)^{1.20} \left(l_P / h_o\right)^{-0.59} + 0.86 \quad [7]$$

$$0.38 \le s_P/h_0 \le 0.60$$
$$2.92 \le l_P/h_0 \le 4.63$$

Firstly, Eq. [7] demonstrates that σ increases linearly in the range of $0.38 \le s_P/h_0 \le 0.60$ and $2.92 \le l_P/h_0 \le 4.63$, which also indicates that σ increases with increasing s_P/h_o and decreasing l_P/h_0. Secondly, σ changes nonlinearly with s_P/h_o and l_P/h_0, and the s_P appears to have more effect on changing the flow regime than l_P does. Furthermore, the upper dash line (σ = 1) in Figure 7 expresses the critical hydraulic jump for $Fr_c^{0.2}\bullet(s_P/h_0)^{1.20}\bullet(l_P/h_0)^{-0.59} \approx 0.2$, whereas the part above the line ($\sigma > 1$) represents the submerged hydraulic jump for $Fr_c^{0.2}\bullet(s_P/h_0)^{1.20}\bullet(l_P/h_0)^{-0.59} > 0.2$ and the part below ($\sigma < 1$) stands for the repelled downstream hydraulic jump for $Fr_c^{0.2}\bullet(s_P/h_0)^{1.20}\bullet(l_P/h_0)^{-0.59} < 0.2$. Therefore, it is efficient to control the flow regimes by altering the basin length and sill height for a given Fr_c in a design application.

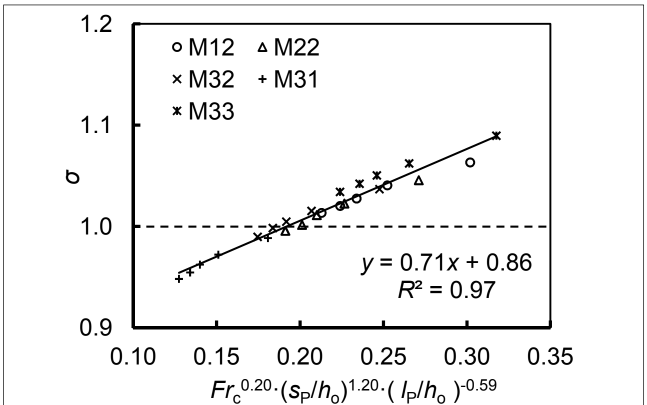

Figure 7. Variation of σ with $Fr_c^{0.2}\bullet(s_P/h_0)^{1.20}\bullet(l_P/h_0)^{-0.59}$.

4.2 Aeration effect

Figure 8 shows air concentration (C) of the outflow over the sill against Y under different Fr_c for case M31, where $Y = (y_i - s_P) / (y_{max} - s_P)$, represents the relative depth above the sill, with y_i as the height from the HJAB bottom to the air concentration probes and y_{max} as the height from the HJAB bottom to the flow surface (as shown in Figure 2). It can be clearly seen that in the process of the flow regime development (as shown in Figure 4), C appears to increase with Y and there is a sharp value surge in the vicinity of Y = 0.5 for Fr_c = 3.76, 3.61 and 3.43. Secondly, the C decreases with the decreasing Fr_c, which implies that the effect of aeration weakens during the transformation of the submerged hydraulic jump into the repelled downstream hydraulic jump under different approach flow conditions.

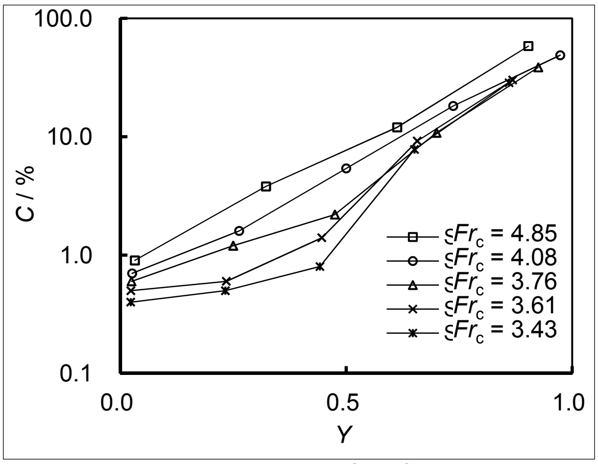

Figure 8. Air concentration of outflow over the sill for different total weir heads (M32).

Figure 9 shows the flow regimes under different approach flow conditions for M33. In this figure, s_P increases from 6.5 cm to 8.0 cm, and the submerged hydraulic jump is observed for all approach flow conditions compared with M31. Figure 10 illustrates the variations of C against Y under different Fr_c for M33, showing the C is larger than the value measured in M31 under identical Fr_c. The better effect of aeration is achieved due to submerged hydraulic jumps, even though Fr_c reaches 3.43.

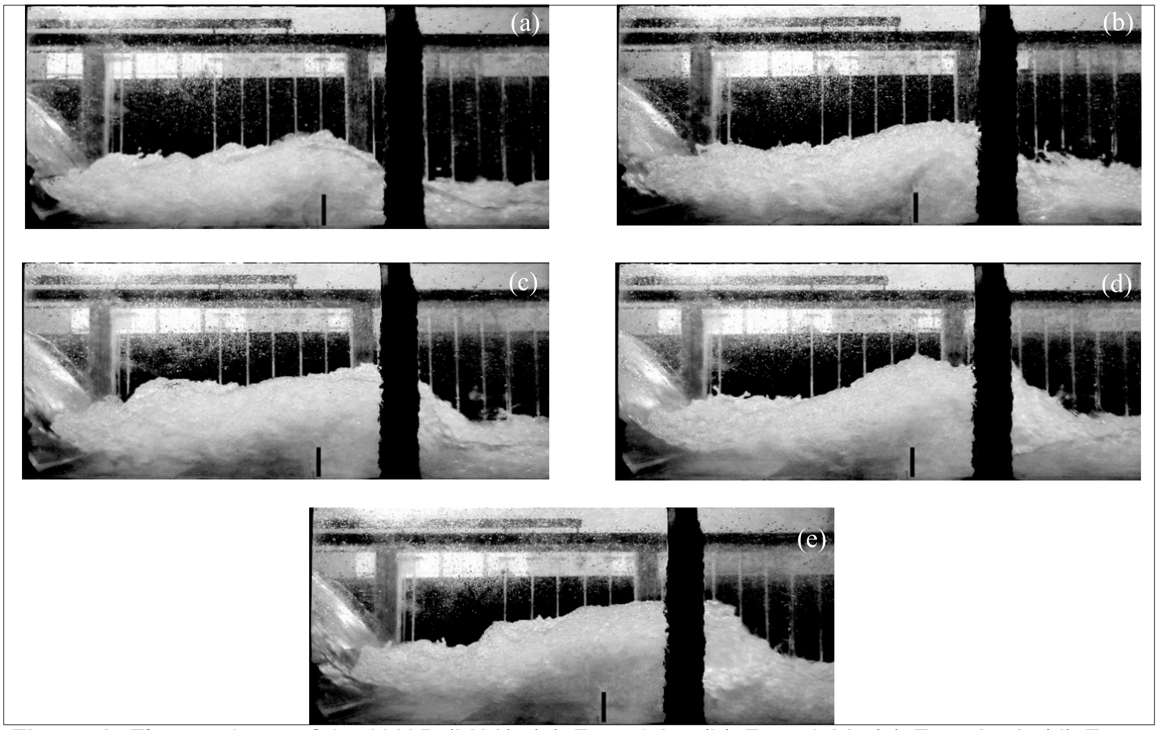

Figure 9. Flow regimes of the HJAB (M33): (a) Fr_c = 4.85; (b) Fr_c = 4.08; (c) Fr_c = 3.76; (d) Fr_c = 3.61; (e) Fr_c = 3.43.

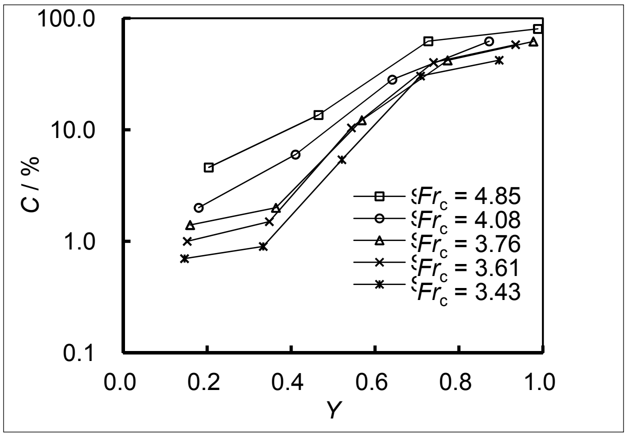

Figure 10. Air concentration of outflow over the sill for different total weir heads (M33).

In addition, the measured air concentration data were analysed concerning the length and sill height of the HJAB. Figure 11 shows the variation of C against *Y* with different s_P under large unit discharges (the prototype unit discharge q_P = 110.00 m^3/(s·m)). Firstly, the larger s_P results in larger *C*. Secondly, it is evident that s_P has a significant effect on the air concentration. For example, the C exhibits a sharp value surge at *Y* = 0.36 for s_P = 8.0 cm, whose results are larger than *Y* = 0.61 for s_P = 5.0 cm.

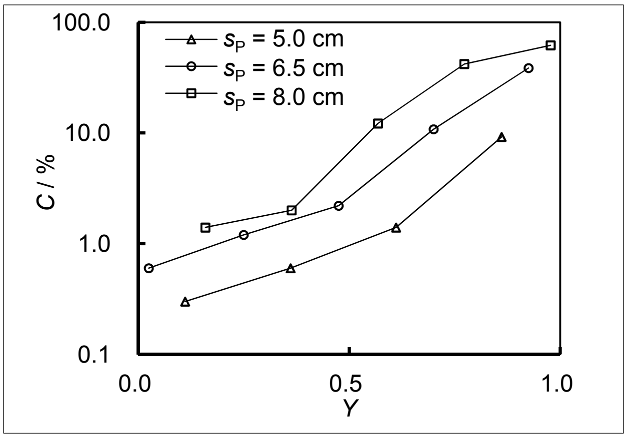

Figure 11. Variation of *C* with *Y* with different s_P and l_P = 70.00 cm (q_P = 110.00 m3/(s·m)).

Figure 12 shows the variation of *C* against *Y* with different l_P under large unit discharges (q_P = 110.00 m^3/(s·m)). Although the submerged hydraulic jump has a larger submergence degree in a shorter HJAB, a longer HJAB results in a higher *C*. The results above are mainly caused by the transfer of roller in a hydraulic jump, which increases the air concentrations above and behind the sill, as is shown in Figure 13 and 14.

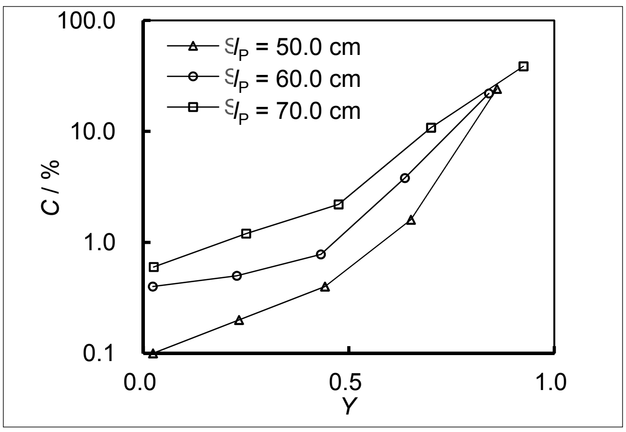

Figure 12. Variation of *C* with *Y* with different l_P and s_P = 6.5 cm (q_P = 110.00 m^3/(s·m)).

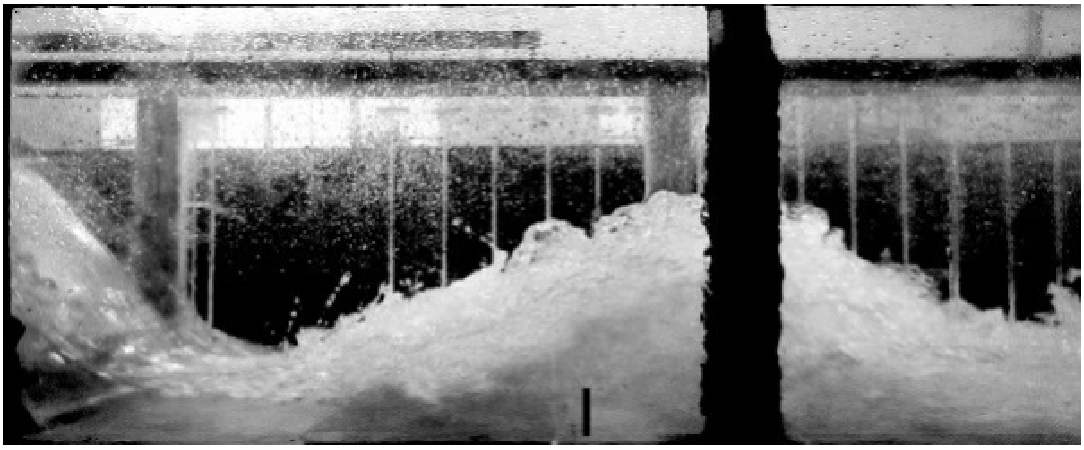

Figure 13. Flow regime of the HJAB for M32 (q_P = 110.00m^3/(s·m)).

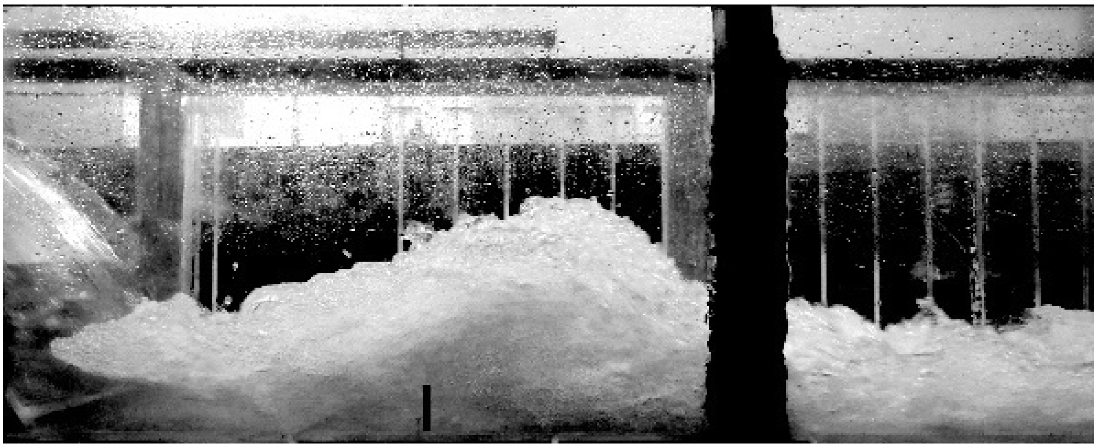

Figure 14. Flow regime of the HJAB for M12 (q_P = 110.00m^3/(s·m)).

5 CONCLUSIONS

In the present work, a novel structure called hydraulic-jump-stepped spillway is introduced and used to prevent cavitation damage inflicted by the absence of air entrainment in the non-aerated region. With respect to this new structure, the hydraulic jump aeration basin (HJAB) plays a role in preaerating the flow by means of a hydraulic jump.

Based on the analysis of flow regimes and aeration effect of the HJAB, the flow regimes of the hydraulic jump change from submerged hydraulic jump to the repelled hydraulic jump with the decrease of the Froude number at the contraction section. Different types of results from different submergence coefficient, which increases with the decreasing length and increasing height of the HJAB. In the study of aeration effect of HJAB, the submerged hydraulic jump compared with other flow regimes has a better effect of aeration and occurs despite that the unit discharge q_P = 110m^3/(s·m) for the prototype.

ACKNOWLEDGEMENTS

This research is supported by the National Natural Science Foundation of China (Grant No. 51479057) and the Research Innovation Program for College Graduates of Jiangsu Province (No. 2015B41714).

REFERENCES

Boes, R.M. & Hager, W.H. (2003). Hydraulic Design of Stepped Spillways. *Journal of Hydraulic Engineering*, 129(9), 671-679.

Chanson, H. (1994). Comparison of Energy Dissipation between Nappe and Skimming Flow Regimes on Stepped Chutes. *Journal of Hydraulic Research*, 32(2), 213-218.

Chanson, M.H. (1995). Predicting the Filling of Ventilated Cavities behind Spillway Aerators. *Journal of Hydraulic Research*, 33(3), 361-372.

Chanson, H. & Brattberg, T. (2000). Experimental Study of the Air-water Shear Flow in a Hydraulic Jump. *International Journal of Multiphase Flow*, 26(4), 583-607.

Chen, Q., Dai, G.Q., Zhu, F.Q. & Yang, Q. (2003). Factors of Influence on the Energy Dissipation Ratio of Stepped Spillways. *Journal of Hydroelectric Engineering*, 22(4), 95-104.

Chinnarasri, C., & Wongwises, S. (2004). Flow Regimes and Energy Loss on Chutes with Upward Inclined Steps. *Canadian Journal of Civil Engineering*, 31(5), 870-879.
Guo, J. & Liu, Z.P. (2002). Prototype Observation of the Flaring Pier Stepped Dam Face Flood Discharging Hydraulics for the Dachaoshan Hydropower Plant. *Yunnan Water Power*, 18(4), 16-20.
Lin, K.J., Han, L. & Deng, Y.G. (2002). Study and Application of the Combined Energy Dissipator of RCC Overflow Dam Flaring Piers and Stepped Dam Face in the Dachaoshan Hydropower Plant. *Yunnan Water Power*, 18(4), 6-15.
Pfister, M., Hager, W.H. & Minor, H.E. (2006). Bottom Aeration of Stepped Spillways. *Journal of Hydraulic Engineering*, 132(8), 850-853.
Qian, S.T., Wu, J.H. & Ma, F. (2016). Hydraulic Performance of Ski-Jump-Step Energy Dissipater. *Journal of Hydraulic Engineering*, 142(10).
Wu, C.G. (2003). *Hydraulics (Vol.2)*, Higher Education Press, Beijing.
Wu, S.R., Zhang, J.M., Xu, W.L. & Peng, Y. (2008). Experimental Investigation on Hydraulic Characteristics of the Flow in the Pre-Aerator Stepped Spillways. *Journal of Sichuan University (Engineering Science Edition)*, 40(3), 37-42.
Xu, W.L., Luo, S.J., Zheng, Q.W. & Luo, J. (2015). Experimental Study on Pressure and Aeration Characteristics in Stepped Chute Flows. *Science China Technological Sciences*, 58(4), 720-726.
Zamora, A.S., Pfister, M. & Hager, W.H. (2008). Hydraulic Performance of Step Aerator. *Journal of Hydraulic Engineering*, 134(2), 127-134.
Zheng, A.M., Zhang, Z.C., Yang, Y.Q., Liu, Y.F. & Dai, G.Q. (2002). Water Flow Regime and Flow Velocity Behaviors in Stepped Spillways with Aerated Piers. *Journal of Xi'an University of Technology*, 18(1), 71-75.

Proceedings of the 37th IAHR World Congress
August 13 – 18, 2017, Kuala Lumpur, Malaysia

RESEARCH AND PRACTICE ON JOINT FLOOD CONTROL OPERATION FOR THE XILUODU-XIANGJIABA-THREE GORGES RESERVOIRS GROUP

TING HU(1), HAI WANG(2) & XING-E HU(3)

(1,2,3) China Three Gorges Corporation, Yichang, China,
hu_ting@ctg.com.cn; wang_hai@ctg.com.cn; hu_xinge@ctg.com.cn

ABSTRACT

The Xiluodu and Xiangjiaba reservoirs of China impounded up to normal water level for the first time in 2013 and 2014, respectively. It marked that the Xiluodu-Xiangjiaba-TGR, an ultra-large type cascade reservoir with 27.7 billion m^3 flood control storage formed on the stem stream of Yangtze River. The research indicated that the flood control standard of emphasis cities on the upstream like Yibin, Luzhou, Chongqing, etc., and the middle-downstream wide areas such as Jing River, Chenglingji could be improved substantially through the joint operation of cascade reservoirs with large storage and well regulation abilities. The flood control pressure of main stem and branch will be alleviated effectively. In 2014 and 2016, two large floods happened in the Yangtze River basin. But, the flood control safety of important cities and areas mentioned above were guaranteed effectively by the preliminary joint operation practice of the cascade. Meanwhile, the flood control benefit of joint operation was remarkable. The research and practice can provide favorable references for the similar cascade reservoirs in the world.

Keywords: Stem stream of Yangtze River; cascade reservoirs group; joint flood control operation.

1 INTRODUCTION

The Yangtze River, the longest river in China and the third longest in the world, is about 6300 km long and has 1.8 million km^2 drainage areas. It contains a huge water resource, however, flood damage occurred frequently and caused huge loss in history. In order to solve the flood control puzzle of Yangtze River basin, the government of China adopted many effective actions, such as reservoirs construction.

As known, the Three Gorges Reservoir (TGR) is the greatest hydro-junction and is a vitally important and backbone flood control project in the Yangtze River basin. It has been operating stably and efficiently for more than 14 years since 2003. With the Xiangjiaba (XJB) and Xiluodu (XLD) reservoirs, which rank in the top 10 biggest reservoir in the world being built up and operated, the XLD-XJB-TGR cascade reservoirs pattern is the stem stream of Yangtze River (Hu et al., 2015) as shown in Figure 1.

The three reservoirs with big storage and well regulate property are all exploited, operated and managed by the China Three Gorges Corporation. Their basic parameters are shown in Table 1. Researches showed that (Liu et al., 2015. Research report, 2014), according to the joint flood control operation of cascade reservoirs, the flood control standard of important cities along Yangtze River can be further improved and the flood control pressure of emphasis reaches can be alleviated. In flood season of 2014 and 2016, the joint operation of XLD-XJB-TGR cascade reservoirs was practiced effectively and successfully.

Table 1. The basic parameters of XLD-XJB-TGR reservoirs.

Reservoirs	Drainage area ($10^4 km^2$)	Reservoir storage capacity ($10^8 m^3$)	Flood control storage ($10^8 m^3$)	Hydropower capacity ($10^4 kW$)
XLD	45.44	115.7	46.5	1386
XJB	45.88	49.77	9.03	640
TGR	100	393	221.5	2250
Total	/	558.47	277.03	4276

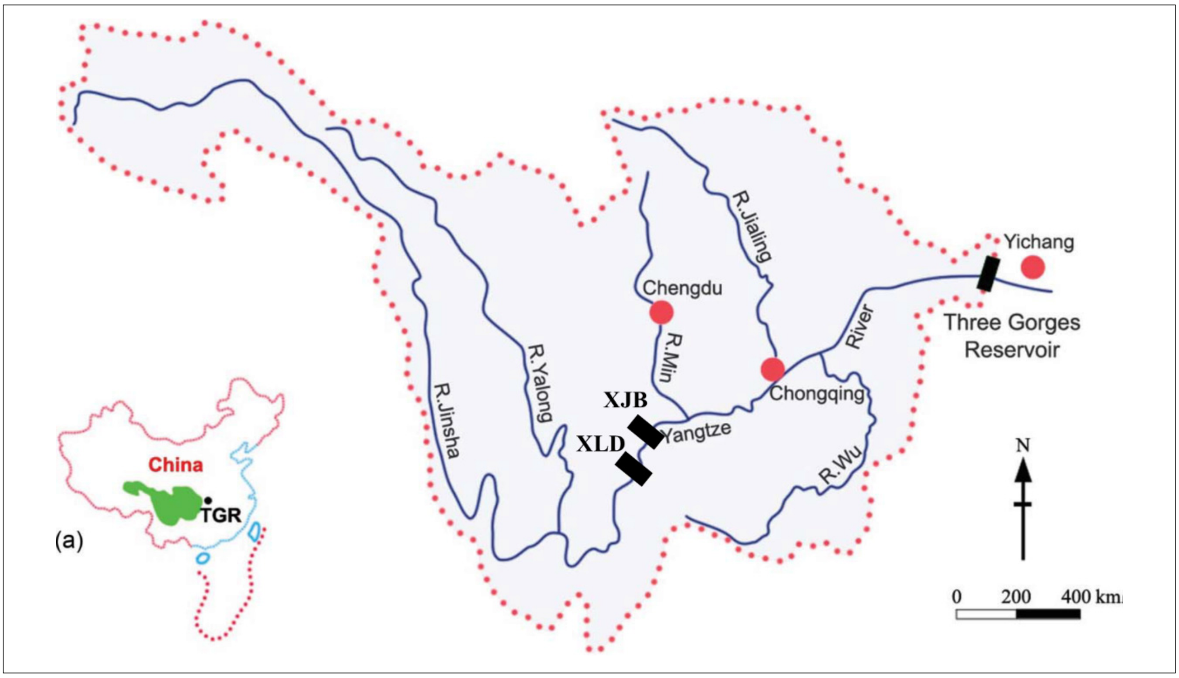

Figure 1. Sketch map of the XLD-XJB-TGR reservoirs in Yangtze River basin.

2 FLOOD CONTROL SITUATIONS OF YANGTZE RIVER

2.1 Flood characteristics and protected areas

The floods of Yangtze River are mainly caused by rainstorm and distributed into a wide range, which have the characteristics, such as large flood peak, coming swiftly and violently, lasting shortly, affected areas are scattered. Sometimes, the regional flood causes truculence disaster of partial area and the mountain torrent disasters always cause a large number of casualties.

The Yangtze River flows through a wide range and flood protected areas are numerous. The downstream Jing River reach of TGR is the most important protected area, which spreads a proverb "million miles of the Yangtze River, the risk in Jing River". Secondly, the protected area is Chenglingji area where the Dongting Lake falls into Yangtze River (He et al., 2013). With the upstream reservoirs being built up, the significant cities along Yangtze River also turn into the important protected areas, such as Yibin, Luzhou, Chongqing city. The sketch map of flood control for the Yangtze River basin is shown in Figure 2.

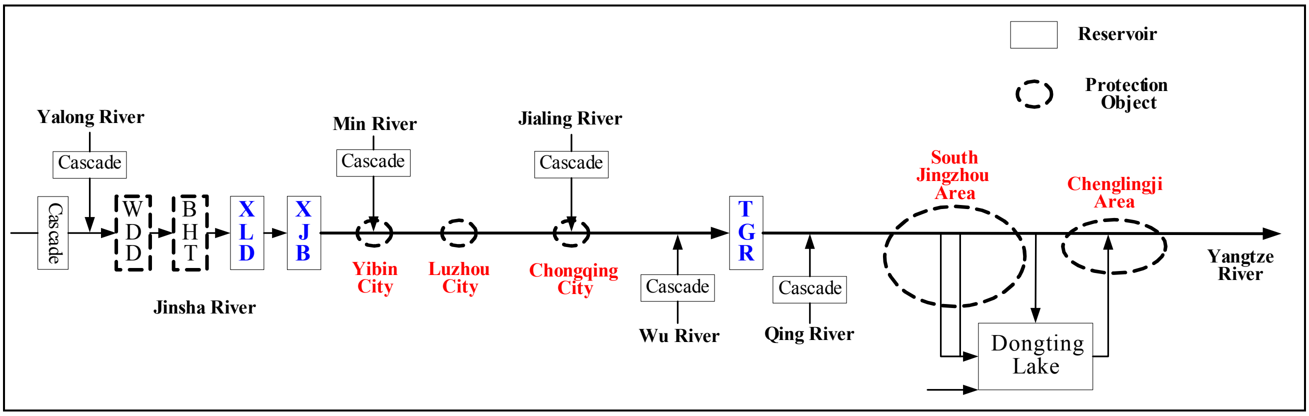

Figure 2. Sketch map of flood control for the Yangtze River basin.

2.2 Flood control measures and standards

The flood volume and scarce drain capacity of channel is the main flood control contradiction in Yangtze River. For decades, through the engineering measures, such as dikes, channels, lakes and reservoirs construction, conservation of water and soil, returning farmland to lake, etc., and non-engineering measures like operation management and research, the Yangtze River basin possess multilayered flood control measures of dikes-reservoirs-flood diversion areas. The flood control capacity was enhanced effectively.

The flood control standard of Yangtze River was low before the construction of TGR and other reservoirs, which was out of keeping with the important economic and society position of Yangtze River area. Before construction of reservoirs, the flood control standards of downstream reaches and upstream cities were 10~15 and 20~50 year return flood respectively depending on dikes. Then after construction of reservoirs, they were enhanced to 50~100 year return flood cooperating with the dikes. The flood control standards of protected areas before and after reservoir construction are shown in Table 2.

Table 2. The flood control standards of protected areas before and after reservoir construction.

Flood control objects	Before reservoir construction	After reservoir construction
Jing River reaches	10-year return	100-year return
Chenglingji area	10~15-year return	Decreasing flood diversion
Yibin city	20-year return	50-year return
Luzhou city	20-year return	50-year return
Chongqing city	50-year return	100-year return

3 JOINT FLOOD CONGTROL OPERATION RESEARCH

3.1 Research design

The flood control storage of 30 billion m^3 can provide solid foundation for the protected areas after XLD-XJB-TGR reservoir group coming into being. Facing such a large span, multi reservoirs and flood protected areas, different protection standards, the main consideration are as follows in the research process of joint flood control operation.

(a) The flood control tasks undertaken by reservoirs should be clearly, and the flood control area must be subdivided. For located closely, the XLD-XJB cascade reservoir is preferential for the flood control of Yibin, Luzhou and Chongqing cities, then for the middle and lower reaches of Yangtze River cooperating with the TGR. The TGR is mainly for the flood control of downstream Jing River and Chenglingji area;
(b) On the basis of existing flood control abilities and standards of the flood protected areas, using the decomposition idea, the reserved flood control storage of upstream reservoirs for the protected areas should be discussed and confirmed when the standard flood occurred;
(c) Analyzing the relationship of various regional flood types and seeking the shared space of flood control capacity, then coordinating the regional flood control;
(d) Determining the overall allocation scheme of flood control storage then targeted to protocol the flood impoundment modes for different protected areas and flood composition.

3.2 Main research results

According to above research ideas and flood routing of different typical flood, the main achievements are as follows:

(a) In order to ensure the 50 years return flood security of Yibin and Luzhou cities in any case of composition, The XLD-XJB reservoirs should reserve the storage capacity of $14.6 \times 10^8 m^3$ in their total capacity of $55.53 \times 10^8 m^3$;
(b) It is consistent in essence that the XLD-XJB reservoirs control flood for Chongqing and for Jing River and Chenglingji areas coordinating with TGR. So, the XLD-XJB reservoirs remainder flood control storage of $40.93 \times 10^8 m^3$ can share with them;
(c) The flood control operation mode of XLD-XJB for upstream cities mainly is “compensation operation by flood peak reduction” and the mode for downstream reaches is “water level compensation operation”;
(d) Coordinating with XLD-XJB reservoirs, the flood control compensation water level of TGR for Chenglingji area can be increased from 155m to 161m. The flood control effect is obviously for the compensation capacity expanded by nearly $42 \times 10^8 m^3$;
(e) When the upstream and downstream flood of Yangtze River meet, the XLD-XJB should control flood for Yibin and Luzhou cities preferentially. Then under the premise of reserving storage of $14.6 \times 10^8 m^3$, they control flood for Chongqing city and middle-lower reaches.

According to above researches, the flood diversion under the joint flood control operation of XLD-XJB-TGR can reduce nearly $24 \times 10^8 m^3$ when encountering the 100-year flood in 1954 (as shown in Table 3).

Table 3. Flood diversion under different conditions in the Yangtze River.

Different conditions	Flood diversion (10^8 m^3)
Before TGR construction	492
Design operation mode of TGR	398
Optimal operation mode of TGR	371
Joint operation of XLD-XJB-TGR	347

4 JOINT FLOOD CONTROL OPERATION PRACTICE

4.1 Practices in 2014

The TGR and upstream XLD-XJB reservoirs were impounding in September 2014. In mid-September, the inflow of TGR was rising constantly for the continuous heavy rainfall. In order to alleviate the flood control pressure of Chongqing city and tail of TGR, the XLD-XJB reservoirs reduced outflow and expedited impoundment process. The flow was reduced 1700m^3/s and the water level was lowered about 0.6m, which relieved the pressure on Chongqing and the tail submerging influence of TGR.

In late September, the TGR was encountered the maximum flood peak of 55000m^3/s. At the same time, the water level of TGR was on the high side for the previous impoundment. In order to avoid the tail submerging of TGR, XLD-XJB reservoirs reduced outflow of 3000m^3/s timely and about 2.5 × $10^8$$m^3$ flood volume for TGR. According to the joint flood control operation, the flood passed TGR successfully and the tail of TGR was safe. The joint flood control operation process in September 2014 is shown in Figure 3.

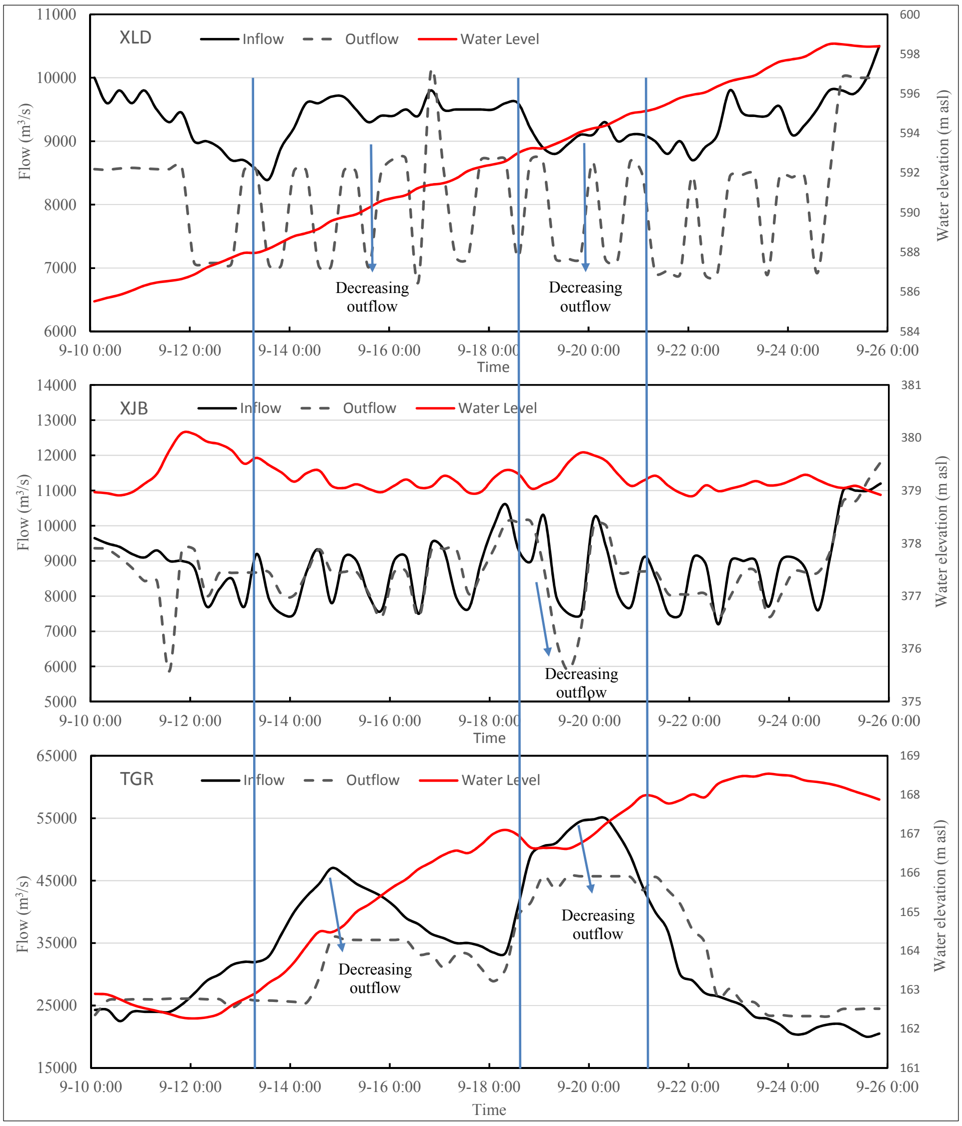

Figure 3. The joint flood control operation process in September 2014.

4.2 Practices in 2016

Affected by the El Nino from June to July, heavy rainfall and urban inland inundation occurred continually, some river level exceeded the critical value in 2016. At the same time, the inflow of TGR increased from 25000m^3/s on June 27th to 50000m^3/s on July 1st for the heavy precipitation weather process, and the level of downstream reaches of Yangtze River continued to rise. So, the flood control situation of Yangtze River was especially severe.

Under the emergency condition, XLD-XJB-TGR cascade reservoirs started the joint flood control operation. XLD began to impound in early July, the maximum flood peak elimination was about 3000m^3/s, the water level of XLD rose from 561.93m on July 1st to 575.5m on July 17th, which the interception volume was 14.5 × 10^{8}m^3. XJB controlled its water level below 374m and coordinated with XLD for the joint flood control operation. TGR eliminated the maximal flood peak of 19000m^3/s, where peak clipping rate was 38%. The interception volume of TGR was 29.5 × 10^{8}m^3 and the maximum flood level was 151.59m.

The inflow of TGR reduction relied on the joint flood retaining, and the further impoundment of TGR avoided the encounter of upstream and downstream flood. The joint operation guaranteed that the Jing River level not exceeding warning value of 43m (the actual value was 41.09m), and the Chenglingji level not exceeding guarantee value of 34.4m (the actual value was 41.29m). The effect of joint flood control operation was shown again. The joint flood control operation process in 2016 is shown in Figure 4.

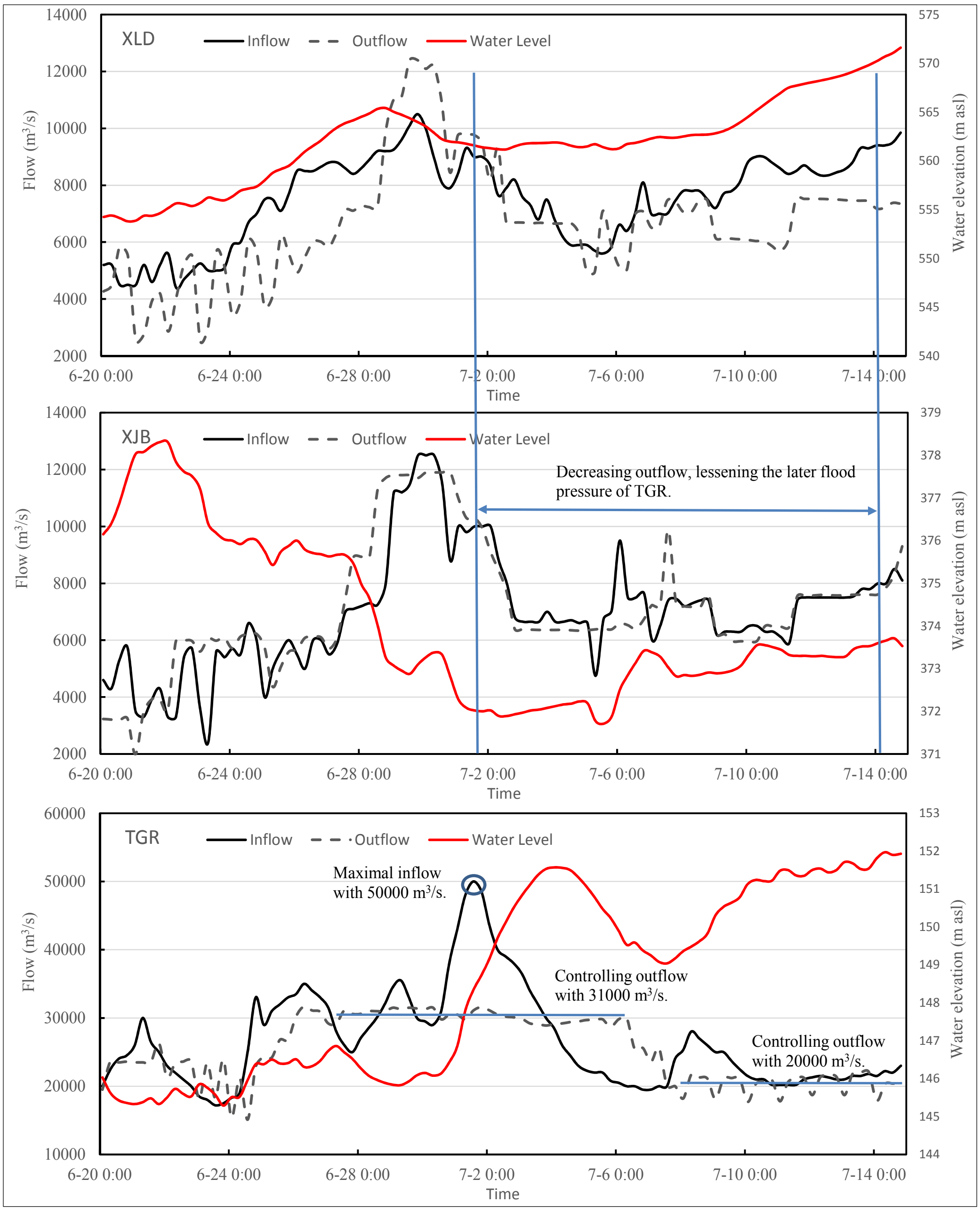

Figure 4. The joint flood control operation process in 2016.

5 CONCLUSIONS

The joint flood control operation of XLD-XJB-TGR is a complex problem for the multi protected areas, wide regions and diverse needs. Through scientific research and practice in recent years, the joint flood control benefits of reservoir group have been realized for the first time. Around the year of 2020, the total flood control storage will be over 50 billion m^3 with the being built up and operation of upstream reservoirs. Then, the flood control situation of Yangtze River will be further improved. Meanwhile, more researches and practices must be done for the accompanying more complex problems in the future.

ACKNOWLEDGEMENTS

This paper was financially supported by the National Key Technologies Research and Development Program of China (2016YFC0402306). The authors would also like to thank the editor and anonymous reviewers for their reviews and comments related to this manuscript.

REFERENCES

He, X.C., Ding, Y. & Li, S.F. (2013). Joint Flood Control Operation Strategy of Three Reservoirs in Middle and Upper Reaches of Yangtze River based on Equal Proportion Water Storage. *Water Resources and Power,* 31(4), 38-41 (in Chinese).

Hu, T., Zhou, M., Wang, H., Hu, X.E. & Gao, Y. (2015). Research on Hierarchical Flood Operation Mode for the Three Gorges Reservoir. *Journal of Hydroelectric Engineering,* 34(4),1-7 (in Chinese).

Liu, P., Li, L., Guo, S.L., Xiong, L.H. et al. (2015). Optimal Design of Seasonal Flood Limited Water Levels and Its Application for the Three Gorges Reservoir. *Journal of Hydrology*, 527(1-2), 1045-1053.

Yangtze River Survey (2014). *Joint Operation Research Report of Xiluodu-Xiangjiaba-Three Gorges Reservoirs*, Planning and Design Co., Ltd, (in Chinese).